Chemical Approaches to Elucidate Lysine Phosphorylation

Dissertation zur Erlangung des akademischen Grades
doctor rerum naturalium
(Dr. rer. nat.)

im Fach Chemie
Spezialisierung: Organische und Bioorganische Chemie

Eingereicht an der
Mathematisch-Naturwissenschaftlichen Fakultät
der Humboldt-Universität zu Berlin

von
M. Sc. Anett Hauser

Präsidentin der Humboldt-Universität zu Berlin
Prof. Dr.-Ing. habil. Dr. Sabine Kunst

Dekan der Mathematisch-Naturwissenschaftlichen Fakultät
Prof. Dr. Elmar Kulke

Gutachter/innen:
1. Prof. Dr. Christian P. R. Hackenberger
2. Prof. Dr. Dorothea Fiedler
3. Prof. Dr. Christian Hedberg

Tag der mündlichen Prüfung: 27.10.2020

Abstract

Post-translational modifications (PTMs) of proteins give access to the huge functional variety required to organize and control cell homeostasis. Reversible phosphorylation is the most prominent PTM and affects all cellular processes. Although it is known to occur on nine amino acids, the *O*-phosphomonoesters of serine, threonine and tyrosine have been considered as the only notable forms since the discovery of post-translational phosphorylation. Recent developments in the field of chemical biology have paved the way to fundamental insights into the biological relevance of labile phosphorylations, e.g. phosphorylation of histidine, arginine and cysteine as well as pyrophosphorylation of serine and threonine. Also, elucidation of phospho-lysine (pLys) was tackled with first, the establishment of a chemoselective synthesis method to obtain site-selectively phosphorylated lysine peptides and second, the development of suitable mass spectrometric protocols to unambiguously identify modification sites. Nonetheless, no endogenous pLys site has been so far described or in-depth investigations of possibly interacting enzymes have been conducted.

In this thesis, several approaches to enhance the knowledge about lysine phosphorylation are introduced. These include the development of novel and advanced methods for the toolbox of chemical biology in general, and specifically studies regarding chemical properties as well as biochemical stability of this PTM. Along these lines, an alternative synthesis route to site-selectively phosphorylated peptides was explored and two stable pLys analogues were designed, synthesized as building blocks for solid-support peptide synthesis and validated with respect to their mimicry potential. Furthermore, the hitherto unproven protonation of the phosphoramidate ϵ-nitrogen was investigated in titration experiments using nuclear magnetic resonance spectroscopy.

Building up on the initial approaches, the interactions between *phospholysine phosphohistidine inorganic pyrophosphate phosphatase* (LHPP) and various phospho-substrates were examined in systematic phosphoramidate hydrolase and phosphatase activity assays. Thereby, distinct selectivity for pLys over other phosphorylation variants, high sequence dependence of LHPP activity and a distinct binding motif were revealed. In addition to that, proteomic methods were evaluated regarding their suitability for pLys peptides and partially optimized. Over the course of this investigation, several pLys immunogens for the generation of monoclonal α-pLys antibodies and a workflow for histone separation and analysis were developed. Furthermore, the chelation-enhanced fluorescence of labeled phospho-peptides was studied as a tool for determining the degree of phosphorylation in enzyme activity or stability assays.

Taken together, the gained knowledge and novel achievements presented in this thesis help to overcome challenges in the quest for endogenous lysine phosphorylation. It could be shown that every previously developed biochemical or proteomic technique needs to be tailored to the peculiar properties of this phosphoramidate. With the tools presented in this thesis, the study of post-translational protein lysine phosphorylation has been bolstered by new potential investigatory routes drawing from the fields of organic synthesis, protein–substrate interaction studies and affinity enrichment.

Kurzzusammenfassung

Posttranslationale Modifikationen (PTMs) von Proteinen ermöglichen den Zugang zur großen funktionellen Vielfalt, die zur Organisation und Kontrolle der Zellhomöostase erforderlich ist. Die reversible Phosphorylierung ist die prominenteste PTM und beeinflusst alle zellulären Prozesse. Die *O*-Phosphomonoester von Serin, Threonin und Tyrosin wurden lange Zeit als die einzigen wichtigen Vertreter angesehen. Jüngste Entwicklungen auf dem Gebiet der chemischen Biologie haben zu grundlegenden Erkenntnissen über labile Phosphorylierungen, z.B. Phosho-Histidin, -Arginin und -Cystein sowie die Pyrophosphorylierung von Serin und Threonin, geführt. Auch die Aufklärung von Phospho-Lysin (pLys) wurde mit der Etablierung einer Synthesemethode von ortsselektiv phosphorylierten Lysinpeptide und der Entwicklung geeigneter massenspektrometrischer Verfahren zur eindeutigen Identifizierung von Modifikationsstellen in Angriff genommen. Dennoch wurde bisher kein endogenes pLys-Protein beschrieben oder Untersuchungen von möglicherweise interagierenden Enzymen durchgeführt.

In dieser Arbeit werden verschiedene Ansätze zur Erforschung der Lysinphosphorylierung vorgestellt. Dazu gehören die Entwicklung neuartiger und verbesserter Methoden für die chemischen Biologie und Studien zu den chemischen Eigenschaften sowie zur biochemischen Stabilität dieser PTM. So wurde ein alternativer Syntheseweg zu ortsselektiv phosphorylierten Peptiden erforscht und es wurden zwei stabile pLys-Analoga entworfen, als Bausteine für die Feststoff-Trägerpeptidsynthese synthetisiert und hinsichtlich ihres Mimikry-Potentials validiert. Darüber hinaus wurde die bisher nicht nachgewiesene Protonierung des Phosphoramidat-Stickstoffs in kernmagnetresonanzspektroskopischen Titrationsexperimenten untersucht.

Aufbauend auf den ersten Berichten darüber wurden die Wechselwirkungen zwischen *Phospholysine phosphohistidine inorganic pyrophosphate phosphatase* (LHPP) und verschiedenen Phospho-Substraten in systematischen Phosphoramidat-Hydrolase- und Phosphatase-Aktivitätsassays untersucht. Dabei zeigten sich eine deutliche Selektivität für pLys gegenüber anderen Phosphorylierungsformen und eine hohe Sequenzabhängigkeit der LHPP-Aktivität. Darüber hinaus wurden proteomische Methoden hinsichtlich ihrer Eignung für pLys-Peptide evaluiert und teilweise optimiert. Im Zuge dessen wurden mehrere pLys-Immunogene zur Generierung von monoklonalen α-pLys-Antikörpern und ein Workflow zur Histonseparation und -analyse entwickelt. Des Weiteren wurde die chelatationsverstärkte Fluoreszenz von markierten Phospho-Peptiden als Werkzeug zur Bestimmung des Phosphorylierungsgrades in Enzymaktivitäts- oder Stabilitätsassays untersucht.

Zusammengenommen helfen die gewonnenen Erkenntnisse und die in dieser Arbeit vorgestellten neuen Errungenschaften, die Herausforderungen bei der Suche nach endogener Lysinphosphorylierung zu erfassen. Es konnte gezeigt werden, dass jede zuvor entwickelte biochemische oder proteomische Technik auf die besonderen Eigenschaften dieses Phosphoramidats zugeschnitten werden muss. Dabei können die hier etablierten Werkzeuge neue Wege zu Anwendungen eröffnen, z.B. in der organischen Synthese, bei Protein-Substrat-Interaktionsstudien oder bei der Affinitätsanreicherung.

"Wir können immer wieder anfangen. Was es dazu braucht? Nicht viel: etwas Haltung, etwas lachenden Mut und nicht zuletzt die Bereitschaft, die Blickrichtung zu ändern, damit es häufiger geschieht, dass wir alle sagen: Wow. So sieht es also aus dieser Perspektive aus."

Carolin Emcke

Erklärung der Autorin

Diese Arbeit wurde vom 01.02.2015 bis zum 15.12.2019 unter Aufsicht von Prof. Dr. Christian P. R. Hackenberger am Leibniz-Forschungsinstitut für Molekulare Pharmakologie angefertigt.
This work was carried out from 01.02.2015 to 15.12.2019 under the supervision of Prof. Dr. Christian P. R. Hackenberger at the Leibniz-Forschungsinstitut für Molekulare Pharmakologie.

Die dargelegten Ergebnisse der Kapitel 4.1, 4.2, 4.3 und 4.4 basieren zum Teil auf folgenden Publikationen:
The results presented in chapter 4.1, 4.2, 4.3 and 4.4 are based partially on the following publications:

- Hauser, A., Hwang, S., Sun, H. and Hackenberger, C.P.R. "Combining free energy calculations with tailored enzyme activity assays to elucidate substrate binding of a phospho-lysine phosphatase", *Chemical Science* **2020**, *11*, 12655-12661. DOI: 10.1039/D0SC03930F
- Hauser, A., Poulou, E., Müller, F., Schmieder, P. and Hackenberger, C.P.R., "Synthesis and evaluation of non-hydrolyzable phospholysine peptide mimics" *Chemistry—A European Journal* **2020**. DOI: 10.1002/chem.202003947

1. Gutachter:	Prof. Dr. Christian P. R. Hackenberger Chemische Biologie II Leibniz-Forschungsinstitut für Molekulare Pharmakologie
2. Gutachterin:	Prof. Dr. Dorothea Fiedler Chemische Biologie I Leibniz-Forschungsinstitut für Molekulare Pharmakologie
3. Gutachter:	Prof. Dr. Christian Hedberg Department of Chemistry UmeåUniversitet

Table of Content

1 | Motivation

Cellular processes in all their variety are predominantly controlled and also conducted by proteins, which as such make a huge fraction of the macromolecular cell mass, e.g. 55% of the dry weight of an average *Escherichia coli* cell.[1] In order to meet the required functional and structural complexity, proteins are most often post-translationally modified. Reversible phosphorylation of proteins is a highly abundant post-translational modification (PTM) and induces with the addition of negative charge to the molecule conformational changes and activation or deactivation of enzymes. Even though hundreds of thousands of phosphorylation sites are known, by far not all of their biological roles have been revealed yet and there are probably many more phosphorylated proteins still to discover. Furthermore, altered phosphorylation regulation can induce severe diseases as, for example, kinase activity is upregulated in most cancer types. Consequently, a deep understanding of this PTM is crucial in order to target specific cellular processes or treat diseases successfully. The apparent ubiquitous involvement of phosphorylation as a PTM is achieved by its incorporation in a variety of nucleophilic amino acid side chains. Among these, the phosphorylation of lysine is one of the most elusive, labile modifications. Despite significant reports on its occurrence in histone H1 more than 45 years ago, no further profound studies on the biological role has come to light so far.

Chemical biology is a powerful research area, representing the interface between design and preparation of synthetic molecules and their application in order to understand and interfere with biological processes. This field encompasses a huge variety of tools from organic synthesis to biological techniques and proteomics, at least one possible strategy for each purpose. Rather general questions regarding the chemical properties of biological substrates and their alterations are the basis of chemical biology.
Beyond that, chemoselective reactions can be utilized to introduce modifications at desired positions in a molecule. With development of the Staudinger-phosphite reaction for biochemical applications about ten years ago, our group has enabled access to site-specifically phosphorylated lysine peptides, which could be investigated regarding their stability.
Besides in the synthesis of model substrates, chemistry stands also at the beginning of antibody generation, as haptens employed during immunization often have to be designed and synthesized with individual properties. Especially if the target is a labile PTM, suitable stable mimics are required to avoid probe degradation during the immunization process. Those generated antibodies can be applied in detection or enrichment of the substrate of interest in biological samples.
In turn, protocols for proteomic sample preparation to identify phosphorylation sites have to be tested for their fitness as well since phosphoramidates disfavor conventional techniques due to

their intrinsic lability. Besides the substrate identification itself, interacting enzymes are key factors to understand the biological importance. Regarding phosphorylation, especially selective kinases and phosphatases indicate the occurrence of certain phospho-amino acids. Another high-potential device are fluorogenic tags as they can be synthetically introduced and offer great sensitivity as biosensors, for example, for phosphorylation during detection and quantification. They can be applied in various studies, e.g. enzyme activity assays, protein–protein interaction experiments or the investigation of certain modifications.

The basic goal of these doctoral studies was the expansion of the chemical toolbox available to scientists for the elucidation of phospho-lysine occurrence in organisms. Our aim was to investigate this modification more closely from different sides. As such, various approaches will be explored further in the context of this thesis. Out of all of the methods for studying life encompassed by the field of chemical biology, chemical peptide synthesis, proteomics, enzyme activity and fluorescent peptide biosensors offered us helpful techniques in the quest for phospho-lysine. We believe that the contributions from our studies reveal further pieces of the phosphorylation PTM puzzle which give reason as well as access to further investigations in this field.

2 Introduction

2.1 Post-Translational Modification of Proteins

Compared to other biological macromolecules, such as carbohydrates, lipids and nucleic acids, proteins exhibit the largest structural diversity and each cell contains several thousand different species. They make up approximately 50% of the dry weight of cells [2] and serve as the executors of biological tasks. [3] As such, proteins are involved in a wide variety of functions, e.g. building structural components (microtubules), transport of molecules (hemoglobin), signal transduction (hormones) and defense mechanisms (antibodies). The majority of proteins performs as enzymes by catalysis of nearly every chemical reaction in biological systems. Depending on the superior objectives, protein families have evolved to varying magnitude of versatility. This means, for core functions as in transport, transcription and translation, proteins have diversified less than for regulatory functions as signaling, metabolic processes and phosphorylation [4] Strikingly, the information for this broad variety in structure and functionality is originated in the relatively small encoding genome, e.g. approximately 19-20,000 genes [5] code more than 9.3 million proteins [6] in humans. Besides alternative splicing, [7] post-translational modifications (PTMs) give predominantly access to this proteome complexity.

Post-translational modification (PTM) of proteins describes the usually enzymatic but occasionally also non-enzymatic [8] alteration of proteins following their biosynthesis. These modifications can be installed directly after formation of the polypeptide chain in order to promote protein folding and stability or at a later stage as a response to changing conditions, for example, in signal transduction, enzyme de- and activation or protein degradation. Statistical analysis has shown that proteins undergoing PTMs commonly participate in more protein–protein interactions and are positioned at more central locations in organisms than non-modified proteins. [9] To date, more than 500 different reversible alterations of proteins [10] have been discovered. PTMs can occur either as small chemical groups (alkylation, acylation, glycosylation, phosphorylation) or large biomolecules (palmitoylation, ubiquitination, SUMOylation), which are covalently attached to functionalities of amino acid (AA) side chains. Thereby, sites, which can serve as a nucleophile during modification, are subject of PTMs. [11] Besides the amino- (*N*-) and carboxyl- (*C*-)termini of proteins, the hydroxyl groups of serine, threonine and tyrosine (Ser, Thr, Tyr), the thiol of cysteine (Cys), the carboxyl groups of aspartate and glutamate (Asp, Glu) and the amines of histidine, arginine and lysine (His, Arg, Lys) are addressed regularly. Among the mentioned residues, Lys exhibits unique properties and can be modified in many ways as outlined below.

2.1.1 Versatility of Lysine

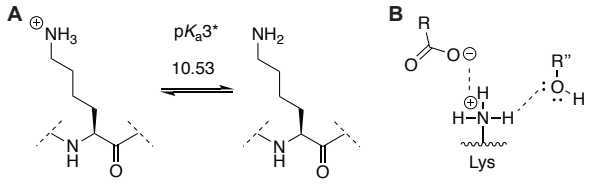

Figure 2.1: **A**. The Lys side chain amine is highly basic [12] and thus protonated under physiological conditions. **B**. It can non-covalently build electrostatic interactions with negatively charged residues or hydrogen bonds with electron lone pairs. * pK_a1 and pK_a2 for the deprotonation of carboxyl group and α-amine, respectively, are not relevant when Lys is bound in a peptide or protein.

His, Arg and Lys represent the proteinogenic AAs with amines in their side chains and even though it is an essential AA, Lys makes up of approximately 6% of all residues in the human proteom. [13] The ϵ-amine of Lys is highly basic with an acid dissociation constant (pK_a) of 10.53 and thus, positively charged under physiological conditions (figure 2.1**A**). [12] Compared to the delocalization in Arg, the charge is located on one atom and can build only one-dimensional interactions with negative charges or free electron pairs (figure 2.1**B**). Nonetheless, the flexibility of its alkyl chain makes Lys a potent binding partner. Due to the positive charge, Lys similar to Arg residues are highly hydrophilic and often located on the surface of proteins to ensure solubility by interaction with water. [3] In fact, observations about the Lys/Arg ratio in various proteins in correlation to their solubility indicated that a higher Lys content is favored by proteins, which are expressed at high concentrations. [14] Opposite to that, Arg residues seem to have a higher influence on protein stability as the guanidinium moiety can form interactions in different directions and also delocalize the positive charge. [15] However, experiments with site-selectively acetylated Lys side chains have demonstrated the importance of electrostatic interaction between ϵ-aminium ions and negative charged residues for protein structural integrity. [16] These interactions might have a similar function to disulfide bonds even though they are much weaker.

Besides localization on the surface of proteins, Lys residues are also found inside of the protein structure and often even in the catalytic center, e.g. in the active sites of protein kinases where they are involved in the phosphate transfer. [17] When buried and being separated from water, the electrostatic bonds are stronger and can indeed influence the structure. [18] Additionally, a high reactivity and ligandability of interior Lys side chains have been mapped with various electrophiles [19] and also shown in inhibitor assays. [20] This accumulation of reactivity might be result of significantly decreased pK_a values of the buried ϵ-amine. Titration studies have revealed pK_a values down to 5.3 instead of 10.5 for Lys inside of protein structures, which indicated an nucleophilicity increase of those residues. [21]

As mentioned above, Lys is the target of many different PTMs (figure 2.2). [22,23] Almost twenty modifications [24] are known, of which hydroxylation [25] was discovered first and polyphosphorylation [26] most recently. Besides in the case of hydroxylation, modifications are introduced at the ϵ-amine of the side chain. Thereby, PTMs mostly are linked *via* an amide bond and only three types of alkylation (methylation, glycation, ADP-ribosylation) and two types of phosphoramidate formation (poly-/phosphorylation) have been reported. Among the known PTMs, only glycation seems to occur without any enzyme being involved.

The main impact of modifications on ϵ-amine is the altered net charge, which is predominantly shifted to neutral, mono- or multi-negative. Together with the substrate size, this effects interactions of Lys with other residues and hence, the protein structure. Especially the combination of different PTMs has regulatory effect on protein activity. [27]

While some PTMs on Lys as acetylation, methylation and ubiquitination are extensively studied and their biological role has been understood to a certain extend, some modifications are barely recognized and the scientific community only starts to dedicate their effort towards them. Among these, Lys phosphorylation is one of the most elusive PTMs as will be depicted later.

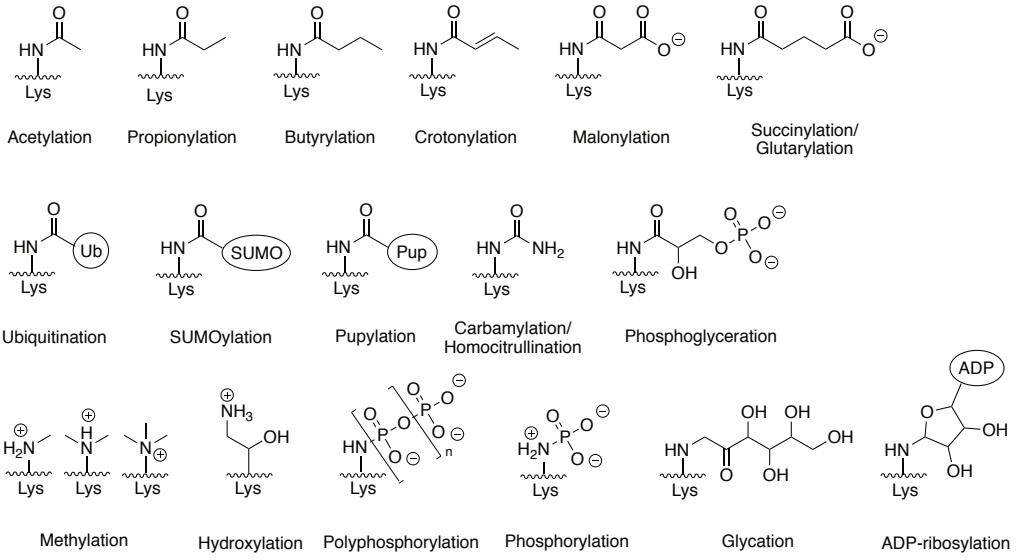

Figure 2.2: Lys residues undergo many types of PTMs. [24]

2.1.2 Phosphorylation of Proteins

Among post-translational modifications, reversible protein phosphorylation is by far the most abundant and occurs on many different AAs due to its versatility and rapid reaction kinetics. [28] Being described first in 1906 by Levene and Alsberg, [29] it took almost another fifty years to reveal this modification as a process controlled by enzymes. [30] In fact, phosphorlyation describes the cellular response to a conditional change by addition of a phosphate group to a nucleophilic AA residue whereby usually a nucleoside triphosphate (adenosine or guanosine triphosphate, ATP or GTP) is consumed. The reverse reaction is a hydrolysis upon which inorganic phosphate (P_i) is released (figure 2.3**A**). This equilibrium is tightly regulated enzymatically by kinases and phosphatases and further an indicator for the health of an organism. In several diseases, e.g. many cancer types, kinase activity is upregulated while phosphatases are suppressed. [31,32]

Upon phosphorylation, two negative charges are introduced to the modified protein at a distinct site, which then presents properties varying from all natural AAs. The chemical state of the protein surface is altered as the phosphate can form either inter- or intramolecularly hydrogen bonds with polar AAs as well as electrostatic interactions with positively charged residues. Especially interactions with Arg are favored as the rigid guanidinium structure can build direct hydrogen bonds with the doubly charged phosphate group (figure 2.3**B**). Indeed, because of the high negative charge density, phospho-AAs build stronger hydrogen bonds to Arg than Asp or Glu. [33]

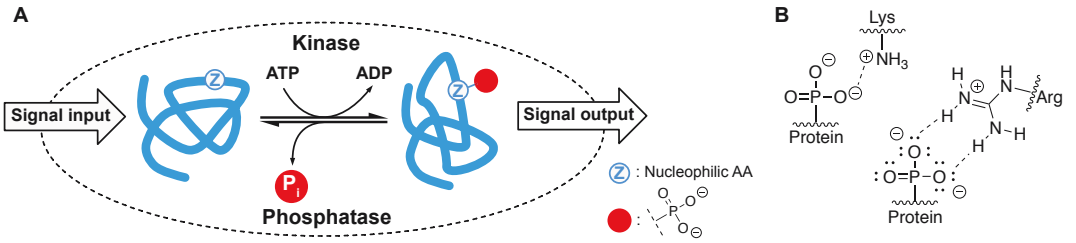

Figure 2.3: **A**. Phosphorylation of proteins is catalyzed by kinases under adenosine triphosphate (ATP) consumption. The reverse reaction is mediated by phosphatases and produces inorganic phosphate (P_i). **B**. The phosphate group can enter electrostatic interactions or hydrogen bonds.

As a result, phosphorylated proteins can undergo conformational change and distribute to another subcellular location. Furthermore, their binding behavior, activity and turnover can be altered.[34] Evaluation of twelve common PTMs has revealed that proteins undergoing phosphorylation are located in central network locations and have a broad spectrum of interactions with other modified proteins. Consequently, phospho-proteins occur in most intracellular compartments and are involved in nearly all biological processes.[9] As an example, phosphorylation has great importance in cell signaling. From transmembrane receptors, e.g. *epidermal growth factor receptor* (EGFR) over various intracellular signaling pathways, e.g. *mitogen-activated protein kinase* pathways (MAPK to MAPKKK) to the final destination, stimuli are forwarded and the cellular response prepared by phosphorylation and dephosphorylation events.[35]

Since phosphorylation occurs in very diverse contexts, its interdependence with other PTMs is rational. Crosstalk between different modifications can occur in a positive or negative feedback. Thereby, positive crosstalk describes the installation or removal of a PTM or also recruitment of a modifying enzyme upon a first modification event. For example, phosphorylation can prime kinase engagement or induce ubiquitination or SUMOylation.[36] Contrary to that, negative crosstalk describes the direct competition of several PTMs over one residue or the indirect effects as one modification prevents the introduction of further PTMs on other AAs. This can be found, for example, in MAPK where acetylation of certain Ser residues inhibits their phosphorylation and blocks the downstream signal transmission.[37] Also the attachment of *O*-linked *N*-acetylglucosamine residues to specific Ser or Thr can inhibit phosphorylation at other sites, e.g. in Tau protein.[38,39] The combined action of phosphorylation, acetylation and further ubiquitination can also be observed in various heart diseases or the response of *tumor protein p53* to genotoxic stress.[40,41] Especially in histones, whole patterns of various PTMs occur, which are not completely understood but have regulatory effects on deoxyribonucleic acid (DNA) packing and gene transcription.[27,42]

It can be seen that phosphorylation as a post-translational event has significant impact on cellular processes by itself or in combination with other PTMS. The highly diverse information gathered so far indicates a ubiquitous involvement of phospho-proteins in organisms and announces even more functions to be discovered within less studied areas.

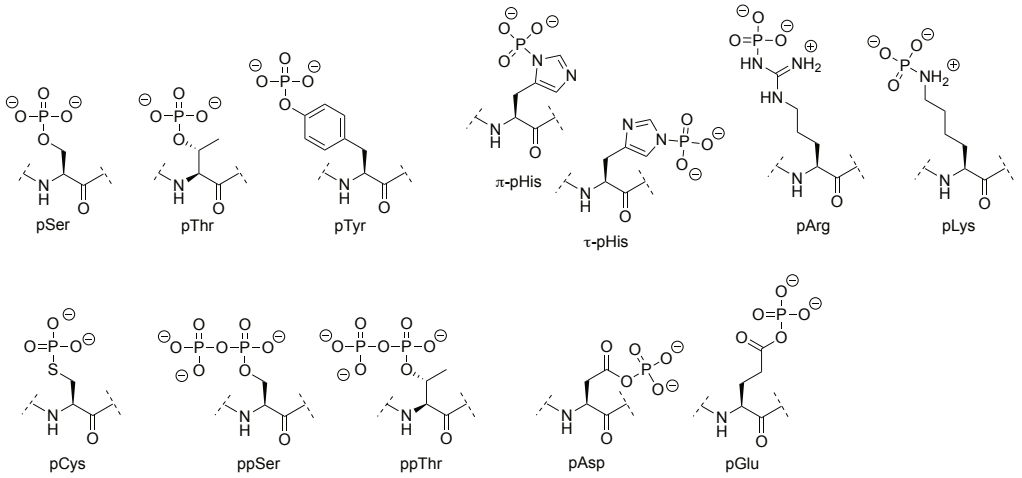

Figure 2.4: Phospho-amino acids with assumed charge under physiological conditions, which have been reported to occur as PTM in proteins.

To date, eleven different phosphorylation events on nine AA residues forming five structural classes are known (figure 2.4):[43,44] the *O*-phosphomonoester of phospho-serine, -threonine and -tyrosine (pSer, pThr, pTyr), the *N*-phosphoramidates of phospho-histidine, -arginine and -lysine (pHis, pArg, pLys), the *S*-phosphorothioate of phospho-cysteine (pCys), the phosphoanhydrides of phospho-aspartate and -glutamate (pAsp, pGlu) and the pyrophosphates of serine and threoine (ppSer, ppThr). This pool of phosphorylation events is usually divided into groups defined by their P–X bond stability under physiological conditions and during conventional phosphoproteomic analysis, which is equivalent to the amount of knowledge about them. While stable phosphorylation includes the *O*-phosphomonoesters of pSer, pThr and pTyr, labile phosphorylation events describes all other phospho-AAs since they are susceptible to hydrolysis under acid treatment or at elevated temperatures. Still, studies on phosphate ester AAs are very valuable for the present work as they guide the way to biological role elucidation of these events. Also, the main understanding about how protein phosphorylation impacts cellular functions, which was described above, is based on research about stable phosphorylations. As mentioned before, pSer and pThr were identified already at the beginning of the 20th century while pTyr was not reported before 1979.[45] The three phosphate esters occur in a significant different ratio from the unphosphorylated AAs even though some protein kinases exhibit Ser and Thr activity. For example, in human, fly, worm and yeast an average of 8.5% Ser, 5.7% Thr and 3.0% Tyr residues are present.[46] Still, the ratio of the phospho-species is 76:15:9 for pSer:pThr:pTyr as annotated by UniProt.[27,47] It seems like most Ser/Thr kinases have a preference for Ser over Thr, whereas pSer/pThr phosphatases act more readily on pThr residues.[48,49]

2.1.3 Labile Phosphorylation Species

Besides *O*-phosphomonoesters, all other known phospho-AAs pertain to the class of labile PTMs. It is known that these phosphorylation events have also biological significance even though the available data is much less.

Although pHis, pArg and pLys are characterized by a phosphoramidate bond, they all exhibit

varying properties regarding chemical as well as physical characteristics and consequently their stability. Since large efforts have been made to study them and the previous knowledge built the basis for this present work, these PTMs will be introduced in the next section (2.1.4). Polyphosphorylated Lys presents a special type of phosphoramidate since the derivatization of AA side chain happens *via* an phosphor-nitrogen (P–N) bond, but the whole PTM functions rather as an anhydride. So far, only one study described the polyphosphorylation of Lys as a non-enzymatic modification in *Saccharomyces cerevisiae* (*S.cerevisiae*).[26]

Phospho-Cys was reported to be the key AA in the catalytic center of various phosphatases, e.g. *protein-tyrosine phosphatases* (PTPs) or phosphatases in regenerating liver.[50,51] Also in bacterial systems, pCys occurs as, for example, in the *phosphoenolpyruvate-dependent phosphotransferase system* within the glycolysis pathway of *Escherichia coli* (*E.coli*)[52] or as crucial effector of bacterial resistance of *Staphylococcus aureus* (*S.aureus*) in the protein family of *staphylococcal accessary regulator A/MarR family global transcriptional regulator* (SarA/MgrA).[53]

Studying the acylphosphates of Asp and Glu is particularly challenging since they are prone to hydrolysis under both, acidic and alkaline conditions. Thus, their occurrence is rather verified indirectly, e.g. by selective reduction and simultaneous tritium labeling with $NaBH_4$/[^{3}H]$NaBH_4$ or by *in situ* trapping with desthiobiotin-linked hydroxylamine (DBHA), which forms stable intermediate with pAsp and can be enriched for mass spectrometric analysis afterwards.[54,55] Compared to pGlu, little more is known about pAsp sites. Temporarily phosphorylated Asp residues can be found in catalytic centers of several enzymes such as members of the *haloacid dehalogenase* (HAD) superfamily or the two-component signaling system.[56–59] Both phosphoanhydrides appear as intermediates in aminoacyl-tRNA biosynthesis and in phospholipids of rat brain.[57,60]

Pyrophosphorylation of Ser and Thr represents another class of mixed anhydrides, which was discovered quite recently. Notably, this PTM is rather stable compared to the other mentioned phospho-AAs. However, under harsh acidic or basic conditions and at elevated temperatures pyrophosphates get hydrolyzed to Ser or Thr residues. The phosphate transfer from hyperphosphorylated inositols as diphosphoinositol pentakisphosphate and bis-diphosphoinositol tetrakisphosphate (IP_7 and IP_8, respectively) to proteins was described in 2004 and later assigned to form pyrophosphorylated Ser on priming pSer residues.[61,62] Strikingly, the phosphorylation of Ser or Thr is catalyzed by kinases but the second phosphate group is incorporated without enzyme activity and only requires magnesium ions to be present.[61,63,64] So far, pyrophosphorylation was mainly reported to occur in yeast but might also play a major role in mammalians.[65,66]

2.1.4 Phosphoramidates

Phosphoramidates represent the most diverse group of labile phosphorylations. Despite the fact that the PTM is introduced on a nitrogen of the AA side chain, the structures of pHis, pArg and pLys differ clearly in their electron distribution and thus, their stability (figure 2.5). For all of them, the P–N bond is higher in energy than P–O bonds, as -12 to -14 kcal·mol^{-1} Gibbs energy are released from phosphoramidates[67–69] compared to -6 to -9 kcal·mol^{-1} from phosphates.[70,71]

Nonetheless, in the cases of pHis or pArg, some stability is gained by partial expansion of the aromatic system *via* the nitrogen lone pair or partial charge delocalization in a six-membered co-

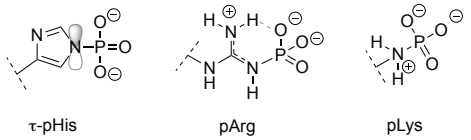

Figure 2.5: Structural situations in pHis, pArg and pLys.[72–74] Figure adapted from Hauser *et al.*.[44]

ordinative ring system, respectively (figure 2.5). Hence, the nitrogens of the P–N bond are not basic. For pLys, the assumed positive charge of the ϵ-nitrogen is localized, thereby weakening the phosphoramidate bond, which will be elaborated more in the next section (2.1.4.1).
Phospho-His was detected almost sixty years ago in radiolabeled mitochondria[75] and mostly connected with phosphate transfer in the two-component signaling system[59,76] until its importance in mammalian cells and tumor tissue got revealed in more detail.[77–79]
Phospho-Arg functions as phosphagen to buffer ATP concentrations in vertebrates.[80] Until the identification of McsB as *protein arginine kinase*, not many studies have been published on this PTM.[81] Since then, a high degree of Arg phosphorylation in *Bacillus subtilis* (*B.subtilis*)[82] and *S.aureus*[83,84] has been reported. Very recently, Arg phosphorylation could be verified in Jurkat cells and with this still hidden details about this modification have been indicated.[85,86]

2.1.4.1 Phosphorylation of Lysine

Phospho-Lys was first identified in cell extracts from rat liver after incubation with [^{32}P]ATP in the late 1960s.[87–89] Within the following ten years, a kinase showing activity towards Lys in histone H1 could be isolated[90,91] and pLys occurrence detected *in vivo* in rat liver as well as in Walker-256 carcinoma (W256).[92,93] Nonetheless, neither the reported kinase has been characterized further nor a distinct pLys site in any protein identified to date.

The main reason for this blank space in biology despite the first promising studies might be the intrinsic high lability of this phosphoramidate under acidic condition, which are commonly applied in phosphoproteomic approaches. As mentioned before, it is assumed that the ϵ-amine of pLys is protonated under physiological conditions (figure 2.4). This expectation is based on titration studies conducted with *N*-(*n*-butyl)phosphoramidate (*n*-BPA) by Benkovic *et al.*[74] The structural situation is thus completely different from the partial aromaticity in pHis. Also, the positive charge can not be delocalized as in pArg. Additionally to that, compared to carbonyl amides, the P–N bond has mostly single bond character.[94,95] As a result, which could be seen in the study of Benkovic *et al.*, the acid dissociation constant of the ϵ-nitrogen remains similar to the unphosphorylated amine (pK_a(Lys) = 10.53[12], pK_a(*n*-BPA) = 9.9[74]). This influence was further investigated with regard to the phosphoramidate hydrolysis rate.[96] As long as one phosphoryl oxygen is protonated (below pH 3[74]), the P–N bond is highly unstable and gets cleaved very fast. At the stage where both phosphoryl oxygens are deprotonated but the amidate nitrogen still protonated (pH 3 to 10), the hydrolysis rate is moderately high. Only after subsequent deprotonation of the nitrogen, phosphoramidates exhibit increased stability.[74] Similar observation were made with pLys peptides by Bertran-Vicente *et al.*[97] While samples incubated at pH 3.2 or below showed half-life times ($t_{1/2}$) of approximately 2.5 hours, the same peptides were stable more than 18 hours at pH values 4.5 or higher. Also the temperature influence at pH 7.4 was investigated and revealed $t_{1/2} \approx$

24 hours at 25 °C and less than one hour at 60 °C or higher. In comparison to, for example, pArg, which shows a similar pH profile but is stable at 60 °C and pH values 7 or higher, [98] the temperature dependence might be the crucial point in feasible Lys phosphorylation examinations.

Very recently, three studies have been published claiming the discovery of several hundred phospho-Lys sites in various proteins from HeLa cells or *E.coli* by the groups of Hunter, Chen and Eyers. [99–101] The value of these results might be doubted since they are based on statistical probability. For once, access to sample sequences or raw data is missing. [101] Furthermore, none of the identified pLys-carrying sequences was evaluated by analysis of according synthetic pLys peptides. [99–101] These studies do indeed hint to pLys occurrence in various organisms but are no unambiguous proof. However, the fact that the success of all three works is based on fast sample preparation at neutral or basic pH speaks for the requirement of adjusted biochemical techniques to the challenging properties of phosphorylated Lys. General and tailored approaches to study protein phosphorylation are introduced in the following section.

2.2 Investigation of Peptide and Protein Phosphorylation

Investigations of elusive modifications involve numerous studies including chemical and physical properties, interaction with enzymes and identification *in vitro* or *in vivo*. Prior to any functional experiment, selectively modified peptides and proteins need to be synthesized and characterized.

2.2.1 Solid-Phase Peptide Synthesis

Synthetic peptides are usually obtained by solid-phase peptide synthesis (SPPS). Primed by the achievements of Fischer and Bergmann who showed the first synthesis of di- and tripeptides in solution [102] and the advantageous utilization of *N*-terminal protection, [103] the principle of SPPS was introduced by Merrifield in 1963. [104,105]

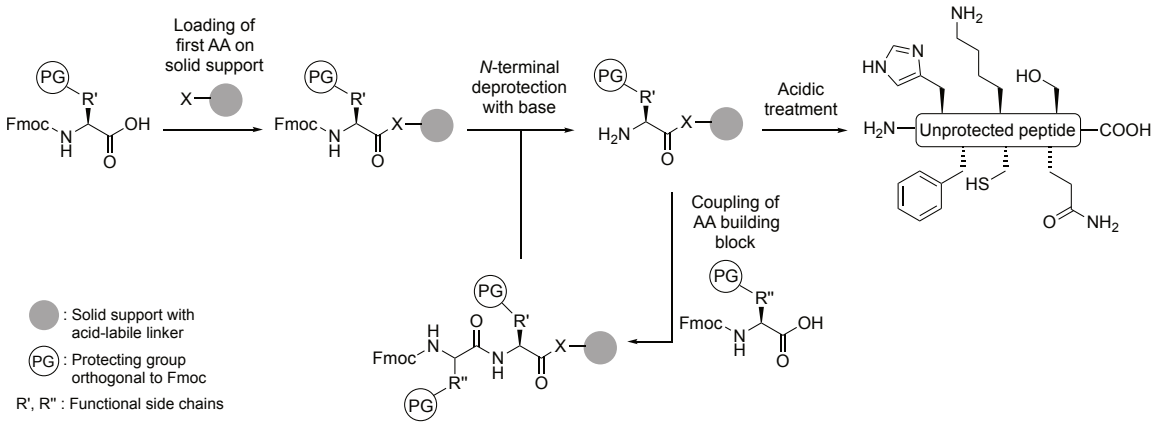

Figure 2.6: General principle of solid-phase peptide synthesis (SPPS) following the Fmoc-protection strategy.

As shown in figure 2.6, by application of a solid support the peptide chain can be built link by link without purification steps in between. Thereby, the employment of orthogonally pro-

tected AA building blocks is a key factor to distinguish the *N*-terminal and AA side chain reactivity. Briefly, an *N*-terminally fluorenylmethyloxycarbonyl- (Fmoc-) and side chain-protected AA is loaded on to the solid support *via* an acid-cleavable linker. Before coupling the next AA building block, the α-amine is deprotected with a nucleophilic base. Coupling occurs upon activation of the *C*-terminal carboxyl group with carbodiimide-, *N*-hydroxybenzotriazole- (HOBt-) or ethyl cyanohydroxyiminoacetate- (Oxyma-)based coupling reagents. [106,107] After final AA conjugation, the peptide is cleaved from the solid support and simultaneously deprotected by treatment with acid (figure 2.6).

By applying SPPS, functionally diverse peptides from desired sequence length can be prepared. [108] Thereby, the combination of different side chain protection strategies allows selective deprotection of certain AA residues and gives access to tailored modifications or branched peptides. Especially the possibility to incorporate not only natural AAs but building blocks with either modified side chains or non-canonical AA character, e.g. halides, alkynes or azides, expanded the scope of functional peptide synthesis significantly. [109,110] Incorporated reactive handles can be applied in further functionalization of the peptide substrate as depicted in the next section. Along these lines, some PTMs can be introduced during SPPS already if the modification is stable against coupling and cleavage conditions. For example, pSer, pThr and pTyr peptides can be prepared conveniently and yield bioactive peptides after cleavage (figure 2.7**A**). [39,108,111] Another phospho-AA whose precursor can be introduced during Fmoc-SPPS is pArg. [112] Hofmann *et al.* developed a 2,2,2-trichloroethoxy- (Tc-)protected phosphoramidate, which was stable enough to withstand coupling, *N*-terminal deprotection and acidic conditions to give a caged pArg peptide upon cleavage from the solid support. Subsequent hydrogenation at basic pH yielded free pArg (figure 2.7**B**). Some more information about this approach can be found in section 4.1.

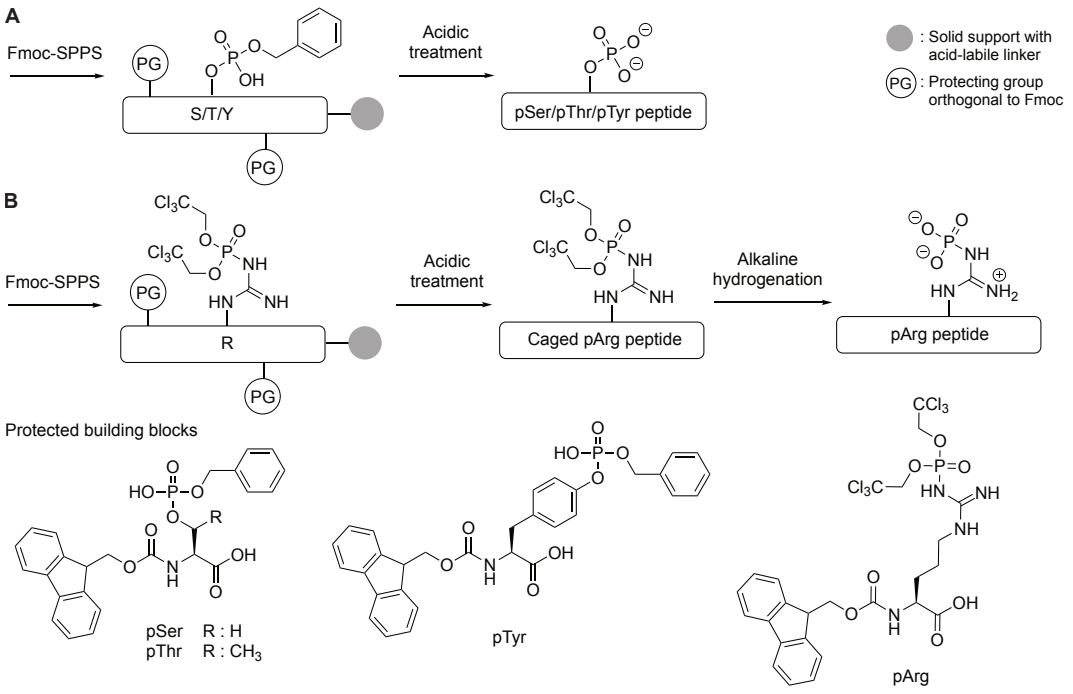

Figure 2.7: SPPS approaches for preparation of phosphorylated peptides. **A**. *O*-phosphomonoesters of pSer, pThr and pTyr can be obtained directly after cleavage from the solid support. [108] **B**. The Fmoc- and Tc-protected phosphoramidate of Arg yields a precursor during SPPS, which can be uncaged by hydrogenation. [112]

2.2.2 Site-Selective Modification of Peptides and Proteins

Crucial for reliable method development and subsequent analysis of proteomic samples directed towards specific PTMs is the preparation of homogenous, defined substrates. In order to obtain such samples, site-selective modifications are ideal.[113,114] Biological techniques to achieve site-selectivity on protein level include incorporation of already modified as well as unnatural AAs for later derivatization by genetic code expansion and Amber codon suppression.[115] By doing so, common Lys PTMs as methylation, acylation and ubiquitination can be addressed for example. While acetylated Lys residues can be introduced directly, methylated or ubiquitinated proteins are obtained by combining genetic code expansion with chemical reactions or a native chemical ligation–desulfurization approach, respectively.[116]

On peptide and protein level, chemical methods are applied to gain site-selectivity. On one hand, this can be done by taking advantage of the unique reactivity of natural occurring residues, e.g. *N*- and *C*-terminus, Cys thiol or Lys amine. For example, Cys can be addressed for elimination and subsequent addition, reaction with maleimides and haloacetamides, disulfide exchange or formation of adducts with phosphonamidates and -thiolates.[117–119] Lys reacts selectively with *N*-hydroxysuccinimide (NHS-)esters, iso(thio)cyanates and aldehydes.[113] Thereby, site-selectivity can only be granted if various residues of the same AA can be clearly discriminated in their reactivity or accessibility.

On the other hand, the introduction of non-canonical AAs with bioorthogonal reactivity and subsequent derivatization is a powerful tool to modify peptides and proteins not only site-selectively, but also chemoselectively. The term of bioorthogonality was introduced by the Bertozzi group and describes chemical reactions, which can take place without interference of cellular processes often to study living systems in real time.[120–122] These chemical reactions are most commonly a type of ligation to introduce, for example, fluorophores, tags, drugs or PTMs or to achieve stabilization of peptides or proteins against structural flexibility or proteases.[113,121] Azides have proven as particularly potent in bioorthogonal approaches as they can undergo cycloaddition[123] and reduction to amines and amides. Thereby, the azide group has great advantages like its small size, which provides bioavailability, stability against degradation and no natural occurrence meaning no competition with other biomolecules or residues.

2.2.2.1 Site-Selective Phosphorylation Approaches

With regard to phosphoproteomics, peptides and proteins containing defined phosphorylation sites are required for method development and evaluation as well as detected phospho-site confirmation. Different techniques have been developed depending on the nature of phosphorylation and substrate. As mentioned in section 2.2.1, *O*-phosphomonoesters of pSer, pThr and pTyr can be introduced into peptides during SPPS. In proteins, genetic engineering applied for *E.coli* has offered the possibility to obtain distinct Ser,[124–126] Thr[124–127] and Tyr[128–130] phosphorylation sites. Especially pTyr presents challenges and researches have developed, for example, an pTyr protected as phosphordiamidate[129] or a Lys-pTyr dipeptide[130] for site-specific incorporation.

Taking a look at labile phosphorylations, different approaches are reported for the installation of these PTMs.[44,131] So far, no synthesis of pAsp and pGlu peptides or proteins is reported. These

phospho-AAs can only be obtained as monomers.

As shown in figure 2.8, methods have been tailored for the individual AA residues and proceed not always site-selectively. Phospho-Cys can be obtained *via* chemoselective reactions on unprotected peptides or proteins. The Hackenberger group developed the two-step reaction wherein the nucleophilic Cys thiol is converted to an electrophilic disulfide and reacts subsequently with phosphites to form a phosphorothioate (figure 2.8**A**). [52] On protein level, oxidative elemination followed by addition of thiophosphate is the only reported synthetic method. [117,132] During this approach, the chiral information at the α-carbon is lost and both enantiomers are formed (figure 2.8**B**). Studies have shown that an approximate ratio of 60:40 (D-:L-form) is obtained independently from the structural environment. [133] It should be noted that both approaches are not site-selective and would convert all Cys in a peptide or protein. Hence, other accessible Cys residues have to be excluded from the sequence during SPPS or by mutation for peptides or proteins, respectively.

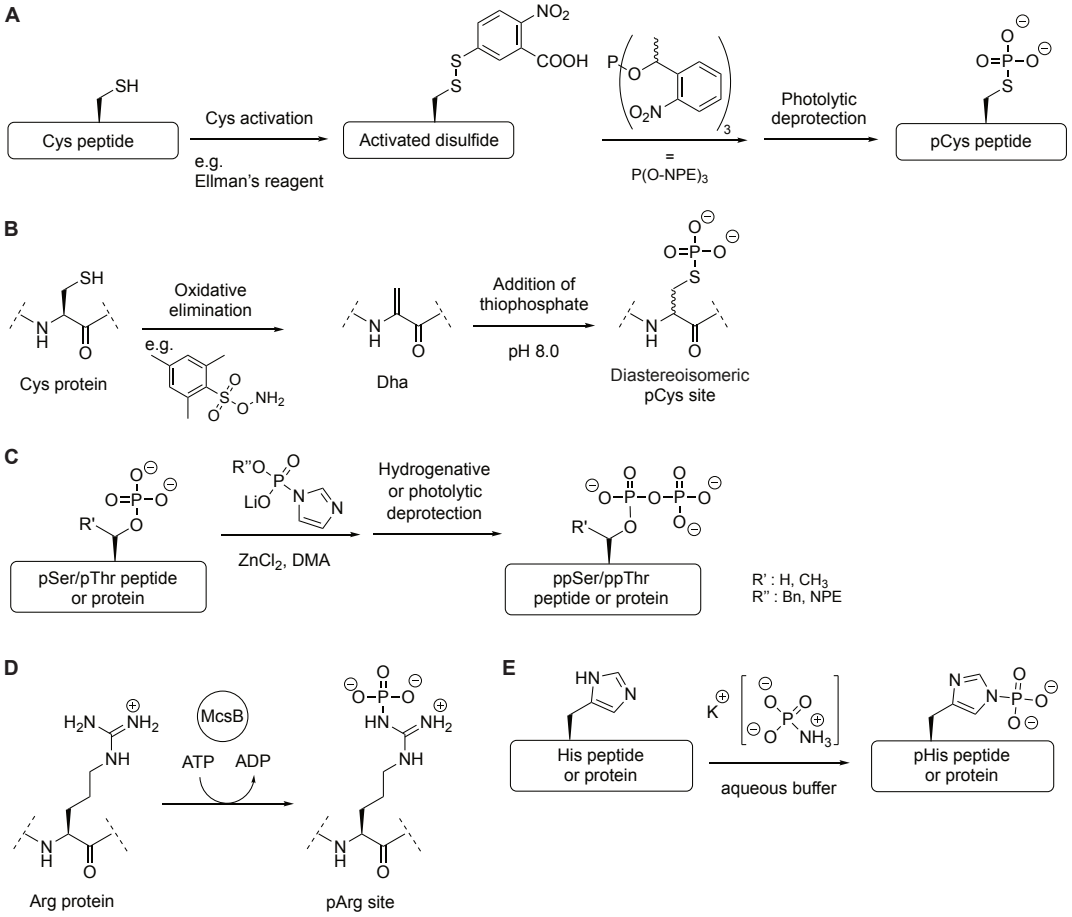

Figure 2.8: Synthetic approaches besides direct incorporation during SPPS to obtain peptides and proteins phosphorylated on Cys (**A** & **B**), pSer and pThr (**C**), Arg (**D**) and His (**E**).

Pyrophosphorylated Ser and Thr peptides or proteins can indeed be obtained in a site-selective fashion. [134,135] Marmelstein *et al.* developed several phosphorimidazolide reagents to chemoselectively functionalize pre-phosphorylated Ser or Thr residues (figure 2.8**C**). Thereby, phospho-Ser and -Thr peptides can be prepared as described in section 2.2.1, while proteins with pSer incorporated were prepared by genetic encoding as reported by the Chin group. [136] Depending on the

protecting group, free ppSer and ppThr was obtained by photolysis or hydrogenation.[134,135]

Also pArg peptides can be synthesized site-selectively as described in the previous section (figure 2.7**B**).[112] Arg residues in peptide and protein sequences can be phosphorylated enzymatically with McsB under ATP consumption (figure 2.8**D**).[137] This approach is not site-selective since McsB does not act sequence-dependently and thus, interacts with every accessible Arg residue.

For installation of pHis in peptides and proteins only global phosphorylation reagents are known. Due to the low pK_a value of the imidazole nitrogen, His can be addressed in presence of free *N*-termini, Lys or Arg (pK_a = 6.00, compared to ~9, 10.53, 12.48 for *N*-termini, Lys, Arg, respectively)[12], whereby side reactions with the other amines cannot be excluded. Incubation with potassium phosphoramidate (K-PA) at basic pH is the most applied phosphorylation technique (figure 2.8**E**).[138] However, it has been claimed by Hu *et al.* that also Lys residues undergo phosphorylation with K-PA.[101] Furthermore, Ruman *et al.* reported phosphorylation of several AAs including His, Arg, Lys and Cys with K-PA.[139] Besides the phosphoramidate, also phosphoryl chloride can be used to phosphorylate His.[138] Again, depending on the pH, also Lys reacts with this reagent.[87] Upon addition of Cu^{II} salt, pArg can be obtained as well.[140] Notably, all variants of pHis – π-pHis, τ-pHis or even 1,3-di-pHis – can be formed and the ratio of products is predominantly dependent on the reaction time and not the chosen reagent.[138,141]

Regarding phosphorylation on Lys, the already mentioned modification with phosphoryl chloride can be applied for the monomer and peptides.[87] On protein level, Ek *et al.* reported ammonium phosphoramidate (NH_4 – PA) to be selective for Lys residues.[142] Both methods are not site-selective and their chemoselectivity has to be doubted as well. The site- and chemoselective preparation of pLys peptides has been established by Bertran-Vicente *et al.* in 2014 as a further development of the Staudinger reaction.[97] This method will be described in the next section.

2.2.2.2 Staudinger-Type Reactions

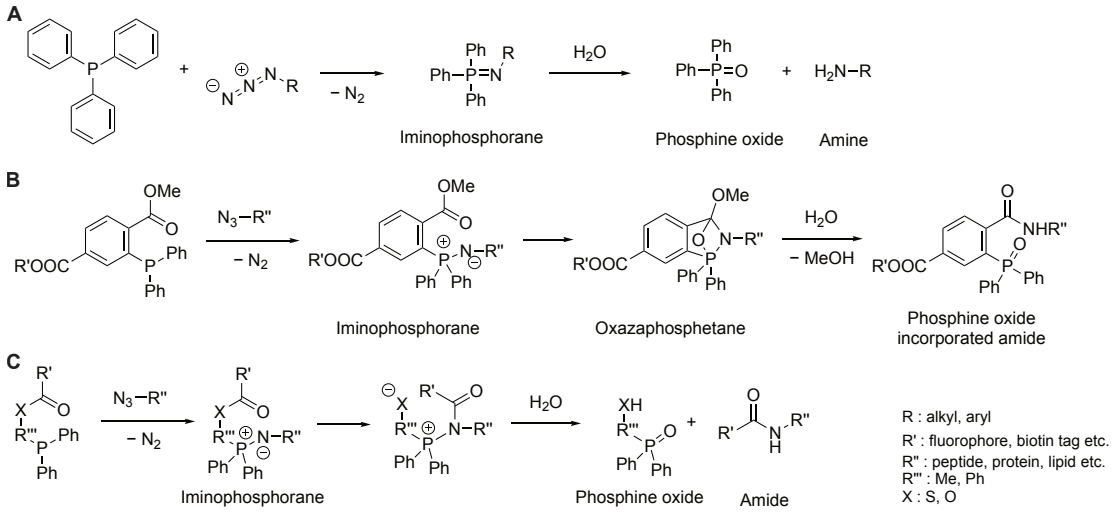

Figure 2.9: **A**. Staudinger reaction with subsequent hydrolysis.[143] **B**. Non-traceless Staudinger ligation to form amide bonds.[144] **C**. Traceless Staudinger ligation, which yields a native peptide bond.[145,146]

The basis for this present study is the synthetic access to pLys peptides. With the effort of several research groups, the chemoselective Staudinger reaction was advanced to a bioorthogonal

ligation and further to the Staudinger-phosphite reaction.

In 1919, Staudinger reported the reaction of phosphines with azides to form iminophosphoranes. These can be further hydrolyzed to stable phosphine oxide and amines (figure 2.9**A**).[143,147] As a further development, the Bertozzi group introduced the non-traceless Staudinger ligation to functionalize biomolecules *via* an amide bonds in 2000 (figure 2.9**B**).[144] Reported in the same year by the Bertozzi and Raines group independently from each other, the traceless Staudinger ligation was introduced, whereby a native peptide bond is formed in the product (figure 2.9**C**).[145,146,148] In both ligations, an iminophosphorane is formed in the first step, which can intramolecularly convert to an oxaphosphetane. Depending on the structure of phosphine, the subsequent hydrolysis yields phosphine oxide with the amide still incorporated (non-traceless) or cleaves both species due to a good leaving group (traceless). Over the years, a vast variety of substrates has been linked together and almost every biomolecule can be addressed, e.g. peptides, lipids, carbohydrates, nucleotides.[148]

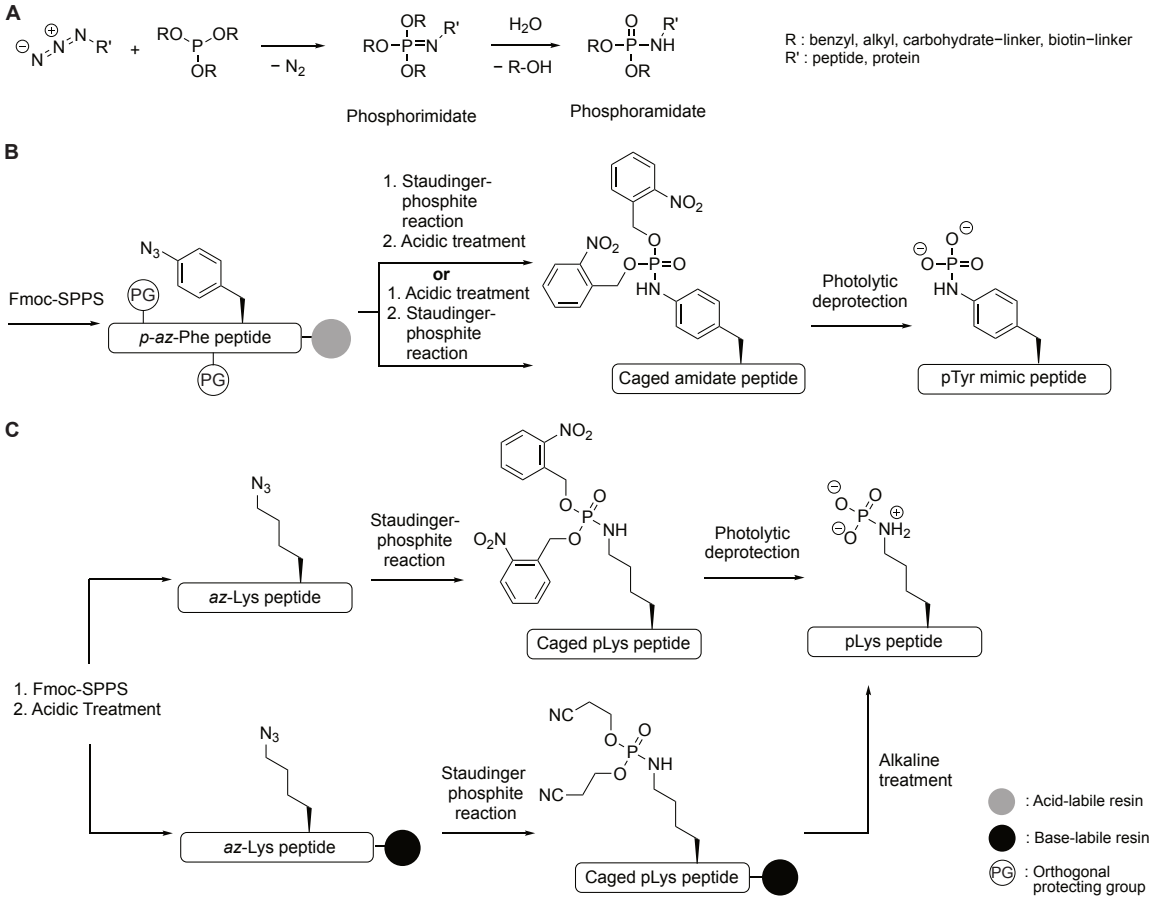

Figure 2.10: **A**. Principle of Staudinger-phosphite reaction for the formation of phosphoramidates.[149,150] **B** & **C**. Selective hydrolysis of phosphoresters leads to phosphoramidic acids, which were applied in preparation of pTyr mimicking peptides and proteins[150–152] (**B**) as well as synthesis of pLys peptides[97,153] (**C**).

Already in the 1950s, the Staudinger-phosphite reaction was described.[149] When reacting an azide with a phosphite instead of a phosphine, a phosphorimidate is formed in the first step from which an alcohol is abstracted upon hydrolysis (figure 2.10**A**). The amine remains bound to the phosphorous due to the fact that the alcohol is a better leaving group. The Hackenberger group recognized the potential of this reaction for bioconjugations[150] and developed several applica-

tions depending on the alkoxy groups, including stabilization of peptides and proteins by PEGylation [154,155] and phosphoglycosylation. [156]

Crucial for the present work was the preparation of post-translationally modified peptides and proteins. As such, *p*-azidophenylalanine (*p*-*az*-Phe) could be incorporated in peptides by SPPS or in proteins by genetic engineering and converted in a caged phosphoramidate by the Staudinger-phosphite reaction in solution or on-resin. Employing phosphites with photolabile alkoxy groups allowed controlled deprotection and yielded a functional pTyr mimic (figure 2.10**B**). [150,151,157]

Some years later, Bertran-Vicente *et al.* expanded the substrate scope to ϵ-azido-Lys (*az*-Lys) and could prepare free pLys peptides in two different syntheis pathways depending on the phosphite employed (figure 2.10**C**). [97,153] For example, the use of *o*-nitrobenzyl acohol or β-cyanoethanol gave access to photolabile [97] or base-labile [153] caged pLys. These different reactivities were taken advantage of in varying synthesis routes, which will be described in more detail in section 4.1.

With the development of these reactions, access to natural, site-specifically phosphorylated Lys peptides was granted. Previously, only low yielding phosphorylations either with phosphoramidates (potassium or ammonium salts, K-PA or NH_4-PA) [138,140,158] or phosphoryl chloride [138] involving no regioselectivity and attack on other amines as side reaction were described. So far, the synthesis of pLys *via* Staudinger-phosphite reaction could not be shown on proteins. On one hand, aliphatic azides are less reactive than aromatic, which would lead to elongated reaction times. On the other hand, the deprotection conditions might be disfavored by proteins as, for example, the β-cyanoethyl groups are cleaved under harsh basic conditions. [153]

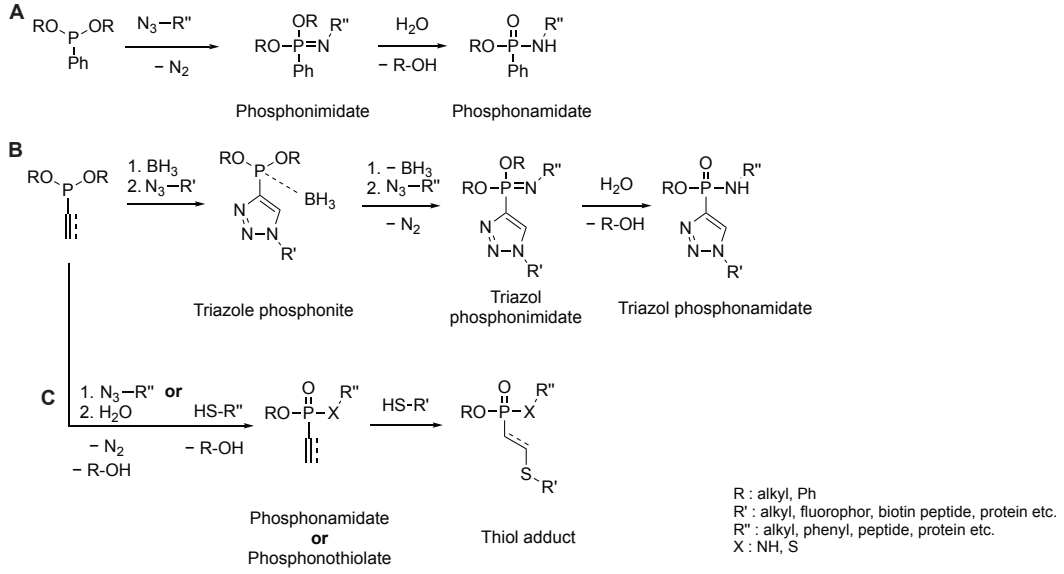

Figure 2.11: **A**. Principle of Staudinger-phosphonite reaction for formation of phosphonamidates. [159] **B** & **C**. Depending on the synthesis sequence, triazole phosphonamidates [160–163] (**B**) or thiol adducts of phosphonamidates [118,164,165] and phosphonothiolates [119] (**C**) can be obtained.

The further expansion of the Staudinger reactant scope to phosphonites [159] (figure 2.11**A**) by the Hackenberger group should also be mentioned here as it gave access to subsequent azide-azide [160–162] (figure 2.11**B**), azide-thiol [118,164,165] and thiol-thiol [119] conjugations (figure 2.11**C**). Hence, two different chemoselective reactions were applied subsequently. These syntheses could

successfully yield stapled peptides,[164,166] a cleavable purification tag for peptides,[163] cell-penetrating protein-peptide conjugates,[118] functional antibody-drug conjugates[165] as well as protein-protein conjugates recognized for ubiquitination[119] and thus, demonstrate the power and versatility of this Staudinger-type reaction.

2.2.3 Phospho-Amino Acid Mimics

Besides natural PTMs, other AA residues are often employed in replacement to study a certain modification.[167] These AAs can be canonical or unnatural depending on their ability to mimic the target structure, electronic environment or properties. For phosphorylation events, analogues are commonly designed as non-hydrolyzable version of the PTM to achieve longer lifetimes in biological systems. With effective mimics in hand, enzyme–substrate interactions can be intervened, binding proteins captured or antibodies (Abs) for further biochemical or proteomic applications raised.

2.2.3.1 Phosphate Analogues

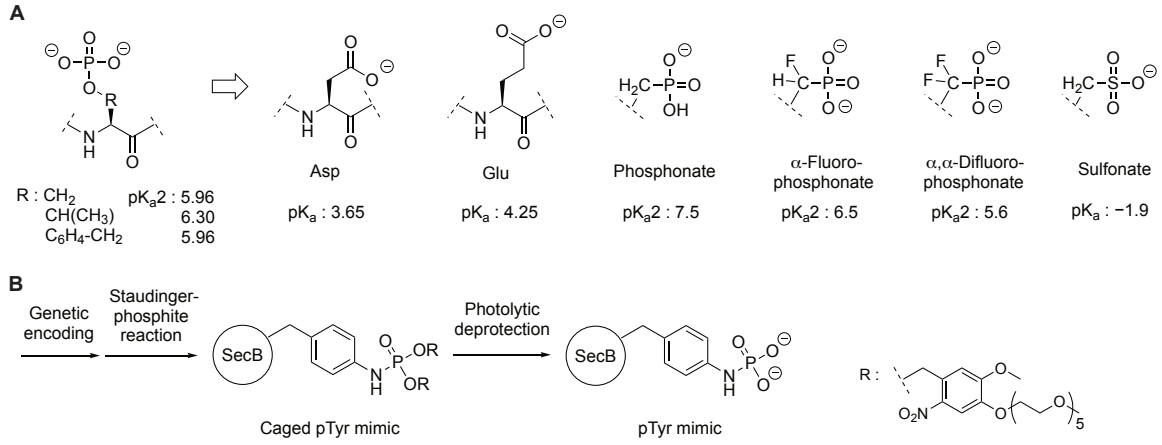

Figure 2.12: **A**. Examples of phosphate mimics with their most probable charge state under physiological conditions.[12,168,169] **B**. Incorporation of a phosphoramidate moiety to mimic pTyr by Staudinger-phosphite reaction.[150,151]

Regarding the phosphates of pSer, pThr and pTyr, a variety of mimics has been established already.[168] The change of phosphorylated AA sites to Asp or Glu by site-directed mutagenesis is an facile method (figure 2.12**A**). Nonetheless, Asp and Glu exhibit pK_a values differing from the phosphates[12,169] and are present only as monoanions at physiological pH.[170] This disproportion could be addressed by incorporation of two vicinal Asp or Glu residues and thus, presentation of two negative charges.[171]

In order to work with structurally very similar residues, the phosphate group can be exchanged, for example, by various phosphonates or sulfonates.[168] Comparing the acid dissociation constants of pSer, pThr and pTyr with methylenephosphonate, fluoromethylenephosphonate, difluoromethylenephosphonate (DFMP), it can be seen that monofluorination results in a pK_a value closest to phosphates (figure 2.12**A**).[168,169] Hence, analogues presenting this moiety should per-

form best as mimics. However, most studies have been conducted either with non- or difluorinated phosphonates. As such, phosphomethylenealanine (Pma) incorporated by Amber codon suppression into *serotonin N-acetyltransferase* instead of pThr could stabilize protein–protein interactions.[172]

Especially Tyr phosphorylation has led to the development of versatile mimic structures, often to inhibit *protein-tyrosine phosphatase 1B* (PTP1B), which plays a role in type 2 diabetes, cancer and Alzheimer's disease.[173] For example, 4-phosphomethyl-phenylalanine (Pmp) and DMFP pTyr analogues were studied in peptidic inhibitors and a 2000-fold higher efficiency could be observed for the difluorinated variant.[174] Also, methylenesulfonate mimics exhibited less potency than DMFP.[175] Obviously, the electronic environment plays a crucial role in the performance as mimic for the natural phosphorylation.

As described in section 2.2.2, Cys phosphorylation was installed on proteins by oxidative elimination and subsequent addition of thiophosphate (figure 2.8**B**).[117,132] However, this was not done to study pCys occurrence itself, but to mimic pSer or pThr sites. Since Cys is less abundant than other AA residues and most often its side chain is involved in disulfides for protein structure formation, the selective mutation of Ser or Thr to Cys is a common technique to study these AAs.

Another approach of phosphate mimicking species was the phosphoramidate developed by the Hackenberger group.[150,151] Genetic encoding of a *p-az*-Phe (figure 2.10**B**) and subsequent chemoselective reaction with a phosphite derivatized with PEGylated, photolabile alkoxy groups yielded a caged phosphoramidate. This could be deprotected by irradiation to give a potent, even though labile pTyr mimic, which could be detected with an α-pTyr-Ab (figure 2.12**B**).[150]

2.2.3.2 Analogues for Labile Phosphorylations

The intrinsic labilites of phosphorothioates, mixed anhydrides and phosphoramidates make it hard to study these PTMs. Several approaches have been made to develop stable analogues, but not for all known natural occurring phospho-AAs a mimic has been reported so far. For example, in the case of pCys, no equivalent has been established even though the usage of pSer as mimic is conceivable.

In replacement of pGlu, other natural AA residues were mutated in proteins to interfere with the structure stabilities. Apart from that, small molecule inhibitors were developed, but no building block for peptide synthesis or protein engineering.[176] Instead, studies on the Che proteins led to different pAsp mimics (figure 2.13**A**). The mutation of corresponding Asp to Cys gave access to first, activation with Ellman's reagent and subsequent substitution with thiophosphate[177,178] or second, direct alkylation of the thiol with phosphonomethyltriflate to yield a phosphonate.[179,180] With these mimics incorporated, into CheB or CheY, the protein conformation could be stabilized, crystallized and high resolution structure determined.[179,181]

With the non-hydrolyzable methylene-bisphosphonate (PCP), the Fiedler group developed a stable mimic for ppSer.[182] As Fmoc- and benzyl-protected building block (figure 2.13**B**), the analogue could be applied in standard SPPS. Peptides obtained were further utilized in ligation reactions or conjugated to immunogenic proteins.[182]

With regard to the present work, the efforts taken in the field of pHis and pArg mimics can be of advantage. Most often, these mimics have been developed to be employed in antibody gener-

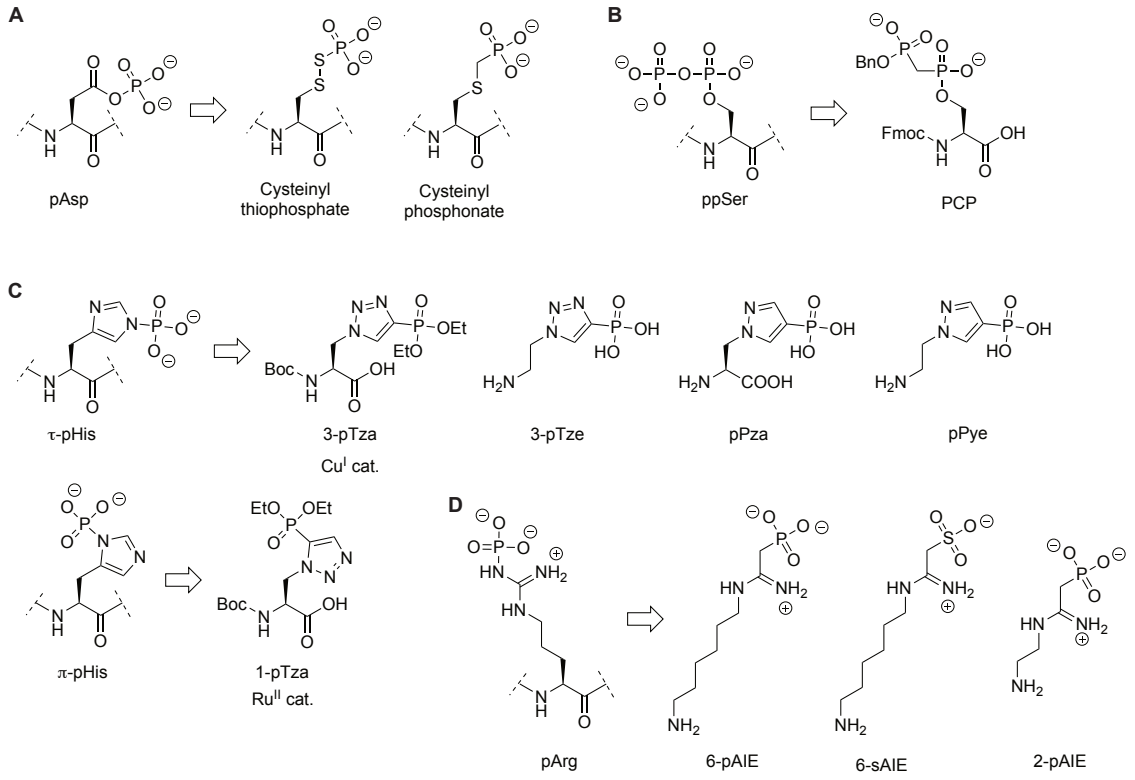

Figure 2.13: Stable analogues developed for pAsp (**A**), ppSer (**B**), pHis (**C**) and pArg (**D**).

ation studies as is described in section 2.2.5.3. Various approaches to mimic pHis are known and with the early developments of furyl or pyrrolyl structure in replacement of the imidazole ring no successful application could be reported.[72,183] Starting ten years ago, a series of pHis analogues has been designed with close similarity to the natural PTM. Alkyne-azide cycloadditions gave access to triazolylalanine (pTza) either as τ- or π-pHis analogue, depending on the chosen catalyst species (figure 2.13**C**).[184] While a copper catalyst yielded the 3-pTza variant, a ruthenium complex led to formation of 1-pTza. As *tert*-butyloxycarbonyl- (Boc-) and ethyl-protected building blocks they could be incorporated into peptides following the Boc-strategy.[184] In order to enable common Fmoc-SPPS, these building blocks have been advanced to Fmoc- and benzyl-protected molecules some years later.[185–187] With phosphoryltriazolylethylamine (3-pTze) it could also be shown, that a carboxylic acid function is not necessary to mimic pHis efficiently.[188] To get even closer to structural and electronic properties of pHis, pyrazole-based mimics presenting two instead of three nitrogen atoms have been developed. Again, potent mimics had either AA character as 4-phosphopyrazol-2-yl alanine[189] (pPza) or no acid function incorporated as phosphonopyrazolylethylamine (pPye).[190]

Phospho-Arg could be successfully mimicked either with phosphonic or sulfonic acids (figure 2.13**D**). Without AA moiety and varying in chain length, (2-((6-aminohexyl)amino)-2-iminoethyl)-phosphonic acid (6-pAIE) and (2-((6-aminohexyl)amino)-2-iminoethane)-1-sulfonic acid (6-sAIE) were developed by Fuhrmann *et al.* and employed as haptens or in phosphatase inhibition assays.[191,192] A phosphonate variant with an even shorter chain length – (2-((2-ammonioethyl)-amino)-2-iminoethyl)-phosphonic acid (2-pAIE) – exhibited also efficient pArg mimicking properties.[193]

So far, no analogue for pLys has been reported. The advances for other labile phosphorylations show the importance of structural and electronic similarity. While the His and Arg side chains exhibit properties of aromaticity and a guanidinium moiety, respectively, Lys has no significant characteristic besides a flexible four carbon chain. Even though the guanidinium group was not part of pArg analogues, the amine-iminium element seemed required. The positively charged ϵ-amine, which is probably present in pLys as well,[74] might play a crucial role in the quest for a potent pLys mimic, either with the charge itself or a similar electron density at this position.

2.2.4 Biochemical Techniques to Study Labile Phosphorylations

Recent breakthroughs in the fields of biochemistry and phosphoproteomics have led to identification of multiple phosphoramidate sites in proteins,[78,83] thereby indicating that the overwhelming significance of *O*-phosphomonoesters might be a side effect of established, standard biochemical detection methods.[194] Even though already in the 1970s it was shown that acid-labile modifications could be detected upon sample preparation at neutral pH, it took more than 40 years to report comprehensive studies with adjusted protocols.[195] Instead of applying one encompassing method, tailored approaches for labile phosphorylation events are crucial. Also among these, no intersectional study combining the various phospho-species and comparing their properties is known.

2.2.4.1 Chemical Stability of Labile Phosphorylations

In order to develop suitable processes, knowledge about the chemical stability of different phospho-species was required. While the general tendencies of acid- and base-stability of phosphorylations belongs to basic knowledge nowadays,[54] detailed studies with peptidic substrates in various buffer systems and at different temperatures were only possible in the recent past after successful development of selective phosphorylation techniques (see section 2.2.2.1). Along these lines, stability of pCys was tested at varying pH values between 2 and 13.[52] For pyrophosphorylation on Ser it was evaluated first in a non-peptidic small molecule[134] and later with two peptides at 25 as well as 37 °C between pH 1 and 13.[196] Approaching primarily the proteomic identification of pHis, model peptides have been incubated only at pH 2.3 for two hours and their decay determined.[78] A pArg model peptide was incubated either at 25 or 60 °C in different buffer systems from pH 1 to 12,[98] to observe P–N bond stability. Lys phosphorylation decay was investigated with a dipeptide at room temperature (r.t.) between pH 1 and 7.5 as well as with a histone H1 derived peptide at temperatures from −78 to 85 °C at pH 7.5.[97] Notably, only one larger peptide in one buffered system was employed in this study. There was no information acquired how this specific sequence would behave at varying pH values or if other AA sequences would show different hydrolysis behavior.

It can be summarized from the various studies, that each phosphorylation has its own stability window. While, for example, ppSer exhibited $t_{1/2} > 24$ hours for almost all conditions,[196] pCys showed similar stability only between pH 6.6 and 9.3.[52] For other substrates much shorter time frames and completely different or very restricted buffer systems were investigated[78,97,98]

and thus, it is hard to compare or combine the results. These reports can give indications about a suitable working window but suggest strongly to optimize the system for each substrate of interest.

2.2.4.2 Kinase and Phosphatase Activity Assays

Protein phosphorylation in cells is regulated by kinases and phosphatases (Pases) to add and remove phosphate groups, respectively (figure 2.3). The fine tuned balance between both enzyme classes is responsible for intact homeostasis and alterations can lead to several diseases. Especially regarding less-studied PTMs, the identification of selective enzymes can help elucidating their biological role. Kinases, which show activity only towards selective AA residues, would indicate an intentional occurrence of this phospho-AA in cells. Phosphatases on the other hand might hydrolyze both, purposed and incorrect phospho-species. Thus, studying both enzymes can help to understand the importance of a specific phosphorylation.

Biologically emphasized approaches work most often with overexpression or knockdown of certain Pases and kinases as well as point mutations in the protein's AA sequence. Consequently, effects on cells and organisms can be revealed and thus, the biological ranking of the altered enzyme concluded. Along these lines, the structure of McsB was elucidated and crucial residues inside the catalytic center shown.[197] On the other hand, *protein-arginine-phosphatase* YwlE was functionalized to a pArg trap by mutation of a key Cys in the enzymatic pocket to Ala.[198] Furthermore, the potential role of *nucleoside diphosphate kinase A* (NME1) as His phosphoramidate hydrolase (PAH) in neuroblastoma was examined by immunoblotting and gene knockdown.[199]

Especially interesting for the presented doctoral studies are recent findings regarding the impact of *phospholysine phosphohistidine inorganic pyrophosphate phosphatase* (LHPP) on tumor cells and tissues. Three research groups have reported the role of LHPP as a tumor suppressor in bladder, cervical and liver cancer, which was investigated either by its overexpression or knockout.[79,200,201] Thereby, the focus for possible phosphorylation sites lay on His residues even though no site identification was conducted and reports on PAH activity with peptidic substrates indicate no affinity of LHPP for pHis.[202] Furthermore, other studies claimed to have identified pLys in proteins, which are potential LHPP substrates.[99] Nonetheless, since the identification of LHPP as hydrolase for pLys, pHis as well as for inorganic phosphate (P_i) or imido diphosphate (PNP),[203–205] no comprehensive study with pLys peptides or proteins as substrates has been conducted and the selectivity and mode of action of LHPP remain to be elucidated.

Approaches using biochemical techniques often apply model peptides or synthetically phosphorylated proteins, which allow precise control over substrate properties and hence, detailed specificity studies. Pase activity is commonly determined by detection of P_i amounts released with diverse reagents (figure 2.14**A**).[206] Furthermore, the substrate itself can be measured over time as done, for example, for ppSer and ppThr peptides by Yates *et al.*[196] Here, sufficient different retention of pyrophosphorylated and hydrolyzed species enabled high performance liquid chromatography coupled with mass spectrometry (HPLC/MS) analysis and quantification (figure 2.14**B**). Notably, standard HPLC conditions imply a risk of losing acid-labile modifications due to acid in the eluent and might not be suitable for less stable phosphorylations as pLys.

Another experimental design, which was applied for McsB detection, is the surface enhance Raman scattering (SERS) assay platform introduced by Cai *et al.*[207] Under physiological conditions positively charged Arg peptides result in high SERS signal intensity, which will subsequently decrease when McsB is present and active (figure 2.14**C**). Even though this set up was utilized in kinase detection it might be applicable in enzyme activity assays as well.

The detection of either kinase or phosphatase activity is possible with 8-hydroxy-5-(*N*,*N*-dimethylsulfonamido)-2-methylquinoline- (Sox-)based probes introduced by the Imperiali group.[208–211] These undergo a fluorescence signal increase due to chelation of magnesium ions upon phosphorylation of the target substrate 2.14**D**). Initially applied for kinase activity assays on Ser, Thr and Tyr residues, the Sox-based chelation-enhanced fluorescence (CHEF) approach was recently expanded to PAH and Pase activity assays with pHis peptides as well as phosphorylation–dephosphorylation experiments with Arg peptides in combination with McsB and YwlE.[202,212] These results indicate great potential for pLys detection in various systems especially very little is known about (p)Lys selective kinases or phosphatases.[213] The Sox-based probes enable real-time measurements at low concentrations without system interference.

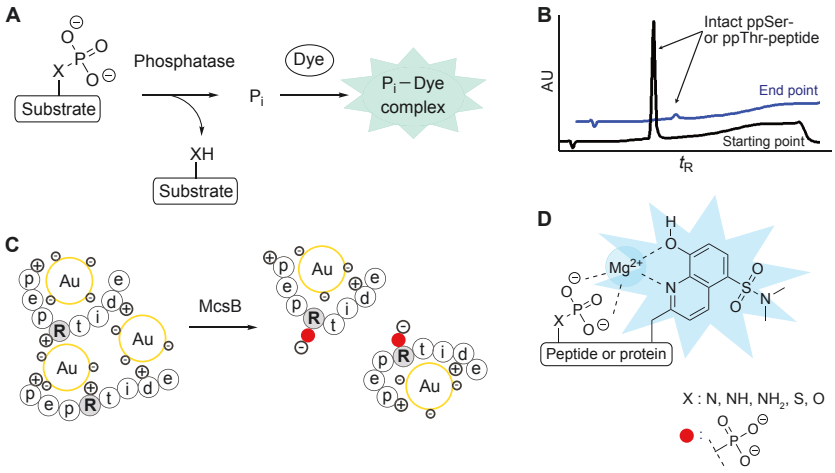

Figure 2.14: Methods for phosphatase and/or kinase activity determination. **A**. Photometric inorganic phosphate (P_i) concentration measurement.[206] **B**. HPLC/MS analysis of substrates.[196] **C**. Phosphorylation induced surface enhanced Raman scattering (SERS) intensity decrease.[207] **D**. 8-hydroxy-5-(*N*,*N*-dimethylsulfonamido)-2-methylquinoline- (Sox-)based chelation-enhanced fluorescence.[202,208–212]

2.2.5 Phosphoproteomics

An essential element of chemical biology, biochemistry and biology is the field of proteomics. It describes the large scale protein analysis regarding protein composition, structure and activity. Since the beginning of protein analysis, techniques have developed from colorimetric methods to determine protein concentration *via* electrophoretic applications for size- or charge-based separation to various sequencing methods including chemical break up or analytical fragmentation.[214] Nowadays, the term proteomics is most often used with regard to protein purification and mass spectrometric analysis. With the large number of proteins per organism and the advanced sensitivity, an huge amount of data is produced, which is processed and evaluated with the help of various databases.[10] Regarding PTMs and their impact on protein activity, proteomics is of spe-

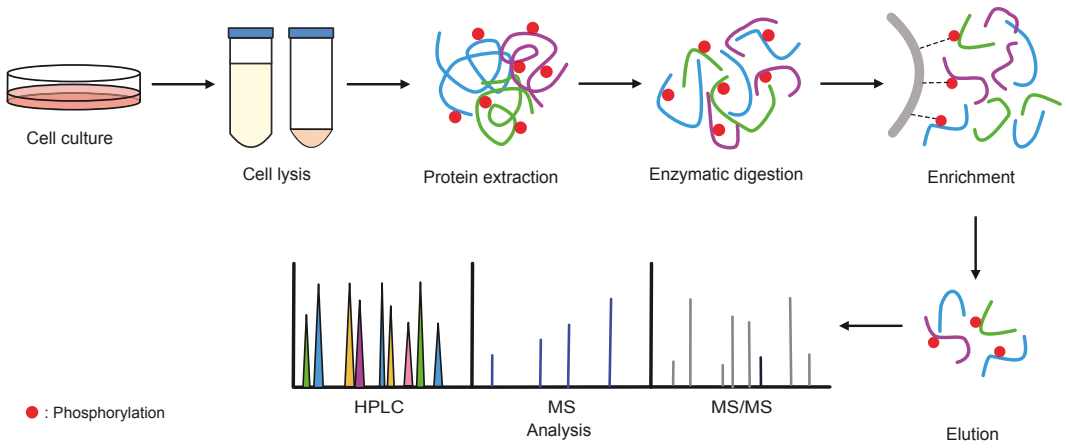

Figure 2.15: Proteomic workflow using phosphorylated substrates as example from cell culture to mass spectrometric analysis including an enrichment step.

cial interest as it can deliver information about PTM site stoichiometry and thus the functional relevance of a distinct PTM. [215]

Phosphoproteomics as a subdivision investigates occurrence and biological role of phosphorylation as a PTM. Most studies apply bottom-up phosphoproteomic approaches (figure 2.15) meaning proteins from lysed cells are digested with one or a combination of several proteases, e.g. trypsin or chymotrypsin, and subsequently analyzed by nano-liquid chromatography coupled to tandem mass spectrometry (nLC-MS/MS). [216] Even though phosphorylation is the most abundant PTM known, phosphorylated peptides often appear in substoichiometric amounts. Chemically, the modification is accompanied with the introduction of two negative charges to the protein site. As a result, ionization efficiency is reduced compared to unmodified counterparts. [217] These conditions have driven the development of various advancements at each step of the bottom-up approach including sampling, usage of proteases, affinity-based enrichment, derivatization, chromatographic separation as well as mass spectrometry parameters. [216] Some of these progresses tailored for phosphorlyation as stable and labile modification of proteins are described in the next sections.

2.2.5.1 Chemical Derivatization

Depending on the study target, investigated proteins might posses properties, which are either unique and can be taken advantage of or unfavorable from the technical feasibility point of view. Derivatization of distinct AA side chain gives access to selective subsequent analysis.

Histones, for example, carry an immense number of PTMs and are as such an interesting subject for research. [27,42] Nonetheless, their AA sequence characteristics comprise high amounts of basic AA residues in the *N*- and *C*-terminal regions, [221] which leads to short peptide fragments upon tryptic digest. These short peptides cannot be analysed by tandem-MS. Furthermore, charged residues lead to poor retention in the nano-LC in a way that the target peptides get washed away during a desalting step. Selective derivatization of the Lys ϵ-amine prevents these two impediments (figure 2.16**A**). Along these lines, acylation with different anhydrides has been established [222] and especially propionylation with propionic anhydride is widely applied. [218] This

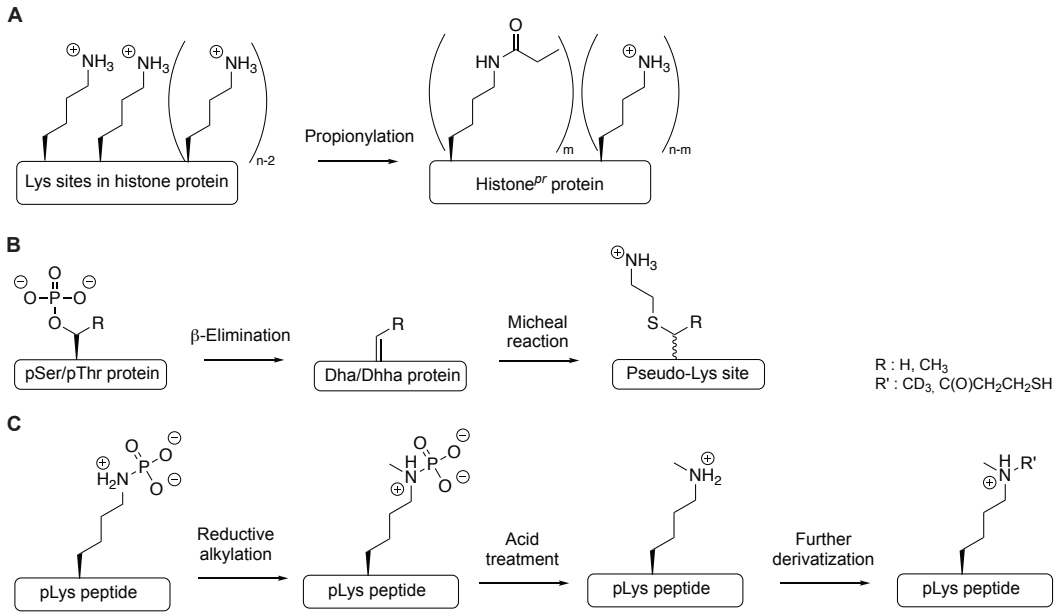

Figure 2.16: Chemical approaches for selective derivatizations of proteins or digest derived peptides. **A**. Propionylation of histones described by the Garcia group.[218] **B**. Elimination-addition with pSer or pThr proteins.[219] **C**. Labeling of pLys peptides by reductive amination or amide formation.[101,220]

modification diminishes the positive charge of Lys and further masks the AA for recognition by trypsin. As a result, longer tryptic peptides with preferred behavior are obtained.[218]

Selective modification of pSer and pThr inducing uncommon trypsin cleavage sites was developed by the Shokat group. Under alkaline conditions at elevated temperature β-elimination of inorganic phosphate occurred and dehydroalanine or dehydrohomoalanine were formed. These alkene species could be converted chemoselectively to aminoethylcysteine and β-methylaminoethylcysteine in a Micheal reaction with 2-aminoethane-1-thiol, which were recognized by trypsin as pseudo-Lys cleavage site and yielded unique peptide fragments (figure 2.16**B**).[219]

Very recently, a labeling strategy for pLys peptides was introduced by the Zhang group. Reductive alkylation of the phosphoramidate nitrogen followed by acidic P–N bond hydrolysis enabled selective further derivatization (figure 2.16**C**). For example, heavy dimethyl labeling with deuterated formaldehyde[101] or acylation with an NHS-ester[220] were shown. For the Zhang group, the rationale for selectivity of this approach lay in the distinct reactivity of primary and secondary amines towards formaldehyde. According to this, already post-translationally methylated Lys side chains would have reacted in the first labeling quantitatively to a tertiary amine and would not be accessible for further derivatization. Hence, false positives resulting from methylation as PTM should be excluded. Nonetheless, the identification of endogenous pLys was based on statistical, database search-based analysis of the recorded data and no spectra information was given. Additionally, the claimed synthesis of reference pLys-peptides with K-PA at pH 8[101] is highly debatable, since the protonated ϵ-amine of Lys is very unreactive.

2.2.5.2 Phospho-Specific Enrichment

As mentioned above, phosphorylation sites occur in low abundance relative to the whole proteome. To improve the ratio of phospho- to residual sites, enrichment techniques selective for this PTM have been developed.[223] As shown in figure 2.17, common enrichment protocols for digestion derived phospho-peptides rely on binding events between functionalized solid support and phosphoryl oxygens. Thus, substrates are bound *via* electrostatic interactions and no discrimination between different phosphorylation species occurs. In order ot prevent cross-reactivity with acidic AAs or *C*-termini, binding is usually performed at low acidic pH when carboxylic acids are protonated. Since these conditions are unfavored for labile phosphorylation, recent advancements have successfully shown that phosphorylated peptides can also be enriched with adjusted pH and hence, labile PTMs investigated as outlined below.[224,225]

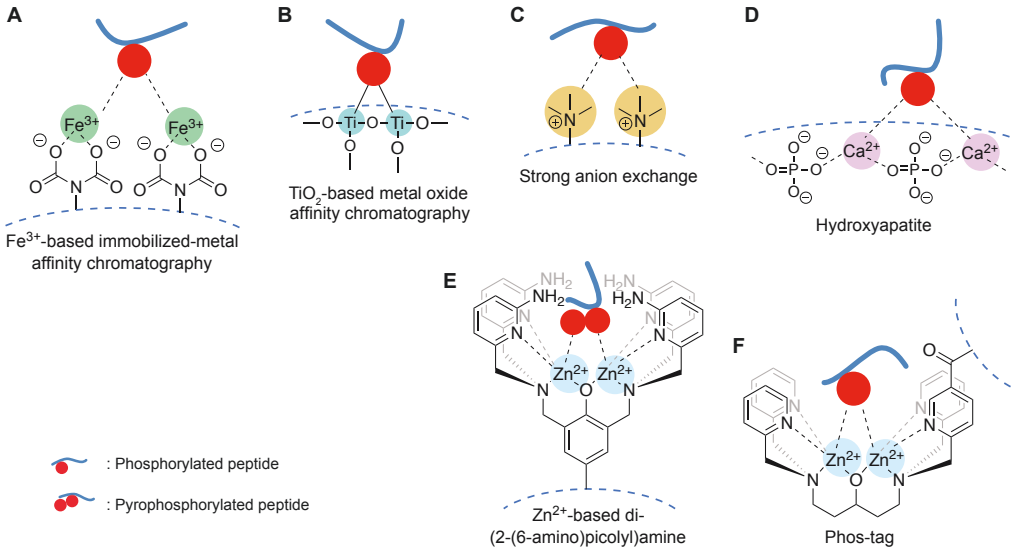

Figure 2.17: Common phospho-selective enrichment methods, partially applied for labile phosphorylation events. **A**. Fe^{3+}-based immobilized-metal affinity chromatography (IMAC). **B**. TiO_2-based metal oxide affinity chromatography (MOAC). **C**. Strong anion exchange (SAX). **D**. Hydroxyapatite (HAP). **E**. Zn^{II}-coordinating di-(2-(6-amino)picolyl)amine (DPA). **F**. Phos-tag.

Immobilized-metal affinity chromatography (IMAC) is based on the interaction between phospho-peptides in solution and transition metal ions - usually Fe^{III} - fixed to a solid support by coordination to nitrilotriacetic acid (NTA) or iminodiacetic acid (IDA) as shown in figure 2.17**A**. Potel *et al.* have reported efficient pHis binding under mild acidic conditions in a way that the phosphoramidate remained intact and no cross-reactivity was observed. Also, elution of bound peptides with ammonium hydroxide did not hydrolyze the P–N bond. As a result, a high number of pHis sites was identified in *E.coli* and their varying levels in different phases of the cell cycle examined.[78]

Titanium dioxide-based metal oxide affinity chromatography (MOAC) is another often applied phospho-enrichment technique (figure 2.17**B**). It can be utilized as beads or column material. In 2018, the Becher group has shown high degree of Arg phosphorylation in *S.aureus* by adjusting conditions during the binding step to pH 2.7 or even 3.2.[83,84] Again, elution with ammonium hydroxide did not harm the phosphoramidate. The IMAC as well as TiO_2-based protocol yielded

better ratios of *N*- to *O*-phosphorylated peptides upon sequential enrichment.[226]

Two approaches applicable for several labile phosphorylation species have been introduced by the Eyers and the Hunter group (figure 2.17**C** & **D**). Strong anion exchange (SAX) chromatography with an optimized triethylammonium phosphate gradient at pH 6.8 led to large scale identification of labile phosphorylation events on Asp, Glu, His, Arg, Lys and Cys.[100] The calcium phosphate variant hydroxyapatite (HAP) is a crystalline compound with the summary formula $Ca_{10}(PO_4)_6(OH)_2$,[227] which could be applied in phospho-peptide enrichment as well. Binding at pH 7.2 and elution at pH 11 led to detection of high amounts of pHis, pArg and pLys, but also pAsp, pGlu and pCys though to smaller extent.[99] Notably, both approaches base their findings on statistical database search with an included level of probability. No additional result evaluation with synthetic phospho-peptides has been conducted.

A selective enrichment of pyrophosphorylated peptides was developed by the Fiedler group. Coordination of Zn^{2+} ions by immobilized di-(2-(6-amino)picolyl)amine (DPA) allowed the binding of ppSer and ppThr sites at pH 7.4 and subsequent elution by displacement with inorganic pyrophosphate (PP_i) at high buffer concentrations (figure 2.17**E**).[228] The chelating DPA moiety is an advancement of the versatile Phos-tag[229] reagent, which is nowadays applied in enrichment of phospho-peptides as well as detection of phospho-proteins during sodium dodecyl sulfate–polyacrylamide gel electrophoresis (SDS-PAGE, figure 2.17**F**). Even though Phos-tag is applied at neutral conditions as well, no application for labile phosphorylations has been reported yet.

2.2.5.3 Immunoaffinity Enrichment

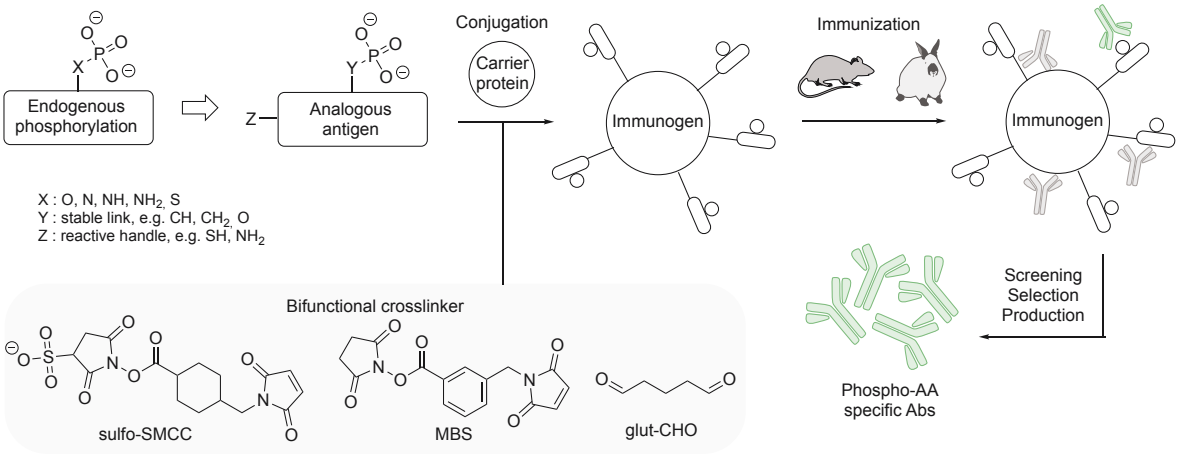

Figure 2.18: Generation of Abs specific for a distinct phospho-AA by employment of stable mimics as antigens is a key technique to elucidate labile phosphorylations. Applied immunogens are most often carrier protein–antigen conjugates linked *via* homo- or heterobifunctional molecules.

Besides recognition of the phosphate group, the whole phospho-AA side chain can be utilized in affinity enrichment. By doing so, a certain class of PTM can be isolated and examined without interference of others. This is of advantage especially for labile phosphorylations since these probably occur to a lower extent than *O*-phosphomonoesters and might be missed with phospho-specific enrichment. Selectivity for a distinct phospho-AA is usually gained with antibodies (Abs)

either as polyclonal or monoclonal variants (pAbs or mAbs). While pAbs include a mixed population of antibodies, which recognize different areas of the target, mAbs are of one genetic species and will bind only to one moiety of the antigen.[230] Thus, they are less tolerant for small changes in the target structure or conformation, but they are infinitely renewable. The general procedure for the generation of Abs is shown in figure 2.18. As a matter of principle, the intrinsic lability of phosphorothioates, mixed anhydrides and phosphoramidates demands potent, stable analogues for these phospho-AAs to successfully generate Abs, some of which will be described below. The hapten size is usually too small to induce a sufficient immune response itself before degradation or clearance. Therefore, they are coupled to carrier proteins in order to increase the immunogenicity significantly *via* bifunctional linkers. *keyhole limpet hemocyanin*, *bovine serum albumin* and *ovalbumin* (KLH, BSA, OVA, respectively) are commonly employed carrier proteins.

So far, no specific Abs have been reported for pCys, pAsp or pGlu and pLys maybe due to the lack of suitable mimics (section 2.2.3). The Fiedler group reported in 2016 the development of PCP as analogue for ppSer. They could show its successful incorporation into peptides and subsequent ligation to maleimide-activated BSA and *glutathione S-transferase* (GST) *via* glutaraldehyde (glut-CHO) and paved the way to α-ppSer antibody generation.[182]

Research on His phosphorylation brought forth several approaches of pAbs and mAbs generation. The first described, pyrrolyl-based pHis mimic led to successful Ab production but only to recognition of the mimic and not pHis.[72,183] The Muir group developed several analogues, which were utilized for Ab generation afterwards. In 2010, a peptide bearing 3-pTza and an *N*-terminal Cys was linked to KLH *via* the heterobifunctional sulfosuccinimidyl-4-(*N*-maleimidomethyl)cyclohexane-1-carboxylate (sulfo-SMCC). With this conjugate the group could raise the first polyclonal, sequence-dependent α-τ-pHis Abs, which detected selectively 3-pTza and pHis.[184] In 2013 and 2015, 3-pTze and pPye, respectively, were conjugated to KLH with glut-CHO and again pAbs generated.[188,190] While the triazole derived Abs exhibited significant cross-reactivity with pTyr, Abs produced from pPye showed distinct selectivity for pHis over pTyr.[190] Another pyrazole-based analogue developed by Lilley *et al.* was also applied in successful α-τ-pHis Ab generation.[189] Again in 2015, the first ever sequence independent Abs against π- and τ-pHis were raised from randomized peptides.[187] As KLH–peptide conjugates linked *via m*-maleimidobenzoyl-*N*-hydroxysuccinimide ester (MBS) mAbs were produced and later applied in immunoblotting for example.[199,231]

Similar to pHis, various approaches to generate α-pArg Abs have been reported. The Clausen group investigated the suitability of pArg itself for immunization but observed only rapid dephosphorylation in serum.[198] Also, *in vitro* phage display was tested. Indeed, Abs could be produced for further *in vitro* studies with recombinant proteins, but their affinity was too low to apply them in cellular studies.[232] The suitability of phosphonates as pArg mimics during Ab generation was shown by Fuhrmann *et al.* and Ouyang *et al.* 6-pAIE or 2-pAIE were conjugated to KLH and employed in immunization of rabbits or mice, respectively.[191,193] Both approaches yielded specific, polyclonal α-pArg Abs and even the first mouse Abs.[193] Notably, Fuhrmann *et al.* also tested the structurally similar sulfonate (6-sAIE), which did not yield potent clones.[191]

2.2.5.4 Tandem Mass Spectrometric Advancements

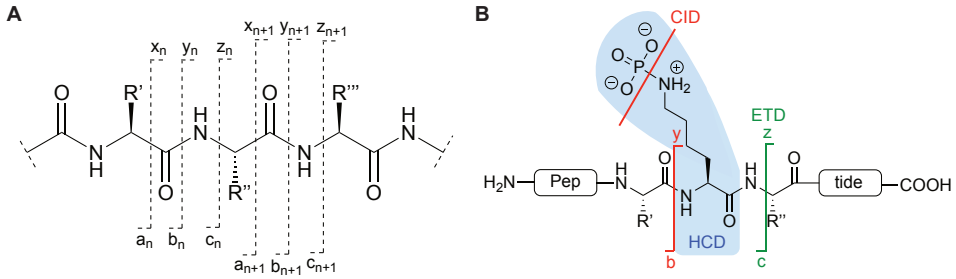

Figure 2.19: **A**. Fragmentation pattern of peptides in tandem-MS containing either the *N*- or *C*-terminus of the precursor peptide and yielding a-/b-/c-ions or x-/y-/z-ions, respectively.[233] **B**. Effect of different fragmentation techniques on pLys peptides. red: collision induced dissociation (CID) induces peptide bond cleavage and loss of phosphorylation; green: electron transfer dissociation (ETD) cleaves the N–C_α bond; blue: electron transfer/higher energy collision dissociation (EThcD) leads to formation of a pLys diagnostic phosphoimmonium ion.

Successful identification of labile phosphorylation sites depends not only on suitable derivatization or enrichment but also on mild MS techniques. Peptide AA sequences can be elucidated unambiguously by a combination of ionization gaining information about the mass-to-charge ratio (m/z) with fragmentation of distinct precursor ions revealing the actual AA sequence. Thereby, the following fragments are obtained along the peptide backbone and termed as proposed by Roepstorff and Fohlmann.[233] As shown in figure 2.19**A**, cleavage of the C_α–C_{CO} bond, C_{CO}–N bond and N–C_α bond leads to a-/x-, b-/y- and c-/z-ions, respectively. While the a-/b-/c-ions contain the *N*-terminus of the precursor peptide ion, the x-/y-/z-ions contain the *C*-terminus.

Depending on the choice of fragmentation technique, labile phosphorylations can be detected or not. Conventional tandem-MS (MS/MS) applies collision induced dissociation (CID), which predominantly cleaves amide bonds. Furthermore, the weakest positions in the peptide are attacked and thus, also P–X bonds (X : O, N, NH, NH_2, S; figure 2.19**B**). This neutral loss is taken advantage of in phosphoproteomics of pSer, pThr and pTyr since also sufficient amounts of intact phospho-peptide can be detected.[194,234] When applied to phosphorothioates, anhydrides or phosphoramidates usually no unambiguous site identification is possible. Only for pHis characterization, the unique triplet of phosphate neutral loss with m/z 80, 96 and 116 Da was utilized before.[234]

A modification of CID is higher-energy collisional dissociation (HCD) where the fragmentation is induced in another part of the mass spectrometer. Nonetheless, labile phosphorylations are usually lost with this fragmentation technique as well.[52] Only recently, investigation of activation energies has led to identification of significant immonium ions for pHis and pLys, which could be taken advantage of as outlined below.[234,235]

With the establishment of electron transfer dissociation (ETD) as soft fragmentation, labile PTMs and especially pLys could be detected eventually.[153] As shown in figure 2.19**B**, ETD leads to cleavage of N–C_α bonds yielding mainly c- and z-ions while leaving the P–N bond intact. Since the dissociation is induced by transfer of an electron to the precursor ion, singly charged ions cannot be detected at all and doubly charged ion fragments only to little extent. This is a serious drawback of this technique since most precursor ions are doubly charged. Furthermore, a phosphate transfer in gas phase was observed at low charge states for pLys peptides.[236]

Recent advancements in tandem-MS is the application of electron transfer/higher energy collision dissociation (EThcD). This fragmentation technique combines ETD with HCD and can induce series of complementary fragment ions. Thereby, an significantly improved sequence coverage is achieved and thus, the unambiguous peptide identification enabled. EThcD was successfully applied on pyrophosphorylated peptides as well as pCys, pHis and pLys substrates. [52,78,235,237,238] Notably, adjustments of the activation energy led to the successful phosphorylation site identification from doubly charged precursor ions. Thereby, the sensitivity of this technique was increased since now the predominant ion species could be analyzed as well. [235] However, one drawback of EThcD is the increased analysis time, which leads to less fragmentation events in the same time compared to CID or HCD. Thus, especially the development of triggered EThcD fragmentation has led to tailored MS analytic approaches. Along these lines, a unique neutral loss pattern of m/z 98, 178 and 196 Da was used to clearly identify ppSer and ppThr sites. [237] Furthermore, pHis yielded a diagnostic immonium ion with m/z 190.0376 Da during HCD, which subsequently triggered EThcD fragmentation for sequence elucidation. [78,238] Of special interest for the present work was the detection of pLys-specific phosphoimmoniumions with m/z 164.047 and 181.074 Da during HCD (figure 2.19**B**). These m/z were utilized as indicator for EThcD fragmentation and hence, distinct pLys site identification. [235,239]

3 | Objectives

As described in section 2.1.4.1 phosphorylation of lysine is a compelling PTM and still enigmatic for researchers despite the initial reports on its occurrence in histone H1 *in vitro* as well as *in vivo* and the very recent publications on incidental detection during proteomic analyses. To date, no comprehensive study has described lysine phosphorylation in the context of its biological relevance and thus, the knowledge about this PTM consists of appealing nuggets occasionally published without sufficient context for making significant conclusions on its biological function. Hence, a high variety of starting points for investigations are present. Probably the major challenge in this regard is the intrinsic lability of the P–N bond of phosphoramidates and the associated risk of losing the modification throughout sample preparation or analysis process. Consequently, conventional methods and protocols are unfavorable for identification, characterization or comprehension of pLys and adjusted conditions are required for every approach. Additionally, since no pLys-presenting protein or interacting proteins are known, the majority of studies are done on model substrates, which have to be obtained from tedious synthesis procedures.

A Novel Synthesis Path for Site-Specifically Phosphorylated Lysine Peptides

Previous efforts in our group put forth the first ever reported synthesis route to obtain site-specifically phosphorylated lysine peptides in solution (see sections 2.2.2.2). Shortly afterwards, the very same method was refined to give free pLys peptides directly upon cleavage from the solid support, thereby saving two purification steps. Despite their great novelty, both approaches exhibit drawbacks, and especially the time consumption from peptide design to its actual receipt can be unpleasant. A generic building block suitable for standard peptide synthesis to obtain site-specific yet still caged pLys peptides during the cleavage step would be an improvement of the available methods. Thus, the synthesis and evaluation of a caged and Fmoc-protected phospho-lysine with an SPPS-suitable stability profile was our aim in this regard.

Investigation of the Amine Protonation in Various Phosphoramidate Species

To understand the lability of the P–N bond in pLys it is crucial to investigate the charge state and electron distribution around the phosphoramidate. Potentiometric titration experiments, which

were conducted with *N*-(*n*-butyl)phosphoramidate, revealed several acid dissociation constants. These findings were rationalized by protonation of the phosphoramidate nitrogen. Since then, a similar pattern has been presumed for pLys despite no studies having been done with the modified amino acid. Thus, we intended to confirm those assumptions during this project. Besides the uncaged phosphoramidate of endogenous pLys, we were highly interested in the various species that occur during the Staudinger-phosphite synthesis pathway. Nuclear magnetic resonance spectroscopy offers the possibility to measure nitrogen protonation directly when applying it on ^{15}N-labeled amines. By means of this, we aimed to track the protonation process of pLys and its precursors with titration experiments.

Development of Stable Mimics for Phospho-Lysine

The aforementioned lability of pLys has hampered the development of appropriate analytical methods and hence, the in-detail investigation of this modification. Especially long term experiments cannot be conducted without a significant extent of hydrolysis occurring. Therefore, the design, synthesis and characterization of stable analogues for pLys was the desired outcome of this project part. Furthermore, these mimics were intended to be employed in the development of novel enrichment techniques.

Investigation of Phospho-Lysine Selective Enzyme

The identification of selective phosphorylation–dephosphorylation processes of lysine residues on proteins would emphasize the biological relevance of this modification. Phosphatases (Pases) cleaving selectively the phosphoramidate – so-called phosphoramidate hydrolases (PAHs) – of pLys would hint to its occurrence in organisms. The only reported pLys hydrolyzing enzyme is *phospholysine phosphohistidine inorganic pyrophosphate phosphatase* (LHPP) whereby its activity has been shown on monomers or poly-pLys only. In this investigation, we aimed for a detailed study about the mode of action and binding motif of LHPP to gain insight into possible pLys substrates for this enzyme.

Development of Novel Enrichment Techniques

Two main factors hamper pLys detection in biological samples: the intrinsic lability of the P–N bond in unprotected phosphoramidates as well as the expected low abundance of pLys in the total proteome. Since the probability is high to miss this modification during conventional proteomic sample preparation and analysis, we investigated different approaches to mitigate those impediments.

Generation of Monoclonal Antibodies Targeting Phospho-Lysine

Application of common and convenient enrichment techniques targeted to the negatively charged phosphate group cannot distinguish between various protein phosphorylation species. As a consequence, proteins or their digestion derived peptides get enriched in the same ratio as they

were present in the lysate at best. More often, highly abundant phosphorylations will be enriched to a larger extent than modifications with low abundance as pLys due to the limited capacity of the employed material. Therefore, we aimed to design, synthesize and characterize immunogens for the generation of a pLys specific monoclonal antibody, which would give access to targeted identification and enrichment of this PTM.

Proteomic Workflow Optimization for Phospho-Lysine Identification

Phosphoproteomics is a well-established research field and great progress has been achieved with regards to efficiency and sensitivity, which are both especially relevant for the analysis of labile phosphorylations. Despite overall general improvements, recent reports have shown the importance of tailored sample preparation and mass spectrometric analysis methods for some PTMs. So far, no published method is available to detect pLys selectively during bottom up proteomics. Thus, our goal is to adjust common proteomic protocols to eventually identify endogenous pLys sites. This includes the re-evaluation of cell lysis and protein extraction as well as phospho-selective enrichment techniques. Furthermore, referring to the first reports on endogenous lysine phosphorylations, we intended to take advantage of the unique properties of histones in the development of customized sample preparation steps.

A Fluorescence Tag to Determine the Degree of Phosphorylation

The accurate identification and quantification of lysine phosphorylation under various conditions is essential in the evaluation of certain processes. Common analysis methods involve distinct disadvantages including prohibitively large sample amount requirements, acidic conditions, long experiment times and lack of real-time analysis. In this project, we intended to establish a fluorescent tag to enable fast, convenient degree of phosphorylation determination in various bio- and chemical experiments by taking advantage of the previously reported chelation-enhanced fluorescence approach (see section 2.2.4.2).

4 | Results and Discussion

4.1 Fmoc-Based Synthesis of Caged Phospho-Lysine Peptides

4.1.1 Outline of the Project

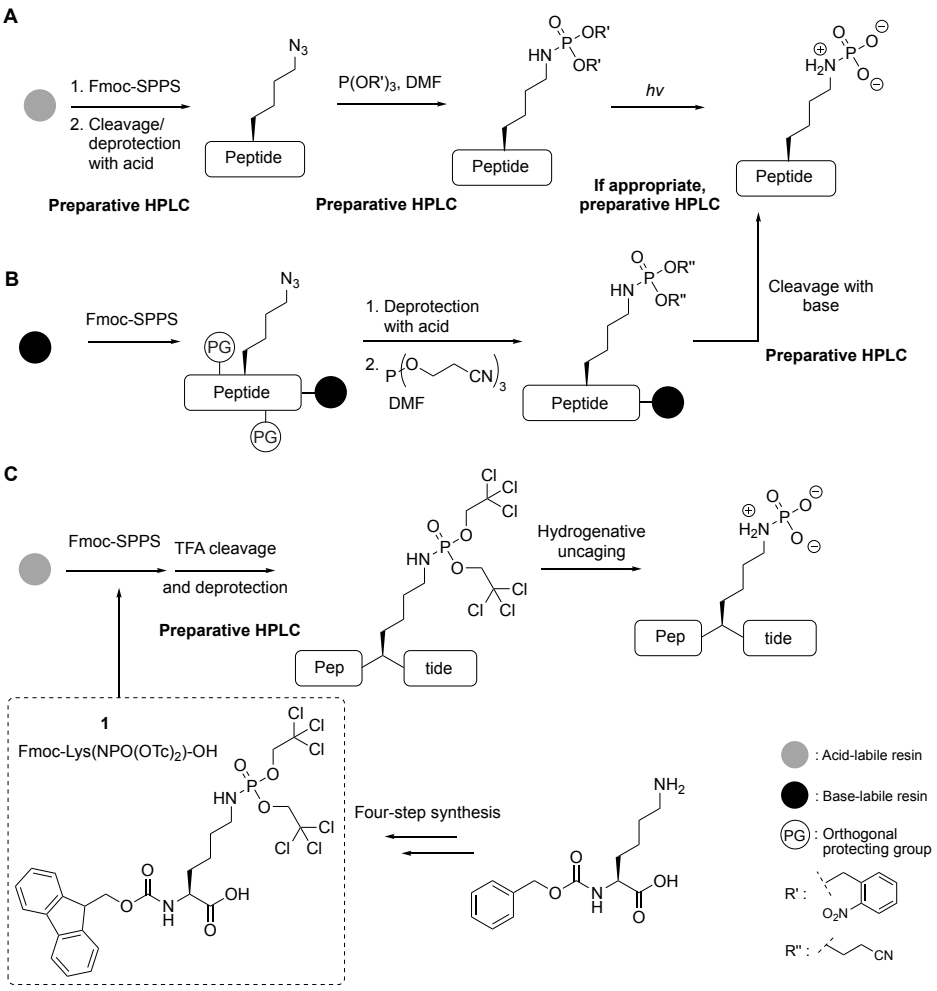

Scheme 4.1: **A** & **B**. Synthesis routes to site-selectively phosphorylated Lys peptides by an in-solution approach [97] (**A**) or on solid support [153] (**B**). **C**. Alternative synthesis approach to caged-pLys peptides.

The development of a reliable synthesis method for site-specifically phosphorylated lysine peptides in 2014 [97] presented the starting point of systematic studies to elucidate this PTM in the Hackenberger group. The synthesis route started from ϵ-azido-Lys (*az-Lys*) and gave access

to model peptides, which could be designed *ad libitum* by taking advantage of the chemoselective Staudinger-phosphite reaction.[150] Furthermore, protected phosphoramidates would be obtained, which can be stored for longer periods and subsequently deprotected when needed, thereby circumventing the lability issue of free pLys substrates. Besides its novelty and possibilities, this approach entailed some drawbacks. In order to prepare caged pLys peptides *via* this route, up to three purification steps were required (scheme 4.1**A**), which would remarkably reduce the overall yield to approximately 3% (preparation of phosphite not taken into account). Additionally, the conversion of *az*-Lys to caged pLys required two days and up to 15 equivalents of phosphite to drive the reaction to completion, due to the aliphatic, electron-rich and hence low-reacting azide moiety in *az*-Lys.
A further development employed a base-labile linkage to the solid support during peptide synthesis, thereby giving direct access to conduction of the Staudinger-phosphite reaction on solid support and preparation of free pLys peptides upon cleavage in 3% isolated yield when applying base-labile phosphoramidate protection. Additionally, two purification steps could be spared (scheme 4.1**B**).[153] Nonetheless, preparation free pLys peptides involved the risk of obtaining a certain amount of hydrolyzed pLys as a side product.

The goal of the first part of this thesis was the suitability evaluation of a 2,2,2-trichloroethoxy- (Tc-) and Fmoc-protected pLys building block **1** for SPPS to obtain caged pLys peptides directly after cleavage from the solid support (scheme 4.1**C**). We envisioned the electron-withdrawing effect of the chlorine atoms in the protecting group to reduce the acid-lability of the P–N bond to sufficient extent. The design was inspired by the work for a caged pArg SPPS building block by Hofmann *et al.*[112] and would be obtained in a facile four-step synthesis starting from commercially available Cbz-protected Lys. This building block would enable a fast on-demand synthesis of caged pLys peptides and also avoid two purification steps.

4.1.2 Responsibility Assignment

The idea to transfer the knowledge about an protected pArg building block developed by the Seebeck group[112] and initial synthesis trials were designed by Anett Hauser. The project proceeded with the help of Eleftheria Poulou (FMP Berlin), who was responsible for the synthetic strategy optimization and peptide synthesis.

4.1.3 Synthesis of Core Building Block 1

For the synthesis of Fmoc-Lys(NPO(OTc)$_2$)-OH **1**, three different, commercially available Lys structures were tested. First, the toluene sulfonic acid salt of benzyloxycarbonyl- (Cbz-) and benzyl- (Bn-)protected Lys was applied to directly form phosphoramidate **3** (scheme 4.2, Route 1). However, due to its salt structure, insufficient solubility of the starting material in various solvent systems was observed, which led to poor yields of maximum 14% even at elevated temperatures (table 4.1, entry **1**-**3**). Also, basic pretreatment of the starting material with caesium carbonate (Cs_2CO_3) or pyridine to induce an *in situ* counter ion exchange did not lead to improved yields (entries **4** and **5**). Separation from the sulfonate anion was only achieved by flash preparative reversed phase

chromatography to obtain the desalted compound **2** in 85% yield, which was then susceptible for phosphoramidate **3** formation.

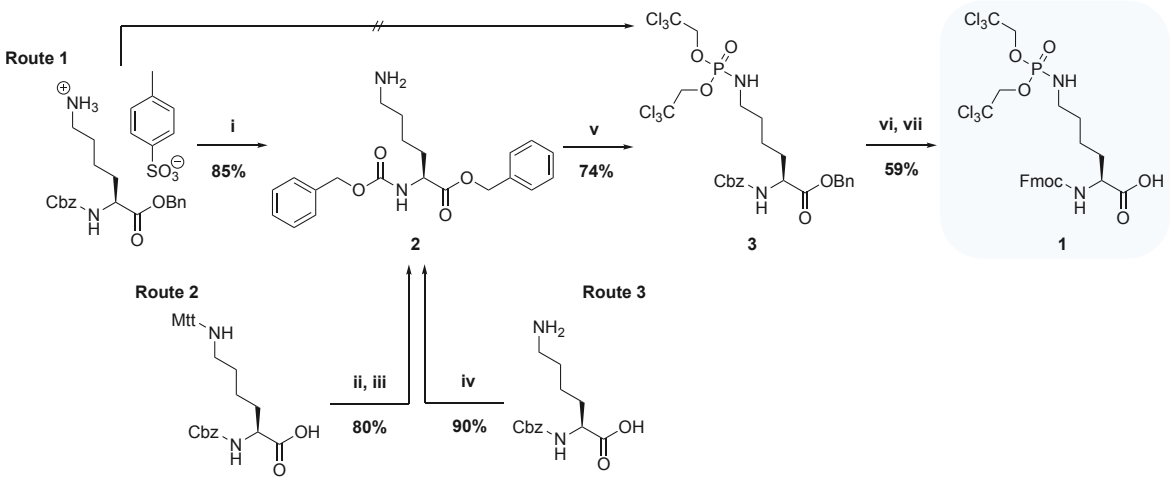

Scheme 4.2: Synthesis route to Fmoc-Lys(NPO(OTc)$_2$)-OH **1** either starting from Cbz- and benzyl-protected Lys 4-methylbenzenesulfonate (Route 1), Mtt- and Cbz-protected Lys (Route 2) or Cbz-protected Lys (Route 3). Reagents and conditions: **i**) flash HPLC; **ii**) Bn-Br (1.1 eq.), Cs_2CO_3 (1 eq.), DMF, r.t., 3.5 h; **iii**) TFA:TIS:DCM (1:1:98, v/v/v), 0 °C, 5 h; **vi**) $SOCl_2$ (5 eq.), Bn-OH (neat), 0 °C to r.t., 2 h; **v**) bis(2,2,2-trichloroethyl) phosphorochloridate (1.2 eq.), Et_3N (4 eq.), ACN, r.t., 5 h; **vi**) H_2, 10% Pd@C, AcOH:TFA:MeOH (5:5:90, v/v/v), r.t., 45 min; **vi**) Fmoc-OSu (1 eq.), Et_3N (1 eq.), H_2O:ACN (1:1, v/v), pH >9, r.t., 90 min.

Table 4.1: Tested reaction conditions to optimize the conversion of Cbz-Lys-OBn·TsOH to **3**.

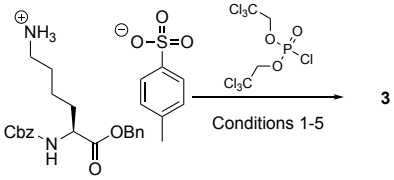

#	Solvent system	c [mM]	Et_3N [eq.]	ϑ [°C]	Pretreatment with	Isolated yield of **3** [%]
1	ACN:DMSO:NMP (69:21:10)	45	8	r.t.	–	3
2	ACN	50	8	r.t.	–	14
3	ACN	25	8	r.t. to 50	–	5
4	ACN	67	5	r.t.	3 eq. Cs_2CO_3	7
5	ACN	67	5	r.t.	1.5 eq. pyridine	6

Side chain 4-methyltrityl- (Mtt-) and Cbz-protected Lys was applied as second starting material (scheme 4.2, Route 2). The *C*-terminal Bn-protection was performed with benzyl bromide (Bn-Br) and Cs_2CO_3 as base within 3.5 hours reaction time. Without purification, the intermediate was side chain deprotected with 1% trifluoroacetic acid (TFA) and 1% triisopropyl silane (TIS) in dichloromethane (DCM) while cooling. Up to 80% **2** were isolated after preparative HPLC purification. This approach presented a feasable synthesis.

Even more facile was the employment of only *N*-terminally Cbz-protected Lys, since the *C*-terminal benzyl ester protection could be realized without cross-reaction of the side chain amine

(scheme 4.2, Route 3). By treating the starting material with thionyl chloride in neat benzyl alcohol (Bn-OH), full conversion to **2** was observed within two hours and up to 90% desired product were isolated.

The phosphoramidate formation with bis(2,2,2-trichloroethyl) phosphorochloridate was conducted in a closely similar fashion to Hofmann *et al.* for caged pArg.[112] The reaction time was increased in order to achieve full consumption of **2**, but the isolated yield of **3** was with 74% higher than described for the caged pArg building block.

Since the P–N bond in pArg displays higher stability than in pLys,[97,98] determined by liquid chromatography mass spectrometry (LC-MS) and nuclear magnetic resonance (NMR) spectroscopy, respectively, different conditions were tested for the simultaneous *N*- and *C*-terminal deprotection by hydrogenation. The protocol of Hofmann *et al.* described the usage of acetic acid (AcOH) and TFA in a 50:50 mixture (v/v) and subsequent acid removal by co-evaporation with ethanol (EtOH) under reduced pressure (rotavap) after filtration of the catalyst. Besides the fact that caged phosphoramidates are more stable than the corresponding phosphoramidic acids, a less acidic system would be preferred for the Lys derivative. Initial tests indicated a higher lability of caged pLys **3** compared to the caged pArg building block,[112] as more than 50% P–N bond hydrolysis of **3** was observed after storage in AcOH:TFA (50:50, v/v) for 16 hours at r.t. During the optimization, deprotection as well as hydrolysis progress were followed by ultra high performance liquid chromatography (UPLC) analysis. However, the final evaluation was based on isolated yield of the subsequent *N*-terminal Fmoc-protection to target compound **1**. The conditions for the latter reaction were not changed throughout the whole study and hence, did not have a significant influence on the outcome.

Table 4.2: Tested reaction conditions to optimize yields during conversion of **3** to **1**.

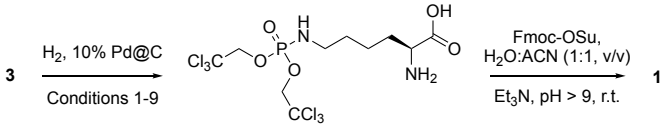

#	Solvent system	*c* [mM]	Reaction time [min]	P–N bond hydrolysis $[\%]_{220\ nm}$	Solvent removal	Isolated yield of **1** [%]
1	AcOH:TFA (50:50)	56	90	5	rotavap	29
2	AcOH:TFA (50:50)	56	90	3	N_2 flush	40
3	AcOH:TFA (50:50)	75	120	10	rotavap	5
4	AcOH:TFA (50:50)	75	45	<5	N_2 flush	33
5	MeOH	20	120	0	rotavap	[a]
6	AcOH:TFA:MeOH (1:1:98)	28	60	3-10	rotavap	22-60
7	AcOH:TFA:MeOH (5:5:90)	28	60	2	rotavap	51
8	AcOH:TFA:MeOH (5:5:90)	70	60	10	rotavap	20
9	AcOH:TFA:MeOH (5:5:90)	75	60	3	N_2 flush	59

[a] no product was formed

As shown in table 4.2, product formation was influenced not only by the acid concentration in the solvent, but also the compound concentration and the work up method. In that way, test reactions with acid gave moderate to good yields while in a system without any acid (entry **5**) no final product **1** was formed at all. The influence of starting material concentration can be seen in entries **7** and **8**, in which the higher dilution led to a decreased P–N bond cleavage during the deprotection and increased yield after Fmoc-protection. The technique used for solvent removal had also an impact on the hydrolysis rate. When comparing entries **1** with **2**, **3** with **4** or **8** with **9** it was observed that nitrogen bubbled through the filtered solution in order to remove solvents was less harmful than evaporation at the rotavap. This was probably related to the lower temperature and faster acid removal during N_2-treatment. In that perspective, especially entries **8** and **9** are promising, since with higher compound concentration during deprotection (entry **9**) significantly higher yield of **1** was achieved (59% compared to 20%). Thus, those latter conditions were used for further resynthesis of **1**.

4.1.4 Application of 1 in Peptide Synthesis

4.1.4.1 Stability of the Phosphoramidate Bond

Table 4.3: Testing of phosphoramidate stability in **3** or **1**.

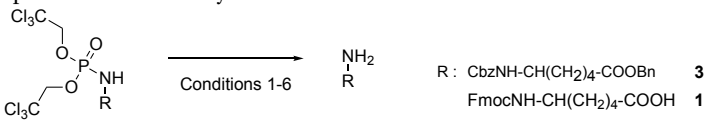

#	Compound	Condition	c [mM]	Time [min]	Intact P–N bond $[\%]_{220\ nm}$
1	**3**	Pip:DMF (20:80)	50	10	100
				90	98
2	**3**	5 eq. HATU, 10 eq. DIPEA in DMF	100	10	100
				90	99
4	**3**	TFA:TIS:H_2O (95:2.5:2.5)	50	45	95
				90	75
				120	50
				960	0
5	**1**	Pip:DMF (20:80)	50	10	100[a]
				60	100[a]
6	**1**	TFA:TIS:H_2O (95:2.5:2.5)	50	30	100
				90	75
				180	66

[a] detected was the compound with free *N*-terminus

Fmoc-Lys(NPO(OTc)$_2$)-OH **1** was envisioned as a building block for Fmoc-based SPPS and thus it was necessary to test its suitability for this purpose. During peptide synthesis, the phos-

phoramidate bond needed to withstand various conditions like piperidine in *N*,*N*-dimethylformamide (20% Pip in DMF), coupling reagents in combination with *N*,*N*-diisopropylethylamine (DIPEA) and TFA-based cleavage cocktails. Either **1** or **3** were treated with different reagents at r.t. and the P–N bond hydrolysis detected by UPLC-MS analysis at distinct time points.

Table 4.3 summarizes the tested conditions and results, which indicated a sufficient stability under standard SPPS conditions. Nonetheless, P–N bond cleavage was observed during prolonged treatment with the acidic deprotection and cleavage cocktail. This phenomenon might be avoided with shorter reaction times along with repetitive treatment, cooling during the deprotection/cleavage step or immediate neutralization of the obtained peptide solution. Furthermore, if the synthesis itself would be high-yielding and faster compared to the established Staudinger-phosphite route, a certain amount of product loss due to P–N bond hydrolysis would be acceptable.

4.1.4.2 Peptide Synthesis

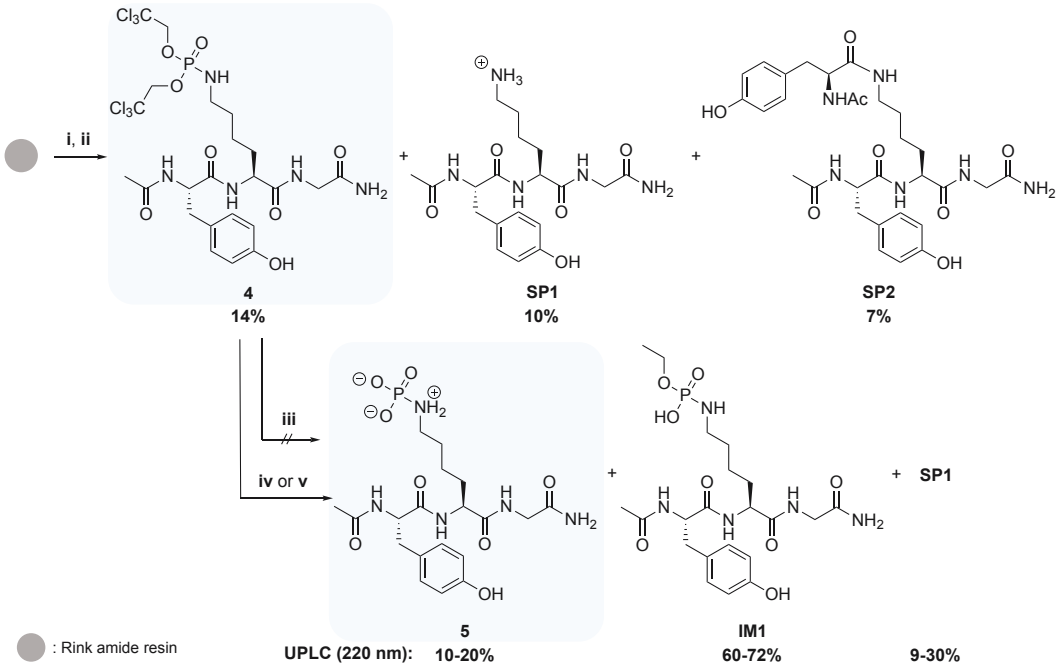

Scheme 4.3: Peptide synthesis routes to ^{Ac}Tyr-Lys(NPO(OTc)$_2$)-Gly^{CONH_2} **4** and subsequent hydrogenative uncaging of the phosphoramidate to ^{Ac}Tyr-pLys-Gly^{CONH_2} **5**. Reagents and conditions: **i**) Fmoc-SPPS; **ii**) TFA:TIS:H_2O (95:2.5:2.5, v/v/v), r.t., 2 h; **iii**) H_2, 10% Pd@C, 100 mM $(NH_4)_2CO_3$, pH 8:EtOH (20:80, v/v), 0 °C, 4 h; **iv**) H_2, 10% Pd@C, 100 mM $(NH_4)_2CO_3$, pH 9.2:EtOH (20:80, v/v), 0 °C, 2 h; **v**) H_2, 10% Pd@C, 100 mM $(NH_4)_2CO_3$, pH 8:EtOH (20:80, v/v), r.t., 6 h.

A Rink amide resin-based tripeptide ^{Ac}Tyr-Lys(NPO(OTc)$_2$)-Gly^{CONH_2} **4** was chosen as model compound to show the successful incorporation of **1** (scheme 4.3). Gly and Tyr were coupled with 2-(6-chloro-1H-benzotriazole-1-yl)-1,1,3,3-tetramethylaminium hexafluorophosphate (HCTU) and ethyl cyanohydroxyiminoacetate (Oxyma) as activating reagents in presence of DIPEA in DMF for 45 minutes each, while **1** was coupled with 1-[bis(dimethylamino)methylene]-1*H*-1,2,3-triazolo[4,5-*b*]pyridinium 3-oxid hexafluorophosphate (HATU) and DIPEA in DMF for two hours. The TNBS test for primary amines (containing picrylsulfonic acid) was used to confirm successful and complete reaction of **1**. Nonetheless, after cleavage from the solid support, not only the desired

product **4** was isolated in 14% yield, but also two major side products (10% **SP1**, 7% **SP2** in scheme 4.3). The masses detected by UPLC-MS indicated hydrolysis of the phosphoramidate (**SP1**) and an additional acetylated Tyr added to **SP1** (**SP2**). The latter case would have been possible only if the P–N bond was not stable under coupling conditions or rather in the Fmoc-deprotection step. NMR analysis of all isolated products confirmed the assumptions.

To further evaluate the alternative synthesis approach for caged pLys peptides, a comparative peptide synthesis was conducted (4.4). As mentioned above, the established synthesis route takes advantage of the chemoselective reaction of azides with phosphites. The (*o*-nitrophenyl)ethyl-(NPE-)protected peptide ^{Ac}Tyr-Lys(NPO(ONPE)$_2$)-Gly^{CONH_2} **7** was synthesized in one step after incorporation of *az*-Lys during SPPS. Phosphite **9** was obtained within two steps starting from 2'-nitroacetophenone in 70% yield over two steps. Reduction with sodium borohydride ($NaBH_4$) yielded alcohol **8**, which was further converted to the desired tris(1-(2-nitrophenyl)ethyl) phosphite **9** with PCl_3 under basic conditions. The overall yield of **7** was 45% without consideration of the phosphite synthesis (and 31% when taking the synthesis of **9** into account). Thus, a significant higher yield was achieved than *via* the Tc-protection route (14%). Nonetheless, considering the required amount of phosphite (7 eq.) and time for the Staudinger-phosphite reaction (48 hours plus purification), the new designed approach for caged pLys peptides proved to be an attractive alternative.

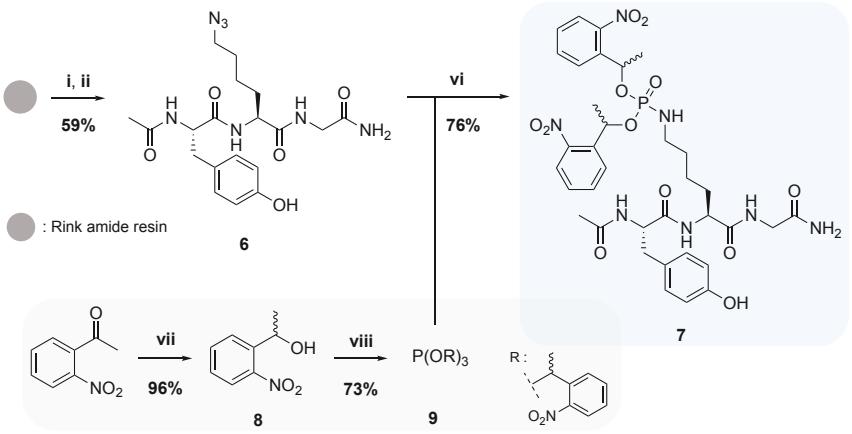

Scheme 4.4: Peptide synthesis route to ^{Ac}Tyr-Lys(NPO(ONPE)$_2$)-Gly^{CONH_2} **7**. Reagents and conditions: **i**) Fmoc-SPPS; **ii**) TFA:TIS:H_2O (95:2.5:2.5, v/v/v), r.t., 2 h; **iii**) **9** (3+2+2 eq.), DMF, 45 °C, 48 h; **iv**) $NaBH_4$ (2.5 eq.), MeOH:dioxane (3:2, v/v), 0 °C to r.t., 16 h; **v**) PCl_3 (0.29 eq.), Et_3N (0.31 eq.), dry THF, Ar, 0 °C to r.t., 18 h.

With the model peptide **4** in hand, the last step to a free pLys peptide **5**, which involved hydrogenative uncaging (scheme 4.3), was tested as well. The caged pArg protocol by Hofmann *et al.* described a hydrogenation at pH 9.2 and r.t.[112] Since the stability of pLys is closely related to both, temperature and pH value, also other conditions were evaluated (table 4.4). In a first approach, the same buffer as described previously for Tc-caged pArg peptides was used, but the reaction was conducted at 0 °C. After two hours, no starting material was left while a large amount of hydrolysis product **SP1** and intermediate **IM1** still bearing one ethyl ester were present besides the desired product **5** (scheme 4.3 & table 4.4, entry **1**). Thus, the basicity of the solvent was reduced to 8.0 and the temperature kept at 0 °C (entry **2**). Under these conditions, no conversion of **4** was observed even with prolonged reaction time. As shown in entry **3**, by adjusting the pH to 8.0 and conducting the reaction at r.t., the phosphoric ester cleavage was achieved to a higher extent while the

P–N bond hydrolysis remained less favored. Nonetheless, longer reaction times subsequently led to increased phosphoramidate degradation to amine **SP1** instead of onward product formation. This observation could also be understood as built product being hydrolyzed afterwards. Furthermore, even until six hours of reaction time, the deprotection did not proceed as the main product remained **IM1** with one ethyl ester at the phosphorous.

Table 4.4: Tested uncaging conditions for the conversion of **4** to **5**.

#	pH	ϑ	c	Time	Compound			
					4	**5**	**IM1**	**SP1**
		[°C]	[mM]	[h]	$[\%]_{220\ nm}$	$[\%]_{220\ nm}$	$[\%]_{220\ nm}$	$[\%]_{220\ nm}$
1	9.2	0	2	2	0	10	60	30
2	8.0	0	2	4	100	0	0	0
3	8.0	r.t.	2	2	0	19	72	9
				3.5	0	19	63	18
				6	0	20	61	19

4.1.5 Conclusion and Outlook

In conclusion, we could show the synthesis and application in SPPS of a novel protected lysine phosphoramidate. The Fmoc-protected SPPS building block **1** could be obtained in a straight forward synthesis in 39% yield over four steps starting from a non-expensive commercial compound. Also, **1** seemed to be stable under peptide synthesis and cleavage conditions when incubated in solution. However, from synthesis of peptide **4**, only 14% desired product besides a large amount of hydrolyzed phosphoramidate (**SP1**, 10%) were isolated. Especially the isolation of side product **SP2** with a Tyr modification on the Lys side chain was striking. These findings indicated more complex circumstances on resin than in solution. The proximity of reactive handles and thus, the high effective concentration might have decreased the stability of the P–N bond. The comparative synthesis of NPE-caged peptide **7** revealed indeed higher yield *via* the two-step Staudinger-phosphite route. Yet, the availability of desired caged peptide from loading of the solid support to **4** or **7** was much faster for the newly envisioned building block **1** since the desired compound could be obtained directly after cleavage from the solid support.

Caged pLys peptides present a convenient way to store pLys compounds for longer time and to have them deprotected readily on demand for functional assays of interest. Thus, the successful deprotection of **4** to the free phosphoramidate **5** was crucial for the evaluation of this approach. In small scale reactions it could be shown, that the desired compound was formed only in 20% yield in relation to starting material, intermediate **IM1** and detected side product **SP1**. Under the chosen conditions, it was not possible to achieve further conversion of **IM1** without simultaneous hydrolysis of **5** in the meantime. These results indicated an increased stability of the monoethyl ester and confirmed again the lability of free pLys at r.t. This observation was made repeatedly during irradiative uncaging of NPE-protected pLs peptides as well. [97]

So far, the only advantage of **1** compared to established protocols is the time saving during

synthesis. It might be sensible to test the latter reaction at larger scale and different conditions such as slightly higher pH while cooling the reaction. Only then, isolation of **5** might be possible to eventually assess the suitability of Fmoc-Lys(NPO(OTc)$_2$)-OH **1** for the generation of pLys peptides.

4.2 Investigation of Amine Protonation in Various Phosphoramidate Species

4.2.1 Outline of the Project

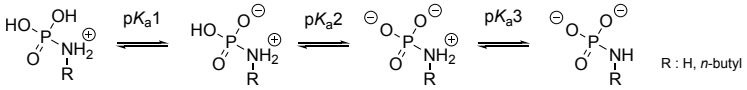

Figure 4.1: Proposed protonation of phosphoramidates according to Gamcsik *et al.* [240] and Benkovic and Sampson. [74]

One element in understanding the properties of pLys is the change in protonation with different pH values (acid dissociation constants, pK_a values). Previous experiments with phosphoramidates have proposed a positively charged nitrogen (pK_a3 in scheme 4.1) at pH values below 8.6 and 9.9 for phosphoramidic acid [240] and *N*-(*n*-butyl)phosphoramidate [74] (*n*-BPA), respectively. Thereby, the pK_a values of phosphoramidic acid were determined by NMR spectroscopy titrations and the pK_a values of *n*-BPA were measured potentiometrically. While these values gave an idea about the protonation of pLys, no study was performed to actually investigate the pK_a values of a pLys peptide. Hence, the goal of this project part was the acid dissociation constants determination of pLys in a peptidic compound. These experiments should be realized in accordance to the assay by Gamcsik *et al.* since NMR spectroscopy offers non-invasive analysis and allows examination of various atom species in one sample. Consequently, the change in protonation can be observed by the changes of chemical shift of phosphorous nuclei (^{31}P), protons (^{1}H) and nitrogen nuclei (^{15}N). While ^{31}P and ^{1}H display sufficient signal intensities to allow low sample concentration, nitrogen NMR is hampered by low natural abundance of ^{15}N. [241] Thus, in order to measure nitrogen *via* NMR spectroscopy, ^{15}N-labeled compounds should be prepared and employed in correlation experiments.

For this project, the previously synthesized peptide ^{Ac}Tyr-Lys(NPO(ONPE)$_2$)-Gly^{CONH_2} **7** was applied after photolysis to peptide **5** (figure 4.2). With this compound in hand, the chemical shifts of the phosphorous and the protons – especially the ϵ-H – at varying pH values were monitored by one- and two-dimensional (1D and 2D) NMR experiments. In a similar fashion, ^{15}N-labeled peptide ^{Ac}Tyr-pLys-$^{15}N_2$-Gly^{CONH_2} **10** was employed in the titration experiments as well to to investigate the presence of protons on the phosphoramidate nitrogen *via* 2D one-bond correlations ($^1J[^1H_\zeta, ^{15}N_\zeta]$).

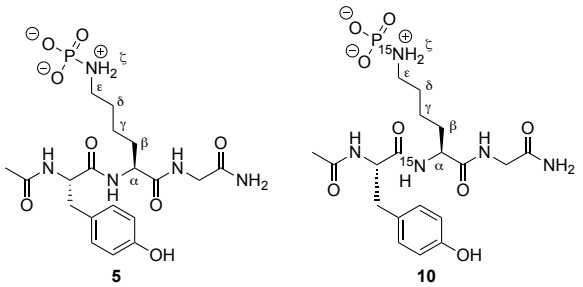

Figure 4.2: Target peptides **5** and **10** for NMR titration experiments to determine the side chain nitrogen pK_a values with nomenclature of pLys side chain positions α to ζ.

4.2.2 Responsibility Assignment

The design of the study was planned by Peter Schmieder (FMP Berlin), Anett Hauser and Christian Hackenberger. The synthesis, purification and characterization of all compounds were conducted by Anett Hauser. The NMR spectroscopy measurements were programmed and supervised by Peter Schmieder. The data analysis and evaluation as well as pK_a values calculations were performed by Anett Hauser and Peter Schmieder.

4.2.3 Synthesis of Target Peptides 5 and 10

4.2.3.1 Photolytic Deprotection of ^{Ac}Tyr-Lys(NPO(ONPE)$_2$)-Gly^{CONH_2} 7

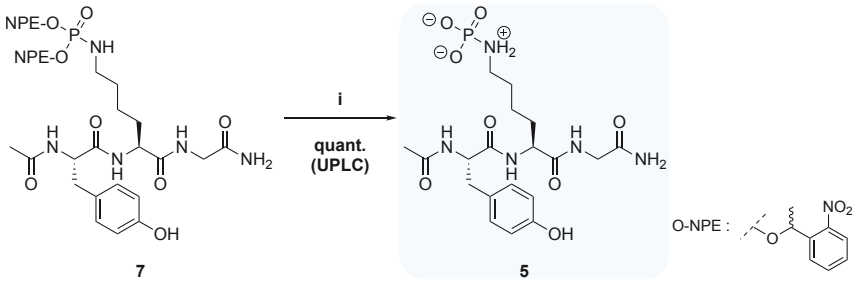

Scheme 4.5: Synthesis route to peptide ^{Ac}Tyr-pLys-Gly^{CONH_2} **5**. Reagents and conditions: **i**) $h\nu$ (297 nm), MeOH, r.t., 45-60 min.

In previous reports, NPE-protected pLys peptides have been uncaged by irradiation with a laser for 30 seconds and purified by preparative HPLC under basic conditions.[97] It was obeserved throughout the experiments that lyophilization was also harmful for pLys and led to a certain amount of P–N bond hydrolysis. Furthermore, the aparatus formerly available could not be used during the recent studies anymore. Thus, the photolysis of **7** was conducted with an ultraviolet (UV-)lamp, which led to increased deprotection times (scheme 4.5). To avoid lyophilization of **5**, different solvent systems like ACN, EtOH, methanol (MeOH) and various mixtures thereof were tested, from which the product could be isolated by precipitation. Eventually, 0.5 µmol aliquots of **7** were dissolved in MeOH to at least 5 mM and irradiated until UPLC-MS analysis indicated full conversion. **5** was separated from the deliberated ketone by precipitation in cold diethyl ether (Et_2O), dried under reduced pressure at r.t. and stored in the freezer until employed in the NMR experiments.

4.2.3.2 Synthesis of Model Peptide ^{Ac}Tyr-pLys-$^{15}N_2$-Gly^{CONH_2} 10

The ^{15}N-labeled target compound was synthesized starting from commercially available side chain Boc- and *N*-terminally Fmoc-protected Lys-$^{15}N_2$ (scheme 4.6). In a first approach, the shortest route was tested, thereby incorporating the building block into the desired tripeptide **11** by standard Fmoc-SPPS with 95% yield. For the subsequent phosphorylation with ammonium phosphoramidate (NH_4 – PA, **16**), the phosphorylation reagent was obtained as previously

described by Buckler and Stock.[158,242] Briefly, activation of ammonium phosphate with ethyl isocyanate was

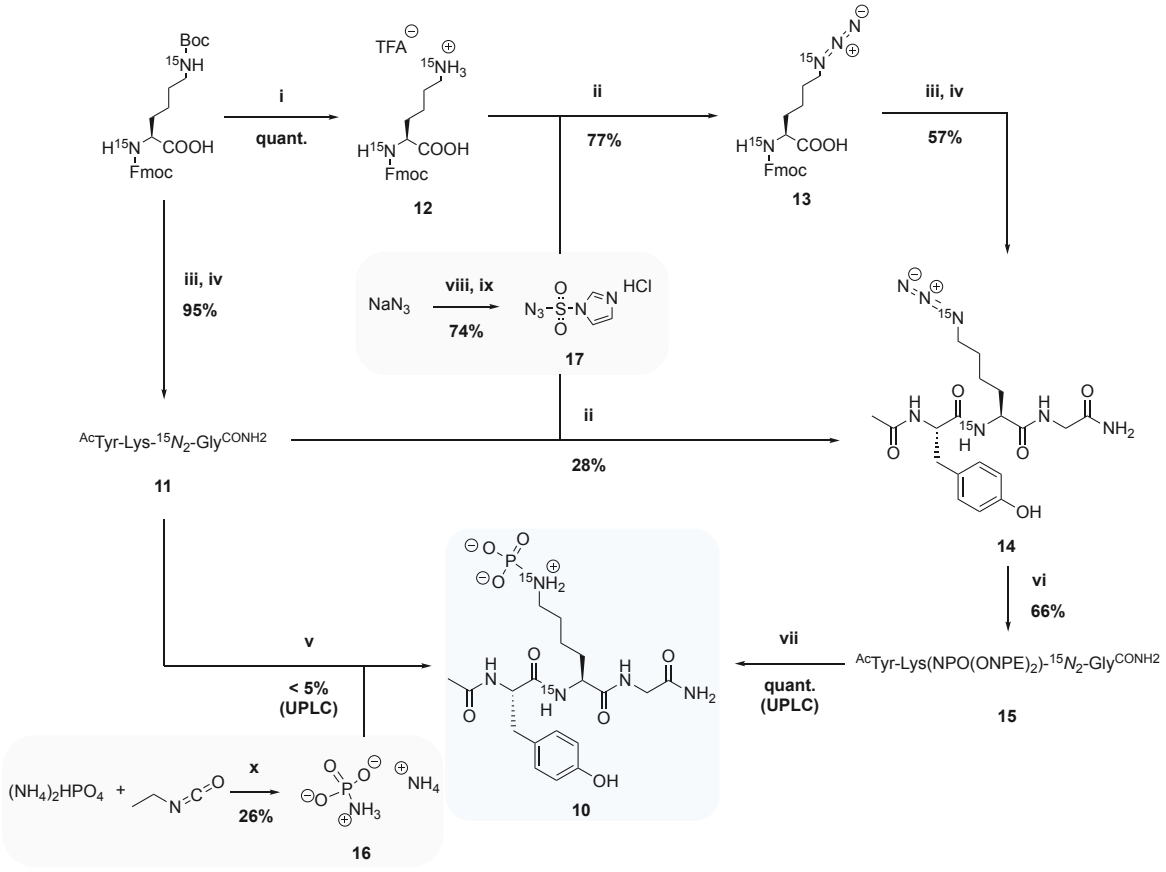

Scheme 4.6: Synthesis route to peptide ^{Ac}Tyr-pLys-$^{15}N_2$-Gly^{CONH_2} **10**. Reagents and conditions: **i**) TFA (neat), r.t., 10 min; **ii**) **17** (1.2 eq.), $NaHCO_3$ (10 eq.), $CuSO_4 \cdot 5H_2O$ (0.01 eq.), MeOH:H_2O (3:1, v/v), r.t., 18 h; **iii**) Fmoc-SPPS; **iv**) TFA:TIS:H_2O (95:2.5:2.5, v/v/v), r.t., 2 h; **v**) **16** (650 eq.), 25 mM Tris, pH 7, r.t., 7 d; **vi**) **9** (3+3+3 eq.), 45 °C, 950 rpm, 48 h; **vii**) *hv* (297 nm), MeOH, r.t., 45-60 min; **viii**) a) SO_2Cl_2 (1 eq.), ACN, 0 °C - r.t., ovn, b) imidazole (2 eq.), 0 °C - r.t.3 h; **ix**) EtOH:Ac-Cl (79:21, v/v), EE, 0 °C, 15 min; **x**) a) ethyl isocyanate (1.6 eq.), H_2O, r.t. - 44 °C, 40 min, b) NH_4OH (conc., 13.3 eq.), r.t. - 50 °C, ovn.

followed by formation of the phosphoramidate with concentrated ammonium hydroxide solution to give **16** in 26% yield. Unfortunately, the phosphorylation of ^{Ac}Tyr-Lys-$^{15}N_2$-Gly^{CONH_2} **11** to give **10** following a procedure introduced by Ek *et al.*,[142] which described the Lys phosphorylation of histone H1 by treatment with **16** at pH 7 and r.t. for 24 hours, did not lead to a sufficient conversion and thus, this synthesis route was abandoned.

In a second approach, the Staudinger-phosphite route was used. The required azide could be formed at two positions in the reaction sequence *via* an azide transfer reaction from imidazole-1-sulfonyl azide hydrochloride **17** to an amine as described by Guo *et al.* for *N*-terminally Boc protected Lys.[243] Reagent **17** was obtained according to a protocol described by Goddard-Borger and Stick from sodium azide in 74% yield.[244] An elaborated NMR spectroscopy study by Pandiakumar *et al.* proposed the retention of the amine nitrogen bound to the carbon within the formed azide, hence, the ^{15}N-label should stay intact during the Staudinger-phosphite reaction.[245]

The first opportunity to install the azide was before peptide synthesis. For this, the purchased building block Fmoc-Lys(Boc)-OH-$^{15}N_2$ was quantitatively side chain deprotected with TFA to **12**

and subsequently applied in the azide transfer reaction to give Fmoc-*az*-Lys(Boc)-OH-$^{15}N_2$ **13** in 77% yield. The building block was incorporated into the model peptide and 57% of **14** were isolated after preparative HPLC.

The second possibility was the conversion of previously synthesized **11** to **14** by azide transfer following the same protocol. However, this reaction led only to unsatisfactory product formation. With **14** in hand, the NPE-caged phosphoramidate was installed as described in section 4.1.4.2 with 66% isolated yield of **15**. Aliquots of ^{Ac}Tyr-Lys(NPO(ONPE)$_2$)-$^{15}N_2$-Gly^{CONH_2} **15** were deprotected to **10** as described in section 4.2.3.1.

4.2.4 NMR Experiments

4.2.4.1 Determination of pK_a Values of Phospho-Lysine

The experiments were inspired by the NMR titration conducted by Gamcsik *et al.* on phosphoramidic acid and other phosphoramides.[240] Samples were prepared at a 1 mM concentration in 40 mM potassium chloride (H_2O + 10% D_2O) and kept at low temperature to reduce P–N bond hydrolysis. The pH of each sample was adjusted before measurement and checked again afterwards. Proton (^{1}H), Phosphorous (^{31}P) 1D as well as ^{1}H-^{31}P-heteronuclear multiple bond coupling (HMBC) NMR spectra (figure 4.3**A**) were recorded from pH 2 to 11 on a 600 MHz (^{1}H frequency) spectrometer at 278 K and subsequently used for calculations of pK_a values.

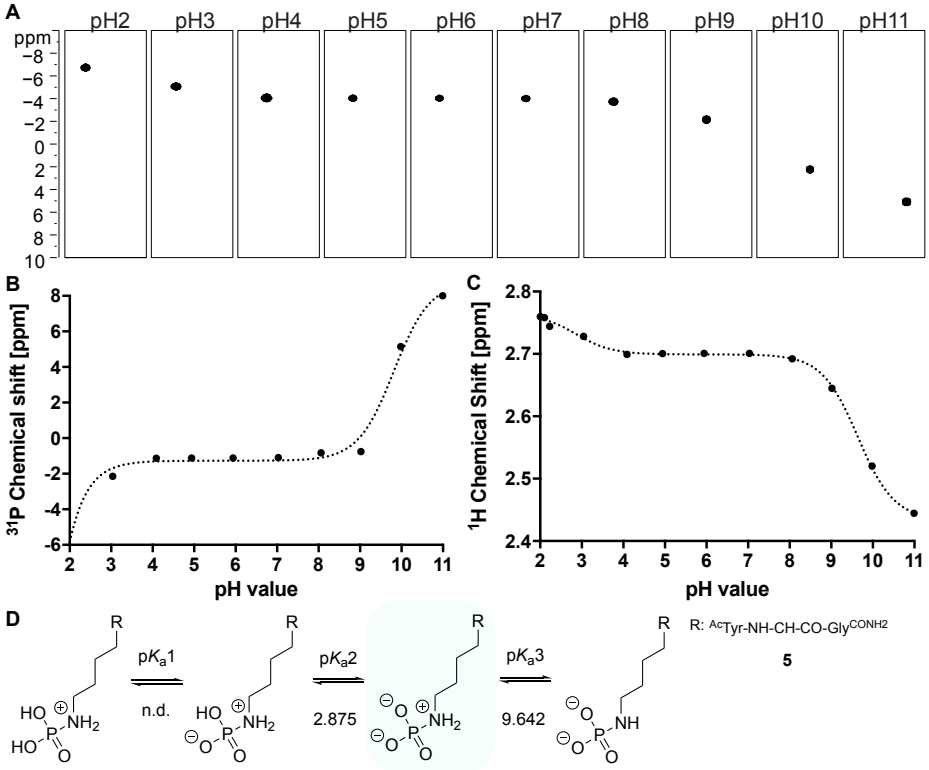

Figure 4.3: **A**. Signals extracted from the ^{1}H-^{31}P-HMBC experiment. **B** & **C**. Graphical visualizations of NMR measurements of ^{31}P chemical shifts (**B**) and ^{1}H$_\epsilon$ chemical shifts (**C**). **D**. Dissociation equilibrium of pLys in a peptide with calculated pK_a values.

In order to do so, the chemical shift of phosphorous in pLys (table 4.5, third column) was plotted against the pH values and the resulting curve fitted with a sigmoidal function wherein pK_a values were obtained from the inflection points (figure 4.3**B**). We further evaluated the data by plotting and fitting the chemical shift of the ϵ-protons (table 4.5, fourth column) against pH values (figure 4.3**C**).

Table 4.5: Measured values for ^{31}P and $^{1}H_{\epsilon}$ chemical shifts at different pH values.

#	pH	$\delta_{^{31}P}$ [ppm]	$\delta_{^{1}H_{\epsilon}}$ [ppm]
1	2.00	-6.021	2.760
2	2.10	-4.722	2.758
3	2.23	-3.812	2.744
4	3.04	-2.150	2.728
5	4.09	-1.132	2.699
6	4.94	-1.125	2.701
7	5.94	-1.124	2.701
8	7.03	-1.091	2.701
9	8.06	-0.822	2.692
10	9.02	-0.760	2.645
11	9.98	5.152	2,520
12	10.99	8.031	2.445

Our findings indicated that the first acid dissociation constant could not be determined (pK_a1 in figure 4.3**D**), because it was below pH 2 and thus, outside of our measurement range. Besides that, it was possible to calculate pK_a2 and pK_a3 at 2.875 ± 0.296 and 9.642 ± 0.067 (R^2 = 0.9995), respectively, which correlated with the complete deprotonation of the phosphoryl oxygens and eventually the deprotonation of the nitrogen. Additionally, the magnitude of change in ppm (Δppm) at the inflection points when compared with the report of Gamcsik *et al.* supported our assignments of charge states. Then, a smaller value indicated protonation change on oxygen while a larger value correlated with the protonation of nitrogen.[240] Consistent with these previous reports, we observed Δppm of 5.09 ppm and 8.82 ppm in the phosphorous spectra for pK_a2 and pK_a3, respectively. In addition to this, our calculations are in the range of the results for *n*-BPA described by Benkovic and Sampson as they reported 2.92 ± 0.06 and 9.88 ± 0.10 as pK_a2 and pK_a3, respectively.[74] Thus, pLys in peptide **5** has a mono-anionic charge state under physiological conditions (figure 4.3**D**).

4.2.4.2 ^{15}N-Nitrogen NMR

Building upon the results with unlabeled peptide **5**, the second approach of this project aimed for the detection of the ζ-proton(s) in pLys. With the ^{15}N-labeled *az*-Lys peptide **14** in hand, a full characterization was conducted, within which the $^{15}N_{\zeta}$-signal was determined from the $^{2}J[^{1}H_{\epsilon}, ^{15}N_{\zeta}]$ and $^{3}J[^{1}H_{\delta}, ^{15}N_{\zeta}]$ correlations in the ^{1}H-^{15}N-HMBC spectrum with a chemical shift of

$\delta_{^{15}N}$ = 71.25 ppm (figure 4.4, left). In addition, these experiments confirmed the desired position of the ^{15}N-label in the azido-group and validated the proposed mechanism for the azide transfer reaction. [245]

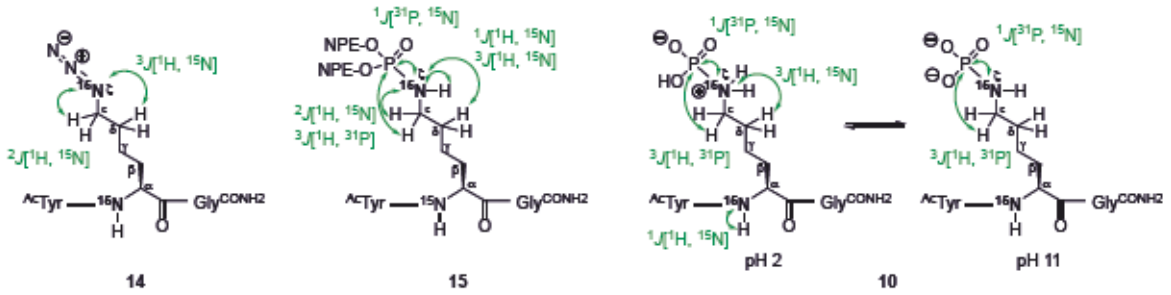

Figure 4.4: Overview of detected correlations in compounds **14**, **15** and **10**.

After the Staudinger-phosphite reaction, the NPE-caged phosphoramidate **15** was obtained, from which the two isomers could be seperated by preparative HPLC. First NMR measurements were conducted in TFA-acidified H_2O with 10% D_2O and 10% CD_3CN and delivered proof for the target structure. Figure 4.4 summarizes the findings, which are further displayed in more detail in figure 4.5**A**-**D** and below.

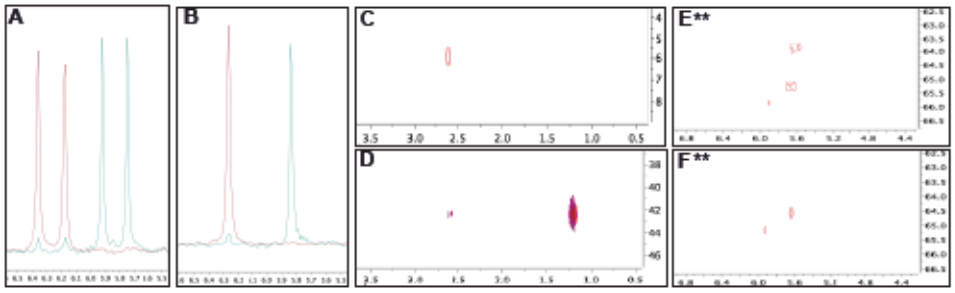

Figure 4.5: NMR spectra obtained from **15** in 0.1% TFA + 10% D_2O + 10% CD_3CN (**A**-**D**) or DMSO-d_6 (**E** & **F**). **A**. Overlay of $^{31}P\{^1H\}$, — isomer 1, — isomer 2. **B**. Overlay of $^{31}P\{^1H, ^{15}N\}$, — isomer 1, — isomer 2. **C**. ^{1}H-^{31}P-HMBC of isomer 2. **D**. ^{1}H-^{15}N-HMBC of isomer 2. **E**. ^{31}P-^{15}N-HMQC, protons not decoupled. **F**. ^{31}P-$^{15}N\{^1H\}$-HMQC. ** The spectrometer calibration was incorrect during these experiments, the scale in ^{15}N-dimension is between 42.1 and 46.1.

The presence of the correct structure was, for example, seen in the proton decoupled ^{31}P, which showed a signal as doublet with J = 41.8 Hz. Running the spectrum again as $^{31}P\{^1H, ^{15}N\}$ resulted in a singlet peak, thereby proving the intact P–^{15}N bond as the previously detected correlation was based on a $^1J[^{31}P, ^{15}N]$ (figure 4.5**A** & **B**). Furthermore, proton correlation spectra with phosphorous (figure 4.5**C**) and nitrogen (figure 4.5**D**) confirmed the structural proximity of ϵ-protons to the phosphoramidate and thus, the ζ-^{15}N. This was shown by the detected $^3J[^1H_\epsilon, ^{31}P]$ (figure 4.5**C**), a small $^2J[^1H_\epsilon, ^{15}N_\zeta]$ as well as a more distinct $^3J[^1H_\delta, ^{15}N_\zeta]$ (figure 4.5**D**). The chemical shift for the side chain ^{15}N is 42.4 ppm in acidic, aqueous medium. Other than expected, no one-bond correlation for the N–H pair in the Lys side chain was detected, neither in a ^{1}H-^{15}N-heteronuclear single quantum coherence (HSQC) nor a ^{1}H-^{15}N-heteronuclear multiple quantum coherence (HMQC) experiment. Both would have proven the existence of one or more ζ-protons bound to the phosphoramidate nitrogen.

Switching the solvent from an aqueous system to dry DMSO-d_6 delivered further insights. As shown in figure 4.5**E** and **F**, the different ^{31}P-^{15}N-HMQC experiments delivered the missing infor-

mation about the protonation on the ζ-nitrogen. Running the correlation experiment without proton decoupling resulted in a peak splitting in the ^{15}N-dimension at approximately $\delta_{^{15}N}$ = 44.1 ppm to a doublet indicating one proton bound to nitrogen (figure 4.5**E**, please note the incorrect calibration of the spectrometer led to a signal shift of +20.1 ppm). This pattern vanished when repeating the experiment with proton decoupling, thereby confirming the indicated N–H bond (figure 4.5**F**). For last measurements with the caged phosphoramidate **15**, some dry TFA was added to the sample dissolved in DMSO-d_6 to acidify the system and induce protonation. Unfortunately, the only detected species was a peptide with a free amine on the Lys side chain resulting from P–N bond hydrolysis.

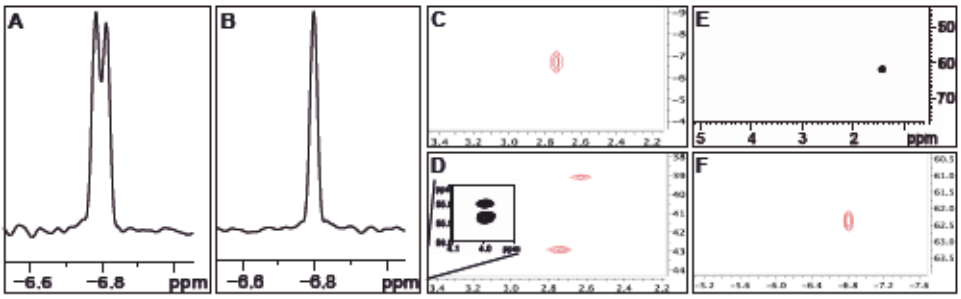

Figure 4.6: NMR spectra obtained from **10** in H_2O + 10% D_2O at pH 2. **A.** $^{31}P\{^1H\}$. **B.** $^{31}P\{^1H, ^{15}N\}$. **C.** ^{1}H-^{31}P-HMBC. **D.** ^{1}H-^{13}C-HSQC. **E.** ^{1}H-^{15}N-HMBC. **F.** ^{31}P-^{15}N-HMQC, protons not decoupled.

With the target compound **10** itself most NMR measurements were conducted in aqueous systems at low pH to ensure nitrogen protonation as indicated by the results from section 4.2.4.1. Figure 4.4 on the right summarizes the observed correlations.

Pleasingly, the proton decoupled ^{31}P experiment gave a doublet signal as compound **15** with $^1J[^{31}P, ^{15}N_\zeta]$ = 7.3 Hz (figure 4.6**A**), which vanished when applying nitrogen decoupling in addition (figure 4.6**B**). Interestingly, this coupling was much smaller compared to the compound with protecting groups. Hence, the phosphoramidate of pLys was intact. Also, a distinct $^3J[^1H_\epsilon, ^{31}P]$ correlation was detected during the ^{1}H-^{31}P-HMBC experiment (figure 4.6**C**).

Besides this evidence for the right structure of pLys peptide **10**, no indication for proton(s) bound to the side chain nitrogen could be obtained. As shown in figure 4.6**D**, the ^{1}H-^{13}C-HSQC experiment without ^{15}N-decoupling in the ^{13}C-dimension indicated the C–N bond for the α-carbon at $\delta_{^{13}C} \approx$ 55.8 ppm with a coupling constant of $^1J[^{13}C_\alpha, ^{15}N_\alpha]$ = 15 Hz. This was in the range of reported values for amide bonds.[246] Nonetheless, no significant splitting due to a ^{13}C-^{15}N coupling was detected for the side chain ϵ-carbon, neither in the intact pLys ($\delta_{^1H} \approx$ 2.75 ppm), nor the hydrolyzed Lys peptide ($\delta_{^1H} \approx$ 2.65 ppm).

Furthermore, the ^{1}H-^{15}N-HMBC spectrum did not show any $^1H_\epsilon$-$^{15}N_\zeta$-correlation. Only a faint signal for the $^3J[^1H_\delta, ^{15}N_\zeta]$ at $\delta_{^{15}N}$ = 62.3 ppm could be observed (figure 4.6**E**). As for the caged pLys peptide **15**, ^{31}P-^{15}N-HMQC experiments with and without proton decoupling in the ^{15}N-dimension were performed. Neither of the resulting peaks was split additionally (figure 4.6**F**) and thus, no indication for one or more protons bound to nitrogen was given. Also, measurements in dry DMF-d_7 did not give signals as obtained for peptide **15**.

Strikingly, during the titration experiments, the one-bond correlation $^1J[^{31}P, ^{15}N_\zeta]$ was observed only at pH 2 and pH 11 with 7.3 Hz and 11.8 Hz, respectively. All other pH values yielded

in singlet peaks for the $^{31}P\{^{1}H\}$ experiments and empty spectra in the ^{31}P-^{15}N-HMQC measurements. Still, the ^{1}H-^{31}P-HMBC spectra showed intact pLys peptide throughout the titration.

4.2.5 Small Molecule for NMR Studies

Several findings from the preceding investigations of peptides **5**, **10** and **15** gave rise to further studies. First, the varying protonation of phosphoramidate nitrogen in the caged and the unprotected state. Second, the difficulties to detect any N–H one-bond correlations ($^{1}J[^{1}H_{\zeta}, ^{15}N_{\zeta}]$) even under acidic conditions. Third, the disappearance and recurrence of the P–N one-bond correlations ($^{1}J[^{31}P, ^{15}N_{\zeta}]$) in the $^{31}P\{^{1}H\}$ experiments from pH 3 to 10. Thus, the mechanistic processes taking place during phosphoramidate formation and subsequent deprotection were of particular interest for us. Additionally, all NMR samples were prepared at a concentration of 1 mM. Since ^{15}N NMR is rather insensitive, higher concentrations could lead to more significant results. At the same time, increased sample concentration might induce P–N bond hydrolysis, an effect, which has never been studied thoroughly before and should be kept in mind.

The preparation of peptide **10** was tedious with high monetary effort for Fmoc-Lys(Boc)-OH-$^{15}N_2$, while yielding only small amounts of target compound eventually. Additionally, the doubly labeled building block resulted in more complex spectra stemming from **10** itself and the hydrolyzed peptide **11**. For studies regarding the events on phosphoramidate nitrogen, no amino acid structure was required. Thus, the synthesis of a small, mono-labeled molecule like *N*-propyl phosphoramidate-^{15}N or *N*-(*n*-butyl)phosphoramidate-^{15}N (*n*-BPA-^{15}N) was targeted. Thereby, *n*-BPA-^{15}N was favored due to its higher boiling point. The synthesis route shown in figure 4.7 was proposed starting from *n*-butylamine-^{15}N. Since *n*-butylamine-^{15}N is not as expensive as Fmoc-Lys(Boc)-OH-$^{15}N_2$ and less synthesis steps are required to obtain the target compound, a higher amount was to be produced and thus, the NMR experiments conducted at higher concentrations. Even though *n*-butylamine-^{15}N has been offered by two suppliers, none of them could deliver any material within the period of this doctoral thesis.

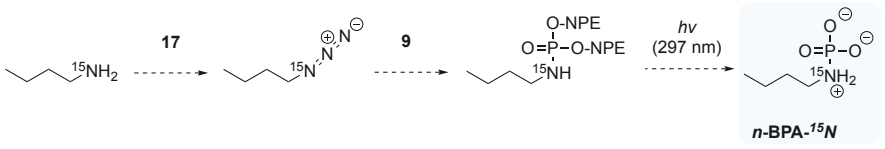

Scheme 4.7: Proposed synthesis route to *n*-BPA-^{15}N.

4.2.6 Conclusion and Outlook

During this project, two closely related peptides (**5** and **10**) were synthesized and applied in elaborated NMR experiments. The unlabeled peptide **5** was used for the determination of the acid dissociation constants of pLys, which has not been reported for pLys compounds before. With $pK_a2 = 2.875 \pm 0.296$ and $pK_a3 = 9.642 \pm 0.067$ ($R^2 = 0.9995$), the results indicated similar pK_a values as described for phosphoramidic acid and *n*-BPA.[74,240]

The ^{15}N-labeled peptide **10** was designed to observe the protonation of the side chain nitrogen throughout the titration. Structure elucidation confirmed indeed the successful synthesis. However, no $^{1}H_{\zeta}$-$^{15}N_{\zeta}$-correlation could be determined in all conducted NMR experiments. Even though a H–N bond could be observed for the caged pLys peptide **15**, no distinct proof for nitrogen protonation could be detected with target peptide **10**. A possible reason could be the self-decoupling of nitrogen. As described for other amines and amino acids, the exchange rate of protons bound to nitrogen with protons in the solvent can be so high that it reaches the magnitude of the ^{1}H-^{15}N coupling constant.[247,248] As a result, the nitrogen nuclei can not distinguish the spin states of the protons. In the spectrum the ^{15}N-signals broaden and no correlation in 2D spectra nor multiplets in 1D spectra can be observed.

To investigate the mechanism of the Staudinger-phosphite reaction in more detail, the synthesis of *n*-BPA-^{15}N was approached but could not be conducted eventually. This plan might be of interest in the future and should not be neglected since it can deliver closer insights into the structural and electronic situation in caged phosphoramidates and their deprotected derivatives. The synthesis strategy is established and could be applied easily to most amines of interest.

Apart from that, NMR measurements at lowered temperature might be useful to reduce the proton exchange and avoid the self-decoupling. In order to do so, another solvent system would be required. A mixture of water and organic solvents could lead to decreased melting temperature and give access to lower experiment temperatures. Unfortunately, those experiments could not be conducted in the facilities of the FMP Berlin, since the required temperatures for a diminished proton exchange can not be reached using a cryogenic probe.

4.3 Design and Synthesis of Stable Phospho-Lysine Mimics

4.3.1 Outline of the Project

Compared with other endogenous phospho-AAs, phosphoramidates and especially pLys exhibit a reduced chemical and thermal stability.[44] Interestingly, phosphoramidates seem to be more stable under basic than acidic conditions. These properties present additional challenges during investigations of pLys proteins or peptides. Precautions have to be taken when it comes to sample treatment, working temperatures and reaction times. A major drawback is the thermal instability,[97] which did not allow to incorporate unprotected pLys substrates into proteins, so far. Stable analogues would present an attractive option to circumvent P–N bond hydrolysis and still be able to study interaction partners of pLys. Hence, two structures were envisioned with varying hydrolytic stability (figure 4.7). First, a phosphonate, which would be non-hydrolyzable substrate and should exhibit the highest chemical and thermal stability. Also, it might function as an enzyme inhibitor in further investigations, especially for phosphatases (Pases) and phosphoramidate hydrolases (PAHs). Second, a phosphate, which was expected to be acid-stable but still labile under certain conditions, e.g. elevated temperatures, at basic pH or under Pase treatment. In order to apply both analogues in peptide synthesis, the structures ought to be developed as benzyl and Fmoc-protected SPPS building blocks. The target structures of Fmoc-hCys(EtPO(OBn)$_2$)-OH **18** and Fmoc-Nle(OPO(OH)(OBn))-OH **19** are shown in figure 4.7.

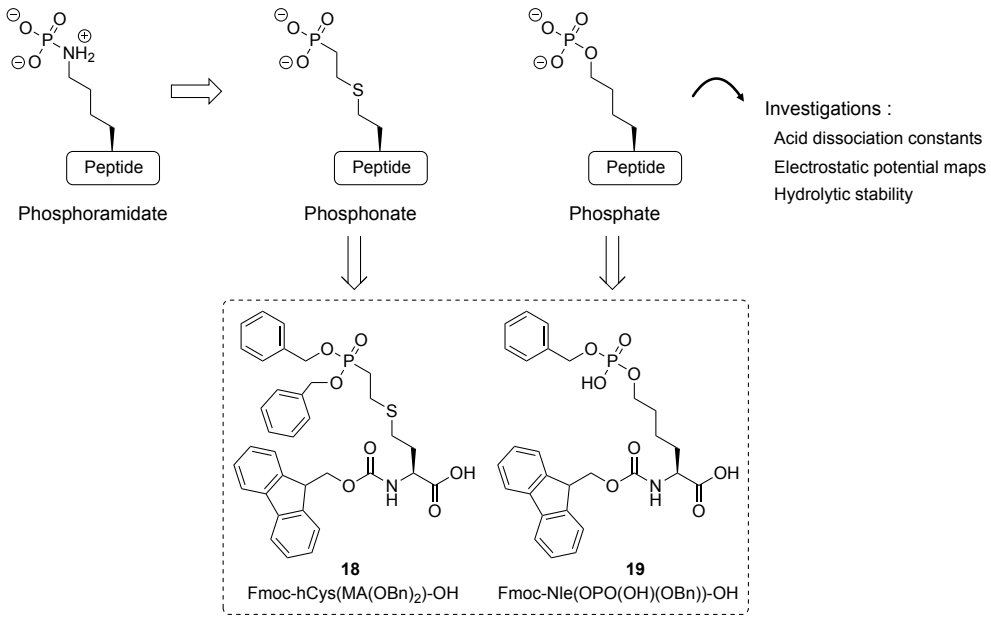

Figure 4.7: Envisioned stable mimics for pLys and proposed investigations to compare their properties.

With **18** and **19** as well as successful peptide synthesis, their pLys mimicking properties were to be estimated. We planned to calculate charge densities for pLys and analogues. In order to do so, the acid dissociation constants (pK_a) of the free phosphonate and phosphate were to be determined in the same fashion as for pLys by the help of NMR titration experiments (see section 4.2).

Derived from the pK_a values, the charge state at physiological conditions could be concluded and employed in structure optimization calculations. The optimized structures were to be visualized as electrostatic potential (ESP) maps, thereby enabling a mathematical and optical comparison of the three molecules. The stability was another criteria to estimate the mimic suitability. Both building blocks were envisioned to be incorporated into peptides. Thus, the acid stability could be proven throughout the synthesis. Besides this, the recognition of interacting enzymes was of interest. For pLys only one specific PAH – *phospholysine phosphohistidine inorganic pyrophosphate phosphatase* (LHPP) – is known so far. [203,204,213,249,250] The altered enzymatic activity of LHPP towards the analogues was to be investigated, whereby a decrease or inactivity was expected for the phosphate or phosphonate, respectively. In addition to LHPP, the hydrolytic stability was to be shown with the promiscuous Pase *bovine alkaline phosphatase* (ALP).

4.3.2 Responsibility Assignment

The project concept was established by Anett Hauser and Christian Hackenberger. The synthesis design and conduction was performed by Anett Hauser. The NMR spectroscopy measurements were programmed and supervised by Peter Schmieder. The data analysis and evaluation as well as pK_a values calculations were performed by Anett Hauser and Peter Schmieder. All molecule structure optimization as well as electrostatic density calculations were planned and executed by Fabian Müller (Humboldt-Universität zu Berlin). The hydrolytic stability towards PAHs and Pases were assayed by Anett Hauser.

4.3.3 Synthesis of Central Compounds 18 and 19

4.3.3.1 Synthesis of Homocysteine-Derived Phosphonate 18

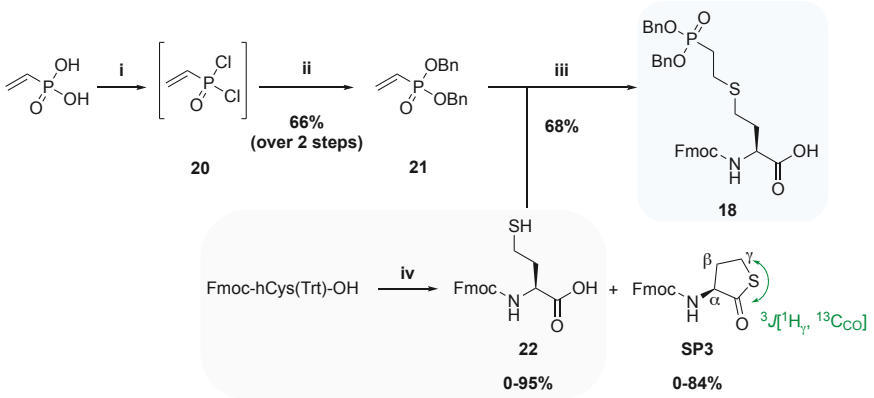

Scheme 4.8: Synthesis route to target compound Fmoc-hCys(EtPO(OBn)$_2$)-OH **18** and side reaction elucidation occurring during Fmoc-hCys(Trt)-OH side chain deprotection. Reagents and conditions: **i**) $(COCl)_2$ (3 eq.), DCM, cat. DMF, 0 °C to r.t., 17.5 h; **ii**) Bn-OH (2.5 eq.), Et_3N (3 eq.), THF, 0 °C to r.t., ovn; **iii**) **22** (0.33 eq.), 50 mM NH_4HCO_3:DMF (2:1, v/v), pH 8.5, 45 °C, 6 h; **iv**) neat TFA:TIS:EDT:DCM (50:2:0.1:47.9, v/v/v/v), 0 °C, 7 min.

Synthetic access to bis-benzyl- and Fmoc-protected building block **18** was intended by a thiol-selective addition reaction examined recently in our group. [118,164,251] Thereby, the central compound **18** was obtained as a thioether of homocysteine (hCys) (scheme 4.8). Starting from vinyl

phosphonic acid, benzyl protection was installed in two steps *via* vinylphosphonic dichloride **20** to give the α,β-unsaturated system of **21** susceptible to thiol addition in 66% yield over two steps.

Commercially available Fmoc-hCys(Trt)-OH was side chain deprotected with TFA in presence of TIS and ethanedithiol (EDT) to give **22**. During the first trityl cleavage attempts, significant amounts of a by-product **SP3** with detected mass-to-charge ratio (m/z) of 362 were obtained after purification, which did not fit to an evident side reaction. By the help of NMR analysis, **SP3** was elucidated as thiolactone[252] with the typical large chemical shift for carbonyl carbons at $\delta_{^{13}C_{CO}}$ = 206 ppm[253] and a distinct $^{1}H_{\gamma}$-$^{13}C_{CO}$-correlation detected in ^{1}H-^{13}C-HMBC experiments, which is only possible in a cyclized structure (scheme 4.8). Considering the prior UPLC-MS analysis, the detected m/z matched the sodium adduct of **SP3** (m/z calc. $[M+Na^+]^+$ = 362.3988).

Table 4.6: Tested reaction conditions to optimize yield of **22**.

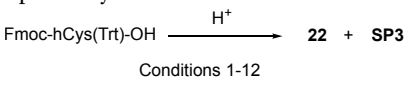

#	Deprotection solution	c	ϑ	Time	Work up	Isolated yield	
						22	**SP3**
		[mM]	[°C]	[min]		[%]	[%]
1	TFA:TIS:EDT:DCM (5:2:1:92)	100	r.t.	30	N_2, 1 d, HPLC	66	29
2	TFA:TIS:EDT:DCM (5:2:1:92)	170	r.t.	30	N_2, 3 d, desalting	26	40
3	TFA:TIS:EDT:DCM (5:2:1:92)	100	r.t.	30	N_2, 6 d, HPLC	4	73
4	TFA:TIS (97.5:2.5)	50	r.t.	30	N_2, lyo., HPLC	35	22
5	TFA:H_2O (97.5:2.5)	50	−10	120*	lyo.	–[a]	–[a]
6	TFA:TIS:ACN (47.5:2.5:50)	50	−10	120*	lyo.	–[a]	–[a]
7	TFA:TIS:ACN (48:2:50)	84	−10	240	lyo., 3 d, HPLC	17	84
8	3 N HCl in MeOH	50	r.t.	2880	lyo., HPLC	0	76
9	TFA:TIS:EDT:DCM (50:2:0.1:47.9)	50	0	15	N_2/0 °C, HPLC	70	18
10	TFA:TIS:EDT:DCM (50:2:0.1:47.9)	40	r.t.	15	N_2/0 °C, HPLC	80	12
11	TFA:TIS:EDT:DCM (50:2:0.1:47.9)	40	0	10	N_2/0 °C, HPLC	87	8
12	TFA:TIS:EDT:DCM (50:2:0.1:47.9)	40	0	7	N_2/0 °C, HPLC	95	0

[a] After lyophilisation, no **22** or **SP3** were detected anymore. * No full conversion was achieved during reaction

In order to minimize **SP3** formation and increase product yield, several reaction conditions were examined (table 4.6). As it turned out, the reaction time had a relative small impact on the outcome compared with the work up protocol. In first approaches, the remaining thiol additive was allowed to evaporate for many hours and up to several days from an flask kept open. Thereby, up to 70% thiolactone **SP3** were isolated after purification (entry **1**-**3**). Removal of solvent by lyophilisation and fast subsequent purification diminished by-product formation, probably due to lower temperatures during the process (entry **4**). A longer waiting period after lyophilization led to an increase of **SP3** yield again (entry **7**). Conditions **5**-**7** showed furthermore, that cooling of the reaction mixture reduced the conversion drastically. Hence, higher substrate concentration and longer reaction times were necessary to drive the deprotection to completion. Switching to a system without TIS or another acid yielded only starting material recovery (entry **5**) or by-product

isolation (entry **8**), respectively. Eventually, ultra short reaction times granted by increased TFA concentration in combination with immediate work up while cooling and purification gave the optimum results (entries **9**-**12**). Following this protocol (50% TFA, 2% TIS and 0.1% EDT in DCM), the isolated yield of **22** could be increased up to 95% (and still 84% after scale up, see experimental part) while no **SP3** was isolated.

Eventually, with enough amounts of side chain deprotected Fmoc-hCys **22** and dibenzyl vinylphosphonate **21** in hand, the thiol addition was performed. Thereby, the reaction conditions were adopted from protocols developed for other α,β-unsaturated P^V systems.[118,164,251] Target compound Fmoc-hCys(EtPO(OBn)$_2$)-OH **18** was obtained under slightly basic conditions at 45 °C within six hours and 68% product were isolated after preparative HPLC.

4.3.3.2 Synthesis of Norleucine-Derived Phosphate 19

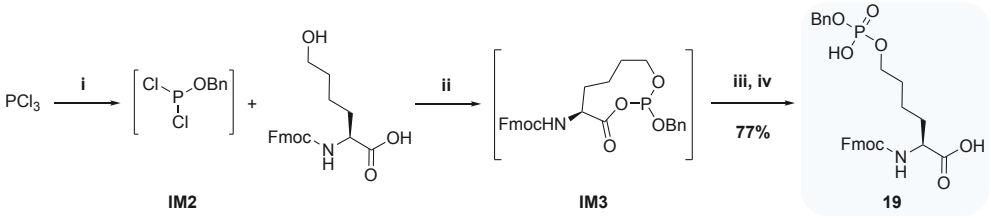

Scheme 4.9: Synthesis route to target compound Fmoc-Nle(OPO(OH)(OBn))-OH **19**. Reagents and conditions: **i**) Bn-OH (1+0.3 eq.), THF, 0 °C, 10 min; **ii**) Fmoc-Nle(6-OH)-OH (0.59 eq.), 2,6-lutidine (2.45 eq.), 0 °C to r.t., 90 min; **iii**) H_2O, 0 °C, 1 min; **iv**) NaBr (1.35 eq.), $NaBrO_3$ (0.3 eq.), 0 °C to r.t., 4 h.

Since common phospho-AAs such as pSer, pThr and pTyr can be incorporated into peptides as mono-benzyl- and Fmoc-protected building blocks, central compound **19** was planned. A published one-pot protocol for pSer derivatives by Petrillo *et al.* was taken as an example for the modification of 6-hydroxynorleucine (scheme 4.9).[254] Starting from phosphorous trichloride, the first chloride atom was exchanged with Bn-OH to **IM2**. Subsequently, commercially available Fmoc-Nle(6-OH)-OH was added under basic conditions to coordinate to proposed intermediate **IM3**.[254] By addition of water and sodium bromide/sodium bromate as oxidant, the mixed phosphite was hydrolyzed to the desired product **19**. This convenient synthesis route gave access to the protected phospho-AA within one day in decent yield of 77%.

4.3.4 Peptide Synthesis and Further Evaluation

With both central compounds in hand, their suitability for standard SPPS as well as their pLys mimicking properties were investigated. The latter included evaluation of structural and electronic similarities as well as their stability towards hydrolyzing enzymes as outlined below.

4.3.4.1 Peptide Synthesis

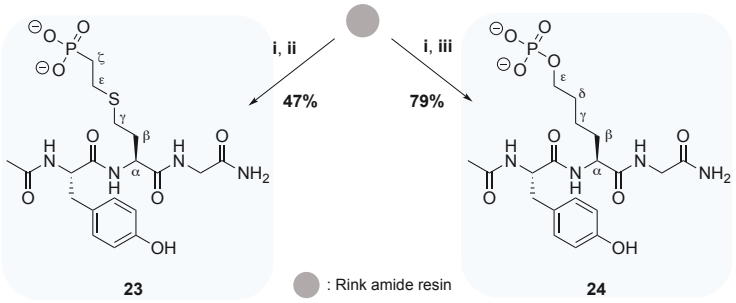

Scheme 4.10: Synthesis route to peptides ^{Ac}Tyr-hCys(EtPO(OH)$_2$)-Gly^{CONH_2} **23** and ^{Ac}Tyr-Nle(OPO(OH)$_2$)-Gly^{CONH_2} **24** with nomenclature of side chain positions α to ζ. Reagents and conditions: **i**) Fmoc-SPPS; **ii**) a) TFA:TIS:H_2O (95:2.5:2.5, v/v/v), r.t., 105 min, b) EDT:TMSBr (17:83, v/v), r.t., 15 min; **iii**) TFA:TIS:H_2O (95:2.5:2.5, v/v/v), r.t., 2 h.

Target peptides **23** and **24** were chosen with closest sequence similarity to the already investigated pLys peptide **5**. Pleasingly, both peptides could be obtained in moderate to good yields without elaborate protocol adjustments (scheme 4.10). The tailored monomers **18** and **19** were coupled with HATU as activating reagent in presence of DIPEA. After two hours reaction time, negative TNBS tests indicated full conversion and the remaining peptide synthesis was accomplished under standard conditions. To avoid thioether oxidation during cleavage and deprotection, an altered procedure was conducted for ^{Ac}Tyr-hCys(EtPO(OH)$_2$)-Gly^{CONH_2}.[255] Beside the standard cleavage solution, ETD and trimethylsilylbromide (TMSBr) were added to the mixture at the end of the reaction time. During following UPLC-MS analysis of the crude peptide, no oxidation to the sulfoxide was detected.

The successful synthesis of ^{Ac}Tyr-hCys(EtPO(OH)$_2$)-Gly^{CONH_2} **23** and ^{Ac}Tyr-Nle(OPO(OH)$_2$)-Gly^{CONH_2} **24** in 47% and 79% yield, respectively, documented the acid stability of unprotected phosphonate and phosphate, since those were obtained directly after cleavage from the solid support under harsh acidic conditions. Thus, the first comparison to pLys could be drawn. While free phosphoramidates in pLys peptides exhibited a half-life of $t_{1/2} \approx 1.75$ hours in 0.1% TFA,[97] the analogues were stable for more than two hours in almost neat TFA and even longer during purification in a 0.1% TFA containing solvent system.

4.3.4.2 Structural and Electronical Comparison with Phospho-Lysine

As mentioned above, the structural and electronical similarities are properties to evaluate the mimic suitability of the designed analogues. Thus, the charge state at physiological conditions was determined. Samples were prepared as described in section 4.2.4.1 (1 mM peptide in 40 mM KCl in H_2O + 10% D_2O) and measured at 278 K in a 600 MHz (^{1}H frequency) spectrometer at pH values from 2 to 11. The detected ^{31}P as well as ^{1}H chemical shifts ($\delta_{^1H_\zeta}$ for **23**, $\delta_{^1H_\epsilon}$ for **24**; table 4.7 & figure 4.8**A**) were used for calculations of pK_a values.

Table 4.7: Measured ^{31}P and ^{1}H chemical shifts for **23** and **24** at different pH values.

#	^{Ac}Tyr-hCys(EtPO(OH)$_2$)-Gly^{CONH_2} **23**			#	^{Ac}Tyr-Nle(OPO(OH)$_2$)-Gly^{CONH_2} **24**		
	pH	$\delta_{^{31}P}$ [ppm]	$\delta_{^{1}H_\zeta}$ [ppm]		pH	$\delta_{^{31}P}$ [ppm]	$\delta_{^{1}H_\epsilon}$ [ppm]
1	2.20	23.781	1.544	**11**	2.01	0.152	3.541
2	3.00	22.310	1.543	**12**	3.00	0.232	3.525
3	3.91	21.940	1.525	**13**	4.05	0.276	3.524
4	4.90	21.920	1.528	**14**	4.97	0.561	3.518
5	6.12	21.493	1.494	**15**	6.01	1.143	3.489
6	7.00	20.342	1.436	**16**	7.00	2.379	3.430
7	7.94	19.030	1.367	**17**	8.12	3.170	3.405
8	9.03	18.491	1.332	**18**	9.03	3.302	3.404
9	9.92	18.453	1.335	**19**	10.06	3.330	3.405
10	11.00	18.450	1.335	**20**	10.96	3.378	3.404

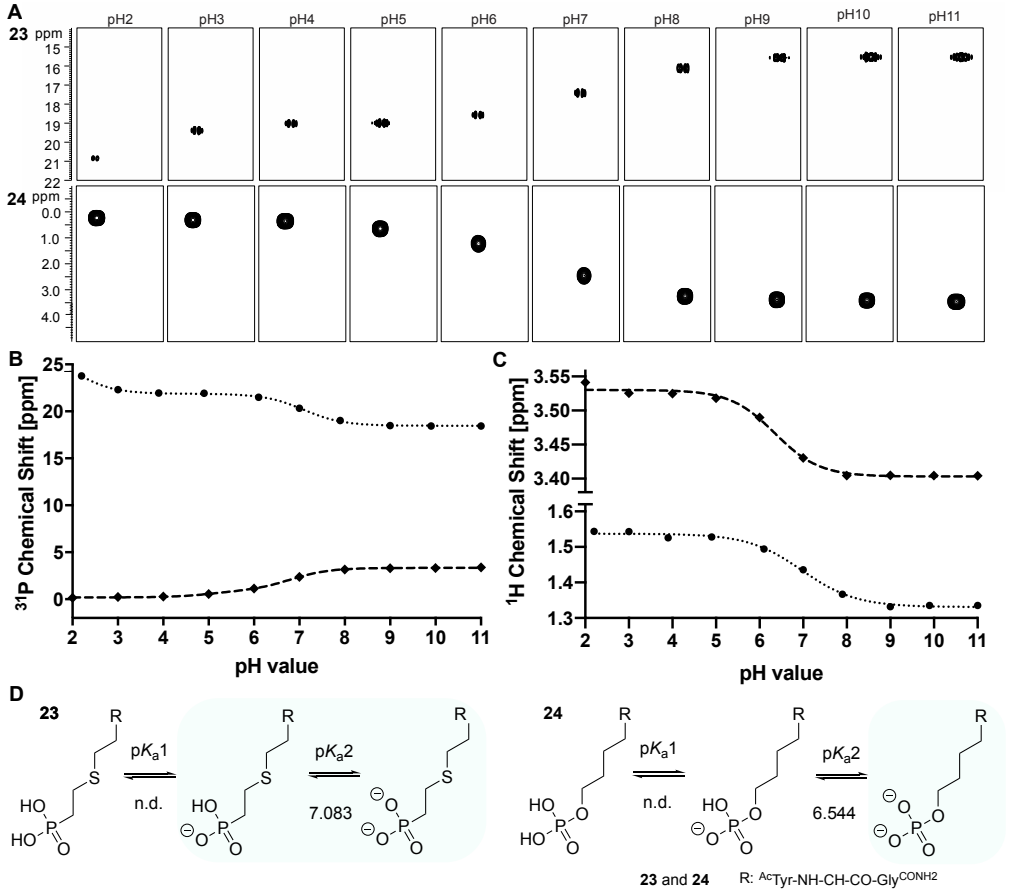

Figure 4.8: **A**. Signals extracted from the ^{1}H-^{31}P-HMBC experiment for peptides **23** (top) and **24** (bottom). **B** & **C**. Graphical visualizations of NMR measurements of ^{31}P chemical shifts (**B**) and ^{1}H chemical shifts (**C**); *dotted* ● peptide **23**, ζ-protons; *dashed* ◆ peptide **24**, ϵ-protons. **D**. Dissociation equilibrium of hCys-derived phosphonate **23** and Nle-derived phosphate **24** in a peptide with calculated pK_a values.

The results indicated that for both analogues the first pK_a values could not be determined, since they were below pH 2 (figure 4.8**B** & **C**). For thioether phosphonate **23**, the pK_a2 value, which describes the equilibrium between mono-protonated phosphoryl oxygen and di-anionic compound, was 7.083 ± 0.031 ($R^2$2 = 0.9999).Thus, both species should be present in a rather balanced ratio under physiological conditions (figure 4.8**D**, left). In case of phosphate peptide **24**, the second pK_a value was 6.544 ± 0.125 (R^2 = 0.9991), thereby demonstrating a charge state of −2 under physiological conditions (figure 4.8**D**, right).

Again, as described in section 4.2.4.1, the magnitude of chemical shift change at the pK_a values (Δppm) fit the observations of Gamcsik *et al.* for a change in oxygen protonation [240] as they reported a Δppm for phosphorous of 3.2 ppm. In the present study, the Δppm for **23** and **24** representing protonation of oxygen are below 3.5 ppm each. Interestingly, increasing pH values resulted in an upfield move of ^{31}P chemical shift for phosphonate **23** but a downfield move for phosphoramidate **5** (figure 4.3**B**) and phosphate **24**. This behavior has been described already for adenosine nucleotide analogues in the early 1980s, in which phosphonate derivatives of triphosphates exhibited the same pattern as observed now. [256–258]

In summary, the net charges at pH 7, were −1, −1 ⇌ −2, and −2 for **5**, **23** and **24**, respectively (figure 4.9**A**).

To visualize the charge distribution at physiological conditions, ESP maps were calculated from optimized structures as shown in figure 4.9**B**. Even though the maps indicated a strong geometrical similarity of all substrates, the charge distribution showed clear differences. While the electron density was well spread over the whole molecule with only a slight concentration at the phosphoryl oxygens in pLys peptide **5** as well as the mono-anion of **23**, the −2 charged species of **23** and **24** exhibited distinct diversity across the structures. Strikingly, even though in all substrates the phosphoryl oxygens are deprotonated, the di-anion of **24** was far more electronegative than **5**. Also, **5** and the mono-protonated species of **23** presented over all less negativity than **24**. This indicated, that a second negative charge had a strong impact on the electron density of the whole molecule, not only the charge localization site; an effect, which was partially balanced by the protonated nitrogen in pLys peptide **5**. This properties indicated the hCys derived phosphonate as the more potent mimic for pLys.

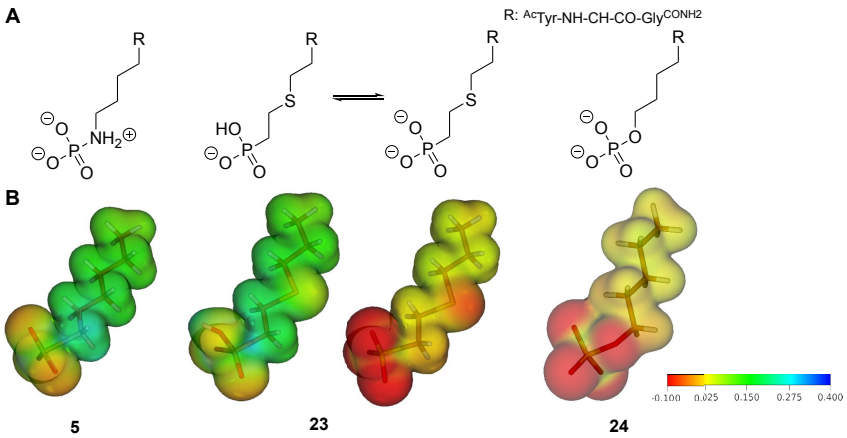

Figure 4.9: **A**. Protonation in **5**, **23** and **24** under physiological conditions. **B**. Calculated ESP maps from optimized structures visualizing the electron densities.

4.3.4.3 Stability Against Phosphoramidate Hydrolases and Phosphatases

The exchange of nitrogen with carbon or oxygen resulted in increased acid stability of **23** and **24** as seen during the peptide synthesis. The obtained altered chemical behavior was examined further with regard to resistance against PAHs and Pases as well. From the literature, LHPP is known to hydrolyze pLys in monomeric AA or poly-pLys peptides (see sections 2.2.4.2 & 4.4).[203,204,213,249,250] It was also shown, that pTyr is not a substrate for LHPP. Thus, clearly decreased enzymatic activity was expected for the novel mimics. This study was the first to investigate LHPP on a site-specific pLys peptide. To gain certainty about, first, the non-hydrolyzable moiety in **23** and, second, the accessible phosphate in **24**, the peptides were treated with the promiscuous Pase ALP as well.

Substrates were tested under optimized conditions for LHPP and ALP and the amount of released inorganic phosphate (P_i) was determined by photometric read-out (see section 4.4 for more details). Briefly, in 50 µL reaction mixtures, peptides **5**, **23** and **24** were dissolved to 1 mM concentration in 50 mM Tris, 1 mM $MgCl_2$, pH 7.8 (LHPP) or in 50 mM Tris, 1 mM $MgCl_2$, 1 mM $ZnCl_2$, pH 8.2 (ALP) and incubated with 0.5 µg LHPP ($3{\cdot}10^{-4}$ eq.) or 0.05 enzyme units (U, with regard to 4-nitrophenyl phosphate) ALP at 30 °C for two hours. After 120 min, an aliquot of the reaction mixture was diluted further to 50 µM concentration into an EDTA-containing sample buffer for UV-detection of P_i amount.

Figure 4.10 shows the amount of enzymatically hydrolyzed substrate, which was calculated by subtraction of detected P_i in reactions without enzyme from the reactions with enzyme being added. Both, LHPP and ALP hydrolyzed the phosphoramidate of **5**, thereby demonstrating the performance of both enzymes. As expected, no P_i was released from phosphonate **23** during incubation with LHPP or ALP, by what the non-hydrolyzability could be proven. Pleasingly, LHPP showed no enzymatic activity towards phosphate **24** either. These results hinted to a specificity of LHPP for P–N over P–O bonds. Treatment of **24** with ALP yielded indeed in a P_i release. Thus, the phosphate was susceptible to Pases.

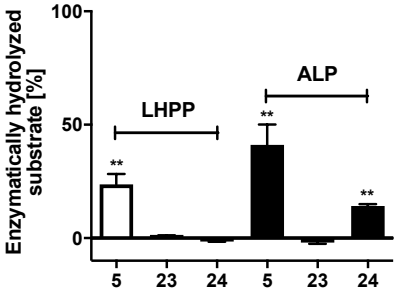

Figure 4.10: Observed hydrolysis of peptides **5**, **23** and **24** after 120 min incubation with LHPP or ALP. ** Background hydrolysis without enzyme being present was subtracted.

4.3.5 Conclusion and Outlook

In this approach, stable mimics for pLys were tested, one containing a phosphonate and the other a phosphate. Two ready-to-install benzyl- and Fmoc-protected building blocks for SPPS – **18** and **19** – could be synthesized from commercially available starting materials in straightforward synthesis routes. In further experiments, the suitability of both central compounds for peptide

synthesis could be demonstrated. Furthermore, their stability during acidic global deprotection and cleavage from the solid support could point out the improved stability profiles of free phosphonates and phosphates compared to pLys.

With P–N, P–C and P–O peptides in hand, comparative investigations were conducted. NMR titration was utilized to determine each net charge under physiological conditions and indeed, peptide **23** was present in an equilibrium between charges -1 and -2 close to pLys peptide **5**, which exhibited a charge of -1. As expected, both phosphoryl oxygens of phosphate **24** were deprotonated at pH 7, therefore having a net charge of -2. These results were visualized in ESP maps, which confirmed the indicated properties. The electron density in the mono-anion of **23** was far more similar to **5** than the di-anions of **23** and **24**. This implied better mimicry of the designed phosphonate than the Nle-derived phosphate.

Additionally, their reactivities in PAH and Pase treatment were assayed. Satisfactorily, the as pLys and pHis selective reported PAH LHPP showed enzymatic activity only towards phosphoramidate peptide **5**. In contrast to that, incubation with ALP led to P_i release from **5** and **24**, thereby proving the stability of **23** and accessibility of **24**.

The different pLys mimics could be further applied for distinct purposes matching their characteristics and the question of each investigation. Other enzymes could be studied in a comparative manner as done with LHPP and ALP. Moreover, protein binding partners could be identified by application of one or the other pLys analogue. Apart from this, proteomic studies of endogenous Lys phosphorylation were to be promoted as the phosphonate and phosphate were to be employed in antibody generation for pLys detection and enrichment experiments, which are described in more detail in section 4.5.

4.4 Investigation of Phosphoramidate Hydrolase Activity of LHPP

4.4.1 Outline of the Project

Reversible phosphorylation is usually regulated by a synergy of kinases and phosphatases (Pases), which are responsible for efficient installation and subsequent release of phosphate groups as required by cellular processes. While no distinct kinase is known to catalyze phosphoramidate formation on Lys residues in proteins, LHPP is the single phosphatase, more precisely phosphoramidate hydrolase (PAH), reported for its reactivity towards pLys and pHis substrates. Thereby, the hydrolysis yield for pLys was higher than for pHis (1.22 *versus* 1.09 $\mu mol \cdot min^{-1} \cdot mg^{-1}$). [203–205] Since it has never been applied in comprehensive studies with selectively phosphorylated Lys peptides, the goal of this project was to gain insight into the mode of operation of LHPP with synthetic model substrates. This issue was addressed in several stages. Considering that no enzyme activity towards reference substrates is known, the assay conditions had to be determined at the very beginning. Then, prominent phospho-AA monomers should be investigated and by this, the selectivity of LHPP for phosphoramidates demonstrated. Afterwards, the substrate scope was elucidated regarding the molecule size and phosphorylation site position. Particularly of interest was the enzyme activity in dependence of the AA adjoining pLys. Differences in P_i release were further reviewed by means of computational chemistry studies. In this approach, interactions between LHPP and its substrates should be visualized and quantitatively evaluated by Gibbs free energy (ΔG) calculations.

4.4.2 Responsibility Assignment

The concept of PAH/Pase activity examination was planned by Christian Hackenberger, Jordi Bertran-Vicente and Anett Hauser. Substrates were designed, synthesized and characterized by Anett Hauser. The PAH/Pase activity assay was, first, optimized and implemented and, second, conducted by Anett Hauser with scientific advise from Maja Köhn (University of Freiburg) and executive support by Alina Nastke (Humboldt-Universität zu Berlin, now Universität Bielefeld) and Jeannine Engelke (University of Konstanz). Data processing was done by Anett Hauser. All computational experiments were planned, supervised and conducted by Han Sun and Songhwan Hwang (both FMP Berlin).

4.4.3 Substrate Choice and Synthesis

In order to investigate LHPP selectivity for *N*- and *O*-phosphorylation, common monomeric phospho-AAs were intended, since initial studies by the Kumon group have been conducted only with phosphoramidate and phosphate monomers (figure 4.11**A**). [203–205]

Apart from this, the main focus of the present approach was devoted to site-specifically phosphorylated, peptidic compounds, which were never assayed with LHPP before. Encouraged by reports about pLys occurrence in histone H1, [90–93] a sequence section was chosen, which contains pSer and pThr in close proximity to Lys residues. These phosphates could have been assigned

incorrectly based on standard proteomic analysis that is disfavored by pLys, a circumstance explained in more detail in section 4.6. Hence, two peptides with pLys adjacent to the endogenous phosphorylation sites were prepared (figure 4.11**B**).

Additionally, to gain more insight in the actual mode of action of LHPP, smaller peptides were designed to systematically study the selectivity (figure 4.11**C**) and sequence dependence (figure 4.11**D**) of the enzyme activity.

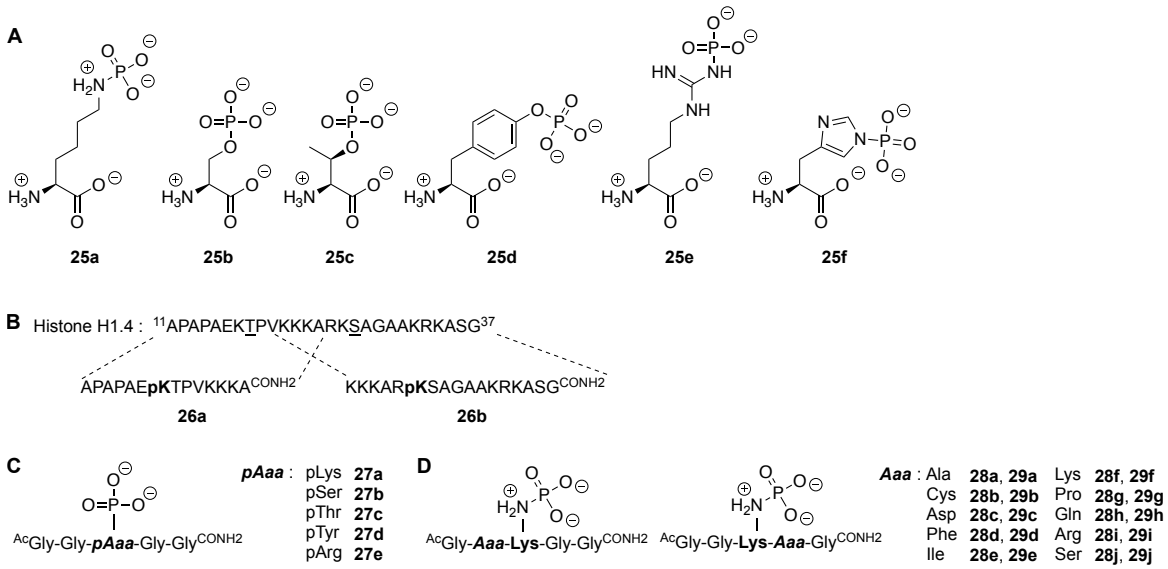

Figure 4.11: Proposed substrates for the PAH/Pase activity assay. Phosphorylation sites in H1.4 are underlined.

Substrates were accessed by established synthesis protocols. All pLys containing substrates (**25a**, **26a**-**b**, **27a**, **28a**-**j** and **29a**-**j**, scheme 4.11**A**) were obtained following the Staudinger-phosphite route explained in section 4.1.4.2. [97] It was nicely shown that also monomeric pLys **25a** can be accessed *via* this protocol starting from commercially available N^6-diazo-*L*-lysine hydrochloride. Phosphoramidate **30** was obtained in 79% yield with less equivalents NPE-caged phosphite **9** than previously described. The synthesis of azido-peptides **31a**-**w**, subsequent conversion to caged pLys peptides **32a**-**w** and final photolytic deprotection were conducted as described in section 4.1.4.2.

The phosphate monomers **25b**-**d** were obtained by global deprotection of the commercially available, benzyl- and Fmoc-protected SPPS building blocks after preparative HPLC (scheme 4.11**B**). Besides that, pSer, pThr and pTyr pentapeptides (**27b**-**d**) were readily prepared during peptide synthesis by installation of the aforementioned building blocks in moderate to good yields (64-85%).

For the synthesis of pArg substrates **25e** and **27e** (scheme 4.11**C**), the Fmoc-protected and Tc-caged pArg **34** was prepared according to the protocol of Hofmann *et al.* as mentioned in section 4.1. [112] Briefly, starting from Cbz-protected Arg, the carboxyl group was benzyl-protected before the phosphoramidate was installed by nucleophilic substitution with bis(2,2,2-trichloroethyl) phosphorochloridate to give product **33** in 83% yield over two steps. [112] Hydrogenation under acidic conditions and subsequent Fmoc-protection yielded 84% of the desired building block **34**. This was either converted to free pArg monomer **25e** by hydrogenation under basic conditions or incorporated into a peptide and deprotected afterwards to give substrate **27e**.

His phosphorylation was accomplished by nucleophilic substitution with potassium phosphoramidate **35** (K-PA), which was prepared as described by Wei and Matthews (scheme 4.11**D**).[138] Therefore, phosphoryl chloride was first, treated with concentrated ammonium hydroxide and second, hydrolyzed with a concentrated potassium hydroxide solution to obtain K-PA **35** in 23% yield. *L*-histidine was incubated with **35** for several days to ensure predominant formation of τ-pHis **25f**[138] and purified by strong anion exchange chromatography at 4 °C. NMR analysis proved the formation of the desired isomer. Initially, also a peptidic pHis substrate was envisioned. However, the only known phosphorylation method for His is the protocol by Wei and Matthews, which was not suitable in our case, since the separation of peptide and K-PA is not possible on small scale reactions.

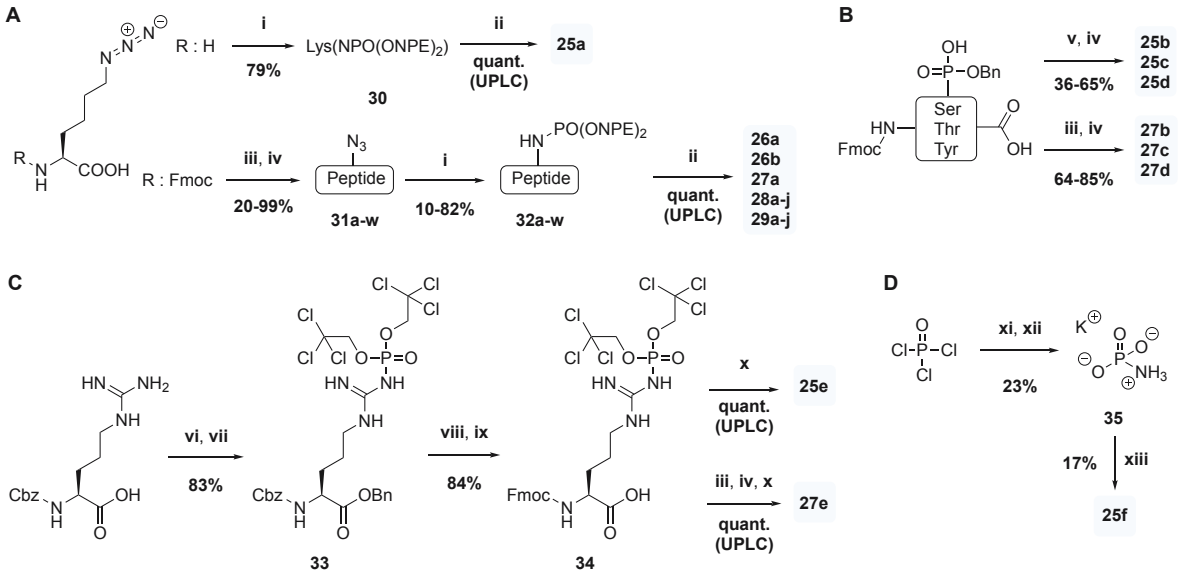

Scheme 4.11: Synthesis routes to phosphorylated compounds applied in the LHPP activity assay. **A**. pLys substrates; **B**. phosphates; **C**. pArg substrates; **D**. pHis. Reagents and conditions: **i**) **9** (3x 1.5 eq.), DMF, 45 °C, 48 h; **ii**) *hv* (297 nm), MeOH, r.t., 45-60 min; **iii**) Fmoc-SPPS; **iv**) TFA:TIS:H_2O (95:2.5:2.5, v/v/v), r.t., 2 h; **v**) neat Pip:DMF (20:80, v/v), r.t., 10 min; **vi**) Bn-Br (1.1 eq.), NMP, Ar, dark, r.t., 17 h; **vii**) bis(2,2,2-trichloroethyl) phosphorochloridate (1.2 eq.), Et_3N (4 eq.), ACN, r.t., 16 h; **viii**) H_2, 10% Pd@C, AcOH:TFA (1:1, v/v), r.t., 60 min; **ix**) Fmoc-OSu (1 eq.), Et_3N (1 eq.), H_2O:ACN (1:1, v/v), pH >9, r.t., 40 min; **x**) H_2, 10% Pd@C, 25 mM $(NH_4)_2CO_3$, pH 9.2:EtOH (80:20, v/v), 0 °C, 60 min; **xi**) NH_4OH (10% in H_2O, 8 eq.), 0 °C, 20 min; **xii**) KOH (50% in H_2O, neat), 55 °C, 15 min; **xiii**) *L*-histidine (0.6 eq.), H_2O, r.t., 5 d.

4.4.4 Phosphoramidate Hydrolase and Phosphatase Activity Assay

4.4.4.1 Assay Optimization

To approach the investigation of LHPP's hydrolase activity as PAH and Pase, some considerations needed to be made. Phosphoramidates and especially pLys are prone to hydrolysis already at room temperature without any enzyme being present. Thus, fast sample preparation, distinct pH adjustment and substrate storage while cooling were crucial. Besides that, kinetic parameters derived from real-time measurements were intended in the present work. According to the reported studies about LHPP–pLys interactions, released P_i was quantified either with Rosenberg's reagent[204] or Malachite green,[203,205] two rather time consuming methods with long delay be-

tween probing and actual read-out. Hence, no real time determination of P_i concentration was possible then. Today, state of the art assaying of Pase activity can be conducted conveniently with enzymatic assay kits in cuvette- or microplate-based experiments, which are suitable for the desired high throughput set up in the present study. The EnzChek® phosphate assay kit enables continuous measurement of released P_i, which induces the formation of 2-amino-6-mercapto-7-methylpurine that is subsequently detected.[259] In order to optimize the previous protocol described by Hiraishi *et al.* and transfer it to a microplate reader, uniformed parameters were required including buffer, reaction time as well as applied substrate and enzyme concentrations.

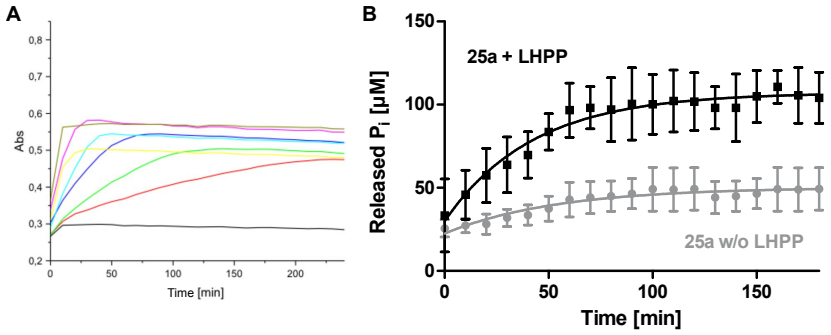

Figure 4.12: Example of reaction from assay optimization. **A**. Absorbance measurements over time of incubation of 100 µM **25a** with varying amounts of LHPP. — no enzyme, — 0.03125 µg, — 0.0625 µg, — 0.125 µg, — 0.25 µg, — 0.5 µg, — 0.75 µg, — 1 µg LHPP added. **B**. Kinetics for 100 µM **25a**. — with 0.25 µg LHPP, — without addition of LHPP.

In order to identify suitable assay conditions, the LHPP activity was assayed with previously reported substrate pLys **25a**.[204] Based on previous reports, the pH-dependencies of pLys stability[97] and LHPP activity[204] were compromised at slightly basic conditions. In an optimization screen with varying concentrations of substrate and enzyme (figure 4.12**A** & Experimental Part, section 6.5), the combination of 100 µM substrate with 0.25 µg LHPP ($7.4{\cdot}10^{-3}$ nmol, $3.7{\cdot}10^{-4}$ eq.) was determined as suitable for satisfying enzyme kinetics within 90 minutes incubation time. To sum up, the assay conditions were chosen as followed: substrates were incubated at a concentration of 100 µM in 50 mM Tris-HCl buffer containing 1 mM $MgCl_2$ at pH 7.8 in the presence or absence of 0.25 µg LHPP ($3.7{\cdot}10^{-4}$ eq.) for the overall phosphate release (enzymatic plus background reaction) or non-enzymatic hydrolysis, respectively. Absorbance was measured every ten minutes for 90 min at 360 nm. Details about the experimental set up and data processing can be found in section 6.5.

Notably, reactions without enzyme being present (background hydrolysis, black graph in figure 4.12**A**) showed significant absorbance already at the starting point of each experiment. This phenomenon was partially derived from the synthesis route, which did not yield pure pLys substrates but rather always a mixture with P–N bond hydrolysis products (Lys + P_i). Additionally, the intrinsic lability of pLys led to P_i release over time even without enzyme being present (figure 4.12**B**). This background reaction had a distinct impact on the calculation of the percentage of enzymatically hydrolyzed substrate, which was obtained as difference between the measured value from incubation with LHPP (black graph in figure 4.12**B**) and the value without enzyme being present (gray graph in figure 4.12**B**). For the given example, approximately 50 µM **25a** were degraded by LHPP, according to 50% enzymatically hydrolyzed substrate, after 60 minutes when the conversion was complete.

Under the mentioned standardized conditions, kinetic parameters, e.g. initial rates (v_0) and first order rate constants (k), were determined as well. As shown in table 4.8 for the sample experiment of 100 µM pLys **25a** with 0.25 µg LHPP, the hydrolysis occurred one magnitude faster with LHPP than without enzyme being present. Thus, despite the fact that P–N bond hydrolysis took place due to intrinsic lability, LHPP accelerated the reaction rate by a factor of ten.

Table 4.8: Initial rates and first order rate constants of the kinetic studies for 100 µM **25a** with 0.25 µg LHPP or without enzyme addition.

Substrate	Without LHPP			
	v_0 [M·s^{-1}]	Error ±	k [s^{-1}]	Error ±
25a	$2.10 \cdot 10^{-9}$	$3.65 \cdot 10^{-10}$	$3.47 \cdot 10^{-5}$	$4.13 \cdot 10^{-6}$
	With LHPP			
	v_0 [M·s^{-1}]	Error ±	k [s^{-1}]	Error ±
25a	$2.00 \cdot 10^{-8}$	$4.43 \cdot 10^{-10}$	$2.25 \cdot 10^{-4}$	$1.86 \cdot 10^{-5}$

4.4.4.2 Selectivity of LHPP

Initial experiments were dedicated to the activity discrimination of LHPP as PAH or Pase. Phospho-AA monomers **25a**-**f** were examined for this purpose (figure 4.13**A**). In accordance with the results published by Hiraishi *et al.*,[204] phosphorylated lysine monomer **25a** was hydrolyzed at a rate of 0.88 µmol·min^{-1}·mg^{-1}, corresponding to 56.26% enzymatically hydrolyzed substrate after 90 min reaction (background hydrolysis subtracted). For the other *N*-phospho-AAs (pArg **25e**, pHis **25f**) and for the phosphates (pSer **25b**, pThr **25c**, pTyr **25d**) drastically lower values for the hydrolyzed substrates were observed (17.57%, 6.64%, 5.75%, 3.67%, 4.81%, respectively, figure 4.13**A**). These results indicated a clear preference of LHPP for pLys over other phospho-AAs.

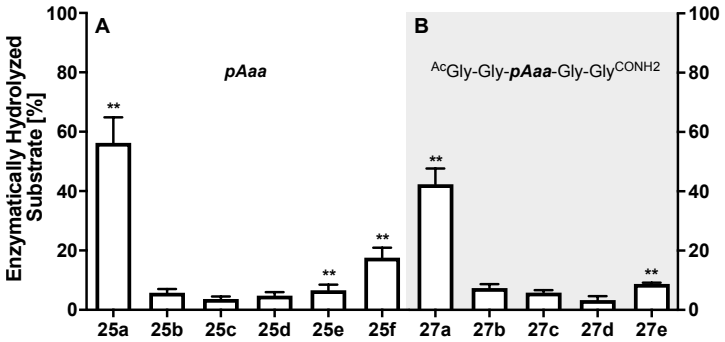

Figure 4.13: **A** & **B**. Percentage of enzymatically hydrolyzed substrates after 90 min of incubation of monomeric phospho-AA **25a**-**f** (**A**) or differently phosphorylated pentapeptides **27a**-**e** (**B**) with LHPP. Experiments have been conducted as biological and technical triplicates. ** Hydrolysis rates without enzyme being present have been subtracted.

Encouraged by these findings, more elaborated substrates were investigated next. Surprisingly, the histone H1.4 derived peptides **26a** and **26b** seemed to not allow any enzymatic activity of LHPP as no increased inorganic phosphate release was detected upon enzyme addition, even with higher amounts. As such, a P_i concentration of approximately 38 µM was detected in each of the experiments with 0, 0.25, 0.5, 1.0 or 2 µg LHPP after 90 min. This means, no enzymatically hydrolyzed substrate was detected.

The contradictory results obtained from monomers and peptides made the mode of action of LHPP a subject of investigation. In order to understand the enzyme–substrate interaction better, smaller peptides were examined. The simple, unpretentious pentapeptides **27a**-**f** confirmed the initial enzyme activity as the pattern obtained with **25a**-**f** could be reproduced here (figure 4.13**B**). As such, high yield of enzymatically hydrolyzed substrate was detected for pLys peptide **27a** (37.90%) and a fairly lower activity for all other substrates (**27b**: 7.37%, **27c**: 5.86%, **27d**: 3.34%, **27e**: 8.78%). These values were further indications for LHPP being a selective phosphoramidate but not a phosphate ester hydrolase. In addition to that, the reasonably decreased hydrolysis yield obtained for **27a** compared to **25a** hinted again towards a length dependence of LHPP's substrate scope.

4.4.4.3 Influence of Adjacent Amino Acids

Both, the results from experiments with histone H1 derived pLys peptides and with the pLys pentapeptide, implied a certain sensitivity of LHPP to substrate size and sequence. While with 14-mer **26a** and 17-mer **26b** no enzymatic activity was observed, the smaller substrate **27a** exhibited a reduced P_i release compared to monomeric pLys **25a**. This could mean that the H1 peptides were too large for the active center of LHPP or their AA sequence did not allow effective interaction with the enzyme. Thus, the influence of AA situated in proximity to the phosphorylation site was investigated. Peptides **28** and **29** presented common structural and electronic environments while keeping the chain length at five links (figure 4.11**D**), e.g. steric hindrance as in Phe **28**/**29d** and Ile **28**/**29e**, nucleophilic character as in Cys **28**/**29b** and Ser **28**/**29j**, positive or negative charge as in Lys **28**/**29f**, Arg **28**/**29i** or Asp **28**/**29c**. The stereochemistry taken into account, AA modifications were introduced *N*- (**28**) or *C*-terminal (**29**) to the phosphorylation site. By doing so, modified substrates exhibited the same AA sequence when rotated, e.g. $N^{\text{mod}}\rightarrow C = C^{\text{mod}}\rightarrow N$, but the side chains pointed in opposite directions.

As shown in figure 4.14**A**, a distinct impact on the PAH activity of LHPP by modifications adjacent to the phosphorylation site was observed. Most of the mutations led to a decrease in P_i release regardless of the sequence positioning. Only very few examples – *N*-terminal Ala **28a**, Arg **28i** and *C*-terminal Lys **29f** – retained or increased the amount of enzymatically hydrolyzed substrate (37.33%, 40.70%, 29.81%, respectively; compared to 37.90% for **27a**). Strikingly, these values were only obtained either for the *N*- or the *C*-terminal incorporation, not in both positions. The complementary peptides **29a**, **29j** and **28f** led to diminished hydrolysis yields. Even though the substrates seemed mirrored from the sequence, their stereochemistry had a noticeable influence on LHPP activity.

Another interesting observation was the reduced PAH activity with negatively charged Asp modifications (**28**/**29c**). Especially in comparison to the stimulating influence of Lys and Arg muta-

tions, this outcome indicated an electrostatic repulsion of the Asp peptides in the binding pocket, which presents a high negative electron density itself (see section 4.4.5). Taken together, the above considerations hinted again at the sensitivity of LHPP activity towards sequence alterations. The enzyme seemed to accept only a limited scope of pLys substrates. Similar findings have been reported recently for LHPP activity on histidine phosphorylations by Choi *et al.* [202]

Focusing on the kinetics of each substrate, the AA sequence did also have a distinct impact on the lability of the phosphoramidate regardless of enzyme presence. Exemplified in figure 4.14**B** for unmutated **27a**, Ala-modified **28a**, Arg-modified **28i** and Ser-modified **28j**, varying AAs adjacent to the phosphorylation site led to different degrees of background hydrolysis (gray graphs in figure 4.14**B**). As up to 40 µM P_i was detected without LHPP addition, a clearly decreased amount of enzymatically hydrolyzed substrate – meaning the difference between reaction with LHPP and reaction without LHPP – was achieved in the end.

Particularly noticeable in figure 4.14**B** is the low intrinsic lability of Ser-modified peptide **28j** compared to the other shown substrates, but especially to the Ala-modified peptide **28a**. Probably, the hydroxyl oxygen of the Ser side chain coordinated to the ζ-protons of pLys. Thereby, the positive charge on the nitrogen was partially reduced and the P–N bond stabilized.

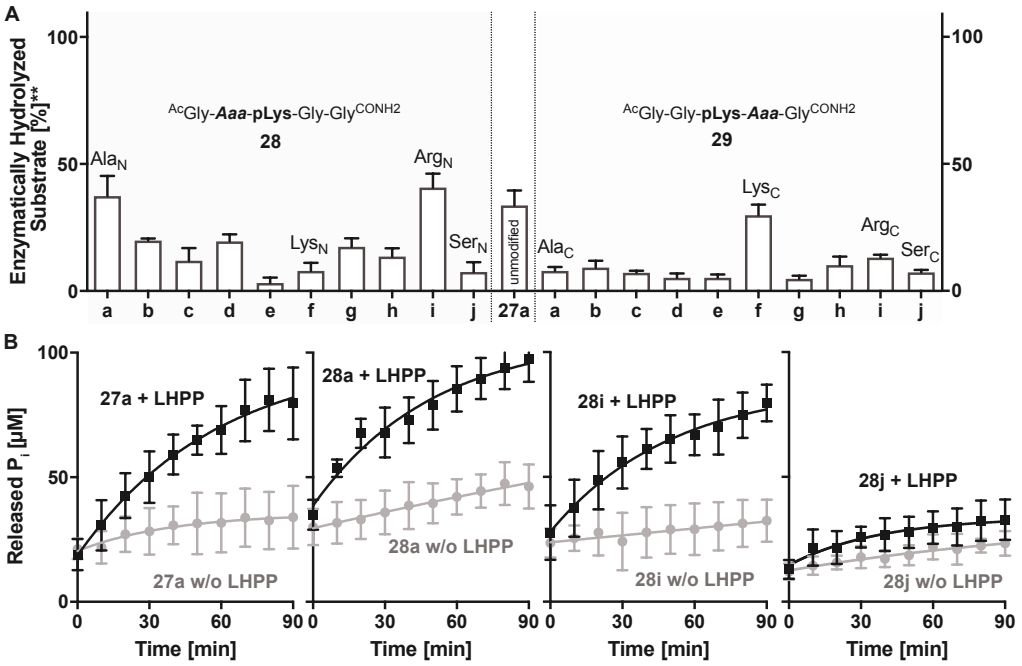

Figure 4.14: **A**. Percentage of enzymatically hydrolyzed substrate after 90 min of incubation of pentapeptides **28a**-**j** and **29a**-**j** with LHPP, in comparison to unmodified **27a**. **B**. Kinetics for **27a**, **28a**, **28i** and **28j**. The rate of background hydrolysis was strongly impaired by the peptide sequence. — with LHPP, — without addition of LHPP. Experiments have been conducted as biological and technical triplicates. ** Hydrolysis rates without enzyme being present have been subtracted in **A**.

Such specific substrate lability was also identified from the kinetic parameters. As shown in table 4.9, the experiment without LHPP gave hints about the background reaction taking place. The initial rate v_0 of unmodified pLys peptide **27a** was considerably higher than of the other examples. Together with the first order rate constant *k*, assumptions on the phosphoramidate lability could be made. As *k* values of **27a** and **28a** were up to 1.6-fold higher than of **28i** and **28j**, less amounts of intact pLys peptide were left to interact with the enzyme. Taking also v_0 and *k* from incubation

with LHPP into account (table 4.9, lower part), this meant that the net amounts of P_i for **27a** and **28a**, which described the enzymatically hydrolyzed substrate, were not clearly higher than for **28i**, even though the reactions were faster and produced more inorganic phosphate in total as already seen in figure 4.14**B**.

Table 4.9: Initial rates and first order rate constants of the kinetic studies for four sample substrates **27a**, **28a**, **28i** and **28j**.

Substrate	Without LHPP			
	v_0 [M·s^{-1}]	Error ±	k [s^{-1}]	Error ±
27a	$4.95 \cdot 10^{-9}$	$2.16 \cdot 10^{-9}$	$3.59 \cdot 10^{-5}$	$4.35 \cdot 10^{-6}$
28a	$2.48 \cdot 10^{-9}$	$1.53 \cdot 10^{-10}$	$5.60 \cdot 10^{-5}$	$2.95 \cdot 10^{-6}$
28i	$3.47 \cdot 10^{-9}$	$1.67 \cdot 10^{-10}$	$2.20 \cdot 10^{-5}$	$2.81 \cdot 10^{-6}$
28j	$3.09 \cdot 10^{-9}$	$2.58 \cdot 10^{-10}$	$2.47 \cdot 10^{-5}$	$2.00 \cdot 10^{-6}$
	With LHPP			
	v_0 [M·s^{-1}]	Error ±	k [s^{-1}]	Error ±
27a	$1.97 \cdot 10^{-8}$	$5.80 \cdot 10^{-11}$	$3.44 \cdot 10^{-4}$	$2.07 \cdot 10^{-5}$
28a	$2.72 \cdot 10^{-8}$	$2.26 \cdot 10^{-9}$	$4.29 \cdot 10^{-4}$	$3.93 \cdot 10^{-5}$
28i	$1.75 \cdot 10^{-8}$	$7.22 \cdot 10^{-10}$	$2.56 \cdot 10^{-4}$	$9.42 \cdot 10^{-6}$
28j	$6.46 \cdot 10^{-9}$	$1.94 \cdot 10^{-9}$	$4.24 \cdot 10^{-5}$	$4.90 \cdot 10^{-6}$

With the results from the AA screen in hand we wondered, if they could explain the observations during preceding experiments as well. For example, from histone derived peptide **26b** with the AA sequence Lys-Lys-Lys-Ala-Arg-**pLys**-Ser-Ala-Gly-Ala-Ala-Lys-Arg-Lys-Ala-Ser-Gly^{CONH_2} (figure 4.11**B**) same amounts of P_i were release with and without enzyme being present. Thus, no enzymatically hydrolyzed substrate was detected at all. The sequence elements of Arg and Ser, *N*- and *C*-terminal to the phosphorylation site, respectively, were also found in peptides **28i** ^{Ac}Gly-***Arg***-**pLys**-Gly-Gly^{CONH_2} and **29j** ^{Ac}Gly-Gly-**pLys**-***Ser***-Gly^{CONH_2}. While for **28i** high hydrolysis with and without LHPP addition was obtained, only a low yields were achieved with **29j** (figure 4.14**A** & **B**). Taking only these two modifications into account, on one hand, Arg might have induced a high intrinsic lability of **26b** to a certain extent. On the other hand, Ser seemed to have a larger influence on the enzymatic activity since the concentration of enzymatically hydrolyzed substrate of **26b** was not only decreased but not present at all. Nonetheless, a more complex interdependence was rather likely. Peptide **26b** was a 17-mer with a diverse sequence compared to **28i** and **29j**. With regard to diminished hydrolysis of pentapeptides compared to monomers, the substrate size of **26b** itself made a successful binding to LHPP questionable. Additionally, **26b** contained seven basic AAs, which could all interact with the negative charge density in the enzyme pocket described above, thereby possibly inhibiting interactions between catalytic center and the pLys site. Taking these considerations together, knowledge gained from short peptides with one

modification could not be transferred to completely different substrates. Gained insights can give an idea which factors to consider, but they cannot be extrapolated or allow well-founded statements.

4.4.5 Computational Chemistry Studies

The empirical data obtained during the activity assays gave insight into the complex mode of action of LHPP. It seemed as if the enzyme was sensitive to changes in substrate size and sequence. As the highest hydrolysis yield was achieved with monomeric pLys and no P_i release could be detected with a 14-mer or 17-mer, the binding pocket and further the enzyme–substrate interaction were assumed to be quite definite. Additionally, the opposite enzymatic activities from substrates with *N*- or *C*-terminal modifications indicated a distinct discrimination based on the peptide stereochemistry. To understand the characteristics better, computational studies with selected pentamers were tested as outlined below. Those molecular dynamic (MD) calculations and simulations were especially challenging, since no such experiments have been conducted with pLys peptides before.

4.4.5.1 Molecular Modeling

First, the enzyme–substrate interaction was probed. Especially the possible energetic differences between unmodified peptide **27a** and the mutated peptides, which had the largest impact on enzyme activity (Ala_N/Ala_C – **28**/**29a**, Lys_N/Lys_C – **28**/**29f**, Arg_N/Arg_C – **28**/**29i** and Ser_N/Ser_C – **28**/**29j**) were of interest. Since no precise binding mode of **27a** or any pLys substrate in complex with LHPP was known, the crystal structure available in the protein database (RCSB PDB, doi: 10.2210/pdb2X4D/pdb) since 2010 was the starting point for the modeling experiments. This structure revealed the catalytic center of the LHPP comprising a phosphate group and a magnesium ion (Mg^{2+}). First, an optimized structure of **27a** was calculated with a small adjustment in the molecule as shown in figure 4.15**A**. Similar to the applied peptide, the *N*-terminus was defined as acetylated but the *C*-terminus was capped set to *N*-methylamide **27a*** instead of a non-methylated amide.

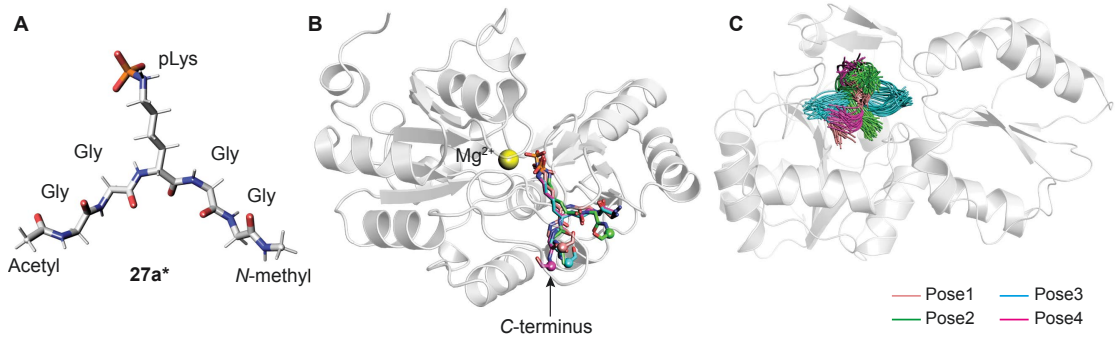

Figure 4.15: **A**. Molecular structure of model substrate **27a***. **B**.Overlaid docking poses of **27a*** in the binding pocket of LHPP, showing pLys interacts with Mg^{2+}. **27a*** peptide in four different docking poses is shown as sticks with the *C*-terminal highlighted as sphere, and the LHPP as cartoon. **C**. Superposition of simulation snapshots of **27a*** starting from four different docking poses. Peptides are shown as ribbon and LHPP as cartoon.

In order to explore possible binding poses of **27a*** within the catalytic center of LHPP, a molecular docking study was performed whereas Mg^{2+} in the catalytic center was defined the midpoint of the docking pocket. Docking of the pentamer into the pocket was carried out using the Glide module [260–262] implemented in the software Schrödinger. Out of ten best docking poses with the highest scores, seven poses exhibited considerable overlap in the phosphoramidate position of pLys with the P_i from the published crystal structure. From these seven poses, we chose four (figure 4.15**B**) that showed significant variation in their binding conformations as the starting structures in the MD simulations. As no force field parameter for phosphorylated Lys can be found in the literature, the AMBER-based force field parameters for pLys were generated using the previously proposed approach for parameterizing pSer, pThr, pTyr, and pHis. [263] More details on the procedure are given in the Experimental Part, section 6.5. For MD simulations, **27a*** was defined as solvated in water. Pleasingly, the energy values remained to be stable during a 100 ns simulation. Furthermore, no obvious molecular distortion was observed during the simulations, additionally verifying these new force field parameters of pLys to be suitable for the MD simulations (figure 4.15**C**).

4.4.5.2 MD-Based Free Energy Calculation of LHPP–Substrate Complexes

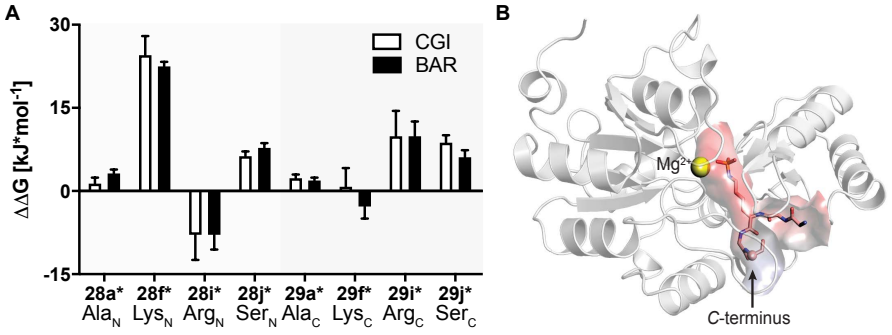

Figure 4.16: **A**. Calculated ΔΔG together with errors of mutated substrates relative to the WT model substrate **27a*** estimated from the MD simulations starting from docking pose 1. Crooks Gaussian Intersection (CGI) and Bennet's Acceptance Ratio (BAR) estimators were employed for the analysis of ΔΔG. **B**. Determined binding mode of **27a*** in complex with LHPP (pose 1). The peptide is shown as ribbon with the *C*-terminus highlighted in sphere. LHPP is shown as cartoon and the electrostatic potential (red: negative, blue: positive) of the binding pocket has been mapped onto the molecular surface.

For the purpose of theoretical evaluation of the free energy changes of different pLys-based pentapeptides, alchemical free energy calculations for **28**/**29a***, **28**/**29f***, **28**/**29i*** and **28**/**29j*** (* indicating *C*-terminal amide *N*-methylation) were employed using **27a*** as the reference. The Ala-, Lys- and Arg-modified peptides were chosen as their introduction either *N*- or *C*-terminal to pLys resulted in large differences in the enzymatic activity of LHPP (figure 4.14**A**). As a comparison, also free energy changes of the Ser-modified pentamers were calculated, since it revealed a remarkably decreased PAH activity regardless of the position in the sequence.

The general idea of MD-based free energy calculation is illustrated in figure S2. The applied method required a combination of equilibrium MD simulations for the non-modified and modified peptides, as well as non-equilibrium transitions from each other. In the MD simulations of **27a*** starting from four different docking poses, the binding conformations of the peptide re-

mained relatively stable and did not interconvert (figure 4.15**C**). In order to evaluate, which docking pose represents the best binding conformation of the peptide, equilibrium simulations for **28**/**29a***, **28**/**29f***, **28**/**29i*** and **28**/**29j*** were performed starting from each of the four poses. The subsequent non-equilibrium alchemical transition simulations were carried out according to previously established protocol [264,265] using a combination of the GROMACS [266,267] and pmx [268,269] software packages. Both CGI and BAR estimators were employed in the analysis of free energy changes ΔΔG. [264] Details of the simulations are given in the Experimental Part, section 6.5.

Results from ΔΔG calculations starting from four different docking poses are summarized in figure 4.16**A** and table S6. It can be seen that the predicted free energy changes upon amino acid changes in the peptide were considerably different for the simulations depending on the starting point. Qualitatively, free energy changes derived from the simulations of the docking pose 1 revealed unambiguously the best agreement with the experimental data (figure 4.16**A** compared to empirical data in figure 4.14**A**). The large difference in ΔΔG between **28f*** and **29f*** as well as **28i*** and**29i*** or the significant decrease of free energy in both, **28j*** and **29j***, compared to the non-modified **27a*** are all well reproduced in the simulations. Nevertheless, the experimental results upon introduction of Ala *N*-terminally to pLys (**28a**) retained the hydrolysis yield while the *C*-terminally counter modification (**29a**) diminished the enzyme activity. This result could not be reflected in the simulation data of **28a*** and **29a***, as slight increases in relative binding free energy were predicted for both compared to **27a***. This might be explained by the size of the mutation. Introducing small steric perturbation in amino acid sequence may require much longer simulation time than that was performed in the current study (a few hundred of nanoseconds) to capture the differences in binding. The simulations results obtained for Ser-modifications could also hint towards that. The hydrolysis yields for **28j** and **29j** were clearly decreased as for *N*-terminal Lys-modification (**28f**). Yet, the calculated ΔΔG values were much higher in case of **28f***. Even if those results could strengthen the experiment trends, their quantitative statement was not correct. Explanations for the varying enzymatic activity of LHPP depending on the modification position in the sequence could be found in the enzyme–substrate complex (figure 4.16**B**). In the best binding mode (pose 1) revealed by the alchemical free energy calculations, the pLys side chain was nicely fitted in a small, negatively charged cavity where it was completely buried from solvent. Within that, the doubly charged magnesium ions did compensate the negative charges both from pLys and the protein environment. In contrast, electronic potential of the binding site for accommodating the substrate main chain with the peptidic backbone was considerably different for *C*- and *N*-terminal regions. As a result, modifications with positively charged side chains (**28**/**29f**, **28**/**29i**) could interact differently with LHPP depending on their sequence position. The Lys side chain was shorter but more flexible compared to Arg and thus, **29f** and **28i** might have reached into the same negative domain of LHPP while their counter molecule did not fit there.

4.4.6 Conclusion and Outlook

In this approach, a systemic study of the LHPP activity profile was conducted. To do so, several sets of model substrates have been synthesized, all of which could be obtained *via* established synthesis routes, except a pHis pentapeptide. Starting from single phospho-AAs, the activity of LHPP as PAH or Pase was investigated. It could be shown that LHPP had a clear discrimination

between P–N and P–O bonds. These observation could be once more found with differently phosphorylated pentamers. As the scope of substrate assayed had been expanded to protein derived, longer pLys peptides – 14-mer and 17-mer, the encouraging results could not be reproduced as no P_i was released upon incubation with the enzyme. This property might hint towards LHPP activity rather on small metabolic substrates than on whole proteins. To further elucidate the capacity of LHPP, the influence of steric and electronic diverse AA mutations adjacent to the phosphorylation site were examined. A clear trend towards activity reduction upon AA variation was detected with some exceptions as Ala or Arg *N*-terminally or Lys *C*-terminally to pLys. These observations indicated a narrow, well defined catalytic center with low flexibility in substrate binding and were explored in a computational chemistry approach. Within this, the possible binding poses of the unmodified pLys peptide in the catalytic center of LHPP were calculated and further evaluated with MD-based free energy calculations. Extending the considerations, MD-simulations were also conducted for four mutated peptides, which gave free energy values relative to the unmodified substrate. These results delivered valuable insight into the sequence dependency of LHPP's enzymatic activity and indicated a distinct binding motif. Apparently, small or positively charged groups flanking the phosphorylation site were favored. Along these lines, the highest activity inducing peptide sequences of unmodified **27a**, Ala_N **28a**, Arg_N **28i** and Lys_C **29f** with considerations of Lys instead of pLys, can be found in 2678, 58, 54 and 40 proteins of the human proteome, respectively.

Building up on the work accomplished in this approach, the combination of *in vitro* biochemical assays and computational simulations could be applied in a comprehensive AA scrambling assay and hence be useful in the search for pLys proteins. Small model substrates might be examined with altered sequences and together with enzyme activity could be transferred to conserved motif quests. The principle itself could also be integrated in studies working on other poorly characterized enzyme–substrate interactions.

4.5 Generation of Monoclonal Anti-Phospho-Lysine Antibody

4.5.1 Outline of the Project

As shown very gracefully for His [187–190] and Arg, [191,193] selective antibodies (Abs) can give access to detection and identification of numerous previously unknown labile phosphorylation sites. Thereby, the process of Ab generation required stable pHis [184–186,189,190] or pArg [191,193] analogues to mimic endogenous PTMs and ensure successful enrichment of the phosphorylated species. The aim of this project was to employ pLys mimics **18** and **19** described in section 4.3 in monoclonal Ab (mAb) generation against pLys. As shown in figure 4.17, organic synthesis was to be utilized to prepare customized pLys mimicking haptens and subsequently conjugate them to carrier proteins of choice. The obtained immunogens were supposed to initiate Ab formation during immunization of rats and mice. After fusion of obtained splenocytes with myeloma cells to hydridoma cells, the potent clones were proposed to be evaluated in enzyme-linked immunosorbent assays and a monoclonal α-pLys Ab was aimed to be produced from the best hit.

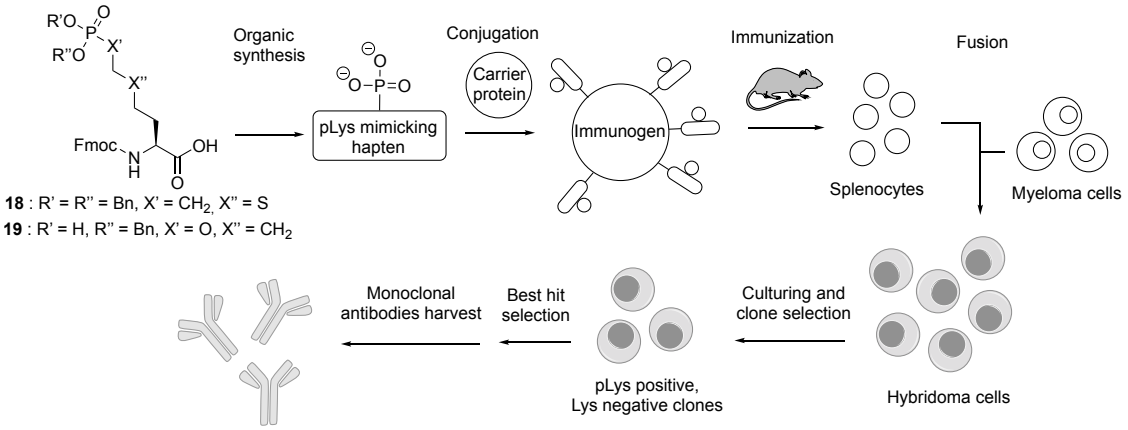

Figure 4.17: Strategy for generation of monoclonal antibodies against pLys.

4.5.2 Responsibility Assignment

The project was anticipated by Anett Hauser and Christian Hackenberger. In close coordination with Regina Feederle and Aloys Schepers from the Helmholtz Zentrum Munich, immunogen architectures were designed. Organic small molecule and immunogen synthesis was performed by Anett Hauser. The process of immunization until primary hybridoma screen was conducted at the Monoclonal Antibody Core Facility of Helmholtz Zentrum Munich under the supervision of Aloys Schepers. Further evaluation of primary supernatents (1°) was completed by Anett Hauser by enzyme-linked immunosorbent assay (ELISA). The required ELISA protocol was designed by Anett Hauser and optimized by Jeannine Engelke with very helpful advise from Hubert Kalbacher (Eberhard Karls Universität Tübingen) and Peter Carl (BAM).

4.5.3 Target Immunogen Architectures

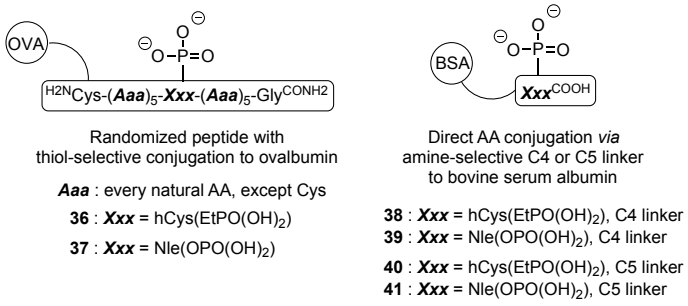

Figure 4.18: Investigated immunogen architectures in the α-pLys Ab generation. Sequence independence could be ensured by conjugation of randomized peptides or only the monomeric AA to carrier proteins.

The immune response to an immunogen administered during immunization could be directed towards several parts of the immunogen. To achieve a response against pLys, the hapten design was crucial. Ideally, unique properties of the desired target (pLys) should be utilized. Since the aim of this project was an mAb against a yet unidentified phosphorylation event, the immunization was required to happen independently from any peptide sequence. Several immunogen architectures were suitable for this approach (figure 4.18).

First, a randomized peptide with pLys mimic as the only conserved site was intended. This structure allowed the recognition of a peptidic backbone similar to a protein moiety and still ensured sequence independence. Additionally, excluding Cys from the randomized part and introducing it *N*-terminally, allowed its employment in chemoselective conjugation to the carrier protein. Several thiol-reactive linker modified carrier proteins were commercially available. *Ovalbumin* (OVA) was an attractive choice since it was known to be immunogenic but less prone to inter-protein cross conjugation than other carrier proteins. Furthermore, the novel designed pLys mimics introduced in section 4.3 have been readily synthesized for incorporation into peptides as benzyl- and Fmoc-protected building blocks **18** and **19**. Thus, the target conjugates **36** and **37** as shown in figure 4.18 were intended.

Second, pLys mimics could be coupled directly to the carrier protein of choice *via* a homobifunctional linker. Later administration of the monomeric AA ensured a sequence independence as well. This approach bore the risk of generating either no specific immune response to such a small modification or predominant recognition of *C*-terminal AA since the antigen was coupled *via* its *N*-terminus and hence, still had a free carboxyl group. By choosing *bovine serum albumin* (BSA) as carrier protein, the loading of antigen and thus, the immunogenicity was to be increased. The restricted recognition to free carboxyl groups could be diminished by amidation of the *C*-terminus. Also, thorough evaluation of yielded clones could eliminate the exclusive *C*-terminal recognition. The standard procedure for homobifunctional linkage is a one-pot incubation of protein, substrate and glutaraldehyde (C5 linker, glut-CHO) together, which is convenient but also leads to high crosslinking and takes away control over the immunogen structure. Variation of the reactants addition sequence could prohibit protein–protein crosslinks to some extent. Another option was the synthesis of the pLys mimic already with the linker attached and subsequent conjugation of this construct to the carrier protein. With this approach, undesired protein–protein conjugates were excluded and the linker could be tailored to the favored length. Target compounds for the

single AA immunogen were as followed (figure 4.18): phosphonate and phosphate derived mimics conjugated to a C4 linker prior to conjugation to BSA (**38** and **39**) or both analogues applied in the glut-CHO conjugation protocol (**40** and **41**).

4.5.4 Synthesis Approaches

4.5.4.1 Randomized Peptides and Thiol-Selective Protein Conjugation

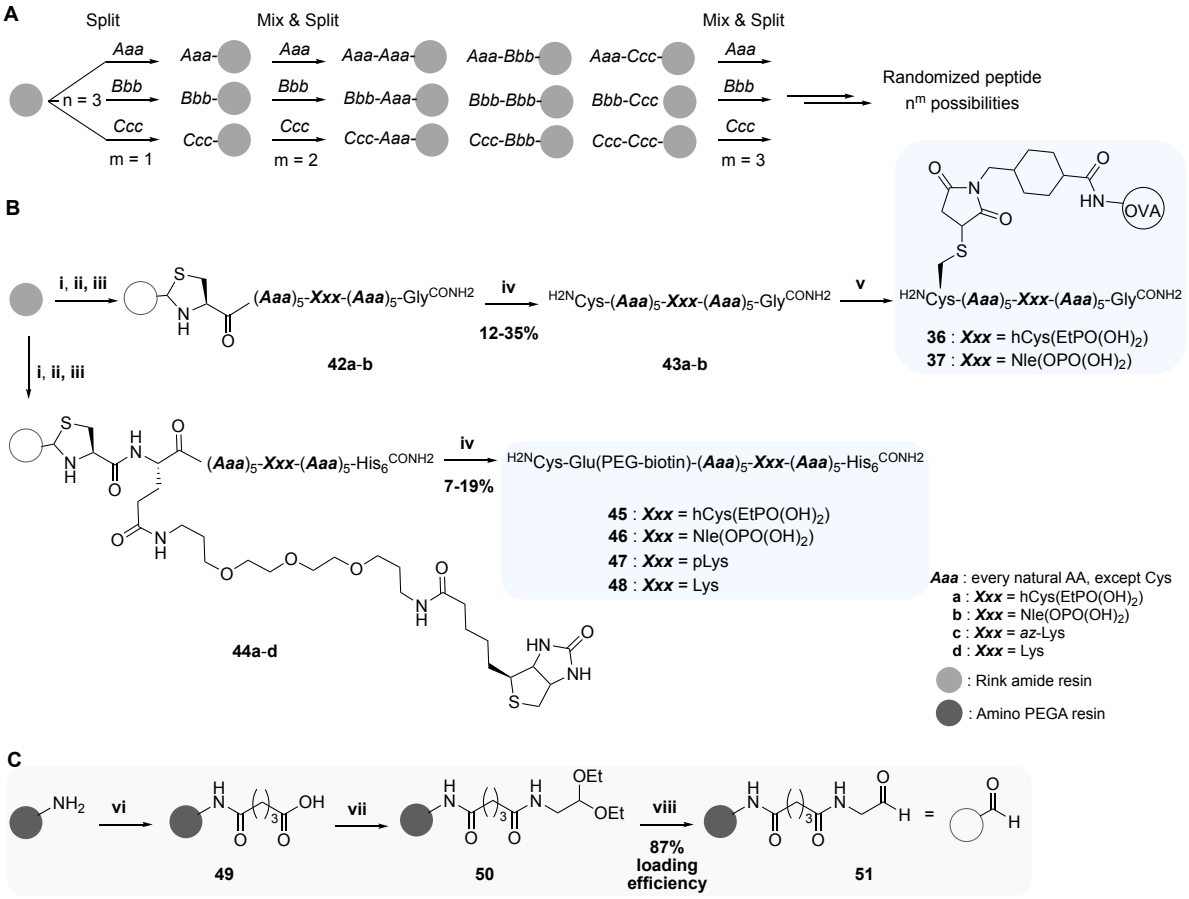

Scheme 4.12: **A**. Combinatorial peptide synthesis via split-and-mix approach. n = number of varied AAs, m = number of coupling steps. **B**. Synthesis route to target conjugates **36** and **37** for immunization as well as peptides **45**-**48** for antibody evaluation. **C**. Aldehyde functionalization of an amino resin. Reagents and conditions: **i**) Fmoc-SPPS with acetylation after each step except *N*-terminal; **ii**) TFA:thioanisole:TIS:H_2O (90:5:2.5:2.5, v/v/v/v), r.t., 2x 2 h; **iii**) **51** (5 eq.), 100 mM MES, 10 mM TCEP, ACN:H_2O (1:1, v/v), pH 6.4, min. 24 h; **iv**) a) 200 mM $MeO-NH_2 \cdot HCl$, ACN:H_2O (1:1, v/v), unbuffered, 4x 8-16 h; b) only for pLys peptide: Staudinger-phosphite reaction with phosphite **9** followed by photolytic deprotection; **v**) Mal-activated OVA (0.4 eq. with regard to Mal functionalities), TCEP (1 eq.), PBS, r.t., 48 h; **vi**) succinic anhydride (10 eq.), HOBt·H_2O (10 eq.), DIPEA (10 eq.), DMF, r.t., 23 h; **vii**) a) CDI (40 eq.), DMF, r.t., 90 min; b) aminoacetaldehyde diethyl acetal (30 eq.), HOBt·H_2O (20 eq.), DMF, r.t., 16.5 h; **viii**) TFA:H_2O (1:1, v/v), r.t., 90 min.

For the first targeted immunogen architecture randomized peptides were synthesized. Among those, two OVA conjugates **36** and **37** were to be administered during immunization, four *N*-terminally biotinylated peptides with a *C*-terminal His-tag **45**-**48** were to be applied in clone evaluation. The randomization was achieved by the combinatorial approach of split-and-mix

(scheme 4.12**A**).[270] Thereby, the solid support was split into portions equal to the amount of different AAs to be scrambled before every coupling step and in each reactor one AA was employed. Hence, bulky AAs could couple without competing with smaller AA for free amino functionalities. After coupling, the whole amount of solid support was mixed well and divided again to the reactors. In this manner, n^m possible peptides were obtained (n being the number of different AAs, m being the number of coupling steps). For the target compounds **36**, **37**, **45**, **46**, **47** and **48** (scheme 4.12**B**), nineteen AAs were scrambled in ten positions and as such, possibly 19^{10} different peptides prepared. Cys was excluded from the randomization procedure since it presented the required chemoselective handle for the protein conjugation with its conserved *N*-terminal positioning.

During randomization, more than $6{\cdot}10^{12}$ species could have been synthesized, the sequences ranging from a peptide containing only Gly with the smallest molecular weight to one having only Trp incorporated with the highest molecular weight. The diversity in structure, aromaticity and polarity made a characterization and distinct purification from truncated peptides not feasible. At this point, the Cys residue was of great benefit as a reactive handle as well. As described by Villain *et al.*, aldehyde functionalized resin **51** (scheme 4.12**C**) was applied in a covalent capture (**42a**-**b**, **44a**-**d**) and release (**43a**-**b**, **45**, **46**, **47** and **48**) strategy of *N*-terminally cysteinylated peptides.[271,272] Starting from Amino-PEGA resin, coupling of succinic anhydride delivered the required carboxyl group in **49** for subsequent functionalization with aminoacetaldehyde diethyl acetal to the protected aldehyde **50**. Short acid treatment yielded the desired resin **51**, which was stable when stored in ACN:H_2O (1:1, v/v).

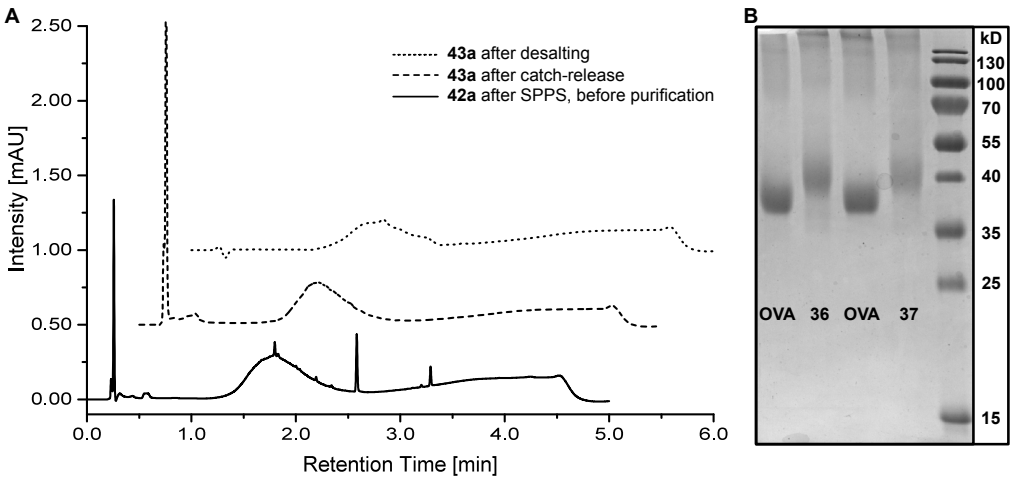

Figure 4.19: **A**. UPLC chromatograms of **43a** at 220 nm. —— crude product after SPPS; – – – after catch and release purification with **51**; ····· after desalting. **B**. Non-reducing SDS-PAGE gel (15%) of conjugation reactions of **43a** and **43b** with Mal-activated OVA to target conjugates **36** and **37**, Coomassie stained.

Covalent capture was achieved under slightly acidic conditions in the presence of tris(2-carboxyethyl)phosphine (TCEP) to ensure reduction of Cys. Treatment of the thiazolidine-linked bound peptides with *O*-methylhydroxylamine hydrochloride ($MeO-NH_2$) resulted in release of bound peptides. Purification of target compounds from truncated ones was possible as long as acetylation was conducted during peptide synthesis after each coupling step except after Cys incorporation. All randomized peptides were separated from remaining $MeOH-NH_2$ by desalting. Figure 4.19**A** shows exemplified for **43a** the purification steps from crude to desalted randomized peptide. The detected broad signal indicated a diverse mixture.

Before immunization, peptides **43a** and **43b** were conjugated to commercially available maleimide- (Mal-)activated OVA. After incubation in phosphate-buffered saline (PBS) in the presence of TCEP, distinct upwards shifts were observed in sodium dodecyl sulfate–polyacrylamide gel electrophoresis (SDS-PAGE), indicating a successful conjugation to target compounds **36** and **37** (figure 4.19**B**). Due to the heterogenicity of the constructs, no further characterization like LC-MS or tandem-MS could be conducted. All samples were rebuffered to sterile PBS and delivered to the collaboration partner for immunization and hybridoma screen.

4.5.4.2 Butanal Based Linkage Strategy

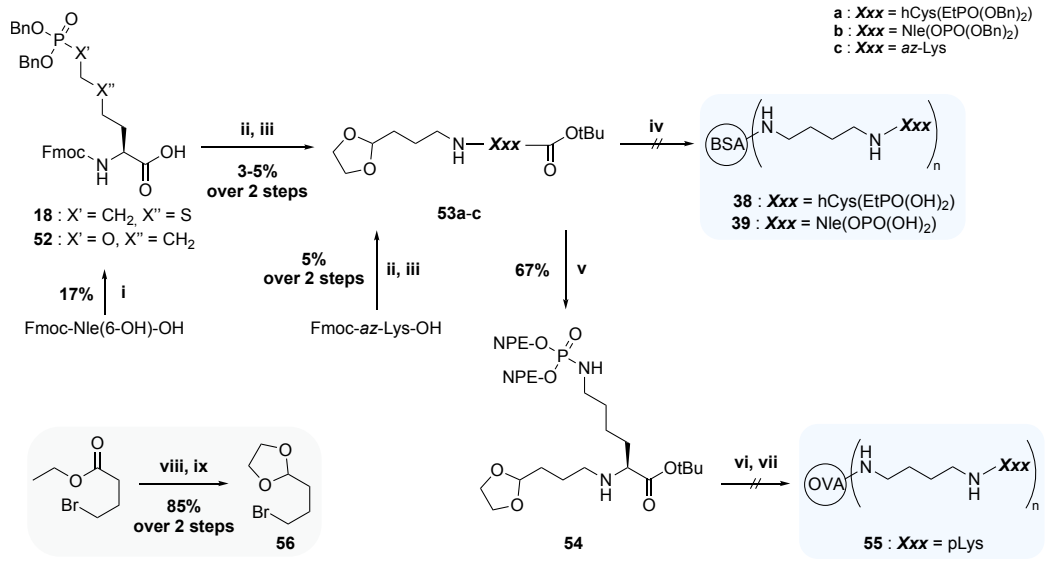

Scheme 4.13: Synthesis routes to target conjugates **38** and **39** for immunization as well as conjugate **55** for clone evaluation. Reagents and conditions: **i**) a) PCl_3 (1.7 eq.), Bn-OH (3.5 eq.), Et_3N (3.5 eq.), THF, 0 °C to r.t., 3 h, b) 2,6-lutidine (4.2 eq.) r.t., 60 min, c) H_2O, NaBr (2.3 eq.), $NaBrO_3$ (0.51 eq.), 0 °C to r.t., 17 h; **ii**) *tert*-butyl 2,2,2-trichloroacetimidate, DCM:Et_2O (1:1, v/v, dry), Ar, r.t., 3 d; **iii**) **56** (0.9 eq.), Cs_2CO_3 (5 eq.), DMF, 80 °C, 48 h; **iv**) a) TFA:H_2O (97:3, v/v), r.t., 20 h, b) BSA (0.01 eq.), 100 mM Na_2CO_3, 150 mM NaCl, pH 8.4, 4 °C, 20 h, c) $NaBH_3CN$ (10 mg·mL^{-1}), 4 °C, 3.5 h; **v**) **9** (2x 3 eq.), DMF, 45 °C, 42 h; **vi**) a) HCl (4 N in dioxane), r.t., dark, 20 h, b) OVA (0.01 eq.), 100 mM Na_2CO_3, 150 mM NaCl, pH 8.4, 4 °C, 20 h, c) $NaBH_3CN$ (10 mg·mL^{-1}), 4 °C, 3.5 h; **vii**) PBS, 297 nm, r.t., 5x 20 min, cooling in between irradiation cycles; **viii**) DIBAL-H (1.14 eq.), DCM, -78 °C; 45 min; **ix**) EDT (3 eq.), *p*-TsOH (0.05 eq.), toluene, reflux, 45 min.

The second tested immunogen architecture was a direct conjugation of AA monomers to the carrier protein. In order to avoid high protein–protein crosslinking degree, this conjugation was tackled with butanal-funtionalized AAs in a first approach. The simplest way to achieve *N*-alkylation would have been reductive amination of an aldehyde. Nonetheless, the Fmoc-protected amines of **18**, **19** or Fmoc-*az*-Lys-OH turned out to be very unreactive towards aldehydes. Furthermore, condensation products of several aldehyde molecules were a possible side reaction. Thus, nucleophilic substitution was desired. First attempts showed that an alkyl bromide did rather attack the carboxyl group or, in case of Nle derived building block **19**, the free phosphoryl hydroxyl group. Therefore, AAs with protected *C*-terminus and intact phosphate esters were required.

In order to obtain bis-benzyl-protected Fmoc-Nle($OP(OBn)_2$)-OH **52**, the synthesis protocol of **19** was adjusted in its first step (see section 4.3.3.2). Instead of 1.7 eq., 3.5 eq. of Bn-OH were applied, which yielded 17% of **52** in the end. The carboxyl groups of **18**, **52** and Fmoc-*az*-Lys-OH

were *tert*-butyl-protected with *tert*-butyl 2,2,2-trichloroacetimidate,[273] which turned out to give the highest conversion and yields compared to activation with sulfuric acid[274] or thionylchloride[275] and reaction with DCC incubated *tert*-butanol[276] or *O*-*tert*-butyl-*N,N'*-diisopropylisourea.[273]

For the nucleophilic substitution with a butyl aldehyde building block, the 4-bromobutyl acetal **56** was obtained in two steps *via* 4-bromobutanal in 85% yield, starting from ethyl 4-bromobutanoate. *N*-alkylation was conducted under basic conditions to ensure reactivity of the carbamate. Thereby, upon incubation with Cs_2CO_3, the Fmoc-group was removed and a more reactive amine obtained intermediately, which proceeded further to the desired amines of **53a**-**c**. The isolated yields of products **53a**-**c** were notably low, which was strongly influenced by the low separation efficiency during preparative HPLC purification. Before protein conjugation, azide **53c** was converted to phosphoramidate **54** by Staudinger-phosphite reaction as described in section 4.1.

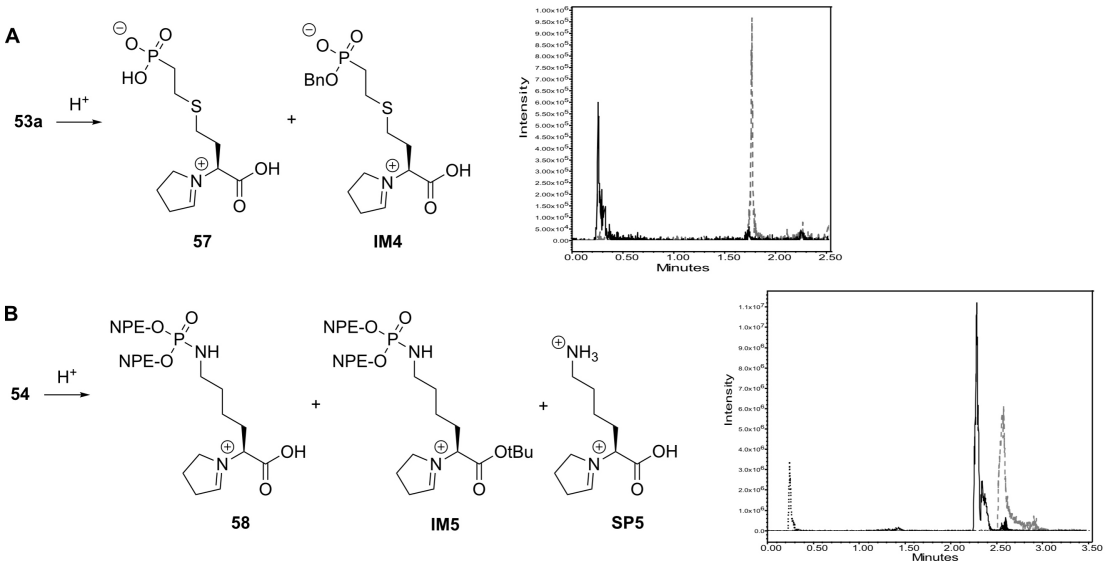

Figure 4.20: **A** & **B**. Products obtained during acidic treatment of **53a** and **54**, which were detected during UPLC-MS analysis. **A**. Mass spectra show extracted target masses of **57** (m/z 296 ——) and **IM4** (m/z 386 – – –). **B**. Mass spectra show extracted target masses of **58** (m/z 577 ——), **IM5** (m/z 633 – – –) and **SP5** (m/z 199 ·····).

Test reactions were conducted with phosphonate **53a** and caged pLys **54** to find the optimal conditions for acetal hydrolysis and subsequent conjugation since their different acid stability required individual treatment. While the building block design of **53a** and **53b** allowed simultaneous deprotection of aldehyde, phosphate ester and carboxylic acid, the phosphoramidate of **54** should remain caged and only the aldehyde and acid deprotected. Thus, hCys-derived **53a** was incubated with a TFA:H_2O (1:1, v/v) mixture and **54** with 4 N HCl in dioxane. For both molecules, immediate cyclization of the deprotected aldehyde to a pyrrole derivative was observed (figure 4.20). Since the closed enamine form was in equilibrium with the open aldehyde form,[277] the compounds **57** and **58** were still applicable for protein conjugation. A major problem was posed by the incomplete deprotections. In case of the phosphonate derivative, the second benzyl ester was not hydrolyzed even after 20 h of reaction time (**IM4**, figure 4.20**A**). For the phosphoramidate, the conditions were too soft to cleave the carboxylic acid ester (**IM5**) on one hand, but too harsh to keep the P–N bond intact over time on the other hand (**SP5**, figure 4.20**B**). Even though for both molecules a certain amount of desired product was detected by UPLC-MS analysis, no pure compounds were obtained

in any trial. Nonetheless, the reaction mixtures were employed in protein conjugations to check the reactivity of the enamines. Therefore, the solutions were neutralized and subsequently added to 0.01 eq. of protein in 100 mM Na_2CO_3, 150 mM NaCl at pH 8.4. Unfortunately, no indication for successful formation of **38** or **55** was observed neither in SDS-PAGE or UPLC-MS analysis.

Taking all the drawbacks of this approach together and having especially the final step in mind, the butanal-derived immunogen architecture was abandoned.

4.5.4.3 Glutaraldehyde Based Protein Modification with Monomers

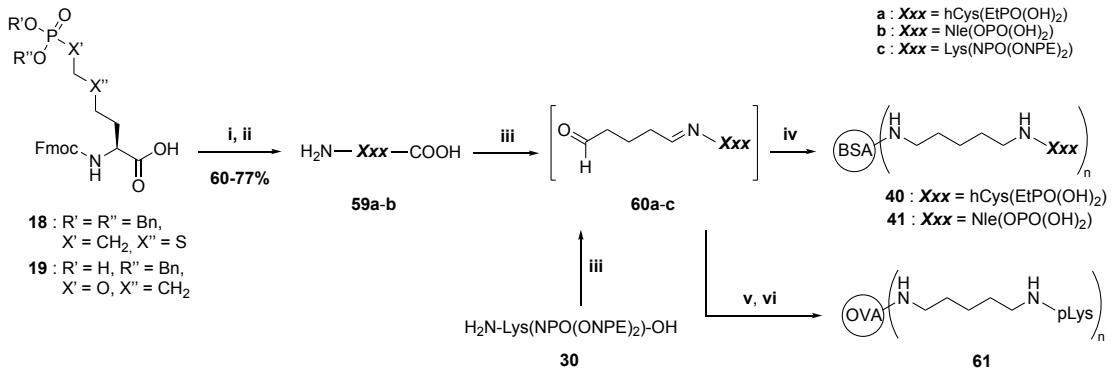

Scheme 4.14: Synthesis routes to target conjugates **40** and **41** for immunization as well as conjugate **61** for antibody evaluation. Reagents and conditions: **i**) Pip:DMF (20:80, v/v), r.t., 3 min; **ii**) for **59a**: TFA:TIS:H_2O:thioanisole (93:2.5:2.5:2, v/v/v/v), for **59b**: TFA:TIS:H_2O (95:2.5:2.5, v/v/v), r.t., 3+2 h; **iii**) glut-CHO (2 eq., 1% (w/v) in final solution), 100 mM Na_2CO_3, 150 mM NaCl, pH 7, 20 °C, 17 h; **iv**) a) BSA (0.02 eq., 2 mg·mL^{-1} final concentration), 100 mM Na_2CO_3, 150 mM NaCl, pH 8.4, 4 °C, 26 h, b) $NaBH_3CN$ (10 mg·mL^{-1} final concentration), 4 °C, 70 min; **v**) a) OVA (0.02 eq., 2 mg·mL^{-1} final concentration), 100 mM Na_2CO_3, 150 mM NaCl, pH 8.4, 4 °C, 26 h, b) $NaBH_3CN$ (10 mg·mL^{-1} final concentration), 4 °C, 70 min; **vi**) PBS, 297 nm, r.t., 5x 20 min, cooling between irradiation cycles.

Besides the butanal-based approach to attach monomeric AAs to carrier proteins, glut-CHO is commonly used as homobifunctional linker. Since the substrate synthesis of the aforementioned strategy did not give the target molecules in satisfying yield or purity, also the connection *via* glut-CHO was investigated.

For the synthesis, previously obtained building blocks **18**, **19** (see section 4.3) and **30** (see section 4.4) could be used. The pLys mimics were globally deprotected by subsequent basic and acidic treatment. In a first approach, **59a** and **59b** were tried to precipitate in cold diethyl ether but within that, Pip could not be removed. Thus, both compounds were purified by preparative HPLC in addition to precipitation.

Popular protein antigen conjugation strategies *via* glut-CHO work either with a one-step or a two-step protocol.[278–280] They differ in the order of reagent addition to the reaction mixture. Either carrier protein, antigen and glut-CHO are incubated together or substrate and glut-CHO are allowed to react before they are added to the carrier protein. The latter technique is supposed to minimize protein–protein crosslinking due to excess glut-CHO. For the synthesis of **40**, **41** and **61**, both protocols were tested. As figures 4.21**A** & **B** show for **40** as an example, distinct differences were observed between the methods. While for the two-step protocol **40^{II}** a distinct band with slight upper shift and only few bands of larger molecular weight were detected, the one-step protocol led to smeared bands and large upwards shift, thereby indicating a more heterogeneous

mixture and higher degree of crosslinking. Thus, the target conjugates were synthesized *via* the two-step approach (see Experimental Part, section 6.6 for a detailed protocol).

Figures 4.21**C**-**E** show the analysis data obtained for the three reactions. For conjugates **40** and **41**, the SDS-PAGE revealed small shifts of the main BSA band but also some smears, which implied a low degree of functionalization and protein–protein crosslinking. The associated UPLC-MS analysis indicated the formation of a heterogeneous mixture as no clear charge envelope could be recognized and no deconvolution was possible of the samples after the reaction (figure 4.21**E** shows the total ion currents (TICs) of injected samples). Interestingly, the applied OVA seemed to be present as a dimer, which was destroyed during sample preparation for SDS-PAGE analysis. The conjugation to **60c** yielded a more heterogeneous construct compared to both BSA–AA conjugates. This could be observed in a more smeared SDS-PAGE band as well as a more cluttered TIC mass spectra. Unfortunately, no exact structures or conjugation yields could be determined for the conjugates. All samples were rebuffered to sterile PBS and delivered to the collaboration partner for immunization experiments and hybridoma screen.

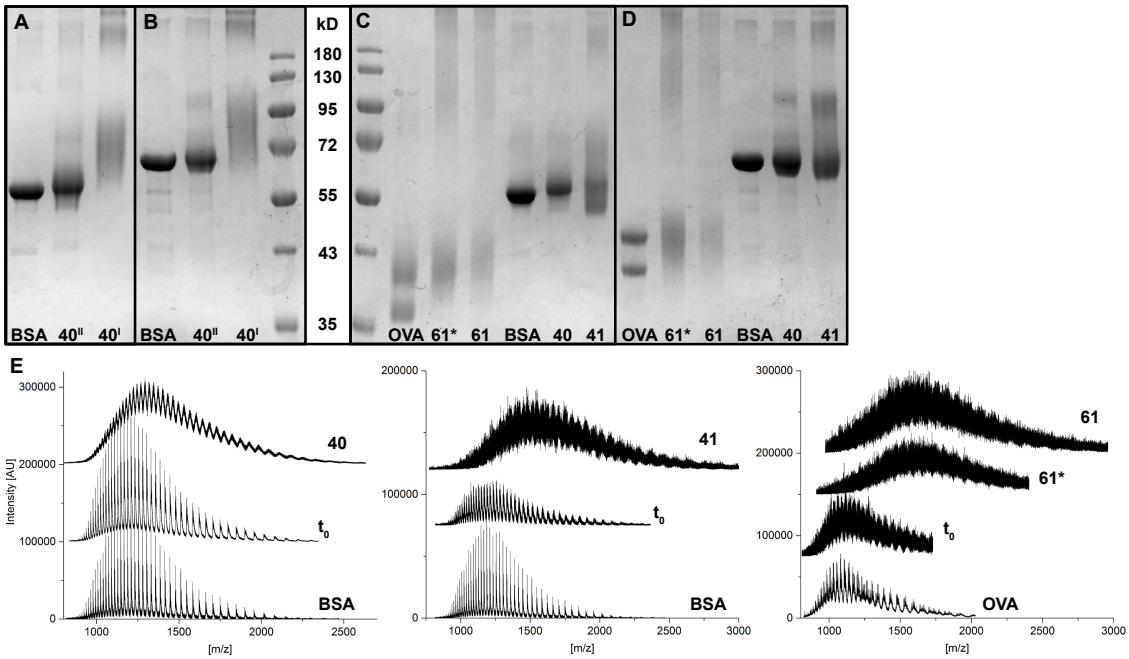

Figure 4.21: **A** & **B**. Non-reducing (**A**) and reducing (**B**) SDS-PAGE analysis (12%) of conjugation reaction of BSA with **59a** either in two steps (**40^{II}**) or in one step (**40^{I}**), Coomassie stained. **C** & **D**. Non-reducing (**C**) and reducing (**D**) SDS-PAGE analysis (12%) of target conjugates **61*** before photolytic deprotection, **61**, **40** and **41**, Coomassie stained. **E**. TIC mass spectra of conjugation reactions: BSA with **60a** (left), BSA with **60b** (middle) and OVA with **60c** including subsequent photolytic uncaging (right).

4.5.5 Immunization and Hybridoma Screen

All immunizations and primary screens to generate α-pLys-mAbs were conducted by the collaboration partners in the Monoclonal Antibodies Core Facility at the Helmholtz Zentrum München. Different species of rats or mice were used for the study. Overall, eight, nine, three and three immunizations have been conducted with conjugates **36**, **37**, **40** and **41**, respectively. Some of them yielded positive immune response against pLys, which could be shown in the primary

screen, but only one clone (*pLysN 5G1 R-2b*) was stable and could be confirmed. This clone was originated from an immunization with the OVA–peptide conjugate **37**, which had the phosphate mimics installed and was evaluated further in the Chemical Biology II department at the FMP in Berlin as outlined below. Furthermore, the *immunoglobbulin G* (IgG) subclass was determined in the Monoclonal Antibodies Core Facility and a matching *horseradish peroxidase*- (HRP-)labeled secondary (2°) Ab (mouse-α-rat-IgG2b-Ab-HRP) delivered to Berlin. More details on the immunization can be found in the Experimental Part, section 6.6.

4.5.5.1 Clone Evaluation

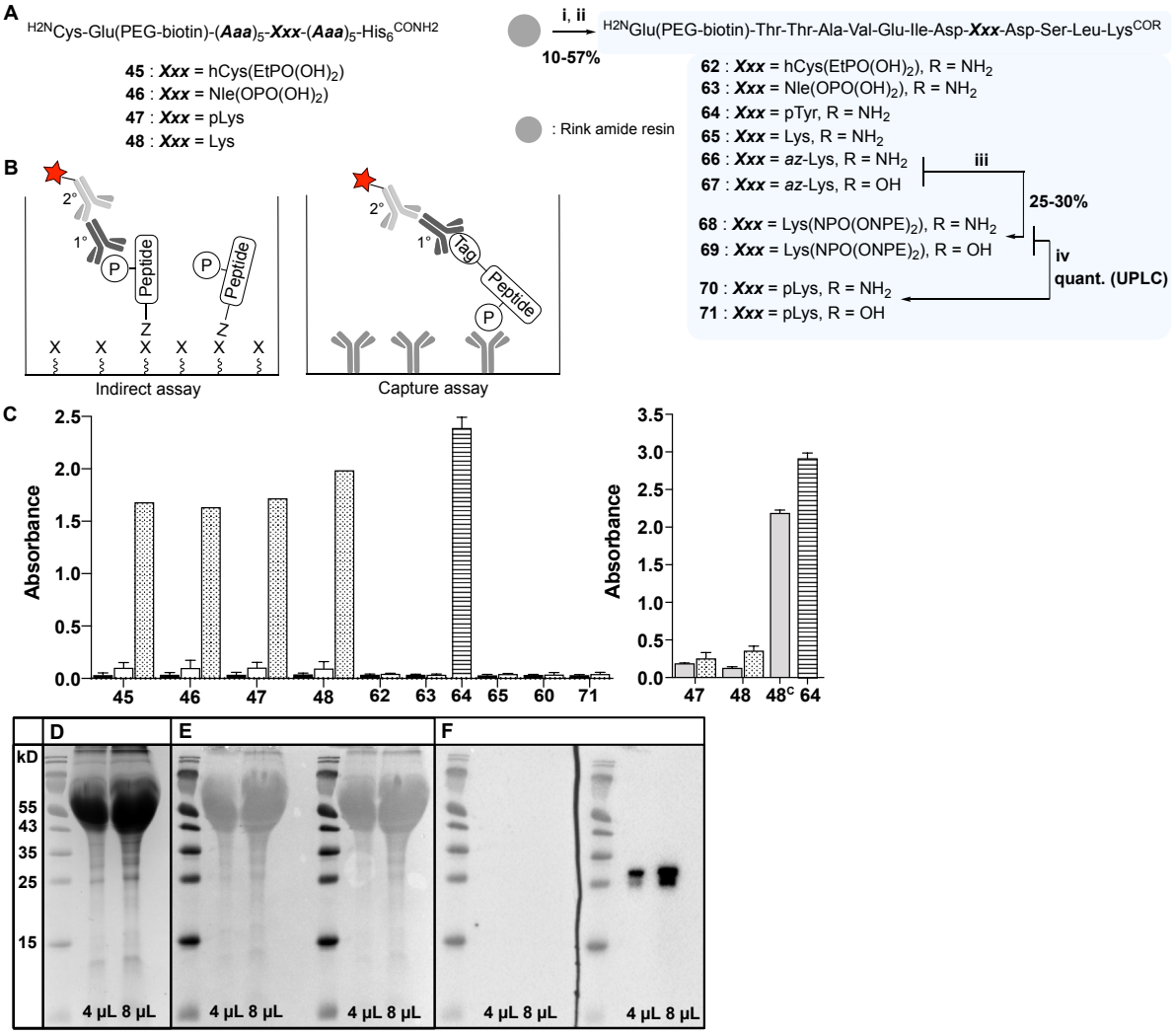

Figure 4.22: **A**. Applied peptides during clone evaluation. Reagents and conditions: **i**) Fmoc-SPPS; **ii**) TFA:TIS:H_2O (95:2.5:2.5, v/v/V), r.t., 2 h; **iii**) **9** (2x 3 eq.), DMF, 45 °C, 48 h; **iv**) MeOH, 297 nm, r.t., 60 min. **B**. Different ELISA strategies to test the clone. Indirect assay (left) and sandwich ELISA (right). **C**. Results of ELISA tests. Indirect assay (left) and sandwich ELISA (right) detected with mouse-α-rat-IgG2b-HRP (black), goat-α-rat-HRP (blank), mouse-α-His-tag-Ab + goat-α-mouse-Ab-HRP (dotted), α-pTyr-HRP (striped) and *streptavidin*-HRP (gray). **D**-**F**. Western blot analysis of 4 or 8 µL delivered supernatant *pLysN 5G1 R-2b* with Coomassie stain (**D**), Ponceau stain (**E**) and chemiluminescence (**F**) after incubation with delivered mouse-α-rat-IgG2b-HRP (left) and goat-α-rat-HRP (right).

The evaluation was done with the purpose to check for several characteristics of the yielded clone. Most important was the selective recognition of pLys peptides over Lys residues. Unphosphorylated Lys is probably the predominant condition of this AA and thus, detection of Lys by the generated mAb would have led to many false positive responses. Secondly, the cross reactivity with other phospho-AAs and acidic residues was part of the evaluation. Since the abundance of pLys is estimated to be rather low compared to other phospho-AAs, this feature was of high interest. Besides that, the sequence independence of the positive clone was crucial. So far, no pLys site in any protein is known and therefore, the newly obtained Ab should have recognized the phosphorylation site in various peptide sequences. Lastly, the sensitivity of the clone was to be determined, so that the required minimum pLys concentration in a sample would be known.

For these objectives, the previously synthesized randomized, biotin- and His-tagged peptides **45**-**48** were applied. Also, further biotin-labeled peptides **62**-**71** with known AA sequence were synthesized (figure 4.22**A**).

As mentioned above, the clone should be investigated by ELISA for its properties (figure 4.22**B**). Therefore, suitable assay conditions were established first with pTyr peptide **64** and a α-pTyr-Ab-HRP conjugate. Since the Ab of interest was supposed to recognize Lys phosphorylation, an indirect assay was tested, in which antigens (peptides) were coated on the plate and the binding efficiency of the generated clone (1° Ab) detected with a 2° Ab. Initially, peptides were supposed to be coated on plates without tag to be independent from *N*- or *C*-terminal modification of the substrates. Nonetheless, the required sample material too high to actually detect signals with a valid, reproducible intensity. Thus, *streptavidin*-coated ELISA plates were used together with biotin-tagged peptides (figure 4.22**B**, with X = *streptavidin*, Z = biotin). Besides that, the coating conditions, buffers, blocking and detection reagents were tested. The optimal conditions are outlined in the Experimental Part, section 6.6.

In addition to the indirect ELISA, also a capture assay (sandwich ELISA, figure 4.22**B**, right) was performed, in which the plate was coated with the generated clone *pLysN 5G1 R-2b* and subsequently incubated with randomized pLys and Lys peptides, **47** and **48**, respectively. This was done, to detect the clone–substrate interaction independently from the supplied 2° Ab. Since **47** and **48** were equipped with an *N*-terminal biotin-tag and a *C*-terminal His-tag, their binding to the 1° Ab could be detected with according reagents as well.

Figure 4.22**C** shows the results of the different ELISA experiments, whereby the detection of pTyr peptide **64** with an α-pTyr-Ab-HRP was used as positive control for a functional assay (striped bars). On the left, the indirect assay is displayed, within which the randomized and defined peptides were coated and detected with various Abs. Very clearly, the coating itself did work, since the mouse-α-His-tag-Ab bound to peptides **45**-**48** and could be detected (dotted bars). Unfortunately, no signal was obtained upon incubation with the generated clone *pLysN 5G1 R-2b*, no matter if it was then treated with the matching, mouse-derived 2° Ab-HRP from Helmholtz Zentrum (black bars) or another, goat-derived 2° Ab-HRP from the FMP (blank bars). These results could have several reasons. On one hand, the 2° Ab might not have recognized the 1° Ab, meaning the clone, due to a wrong subclass of the mouse-α-rat-IgG2b-Ab-HRP from Munich or a low specificity of the goat-α-rat-Ab-HRP from the FMP stock. On the other hand, the clone could not have recognized the peptides and thus have been washed away and no detection was possible anymore.

In order to eliminate the variable of the 2° Ab and with it a possible mismatch, the sandwich

ELISA was conducted as described above. The results shown in figure 4.22**C** on the right indicated again no interaction of peptide and clone. Since the pTyr peptide **64** was detected, the coating process of the plate did work for certain and *pLysN 5G1 R-2b* should be bound to the plate. Furthermore, a second positive control of coating mouse-α-His-tag-Ab as capture Ab, binding peptide **48** and detection of the *N*-terminal biotin-tag gave a high signal (**48**$^{\mathbf{C}}$ in the figure). Nonetheless, neither the detection with *streptavidin*-HRP conjugate (gray bars), nor with mouse-α-His-tag-Ab + goat-α-mouse-Ab-HRP (dotted bars) resulted in a considerable signal during the actual experiment. Thus, no peptide **47** or **48** was found to be bound to clone *pLysN 5G1 R-2b*.

Another conducted analysis method was Western blot (figure 4.22**D**-**F**) ran with the clone and visualized with the two different 2° Ab-HRP. This was done first, to proof the presence of Abs in the delivered supernatent and second, to show the matching of 2° Abs to the clone. Figures 4.22**D** and **E** show the Coomassie and Ponceau staining, respectively, which confirmed proteins being present on the gel and also successfully transferred to the membrane. The results of the chemiluminescence of the Western blot indicated clearly no interaction of *pLysN 5G1 R-2b* with the IgG2b-HRP from Munich (figure 4.22**F**, left) but instead with the 2° Ab-HRP from the FMP (4.22**F**, right). Consequently, there were Abs present in the supernatent, but none of the subclass, which was determined at the Helmholtz Zentrum before.

All observations from the various ELISA experiments as well as the Western blot taken together led to the conclusion, that it was not possible to detect any substrate interaction with the Ab pair delivered from the collaboration partners and furthermore, that probably no recognition of the target substrates took place at all. Hence, the primary screen conducted at the Helmholtz Zentrum Munich was repeated and revealed indeed no positive immune response to pLys peptide **47** or the mimics anymore. Apparently, the generated clone was not stable and lost over time.

4.5.6 Conclusion and Outlook

The goal of this project was the generation of a monoclonal α-pLys-Ab with the help of prior designed pLys mimicking molecules. Three different immunogen architectures were approached, but only two of them could be successfully synthesized. It turned out, that a controlled homobifunctional linkage targeting amines was challenging regarding protection group strategy and final conjugation reaction.

Alternative to an aldehyde-based linker, squaric acid diesters also enable the conjugation of two amines (figure 4.23**A**) and could have been tested as well. Their selective reactivity for amino- over other functional groups has been introduced by Tietze *et al.* in 1991 and since then developed for the preparation of glycoproteins as vaccines.[281,282] Particularly appealing for working with proteins are the mild reaction conditions and the high control over the conjugation sequence. While the first ester reacts at pH 7, the second is modified only at basic conditions and hence, a low amount crosslinking products is expected. Nonetheless, no systematic study is known, which deals with the suitability of squaric acid derivatives for Ab generation with regard to conjugation efficiency, conjugate stability or immunogenicity of the cyclobutenedione moiety. However, a recent study by Straßburger *et al.* applied this very concept to immunize mice with a *mucin 1*-derived glycopeptide, which was linked at its *N*-terminus *via* squaric acid to *tetanus toxoid* as carrier protein. Thereby, the rigidity resulting from the cyclobutenedione ring was lowered by incorporation of a

PEG-linker between glycopeptide and squaric acid. [283]

Instead of the connection of two amine functionalites, it could have been more elegant to choose a heterobifunctional linkage, which connects the carboxylic acid of the mimic to ϵ-amines of Lys residues on the carrier protein. By doing so, the *N*-terminus of the AA could have been acetylated and thereby being protected from an attack by the linker. The linker itself could have been installed as ester or amide depending on the desired antigen properties (figure 4.23**B**).

Besides the linker strategy, the immunogen architecture was strongly influenced by the choice of the carrier protein. An alternative approach to the application of proteins for increased immunogenicity might be presented by the supramolecular structures formed with branched peptide–carbohydrate conjugates. [284] Thereby, the monomers are synthetically obtained and can be tailored to the requirements of each immunization target. Haptens can be introduced to the self-assembling molecules *via* reactive handles such as alkynes. It could be shown that supramolecular polymers originating from peptide–carbohydrate monomers show low toxicity and efficient cellular uptake facilitated by the carbohydrate units. [284]

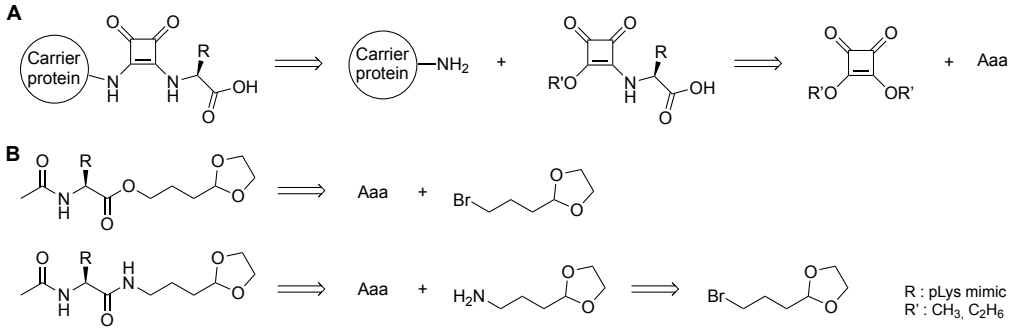

Figure 4.23: **A**. Squaric acid-based homobifunctional linkage strategy for subsequent coupling of antigen and carrier protein. **B**. Possibilities for alternative antigen design by coupling the linker to the *C*-terminus of the AA.

With the immunogens, more than twenty different immunizations were conducted at the Helmholtz Zentrum Munich, from which only one clone recognizing pLys but not Lys could be generated. This clone was evaluated at the FMP in elaborated ELISA studies, which have been designed and optimized for this purpose. Unfortunately, the indirect as well as the capture assay indicated no recognition of any substrate by the obtained clone. Further analysis by Western blot revealed no Ab of the previously determined subclass in the supernatent. These negative results were confirmed in repeated screens of the hybridoma cells, which proved the loss of the generated clone.

Besides the two applied analogues, other structures could be utilized as pLys mimics, e.g. sulfonates or fluorophosphonates. Since this project was primarily directed towards immunization with the hCys-derived phosphonate and the Nle-derived phosphate in various immunogen architectures, other possible haptens will be discussed in chapter 5.

In case this project will be resumed at one point or other targets for Ab generation will be defined, the knowledge gained during the present study could be applied again, may it be the synthetic findings, the established ELISA protocols or the preliminary thoughts about a possible high throughput evaluation by microarray analysis. Since the desired Ab was to be sequence-independent, a large variety of peptides was supposed to be tested during evaluation phase. For this emergence, immunogen microarray offers a technique to analyze many samples in a short

amount of time and with minimum material input. A possible collaboration with the BAM Berlin was heralded and could be continued then.

A last reasonable conclusion from this project might be to realize the extent of a challenge the generation of Abs poses. A very precise design of antigens as well as immunogens is necessary to find the suitable answer for a mostly unknown question. Also, the importance of thorough evaluation was revealed as many error sources are hidden within the analysis process and need to be examined from several different angles. The smart combination of various techniques can help to find not only suitable but also correct answers eventually.

4.6 Development and Optimization of Proteomic Protocols for Phospho-Lysine Detection

4.6.1 Outline of the Project

The quest for novel proteins or PTMs is based on cell extract preparation and analysis. The intrinsic acid and thermal lability of phosphoramidates has created an additional challenge since conventional protocols involve acidic treatment and protein digestion at elevated temperatures among other things. Recently, large efforts have been made to adjust existing or develop new protocols which are suitable for pHis [78,234,238] or pArg [83,84] site identification in cell samples. Besides the sample preparation, mass spectrometric methods have a huge impact on the possibility to detect labile PTMs. In this context, mild fragmentation techniques with fine-tuned parameters could help to identify pLys on synthetic peptides. [97,153,235,239] Nonetheless, no encompassing strategy which enables pLys identification *in vitro* or *in vivo* is known so far.

The aim of this project was the evaluation and optimization of existing proteomic protocols for their practicality for Lys phosphorylation. The first part of this work dealt with histone-focused cell extracts based on preliminary reports from Smith *et al.* on the pLys occurrence in histone H1 in the early 1970s. [90–93] The goal was the establishment of a workflow from cell culture to nano-LC/MS analysis. Thereby, cell extract preparation, selective enrichment and derivatization were included and examined on their pLys suitability.

The second focus of this part lied on phospho-specific enrichment techniques. As mentioned above, powerful procedures have been developed for pHis [78,234,238] as well as pArg [83,84] recently, thus, the investigations for the present study were based on those. To begin with, the main interests were the establishment of analytic techniques in the FMP facilities and determination of limit of detection for pLys samples.

4.6.2 Responsibility Assignment

This project was highly interdisciplinary and characterized by strong cooperative work with Martin Penkert (FMP Berlin, now BASF AG). The concepts of both project parts were developed together with Eberhard Krause (FMP Berlin) and Christian Hackenberger. Syntheses either small molecule, peptide or protein related and cell culture as well as cell extract preparation were conducted by Anett Hauser. Different high pressure LC-based enrichment techniques were elaborated by Martin Penkert. Also, mass spectrometric methods were optimized and data processing supervised by him. The beads-based enrichment of phospho-peptides was done by Anett Hauser with great advise from Sabryna Junker (University of Greifswald).

4.6.3 Optimization of Histone Extraction and Preparation for Tandem-MS Analysis

As mentioned above, research from the Smith group showed pLys occurrence on histone H1. [90–93] However, no profound study regarding the exact phosphorylation site identification is known to date. Targeted isolation and analysis of histones from cells under conditions tolerated by

labile PTMs were the main concerns in this work. First, a workflow was designed and the individual steps investigated. Figure 4.24 shows the envisioned sample preparation process. During cell culture, no favorable adjustments regarding lower temperature could be made since this would interfere with the homeostasis of cells. From obtained cell extracts, fractions of lysate proteins and nuclear proteins were to be prepared (see section 4.6.3.1). In order to separate histones from nuclear debris, a weak cation exchange (WCX) chromatography was to be employed. This principle was used by Chen *et al.*[92] and should be transferred to state of the art instruments and sample amounts (see section 4.6.3.2). With enriched histones in hand, tandem-MS was supposed to be approached. In order to do so, enzymatic digestion of the proteins was necessary. Trypsin, which cuts *C*-terminal to Lys and Arg residues, was the protease of choice. Due to the fact that histone sequences are rich in basic AA residues, trypsin treatment of histones would have led to short and highly positively charged peptidic fragments eluting in the desalting step of the subsequent LC and therefore not being analyzed *via* MS/MS. Thus, a derivatization technique for histones was examined, which would result in masked Lys residues and yield longer, more hydrophobic peptides during proteolysis (see section 4.6.3.3). The analytical separation method by nano-LC has been optimized already[97] and further adjustments of the fragmentation parameters during tandem-MS have been evaluated.[235,239]

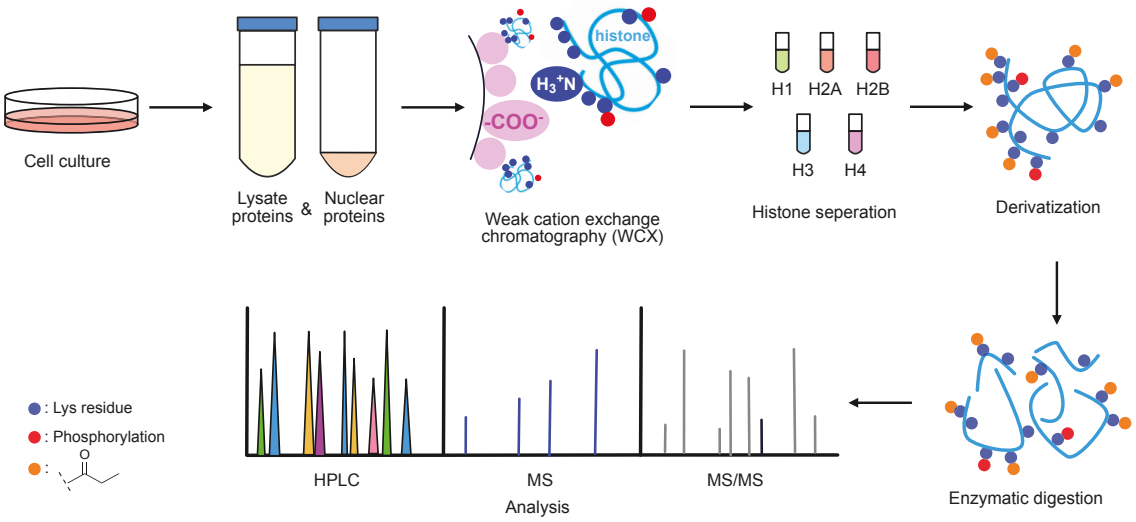

Figure 4.24: Envisioned procedure of selective histone extraction from cell culture.

4.6.3.1 Comparison of High-Salt and Acidic Isolation Protocols

In 2007, Shechter *et al.* published a comparative study regarding extraction of histones.[285] Within that, a conventional acidic and a high-salt treatment during cell lysis were described. Thereby, the acid applied was 0.2 M sulfuric acid, while 2.5 M sodium chloride was used for the high-salt extraction. These two procedures were exercised with Walker-256 rat tumor (W256) cells, from which pLys containing histone H1 had been isolated previously.[92,93] Throughout the experiments, some distinct differences were observed for the acidic and the high-salt extraction. First, the high-salt protocol required more steps and thus, longer sample preparation time. Second, the pellets formed during centrifugation steps were more dense and firm for the acidic treatment. As

a consequence, each separation of supernatant and insoluble pellet was more difficult with the high-salt procedure. Third, after the final isolation of histones from nuclear debris, dialysis and lyophilization were conducted, which yielded acidic samples with a pH of 3-4 for the acid extraction and slightly basic samples of about pH 8 for the high-salt extraction. Subsequent SDS-PAGE analysis revealed some differences as well (figure 4.25). Not only the concentration of proteins obtained by acidic treatment (lane **A**) was higher than in the sample of high-salt extraction (lane **B**), the total number of proteins also seemed higher. Besides that, a proper enrichment of histones was not observed except H2B (band **4**) and H4 (band **6**). On the other side, the high-salt protocol delivered less proteins in a lower concentration. Nonetheless, the bands for all histones were clearly distinguishable from the residue sample. In summary, the acidic isolation procedure was faster and more convenient in general. But, considering the intrinsic lability of phosphoramidates, this protocol cannot be applied for histone enrichment with regard to pLys identification.

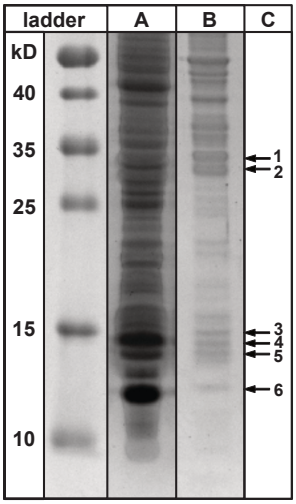

Figure 4.25: **A** & **B**. SDS-PAGE (15%, Coomassie stained) analysis of acid extraction (**A**) and high-salt isolation (**B**) of histones. **C**. Identified bands by band excision, in-gel digest and MS/MS analysis; **1**: H1, **2**: H1, **3**: H3, **4**: H2B, **5**: H2A, **6**: H4.

4.6.3.2 Establishment of Weak Cation Exchange Chromatography

The basic principle of cation exchange chromatography is increased retention of positively charged molecules compared to negatively charged or neutral ones. Thereby, strong cation exchange (SCX) is usually applied for peptides and small molecules, while WCX can be utilized to separate proteins.

The main work for this project part was conducted by Martin Penkert and thus, is summarized and published within his doctoral thesis.[239] Briefly, starting from a mixture of proteins with various isoelectric points (pIs), a 2-(*N*-morpholino)ethanesulfonic acid- (MES-)buffered gradient system with increasing sodium chloride concentration over time was established. A mixture of five proteins was chosen for method development: *β-casein*, BSA, *β-lactoglobulin*, *myglobin* and *cytochrom c* (cit *c*) with pI 4.5, 4.7, 5.1, 7.1 and 10.2, respectively. According to these values, four proteins exhibited a pI lower than histones and only cyt *c* had its isoelectric point in the range of histones.[286,287] Indeed, as shown in figure 4.26, cyt *c* was eluted from the stationary phase much

later than proteins with lower pI. Nonetheless, these promising results could not be transferred to samples containing histone H1, H2A or H2B. These proteins were injected either individually or in spike-in experiments and from none of the injections histones were detected in any collected fractions. This unsatisfying recovery indicated a very strong interaction of the histones with the stationary phase. This might be due to the unique charge distribution within the histones. Their *N*- and *C*-terminal domains are highly positively charged, so their 'local' pI is probably much higher than the reported pIs for the whole proteins. In accordance with that, it seemed that the histones were not eluted from the column at all. This assumption could be shown by increasing the salt concentration and thereby initiate the histone basic residues displacement from the stationary phase. Unfortunately, these experiments have never been conducted so far.

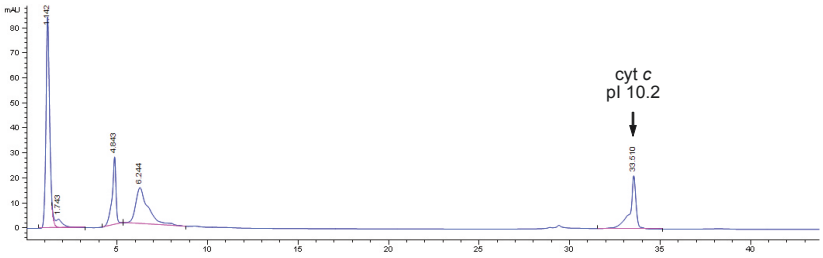

Figure 4.26: Chromatogram of the WCX separation of *myoglobin*, BSA, *β-casein*, *β-lactoglobulin* and cyt *c* with a clear retention time difference to the other proteins. Figure adopted from Penkert. [239]

4.6.3.3 Derivatization of Lysine Side Chains and *N*-terminal Amines in Peptides and Histone H1 by Propionylation

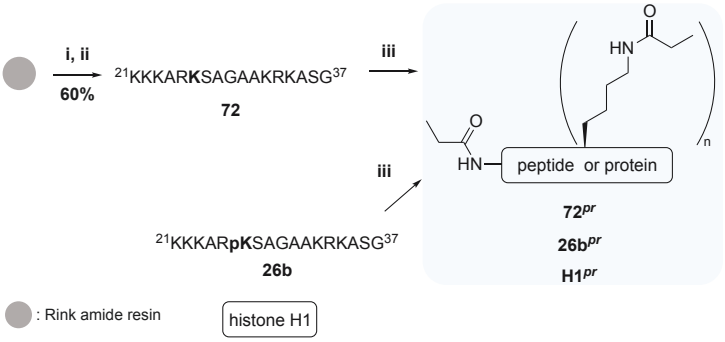

Scheme 4.15: Synthesis route to propionylated peptides **72**^{pr}, **26b**^{pr} and protein **H1**^{pr}. Reagents and conditions: **i**) Fmoc-SPPS; **ii**) TFA:TIS:H_2O (95:2.5:2.5, v/v/v), r.t., 2 h; **iii**) $Prop_2O$:MeOH (75:25, v/v), 100 mM NH_4HCO_3, pH 8, 30 °C, 20 min.

Derivatization of basic residues in histones is a common principle to alter the retention behavior and proteolytic fingerprint of these proteins. By amidation of lysine side chains, their charge is neutralized and their hydrophilic character diminished.[218,288] Propionic anhydride ($Prop_2O$) is commonly applied to obtain proteins wherein the modification can be distinguished from common PTMs, especially Lys acetylation.

The protocol was transferred in several steps within the present study. First, a histone H1 derived peptide presenting six Lys residues and over all seven possible derivatization sites was chosen. This sequence was either applied as unmodified **72** or mono-phosphorylated peptide **26b** (see

section 4.4) Second, full length histone H1 was propionylated. Since to date no synthesis method is known to produce site-selective Lys phosphorylation on proteins, only unmodified H1 was derivatized. All substrates could be propionylated to sufficient extend within thirty minutes incubation under slightly basic conditions (scheme 4.15).

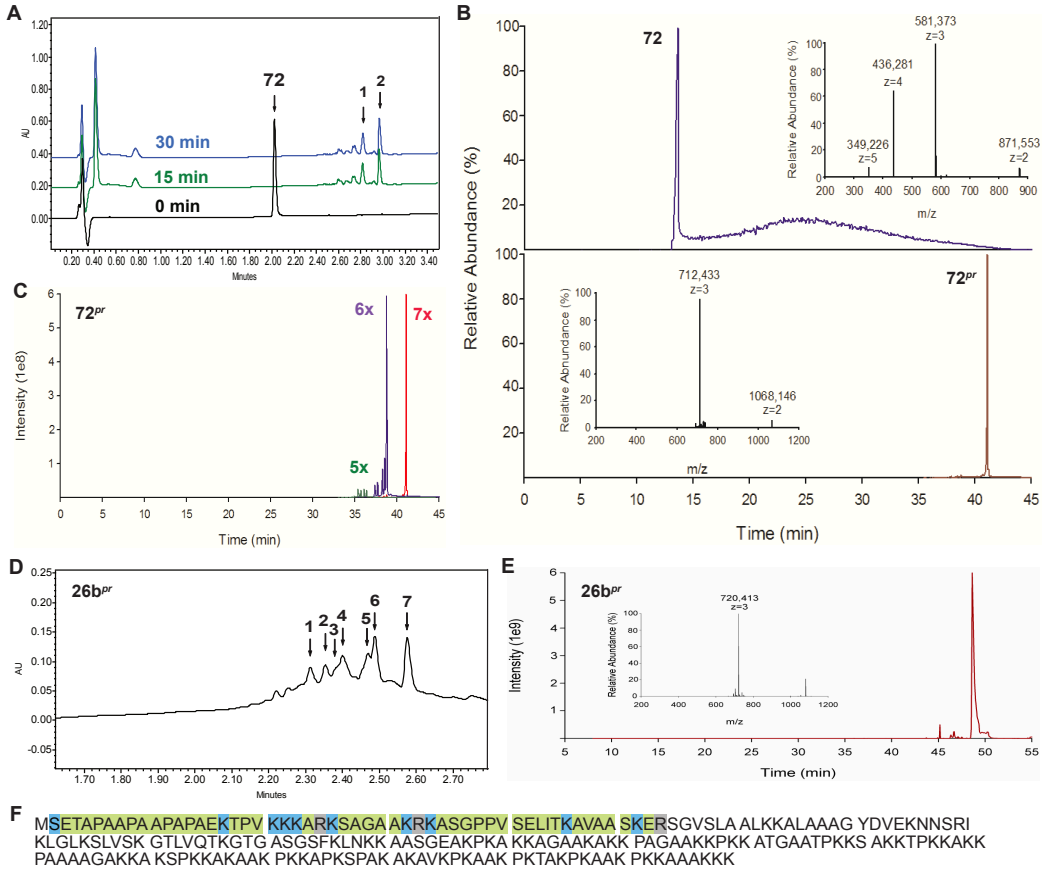

Figure 4.27: Results of derivatization experiments with histone derived peptides **72** and **26b** as well as histone H1. **A**. UPLC chromatograms of the propionylation of **72**. — time zero, — 15 min, — 30 min; **1** six times, **2** seven times modified. **B** Nano-LC TIC curves for **72** and $\mathbf{72}^{pr}$. **C**. Abundance of propionylation events in $\mathbf{72}^{pr}$ by XIC. — five times, — six times, — seven times modified. **D**. UPLC chromatogram of $\mathbf{26b}^{pr}$ after 30 min reaction time. **1** three propionylations, pLys intact; **2** four propionylations, pLys intact; **3** five propionylations, no pLys; **4** five propionylations, pLys intact; **5** six propionylations, no pLys; **6** six propionylations, pLys intact; **7** seven propionylations, no pLys. **E**. Nano-LC TIC curve of $\mathbf{26b}^{pr}$. **F**. Sequence of analyzed, propionylated histone $\mathbf{H1}^{pr}$ after pseudo-ArgC digest with indices for sequence coverage (green), propionylation sites (blue) and cleavage positions (gray). Figure **B**, **C**, **E** and **F** adopted from Penkert. [239]

Figure 4.27 summarizes the results of these experiments. It could be shown, that on the peptide level, full conversion was already achieved after 15 minutes since no change in the UPLC chromatogram was observed between 15 and 30 minutes reaction time (figure 4.27**A**). Furthermore, a distinct retention time shift was observed during UPLC and nano-LC analysis proving the higher hydrophobicity of $\mathbf{72}^{pr}$ (figure 4.27**B**). Also, UPLC and nano-LC showed the formation of several propionylation species wherein the completely modified peptide was the most abundant (figure 4.27**C**). Derivatization of pLys peptide **26b** yielded also several species as shown in figure 4.27**D**. Partial hydrolysis of the P–N bond led to a higher complexity in the chromatogram. As revealed by MS, the most abundant species were the one with six propionylations and intact phosphoramidate and the peptide with seven propionylations after loss of the phosphorylation (peak **6** and **7** in figure 4.27**C**, respectively). Tandem-MS confirmed the presence of desired prod-

uct with the sequence Lys^{pr}2-Lys^{pr}-Lys^{pr}-Ala-Arg-**pLys**-Ser-Ala-Gly-Ala-Ala-Lys^{pr}-Arg-Lys^{pr}-Ala-Ser-Gly^{CONH_2} (figure 4.27**E**).

Modification of H1 and subsequent enzymatic digestion with trypsin led to peptides originating from a pseudo-Arg-C digest. Figure 4.27**F** shows the detected sequence of **H1**^{pr} with all Lys residues being propionylated (blue highlights). Thereby, longer peptides were generated since trypsin could not cleave after Lys^{pr} but only after Arg residues (gray highlights). This peptide length was suitable for fragmentation to determine the sequence. Besides satisfying sequence coverage in the *N*-terminal region, no further cleavage was observed in the rest of **H1**^{pr}. The only remaining Arg^{79} had not been recognized by trypsin. Thus, no peptides from the globular or *C*-terminal region have been generated. For a higher sequence coverage in this part of **H1**^{pr} another protease should be applied in addition to trypsin.

4.6.4 Evaluation of Phospho-Specific Enrichment Techniques

Besides a tailored workflow for histone focused proteomics, phospho-selective enrichment protocols were tested. Among these, recently published studies on pHis enrichment with Fe^{3+}-based immobilized metal affinity chromatography (IMAC) [78,234,238], non-canonical phosphorylation detection by strong anion exchange (SAX) [100] and pArg identification by titanium dioxide-based metal oxide affinity chromatography (MOAC) [83,84] were of interest (figure 4.28). The experiments to introduce IMAC as well as SAX to the MS facility have been conducted by Martin Penkert and thus, were summarized in his doctoral thesis. [239] Briefly, both chromatography techniques were established and applied for different cell lines. Indeed, an enrichment of phosphorylated over non-phosphorylated peptides was achieved. Nonetheless, neither endogenous pLys substrate was detected nor spiked-in model pLys peptides were recovered. These results indicated a loss of phosphoramidate throughout the process.

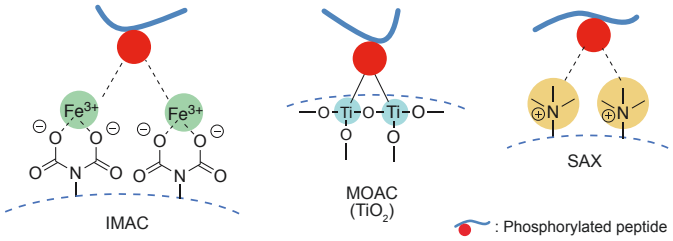

Figure 4.28: Possible enrichment methods for phosphorylated Lys proteins and peptides.

4.6.4.1 Applicability Testing of a Titanium Dioxide-Based Enrichment

The TiO_2-based phospho-peptide enrichment was conducted in accordance to the published protocol by Junker *et al.* [83] Cell extracts from different cell lines such as HeLa, HEK293 and W256 were prepared following a procedure suitable for labile phosphorylations as shown by Potel *et al.* [78] Adjustments have been made mainly regarding the centrifugation steps to ensure proper sedimentation of the beads and later complete elution (see Experimental Part, section 6.7).

The peptides obtained after enzymatic digest were redissolved in buffer of either pH 2.7 or 3.2 and incubated with TiO_2 beads (figure 4.29). After centrifugation and separation of the layers, the

supernatent was employed in further iterations to catch low abundant phospho-peptides as well. From the residual beads, the peptides were eluted under basic conditions into acidic media to immediately neutralize the samples. After evaporation of solvent by vacuum centrifugation, the samples were analyzed by nano-LC/MS.

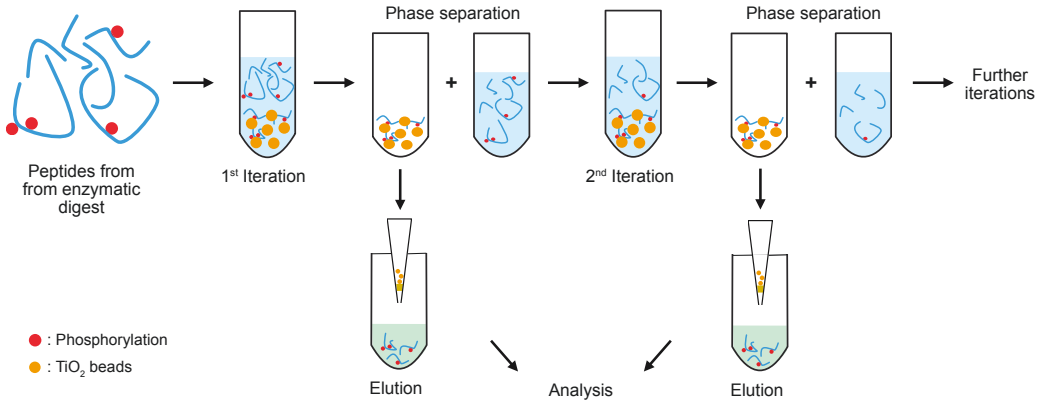

Figure 4.29: Workflow of phospho-specific, TiO_2-based enrichment.

Unfortunately, no distinct enrichment of phospho-peptides was observed as mostly non-phosphorylated peptides were detected. Furthermore, also synthetic, spiked-in pLys substrates were not recovered. Since not even the non-phosphorylated model peptides could be detected, P–N bond hydrolysis did probably occur during the binding step as the peptides remained in the solution phase throughout the whole experiment. Taking the time consumption and results into account, the TiO_2 beads-based strategy was not suitable for a selective pLys enrichment.

4.6.5 Conclusion and Outlook

The two main goals of this project were the establishment of a histone focused cell extraction procedure and the evaluation of recently published phospho-selective enrichment protocols.

The first part was devoted to systematically develop a pLys-suitable strategy for histone enrichment. Even though a functioning cell extraction protocol was adopted [285] and the downstream WCX established as well as a derivatization procedure implemented, some flaws remained elusive. The recovery of histones from WCX separation has not been shown and the unknown whereabouts were not clarified. In order to to so, other solvent compositions could be tested. Regarding the propionylation, histone H1 phosphorylated on Lys has not been tested. This experiment should be done to evaluate suitability for labile phosphorylations also on the protein level.

A completely different strategy would be to take up the histone isolation applied by the Smith group to show pLys occurrence. [93] This protocol included also a high-salt extraction with 1 M NaCl and further precipitation steps to separate nucleotides and nucleic acids from nuclear proteins. [289] By adopting the previously successful protocol, the results might be reproduced and further elucidated regarding the phosphorylation sites.

The second part of this project was dedicated to phospho-selective enrichment methods. Three different techniques were established either by Martin Penkert [239] or Anett Hauser. Focusing on the TiO_2-based MOAC approach, no suitability for the labile Lys phosphorylation could be shown. Future experiments to explain those observations could apply higher amount of spiked-in pLys

peptides to find a critical concentration, above which pLys can be recovered, thus the limit of detection. Other tests could include successive analysis of every step to find the weak point in the protocol. It could be that the P–N bond hydrolysis occurs upon interaction of phosphoryl oxygen with the beads and the accompanying change of electronic environment. To proof this hypothesis, samples should be analyzed in presence and in absence of TiO_2 beads.

As conclusion for pLys-focused proteomics, the presented studies showed, which conditions are not applicable for the labile modification. Even though some advancement in the histone analysis has been made, no omnipotent strategy was found. Also other known phospho-specific enrichment methods, [99,228,229] which were discussed in the Introduction, section 2.2.5 and tested in the meantime were not useful for Lys phosphorylated peptides. So far, it is only known with which strategies pLys can not be isolated and identified.

4.7 A Fluorescence Tag for Phosphorylation Degree Determination

4.7.1 Outline of the Project

Tracking phosphorylation and dephosphorylation events in real time is a powerful tool to study enzyme–substrate interactions or the stability of proteins and peptides. With the introduction of 8-hydroxy-5-(*N*,*N*-dimethylsulfonamido)-2-methylquinoline, or sulfonamidoxine (Sox) into peptide and protein sequences, the Imperiali group presented a chelation-enhanced fluorescence (CHEF) kinase activity probe for Ser, Thr or Tyr residues,[208–211] which could be applied for the detection of pHis and pArg events very recently as well.[202,212]

In accordance wit these reports, the aim of this project was the expansion of the Sox-based CHEF to pLys substrates (figure 4.30). Thereby, model peptides containing Lys residues and Sox were designed to show the fluorescence increase upon phosphorylation of Lys. So far, no Lys-selective kinase is known so the phosphorylation was to be introduced chemically. The Sox probes were envisioned to be applied in PAH activity or other P–N bond hydrolysis assays, whereby CHEF was supposed to allow a real-time detection of the phosphorylation degree on Lys at low concentrations. Compared to photometric read-out or analysis by UPLC-MS, this principle required very few sample amount and no additional preparation step.

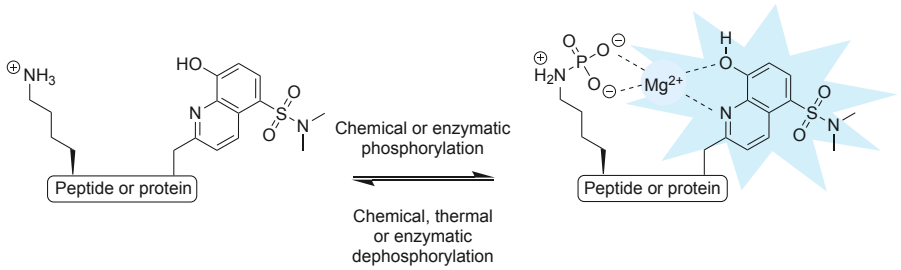

Figure 4.30: Possible chelation-enhanced fluorescence (CHEF) upon phosphorylation of Lys residues.

4.7.2 Responsibility Assignment

The concept was planned by Anett Hauser and Christian Hackenberger. Substrate design and synthesis as well as fluorescence measurements were carried out by Anett Hauser with executive help from Eleftheria Poulou. Structure elucidation by NMR spectroscopic analysis was conducted by Peter Schmieder. Data was processed and evaluated by Anett Hauser.

4.7.3 Design and Synthesis of Sox-Tagged Probes

CHEF probes were to be arranged in that way to investigate two properties initially: first, the event of increased fluorescence upon interaction of Sox with pLys and second, the distance dependence of fluorescence intensity enhancement. Thus, peptides with varying number of AAs between the phosphorylation site and Sox were aimed for.

Conveniently, the phosphoramidate should be installed *via* the Staudinger-phosphite reaction to ensure site-selective phosphorylation. As described in section 4.1, caged phosphoramidates

were usually prepared with photo- or base-labile protecting groups requiring either irradiation or treatment with 250 mM sodium hydroxide solution to generate the free pLys, respectively.[97,153] Another approach would have been the incorporation of the novel, Tc-caged pLys **1** during SPPS (section 4.1), which could be deprotected by hydrogenation under slightly basic conditions. In order to decide which strategy fitted best, a test peptide generously provided by Barbara Imperiali was incubated under various conditions and its stability evaluated by UPLC-MS analysis.

Table 4.10: Testing of Sox stability under Staudinger-phosphite reaction and various deprotection conditions.

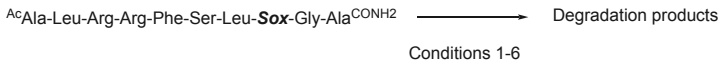

#	Condition	c [mM]	ϑ [°C]	Time [min]	Degradation product [UPLC-MS]
1	DMF	25	45	2880	*
2	3 eq. **9**, DMF	25	45	2880	*
3	297 nm, MeOH	7.5	r.t.	20	*N*-oxidation
4	250 mM NaOH, dioxane	10	r.t.	15	fluorophore elimination
5	H_2, Pd@C, $(NH_4)_2CO_3$, EtOH, pH 9	2	4	120	fluorophore elimination
6	H_2, Pd@C, $(NH_4)_2CO_3$, EtOH, pH 7.5	2	4	120	ring hydrogenation

* no degradation was detected

Table 4.10 summarizes these experiments. It could be shown that during the Staudinger-phosphite reaction (entries **1** and **2**), no change in UV intensity for the test peptide was observed. Unfortunately, the uncaging conditions for both, a photo- and a base-labile phosphoric ester (entries **3** and **4**, respectively), were not suitable with the Sox peptide. Among other masses, *N*-oxidation of the pyridine moiety as well as fluorophore elimination were observed. Also, Tc-deprotection conditions led to degradation of the test peptide, either at pH 9 or at pH 7.5, whereby the latter would probably not yield in Tc-cleavage at all as discussed in section 4.1.

Scheme 4.16: Synthesis route to Sox probes **73**-**79**. Reagents and conditions: **i**) Fmoc-SPPS; **ii**) TFA:TIS:H_2O (95:2.5:2.5, v/v/v), r.t., 2 h; **iii**) **A**: **35** (200 eq.), 50 mM NaH_2PO_4, pH 8, 21 °C, 3 d or **B**: **35** (1,000 eq.), 10 mM KOH, pH 10, 21 °C, 5 d.

According to the stability tests, no known procedure for the site-specific introduction of pLys was appropriate with the Sox residue. Thus, the global phosphorylation with phosphoramidate **35** (K-PA, see section 4.4) was applied. Therefore, peptides **73**-**77** were designed in a way that no K-PA reactive AA was included in the sequence as shown in scheme 4.16. While **73**, **74** and **75** were synthesized to investigate the distance dependence of Mg^{2+}-induced CHEF, peptides **76** and **77** were

prepared to ensure phosphorylation on Lys and not on the *N*-terminus or Tyr. The phosphorylation itself was carried out following two different procedures described recently by Choi *et al.*[202] (**A**) and Hu *et al.*[101] (**B**) for His and Lys phosphorylation, respectively. Pleasingly, for all peptides mass-to-charge ratios (m/z) according to phosphorylated species could be detected by UPLC-MS analysis, even though the conversion was higher for the non-acetylated substrates.

Peptides **78** and **79** were synthesized as positive and negative controls for the CHEF effect with one AA between Sox and pSer (or Ser), which had been described as an efficient distance for increased fluorescence yield.[211]

4.7.4 Fluorescence Measurements

Fluorescence measurements were conducted according to the previously described procedure.[211] Peptide stock solutions were prepared in ddH_2O and their concentration photometrically determined to set up phosphorylation reactions under precisely defined conditions. For fluorescence assays, the stock or reaction solutions were diluted to 15 µM with sample buffer containing 20 mM HEPES and 10 mM magnesium chloride.

In a first experiment, the reference peptides **78** and **79** were measured to test the functionality of the set up (figure 4.31**A**). Indeed, a 3.2-fold increase in fluorescence was observed upon phosphorylation of Ser.

Next, the suitability of reaction solutions for CHEF was tested since the chosen synthesis approach involved additional challenges for the fluorescence measurements. Purification of the phosphorylation reactions was avoided to give access to real-time analysis. This meant that fluorescence measurements were done with samples containing significant amounts of **35** and monosodium phosphate, indeed these reagents were present in higher concentrations than the substrates themselves. Thus, prior to the actual experiment itself, any disturbance based on the reaction solution was excluded. Therefore, Lys containing substrates **73**, **74** and **75** were dissolved only in water (figure 4.31**B**, – – –) or together with K-PA **35** and NaH_2PO_4 (figure 4.31**B**, ·····). The fluorescence spectra showed only very little change in intensity due to the reagents being present, and hence, the reaction solutions could be utilized directly in the assay.

Figures 4.31**C**-**H** show the fluorescence spectra of Lys substrates **73**-**78** before (·····) and after treatment with K-PA **35** (——). Exemplified for peptide **73**, also the mandatory presence of magnesium in the sample buffer to detect CHEF was shown. While dilution of samples in buffer containing Mg^{2+} led to 4.4-fold signal intensity (figure 4.31**C**), fluorescence values before and after **35** addition were almost identical when no $MgCl_2$ was added to the sample buffer figure 4.31**D**. Also with one and two AAs between Sox and Lys as in **74** and **75**, respectively, fluorescence intensity was increased approximately 3-fold upon incubation with **35** (figure 4.31**E** & **F**). Surprisingly, the *N*-terminally acetylated probes **76** and **77** exhibited almost no difference in fluorescence between K-PA-treated and untreated samples. The achieved increase was maximum 1.1-fold, which indicated no successful CHEF (figure 4.31**G** & **H**). This could be based on the fact that no phosphorylation occurred.

Since the difference between probes **73**-**75** showing successful fluorescence increase and **76**-**77** was particularly the acetylation of *N*-termini, a phosphorylation event on the α-amine of Glu instead of Lys side chain seemed likely. This phenomenon was investigated by NMR and tandem-

MS analysis, whereby the latter could not deliver conclusive results. Observation made during NMR experiments are discussed in the next section.

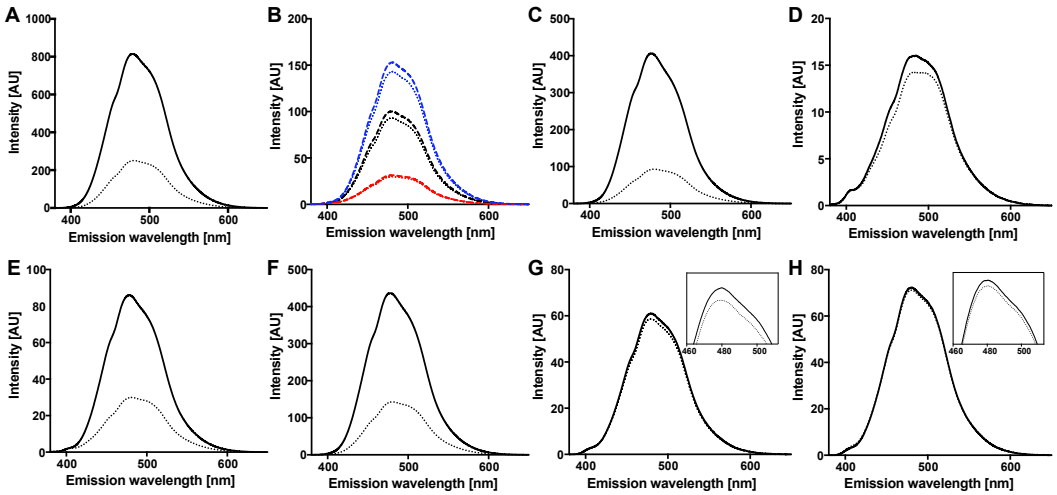

Figure 4.31: Fluorescence spectra of phosphorylated (——) and non-phosphorylated (····· or – – –) Sox-probes. λ_{Ex} 360 nm; λ_{Em} 380-650 nm. **A**. Reference values of pSer peptide **78** and Ser peptide **79**. **B**. Influence of K-PA **35** and NaH_2PO_4 on fluorescence of **73** (—), **74** (—) and **75** (—); ····· reaction solution; – – – ddH_2O. **C**-**H**. Fluorescence spectra of phosphorylation reactions of **73** in sample buffer with 10 mM $MgCl_2$ (**C**) or without Mg^{2+} being present (**D**) as well as of **74** (**E**), **75** (**F**), **76** (**G**) and **77** (**H**).

4.7.5 Phosphorylation Site Determination

Structure elucidation was conducted with three substrates: peptide **73** was chosen as reference for probes with free *N*-terminus, peptides **76** and **77** as acetylated ones. Figures 4.32**A** and **B** show the possible products, which could be obtained from incubation with K-PA **35**. Even though it has not been particularly reported and non-acetylated peptides have been employed for this procedure previously,[101,220] the possible by-product in the reaction of **73** is the formation of a phosphoramidate at the *N*-terminus.

The ^{1}H-^{31}P-HMBC revealed two distinct correlations in **73**, from one phosphorous species (δ = −6.86 ppm) to Glu_α and from another at δ = 0.44 ppm to Lys_ϵ. Nonetheless, this observation could not be confirmed from the 1D-^{31}P spectrum as no signal was visible at 0.44 ppm (figure 4.32**C**). These results indicated that pLys was present in the mixture but only to an insignificant amount. Similar information was obtained from NMR studies with the acetylated peptides **76** and **77**. Clear $^{3}J[^{1}H_\epsilon, ^{31}P]$ couplings were detected in the 2D experiments, but no or a very small signal was obtained from the ^{31}P experiments (figure 4.31**D** & **E**). Again, these observations confirmed small abundance of pLys in the samples.

With these results in hand, the contrary fluorescence intensities for non- and acetylated probes could be explained. In reactions with **73**-**75**, K-PA **35** attacked primarily the *N*-terminus and a phosphoramidate was formed successfully leaving the Lys side chain unnoticed. **76** and **77** did not exhibit an accessible amine at Glu and thus, only the Lys side chain could react. Apparently, this was way less reactive than an α-amine. Consequently, only small amounts of pLys were formed and negligibly small CHEF was detected. The lower reactivity could have several reasons. First, Lys was located in the sequence adjacent to Sox, which was bulky and could block the access to the

ϵ-amine. Second, the nucleophilicities of the relevant amines were different. The pK_a values of α-amine in Glu and ϵ-amine in Lys are in the same range, whereby the one of Glu is at 9.67 and Lys at 10.53.[290] Thus, the α-amine of Glu displayed a stronger nucleophile than the Lys side chain and was supposed to be more reactive in the phosphorylation reaction. Even though the pH was set to 8 and both amines were most probably protonated at this value, the α-amine was more likely to be partially deprotonated. By means of these two explanations, the different observations in the fluorescence assay could elucidated.

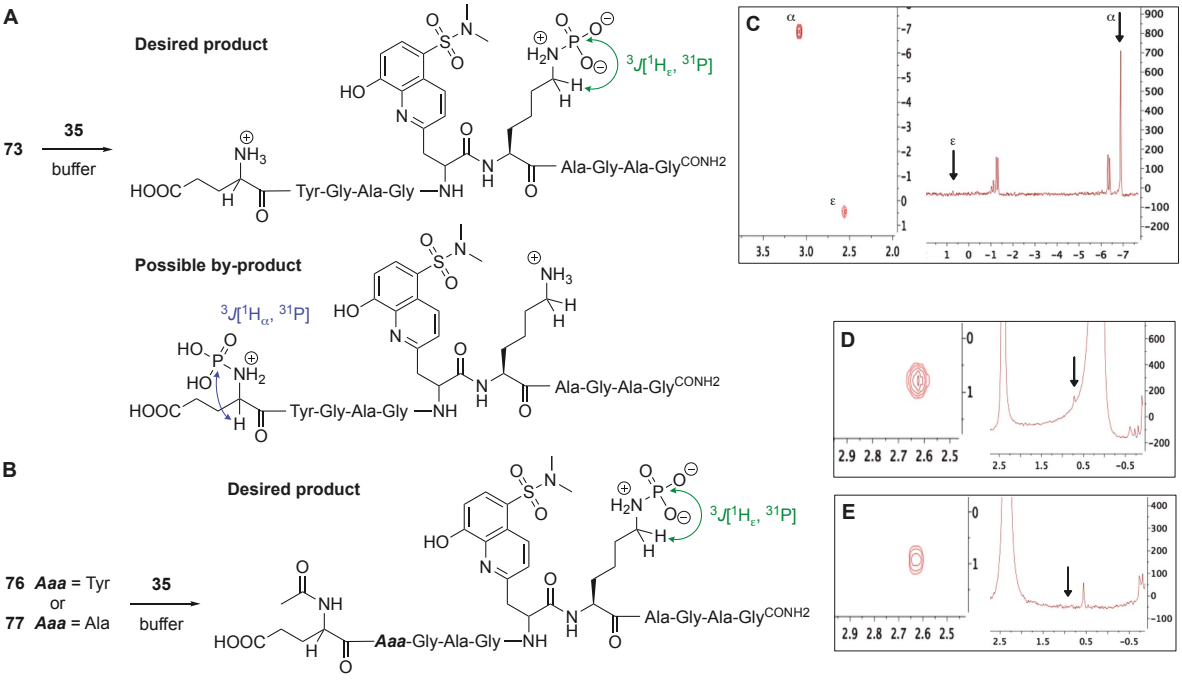

Figure 4.32: **A** & **B**. Structures of possible products from phosphorylation reactions with **73** (**A**), **76** and **77** (**B**) and characteristic ^3J couplings to identify the phosphorylation sites. **C**-**E**. ^{1}H-^{31}P-HMBC and ^{31}P spectra of **73** (**C**), **76** (**D**) and **77** (**E**). Arrows indicate where the peaks in the phosphorous spectra should occur.

4.7.6 Conclusion and Outlook

The aim of this project was the synthesis and application of pLys containing Sox probes. Since the convenient strategies for site-selective phosphorylation on Lys were not feasible in this study, a global phosphorylation approach with K-PA **35** was tested. Based on previous reports for pLys introduction with this reagent,[101,220] the substrates were designed, synthesized and tested. Highly deviating in fluorescence measurements and subsequent NMR experiments revealed poor reactivity of Lys side chains compared to high reactivity of α-amine in Glu. Hence, substrates exhibiting large CHEF were phosphorylated on their *N*-termini instead of Lys. Opposite to that, substrates with acetylated *N*-terminus were susceptible to Lys phosphorylation. Since this reaction proceeded to a very low extent, only small fluorescence intensity increases were detected.

In summary, the results indicated strongly that the published synthesis procedure[101,220] was not robust enough to transfer it to other Lys peptides or that the reported data on successful pLys formation is questionable. Besides that, observations during the fluorescence assay hinted to-

wards a larger scope for Sox-based CHEF. Between the *N*-terminus and Sox four AAs were incorporated. Still a fluorescence increase up to 4.4-fold was detected upon phosphorylation. The distance itself lied in the range of previously reported studies with Sox probes,[202,208–212] but so far no *N*-terminal phosphorylation was examined. Hence, the present study revealed another type of phosphoramidate exhibiting CHEF even though it was not the desired pLys.

Future experiments should focus on establishing another phosphorylation strategy, which is reliable and favored by Sox. Employing acetylated peptides was the first, crucial step. But since Lys was too inert even at pH 10, only an increased pH might enable successful phosphorylation with K-PA. This measure would not be suitable for Sox and thus, should not be applied. Another approach could be the installation of a photo-caged phosphoramidate, which can be cleaved faster or at a different wavelength. Maybe, the NPE-protected pLys can be applied with Sox when being deprotected with a laser instead of the UV lamp. Since a laser works more efficient, the reaction would be done much faster[97] and thereby, the Sox might stay intact allowing fluorescence real-time measurements of phosphorylation decay after all.

5 | Summary

The presented research was dedicated to Lys phosphorylation. Preliminary reports of its occurrence on histone H1 [91–93] hinted at the need to elucidate its biological function. Thereby, the intrinsic lability of phosphoramidates under elevated temperature or acidic conditions presented the main limiting factor in the application of conventional bio- as well as chemical strategies and proteomic protocols. Thus, this work tried to address the quest from different angles with the development and investigation of novel resources for the biochemical and biological toolbox. Along the lines of pLys endogenous site identification and characterization, several weak points were identified and tackled.

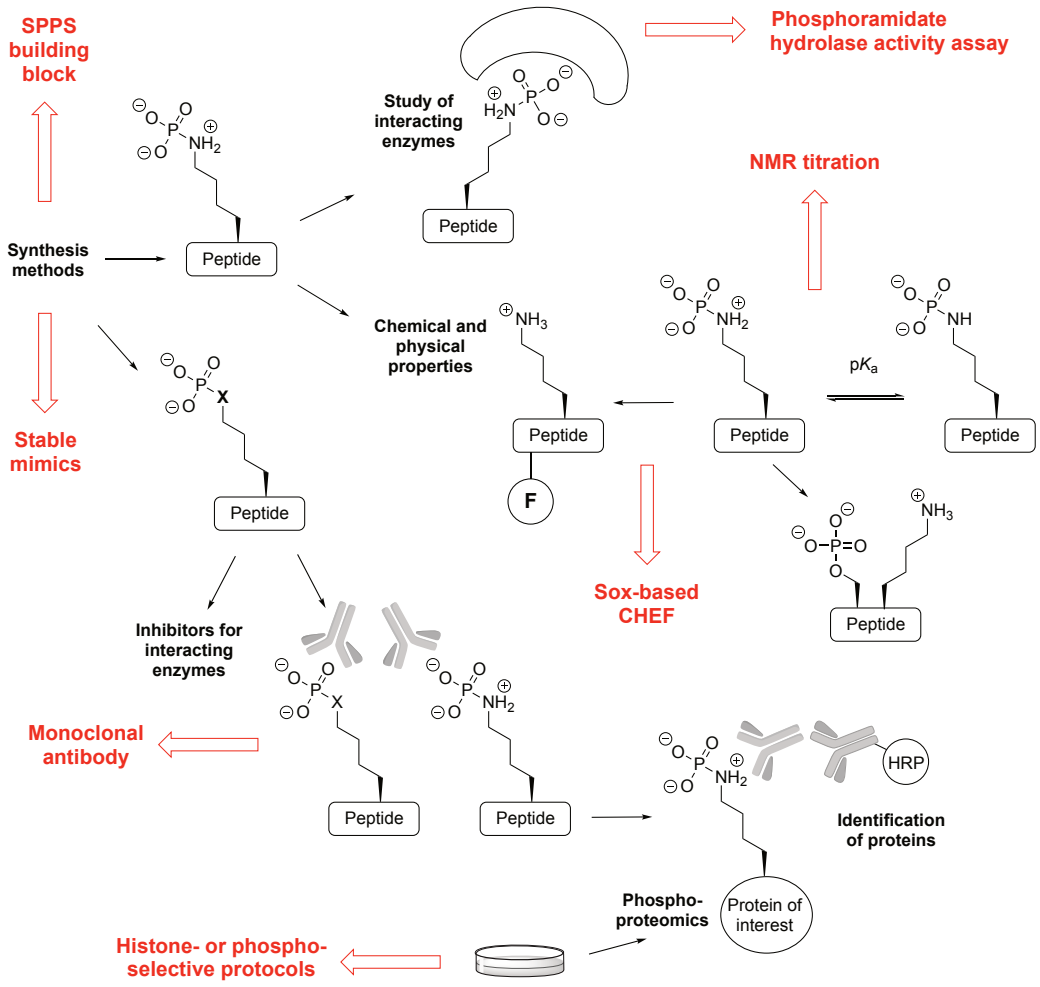

Figure 5.1: Study sites in the quest for Lys phosphorylation with different projects of this work being highlighted.

Throughout the whole work, synthesis design and optimization have been crucial. First, an alternative synthetic approach for pLys was tested, within which pLys introduction into peptides occurred during SPPS as a Tc-caged residue. Therefore, the Tc- and Fmoc-protected building block **1** was synthesized and tested. It could be shown that **1** is applicable for SPPS, and furthermore the subsequent hydrogenative deprotection could deliver free pLys peptides. Nonetheless, several by-products were formed during the synthesis steps, which indicated a narrow stability window of the Tc-caged peptides. As such, an attack of subsequent AAs during SPPS on the Lys side chain (**SP2**) and significant amounts of P–N bond-hydrolyzed peptide (**SP1**) were obtained. Even though the novel building block was ready to use and could deliver caged pLys peptides in a short time using less purification steps, it would not be the method of choice when aiming for high yielding syntheses.

Synthesis of model peptides has accompanied several studies of this work. In the second project, the protonation of ϵ-amine in pLys was investigated, which has never been done before. In order to do so, tripeptide **5** was prepared and subjected to NMR measurements at different, distinct pH values. As a result, two pK_a values could be calculated describing the deprotonation of phosphoryl oxygen and ϵ-nitrogen at pH 2.9 and 9.6, respectively, confirming an overall charge of -1 under physiological conditions as depicted in figure 5.1. This was in accordance with experiments conducted with *N*-(*n*-butyl)phosphoramidate.[74] The protonation of the side chain in pLys ought to be shown by a ^{15}N-NMR study with the labeled, same-sequence peptide **10**. This hypothesis was based on an expected significant change in the chemical shift of nitrogen upon protonation. Unfortunately, no one-bond correlations ($^1J[^1\mathrm{H}_\zeta,\ ^{15}\mathrm{N}_\zeta]$) were detected in any experiment and thus, no distinct proof for phosphoramidate nitrogen protonation obtained. Self-decoupling because of a high exchange rate of bound protons with protons in solution might have been responsible for this phenomenon. Future experiments with small molecules should circumvent complex NMR spectra and allow higher sample concentration. These experiments would be interesting not only for pLys investigation but for further mechanistic studies of the Staudinger-phosphonite and -phosphite reactions, because so far no distinct information about intermediate structures and bond formation is known.[150,160]

Besides chemical and physical properties of Lys phosphorylation, the selective interaction of the enzyme LHPP with various peptidic substrates was one research focus. On the basis of results from the 1990s,[203,204,249] the enzyme activity was proven to be significantly higher towards pLys substrates than other phosphoramidates – pArg and pHis – or common phosphates – pSer, pThr and pTyr – regardless of whether the pLys was presented as a monomeric AA **25a**-**f** or incorporated in a short peptide **27a**-**e**. A systematic study including AA mutations adjacent to the phosphorylation site presented here revealed a strong discrimination between peptide length and sequence. As such, longer peptides with a diverse AA sequence **26a** and **26b** suppressed the enzymatic activity completely. Furthermore, while substrate **27a**, which had only Gly and pLys in its sequence, led to approximately 38% enzymatically hydrolyzed substrate, only three out of twenty modified peptides – **28a**, **28i** and **29f** – exhibited a similar hydrolysis yield. These accessible peptides carried *N*-terminal Ala, Arg or *C*-terminal Lys modification. Thereby, the site of modification seemed to have a distinct influence and therefore, computational chemistry studies were conducted to investigate the substrate binding mode by free energy changes upon mutation from Gly to ***Aaa***. Indeed,

a trend was detectable reflecting the results of the modification's impact on enzymatic activity. Taking the results together, LHPP exhibited selective activity towards pLys in short peptides and hence, might be involved rather in metabolic processes than in protein synthesis. Another striking observation was the partially high P–N bond hydrolysis without enzyme being present. This phenomenon left less substrate to interact with LHPP and yielded decreased amounts of enzymatically hydrolyzed substrate. It also confirmed predictions of a correlation between phosphoramidate stability and the AA sequence surrounding the PTM. .

With the information gathered to this point, the potential of stable pLys mimics for the examination of Lys phosphorylation *in vitro* and *in vivo* became clear. Therefore, the design, synthesis and comparative characterization of two mimics were the goal of the next project. A hCys-derived phosphonate **18** and Nle-derived phosphate **19** were prepared as benzyl- and Fmoc-protected SPPS building blocks. Their improved stability compared to pLys could be proven directly during peptide synthesis as they were obtained with free phosphoryl oxygens after acidic cleavage from the solid support and were stored at room temperature for extended periods without degradation. Besides acid and thermal stability, their susceptibility towards PAHs and Pases was tested. It could be shown that the phosphonate peptide **23** was not hydrolyzed by LHPP or the promiscuous ALP, while the phosphate peptide **25** was stable against LHPP but could be addressed by ALP. Furthermore, a structural and electronic comparison with pLys was desired. This was approached by NMR titration experiments with **23** and **24** as already conducted with pLys peptide **5**. For both mimics, only the pK_a values for the deprotonation of the second phosphoryl oxygen could be calculated. Thereby, the results indicated phosphonate **23** being present in a balanced equilibrium between charges -1 and -2 and phosphate **24** being completely di-anionic under physiological conditions. Further calculations of electron densities and visualization in ESP maps revealed a higher similarity of monoanion phosphonate than phosphate with pLys. As such, two mimics exhibiting significant varying behavior were obtained. These could be applied for versatile approaches as, for example, protein inhibitory studies. With an additional feature, pull-down experiments would also be possible. As shown by Yang *et al.*, a diazirine moiety in Lys residues could be applied for capture of proteins interacting with post-translationally modified Lys. [291]

The project aiming for the generation of monoclonal, sequence independent antibodies against pLys for later affinity enrichment and identification represented another great application of the stable pLys mimics. In two different approaches, the antigen architecture as well as the carrier protein linkage were varied. First, highly randomized peptides with only one conserved site were synthesized to ensure sequence independence and recognition of amide bonds. Second, monomers were conjugated directly *via* glut-CHO, which facilitated sequence independence but lacked peptidic backbone properties. From various immunizations in rats or mice either with randomized OVA–phosphonate **36** and OVA–phosphate **37** or with monomeric BSA–phosphonate **40** and BSA–phosphate **41** only one clone was obtained, which showed an immune response towards pLys but not Lys substrates. This clone was to be tested for its selectivity, cross-reactivity, sensitivity and sequence independence by ELISA. Therefore, the conditions for indirect and capture ELISA were adjusted and optimized first. Throughout several experiments with His-tag- or biotin-labeled peptides, no recognition of pLys or any mimic was detected, while the positive controls for a functioning assay were successful. Western blot analysis and repeated examination at the collaborating

facilities revealed the loss of the generated clone, probably due to instability over time. To approach the generation of mAbs against pLys, several strategies are possible. With the same mimics, peptides randomized only in Gly and Ala instead of nineteen AAs could be applied. This was successful for Fuhs *et al.*, who generated the first mAbs against pHis.[187] It should be mentioned, that the Ala-Gly randomization itself was not chosen completely by accident but was rather similar to a sequence motif of *ATP-citrate lyase* (ACLY), which exhibits His phosphorylation. Besides that, different mimics could be designed as well to achieve higher congruence with pLys. As such, sulfonates are often applied to mimic phosphate groups as, for example, by Fuhrmann *et al.* during Ab generation against pArg.[191] α-Difluorophosphonates could in principle mimic electron density around the phosphoramidate nitrogen as they do as pSer and pTyr analogues.[292] But, since the results during NMR titration experiments indicated a positive charge on the ϵ-nitrogen (section 4.2), those difluoro compounds might also have lower mimicking properties and an electropositive group could be more beneficial. Silicium-phosphanes and -phosphonates have been described in the literature very poorly,[293,294] so they might present an interesting thought experiment as silicium originates from the same group in the periodic table as carbon but exhibits lower electronegativity.

Along with antibody affinity enrichment, several other techniques are known to approach proteomics and their suitability for phosphorylated Lys substrates was investigated during this work as well in a highly collaborative project. In accordance with initial reports of pLys occurrence in histone H1,[91–93] a tailored, histone-focused workflow was created and tested. This included the evaluation of different cell extraction protocols, establishment of enrichment as well as separation of histones by WCX and testing the derivatization of basic side chains. It could be shown that histones were enriched with high-salt extraction. WCX could separate proteins of varying pI values but no histone was successfully eluted from the solid phase. Derivatization of Lys-rich peptides with $Prop_2O$ kept phosphoramidates intact, led to longer retention during nano-LC and enabled high sequence coverage for the *N*-terminal region of H1. Even though good progress has been made so far for each step individually, no combination of all stages was achieved. Besides focusing on one protein class, also phospho-selective enrichment techniques like Fe^{3+}-based IMAC,[78] TiO_2-based MOAC[83] and SAX[100] were implemented at our laboratories and tested with pLys substrates. Strikingly, no Lys phosphorylation was identified with any of these methods and no spiked-in pLys peptide was recovered. So far, it is not known if a minimum concentration exists, above which Lys phosphorylation is detectable. Thus, the conclusion from those experiments was that there is no protocol reported yet, which is suitable for this labile phosphorylation.

To study pLys in low concentrations, the Sox-based CHEF was evaluated.[211] These kinds of probes would enable real-time measurements of the degree of phosphorylation in stability or kinase and PAH activity studies. For this purpose, several Sox probes were synthesized and phosphorylated with the global phosphorylation reagent K-PA **35**. In fluorescence measurements, a signal increase could be detected upon phosphorylation when Mg^{2+} was present. Nonetheless, structure examination revealed phosphorylation of *N*-termini instead of the desired Lys side chain. Even though no chelation to pLys could be shown, a novel type of phosphoramidate and its suitability for CHEF was demonstrated. These results displayed one drawback of the strategy. The Sox probes could not give information about the type and site of phosphorylation. Thus, only well defined

substrates should be applied. It might be worth investigating this observation to maybe find different criteria for distinguishing between several species like the fluorescence intensity, magnitude of increase and maximum emission wavelength. With this information in hand, more complex substrates could be examined, which present several possible phosphorylation sites. Regarding the synthesis of distinct pLys peptides, other phosphites or deprotection strategies, which are tolerated by Sox, could give access to a site-selective Staudinger-phosphite protocol.

Opportunities for Further Studies

As depicted above, very diverse approaches were taken to get closer to pLys identification and elucidation. Nonetheless, the toolbox of chemical biology has no profound method for addressing this challenge. And still, other strategies are possible for widening the methodological span. One striking observation, which was never investigated thoroughly so far, is the ability of the phosphate group to migrate in solution from Lys to other nucleophilic AAs. This phenomenon is known to occur in the gas phase during tandem-MS measurements [236] but has not been described as a way to form stable phosphorylation in solution. Mobile phosphate groups appear interesting regarding the stability of pLys substrates and the reliability of experiments over longer time periods. Also the mechanistic background should be investigated. It would be crucial to know if it is possible that inorganic phosphate attacks, for example, the Ser side chain or if the migration occurs as a direct transfer from pLys to Ser with an intermediate where both residues are coordinated.

Another approach to study Lys phosphorylation in a more complex environment would be the incorporation of a caged pLys into proteins. For example, by Amber codon suppression, this residue could be introduced at any position of choice. With such a protein in hand, stability studies could be conducted and the dependence of Lys phosphorylation stability on the substrate size investigated. It might also give access to important information about critical points during proteomic sample preparation. Furthermore, PAH activity assays could be expanded to another substrate class. Preliminary experiments have shown that, for example, the mCherry protein would be stable under the conditions of basic deprotection of β-cyano ethyl-caged pLys.

With powerful tools developed, the goal above all is the identification of pLys sites in endogenous proteins. Since extraction and enrichment protocols have not been successful so far, the isolation of selectively active enzymes would give additional hints towards pLys occurrence. The earliest reports about pLys were based on experiments with a kinase isolated from rat tissue. [91–93] To date, this kinase has never been purified again and characterized completely. Thus, the identification of this enzyme would be a breakthrough in this research field. Since the protocols from the 1970s are very different from the state of the art methods, another strategy is required. The W256 cell line could give access to the protein of interest. Starting from the crude cell extracts, enzymatic activity towards Lys substrates could be tested. Subsequent purification and repeated kinase activity tests would narrow the amount of possible proteins and enable characterization in the end. The existence of a kinase selectively phosphorylating Lys residues could be equated with a purposeful occurrence of pLys in cells and would lead the way to the discovery of endogenous Lys phosphorylation sites.

6 | Experimental Part

6.1 Materials and Methods

General

Reagents and solvents were, unless stated otherwise, commercially available as reagent grade and did not require further purification. Chemicals were purchased either from Sigma-Aldrich Chemie GmbH (Munich, Germany) or TCI (TCI Deutschland GmbH, Eschborn, Germany). Resins, coupling reagents and amino acids suitable for SPPS were purchased either from IRIS Biotech GmbH (Marktrewitz, Germany) or Novabiochem© (Merck KGaA, Darmstadt, Germany). Fmoc and TBDPS-protected Sox building block was generously provided by Prof. Imperiali. Aliquots from *bovine alkaline phosphatase* (ALP, Sigma-Aldrich) were kindly provided by Prof. Fiedler. An aliquot of goat-α-rabbit Ab (Jackson ImmunoResearch Europe Ltd, Cambridgeshire, UK) was kindly provided by Prof. Haucke. All water- and air-sensitive reactions were performed under Schlenk conditions.

Peptide Synthesis

Peptides were prepared using the Fmoc solid phase strategy unless specifically noted either by manual peptide synthesis in 8 mL Extract Clean^{TM} reservoirs (Grace Davison Discovery Sciences, Deerfield, Illinois, USA) of 40 mL reactors (Activotec, Cambridge, UK) both equipped with fitting teflon frits or by automated synthesis in a Syro parallel synthesizer (MultiSynTech GmbH, Witten, Germany) in 5 mL syringe reactors equipped with a fritted disc (MultiSynTech GmbH).

Coupling of first amino acid on Rink amide resin

Swelling: 3.5 g Rink Amide resin (Novabiochem, 100-200 mesh, Fmoc on, average loading: 0.73 mmol·g^{-1}) were swollen in DMF for 45 min.

Fmoc deprotection: After 2x 10 min shaking, each with 10 mL of piperidine (Pip):DMF (1:4, v/v) the resin was washed with 5x DMF, 5x DCM, 5x DMF.

Coupling: A 0.1 M solution of 0.4 eq. (1 mmol) Fmoc-protected AA, 0.4 eq. (1 mmol) PyBop and 0.8 eq. (2 mmol) DIPEA in DMF was added to the resin. After 2 h of shaking at r.t., the resin was washed (5x DMF, 5x DCM, 5x DMF).

Capping: A solution of Ac_2O:2,6-lutidine:DMF (5:6:89, v/v/v, 10 mL) was added and the mixture shaken for 10 min. The resin was washed (5x DMF, 10x DCM) and dried completely under reduced

pressure.
The loading was determined photometrically as described in the UV/Vis spectroscopy section.

Table S1: Loading of applied Rink amide resins

Resin	*Sequence*	Loading [µmol·mg^{-1}]
80	^{Fmoc}Gly-resin	0.4385
81	^{Fmoc}His^{Trt}-resin	0.3428
82	^{Fmoc}Ala-resin	0.3585
83	^{Fmoc}Lys^{Boc}-resin	0.3563

Coupling of first amino acid on Wang resin
Swelling: 1.5 g Wang resin (Novabiochem, 100-200 mesh, average loading: 0.22 mmol·g$^-$1) were swollen in DCM:DMF (9:1, v/v) for 45 min.
Coupling: 2.5 eq. (825 µmol) Fmoc-protected AA and 2.5 eq. (825 µmol) HOBt·H_2O were dissolved in DMF to a 0.28 M solution. Some solvent was removed from the reactor and the AA–HOBt mixture added. Subsequently, 2.5 eq. (825 µmol) DIC and 0.1 eq. 33 µmol DMAP (0.65 M in DMF) were added to the resin and the reaction kept for 3 h at r.t. *Capping:* A solution of 2 eq. Ac_2O and 2 eq. pyridine (660 µmol each) was added to the mixture and the resin capped for 30 min at r.t., the resin was washed (5x DMF, 10x DCM) and dried completely under reduced pressure.
The loading was determined photometrically as described in the UV/Vis spectroscopy section.

Table S2: Loading of applied Wang resin

Resin	*Sequence*	Loading [µmol·mg^{-1}]
84	^{Fmoc}Lys^{Boc}-resin	0.1077

Manual peptide synthesis
Swelling: The corresponding amount of resin for a 100 µmol scale was swollen in DMF (2,000 µL) for 30 min.
Fmoc deprotection: Pip:DMF (1:4, v/v, 1,000 µL) was added to the resin. After 5 min, the solution was discarded and another portion of Pip:DMF (1:4, v/v, 1,000 µL) was added to the resin. After 5 min, the solution was discarded and the resin washed with DMF, DCM, DMF (3x 1,000 µL each).
Coupling: AAs were dissolved together with HCTU (500 µmol, 5 eq.) and Oxyma (500 µmol, 5 eq.) to a 0.2 M solution in DMF. Directly before adding the mixture to the resin, DIPEA (1,000 µmol, 10 eq.) was added. The resulting reaction mixture was shaken for 45 min at r.t., the resin then filtered and washed with DMF, DCM, DMF (3x 1,000 µL each).
Fmoc-Lys(N_3)-OH, Fmoc-hCys(EtPO($OBn)_2$)-OH **18**, Fmoc-Nle(OPO(OH)(OBn))-OH **19**, Fmoc-Ser(PO(OBzl)OH)-OH, Fmoc-Thr(PO(OBzl)OH)-OH, Fmoc-Tyr(PO(OBzl)OH)-OH, Fmoc-Arg(NPO($OTc)_2$)-OH **34**, Fmoc-Glu(biotinyl-PEG)-OH, and Fmoc-Sox(TBDPS)-OH were incorporated by using 2 eq. AA, 1.95 eq. HATU and 4 eq. DIPEA in DMF and reacting the mixture for 2 h at r.t.
Acetylation: *N*-terminal acetylation was performed by treating the resin with a mixture of Ac_2O:2,6-

lutidine:DMF (5:6:89, 1,000 µL) for 10 min at r.t., after which the resin was washed with DMF, DCM, DMF (3x 1,000 µL each).
Final cleavage: The resin was either washed with DCM (10x 1,000 µL) or used dry and treated with 4 mL of the cleavage cocktail (TFA:TIS:H_2O – 95:2.5:2.5, v/v/v) for 2 h. Peptides containing Cys in the sequence were cleaved with a mixture of TFA:TIS:H_2O:EDT (94:2.5:2.5:1, v/v/v/v). Peptides containing the hCys-derivative **18** were treated for 105 min with the standard cleavage cocktail, before a solution of 60 µL EDT and 300 µL TMSBr was added and the mixture shaken for further 15 min. The resin was filtered off, the TFA filtrate collected in a 10-fold excess of deep-frozen Et_2O and let sit for precipitation in the freezer. After at least 15 min, the mixture was centrifuged, the solution decanted, the precipitate dried under nitrogen and re-dissolved in ACN/H_2O for UPLC analysis and preparative HPLC.

Automated peptide synthesis

Swelling: The corresponding amount of resin for a 50 µmol scale was swollen in DMF (500 µL) for 30 min.
Fmoc deprotection: Pip:DMF (1:4, v/v, 400 µL) was added to the resin. After 5 min, the solution was discarded and the resin washed with DMF (4x 1,000 µL).
Coupling: AAs were coupled by charging the reactor with a solution of the corresponding Fmoc- and side chain-protected AA (0.67 M in DMF, 4 eq.), PyBOP (0.95 M in DMF, 3.98 eq.), NMM (3.99 M in DMF, 7.94 eq.). The resulting solution was shaken for 30 min at r.t., the resin then filtered and subjected to a second coupling following the same procedure.
Fmoc-Lys(N_3)-OH, Fmoc-hCys(EtPO($OBn)_2$)-OH **18**, Fmoc-Nle(OPO(OH)(OBn))-OH **19**, Fmoc-Ser(PO(OBzl)OH)-OH, Fmoc-Thr(PO(OBzl)OH)-OH, Fmoc-Tyr(PO(OBzl)OH)-OH, Fmoc-Arg(NPO($OTc)_2$)-OH **34**, Fmoc-Glu(biotinyl-PEG)-OH, and Fmoc-Sox(TBDPS)-OH were incorporated by using 2 eq. AA, 1.95 eq. HATU and 4 eq. DIPEA in DMF and reacting the mixture for 2 h at r.t.
Acetylation: *N*-terminal acetylation was performed by treating the resin with a mixture of Ac_2O:2,6-lutidine:DMF (5:6:89, 1,000 µL) for 10 min, after which the resin was washed 5x with DMF.
Final cleavage: The resin was either washed with DCM (10x 1,000 µL) or used dry and treated with 2 mL of the cleavage cocktail (TFA:TIS:H_2O – 95:2.5:2.5, v/v/v) for 2 h at r.t. Peptides containing Cys in the sequence were cleaved with a mixture of TFA:TIS:H_2O:EDT (94:2.5:2.5:1, v/v/v/v). Peptides containing the hCys-derivative **18** were treated for 105 min with the standard cleavage cocktail before a solution of 60 µL EDT and 300 µL TMSBr was added and the mixture shaken for further 15 min. The resin was filtered off, the TFA filtrate collected in a 10-fold excess of deep-frozen Et_2O and let sit for precipitation in the freezer. After at least 15 min, the mixture was centrifuged, the solution decanted, the precipitate dried under nitrogen and re-dissolved in ACN/H_2O for UPLC analysis and preparative HPLC.

Analytical UPLC

UPLC®-UV traces for peptides and small molecules were obtained on an ACQUITY H-class instrument (Waters Corporation, Milford, Massachusetts, USA) equipped with an ACQUITY UPLC®-BEH C18 1.7 µm, 2.1x50 mm column (Waters Corporation), applying a flow rate of 0.6 mL·min^{-1} and using eluents A (99.9% H_2O, 0.1% TFA) and B (99.9% ACN, 0.1% TFA) in the corresponding linear gradient. UPLC-UV chromatograms were recorded at 220 nm.

Gradients	I	5% to 95% B in 13 min
	II	0.5% to 60% B in 13 min

UPLC®-UV and -MS traces of proteins were obtained on an ACQUITY H-class instrument (Waters Corporation) equipped with an ACQUITY UPLC®-Protein BEH C4, 300 Å, 1.7 µm, 2.1x50 mm column (Waters Corporation), applying a flow rate of 0.3 $mL \cdot min^{-1}$ and using eluents A (99.95% H_2O, 0.05% FA) and B (99.95% ACN, 0.05% TFA) in the corresponding linear gradient. UPLC-UV chromatograms were recorded at 220 nm. Mass spectra were recorded with an ESI-MS Xevo® G2-XS QTof spectrometer (Waters Corporation).

High resolution masses were recorded on an ACQUITY H-class instrument (Waters Corporation) equipped with an ESI-MS Xevo® G2-XS QTof spectrometer (Waters Corporation).

TLC analysis

The thin layer chromatography (TLC) was performed on silica gel plates with fluorescence indicator F254 (Merck KGaA). Detection was performed at 254 or 366 nm. Compounds without any chromophore were stained with any of staining solutions such as Potassium permanganate solution, Ninhydrin or Vanillin reagent.

Purification

Peptidic substrates were purified by preparative, semi-preparative or analytical HPLC, performed either on a Gilson PLC 2020 system (Gilson Inc., Middleton, Wisconsin, USA), a Shimadzu Prominence 20A system or a Shimadzu Prominence 8A system (both Shimadzu Corporation, Kyoto, Japan) equipped with columns as followed: preparative column – Nucleodur C18 HTec, 5 µm, 250x32 mm; semi-preparative column – Nucleodur C18 HTec, 5 µm, 250x21 mm; analytical column – Nucleodur C18 HTec, 5 µm, 250x10 mm (all columns purchased from Macherey-Nagel, GmbH & Co. KG, Düren, Germany). Eluents A (99.9% H_2O, 0.1% TFA) and B (B**I**: 99.9% ACN, 0.1% TFA or B**II**: 9.9% ACN, 20% H_2O, 0.1% TFA) were applied in the corresponding linear gradient. Peak detection was performed at 220 nm.

Small molecules were purified by silica gel column chromatography (VWR Chemicals, Normasil 60 Å, 40-63 µm). The samples were applied pre-absorbed on silica gel or, if liquid, directly diluted with suitable solvents.

Desalting of small molecules or peptides was performed with Sep-Pak® Vac C18 cartridges (Waters Corporation). Samples were loaded with maximum 10% ACN in H_2O, washed 3x with 3 column volumes H_2O and eluted with increasing ACN concentration.

FPLC purification was performed at 4 °C on an NGCTM Quest 10 Chromatography System (Bio-Rad Laboratories GmbH, Feldkirchen, Germany) equipped with a BioFrac fraction collector and a HiPrep Q HP 16/10 strong anion exchange column (GE Healthcare UK Limited, Buckinghamshire, England). Eluents A (0.1 M Tris, pH 8.25, 4 °C) and B (0.1 M Tris, 1 M LiCl, pH 8.25, 4 °C) were applied in the corresponding linear gradient. Peak detection was performed at 255 nm.

NMR

NMR spectra were recorded either with a Bruker Ultrashield 300 MHz spectrometer or a Bruker Ultrashield 600 MHz spectrometer (both Bruker Corporation, Billerica, Massachusetts USA) at ambient temperature if not stated differently. The chemical shifts are reported in ppm relative to the shift of tetramethylsilane.

NMR titration experiments

Typically, samples were dissolved in 40 mM KCl to a concentration of 1 mM. The solutions were immediately cooled in an ice-water bath. The pH meter was calibrated at 20 °C; however, all sample readings were performed in an ice-water bath. The pH of the samples were taken before and after the NMR experiment and agreed to within 0.01 pH unit. The pH values used for calculations are the average of the two readings and are not corrected for the temperature. Solutions were then transferred into a 5 mm sample tubes and sealed capillaries filled with D_2O were added. The samples were measured sequentially using an automatic sample changer and were thus kept a room temperature for most of the time, the temperature for the experiments was adjusted only after insertion into the magnet.
Experiments were performed at 278 K on a AV-III-600 NMR-spectrometer (600 MHz ^{1}H frequency, Bruker Biospin, Karlsruhe, Germany) equipped with a 60-slot BACS sample changer using a QCI cryoprobe equipped with a cooled ^{31}P coil and preamp and a one-axis self-shielded gradients. The samples were inserted sequentially and 10 min were given for temperature equilibration. Temperatures had been calibrated using d_4-methanol.[295] Topspin 3.2 was used to control the spectrometer. One-dimensional (1D) ^{31}P experiments were recorded using 64k complex points with an acquisition time $t_{P,max}$ = 2.62 sec (i.e. a spectral window of 25,000 Hz was used), a relaxation delay of 2.5 sec and 256 scans. Two-dimensional (2D) ^{1}H,^{31}P-HMBC experiments[296,297] were performed using a gradient version of the experiment in which a WATERGATE[298] water suppression had been implemented. 2,048(^{1}H)·64(^{31}P) complex points were acquired, with acquisition times $t_{H,max}$ = 204.8 ms and $t_{P,max}$ = 6.4 ms (i.e. a spectral window of 10,000 Hz was used in each dimension) and 16 scans. NMR data were processed and spectra viewed using topspin 3.2 (Bruker Biospin).

Photodeprotection

UV-irradiation was carried out with a Hg (Xe) arc lamp (LOT-QuantumDesign GmbH, Darmstadt, Germany) using a 297 nm filter with 15% transmission (Andover Inc., Salem, New Haven, USA). Samples were dissolved in MeOH at a concentration of 7.5 mM, positioned in 20 cm distance to the source and irradiated while stirring. The deprotection progress was followed by UPLC analysis. Upon complete conversion, a 10-fold excess of deep-frozen Et_2O was added and the mixture let sit in the freezer for 10 min. After centrifugation, the liquid phase was discarded and the precipitate re-suspended in the same amount of deep-frozen Et_2O. The mixture was kept in the freezer again for 10 min, centrifuged, decanted and the precipitate dried under reduced pressure for 15 min. Deprotected pLys substrates were stored in the freezer until applied in the assay.

Phosphatase and Phosphoramidate Hydrolase Activity Assay

Phosphoramidate hydrolase as well as phosphatase activities were determined on a SAFIRE^2 microplate reader (Tecan Group Ltd., Männedorf, Switzerland) by photometric detection at 360 nm of released inorganic phosphate with the EnzCheck™ Phosphatase Assay Kit (Thermo Fisher Scientific™, Waltham, Massachusetts, USA) following the protocol for enzymatic kinetics.[259] Briefly, substrates were incubated at a concentration of 100 µM in 50 mM Tris-HCl buffer containing 1 mM $MgCl_2$ at pH 7.8 in the presence or absence of 0.25 µg LHPP ($3.7 \cdot 10^{-4}$ eq., purchased at ProSpec-Tany TechnoGene Ltd. International, Ness-Ziona, Israel) for the overall phosphate release (enzymatic plus background reaction, $[E+BG]_{\mathrm{wBL}}$) or the non-enzymatic hydrolysis ($[BG]_{\mathrm{wBL}}$), respectively. The absorbance values of microplate, buffer, EnzCheck™ reagent and LHPP were determined in separated wells without adding substrate to the solution, considered as baseline ($[BL]_{\mathrm{wLHPP}}$ and $[BL]_{\mathrm{w/oLHPP}}$). Reactions were run for 90 min in total, UV-absorbance was measured every 10 min. The enzymatic hydrolysis yield $[E]$ was determined by subtraction of $[BG]_{\mathrm{w/oBL}}$ from $[E+BG]_{\mathrm{w/oBL}}$.

$$\begin{aligned}[E] &= [E+BG]_{\mathrm{w/oBL}} - [BG]_{\mathrm{w/oBL}} \\ &= ([E+BG]_{\mathrm{wBL}} - [BL]_{\mathrm{wLHPP}}) - ([BG]_{\mathrm{wBL}} - [BL]_{\mathrm{w/oLHPP}})\end{aligned} \tag{6.1}$$

$[E]$: enzymatically hydrolyzed substrate in mol·L^{-1}, $[E+BG]_{\mathrm{w/oBL}}$: total amount of hydrolyzed substrate in mol·L^{-1} baseline subtracted, $[BG]_{\mathrm{w/oBL}}$: background hydrolysis in mol·L^{-1} baseline subtracted, $[E+BG]_{\mathrm{wBL}}$: total amount of hydrolyzed substrate in mol·L^{-1}, $[BL]_{\mathrm{wLHPP}}$ baseline absorbance with enzyme being present in mol·L^{-1}, $[BG]_{\mathrm{wBL}}$: background hydrolysis in mol·L^{-1}, $[BL]_{\mathrm{w/oLHPP}}$ baseline absorbance without enzyme being present in mol·L^{-1}.

UV/Vis Spectroscopy

UV/Vis spectra and absorbance values were determined either on a V-630 spectrophotometer at r.t. or a V-550 UV/Vis spectrophotometer equipped with an ETC-505T temperature controller at 20 °C (both Jasco, Tokyo, Japan).

Determination of resin loading for peptide synthesis

1-2 mg dried resin were weighed into a microcentrifuge tube and covered with 1 mL Fmoc-deprotection solution (Pip:DMF, 1:4, v/v). After 10 min of shaking at r.t., the loading was determined in a 1 mL quartz cuvette. An aliquot of the deprotection solution was diluted to such an extend that the expected resulting absorbance was approx. 0.3. From the actually measured absorbance the loading was calculated by the help of the following equations:

$$A_\lambda = \epsilon_\lambda \cdot c \cdot d \tag{6.2}$$

A: absorbance at given wavelength, ϵ: molar attenuation coefficient at given wavelength in L·mol^{-1}·cm^{-1} (ϵ_{301nm} = 7,800 L·mol^{-1}·cm^{-1} for 1-((9*H*-fluoren-9-yl)methyl)piperidine), c: concentration in mol·L^{-1}, d: cuvette length in cm.

$$L_{resin} = \frac{A \cdot V_{deprotection} \cdot V_{cuvette}}{\epsilon_{301nm} \cdot d \cdot V_{aliquot} \cdot m_{resin}} \tag{6.3}$$

L_{resin}: loading in µmol·mg^{-1}; A: absorbance at 301 nm; $V_{deprotection}$: volume of Fmoc-deprotection solution in µL (1,000 µL); $V_{cuvette}$: total volume in cuvette for measuring in µL; ϵ_{301nm} = 7,800 µL·µmol^{-1}·cm^{-1}; d: cuvette length in cm; m_{resin}: weighed amount in mg.

Determination of concentration of Sox-tagged peptide solutions [211]

Approx. 0.5 mg peptide (see section 6.8.1.2) were dissolved in 100 µL ddH_2O. The concentration was determined at 20 °C. An aliquot of the stock solution was diluted to such an extend that the expected resulting absorbance was approx. 0.3. From the actually measured absorbance the concentration was calculated by the help of the following equation:

$$c_{Sox-peptide} = \frac{A \cdot V_{cuvette} \cdot 1,000}{\epsilon_{355nm} \cdot d \cdot V_{aliquot}} \tag{6.4}$$

$c_{Sox-peptide}$: concentration in mmol·L^{-1}; A: absorbance at 355 nm; $V_{cuvette}$: total volume in cuvette for measurement in µL (75 µL); ϵ_{355nm} = 8,247 µL·µmol^{-1}·cm^{-1} in 0.1 M NaOH, 10 mM EDTA; d: cuvette length in cm; $V_{aliquot}$: volume of stock used for dilution in µL.

Fluorescence Spectroscopy

Fluorescence spectra were recorded at 20 °C using a FP-6500 spectrofluorometer equipped with an ADP-303T temperature controller (Jasco, Tokyo, Japan).

Determination of aldehyde functionalization of Amino-PEGA resin

The amount of aldehyde functions on resin was determined as previously described. [299] Briefly, a small amount of resin was rinsed (5x) and washed (3x 10 min) with ACN and DCM and dried completely under reduced pressure. From the dried resin, a distinct amount was weighed in a small syringe reactor and swollen in DMF for 30 min. In the meantime, a 12.5 mM solution of dansylhydrazine in AcOH:DMF (1:2, v/v) was prepared. The resin was filtered and sucked 'dry' for 30 s before an aliquot of 200 µL (2.5 µmol) the dansyl hydrazine stock was added and the mixture incubated for 90 min at r.t. on the shaker. The resin was filtered and from the filtrate the amount of unreacted dansylhydrazine determined *via* fluorescence spectroscopy with the following settings: emission mode, band width (Ex) 3 nm, band width (Em) 3 nm, response time 1 s, sensitivity high, excitation wavelength 354.0 nm, emission measurement range 410-650 nm. Aliquots were prepared with their highest emission (of starting solution) not exceeding 800 fluorescence intensity units. The non-specific binding was determined with the same procedure on a distinct amount of starting material. The emission values of cuvette and solvents were considered as baseline emission and subtracted from all other values before calculation. The amount of loading was calculated with the following equations:

$$L_{non-specific} = \frac{n_{\text{non-specific}}}{m_{\text{A}}} = \frac{\frac{[F]_{\text{non-specific}} \cdot 2.5\ \mu mol}{[F]_{\text{D}}}}{m_{\text{A}}} = \frac{\frac{([F]_{\text{A}} - [F]_{\text{D}}) \cdot 2.5\ \mu mol}{[F]_{\text{D}}}}{m_{\text{A}}} \tag{6.5}$$

$$L_{spec.+non-spec.} = \frac{n_{\text{spec.+non-spec.}}}{m_{\text{rct}}} = \frac{\frac{[F]_{\text{spec.+non-spec.}} \cdot 2.5\ \mu mol}{[F]_{\text{D}}}}{m_{\text{rct}}} = \frac{\frac{([F]_{\text{rct}} - [F]_{\text{D}}) \cdot 2.5\ \mu mol}{[F]_{\text{D}}}}{m_{\text{rct}}} \tag{6.6}$$

$$L_{resin} = L_{\text{spec.+non-spec.}} - L_{\text{non-specific}} \tag{6.7}$$

L: loading in µmol·mg^{-1}, F: fluorescence at 354 nm(Ex)/513 nm(Em), m: weighed amount of resin in mg, A: unreacted Amino-PEGA resin, D: dansylhydrazine at t_0 (equals 12.5 mM), rct: reacted resin.

Gel Electrophoresis

SDS–PAGE gels were prepared using standard protocols. Unless stated otherwise, all probes were boiled in SDS sample buffer containing β-mercaptoethanol prior to loading. Gels were run in a Mini-PROTEAN system (Bio-Rad Laboratories GmbH) at 250 V for indicated times. Bands were detected with standard Coomassie stain using Comassie Brilliant Blue G-250 (Thermo Scientific™) in a ChemiDoc Imaging System 8 (Bio-Rad Laboratories GmbH).

Western Blots

WBs were performed directly after SDS-PAGE. The gels were incubated in transfer buffer and then transferred to a NC membrane in a Mini-Trans Blot chamber (Bio-Rad Laboratories GmbH) at 250 A for 1 h. The membrane was blocked with Roti®Block (Carl Roth GmbH + Co. KG, Karlsruhe, Germany) ovn at r.t. and then washed with PBS + 0.05% Tween (PBS-T, 3x 10 min), following incubation with the respective Ab (1:1,000 mouseα-rat, 1:10,000 goatα-rat) for 90 min at 4 °C. The membrane was then washed with PBS-T (2x 5 min) and PBS (2x 5 min). All Ab used were directly tagged with HRP. The membrane was treated with Western ECL Blotting substrates (Santa Cruz Biotechnology, Inc., Heidelberg, Germany) for visualization and the bands were detected with a ChemiDoc Imaging System 8 (Bio-Rad Laboratories GmbH).

6.2 Fmoc-Based Synthesis of Caged Phospho-Lysine Peptides

6.2.1 Synthesis of Core Building Block 1

6.2.1.1 Synthesis overview

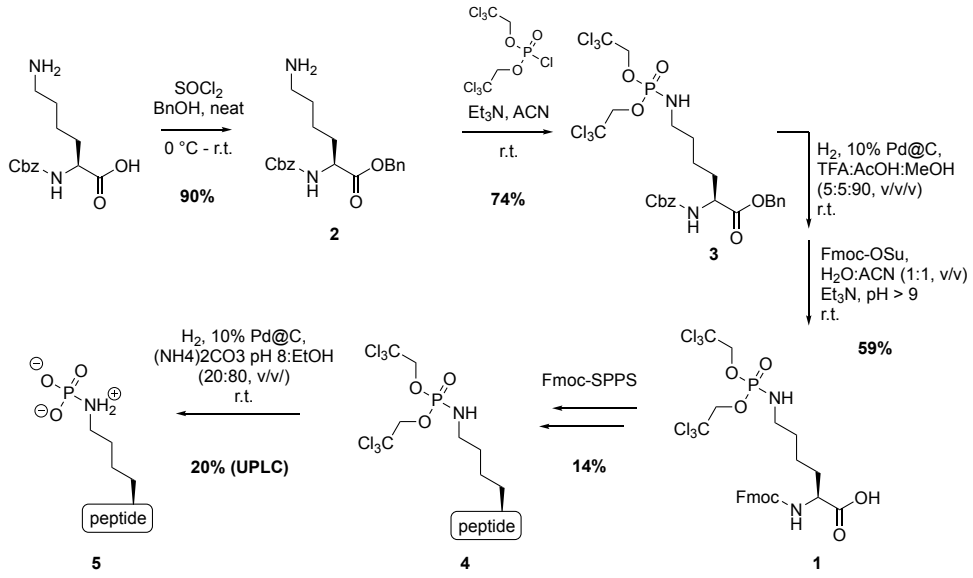

6.2.1.2 Benzyl ((benzyloxy)carbonyl)-*L*-lysinate, Z-Lys-OBn (2)

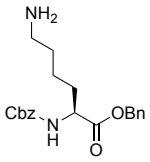

Benzyl protection of ((benzyloxy)carbonyl)-*L*-lysine was achieved by nucleophilic substitution. 1 g (3.6 mmol) Z-Lys-OH was dissolved in benzyl alcohol to a 0.8 M solution and chilled in an ice-bath for 5 min. 1.4 mL (18 mmol, 5 eq.) thionyl chloride were added dropwise to the mixture. After complete addition, the reaction was stirred for 2 h at r.t. until UPLC analysis indicated complete conversion. The mixture was concentrated under reduced pressure and purified *via* silica column chromatography (100% EE+1% Et_3N → MeOH/EE 25/25+1% Et_3N, product eluting at 25% MeOH, silica filtered off after solvent evaporation). 1.20 g (3.2 mmol, 90%) product were obtained as colorless oil. ^{1}H NMR (600 MHz, CD_3CN) δ 7.43 – 7.25 (m, 10H), 6.27 (d, J = 8.1 Hz, 1H), 5.15 (q, J = 12.7 Hz, 2H), 5.08 (q, J = 12.6 Hz, 2H), 4.22 (td, J = 8.6, 4.9 Hz, 1H), 2.88 (t, J = 7.7 Hz, 2H), 1.85 – 1.65 (m, 2H), 1.63 (ddd, J = 21.0, 11.5, 4.3 Hz, 2H), 1.40 (qd, J = 9.2, 8.1, 5.1 Hz, 2H). ^{13}C NMR (151 MHz, CD_3CN) δ 175.01, 163.84, 163.61, 163.39, 163.16, 159.17, 158.56, 139.78, 138.81, 131.84, 131.80, 131.74, 131.55, 131.50, 131.46, 131.34, 131.29, 131.25, 131.04, 131.01, 130.95, 130.78, 130.73, 130.68, 130.44, 130.24, 130.17, 129.95, 129.92, 129.88, 122.56, 120.61, 118.67, 116.72, 70.31, 69.98, 69.32, 69.00, 68.33, 68.02, 57.35, 56.41, 43.02, 42.07, 41.12, 34.22, 33.36, 32.51, 30.06, 29.22, 28.37, 25.82, 24.99, 24.14. R_f (EE/MeOH 3/1+1% Et_3N) = 0.10. HR-MS for $C_{21}H_{26}N_2O_4$: m/z calc. $[M+H^+]^+$ = 371.1966, m/z obs. $[M+H^+]^+$ = 371.1971

6.2.1.3 Benzyl N^2-((benzyloxy)carbonyl)-N^6-(bis(2,2,2-trichloroethoxy)phosphoryl)-*L*-lysinate, Z-Lys(NPO(OTc)$_2$)-OBn (3)

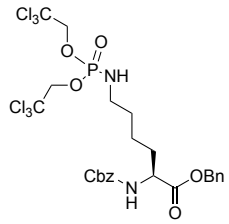

Compound **3** was synthesized in accordance to the previously described protocol by the Seebeck group.[112] Briefly, 1.20 g (3.24 mmol) **2** were dissolved to a 60 mM solution in ACN (54 mL) and 4 eq. Et_3N (13 mmol, 1.8 mL) were added and the pH checked for basicity. 1.47 g (3.88 mmol, 1.2 eq.) bis(2,2,2-trichloroethyl) phosphorochloridate were added in three equal portions of 491 mg each every 2 h while stirring at r.t. The reaction was kept at r.t. ovn and TLC indicated full conversion. Solvents were evaporated under reduced pressure and the crude product purified *via* silica column (hex/EE 8/2+0.25% FA → hex/EE 3/7+0.25% FA, product eluting at 40-50% EE). Fractions containing **3** were concentrated under reduced pressure and residue formic acid removed by lyophilization. The product was obtained as a colourless oil (1.71 g, 2.40 mmol, 74%). ^{1}H NMR (600 MHz, CD_3CN) δ 7.43 – 7.26 (m, 10H), 6.08 (d, J = 8.1 Hz, 1H), 5.13 (q, J = 9.3 Hz, 2H), 5.07 (q, J = 8.1 Hz, 2H), 4.59 (dd, J = 6.2, 1.4 Hz, 4H), 4.24 – 4.15 (m, 1H), 3.92 (dt, J = 13.4, 6.9 Hz, 1H), 2.95 (dddd, J = 13.8, 11.8, 6.8, 1.2 Hz, 2H), 1.83 – 1.61 (m, 2H), 1.58 – 1.44 (m, 2H), 1.43 – 1.36 (m, 2H). ^{31}P NMR (243 MHz, CD_3CN) δ 4.52, 4.50, 4.48, 4.45, 4.43. ^{13}C NMR (151 MHz, CD_3CN) δ 175.07, 158.98, 139.85, 138.86, 131.82, 131.77, 131.72, 131.47, 131.27, 131.20, 130.95, 130.76, 130.71, 130.65, 130.40, 130.21, 129.90, 98.14, 98.06, 79.79, 79.76, 78.75, 78.73, 77.72, 77.69, 70.17, 69.85, 69.19, 68.87, 68.20, 67.89, 57.43, 56.49, 44.39, 43.47, 42.55, 34.43, 34.12, 33.55, 33.28, 32.71, 32.46, 25.84, 25.03, 24.20. R_f (hex/EE 7/3+0.25% FA) = 0.37. HR-MS for $C_{25}H_{29}Cl_6N_2O_7P$: m/z calc. $[M+H^+]^+$ = 710.9917, m/z obs. $[M+H^+]^+$ = 710.9915.

6.2.1.4 N^6-(bis(2,2,2-trichloroethoxy)phosphoryl)-*L*-lysine, H_2N-Lys(NPO(OTc)$_2$)-OH

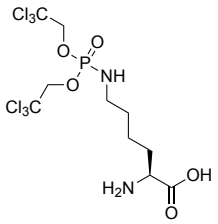

N- and *C*-terminal deprotection was achieved with hydrogenation. 600 mg (850 µmol) **3** were weighed into a Schlenk flask, dissolved to a 75 mM solution with AcOH:TFA:MeOH (5:5:90, v/v/v, 11 mL) and kept under vacuum for 5 min. In inert atmosphere, 96 mg Pd on activated charcoal (10% Pd, 113 mg per mmol starting material) were added and the gas exchanged with H_2. The mixture was stirred for 45 min in H_2 atmosphere until UPLC analysis indicated full conversion. The catalyst was filtered off and washed with MeOH. Solvents were evaporated by bubbling N_2

through the solution and residual acid removed by lyophilization. The crude product was applied in the next step without further purification.

6.2.1.5 N^2-(((9*H*-fluoren-9-yl)methoxy)carbonyl)-N^6-(bis(2,2,2-trichloroethoxy)phosphoryl)-*L*-lysine, Fmoc-Lys(NPO(OTc)$_2$)-OH (1)

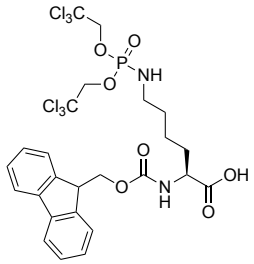

850 µmol crude product of H_2N-Lys(NPO(OTc)$_2$)-OH were dissolved in 2.1 mL H_2O to a 0.4 M solution and 120 µL (850 µmol, 1 eq.) Et_3N were added. The pH was adjusted to 9 and a 0.4 M solution of 287 mg (850 µmol, 1 eq.) Fmoc-OSu in ACN (2.1 mL) was added while keeping the pH above 9 by further Et_3N addition. The reaction was allowed to proceed until the pH stabilized at pH 9.2. Subsequently, the pH was adjusted to 3.5 with AcOH and the mixture extracted 3x with $CHCl_3$. The combined organic layers were dried over Na_2SO_4 and solvents evaporated under reduced pressure. The crude product was purified *via* flash silica column (1. wash impurities off with hex/EE 45/55+0.25% FA, 2. elution of product with hex/EE 35/65+0.25% FA). After evaporation and lyophilization, 357 mg (502 µmol, 59%) product were obtained as white powder. ^{1}H NMR (600 MHz, CD_3CN) δ 7.83 (d, J = 7.7 Hz, 2H), 7.68 (t, J = 6.6 Hz, 2H), 7.42 (t, J = 7.6 Hz, 2H), 7.36 – 7.31 (m, 2H), 6.07 (d, J = 8.0 Hz, 1H), 4.60 (d, J = 6.2 Hz, 4H), 4.33 (d, J = 7.2 Hz, 2H), 4.23 (t, J = 7.0 Hz, 1H), 4.13 – 4.05 (m, 1H), 3.94 (dt, J = 13.4, 6.9 Hz, 1H), 2.99 (dq, J = 13.4, 6.9 Hz, 2H), 1.84 – 1.62 (m, 1H), 1.59 – 1.47 (m, 2H), 1.43 (q, J = 8.2, 7.3 Hz, 2H). ^{31}P NMR (243 MHz, CD_3CN) δ 4.59, 4.57, 4.54, 4.52, 4.49, 4.46, 4.44, 4.41, 4.39. ^{13}C NMR (151 MHz, CD_3CN) δ 176.08, 158.93, 146.86, 143.86, 130.95, 130.35, 129.89, 129.30, 123.27, 123.21, 122.15, 98.11, 79.77, 78.73, 77.70, 68.97, 57.03, 56.11, 50.21, 49.49, 49.34. R_f (hex/EE: 1/1+0.25% FA) = 0.47. HR-MS for $C_{25}H_{27}Cl_6N_2O_7P$: m/z calc. $[M+H^+]^+$ = 708.9760, m/z obs. $[M+H^+]^+$ = 708.9764.

6.2.2 Peptide Synthesis

6.2.2.1 ^{Ac}Tyr-Lys(NPO(OTc)$_2$)-Gly^{CONH_2} (4)

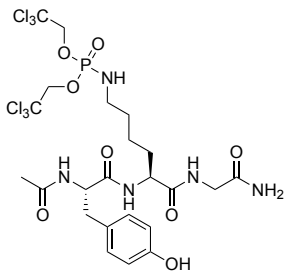

Peptide **4** was synthesized as described in section 6.1 on a 20 µmol scale with resin **20**. Incorporation of building block **1** was conducted as followed: 2.1 eq. AA (42 µmol, 30 mg) and 2 eq. HATU (40 µmol, 15 mg) were dissolved in 200 µL DMF to give a 0.2 M solution. Directly before adding the mixture to the Fmoc-deprotected resin, 14 µL (4 eq., 80 µmol) DIPEA were added. The mixture was shaken at r.t. for 2 h, when the 2,4,6-trinitrobenzene-sulphonic acid (TNBS) test[300] indicated full conversion. The peptide was capped before continuation of the peptide coupling. The crude product was purified on an analytical HPLC column to give 2.1 mg (2.8 µmol, 14% with regard to initial resin loading) white powder of desired peptide **4**. ^{1}H NMR (600 MHz, CD_3CN+10% D_2O) δ 7.14 (d, J = 8.5 Hz, 2H), 6.80 (d, J = 8.5 Hz, 2H), 4.69 (dd, J = 6.1, 1.7 Hz, 4H), 4.53 – 4.47 (m, 1H), 4.19 (dd, J = 9.2, 4.8 Hz, 1H), 3.78 (dd, J = 25.2, 17.0 Hz, 2H), 2.90 (dd, J = 14.0, 8.1 Hz, 2H), 1.95 (s, 3H), 1.88 – 1.81 (m, 2H), 1.66 (dtd, J = 14.2, 9.7, 5.1 Hz, 2H), 1.57 (ddt, J = 17.7, 9.1, 6.8 Hz, 2H), 1.40 – 1.32 (m, 2H). ^{31}P NMR (243 MHz, CD_3CN+10% D_2O) δ 4.83, 4.81, 4.79, 4.76, 4.74, 4.71, 4.69. ^{13}C NMR (151 MHz, CD_3CN) δ 175.24, 174.98, 174.85, 174.24, 158.50, 133.13, 130.46, 117.84, 97.89, 78.80, 58.04, 56.40, 44.68, 43.38, 38.92, 33.28, 32.99, 25.03, 24.57. HR-MS for $C_{23}H_{32}Cl_6N_5O_8P$: m/z calc. $[M+H^+]^+$ = 748.0193, m/z obs. $[M+H^+]^+$ = 748.0192. t_R (gradient **I**) = 6.179 min.

6.2.2.2 ^{Ac}**Tyr-Lys**^{N_3}**-Gly**^{CONH_2} **(6)**

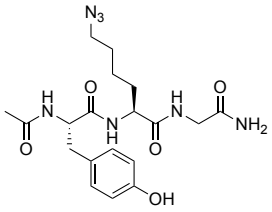

Peptide **6** was synthesized as described in section 6.1 on a 20 µmol scale with resin **80**. Incorporation of Fmoc-*az*-Lys-OH was conducted as described in section 6.1 with HATU as activating reagent. The mixture was shaken at r.t. for 2 h, when the TNBS test indicated full conversion. The peptide was capped before continuation of the peptide coupling. The crude product was purified on an analytical HPLC column to give 5.11 mg (11.8 µmol, 59% with regard to initial resin loading) white powder of desired peptide **6**. HR-MS for $C_{19}H_{27}N_7O_5$: m/z calc. $[M+H^+]^+$ = 433.2074, m/z obs. $[M+H^+]^+$ = 433.2079. t_R (gradient **II**) = 3.458 min.

6.2.2.3 1-(2-Nitrophenyl)ethanol (8)

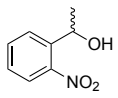

1-(2-nitrophenyl)ethanol was synthesized as previously described.[301] Briefly, in a 500 mL round-bottom flask 10 g (60.6 mmol) 2'-nitroacteophenone were dissolved in 100 mL MeOH:dioxane (3:2, v/v) and cooled with an ice bath. Under vigorous stirring, 2.5 eq. sodium borohydride (151.4 mmol, 5.7 g) were added portionwise over 90 min. The resulting mixture was equipped with septum and balloon and left to reach r.t. ovn while stirring. After 16 h residual $NaBH_4$ was

quenched by the addition of 50 mL of acetone and the solvents evaporated under reduced pressure. The residue was diluted with H_2O and EE and the layers separated. The organic layer was washed twice with water, the combined aqueous layers were washed once with EE, eventually, the combined organic layers were washed with brine, dried over $MgSO_4$ and the filtered solution concentrated under reduced pressure. The residual solvent was evaporated under high vacuum ovn. The product (9.7 g, 58.2 mmol, 96%) was obtained as a yellow oil. ^{1}H-NMR (600 MHz, CD_3CN) δ 7.86 (dd, J = 8.1, 1.4 Hz, 2H), 7.71 (td, J = 7.6, 1.3 Hz, 1H), 7.47 (ddd, J = 8.7, 7.4, 1.5 Hz, 1H), 5.30 (qd, J = 6.4, 4.1 Hz, 1H), 3.55 (dd, J = 4.2, 1.3 Hz, 1H), 1.48 (d, J = 6.4 Hz, 3H). ^{13}C-NMR (151 MHz, CD_3CN) δ 147.84, 141.58, 133.31, 127.91, 127.62, 123.75, 64.64, 24.19. HR-MS for $C_8H_9NO_3$: m/z calc. $[M+H^+]^+$ = 166.0499, m/z obs. $[M+H^+]^+$ = 166.0505.

6.2.2.4 Tris(1-(2-nitrophenyl)ethyl) phosphite (9)

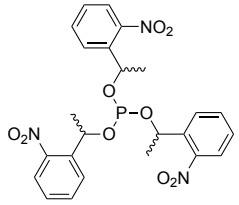

Phosphite **9** was synthesized by the condensation of trichlorophosphane and the alcohol **8** under inert conditions. A Schlenk flask was equipped with 1.7 g 1-(2-nitrophenyl)ethanol **8** (10.2 mmol, 3.4 eq.) and magnetic stir bar and set under high vacuum for 10 min. After balancing the pressure with argon, 10 mL dry THF were added and the solution cooled in an ice bath for 5 min. 1.33 mL Et_3N (9.6 mmol, 3.2 eq.) were added, the mixture left for another 2 min, while preparing a 0.6 M solution of 0.27 mL trichlorophosphane (3 mmol, 1.0 eq.) in dry THF (5 mL). The PCl_3 solution was added dropwise to the Schlenk flask, whereby a white precipitate was formed. After complete addition the mixture was kept in the ice bath for another 15 min, then stirred at r.t. under exclusion of light ovn. After 18 h the precipitate was filtered, washed with EE and the filtrate concentrated under reduced pressure. 1.03 g (2.19 mmol, 73%) product were obtained after column chromatography (hex/EE 9/1+1% Et_3N → hex/EE 7/3+1% Et_3N, the product eluting at 25% EE) as yellow oil and kept under argon, protected from light in the freezer until further usage. ^{1}H-NMR (300 MHz, CD_3CN) δ 7.92 – 7.74 (m, 3H), 7.70 – 7.34 (m, 9H), 5.84 – 5.57 (m, 3H), 1.52 – 1.37 (m, 6H), 1.29 – 1.19 (m, 3H). ^{31}P-NMR (122 MHz, CD_3CN) δ 137.82, 135.97. ^{13}C-NMR (75 MHz, CD_3CN) δ 146.95, 146.86, 146.71, 146.44, 139.09, 139.04, 138.92, 138.89, 133.75, 133.73, 128.51, 128.42, 128.29, 128.02, 127.98, 127.90, 127.68, 124.10, 124.07, 124.06, 67.01, 66.83, 66.76, 66.64, 66.61, 66.50, 24.33, 24.28, 24.24, 24.20, 24.18, 24.13, 24.03, 23.98. R_f (hex/EE 3/1+1% Et_3N) = 0.57.

6.2.2.5 ^{Ac}Tyr-Lys(NPO(ONPE)$_2$)-Gly^{CONH_2} (7)

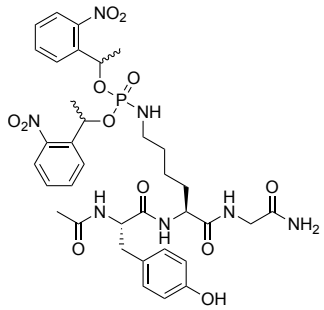

Formation of the phosphoramidate was achieved as previously described.[97] Briefly, 5.1 mg (11.8 µmol) azido-peptide **6** were dissolved in 400 µL dry DMF. 18.7 mg (35.4 µmol, 3 eq.) phosphite **9** were dissolved in 72 µL dry DMF and added to the azide (final azide concentration 25 mM). The reaction was kept at 45 °C and samples taken for UPLC analysis at distinct time points. After 7 h and 26 h additional 2 eq. phosphite **9** were added to the reaction in order to drive it to completion. After 48 h, the solvents were evaporated under reduced pressure and residual DMF removed during lyophilization. The product was obtained as a white powder after purification *via* analytical HPLC (7.0 mg, 9.0 µmol, 76%). HR-MS for $C_{35}H_{44}N_7O_{12}P$: m/z calc. $[M+H^+]^+$ = 786.2865, m/z obs. $[M+H^+]^+$ = 786.2870. t_R (gradient **I**) = 6.212 min.

6.3 Investigation of Amine Protonation in Various Phosphoramidate Species

6.3.1 Synthesis of $^{15}N_2$-Labeled Fmoc-Protected Azido-Lysine 13

6.3.1.1 Synthesis overview

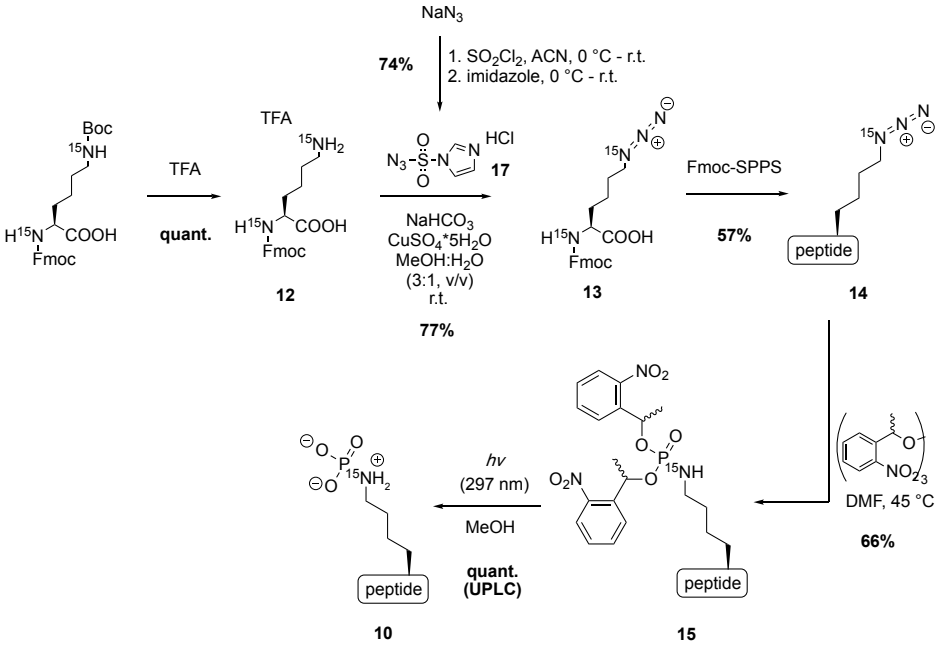

6.3.1.2 1*H*-imidazole-1-sulfonyl azide hydrochloride (17)

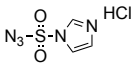

The azide transfer reagent was prepared as previously described.[244,302] Briefly, 3.3 g (50.8 mmol) sodium azide were suspended in 63.5 mL ACN (0.8 M) and cooled with an ice-bath. Slowly, 4.1 mL (50.8 mmol, 1 eq.) sulfuryl chloride were added dropwise whereby a white precipitate formed. The resulting mixture was stirred ovn at r.t., before it was cooled again in an ice-bath and imidazole was added portionwise. During subsequent stirring at r.t., the reaction mixture turned yellow. After 3 h, 100 mL EE and 65 mL H_2O were added to the flask, upon which the precipitate dissolved. The layers were seperated and the organic layer washed with H_2O and twice with $NaHCO_3$, sat. 65 mL each. The organic layer was dried over $MgSO_4$, filtered and the filter cake washed with a small amount of EE. The filtrate was cooled in an ice-bath for 10 min, while an ice-cold mixture of 20 mL EtOH and 5.4 mL CH_2COCl was prepared and kept for 5 min in an ice-bath as well. The mixture was added dropwise to the cooled filtrate while stirring gently. The formed white precipitate was kept cold for 15 min, filtered and washed 4x with 20 mL of cold EE each. 7.88 g (37.6 mmol, 74%) product were obtained as white solid after drying under reduced pressure. ^{1}H NMR (300 MHz, D_2O) δ 9.45 (t, J = 1.5 Hz, 1H), 8.02 (dd, J = 2.2, 1.6 Hz, 1H), 7.62 (dd, J

= 2.2, 1.3 Hz, 1H). ^{13}C NMR (151 MHz, D_2O) δ 140.38, 125.50, 122.99. HR-MS for $C_3H_3N_5O_2S$: m/z calc. $[M+H^+]^+$ = 174.0080, m/z obs. $[M+H^+]^+$ = 174.0079.

6.3.1.3 (((9*H*-fluoren-9-yl)methoxy)carbonyl)-*L*-lysine-$^{15}N_2$ (12)

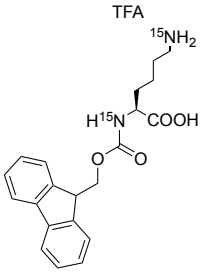

50 mg (106.7 µmol) Fmoc-Lys(Boc)-OH-$^{15}N_2$ were dissolved in 1 mL TFA and kept at r.t. for 5 min. UPLC analysis indicated full conversion. The TFA was evaporated with nitrogen flush and the product obtained as white solid after double lyophilization (49.8 mg, 106.7 µmol, 100%) and used for the next step without further purification.

6.3.1.4 N^2-(((9*H*-fluoren-9-yl)methoxy)carbonyl)-N^6-diazo-*L*-lysine-$^{15}N_2$ (13)

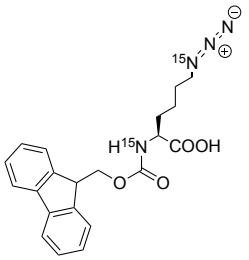

49.8 mg (107 µmol) Fmoc-Lys-OH **12** were dissolved in 3.1 mL MeOH:H_2O (3:1, v/v) to give a 35 mM solution. 90 mg (1.07 mmol, 10eq.) $NaHCO_3$ and 0.25 mg (1 µmol, 0.01 eq.) $CuSO_4 \cdot 5H_2O$ were added and a light blue suspension was formed. 26.9 mg (128.4 µmol, 1.2 eq.) of 1*H*-imidazole-1-sulfonyl azide hydrochloride **17** were added and the reaction stirred for 45 h until UPLC analysis indicated no further progress. Solvents were evaporated under reduced pressure and the crude product purified using semipreparative HPLC. 32.4 mg (82.4 µmol, 77%) product were obtained as white powder. ^{1}H NMR (600 MHz, CD_3CN) δ 7.83 (d, J = 7.5 Hz, 2H), 7.67 (t, J = 6.7 Hz, 2H), 7.38 (dt, J = 49.1, 7.5 Hz, 4H), 5.99 (dd, J = 92.4, 8.2 Hz, 1H), 4.34 (d, J = 8.0 Hz, 2H), 4.24 (t, J = 7.0 Hz, 1H), 4.13 (td, J = 8.6, 4.8 Hz, 1H), 3.29 (d, J = 13.8 Hz, 2H), 1.85 – 1.64 (m, 2H), 1.58 (qd, J = 8.7, 7.2, 3.6 Hz, 2H), 1.43 (ddt, J = 12.7, 9.7, 4.5 Hz, 2H). ^{15}N NMR (61 MHz, CD_3CN) δ 85.93, 71.25. ^{13}C NMR (151 MHz, CD_3CN) δ 173.14, 156.40, 156.22, 144.26, 144.18, 141.27, 127.83, 127.22, 125.32, 66.43, 53.80, 53.71, 51.02, 50.99, 47.17, 30.87, 28.11, 22.79. HR-MS for $C_{21}H_{22}N_2{}^{15}N_2O_4$: m/z calc. $[M+H^+]^+$ = 397.1655, m/z obs. $[M+H^+]^+$ = 397.1650.

6.3.2 Peptide Synthesis

6.3.2.1 ^{Ac}Tyr-pLys-Gly^{CONH_2} (5)

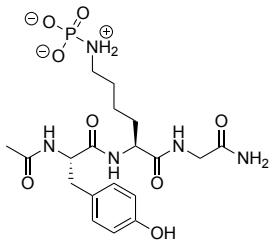

0.5 µmol caged-pLys peptide **7** (0.39 mg) was deprotected and worked up as described in the photodeprotection section 6.1. HR-MS for $C_{19}H_{30}N_5O_8P$: m/z calc. $[M+H^+]^+ = 488.1911$, m/z obs. $[M+H^+]^+ = 488.1923$. t_R (gradient **II**) = 1.537 min.

6.3.2.2 ^{Ac}Tyr-Lys^{N_3}-$^{15}N_2$-Gly^{CONH_2} (14)

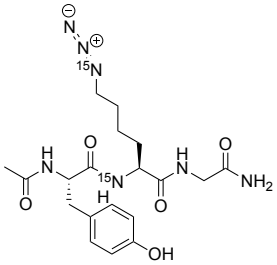

Peptide **14** was synthesized as described in section 6.1 on a 35 µmol scale with resin **80**. Incorporation of building block **13** was conducted as followed: 1.5 eq. AA (52.5 µmol, 21 mg) and 1.49 eq. HATU (52 µmol, 19.8 mg) were dissolved in 262 µL DMF to give a 0.2 M solution. Directly before adding the mixture to the Fmoc-deprotected resin, 17 µL (3 eq., 105 µmol) DIPEA were added. The mixture was shaken at r.t. for 2 h, when the TNBS test indicated full conversion. The peptide was capped before continuing with the peptide coupling. The crude product was purified on an analytical HPLC column to give 8.75 mg (20.0 µmol, 57% with regard to initial resin loading) white powder of desired peptide **14**. ^{1}H NMR (600 MHz, CD_3CN) δ 7.12 – 7.06 (m, 2H), 7.04 (dd, J = 92.2, 6.9 Hz, 1H), 6.78 – 6.74 (m, 2H), 6.51 (s, 1H), 5.75 (s, 1H), 4.40 (dt, J = 8.0, 6.5 Hz, 1H), 4.12 – 4.06 (m, 1H), 3.71 (ddd, J = 30.0, 17.3, 6.0 Hz, 2H), 3.30 (td, J = 7.0, 1.2 Hz, 2H), 2.93 (ddd, J = 73.6, 14.5, 6.3 Hz, 2H), 1.90 (s, 3H), 1.87 – 1.61 (m, 2H), 1.57 (ddtd, J = 16.4, 13.4, 6.6, 2.9 Hz, 2H), 1.37 – 1.27 (m, 2H). ^{15}N NMR (61 MHz, CD_3CN) δ 116.87, 71.25. ^{13}C NMR (151 MHz, CD_3CN) δ 172.28, 172.18, 171.68, 171.25, 170.85, 155.73, 130.40, 128.09, 115.13, 55.57, 55.52, 53.87, 53.80, 50.95, 50.93, 42.22, 36.15, 30.26, 28.06, 22.77, 21.93. HR-MS for $C_{19}H_{27}N_5{}^{15}N_2O_5$: m/z calc. $[M+H^+]^+ = 436.2087$, m/z obs. $[M+H^+]^+ = 436.2089$. t_R (gradient **II**) = 3.854 min.

6.3.2.3 ^{Ac}Tyr(NPO(ONPE)$_2$)-$^{15}N_2$-Gly^{CONH_2} (15)

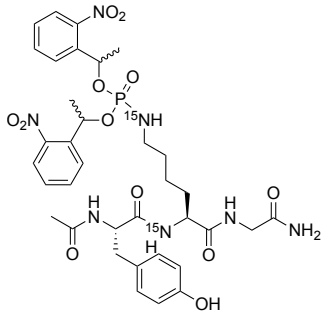

Formation of the phosphoramidate was achieved as previously described.[97] Briefly, 5.2 mg (12 µmol) azido-peptide **14** were dissolved in 400 µL dry DMF. 19 mg (36 µmol, 3 eq.) phosphite **9** were dissolved in 80 µL dry DMF and added to the azide (final azide concentration 25 mM). The reaction was kept at 45 °C and samples taken for UPLC analysis at distinct time points. After 6.5 h and 23.5 h additional 3 eq. phosphite **9** were added to the reaction in order to drive it to completion. After 48 h, solvents were evaporated under reduced pressure and residual DMF removed during lyophilization. The product was obtained as a white powder after purification *via* analytical HPLC (6.2 mg, 7.o9 µmol, 66%). The stereo isomers could be seperated and were present in a ratio of 77:23 but were employed in the next step together. ^{1}H-NMR (600 MHz, 0.1%TFA+10% D_2O+10% CD_3CN) Isomer1: δ 8.43 – 6.85 (m, 14H), 5.98 – 5.82 (m, 1H), 4.23 (q, J = 9.8, 6.3 Hz, 1H), 4.01 – 3.83 (m, 2H), 3.06 (q, J = 6.2, 5.1 Hz, 2H), 2.99 – 2.61 (m, 2H), 2.04 (s, 3H), 1.80 – 1.12 (m, 12H).; Isomer2: δ 8.33 – 6.85 (m, 14H), 6.02 – 5.85 (m, 1H), 4.18 (q, J = 8.8, 8.4, 6.7 Hz, 1H), 3.99 – 3.84 (m, 2H), 3.05 (d, J = 7.8 Hz, 2H), 2.61 (q, J = 8.6 Hz, 2H), 2.04 (s, 3H), 1.75 – 1.00 (m, 12H). ^{31}P-NMR (243 MHz, 0.1% TFA+10% D_2O+10% CD_3CN) Isomer1: δ 6.27; Isomer2 δ 5.84. ^{15}N-NMR (61 MHz, 0.1% TFA+10% D_2O+10% CD_3CN) Isomer1: δ 123.64, 42.03; Isomer2 δ 123.86, 42.36. HR-MS for $C_{35}H_{44}N_5{}^{15}N_2O_{12}P$: m/z calc. $[M+H^+]^+$ = 788.2799, m/z obs. $[M+H^+]^+$ = 788.2780. t_R (gradient **I**) = 6.112 min.

6.3.2.4 ^{Ac}Tyr-pLys-$^{15}N_2$-Gly^{CONH_2} (10)

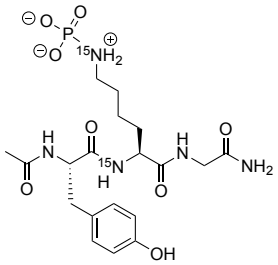

0.5 µmol caged-pLys peptide **15** (0.52 mg) was deprotected and worked up as described in the photodeprotection section 6.1. ^{1}H-NMR (600 MHz, 0.1%TFA+10% D_2O) δ 8.24 – 8.18 (m, 1H), 7.40 (q, J = 5.8 Hz, 1H), 7.29 (q, J = 7.3, 6.7 Hz, 1H), 6.92 (d, J = 8.7 Hz, 2H), 6.60 (d, J = 8.5 Hz, 1H), 4.28 – 4.19 (m, 1H), 4.00 (q, J = 8.0 Hz, 1H), 3.64 – 3.51 (m, 1H), 3.32 (p, J = 7.3 Hz, 2H), 2.85 – 2.75 (m, 2H), 2.70 (tt, J = 15.0, 7.1 Hz, 2H), 1.75 (s, 3H), 1.63 – 1.33 (m, 4H), 1.10 (m, 2H). ^{31}P-NMR (243 MHz, 0.1% TFA+10% D_2O) δ -6.85. ^{15}N-NMR (61 MHz, 0.1% TFA+10% D_2O) δ 125.37, 62.36. HR-MS for

$C_{19}H_{30}N_3{}^{15}N_2O_8P$: m/z calc. $[M+H^+]^+$ = 490.1846, m/z obs. $[M+H^+]^+$ = 490.1829. t_R (gradient **II**) = 1.697 min.

6.4 Design and Synthesis of Stable Phospho-Lysine Mimics

6.4.1 Synthesis of Homocysteine-Derived Phosphonate 18

6.4.1.1 Synthesis overview

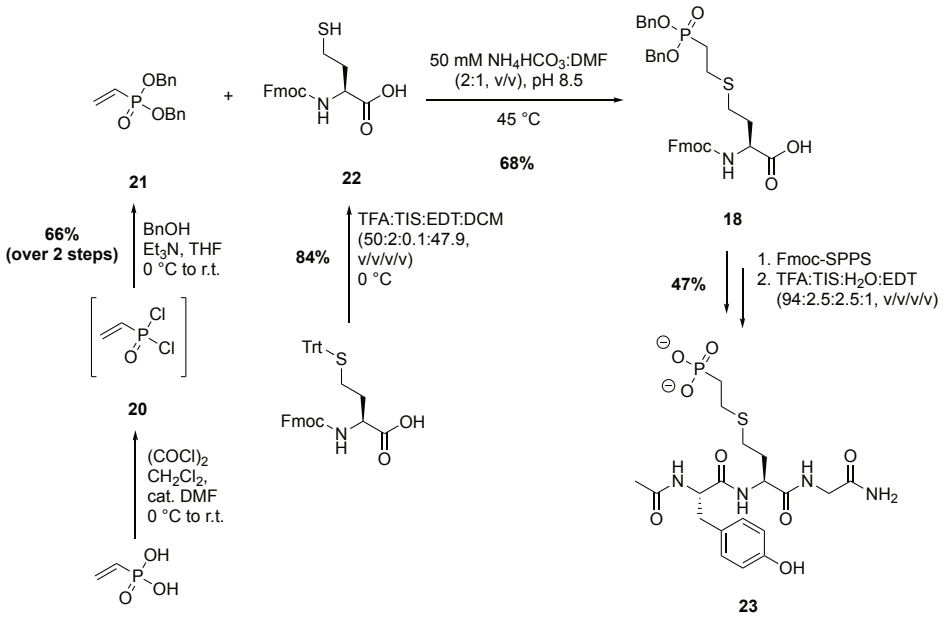

6.4.1.2 Vinylphosphonic dichloride (20)

Vinylphosphonic dichloride was synthesized as described before with minor adjustments.[303] Briefly, in a heated Schlenk flask under Ar, 19 mL of dry DCM were cooled in an ice bath for 5 min. 1.34 mL (17.3 mmol) vinylphosphonic acid were added and cooled for 5 min before 5 drops of dry DMF were added. Under vigorous stirring, 4.47 mL (52.1 mmol, 3 eq.) oxalyl dichloride were added dropwise and the resulting orange mixture kept in the ice bath for further 15 min and then at rt. ovn. After 17.5 h solvents and oxalyl dichloride were evaporated under reduced pressure. The crude product was obtained as a orange-brown oil and used for the next step without further purification. ^{1}H NMR (300 MHz, $CDCl_3$) δ 6.65 – 6.61 (m, 1H), 6.52 – 6.21 (m, 2H). ^{31}P NMR (122 MHz, $CDCl_3$) δ 31.31.

6.4.1.3 Dibenzyl vinylphosphonate (21)

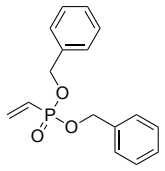

In a heated flask and in Ar atmosphere, 50 mL dry THF were pre-cooled. Subsequently, 4.5 mL (43.25 mmol, 2.5 eq.) benzyl alcohol and 7.2 mL (52.1 mmol, 3 eq.) Et_3N were added and cooled as well. 17.3 mmol (1 eq.) vinylphosphonic dichloride **20** were dissolved in 10 mL dry THF and added dropwise to the pre-cooled mixture, upon which a white precipitate was formed. The reaction was stirred for 15 min in an ice bath and ovn at r.t. The next day, the precipitate was filtered off, solvents evaporated under reduced pressure and the crude product purified by silica column chromatography (100% DCM → DCM/EE 8/2, product eluting at 10% EE). The product was obtained as orange oil (3.24 g, 11.4 mmol, 66%). ^{1}H NMR (600 MHz, CD_3CN) δ 7.43 – 7.31 (m, 10H), 6.29 – 6.05 (m, 3H), 5.07 – 4.96 (m, 4H). ^{31}P NMR (243 MHz, CD_3CN) δ 14.70, 14.67. ^{13}C NMR (151 MHz, CD_3CN) δ 139.44, 139.30, 138.27, 138.22, 137.19, 137.13, 131.83, 131.79, 131.58, 131.53, 131.18, 131.15, 131.12, 130.76, 130.73, 130.56, 130.54, 130.51, 130.48, 130.45, 130.12, 130.09, 130.06, 129.79, 128.69, 128.58, 127.50, 70.76, 69.80, 69.77, 68.79. R_f (DCM/EE 7/3, $KMnO_4$ stain) = 0.50. HR-MS for $C_{16}H_{17}O_3P$: m/z calc. $[M+H^+]^+$ = 289.0988, m/z obs. $[M+H^+]^+$ = 289.0994.

6.4.1.4 (((9*H*-fluoren-9-yl)methoxy)carbonyl)-*L*-homocysteine (22)

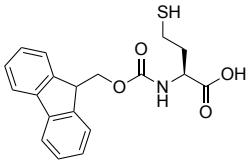

At 0 °C, 480 mg (0.8 mmol) Fmoc-hCys(Trt)-OH were dissolved in 2.4 mL DCM and 2.6 mL of a mixture of TFA:TIS:EDT (96:3.8:0.2, v/v/v) was added. Within 1 min the mixture turned yellow and back to colourless. UPLC analysis after 7 min indicated full conversion. Solvents were evaporated with nitrogen flush, while keeping the mixture in an ice bath. Immediate purification on preparative HPLC gave 240 mg (0.67 mmol, 84%) of desired compound as white powder. ^{1}H NMR (600 MHz, CD_3CN) δ 7.92 (d, J = 7.5 Hz, 2H), 7.76 (t, J = 7.0 Hz, 2H), 7.51 (t, J = 7.5 Hz, 2H), 7.43 (tt, J = 7.5, 1.5 Hz, 2H), 6.07 (d, J = 8.4 Hz, 1H), 4.44 (d, J = 7.2 Hz, 2H), 4.39 (td, J = 8.8, 4.5 Hz, 1H), 4.33 (t, J = 7.0 Hz, 1H), 2.71 – 2.57 (m, 2H), 2.16 – 2.03 (m, 2H). ^{13}C NMR (151 MHz, CD_3CN) δ 175.35, 158.97, 146.81, 143.89, 131.00, 130.95, 130.40, 130.35, 129.94, 129.89, 129.33, 129.29, 128.46, 127.38, 123.27, 123.22, 122.22, 122.17, 69.08, 55.53, 54.59, 50.22, 49.36, 39.08, 38.21, 37.36, 24.21, 23.25. HR-MS for $C_{19}H_{19}NO_4S$: m/z calc. $[M+H^+]^+$ = 358.1108, m/z obs. $[M+H^+]^+$ = 358.1119.

6.4.1.5 *N*-(((9*H*-fluoren-9-yl)methoxy)carbonyl)-*S*-(2-(bis(benzyloxy)phosphoryl) ethyl)-*L*-homocysteine, Fmoc-hCys(EtPO(OBn)$_2$)-OH (18)

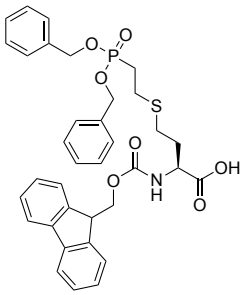

Thiol addition of Fmoc-hCys-OH **22** with alkene **21** was performed at basic pH as followed. 100 mg (280 µmol) AA and 242 mg (840 µmol, 3 eq.) alkene were dissolved in 1.5 mL DMF. After addition of 5 mL 50 mM AmBic buffer, pH 8.5 and pH adjustment to 8.7, the formed precipitate was redissolved with 1.2 mL additional DMF (final concentration of AA 45 mM). The reaction was stirred at 45 °C for 6 h until no starting material could be detected by UPLC analysis anymore. Solvents were evaporated under reduced pressure and by lyophilization and the crude mixture purified by preparative HPLC. 122.9 mg (190.4 µmol, 68%) of desired product were obtained as white powder. ^{1}H NMR (600 MHz, CD_3CN) δ 7.81 (d, J = 7.5 Hz, 2H), 7.65 (dd, J = 7.5, 4.5 Hz, 2H), 7.44 – 7.26 (m, 14H), 6.17 (d, J = 8.4 Hz, 1H), 5.10 – 4.92 (m, 4H), 4.31 (d, J = 6.9 Hz, 2H), 4.29 - 4.24 (m, 1H), 4.20 (t, J = 7.0 Hz, 1H), 2.71 – 2.58 (m, 2H), 2.59 - 2.50 (m, 2H), 2.19 – 1.83 (m, 4H). ^{31}P NMR (243 MHz, CD_3CN) δ 30.15. ^{13}C NMR (151 MHz, CD_3CN) δ 173.07, 156.28, 144.11, 144.01, 141.13, 136.53, 136.45, 128.61, 128.44, 127.99, 127.73, 127.14, 125.24, 120.00, 67.46, 67.44, 67.37, 67.35, 66.35, 52.79, 47.02, 31.04, 27.44, 27.18, 25.40, 23.88, 23.83. HR-MS for $C_{35}H_{36}NO_7PS$: m/z calc. $[M+H^+]^+$ = 646.2043, m/z obs. $[M+H^+]^+$ = 646.2042.

6.4.2 Synthesis of Norleucine-Derived Phosphate 19

6.4.2.1 Synthesis overview

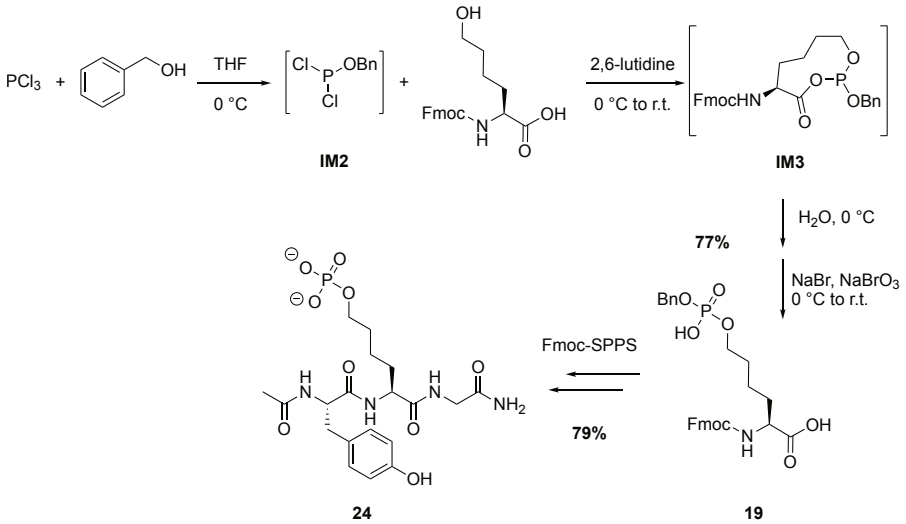

6.4.2.2 (2*S*)-2-((((9*H*-fluoren-9-yl)methoxy)carbonyl)amino)-6-(((benzyloxy)(hy-droxy)phosphoryl)oxy)hexanoic acid, Fmoc-Nle(OPO(OH)(OBn))-OH (19)

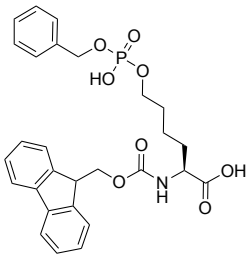

Fmoc-Nle(OPO(OH)(OBn))-OH **19** was prepared as previously described for the pSer derivative.[254] Briefly, in a heated flask and under Ar, 16.5 mL dry THF were cooled in an ice bath for 5 min. 201 µL (2.29 mmol, 1.7 eq) phosphorous trichloride were added and cooled for 2 min as well. While cooling, 238 µL (2.29 mmol, 1.7 eq.) benzyl alcohol were added dropwise and the resulting solution kept at 0 °C for 5 min. Since ^{31}P NMR indicated some PCl_3 left, further 0.3 eq. (0.4 mmol, 42 µL) benzyl alcohol were added and the mixture stirred for 5 min at 0 °C. Upon the addition of 490 µL (4.23 mmol, 3.1 eq.) 2,6-lutidine, a white precipitate was formed, to which a mixture of 500 mg (1.35 mmol, 1 eq.) Fmoc-Nle(6-OH)-OH, 2.8 mL dry THF and 167 µL (1.44 mmol, 1.07 eq.) 2,6-lutidine was dropped within 5 min. The flask was washed with 0.6 mL dry THF to give a final concentration of AA of 65 mM. The reaction was kept for 10 min cooled and then stirred at r.t. until UPLC analysis indicated full consumption of the AA (90 min). Successively, 1.7 mL H_2O, 321 mg (3.12 mmol, 2.3 eq) sodium bromide and 510 µL of a 20% sodium bromate solution (containing 102 mg, 0.7 mmol, 0.51 eq $NaBrO_3$) were added, upon which the mixture turned orange. After 5 min cooling with ice, the reaction was stirred at r.t. for 4 h, when UPLC analysis indicated formation of the desired product. Remaining oxidation reagent was quenched with 10 mL of a 10% $Na_2S_2O_5$ solution as could be observed by destaining of the mixture. The crude product was obtained after evaporation of the solvents under reduced pressure and with lyophilization. 561 mg (1.04 mmol, 77%) of monobenzyl/Fmoc protected phospho-AA **19** were obtained after purification using preparative HPLC. ^{1}H NMR (600 MHz, CD_3CN) δ 7.81 (d, J = 7.6 Hz, 2H), 7.65 (t, J = 6.7 Hz, 2H), 7.41 – 7.37 (m,2H), 7.37 – 7.34 (m, 5H), 7.33 – 7.29 (m, 2H), 6.05 (s, 1H), 5.02 (dd, J = 8.1, 2.2 Hz, 2H), 4.33 – 4.28 (m, 2H), 4.20 (t, J = 7.0 Hz, 1H), 4.12 (d, J = 7.5 Hz, 1H), 3.98 (q, J = 6.6 Hz, 2H), 1.84 – 1.55 (m, 4H), 1.41 (dq, J = 15.7, 7.4 Hz, 2H). ^{31}P NMR (243 MHz, CD_3CN) δ -3.40. ^{13}C NMR (151 MHz, CD_3CN) δ 176.05, 160.46, 160.19, 159.00, 146.78, 143.85, 138.96, 131.84, 131.79, 131.69, 131.13, 130.99, 130.94, 130.77, 130.73, 130.62, 130.39, 130.35, 130.06, 129.93, 129.88, 129.33, 129.29, 128.45, 127.40, 123.26, 123.20, 122.20, 122.15, 71.61, 70.62, 70.06, 69.10, 56.90, 55.98, 50.17, 49.30, 32.03, 24.21. HR-MS for $C_{28}H_{30}NO_8P$: m/z calc. $[M+H^+]^+$ = 540.1782, m/z obs. $[M+H^+]^+$ = 540.1784.

6.4.3 Peptide Synthesis

6.4.3.1 ^{Ac}Tyr-hCys(EtPO(OH)$_2$)-Gly^{CONH_2} (23)

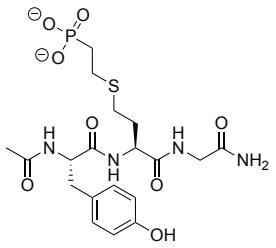

Peptide **23** was synthesized as described in section 6.1 on a 50 µmol scale with resin **80**. Incorporation of building block **18** was conducted as followed: 2 eq. AA (100 µmol, 65 mg) and 1.95 eq. HATU (97.5 µmol, 37.1 mg) were dissolved in 500 µL DMF to give a 0.2 M solution. Directly before adding the mixture to the Fmoc-deprotected resin, 34 µL (4 eq., 200 µmol) DIPEA were added. The mixture was shaken at r.t. for 2 h, when the TNBS test indicated full conversion. The peptide was capped before continuing the peptide coupling. The crude product was purified on an analytical HPLC column to give 11.7 mg (23.5 µmol, 47% with regard to initial resin loading) white powder of desired peptide **23**. ^{1}H NMR (600 MHz, H_2O+10% D_2O, pH 2) δ 8.27 (d, J = 7.5 Hz, 1H), 8.13 (d, J = 5.8 Hz, 1H), 7.31 (t, J = 6.2 Hz, 1H), 7.18 (s, 1H), 6.89 (s, 1H), 6.83 (d, J = 8.5 Hz, 2H), 6.51 (d, J = 8.5 Hz, 2H), 4.10 (m, 1H), 3.58 – 3.39 (m, 2H), 2.65 (ddd, J = 70.4, 13.8, 7.9 Hz, 2H), 2.40 – 2.32 (m, 2H), 2.14 (ddt, J = 96.9, 14.6, 7.8 Hz, 2H), 1.85 (s, 1H), 1.66 (s, 3H), 1.64 (s, 1H), 1.57 (dtt, J = 18.4, 8.9, 3.8 Hz, 3H). ^{31}P NMR (243 MHz, H_2O+10% D_2O, pH 2) δ 23.13. ^{13}C NMR (151 MHz, D_2O) δ 176.90, 176.54, 176.50, 176.04, 157.29, 133.31, 130.46, 118.24, 118.19, 58.37, 55.18, 44.83, 38.69, 32.70, 30.83, 29.96, 29.67, 27.27, 27.25, 24.26. HR-MS for $C_{19}H_{29}N_4O_8PS$: m/z calc. $[M+H^+]^+$ = 505.1517, m/z obs. $[M+H^+]^+$ = 505.1521. t_R (gradient **II**) = 3.691 min.

6.4.3.2 ^{Ac}Tyr-Nle(OPO(OH)$_2$)-Gly^{CONH_2} (24)

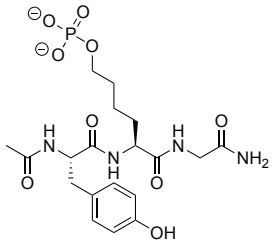

Peptide **24** was synthesized as described in section 6.1 on a 50 µmol scale with resin **80**. The incorporation of building block **19** was conducted as followed: 2 eq. AA (100 µmol, 54 mg) and 1.95 eq. HATU (97.5 µmol, 37.1 mg) were dissolved in 500 µL DMF to give a 0.2 M solution. Directly before adding the mixture to the Fmoc-deprotected resin, 34 µL (4 eq., 200 µmol) DIPEA were added. The mixture was shaken at r.t. for 2 h, when the TNBS test indicated full conversion. The peptide was capped before continuation of the peptide coupling. The crude product was purified on an analytical HPLC column to give 19.3 mg (39.5 µmol, 79% with regard to initial resin loading) white powder of desired peptide **24**. ^{1}H NMR (600 MHz, D_2O) δ 7.13 – 7.07 (m, 2H), 6.82 – 6.77

(m, 2H), 4.51 – 4.45 (m, 1H), 4.21 – 4.16 (m, 1H), 3.88 – 3.83 (m, 2H), 3.78 (dq, J = 24.3, 1.7 Hz, 2H), 2.97 – 2.89 (m, 2H), 1.93 (s, 3H), 1.80 – 1.52 (m, 4H), 1.37 – 1.22 (m, 2H). ^{31}P NMR (243 MHz, D_2O) δ 0.28. ^{13}C NMR (151 MHz, D_2O) δ 176.87, 176.75, 176.63, 176.39, 157.24, 133.29, 130.57, 118.19, 68.94, 68.90, 58.14, 56.46, 44.81, 38.80, 32.83, 31.82, 31.78, 24.26, 23.91. HR-MS for $C_{19}H_{29}N_4O_9P$: m/z calc. $[M+H^+]^+$ = 489.1745, m/z obs. $[M+H^+]^+$ = 489.1740. t_R (gradient **II**) = 1.591 min.

6.4.4 Electrostatic Potential Maps

Electrostatic potential (ESP) maps were prepared by Fabian Müller (HU Berlin) and calculated relying on density functional theory (DFT) optimized molecular structures. The exchange correlation functional B3LYP [304–306] together with the polarized triple zeta basis set def2-TZVPP [307,308] on all atoms was employed and subsequent harmonic vibrational frequency analysis was carried out in order to check if a real local minimum on the potential energy surface was found. From the created electron densities the electrostatic potential was calculated and mapped on the respective density plot for a contour value of 0.01. The Turbomole program package V7.0.2 [309–311] was used for all DFT electronic structure and geometry optimizations. ESP evaluations and visualizations were done with Molden 5.9. [312,313]

6.5 Investigation of Phosphoramidate Hydrolase Activity of LHPP

6.5.1 Synthesis of Phospho-Lysine Substrates 25a, 26a-b, 27a, 28a-j and 29a-j

6.5.1.1 Sythesis overview

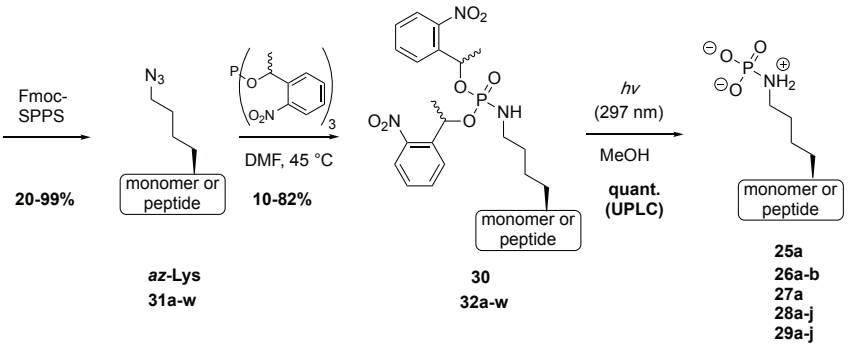

6.5.1.2 Azido-lysine containing peptides (31a-w)

Peptides containing azido-lysine were obtained as described in the peptide synthesis section on a 100 µmol scale on resin **80** or **82**. The crude peptides were used in the next step without further purification.

Table S3: Overview over synthesized azido-lysine peptides including yields (with regard to initial resin loading), high resolution masses and retention times.

#	Sequence	Yield [%]	m/z calc. $[M+H^+]^+$	m/z obs. $[M+H^+]^+$	t_R [min]
31a	^{H_2N}APAPAEK^{N_3}TPVKKKA^{CONH_2}	44	730.9385[a]	730.9388[a]	3.552*
31b	^{H_2N}KKKARK^{N_3}SAGAAKRKASG^{CONH_2}	30	884.5481[a]	884.5491[a]	4.469**
31c	^{Ac}GGK^{N_3}GG^{CONH_2}	99	442.2152	442.2164	4.066**
31d	^{Ac}GAK^{N_3}GG^{CONH_2}	57	456.2314	456.2314	4.450**
31e	^{Ac}GCK^{N_3}GG^{CONH_2}	60	488.2034	488.2033	4.727**
31f	^{Ac}GDK^{N_3}GG^{CONH_2}	52	500.2212	500.2217	4.053**
31g	^{Ac}GFK^{N_3}GG^{CONH_2}	68	532.2627	533.2628	6.446**
31h	^{Ac}GIK^{N_3}GG^{CONH_2}	56	498.2783	498.2787	6.034**
31i	^{Ac}GKK^{N_3}GG^{CONH_2}	20	513.2892	513.2894	4.017**
31j	^{Ac}GPK^{N_3}GG^{CONH_2}	41	482.2470	482.2475	4.910**
31k	^{Ac}GQK^{N_3}GG^{CONH_2}	78	513.2528	513.2534	3.937**
31l	^{Ac}GRK^{N_3}GG^{CONH_2}	52	541.2954	541.2955	4.149**
31m	^{Ac}GSK^{N_3}GG^{CONH_2}	99	472.2263	472.2267	3.854**
31n	^{Ac}GGK^{N_3}AG^{CONH_2}	62	456.2314	456.2316	4.333**
31o	^{Ac}GGK^{N_3}CG^{CONH_2}	55	488.2034	488.2040	4.870**
31p	^{Ac}GGK^{N_3}DG^{CONH_2}	28	500.2212	500.2214	3.949**
31q	^{Ac}GGK^{N_3}FG^{CONH_2}	60	532.2627	532.2631	6.693**
31r	^{Ac}GGK^{N_3}IG^{CONH_2}	56	498.2783	498.2788	5.945**
31s	^{Ac}GGK^{N_3}KG^{CONH_2}	23	513.2892	513.2893	3.754**
31t	^{Ac}GGK^{N_3}PG^{CONH_2}	66	482.2470	482.2473	4.812**
31u	^{Ac}GGK^{N_3}QG^{CONH_2}	51	513.2528	513.2527	3.716**
31v	^{Ac}GGK^{N_3}RG^{CONH_2}	44	541.2954	541.2965	3.784**
31w	^{Ac}GGK^{N_3}SG^{CONH_2}	68	472.2263	472.2267	3.643**

[a] m/z $[M+2H^+]^{2+}$ * gradient **I** ** gradient **II**

6.5.1.3 N^6-(bis(1-(2-nitrophenyl)ethoxy)phosphoryl)-*L*-lysine, NH_2-Lys(NPO(ONPE)$_2$)-OH (30)

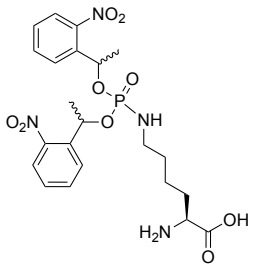

20.8 mg N^6-diazo-*L*-lysine hydrochloride (100 µmol) and 79.4 mg phosphite **9** (150 µmol, 1.5 eq.) were dissolved to a 50 mM solution in dry DMF (with regard to AA) in a round-bottom flask and Ar was bubbled through the solution for 5 min. After that, the flask was closed with a

septum equipped with Ar filled balloon and the mixture was stirred at 45 °C, while subsequently more phosphite (1.5 eq. each time) was added after 6 and 24 h until UPLC showed full consumption of the AA (48 h). DMF was evaporated under reduced pressure, residual solvent was removed *via* lyophilization and the crude product purified *via* preparative HPLC. The product was obtained as yellow sticky oil (41.4 mg, 79 µmol, 79%). ^{1}H NMR (300 MHz, CD_3CN) δ 8.02 – 7.42 (m, 8H), 5.94 – 5.68 (m, 2H), 3.91 (ddd, J = 18.4, 14.2, 6.1 Hz, 2H), 2.66 (d, J = 7.7 Hz, 2H), 1.95 – 1.15 (m, 12H). ^{31}P NMR (122 MHz, CD_3CN) δ 8.13, 7.79, 7.43. ^{13}C NMR (151 MHz, CD_3CN) δ 171.24, 160.23, 159.99, 146.96, 146.79, 137.49, 134.03, 133.95, 129.01, 128.91, 128.83, 127.93, 127.81, 127.64, 124.32, 124.29, 124.26, 70.98, 70.81, 70.71, 53.16, 39.85, 39.65, 39.56, 30.14, 30.02, 29.16, 28.99, 23.58, 21.07, 20.96, 20.85. HR-MS for$C_{22}H_{29}N_4O_9P$: m/z calc. $[M+H^+]^+$ = 525.1745, m/z obs. $[M+H^+]^+$ = 525.1756. t_R (gradient **I**) = 5.605 min.

6.5.1.4 NPE-caged phospho-lysine (cpK) peptides (32a-w)

Caged phosphoramidates peptide were synthesized as described above with following changes. 10 µmol azido-peptide and 30 µmol phosphite **9** (3 eq., 15.9 mg) were dissolved to 25 mM in dry DMF (400 µL) and shaken at 950 rpm at 45 °C. After 6 h and 24 h, 3 eq. phosphite were added again. The solvent was evaporated under reduced pressure after 48 h and residuals removed during lyophilisation. The final product was obtained as white powder after purification *via* semi-preparative HPLC.

Table S4: Overview over synthesized NPE-caged phospho-lysine peptides including yields, high resolution masses and retention times.

#	Sequence	Yield [%]	m/z calc. $[M+H^+]^+$	m/z obs. $[M+H^+]^+$	t_R [min]
32a	^{H_2N}APAPAEcpKTPVKKKA^{CONH_2}	48	906.9741[a]	906.9749[a]	5.224*
32b	^{H_2N}KKKARcpKSAGAAKRKASG^{CONH_2}	56	1,060.5837[a]	1,060.5833[a]	4.691*
32c	^{Ac}GGcpKGG^{CONH_2}	82	794.2864	794.2885	5.621*
32d	^{Ac}GAcpKGG^{CONH_2}	16	808.3022	808.3034	5.696*
32e	^{Ac}GCcpKGG^{CONH_2}	20	840.2742	840.2742	5.819*
32f	^{Ac}GDcpKGG^{CONH_2}	42	852.2920	852.2918	5.662*
32g	^{Ac}GFcpKGG^{CONH_2}	62	884.3335	884.3325	6.379*
32h	^{Ac}GIcpKGG^{CONH_2}	79	850.3491	850.3493	6.212*
32i	^{Ac}GKcpKGG^{CONH_2}	59	865.3600	865.3610	5.460*
32j	^{Ac}GPcpKGG^{CONH_2}	58	834.3178	831.3177	5.844*
32k	^{Ac}GQcpKGG^{CONH_2}	62	865.3236	865.3236	5.523*
32l	^{Ac}GRcpKGG^{CONH_2}	48	893.3662	893.3664	5.508*
32m	^{Ac}GScpKGG^{CONH_2}	26	824.2971	824.2971	5.579*
32n	^{Ac}GGcpKAG^{CONH_2}	12	808.3022	808.3022	5.684*
32o	^{Ac}GGcpKCG^{CONH_2}	10	840.2742	840.2740	5.867*
32p	^{Ac}GGcpKDG^{CONH_2}	57	852.2920	852.2920	5.625*
32q	^{Ac}GGcpKFG^{CONH_2}	53	884.3335	884.3325	6.464*

32r	^{Ac}GGcpKIG^{CONH_2}	59	850.3491	850.3491	6.190*
32s	^{Ac}GGcpKKG^{CONH_2}	49	865.3600	865.3596	5.410*
32t	^{Ac}GGcpKPG^{CONH_2}	37	834.3178	834.3177	5.739*
32u	^{Ac}GGcpKQG^{CONH_2}	73	865.3236	865.3237	5.486*
32v	^{Ac}GGcpKRG^{CONH_2}	60	893.3662	893.3663	5.430*
32w	^{Ac}GGcpKSG^{CONH_2}	42	824.2971	824.2971	5.556*

[a] m/z [M+2H$^+$]$^{2+}$ * gradient **I** ** gradient **II**

6.5.1.5 N^6-phosphono-*L*-lysine, pLys (25a)

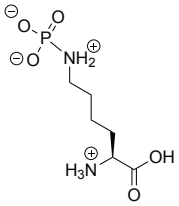

1 µmol caged-pLys **30** (0.52 mg) was deprotected and worked up as described in the photodeprotection section under 6.1. ^{1}H NMR (300 MHz, H_2O) δ 3.43 (t, J = 6.5 Hz, 1H), 2.73 (td, J = 8.2, 4.4 Hz, 2H), 1.48 (ddt, J = 113.3, 16.2, 9.1 Hz, 4H), 1.13 (dddt, J = 31.0, 21.7, 15.9, 8.7 Hz, 2H). ^{31}P NMR (122 MHz, H_2O) δ −1.06. ^{13}C NMR (151 MHz, H_2O) δ 157.86, 54.35, 42.69, 29.74, 26.30, 21.10. HR-MS for $C_6H_{15}N_2O_5P$: m/z calc. [M+H$^+$]$^+$ = 227.0792, m/z obs. [M+H$^+$]$^+$ = 227.0794. t_R (gradient **II**) = 0.545 min.

6.5.1.6 Phospho-lysine peptides (26a-b, 27a, 28a-j, 29a-j)

pLys-peptides were obtained as described in the photodeprotection section (6.1) on a 1 µmol scale.

Table S5: Overview over synthesized phospho-lysine peptides including high resolution masses and retention times.

#	Sequence	m/z calc. [M+H$^+$]$^+$	m/z obs. [M+H$^+$]$^+$	t_R [min]
26a	^{H_2N}APAPAEpKTPVKKKA^{CONH_2}	757.9264[a]	757.9271	4.372**
26b	^{H_2N}KKKARpKSAGAAKRKASG^{CONH_2}	911.5360[a]	911.5367[a]	3.718**
27a	^{Ac}GGpKGG^{CONH_2}	496.1911	496.1956	0.481**
28a	^{Ac}GApKGG^{CONH_2}	510.2068	510.2074	0.450**
28b	^{Ac}GCpKGG^{CONH_2}	542.1788	542.1791	0.347**
28c	^{Ac}GDpKGG^{CONH_2}	554.1966	554.1981	0.349**
28d	^{Ac}GFpKGG^{CONH_2}	586.2381	586.2385	0.373**
28e	^{Ac}GIpKGG^{CONH_2}	552.2537	552.2545	0.374**
28f	^{Ac}GKpKGG^{CONH_2}	567.2646	567.2653	0.355**
28g	^{Ac}GPpKGG^{CONH_2}	536.2224	536.2245	0.675**
28h	^{Ac}GQpKGG^{CONH_2}	567.2282	567.2299	0.347**

28i	^{Ac}GRpKGG^{CONH_2}	595.2708	595.2714	0.509**
28j	^{Ac}GSpKGG^{CONH_2}	526.2017	526.2018	0.345**
29a	^{Ac}GGpKAG^{CONH_2}	510.2068	510.2070	0.574**
29b	^{Ac}GGpKCG^{CONH_2}	542.1788	542.1789	0.374**
29c	^{Ac}GGpKDG^{CONH_2}	554.1966	554.1985	0.347**
29d	^{Ac}GGpKFG^{CONH_2}	586.2381	586.2388	0.373**
29e	^{Ac}GGpKIG^{CONH_2}	552.2537	552.2542	0.458**
29f	^{Ac}GGpKKG^{CONH_2}	567.2646	567.2652	0.494**
29g	^{Ac}GGpKPG^{CONH_2}	536.2224	536.2228	0.683**
29h	^{Ac}GGpKQG^{CONH_2}	567.2282	567.2286	0.347**
29i	^{Ac}GGpKRG^{CONH_2}	595.2708	595.2719	0.436**
29j	^{Ac}GGpKSG^{CONH_2}	526.2017	526.2018	0.433**

[a] m/z [M+2H$^+$]$^{2+}$ * gradient **I** ** gradient **II**

6.5.2 Synthesis of Phospho-Serine, -Threonine and -Tyrosine Substrates 25b-d and 27b-d

6.5.2.1 Synthesis overview

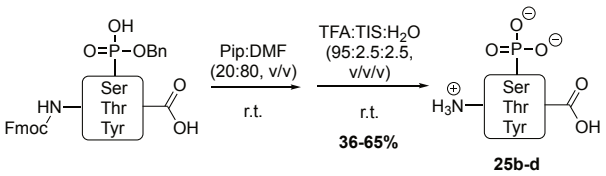

6.5.2.2 *O*-phosphorylated monomers, pSer, pThr and pTyr (25b-d)

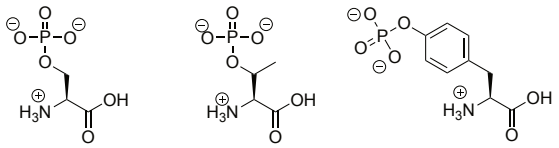

Phosphate amino acids **25b**, **25c** and **25d** were obtained by subsequent global deprotection of commercially available the SPPS-building blocks Fmoc-Ser(PO(OBzl)OH)-OH, Fmoc-Thr(PO(OBzl)OH)-OH, and Fmoc-Tyr(PO(OBzl)OH)-OH. Briefly, 100 µmol AA were dissolved to a 50 mM solution in Pip:DMF (20:80, v/v) and shaken at r.t. for 10 min. The solvent was evaporated under reduced pressure and residuals removed *via* lyophilization. The product was purified from the fluoren adduct *via* flash prep HPLC, concentrated under reduced pressure and directly treated with 1 mL TFA:TIS:H_2O (95:2.5:2.5, v/v/v)) for 90 min. The crude product was precipitated in a 10-fold excess of cold Et_2O, kept in the freezer for 10 min, separated from the ether by centrifugation and purified by semi-preparative HPLC.

pSer **25b**: white powder, 11.6 mg (65 µmol, 65%). ^{1}H NMR (600 MHz, D_2O) δ 4.28 (dt, J = 11.6, 5.7 Hz, 1H), 4.25 – 4.19 (m, 2H). ^{31}P NMR (243 MHz, D_2O) δ -0.28. ^{13}C NMR (151 MHz, D_2O) δ

169.83, 62.96, 62.93, 53.87, 53.81. HR-MS for $C_3H_8NO_6P$: m/z calc. $[M+H^+]^+$ = 186.0162, m/z obs. $[M+H^+]^+$ = 186.0171. t_R (gradient **II**) = 0.359 min.

pThr **25c**: white powder, 7.2 mg (36 µmol, 36%). ^{1}H NMR (600 MHz, D_2O) δ 4.70 (s, 1H), 3.95 (ddd, J = 4.0, 2.6, 1.3 Hz, 1H), 1.41 (d, J = 6.6 Hz, 3H). ^{31}P NMR (243 MHz, D_2O) δ -1.29. ^{13}C NMR (151 MHz, D_2O) δ 170.46, 70.31, 58.58, 18.26. HR-MS for $C_4H_{10}NO_6P$: m/z calc. $[M+H^+]^+$ = 200.0318, m/z obs. $[M+H^+]^+$ = 200.0326. t_R (gradient **II**) = 0.327 min.

pTyr **25d**: white powder, 15.1 mg (58 µmol, 58%). ^{1}H NMR (600 MHz, D_2O) δ 7.32 (d, J = 8.5 Hz, 2H), 7.25 – 7.20 (m, 2H), 4.25 (dd, J = 8.1, 5.2 Hz, 1H), 3.39 – 3.16 (m, 2H). ^{31}P NMR (243 MHz, D_2O) δ -3.95. ^{13}C NMR (151 MHz, D_2O) δ 172.19, 151.60, 151.56, 130.61, 129.95, 121.03, 121.00, 54.70, 35.11. HR-MS for $C_9H_{12}NO_6P$: m/z calc. $[M+H^+]^+$ = 262.0475, m/z obs. $[M+H^+]^+$ = 262.0486. t_R (gradient **II**) = 0.391 min.

6.5.2.3 *O*-phosphorylated peptides (27b-d)

Peptides **27b**, **27c** and **27d** were obtained as described in the peptide synthesis section on a 50 µmol scale on resin **80** and purified by semi-preparative HPLC.

^{Ac}GGpSGG^{CONH_2} **27b**: 14.5 mg (32 µmol, 64%). HR-MS for $C_{13}H_{23}N_6O_{10}P$: m/z calc. $[M+H^+]^+$ = 455.1282, m/z obs. $[M+H^+]^+$ = 455.1290. t_R (gradient **II**) = 0.341 min.

^{Ac}GGpThrGG^{CONH_2} **27c**: 18.8 mg (40 µmol, 80%). HR-MS for $C_{14}H_{25}N_6O_{10}P$: m/z calc. $[M+H^+]^+$ = 469.1438, m/z obs. $[M+H^+]^+$ = 469.1444. t_R (gradient **II**) = 0.367 min.

^{Ac}GGpTyrGG^{CONH_2} **27d**: 22.6 mg (42.5 µmol, 85%). HR-MS for $C_{19}H_{27}N_6O_{10}P$: m/z calc. $[M+H^+]^+$ = 531.1595, m/z obs. $[M+H^+]^+$ = 531.1602. t_R (gradient **II**) = 0.408 min.

6.5.3 Synthesis of Phospho-Arginine Substrates 25e and 27e

6.5.3.1 Synthesis overview

The SPPS-compatible building block Fmoc-Arg(NPO(OTc)$_2$)-OH **34** was synthesized as previously described [112] with minor adjustments as outlined below.

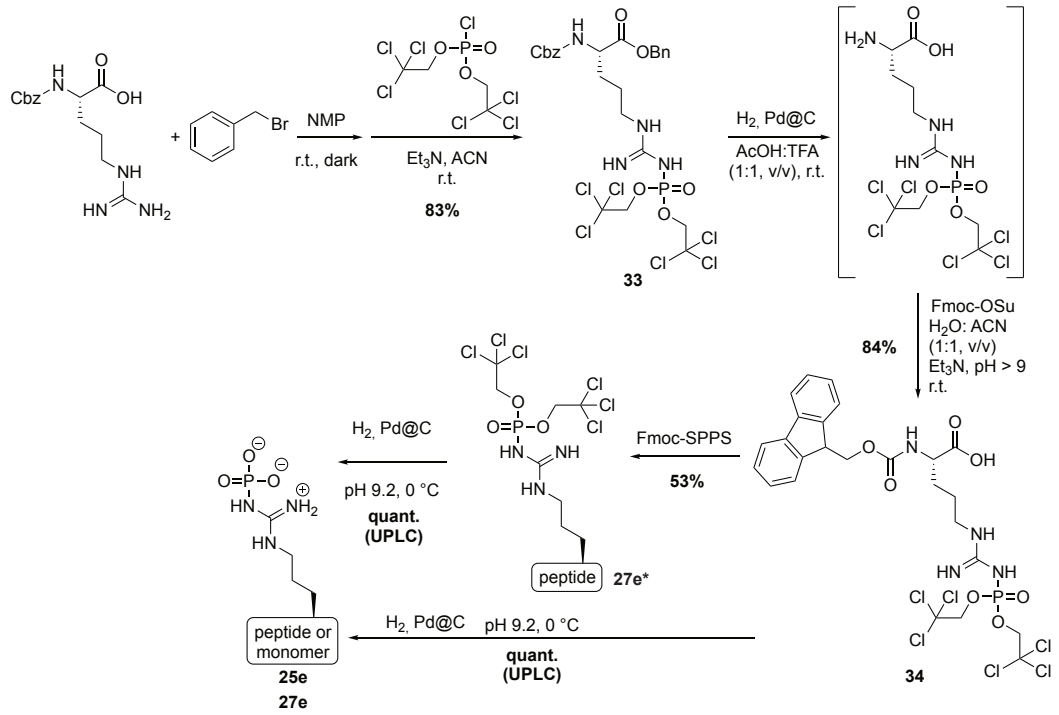

6.5.3.2 Benzyl N^2-((benzyloxy)carbonyl)-N^ω-(bis(2,2,2-trichloroethoxy)phosphoryl)-*L*-arginate (33)

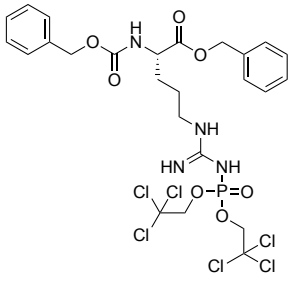

Z-Arg(NPO(OTc)$_2$)-OBn **33** was synthesized from Z-Arg-OH. Briefly, 2.5 g Z-Arg-OH (8.1 mmol) were suspended to 0.25 M in NMP and Ar was bubbled through the suspension for 15 min. Equipped with septum and Ar-balloon, the mixture was heated to 90 °C bath temperature until the AA had dissolved completely. After cooling the mixture to r.t., 1.1 mL benzyl bromide (8.91 mmol, 1.1 eq.) were added dropwise and the mixture left stirring in the dark under Ar overnight. NMP was removed under reduced pressure and the resulting yellow oil dissolved to 67 mM in ACN. Upon addition of 4.52 mL Et$_3$N (32.4 mmol, 4 eq.), the yellow solution turned colourless. 3.7 g (9.7 mmol, 1.2 eq.) Bis(trichloroethyl)phosphoryloxychloride were added in three equal portions at 0, 60 and 120

min and the reaction stirred at r.t. Since UPLC analysis after 6 h indicated still some intermediate left, 0.1 eq. of the phosphorylation reagent were added and the reaction left ovn at r.t. The solvents were evaporated under reduced pressure and the crude product adsorbed to silica gel for purification *via* column chromatography (hex/EE 7/3+1% FA → hex/EE 4/6+1% FA, the product eluting at 50% EE). 5.0 g (6.7 mmol, 83%) of a colorless oil were obtained as product. ^{1}H NMR (600 MHz, acetone-d_6) δ 7.43 – 7.27 (m, 10H), 6.75 (d, J = 8.0 Hz, 1H), 6.59 – 6.47 (m, 1H), 6.39 (s, 1H), 5.17 (s, 2H), 5.12 – 5.01 (m, 2H), 4.61 (q, J = 11.2, 8.1 Hz, 4H), 4.31 (td, J = 8.7, 5.0 Hz, 1H), 3.32 (s, 2H), 1.86 (ddtd, J = 88.4, 14.2, 9.7, 9.1, 5.8 Hz, 2H), 1.74 – 1.62 (m, 2H). ^{31}P NMR (243 MHz, acetone-d_6) δ 5.50. ^{13}C NMR (151 MHz, acetone-d_6) δ 172.01, 159.06, 159.00, 156.28, 137.18, 136.19, 128.46, 128.34, 128.19, 128.06, 127.94, 127.80, 127.77, 96.31, 96.23, 76.46, 76.43, 66.29, 66.11, 65.99, 54.09, 40.25, 25.94. HR-MS for $C_{25}H_{29}Cl_6N_4O_7P$: m/z calc. $[M+H^+]^+$ = 738.9978, m/z obs. $[M+H^+]^+$ = 738.9932. R_f (hex/EE 4/6+1% FA) = 0.33.

6.5.3.3 N^2-(((9*H*-fluoren-9-yl)methoxy)carbonyl)-N^{ω}-(bis(2,2,2-trichloroethoxy) phosphoryl)-*L*-arginine (34)

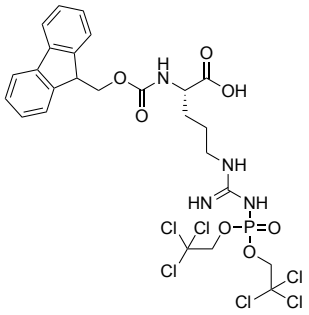

2.5 g Z-Arg(NPO(OTc)$_2$)-OBn **34** (3.37 mmol) were dissolved to a 75 mM solution in AcOH:TFA (1:1, v/v) and set under inert atmosphere. After addition of 375 mg palladium on charcoal (10% wt Pd), Ar was exchanged with hydrogen and the reaction mixture stirred under hydrogen atmosphere at r.t. UPLC analysis after 60 min indicated full Cbz and benzyl deprotection. The catalyst was filtered off, washed with AcOH:TFA (1:1, v/v) and the solvent evaporated under reduced pressure. Residual acid was removed by coevaporation with EtOH and under high vaccum ovn. The crude intermediate was suspended in 8.5 mL H_2O and 471 µL Et_3N (3.37 mmol, 1 eq.) were added. Upon adjustment of the pH to 9 by the addition of more Et_3N, the solution became clear. A solution of 1.14 g Fmoc-OSu (3.37 mmol, 1 eq.) in 8.5 mL ACN was added dropwise while the pH was maintained above 8.0 by the addition of further Et_3N. With a stabilized pH of 9.0 after 40 min, UPLC analysis indicated full conversion. The pH was adjusted to 3.5 with AcOH and an equal volume of brine added under vigorous stirring. The mixture was washed 3x with $CHCl_3$, the combined organic layers were dried over Na_2SO_4 and the filtrate concentrated under reduced pressure. The product was obtained after silica column chromatography (hex/EE 5/5+1% FA → EE 100%+1% FA, the product eluting at 85% EE) as white powder (2.01 g, 2.83 mmol, 84%). ^{1}H NMR (600 MHz, CD_3CN+TFA-d_1) δ 8.83 (d, J = 5.6 Hz, 1H), 7.87 (d, J = 7.5 Hz, 2H), 7.70 (t, J = 7.6 Hz, 2H), 7.45 (t, J = 7.5 Hz, 2H), 7.37 (t, J = 7.4 Hz, 2H), 6.18 (d, J = 8.2 Hz, 1H), 4.84 (qd, J = 11.2, 4.5 Hz, 4H), 4.39 (d, J = 7.1 Hz, 2H), 4.28 (t, J = 7.0 Hz, 1H), 4.20 (d, J = 9.9 Hz, 1H), 3.35 – 3.21 (m, 2H), 1.93 (d, J = 10.2 Hz, 1H), 1.74 (dq, J = 14.4, 7.6 Hz, 3H). ^{31}P NMR (243 MHz, CD_3CN+TFA-d_1) δ -3.71. ^{13}C NMR

(151 MHz, CD_3CN+TFA-d_1) δ 156.47, 155.02, 144.10, 144.01, 141.17, 127.74, 127.13, 125.20, 120.02, 116.18, 114.28, 112.38, 94.15, 94.08, 76.87, 76.84, 66.51, 53.10, 53.00, 47.04, 41.45, 41.33, 28.40, 28.36, 23.89. HR-MS for $C_{25}H_{27}Cl_6N_4O_7P$: m/z calc. $[M+H^+]^+$ = 736.9822, m/z obs. $[M+H^+]^+$ = 736.9828. R_f (EE: 100%+1% FA) = 0.50.

6.5.3.4 ^{Ac}Gly-Gly-Arg(NPO(OTc)$_2$)-Gly-Gly^{CONH_2} (27e*)

2,2,2-Trichloroethyl-protected pArg peptide was obtained as described in the peptide synthesis section on a 50 µmol scale on resin **80**. The crude product was purified by semi-preparative HPLC to give 21 mg (11.5 µmol, 53% with regard to initial resin loading) of a white powder as desired product. HR-MS for $C_{20}H_{32}Cl_6N_9O_9P$: m/z calc. $[M+H^+]^+$ = 784.0261, m/z obs. $[M+H^+]^+$ = 784.0262. t_R (gradient **I**) = 5.291 min.

6.5.3.5 N^{ω}-phosphono-*L*-arginine, pArg (25e)

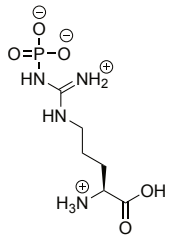

pArg was obtained by global deprotection of Fmoc-Arg(NPO(OTc)$_2$)-OH **34**. Briefly, to 7.4 mg **34** (10 µmol) in 4 mL 25 mM $(NH_4)_2CO_3$ at pH 9.2 18 mg palladium on charcoal (10% wt Pd) were added under Ar. After addition of 1 mL EtOH, the atmosphere was exchanged to hydrogen and the reaction stirred for 60 min in an ice bath until UPLC indicated full conversion. The catalyst was filtered off, washed with low amount of water and the solvents removed by lyophilization. Deprotected pArg was stored in the freezer until applied in the assay. ^{1}H NMR (600 MHz, D_2O) δ 3.78 (t, J = 6.2 Hz, 1H), 3.29 (t, J = 6.9 Hz, 2H), 1.99 – 1.87 (m, 2H), 1.80 – 1.63 (m, 2H). ^{31}P NMR (243 MHz, D_2O) δ -3.59. ^{13}C NMR (151 MHz, D_2O) δ 174.65, 155.77, 54.36, 40.42, 27.72, 23.99. HR-MS for $C_6H_{15}N_4O_5P$: m/z calc. $[M+H^+]^+$ = 255.0853, m/z obs. $[M+H^+]^+$ = 255.0860. t_R (gradient **II**) = 0.345 min.

6.5.3.6 ^{Ac}Gly-Gly-Arg(NPO(OH)$_2$)-Gly-Gly^{CONH_2} (27e)

4.3 mg ^{Ac}Gly-Gly-Arg(NPO(OTc)$_2$)-Gly-Gly^{CONH_2} were dissolved in 550 µL 100 mM $(NH_4)_2CO_3$, pH 9.2 under Ar atmosphere. 10 mg palladium on charcoal (10% wt Pd) were added together with 2.2 mL EtOH, the Ar exchanged with hydrogen and the mixture stirred in an ice bath until UPLC indicated full conversion, usually after 1 h. The catalyst was filtered off, washed with little amount of water and the solvents removed by lyophilization. Deprotected pArg peptide was stored in the freezer until applied in the assay. HR-MS for $C_{16}H_{30}N_9O_9P$: m/z calc. $[M+H^+]^+$ = 524.1973, m/z obs. $[M+H^+]^+$ = 524.1976. t_R (gradient **II**) = 0.420 min.

6.5.4 Synthesis of Phospho-Histidine Substrate 25f

6.5.4.1 Synthesis Overview

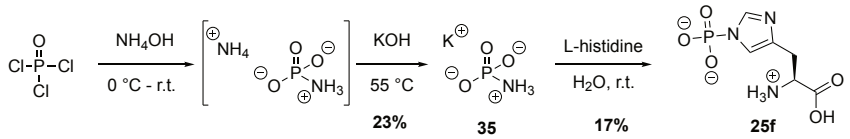

6.5.4.2 Potassium phosphoramidate (K-PA, 35)

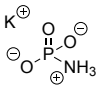

Potassium phosphoramidate (K-PA) was synthesized as previously described.[138] Under vigorous stirring, 4.6 mL phosphorus oxychloride (50 mmol) were added dropwise to 75 mL of precooled 10% ammonium hydroxide in water (396 mmol, 8 eq.) and kept in an ice bath until steam formation ceased. 250 mL acetone were added and the layers separated. The aqueous layer was acidified to pH 6 with AcOH, at which a white precipitate formed. After resting the mixture at r.t. for 60 min, the precipitate was filtered, washed with EtOH and Et_2O, dried under reduced pressure and left under the hood ovn. To the intermediate ammonium salt (1.36 g, 24%) 4 mL 50% KOH in water were added. The bubbling mixture was stirred at 55 °C bath temperature for 15 min to allow ammonia release. After cooling to 5 °C, the mixture was acidified to pH 6 with AcOH and poured into 300 mL EtOH. Gently stirring at r.t. for 60 min led to formation of white precipitate, which was filtered off, washed with cold EtOH and dried under the hood ovn to give the product as white solid (1.55 g, 11.5 mmol, 23%). ^{31}P NMR (122 MHz, D_2O) δ -2.98. HR-MS for H_3NO_3P: m/z calc. $[M+H^+]^+ = 98.0002$, m/z obs. $[M+H^+]^+ = 97.9998$.

6.5.4.3 N^τ-phosphono-*L*-histidine, pHis (25f)

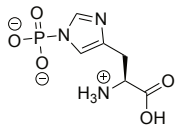

Phosphorylation of histidine was accomplished as described previously.[138] Briefly, 250 mg *L*-histidine (1.6 mmol) and 370 mg K-PA (2.7 mmol, 1.7 eq.) were dissolved in 6.25 mL H_2O and stirred at r.t. for five days. The reaction mixture was purified by SAX on an FPLC system at 4 °C. Fractions giving positive TNBS test result were pooled and diluted with 0.1 M Tris, 0.5 M LiCl (pH 8.25, 4 °C) until addition of three volumes of cold EtOH induced precipitation. The mixture was stirred gently at 4 °C for 5 min and centrifuged 10 min (4,000 × *g*). The precipitate was dried under reduced pressure, while to the supernatant four volumes of cold EtOH were added and resulting mixture left at 4 °C ovn to induce and evolve precipitation. The product was obtained after filtration and drying of the second precipitate under reduced pressure as white solid (63.9 mg, 272 µmol,

17%). Coupling of phosphorous to both aromatic protons detected by ^{1}H,^{31}P-HMBC indicated the formation of τ-pHis. ^{1}H NMR (600 MHz, D_2O) δ 7.60 (d, J = 1.1 Hz, 1H), 6.92 (d, J = 1.4 Hz, 1H), 3.76 (dd, J = 8.6, 4.6 Hz, 1H), 2.99 (d, J = 4.6 Hz, 1H), 2.85 (dd, J = 15.3, 8.5 Hz, 1H). ^{31}P NMR (243 MHz, D_2O) δ -4.49. ^{13}C NMR (151 MHz, D_2O) δ 174.47, 139.20, 136.27, 134.43, 131.89, 118.43, 118.40, 117.09, 54.68, 28.71. HR-MS for $C_6H_{10}N_3O_5P$: m/z calc. $[M+H^+]^+$ = 236.0431, m/z obs. $[M+H^+]^+$ = 236.0428.

6.5.5 Optimization of Assay Conditions

In order to gain valuable kinetic data within less than 120 min reaction time, optimal substrate as well as enzyme concentrations needed to be determined. Therefore, varying amounts of pLys **25a** (0 to 250 µmol·L^{-1}) were incubated with varying amounts of LHPP (0 to 1 µg, purchased at ProSpec-Tany TechnoGene Ltd. International, Ness-Ziona, Israel) for 240 min. Absorbance at 360 nm was recorded every ten minutes. Substrate—LHPP combinations were evaluated regarding their kinetic profile within 90 min reaction time. Hence, 100 µM substrate **25a** with 0.25 µg enzyme (7.4·10^{-3} nmol, 3.7·10^{-4} eq.) were identified as the optimal standard conditions.

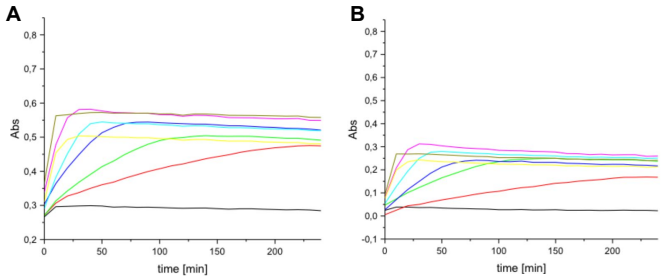

Figure S1: Example of reaction from assay optimization. Absorbance measurements over time of incubation of 100 µM **25a** with varying amounts of LHPP before **A** and after **B** background subtraction. — no enzyme, — 0.03125 µg, — 0.0625 µg, — 0.125 µg, — 0.25 µg, — 0.5 µg, — 0.75 µg, — 1 µg.

6.5.6 Computational Methods

All calculations for the molecular docking as well as molecular dynamic (MD) simulations were conducted by Han Sun (FMP Berlin).

6.5.6.1 Molecular docking

Molecular docking was performed to explore possible binding poses of GGpKGG with the LHPP, where the residues around the catalytic center (Mg^{2+}) of the crystal structure (PDB ID: 2x4d) were defined as the center of the docking pocket. A receptor grid was calculated for LHPP with a box size of 10 Å x 10 Å x 10 Å and an atomistic structure of GGpKGG using the software Schrödinger with both *C*- and *N*-termini capped with *N*-methyl (NME) and acetyl (ACE) groups as **27a***. With an energy minimized structure, docking of the GGpKGG into the pocket was carried out using the Glide module [260–262] implemented in the program Schrödinger. Out of ten docking poses with highest scores, those poses were chosen, which exhibited highest overlap of phosphoramidate group

with phosphate in the known crystal structure. Subsequent MD simulations were performed with structures showing significant variation in the binding conformation of GGpKGG to LHPP.

6.5.6.2 MD simulations

For the MD simulations, dimeric structure of LHPP (PDB ID: 2x4d) with one GGpKGG peptide chain bound at chain A of LHPP was used. In the starting structure the peptide was manually mutated in Pymol.[314] and one Mg^{2+} at its crystallographic position in the catalytic center added. For the equilibration, a 10 ns simulation was performed starting from each docking poses.

For each equilibrium simulation of 100 ns the first 10 ns were discarded. From the remaining trajectory one frame was extracted after every 1.8 ns, so that in total 50 frames were obtained. Hybrid structures and topologies were generated comprising the states before and after the mutation (figure S2). The generated hybrid structures were firstly energy-minimized using steepest descent algorithm. Subsequently, 20 ps of equilibrium simulations were carried out. Starting from the end states of the equilibrium simulations, 100 ps of non-equilibrium transitions were performed from the non-modified to the mutated state, e.g. GGpKGG→GApKGG, and back, e.g. GApKGG→GGpKGG. Expect otherwise stated, in the non-equilibrium simulations all the parameters kept the same as they were in the equilibrium simulations described above. From the output of the work values obtained from the non-equilibrium simulations, free energy differences were estimated using Crooks Gaussian Intersection (CGI) and Bennet's Acceptance Ratio (BAR) methods[315] that are implemented in the pmx[268,316] (table S6).

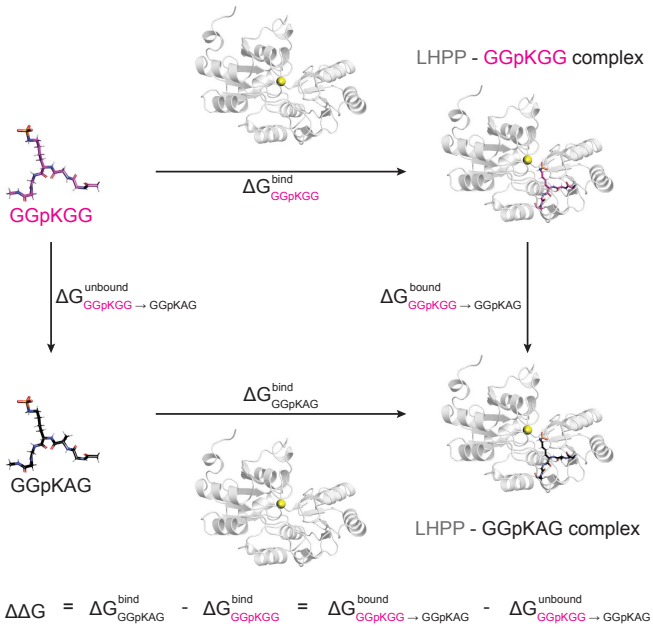

Figure S2: Thermodynamic cycle used in this study to calculate the free energy difference between **27a*** and other mutated peptides

Table S6: Calculated ΔΔG and errors of four mutated substrates relative to the wild type model substrate **27a** estimated from the MD simulations starting from four different docking poses. CGI and BAR estimators were employed for the analysis of ΔΔG.

Substrate	Description	Docking pose	$\Delta\Delta G_{CGI}$ [kJ·mol^{-1}]	Error ±	$\Delta\Delta G_{BAR}$ [kJ·mol^{-1}]	Error ±
28a*	Ala_N	**1**	1.34	1.07	3.18	0.69
		2	-2.41	1.06	-0.55	0.44
		3	-0.77	1.02	-0.03	1.34
		4	3.00	1.03	4.69	0.51
28f*	Lys_N	**1**	24.49	3.45	22.49	0.83
		2	-15.32	2.45	-9.70	0.82
		3	-15.57	2.17	-11.58	0.83
		4	27.26	2.31	21.83	0.98
28i*	Arg_N	**1**	-7.89	4.53	-7.89	2.67
		2	-4.99	3.80	-4.38	2.70
		3	-0.9	5.57	-0.5	2.57
		4	22.43	4.46	13.28	2.22
28j*	Ser_N	**1**	6.27	0.88	7.79	0.87
		2	-1.04	0.84	1.66	0.83
		3	-1.25	0.83	0.21	0.67
		4	8.27	0.85	7.79	0.63
29a*	Ala_C	**1**	2.30	0.69	1.89	0.54
		2	-2.15	0.62	-1.14	0.46
		3	0.36	0.60	0.70	0.47
		4	3.59	0.59	4.80	0.38
29f*	Lys_C	**1**	0.75	3.41	-2.78	2.20
		2	-14.58	2.48	-10.92	2.04
		3	-18.96	2.75	-15.38	1.97
		4	-13.84	2.49	-11.95	1.84
29i*	Arg_C	**1**	9.88	4.58	9.88	2.65
		2	0.53	3.22	-1.68	1.60
		3	9.16	3.35	2.95	2.46
		4	22.33	4.32	10.61	2.74
29j*	Ser_C	**1**	8.73	1.35	6.11	1.24
		2	-0.62	1.17	-2.07	0.64
		3	-4.10	1.20	-4.93	0.82
		4	1.89	1.34	-2.31	0.60

6.6 Generation of Monoclonal Anti-Phospho-Lysine Antibody

6.6.1 Randomized Peptide Synthesis for First Immunization Approach

6.6.1.1 Synthesis overview

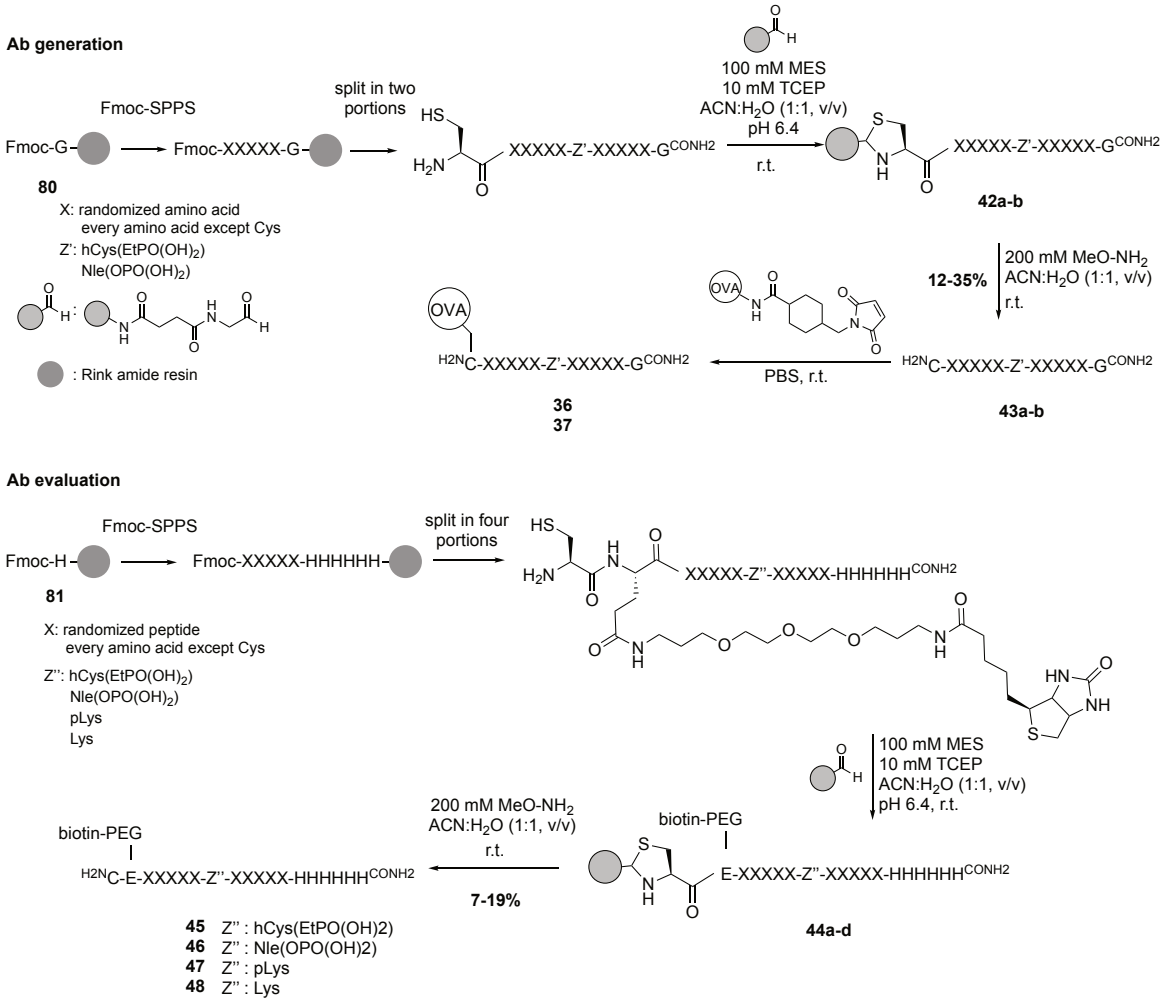

6.6.1.2 Aldehyde functionalization of Amino-PEGA resin (51)

figure aldehyde resin

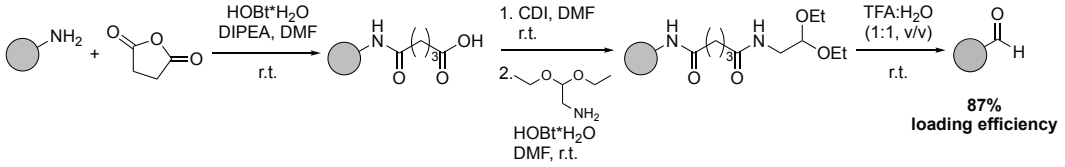

Introduction of an aldehyde function on resin was conducted as previously described for amino-functionalized resin.[271,272] Briefly, one batch of Amino-PEGA resin (Novabiochem®) containing 1 g resin (dry weight, dry loading: 0.34 mmol·g^{-1}, 0.34 mmol, stored in EtOH) was rinsed with DMF and shaken 3x 10 min in DMF to completely exchange the solvent. A mixture of 342 mg

(3.4 mmol, 10 eq.) succinic anhydride, 524 mg (3.4 mmol, 10 eq.) HOBt·H_2O and 578 µL (3.4 mmol, 10 eq.) DIPEA in 10 mL DMF was added and left to react on the shaker at r.t. ovn (23h). Subsequently, the resin was filtered, rinsed with DMF and washed with DMF (3x 10 min). The free acid function was activated at r.t. with 2.2 g (13.6 mmol, 40 eq.) carbonyldiimidazole (CDI) for 90 min in 10 mL DMF. After filtration and washing with DMF (3x 10 min), 1.48 mL (10.2 mmol, 30 eq.) aminoacetaldehyde diethyl acetal were added with 1.1 g (6.8 mmol, 20 eq) HOBt·H_2O in 10 mL DMF and left at r.t. ovn (16.5 h). The resin was filtered and rinsed with DMF and subsequently washed with DMF (2x 10 min), ACN (3x 10 min) and H_2O (3x 10 min). The acetal was cleaved upon addition of 10 mL TFA:H_2O (1:1, v/v) within 90 min at r.t. Afterwards, the resin was rinsed with H_2O and ACN:H_2O (1:1, v/v) and washed with ACN:H_2O (1:1, v/v) (3x 10 min). The degree of functionalization was determined as described in section 6.1 (L_{51} = 0.2946 µmol·mg^{-1}, 87%) and the resin stored in ACN:H_2O (1:1, v/v) in the fridge.

6.6.1.3 Purification strategy for randomized peptides

Randomized peptides were purified from truncated peptides by capture–release strategy.[272] *N*-terminal Cys introduction before cleavage from the solid support enabled the capture of desired product peptides on aldehyde resin. Briefly, 5 eq. of aldehyde functionalized resin **51** (with regard to peptide amount) were weighed into a syringe reactor, rinsed and washed (3x 10 min) with a buffer containing 100 mM MES, 10 mM TCEP pH 6.4 in ACN:H_2O (1:1, v/v). 5-10 µmol peptide were dissolved in 1 mL of buffer to a concentration of 5-2.5 mM and added to the pre-washed resin together with 3 volumes buffer (final peptide concentration 2.5-1.25 mM). The mixture was shaken at r.t. for at least 24 h before the resin was drained and washed 3x 10 min with buffer (4 mL each). Bound peptides were cleaved from the solid support by incubation with 4 mL of 200 mM $MeO-NH_2$ (unbuffered, pH approx. 1.9) in ACN:H_2O (1:1, v/v) in several iterations, usually four iterations à 8 h, 16 h, 8 h, 16 h. Combined cleavage fractions were dried by lyophilization and desalted as described in section 6.1 on 500 mg cartridges. Fractions indicating peptidic content detected by UPLC analysis were pooled and dried by lyophilization.

6.6.1.4 Randomized peptides for immunogen synthesis (43a-b)

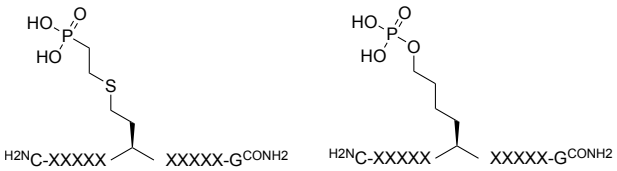

Randomized peptides were obtained following the split-and-mix approach in a semi-automated fashion. Peptides for immunogen synthesis were obtained starting from a 190 µmol scale on Fmoc-Gly-preloaded Rink amide resin **80**. For each coupling step the amount of swollen resin was split in 19 equal portions into separate syringe reactors (1.05 µmol/reactor). Fmoc deprotection, couplings and capping were conducted on a peptide synthesizer. The Fmoc-protecting group was removed with 500 µL Pip:DMF (20:80, v/v) for 3 min and the resin was washed 3x with DMF. The resin in each reactor was reacted with one of the natural AAs, except Cys, employing 5 eq. AA

(0.5 M in DMF), 5 eq. Oxyma (0.5 M in NMP), 5 eq. HCTU (0.7 M in DMF) and 10 eq NMM (2.9 M in DMF) applying double coupling for 30 min each, after which the resin washed 3x with DMF. *N*-terminal acetylation was achieved with 500 µL Ac_2O:2,6-lutidine:DMF (5:6:89, v/v/v) for 5 min. After capping, before the next coupling cycle, the resin was washed with DMF and content of all reactors combined, mixed and split again to the 19 reactors. After 5 cycles of randomized AA coupling, the resin was split into two main portions (each approx. 95 µmol) and stable pLys mimics (**18** and **19**, see sections 6.4.1 and 6.4.2) were coupled as followed. For **43a**, 123 mg (190 µmol, 2 eq.) Fmoc–hCys(EtPO$(OBn)_2$)–OH **18** and 72 mg (190 µmol, 2 eq.) HATU were dissolved in 1 mL DMF and 65 µL (380 µmol, 4 eq.) DIPEA were added directly before coupling. The mixture as given to the Fmoc deprotected resin and shaken for 3 h until TNBS test indicated full conversion. For **43b**, 103 mg (190 µmol, 2 eq.) Fmoc–Nle(OPO(OH)(OBn))–OH **19** and 72 mg (190 µmol, 2 eq.) HATU were dissolved in 1 mL DMF and 65 µL (380 µmol, 4 eq.) DIPEA were added directly before coupling. The mixture as given to the Fmoc deprotected resin and shaken for 3 h until TNBS test indicated full conversion. The resin was acetylated, washed with DMF (3x) and DCM (10x) and dried completely under reduced pressure. The following synthesis steps were conducted for **43a** and **43b** in the same manner in parallel. First, 5 cycles of randomized AA couplings as described above were applied. Second, after mixing the 19 portions again, 5 eq (475 µmol, 280 mg) Fmoc-Cys(Trt)-OH, 5 eq. (475 µmol, 200 mg) HCTU and 5 eq. (475 µmol, 70 mg) Oxyma were dissolved in 2.3 mL DMF and added to the Fmoc deprotected resin together with 10 eq. (950 µmol, 165 µL) DIPEA. The reaction was allowed to proceed 50 min at r.t. and subsequently possibly unreacted *N*-termini capped. After Fmoc deprotection, the peptides were cleaved from the solid support twice with 3 mL of a mixture of TFA:DTT:thioanisole:TIS (90:4.5:4.5:1, v/v/v/v) for 2 h. Solvent amount was reduced to approx. 1 mL with a N_2-flow and the peptides precipitated in a 10-fold excess of cold Et_2O. Due to the usage of DTT in the cleavage cocktail, the crude product mixture was pre-purified by flash preparative HPLC to seperate it from the thiol. Fractions indicating peptide content at the UPLC were pooled and dried by lyophilization. To purify the desired full-length from truncated peptides, the products were purified with aldehyde functionalized resin as described in section 6.6.1.3 on a 10 µmol scale to give 3.4 mg (1.5-3.5 µmol, 15-35%, calculated from the possibilities that all *Xxx* were either Gly or Trp) ^{H_2N}Cys–Xxx_5–hCys(EtPO$(OH)_2$)–Xxx_5–Gly^{CONH_2} **43a** and 3.1 mg (1.4 µmol-3.2 µmol, 14-32%, calculated from the possibilities that all *Xxx* were either Gly or Trp) ^{H_2N}Cys–Xxx_5–Nle(OPO$(OH)_2$)–Xxx_5–Gly^{CONH_2} **43b**.

6.6.1.5 Randomized peptides for hit evaluation (45, 46, 47, 48)

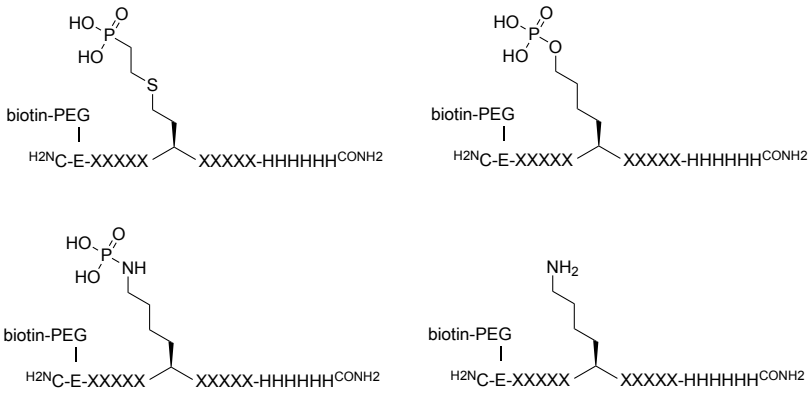

Peptides applied in the hit evaluation process were synthesized in a semi-automated fashion starting from Fmoc-His(Trt) preloaded Rink amide resin **81** on a 500 µmol scale. Five additional His residues were coupled as described in section 6.1. The approximate overall yield was determined by Fmoc-monitoring as described in section 6.1 UV/Vis photometry (loading Fmoc–His_6: 0.18 µmol/mg, according to 265 µmol His-tag, 53% yield). The randomized part of peptides was synthesized as described before (section 6.6.1.4) with minor adjustments. At the conserved position after 5 random AAs, either Fmoc-hCys(EtPO$(OBn)_2$)-OH **18**, Fmoc-Nle(OPO(OH)(OBn))-OH **19** (as described in 6.6.1.4), Fmoc-Lys^{N_3}-OH (3 eq. AA, 3 eq. HATU, 6 eq. DIPEA, 3 h, r.t.) or Fmoc-Lys(Boc)-OH (5 eq. AA, 5 eq. HCTU, 5 eq. Oxyma, 10 eq. DIPEA, 1 h, r.t.) were introduced on a 65 µmol scale. The biotinylation was obtained by coupling of Fmoc-Glu(biotinyl-PEG)-OH (3 eq. AA, 3 eq. HATU, 6 eq. DIPEA, 3 h, r.t.). *N*-terminal Cys-coupling was achieved as described before. Peptides were cleaved from the solid support 2x 2 h with 2 mL of a mixture of TFA:thioanisole:H_2O:TIS (90:5:2.5:2.5, v/v/v/v), solvent amount reduced to approx. 1 mL with nitrogen and the crude products precipitated in a 10-fold excess of cold Et_2O.

The peptides carrying *az*-Lys as conserved site were directly applied in the Staudinger-phosphite reaction with 3 eq. phosphite **9** in DMF at 45 °C (subsequent addition of 4x 3 eq. phosphite at starting point and after 6, 24 and 32 h). After 48 h, DMF was evaporated under reduced pressure and residual solvent removed by lyophilization.

The desired full-length peptides were purified from truncated peptides as described in section 6.6.1.3 on a 10 µmol scale to yield:

3.4 mg (0.95-1.5 µmol, 10-15%, calculated from the possibilities that all *Xxx* were either Gly or Trp) ^{H_2N}Cys–Glu^{biotin}–Xxx_5–hCys(EtPO$(OH)_2$)–Xxx_5–$His_6{}^{CONH_2}$ **45**,

4.5 mg (1.3-1.9 µmol, 13-19%, calculated from the possibilities that all *Xxx* were either Gly or Trp) ^{H_2N}Cys–Glu^{biotin}–Xxx_5–Nle(OPO$(OH)_2$)–Xxx_5–$His_6{}^{CONH_2}$ **46**,

2.1 mg (0.55-0.83 µmol, 6-8%, calculated from the possibilities that all *Xxx* were either Gly or Trp) ^{H_2N}Cys–Glu^{biotin}–Xxx_5–cpLys^{NPE-} Xxx_5–$His_6{}^{CONH_2}$ **47***

and 2.3 mg (0.66-1.0 µmol, 7-10% calculated from the possibilities that all *Xxx* were either Gly or Trp)

^{H_2N}Cys–Glu^{biotin}–Xxx_5–Lys–Xxx_5–$His_6{}^{CONH_2}$ **48**.

Peptides **47*** were deprotected as described in the photodeprotection section 6.1 to give

^{H_2N}Cys – Glu^{biotin} – Xxx_5 – pLys – Xxx_5 – His$_6{}^{CONH_2}$ **47** before sending them to the collaboration partners.

6.6.1.6 Immunogen synthesis of 36 and 37 *via* thiol-selective conjugation

Immunogens applied in the first round of immunization were obtained as protein–peptide conjugates by functionalization of ovalbumin (OVA). For this purpose, sulfosuccinimidyl 4-(*N*-maleimidomethyl)cyclohexane-1-carboxylate (Sulfo-SMCC) activated OVA (Thermo Scientific^{TM} Imject^{TM} Maleimide-Activated) was reconstituted with ddH_2O to a concentration of 10 mg/mL in PBS. This stock solution was stored at 4 °C. 1 mg OVA (0.222 µmol Mal, 100 µL stock) was reacted with 0.5 µmol peptide **43a** or **43b** (2.25 eq. with regard to maleimide functionalities) 2.5 mM in PBS (200 µL) for 48 h at r.t. and subsequently purified by spin filtration with Amicon Ultra centrifugal filters (Merck KGaA 10 kDa cut-off). The conjugation success was estimated by SDS-PAGE gel analysis, protein concentration adjusted to 250 µg·mL^{-1} with sterilized PBS and sent frozen in 100 µg aliquots to the collaboration partners.

6.6.2 Glutaraldehyde Linkage for Second Immunization Approach

6.6.2.1 Synthesis overview

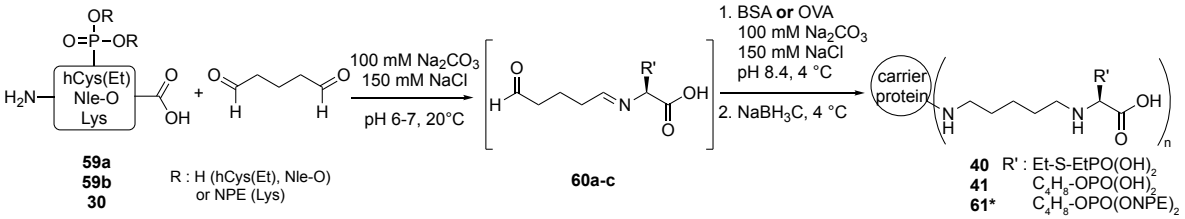

6.6.2.2 Synthesis of mimics 59a-b

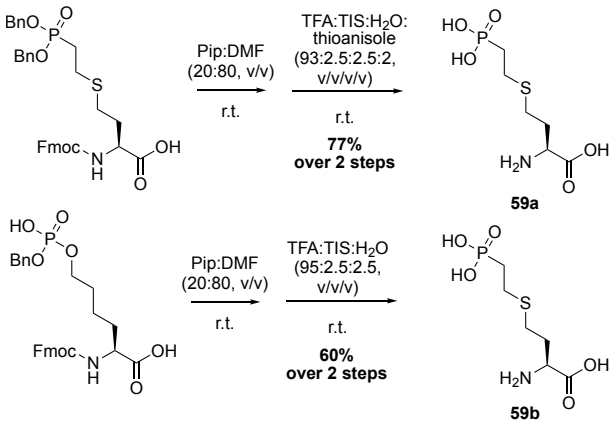

Phospho-AAs **59a** and **59b** were obtained by subsequent global deprotection of the SPPS-building blocks Fmoc-hCys(EtPO(OBn)$_2$)-OH **18** and Fmoc-Nle(OPO(OH)(OBn))-OH **19** (see sections 6.4.1 and 6.4.2). Briefly, 62 or 93 µmol AA were dissolved to a 40 mM solution in Pip:DMF (20:80,

v/v) and shaken at r.t. for 3 min. The solvent was evaporated under reduced pressure and residuals removed *via* lyophilization. Benzyl deprotection was achieved by double treatment of the crude product with a mixture of TFA:H_2O:TIS:thioanisole (93:2.5:2.5:2, v/v/v/v) for **59a** and TFA:H_2O:TIS (95:2.5:2.5, v/v/v) for **59b** (AA concentration 20 mM), 3 h first treatment, 2 h second treatment. Solvents were evaporated under N_2-flow and by lyophilization and the crude product purified using semi-preparative HPLC. Residual Pip was removed by ether precipitation. Therefore, the dried product fractions were suspended in a 600 µL ACN:MeOH (1:2, v/v) and 10 drops TFA added to dissolve the peptide before precipitating it again with a 10-fold excess of cold Et_2O. After 10 min in the freezer, the peptide was obtained by centrifugation, decantation and drying under reduced pressure.

hCys(EtPO$(OH)_2$)-OH **59a**: white powder, 11.6 mg (47.7 µmol, 77%). ^{1}H NMR (600 MHz, D_2O) δ 4.16 (q, J = 6.3 Hz, 1H), 2.86 – 2.74 (m, 4H), 2.36 – 2.17 (m, 2H), 2.05 – 1.95 (m, 2H). ^{31}P NMR (243 MHz, D_2O) δ 23.86. ^{13}C NMR (151 MHz, D_2O) δ 172.39, 52.40, 29.54, 28.44, 27.58, 26.35, 24.80, 24.78. HR-MS for $C_6H_{14}NO_5PS$: m/z calc. $[M+H^+]^+$ = 244.0403, m/z obs. $[M+H^+]^+$ = 244.0397.

Nle(OPO$(OH)_2$)-OH **59b**: white powder, 12.6 mg (55.8 µmol, 60%). ^{1}H NMR (600 MHz, D_2O) δ 4.09 – 4.03 (m, 1H), 3.97 – 3.89 (m, 2H), 2.09 – 1.92 (m, 2H), 1.72 (qd, J = 7.5, 3.4 Hz, 2H), 1.63 – 1.47 (m, 2H). ^{31}P NMR (243 MHz, D_2O) δ 0.37. ^{13}C NMR (151 MHz, D_2O) δ 172.56, 65.30, 53.08, 29.36, 29.15, 29.10, 20.63. HR-MS for $C_6H_{14}NO_6P$: m/z calc. $[M+H^+]^+$ = 228.0632, m/z obs. $[M+H^+]^+$ = 228.0638.

6.6.2.3 Protein–amino acid conjugate synthesis of 40, 41 and 61 *via* glutaraldehyde linkage

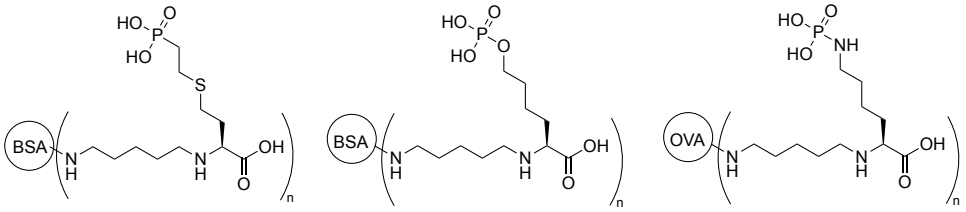

Bovine serum albumin (BSA, Sigma-Aldrich) and OVA (Thermo Scientific^{TM} Imject^{TM}) were linked to the haptens **59a**, **59b** and **30** *via* amine selective glutaraldehyde (glut-CHO) following the two-step protocol.[279,280] Briefly, for the modification of 2 mg protein ($3\cdot10^{-8}$ mol BSA, $4.5\cdot10^{-8}$ mol OVA), 50 eq. AA (1.5 µmol **59a** and **59b**, 2.3 µmol **30**, see section 6.5.1.5) were used. The AA was dissolved to 50 mM in buffer (100 mM Na_2CO_3, 150 mM NaCl, pH 8.5) and an aliquot of glut-CHO (10% in H_2O, freshly prepared) was added so that the final glut-CHO concentration was 1%. After pH adjustment to 6-7 with 0.1 N HCl, the mixture was shaken at 20 °C ovn (17 h). For the next step, 2 mg protein were dissolved to 5 mg·mL^{-1} with buffer and the AA–glut-CHO solution added. The pH was adjusted to 8.4 with 0.1 N HCl and the reaction allowed to proceed at 4 °C ovn (26 h) while shaking gently. Reduction of formed imine was achieved by addition of $NaBH_3CN$ to a final concentration of 10 mg·mL^{-1} and gentle shaking at 4 °C for 70 min. Afterwards, the protein was rebuffered to sterile PBS by spin-filtration (10 kDa cut-off), in the last step diluted to approx. 5 mg·mL^{-1}. The modification success was estimated by SDS-PAGE gel and UPLC-MS(QTof) analysis.

The OVA–cpLys^{NPE} conjugate **61*** was deprotected by photoirradiation as described in section 6.1 with slight adjustments to give **61**. 1.5 mg conjugate in PBS (300 µL) were irradiated 5x for 20 min while cooling the reaction between the cycles for 3 min in ice. Afterwards, the solution was purified *via* spin-filtration with sterile PBS (3x 400 µL).
For all conjugates (**40**, **41** and **61**) the concentration was adjusted to 1 mg·mL^{-1} with sterile PBS and frozen aliquots of 0.1 mg sent to the collaboration partners.

6.6.3 Antibody Generation

All immunizations and primary screens to generate monoclonal antibodies directed against pLys were conducted in the Monoclonal Antibodies Core Facility, Helmholtz Zentrum München. For this purpose, Lou or Winstar rats as well as Balb/C mice were immunized with synthetically obtained pLys mimic conjugates (OVA–randomized peptides **36** and **37** in the first approach, BSA–mimics **40** and **41** in the second approach). Subsequently, splenocytes from sacrificed rats and mice were collected and prepared for fusion with the mouse myeloma cell line P3X63-Ag8.653 to hybridoma cells. In detail, the immunization and preparation of hybridomas were conducted as followed.
Immunization of the animals with 50 µg conjugate, 5 nmol CpG 2006 (rat, TIB MOLBIOL, Berlin) or CpG 1668 (mouse, TIB MOLBIOL, Berlin) in 500 µL PBS + 500 µL Incomplete Freund's adjuvant (IFA) (or 250 µL PBS + 250 µL IFA for mouse). At least six weeks later, a boost injection with 50 µg conjugate and 5 nmol CpG 2006 was applied. Three days later, splenocytes from scarified rats and mice were collected fused with the mouse myeloma cell line P3X63-Ag8.653 to hybridoma cells. Fused cells were plated in 96-well plates in HAT selection media [317] and incubated for 10 d at 37 °C. Supernatents were tested for the presence of IgG Abs directed against the biotin-conjugated, randomized pLys peptides **47** (positive control), a non-phosphorylated Lys conjugate **42** (negative control) and co-immunized antigens **45** and **46** by ELISA.
All positively scored clones were expanded and cryostored. Furthermore, the IgG subclass was determined with HRP-conjugated mAbs against the rat or mouse IgG isotypes (anti-rat:TIB173 IgG2a, TIB174 IgG2b, TIB170 IgG1 all from ATCC, IgG2c own batch; anti-mouse: IgG1; IgG2a; IgG2b all own batch, HB128 IgG3 from ATCC). 4 mL of supernatant of the positive clone were delivered for further validation to the labs of Prof. Hackenberger.

6.6.4 Clone Evaluation

6.6.4.1 Biotinylated peptide synthesis

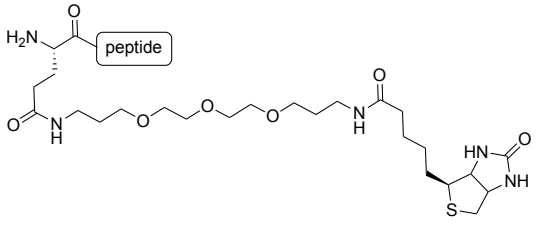

Peptides for ELISA were synthesized in an automated fashion as described in section 6.1 on

Fmoc-Lys(Boc)-preloaded Rink amide resin **83** or Wang resin **84**. Non-natural AAs as well as *N*-terminal biotin-tag (as Fmoc-Glu(biotinyl-PEG)-OH) were introduced manually with 2 eq. AA, 1.95 eq. HATU, 4 eq. DIPEA (0.2 M in DMF with regard to AA) for 2 h at r.t. After *N*-terminal Fmoc-deprotection, peptides were cleaved, precipitated and purified as described in the peptide synthesis section of 6.1.
Azido-Lys peptides were converted to caged pLys peptides by Staudinger-phosphite reaction with phosphite **9** as described in section 6.3 and subsequently deprotected before usage as described in the photodeprotection section on a 0.5 µmol scale.

Table S7: Overview over synthesized biotin-tagged peptides including reaction scale, yields, high resolution masses and retention times.

#	Sequence	Scale [µmol]	Yield [%]	m/z calc. $[M+2H^+]^{2+}$	m/z obs. $[M+2H^+]^{2+}$	t_R [min]
62	^{H_2N}biotin-TTAVEID*hC*DSLK^{CONH_2}	6	22[a]	986.9722	986.9730	4.518*
63	^{H_2N}biotin-TTAVEID*Nle*DSLK^{CONH_2}	6	17[a]	978.9837	978.9832	4.497*
64	^{H_2N}biotin-TTAVEIDpYDSLK^{CONH_2}	12.5	10[a]	995.9758	995.9761	4.556*
65	^{H_2N}biotin-TTAVEIDKDSLK^{CONH_2}	15	30[a]	938.5085	938.5090	4.307*
66	^{H_2N}biotin-TTAVEIDK^{N_3}DSLK^{CONH_2}	40	50[a]	951.5037	951.5033	3.797*
67	^{H_2N}biotin-TTAVEIDK^{N_3}DSLK^{COOH}	25	57[a]	951.9957	951.9952	5.116*
68	^{H_2N}biotin-TTAVEIDcpKDSLK^{CONH_2}	2.6	25	1127.5393	1127.5396	6.127*
69	^{H_2N}biotin-TTAVEIDcpKDSLK^{COOH}	2.6	30	1128.0313	1128.0311	6.169*
70	^{H_2N}biotin-TTAVEIDpKDSLK^{CONH_2}	0.5	quant.	978.4916	978.4914	3.552**
71	^{H_2N}biotin-TTAVEIDpKDSLK^{COOH}	0.5	quant.	978.9837	978.9840	3.786**

[a] yield with regard to initial resin loading * gradient **I** ** gradient **II** *hC* hCys(EtPO(OH)$_2$) *Nle* Nle(OPO(OH)$_2$)

6.6.4.2 Indirect ELISA

Indirect ELISA was performed with biotinylated peptides from sections 6.6.1.5 and 6.6.4.1 on Pierce^{TM} *Streptavidin* Coated Plates, Clear, 96-Well (Thermo Scientific^{TM}). Peptides were dissolved to a concentration of 1 µg·mL^{-1} in 100 mM carbonate/bicarbonate buffer pH 9. A standard protocol was conducted as outlined below. Abs were used in following dilutions in PBS + 0.05% Tween (PBS-T): Detecting Abs (1°): Supernatent from collaborator – *pLysN 5G1 R-2b* 1:10; mouse-α-His-tag (Santa Cruz) 1:1,000; HRP conjugates (2°): mouse-α-rat IgG2b Ab (provided by collaborator) 1:400; goat-α-rat-Ab (Jackson Immuno Research) 1:5,000; goat-α-mouse-Ab (Abcam) 1:5,000;
α-pTyr-Ab (Invitrogen^{TM}) 0.5 µg·mL^{-1}; *streptavidin* (BioLegends) 50 mU·mL^{-1}. As positive control for plates functioning the pTyr peptide **64** was included in every experimented plate.

- 100 µL (100 ng) peptide were coated ovn at 4 °C (approx. 16 h).
- Each well was washed 3x with 200 µL *washing buffer* (PBS + 0.05% Tween, PBS-T) and tapped upside down on a paper towel in between.
- The plate was blocked with 200 µL *blocking buffer* (2% BSA in PBS) for 90 min at r.t.

- Washed plate 3x with 200 µL washing buffer and tapped upside down on a paper towel in between.
- Incubated with 100 µL 1° Ab for 90 min at r.t.
- Plate was washed 5x with 200 µL washing buffer and tapped upside down on a paper towel in between.
- Incubated with 100 µL 2° Ab for 90 min at r.t.
- Plate was washed 5x with 200 µL washing buffer and tapped upside down on a paper towel in between.
- 100 µL TMB (Thermo Scientific^{TM} 1-Step^{TM} Ultra TMB-ELISA Substrate Solution) were added for detection.
- Detection reaction was quenched latest 30 min after TMB addition by addition of 100 µL 2 M H_2SO_4 and absorbance immediately measured on a microplate reader (Tecan Group Ltd.) at 405 nm.

6.6.4.3 Indirect Sandwich ELISA

In order to be independent from secondary antibody delivered from Helmholtz Zentrum München, also sandwich ELISA was performed on Nunc^{TM}-Immuno Plates Maxisorp (Thermo Scientific^{TM}). Applied substrates, Abs and buffers were the same as mentioned in the previous section (6.6.4.2). A protocol as outlined below was followed. Coating with mouse-α-His-tag-Ab as capture Ab for randomized peptide **48** and detection with *streptavidin*-HRP conjugate was used as positive control for the method itself. As positive control for plates functioning the pTyr peptide **64** was included in every experimented plate.

- 100 µL supernatent from collaborator (*pLysN 5G1 R-2b*) were coated ovn at 4 °C (approx. 20 h).
- Each well was washed 3x with 200 µL washing buffer and tapped upside down on a paper towel in between.
- The plate was blocked with 200 µL blocking buffer for 90 min at r.t.
- Washed plate 3x with 200 µL washing buffer and tapped upside down on a paper towel in between.
- Incubated with 100 µL (100 ng) peptides ovn at 4 °C (approx. 16 h).
- Plate was washed 3x with 200 µL washing buffer and tapped upside down on a paper towel in between.
- Incubated with 100 µL mouse-α-His-tag-Ab (**A**) or *streptavidin*-HRP conjugate (**B**) for 90 min at r.t.
- Plate was washed 5x with 200 µL washing buffer and tapped upside down on a paper towel in between.
- Wells **A** were incubated with 100 µL goat-α-mouse-Ab-HRP conjugate for 90 min at r.t.
- Wells **A** were washed 5x with 200 µL washing buffer and tapped upside down on a paper towel in between.
- 100 µL TMB were added to wells **A** and **B** for detection.

- Detection reaction was quenched latest 30 min after TMB addition by addition of 100 µL 2 M H_2SO_4 and absorbance immediately measured on a microplate reader at 405 nm.

6.7 Development and Optimization of Proteomic Protocols for Phospho-Lysine Detection

6.7.1 Optimization of Histone Extraction and Preparation for Tandem-MS Analysis

6.7.1.1 Synthesis overview

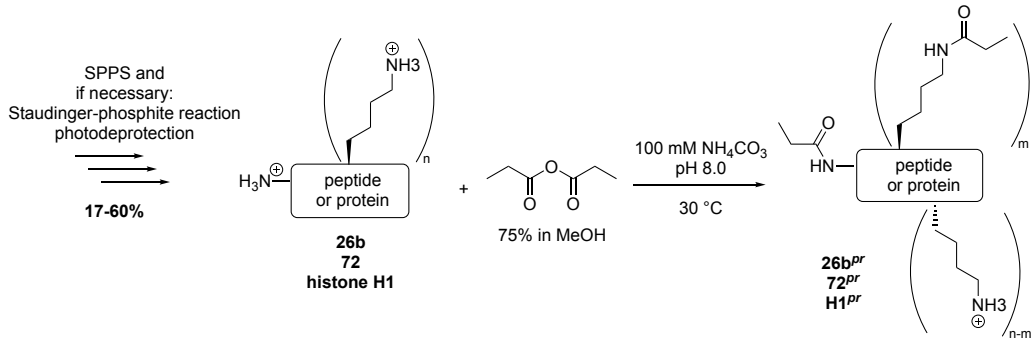

6.7.1.2 Peptide synthesis

As described in section 6.1, peptides were synthesized on a 50 µmol scale on Rink amide resin **80**, the Staudinger-phosphite reactions were conducted on a 10 µmol scale with phosphite **9** and photodeprotection was achieved as usual on a 1 µmol scale.
Details for peptide ^{H_2N}KKKARpKSAGAAKRKASG^{CONH_2} **26b** can be found in section 6.5.

^{H_2N}KKKARKSAGAAKRKASG^{CONH_2} **72**: 52.2 mg (30 µmol, 64%). HR-MS for $C_{73}H_{140}N_{30}O_{19}$: m/z calc. $[M+2H^+]^{2+}$ = 871.5529, m/z obs. $[M+2H^+]^{2+}$ = 871.5521. t_R (gradient **II**) = 3.653 min.

6.7.1.3 Derivatization of basic lysine side chains and *N*-terminal amines in peptides and proteins by propionylation

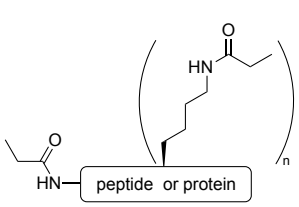

Propionylation was conducted as previously described with some adjustments.[218] For *Peptides*, 0.1 µmol substrate was dissolved to a 1 mM solution in 100 mM ammonium bicarbonate buffer (AmBic), pH 8.0 (100 µL) and 1 µL conc. NH_4OH was added. 2 µL (12 µmol, 120 eq.) of a

freshly prepared mixture of propionic anhydride ($Prop_2O$) in MeOH (75:25, v/v) were added to the peptide and, if necessary, the pH adjusted to 8-8.5 with conc. NH_4OH. The reaction was incubated at 30 °C for 20 min and analyzed using UPLC-MS. A small aliquot was submitted for MS/MS analysis. *Proteins* were propionylated in a similar fashion. 5 µg of chemically phosphorylated H1 (stock of 5 mg·mL^{-1} in Tris-HCl, pH 7.2) were diluted with 5 µL 100 mM Ambic, pH 8.0 and 2 µL conc. NH_4OH. After the addition of 20 µL freshly prepared $Prop_2O$:MeOH (75:25, v/v), the pH was adjusted to 8 with conc. NH_4OH and the reaction incubated at 30 °C for 20 min. The reagents were removed by spin-filtration (10 kDa cut-off) at 4 °C and washed 2x with 20 mM AmBic, pH 8.3. The resulting protein solution was concentrated to approx. 10 µL using a SpeedVac Savant™ SPD1010 (Thermo Scientific™). The protein was digested with trypsin (1:10, w/w, Promega) ovn at 25 °C and analyzed *via* MS/MS by Dr. Penkert.[239]

6.7.2 Evaluation of Phosphate Specific Enrichment Techniques

6.7.2.1 Cell extract preparation

HeLa cells were cultured in Dubelcco's Modified Eagle Medium (DMEM, BioChrom), supplemented with 10% fetal calf serum (FCS) and 1% penicillin/streptomycin (pen/strep), without phenol red indicator at 37 °C and 5% CO_2. *W256* cells were cultured in RPMI 1640 (BioWest), supplemented with 10% FCS and 1% pen/strep, without phenol red indicator at 37 °C and 5% CO_2.
For cell lysis, cells were cultured in 150 cm^2 dishes, harvested with a cell scraper and centrifuged 5 min at 300 × *g*. The pellet was washed once with PBS, centrifuged 5 min, 300 × *g* and the cell pellet volume (CV) measured. The pellet was resuspended in 2 CV lysis buffer (8 M urea in 50 mM AmBic, pH 8.5, supplemented with phosphatase and protease inhibitors: cOmplete™ Ultra Mini EDTA-free and PhosStop™, both Roche) and treated 3x 10 s in ultrasonic bath. After centrifugation for 20 min at 20,000 × *g*, the protein concentration in the supernatent was determined by BCA assay. Aliquots of 1-1.5 mg proteins were used for reduction with 3 mM DTT (final concentration, 100 mM stock) in 50 mM AmBic, pH 8.5 for 60 min at r.t. and under exclusion of light. Thiols were alkylated with 2-iodoacetamide (IAA, 14 mM final concentration from a 400 mM stock in 50 mM AmBic, pH 8.5) for 60 min at r.t. in the dark. DTT was added to a final concentration of 7 mM to quench the reaction. The mixture was diluted with 50 mM AmBic, pH 8.5 to reduce the initial concentration of urea from 8 M to 2 M. Tryptic digest was conducted with 2% (w/w) trypsin (Promega) at r.t. ovn in the dark and stopped next morning by cooling the samples in an ice bath. For desalting, samples were acidified to pH 3.5 with 10% FA, vortexed 5x and centrifuged 5 min at 14,000 × *g* and 4 °C. The supernatent was loaded on a 0.1% FA (H_2O)-equilibrated 200 mg Sep-Pak®, washed 2x with 1 mL cold 0.1% FA (H_2O) and eluted with 500 µL cold ACN:H_2O (30:70, v/v) and 500 µL cold ACN:H_2O (50:50, v/v) directly into 15 µL cold 5% NH_4OH (H_2O) to neutralize the pH. The solution was concentrated by SpeedVac and used for the enrichment protocol.

6.7.2.2 Titanium dioxide beads-based enrichment

TiO_2 beads (Titansphere TiO, GL Sciences) were pre-incubated for 10 min at r.t. in the dark with 2,5-dihydroxybenzoic acid (DHB, stock 30mg·mL^{-1} in ACN:H_2O, 8:2, v/v) at concentration of 50 µL DHB-stock per 5 mg beads. In the meantime, desalted lysate was redissolved to approx. 5 mg·mL^{-1} with 50 mM AmBic, pH 8.5. For the *first iteration*, a 0.5 mg protein aliquot was diluted with 1,450 µL wash-I buffer (ACN:H_2O, 30:70, v/v, pH 3.2 or 2.7 (TFA)) in a 2 mL-microcentrifuge tube (Eppendorf® LoBind microcentrifuge tubes, eppi) and incubated with 50 µL TiO_2/DHB for 30 min at r.t. in the dark using an overhead shaker. After centrifugation of the mixture for 2 min at 1,050 × *g* and 12 °C, the supernatent was employed in *further iterations* whilst the beads were used for washing and elution. *Wash-I*: The beads were resuspended in 1,500 µL wash-I buffer and shaken in an overhead shaker for 10 min at r.t. in the dark. The mixture was centrifuged 2 min at 1,050 × *g* and 12 °C, the supernatent was discarded and the beads treated again with wash-I in the same manner. *Wash-II*: The beads were resuspended in 1,500 µL wash-II buffer (ACN:H_2O, 80:20, v/v, pH 3.2 (TFA)), incubated 10 min at r.t. in the dark in an overhead shaker, centrifuged 2 min at 1,050 × *g* and 12 °C and the supernatent discarded. The beads were resuspended in 100 µL wash-II buffer and transferred to a StageTip equipped with an extra layer of C_8 material (Empore™ Octyl Solid Phase Extraction disks, Supelco) and centrifuged at 1,050 × *g* and 12 °C until the tip was dry. *Elution*: 300 µL conc. NH_4OH:H_2O (40:60, v/v) were added to the tip in three portions, the tip centrifuged inbetween (3 min, 3 min, 1,050 × *g*, 12 °C) to lower the level and eventually until the tip was dry. The eluate was put on ice until all iterations were finished, then concentrated in a SpeedVac to 50 µL, transferred to a sample vial, dried completely and redissolved in ACN:H_2O (3:97, v/v) for LC/MS analysis.

6.8 A Fluroscence Tag for Phosphorylation Degree Determination

6.8.1 Synthesis of Sox-Tagged Phosphorylation Probes

6.8.1.1 Synthesis overview

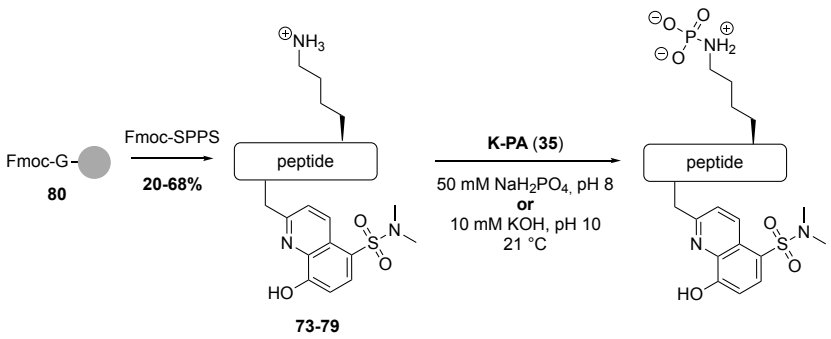

6.8.1.2 Peptide synthesis

Peptides with Sox-tag were obtained as described in the peptide synthesis section on a 5 or 10 µmol scale on resin **80**. Fmoc-Sox(TBDPS)-OH was generously provided by the Imperiali group. Crude peptides were purified using analytical HPLC. After lyophilization and yield determination, a small amount of peptide was dissolved in ddH_2O, the concentration determined as described previously [211] and adjusted to 500 µM with ddH_2O.

Table S8: Overview over synthesized Sox-tagged peptides including scale, yields (with regard to initial resin loading), high resolution masses and retention times.

#	Sequence	Scale [µmol]	Yield [%]	m/z calc. $[M+H^+]^+$	m/z obs. $[M+H^+]^+$	t_R [min]
73	^{H_2N}EYGAG*Sox*KAGAG^{CONH_2}	10	64	1,200.5103	1,200.5146	3.637*
74	^{H_2N}EYGAG*Sox*GKGAG^{CONH_2}	10	67	1,186.4946	1,186.4943	3.617*
75	^{H_2N}EYGAG*Sox*GAKAG^{CONH_2}	10	55	1,200.5103	1,200.5101	3.693*
76	^{Ac}EYGAG*Sox*KAGAG^{CONH_2}	10	26	1,242.5208	1,242.5222	3.870*
77	^{Ac}EAGAG*Sox*KAGAG^{CONH_2}	10	20	1,150.4946	1,150.4919	3.603*
78	^{H_2N}EYGAG*Sox*G**pS**GAG^{CONH_2}	5	68	1,225.3980	1,225.3981	3.443*
79	^{H_2N}EYGAG*Sox*G**S**KAG^{CONH_2}	5	25	1,145.4317	1,145.4324	3.663*

* gradient **I** ** gradient **II**

6.8.1.3 Phosphorylation reaction with K-PA 35

Lysine peptides were phosphorylated with K-PA **35** (6.5.4.2) in adopted protocols either from Choi *et al.* [202] (**A**) or Hu *et al.* [101] (**B**).
In an microtube, 0.1 µmol peptide was diluted to 1 mM with 50 mM NaH_2PO_4 (**A**, final concentration) or 10 mM KOH (**B**, final concentration) and 200 eq. or 1,000 eq. K-PA (**A** or **B**, respectively) were added, usually not dissolving completely. The pH of the mixture was adjusted to 8 (**A**) or 10 (**B**) and the mixture was shaken at 21 °C for 3-5 days and analyzed by HR-UPLC-MS in between. The reaction mixture was applied in further experiments without any workup.

6.8.1.4 Fluorescence measurements

Only phosphorylation reactions from protocol **A** were applied for fluorescence measurements. Those were conducted as described in section 6.1 with following instrument adjustments: emission mode, bandwidth (Ex) 3 nm, bandwidth (Em) 5 nm, response 2 s, sensitivity medium, excitation wavelength 360 nm, emission measurement range 380-650 nm, speed 200 nm·min^{-1}, data pitch 0.1 nm. Samples were used at a concentration of 500 µM in ddH_2O (peptide stock) or K-PA/NaH_2PO_4 (reactions; diluted 1:1 with ddH_2O) and in order to adjust salt content of peptide stock and reactions, equal amounts of K-PA/NaH_2PO_4 and ddH_2O were added during further dilution, respectively. Fluorescence was measured at a peptide concentration of 15 µM in 20 mM HEPES buffer, pH 7.4 containing 10 mM $MgCl_2$ for chelation based fluorescence determination

or no $MgCl_2$ for background fluorescence measurement. As an example, t_0: 3.6 µL peptide stock (500 µM) + 3.6 µL K-PA/NaH_2PO_4 (100 mM/25 mM) + 112.8 µL HEPES/$MgCl_2$ (20 mM/10 mM, pH 7.4); $t_{0-background}$: 3.6 µL peptide stock (500 µM) + 3.6 µL K-PA/NaH_2PO_4 (100 mM/25 mM) + 112.8 µL HEPES (20 mM, pH 7.4). Background fluorescence from cuvette, buffers and K-PA was subtracted from all measurements prior to processing.

6.8.1.5 NMR measurements

For NMR analysis, phosphorylation reactions were conducted with deuterated buffers. 0.5 µmol peptide (**73**, **76**, **77**; 0.59 mg, 0.62 mg, 0.57 mg, respectively) were dissolved together with 500 µmol K-PA **35** (68 mg, 1000 eq.) in 10 mM KOH (D_2O) to a concentration of 1 mM with regard to the peptide. The pH was adjusted to 8.5 with 1 M KOH (D_2O) and the mixture shaken at 21 °C for 3 d. The mixture was transferred to an NMR glass tube and measured as described in section 6.1.

7 | Abbreviations

Amino acids have been abbreviated by the commonly used one-letter or three-letter code.

°C	degree Celcius
1°	primary
1D	one-dimensional
2-ME	2-mercaptoethanol
2-pAIE	(2-((2-ammoniuethyl)amino)-2-iminoethyl)-phosphonic acid
2°	secondary
2D	two-dimensional
6-pAIE	(2-((6-aminohexyl)amino)-2-iminoethyl)-phosphonic acid
6-sAIE	(2-((6-aminohexyl)amino)-2-iminoethane)-1-sulfonic acid
A	area under the curve [mAU·s]
A	absorbance [1]
AA	amino acid
Ab	antibody
Ac	acetyl-
Ac_2O	acetic anhydride
ACLY	*ATP-citrate lyase*
ACN	acetonitrile
AcOH	acetic acid
ALP	*alkaline phosphatase*
AmBic	ammonium bicoarbonate buffer, NH_4HCO_3
approx.	approximately
Ar	argon
ATP	adenosine triphosphate
AU	arbitrary unit
az-Lys	ϵ-azidolysine
β-ME	2-ME
B.subtilis	*Bacillus subtilis*
BAR	Bennet's Acceptance Ratio
Bn	benzyl-
Bn-Br	benzyl bromide
Bn-OH	benzyl alcohol

Boc ..... *tert*-butyloxycarbonyl-
BSA ..... *bovine serum albumin*
c ..... concentration [mol·L^{-1}]
C ..... carboxy-
calc. ..... calculated
cat. ..... catalytic
Cbz ..... benzyloxycarbonyl-
CDI ..... carbonyldiimidazole
CGI ..... Crooks Gaussian Intersection
CHEF ..... chelation-enhanced fluorescence
CID ..... collision induced dissociation
cpK ..... caged pLys
cpR ..... caged pArg
cyt *c* ..... *cytochrom c*
d ..... path length [cm]
δ ..... chemical shift [ppm]
$\Delta\Delta G$ ..... Gibbs free energy difference [kJ·mol^{-1}]
ΔG ..... Gibbs free energy [kJ·mol^{-1}]
DNA ..... deoxyribonucleic acid
DBHA ..... desthiobiotin-linked hydroxylamine
DCM ..... methylene chloride
ddH_2O ..... double-distilled water
DFMP ..... difluoromethylenephosphonate
DHB ..... 2,5-dihydroxybenzoic acid
DIC ..... *N,N*'-diisopropylcarbodiimide
DIPEA ..... *N,N*-diisopropylethylamine
DMAP 4-dimethylaminopyridine
DMEM ..... Dubelcco's Modified Eagle Medium
DMF ..... *N,N*-dimethylformamide
DPA ..... di-(2-(6-amino)picolyl)amine
DTT ..... dithiothreitol
ϵ ..... molar attenuation coefficient [L·mol^{-1}·cm^{-1}]
E.coli ..... *Escherichia coli*
e.g. ..... *exempli gratia*, for example
EDT 1,2-ethanedithiol
EDTA ..... ethylenediaminetetraacetic acid
EE ..... ethyl acetate
EGFR ..... *epidermal growth factor receptor*
ELISA ..... enzyme-linked immunosorbent assay
Em ..... emission
eq. ..... equivalents
ESI ..... electrospray ionisation
ESP ..... electrostatic potential

Et_2O ..... diethyl ether
Et_3N ..... triethylamine
ETD ..... electron transfer dissociation
EThcD ..... electron transfer/higher energy collision dissociation
EtOH ..... ethanol
Ex ..... excitation
FA ..... formic acid
FCS ..... fetal calf serum
Fmoc ..... fluorenylmethyloxycarbonyl-
Fmoc-Sox-OH ..... (*S*)-2-amino-*Nα*-Fmoc-3-(8-hydroxy-5-(*N*,*N*-dimethyl)quinoline-2-yl)
..... propionic acid
glut-CHO ..... glutaraldehyde
GST ..... *glutathione S-transferase*
GTP ..... guanosine triphosphate
h ..... hour(s)
h ..... Planck constant [$6.62607015 \cdot 10^{-34}$ J·s]
H_2O ..... water
HAD ..... *haloacid dehalogenase*
HATU .. 1-[bis(dimethylamino)methylene]-1*H*-1,2,3-triazolo[4,5-*b*]pyridinium 3-oxid hexafluoro-
..... phosphate
HCD ..... higher-energy collisional dissociation
HCTU ..... 2-(6-chloro-1H-benzotriazole-1-yl)-1,1,3,3-tetramethylaminium hexafluorophosphate
HeLa ..... cervical cancer cell line derived from Henrietta Lacks
HEPES ..... 4-(2-hydroxyethyl)-1-piperazineethanesulfonic acid
hex ..... *n*-hexane
Hg ..... mercury
HMBC ..... heteronuclear multiple bond coupling
HMQC ..... heteronuclear multiple quantum coherence
HOBt ..... *N*-hydroxybenzotriazole
$HOBt \cdot H_2O$ ..... 1-hydroxybenzotriazole hydrate
HPLC ..... high performance liquid chromatography
HRP ..... *horseradish peroxidase*
HSQC ..... heteronuclear single quantum coherence
Hz ..... Hertz
IAA 2-iodoacetamide
IDA ..... iminodiacetic acid
IFA ..... Incomplete Freund's adjuvant
IgG ..... *immunoglobulin G*
IMAC ..... immobilized-metal affinity chomatography
IP_7 ..... diphosphoinositol pentakisphosphate
IP_8 ..... bis-diphosphoinositol tetrakisphosphate
J ..... joule [$kg \cdot m^2 \cdot s^{-2}$]
K ..... Kelvin

k ..... first order rate constant [s^{-1}]
K-PA ..... potassium phosphoramidate
kD ..... kilodalton
K_d ..... dissociation constant [µmol·L^{-1}]
KLH ..... *keyhole limpet hemocyanin*
L ..... liter
LC ..... liquid chromatography
LHPP ..... *phospholysine phosphohistidine inorganic pyrophosphate phosphatase*
lyo ..... lyophilization
m ..... mass
M ..... molar [mol·L^{-1}]
m/z ..... mass-to-charge ratio
mAb ..... monoclonal antibody
Mal ..... maleimide
MAP ..... *mitogen-activated protein*
MAPK ..... *MAP kinase*
MAPKKK ..... *MAP kinase kinase kinase*
McsB ..... *protein-arginine kinase*
MD ..... molecular dynamic
Me ..... methyl-
MeO – NH_2 ..... methoxyamine
MeOH ..... methanol
MES ..... 2-(*N*-morpholino)ethanesulfonic acid
$MgCl_2$ ..... magnesium chloride
min ..... minute(s)
MOAC ..... metal oxide affinity chromatography
mol ..... mole
MS ..... mass spectrometry
MS/MS ..... tandem-MS
MS^2 ..... MS/MS
Mtt 4-methyltrityl-
N ..... amino-
ν ..... frequency [Hz]
n-BPA ..... *N*-(*n*-butyl)phosphoramidate
NC ..... nitrocellulose
NH_4-PA ..... ammonium phosphoramidate
NHS ..... *N*-hydroxysuccinimide
nLC ..... nano-liquid chromatography
NME1 ..... *nucleoside diphosphate kinase A*
NMM ..... *N*-methylmorpholine
NMP ..... *N*-methylpyrrolidone
NMR ..... nuclear magnetic resonance
NPE ..... (*o*-nitrophenyl)ethyl-

NTA ..... nitrilotriacetic acid
obs. ..... observed
OVA ..... *ovalbumin*
ovn ..... over night
Oxyma ..... ethyl cyanohydroxyiminoacetate
P–N ..... phosphor-nitrogen
P–O ..... phosphor-oxygen
P–S ..... phosphor-sulfur
p-az-Phe ..... *p*-azidophenylalanine
p-TsOH ..... *p*-toluenesulfonic acid
pAb ..... polyclonal Ab
PAH ..... phosphoramidate hydrolase
pArg ..... phospho-arginine
Pase ..... phosphatase
pAsp ..... phospho-aspartate
PBS ..... phosphate-buffered saline
PBS-T ..... PBS + 0.05% Tween
PCP ..... methylene-bisphosphonate
pCys ..... phospho-cysteine
pGlu ..... phospho-glutamate
Ph ..... phenyl-
pHis ..... phospho-histidine
pI ..... isoelectric point
P_i ..... inorganic phosphate
Pip ..... piperidine
pK_a ..... acid dissociation constant [1]
pLys ..... phospho-lysine
Pma ..... phosphomethylenealanine
Pmp 4-phosphomethyl-phenylalanine
PNP ..... imido diphosphate
PP_i ..... inorganic pyrophosphate
ppm ..... parts per million
ppSer ..... pyrophosphorylated serine
ppThr ..... pyrophosphorylated threonine
pPye ..... phosphonopyrazolylethylamine
pPza ..... 4-phosphopyrazol-2-yl alanine
$Prop_2O$ ..... propionic anhydride
pSer ..... phospho-serine
pThr ..... phospho-threonine
PTM ..... post-translational modification
PTP ..... *protein-tyrosine phosphatase*
PTP1B ..... *protein-tyrosine phosphatase 1B*
pTyr ..... phospho-tyrosine

pTza ..... phosphoryltriazolylalanine
pTze ..... phosphoryltriazolylethylamine
PyBOP ..... benzotriazol-1-yl-oxytripyrrolidinophosphonium hexafluorophosphate
quant. ..... quantitative
r.t. ..... room temperature
RAM ..... Rink amide
RCF ..... relative centrifugal force
R_f ..... retention factor [1]
RP ..... reversed phase
s ..... second(s)
S.aureus ..... *Staphylococcus aureus*
S.cerevisiae ..... *Saccharomyces cerevisiae*
SarA/MgrA ..... *staphylococcal accessary regulator A/MarR family global transcriptional regulator*
sat. ..... saturated
SAX ..... strong anion exchange
SCX ..... strong cation exchange
SDS-PAGE ..... sodium dodecyl sulfate–polyacrylamide gel electrophoresis
SERS ..... surface-enhanced Raman scattering
Sox ..... 8-hydroxy-5-(*N*,*N*-dimethylsulfonamido)-2-methylquinoline, sulfonamidoxine
SPPS ..... solid-phase peptide synthesis
sulfo-SMCC ..... sulfosuccinimidyl-4-(*N*-maleimidomethyl)cyclohexane-1-carboxylate
t ..... time [s; min]
TBDPS ..... tert-butyldiphenylsilyl-
Tc 2,2,2-trichloroethoxy-
TCEP ..... tris(2-carboxyethyl)phosphine
TFA ..... trifluoroacetic acid
THF ..... tetrahydrofurane
TIC ..... total ion current
TIS ..... triisppropylsilane
TMB ..... 3,3',5,5'-tetramethylbenzidine
TMSBr ..... trimethylbromosilane
TNBS ..... 2,4,6-trinitrobenzene-sulphonic acid
TOF ..... time-of-flight
t_R ..... retention time
Tris ..... tris(hydroxymethyl)aminomethane
Trt ..... trityl-
UPLC ..... ultra high performance liquid chromatography
U ..... enzyme unit [$\mu mol \cdot min^{-1}$]
UV ..... ultraviolet
v_0 ..... initial velocity [$M \cdot s^{-1}$]
VIS ..... visible
w/o ..... without
W256 ..... Walker-256 rat tumor

WB ..... Western blot
× g ..... times gravity
YwlE ..... *protein-arginine-phosphatase*
Z ..... see Cbz
z ..... charge

8 | References

[1] A. H. Stouthamer, "A theoretical study on the amount of atp required for synthesis of microbial cell material," *Antonie van Leeuwenhoek*, vol. 39, no. 1, pp. 545–565, 1973.

[2] R. Milo, "What is the total number of protein molecules per cell volume? a call to rethink some published values," *BioEssays*, vol. 35, no. 12, pp. 1050–1055, 2013.

[3] G. Cooper, *The Molecular Composition of Cells*. Sunderland: Sinauer Associates, 2nd ed., 2000.

[4] M. Beck, A. Schmidt, J. Malmstroem, M. Claassen, A. Ori, A. Szymborska, F. Herzog, O. Rinner, J. Ellenberg, and R. Aebersold, "The quantitative proteome of a human cell line," *Molecular Systems Biology*, vol. 7, no. 1, pp. 549–556, 2011.

[5] I. Ezkurdia, D. Juan, J. M. Rodriguez, A. Frankish, M. Diekhans, J. Harrow, J. Vazquez, A. Valencia, and M. L. Tress, "Multiple evidence strands suggest that there may be as few as 19 000 human protein-coding genes," *Human Molecular Genetics*, vol. 23, no. 22, pp. 5866–5878, 2014.

[6] L. P. Kozlowski, "Proteome-pi: proteome isoelectric point database," *Nucleic Acids Research*, vol. 45, no. D1, pp. D1112–D1116, 2016.

[7] X. Yang, J. Coulombe-Huntington, S. Kang, G. Sheynkman, T. Hao, A. Richardson, S. Sun, F. Yang, Y. Shen, R. Murray, K. Spirohn, B. Begg, M. Duran-Frigola, A. MacWilliams, S. Pevzner, Q. Zhong, S. Trigg, S. Tam, L. Ghamsari, N. Sahni, S. Yi, M. Rodriguez, D. Balcha, G. Tan, M. Costanzo, B. Andrews, C. Boone, X. Zhou, K. Salehi-Ashtiani, B. Charloteaux, A. Chen, M. Calderwood, P. Aloy, F. Roth, D. Hill, L. Iakoucheva, Y. Xia, and M. Vidal, "Widespread expansion of protein interaction capabilities by alternative splicing," *Cell*, vol. 164, no. 4, pp. 805–817, 2016.

[8] R. Harmel and D. Fiedler, "Features and regulation of non-enzymatic post-translational modifications," *Nature Chemical Biology*, vol. 14, p. 244, 2018.

[9] G. Duan and D. Walther, "The roles of post-translational modifications in the context of protein interaction networks," *PLoS computational biology*, vol. 11, no. 2, pp. e1004049–e1004049, 2015.

[10] W. He, L. Wei, and Q. Zou, "Research progress in protein posttranslational modification site prediction," *Briefings in Functional Genomics*, vol. 18, no. 4, pp. 220–229, 2018.

[11] C. T. Walsh, *Posttranslational modification of proteins : expanding nature's inventory*. Greenwood Village, CO: Roberts & Company Publishers, 2006.

[12] R. Bischoff and H. Schlüter, "Amino acids: Chemistry, functionality and selected non-enzymatic post-translational modifications," *Journal of Proteomics*, vol. 75, no. 8, pp. 2275–2296, 2012.

[13] F. Tekaia, E. Yeramian, and B. Dujon, "Amino acid composition of genomes, lifestyles of organisms, and evolutionary trends: a global picture with correspondence analysis," *Gene*, vol. 297, no. 1, pp. 51–60, 2002.

[14] J. Warwicker, S. Charonis, and R. A. Curtis, "Lysine and arginine content of proteins: Computational analysis suggests a new tool for solubility design," *Molecular Pharmaceutics*, vol. 11, no. 1, pp. 294–303, 2014.

[15] S. Sokalingam, G. Raghunathan, N. Soundrarajan, and S.-G. Lee, "A study on the effect of surface lysine to arginine mutagenesis on protein stability and structure using green fluorescent protein," *PLOS ONE*, vol. 7, no. 7, p. e40410, 2012.

[16] I. Buchholz, P. Nestler, S. Köppen, and M. Delcea, "Lysine residues control the conformational dynamics of beta 2-glycoprotein i," *Physical Chemistry Chemical Physics*, vol. 20, no. 42, pp. 26819–26829, 2018.

[17] A. C. Carrera, K. Alexandrov, and T. M. Roberts, "The conserved lysine of the catalytic domain of protein kinases is actively involved in the phosphotransfer reaction and not required for anchoring atp," *Proceedings of the National Academy of Sciences*, vol. 90, no. 2, pp. 442–446, 1993.

[18] G. Karp, *The Chemical Basis of Life*, pp. 34–35. Hoboken: Wiley, 2nd ed., 1998.

[19] S. M. Hacker, K. M. Backus, M. R. Lazear, S. Forli, B. E. Correia, and B. F. Cravatt, "Global profiling of lysine reactivity and ligandability in the human proteome," *Nature Chemistry*, vol. 9, no. 12, pp. 1181–1190, 2017.

[20] L. Gambini, C. Baggio, P. Udompholkul, J. Jossart, A. F. Salem, J. J. P. Perry, and M. Pellecchia, "Covalent inhibitors of protein–protein interactions targeting lysine, tyrosine, or histidine residues," *Journal of Medicinal Chemistry*, vol. 62, no. 11, pp. 5616–5627, 2019.

[21] D. G. Isom, C. A. Castañeda, B. R. Cannon, and B. García-Moreno E., "Large shifts in pk_a values of lysine residues buried inside a protein," *Proceedings of the National Academy of Sciences*, vol. 108, no. 13, pp. 5260–5265, 2011.

[22] A. P. Loboda, S. M. Soond, M. Piacentini, and N. A. Barlev, "Lysine-specific post-translational modifications of proteins in the life cycle of viruses," *Cell Cycle*, vol. 18, no. 17, pp. 1995–2005, 2019.

[23] C. Kontaxi, P. Piccardo, and A. C. Gill, "Lysine-directed post-translational modifications of tau protein in alzheimer's disease and related tauopathies," *Frontiers in Molecular Biosciences*, vol. 4, pp. 56–69, 2017.

[24] C. Azevedo and A. Saiardi, "Why always lysine? the ongoing tale of one of the most modified amino acids," *Advances in Biological Regulation*, vol. 60, pp. 144–150, 2016.

[25] D. Van Slyke and S. FM, "The course of hydroxylation of lysine to form hydroxylysine in collagen," *Journal of Biological Chemistry*, vol. 232, no. 2, pp. 797–806, 1958.

[26] C. Azevedo, T. Livermore, and A. Saiardi, "Protein polyphosphorylation of lysine residues by inorganic polyphosphate," *Molecular Cell*, vol. 58, no. 1, pp. 71–82, 2015.

[27] P. Beltrao, P. Bork, N. J. Krogan, and V. van Noort, "Evolution and functional cross-talk of protein post-translational modifications," *Molecular Systems Biology*, vol. 9, no. 1, pp. 714–726, 2013.

[28] T. Hunter, "Why nature chose phosphate to modify proteins," *Phil. Trans. R. Soc. B.*, vol. 367, no. 1602, pp. 2513–2516, 2012.

[29] P. A. Levene and C. L. Alsberg, "The cleavage products of vitellin," *J. Biol. Chem.*, vol. 2, pp. 127–133, 1906.

[30] G. Burnett and E. P. EKennedy, "The enzymatic phosphorylation of proteins," *J. Biol. Chem.*, vol. 211, pp. 969–980, 1954.

[31] J. Cicenas, E. Zalyte, A. Bairoch, and G. P, "Kinases and cancer," *Cancers*, vol. 10, no. 3, pp. 63–70, 2018.

[32] J. Stebbing, L. C. Lit, H. Zhang, R. S. Darrington, O. Melaiu, B. Rudraraju, and G. Giamas, "The regulatory roles of phosphatases in cancer," *Oncogene*, vol. 33, no. 8, pp. 939–953, 2014.

[33] D. J. Mandell, I. Chorny, E. S. Groban, S. E. Wong, E. Levine, C. S. Rapp, and M. P. Jacobson, "Strengths of hydrogen bonds involving phosphorylated amino acid side chains," *Journal of the American Chemical Society*, vol. 129, no. 4, pp. 820–827, 2007.

[34] S. J. Humphrey, D. E. James, and M. Mann, "Protein phosphorylation: A major switch mechanism for metabolic regulation," *Trends in Endocrinology & Metabolism*, vol. 26, no. 12, pp. 676–687, 2015.

[35] T. Hunter, "Signaling—2000 and beyond," *Cell*, vol. 100, no. 1, pp. 113–127, 2000.

[36] T. Hunter, "The age of crosstalk: Phosphorylation, ubiquitination, and beyond," *Molecular Cell*, vol. 28, no. 5, pp. 730–738, 2007.

[37] S. Mukherjee, G. Keitany, Y. Li, Y. Wang, H. L. Ball, E. J. Goldsmith, and K. Orth, "Yersinia yopj acetylates and inhibits kinase activation by blocking phosphorylation," *Science*, vol. 312, no. 5777, pp. 1211–1214, 2006.

[38] X. Li, F. Lu, J.-Z. Wang, and C.-X. Gong, "Concurrent alterations of o-glcnacylation and phosphorylation of tau in mouse brains during fasting," *European Journal of Neuroscience*, vol. 23, no. 8, pp. 2078–2086, 2006.

[39] O. Reimann, *Tag-free semisynthetic tau proteins and novel antibodies targeted against phospho-tau.* Thesis, Freie Universität Berlin, 2017.

[40] J. Habibian and B. Ferguson, "The crosstalk between acetylation and phosphorylation: Emerging new roles for hdac inhibitors in the heart," *International Journal of Molecular Sciences*, vol. 20, no. 1, pp. 102–117, 2018.

[41] C. L. Brooks and W. Gu, "Ubiquitination, phosphorylation and acetylation: the molecular basis for p53 regulation," *Current Opinion in Cell Biology*, vol. 15, no. 2, pp. 164–171, 2003.

[42] S. Brabencová, I. Ihnatová, D. Potěšil, M. Fojtová, J. Fajkus, Z. Zdráhal, and G. Lochmanová, "Variations of histone modification patterns: Contributions of inter-plant variability and technical factors," *Frontiers in plant science*, vol. 8, pp. 2084–2094, 2017.

[43] S. Loroch, C. Dickhut, R. P. Zahedi, and A. Sickmann, "Phosphoproteomics–more than meets the eye," *Electrophoresis*, vol. 34, no. 11, pp. 1483–1492, 2013.

[44] A. Hauser, M. Penkert, and C. P. R. Hackenberger, "Chemical approaches to investigate labile peptide and protein phosphorylation," *Accounts of Chemical Research*, vol. 50, no. 8, pp. 1883–1893, 2017.

[45] W. Eckhart, M. A. Hutchinson, and T. Hunter, "An activity phosphorylating tyrosine in polyoma t antigen immunoprecipitates," *Cell*, vol. 18, no. 4, pp. 925–933, 1979.

[46] J. A. Ubersax and J. E. Ferrell Jr, "Mechanisms of specificity in protein phosphorylation," *Nature Reviews Molecular Cell Biology*, vol. 8, no. 7, pp. 530–541, 2007.

[47] J. V. Olsen, B. Blagoev, F. Gnad, B. Macek, C. Kumar, P. Mortensen, and M. Mann, "Global, in vivo, and site-specific phosphorylation dynamics in signaling networks," *Cell*, vol. 127, no. 3, pp. 635–648, 2006.

[48] L. A. Pinna and A. Donella-Deana, "Phosphorylated synthetic peptides as tools for studying protein phosphatases," *Biochimica et Biophysica Acta (BBA) - Molecular Cell Research*, vol. 1222, no. 3, pp. 415–431, 1994.

[49] L. A. Pinna and M. Ruzzene, "How do protein kinases recognize their substrates?," *Biochimica et Biophysica Acta (BBA) - Molecular Cell Research*, vol. 1314, no. 3, pp. 191–225, 1996.

[50] D. Asthagiri, T. Liu, L. Noodleman, R. L. Van Etten, and D. Bashford, "On the role of the conserved aspartate in the hydrolysis of the phosphocysteine intermediate of the low molecular weight tyrosine phosphatase," *Journal of the American Chemical Society*, vol. 126, no. 39, pp. 12677–12684, 2004.

[51] I. Gulerez, Y. Funato, H. Wu, M. Yang, G. Kozlov, H. Miki, and K. Gehring, "Phosphocysteine in the prl-cnnm pathway mediates magnesium homeostasis," *EMBO reports*, vol. 17, no. 12, pp. 1890–1900, 2016.

[52] J. Bertran-Vicente, M. Penkert, O. Nieto-Garcia, J.-M. Jeckelmann, P. Schmieder, E. Krause, and C. P. R. Hackenberger, "Chemoselective synthesis and analysis of naturally occurring phosphorylated cysteine peptides," *Nature Communications*, vol. 7, p. 12703, 2016.

[53] F. Sun, Y. Ding, Q. Ji, Z. Liang, X. Deng, C. C. L. Wong, C. Yi, L. Zhang, S. Xie, S. Alvarez, L. M. Hicks, C. Luo, H. Jiang, L. Lan, and C. He, "Protein cysteine phosphorylation of sara/mgra family transcriptional regulators mediates bacterial virulence and antibiotic resistance," *Proceedings of the National Academy of Sciences*, vol. 109, no. 38, pp. 15461–15466, 2012.

[54] A. Sickmann and H. E. Meyer, "Phosphoamino acid analysis," *PROTEOMICS*, vol. 1, no. 2, pp. 200–206, 2001.

[55] J. W. Chang, J. E. Montgomery, G. Lee, and R. E. Moellering, "Chemoproteomic profiling of phosphoaspartate modifications in prokaryotes," *Angewandte Chemie International Edition*, vol. 57, no. 48, pp. 15712–15716, 2018.

[56] S. Napper, P. M. Wolanin, D. J. Webre, J. Kindrachuk, B. Waygood, and J. B. Stock, "Intramolecular rearrangements as a consequence of the dephosphorylation of phosphoaspartate residues in proteins," *FEBS Letters*, vol. 538, no. 1, pp. 77–80, 2003.

[57] P. V. Attwood, P. G. Besant, and M. J. Piggott, "Focus on phosphoaspartate and phosphoglutamate," *Amino Acids*, vol. 40, no. 4, pp. 1035–1051, 2011.

[58] J. D. Lapek, G. Tombline, K. A. Kellersberger, M. R. Friedman, and A. E. Friedman, "Evidence of histidine and aspartic acid phosphorylation in human prostate cancer cells," *Naunyn-Schmiedeberg's Archives of Pharmacology*, vol. 388, no. 2, pp. 161–173, 2015.

[59] C. P. Zschiedrich, V. Keidel, and H. Szurmant, "Molecular mechanisms of two-component signal transduction," *Journal of molecular biology*, vol. 428, no. 19, pp. 3752–3775, 2016.

[60] T. Omori, A. Honda, H. Mihara, T. Kurihara, and N. Esaki, "Identification of novel mammalian phospholipids containing threonine, aspartate, and glutamate as the base moiety," *Journal of Chromatography B*, vol. 879, no. 29, pp. 3296–3302, 2011. Analysis and Biological Relevance of D-Amino Acids and Related Compounds.

[61] A. Saiardi, R. Bhandari, A. C. Resnick, A. M. Snowman, and S. H. Snyder, "Phosphorylation of proteins by inositol pyrophosphates," *Science*, vol. 306, no. 5704, pp. 2101–2105, 2004.

[62] R. Bhandari, A. Saiardi, Y. Ahmadibeni, A. M. Snowman, A. C. Resnick, T. Z. Kristiansen, H. Molina, A. Pandey, J. K. Werner, K. R. Juluri, Y. Xu, G. D. Prestwich, K. Parang, and S. H. Snyder, "Protein pyrophosphorylation by inositol pyrophosphates is a posttranslational event," *Proceedings of the National Academy of Sciences*, vol. 104, no. 39, pp. 15305–15310, 2007.

[63] M. Chanduri, A. Rai, A. B. Malla, M. Wu, D. Fiedler, R. Mallik, and R. Bhandari, "Inositol hexakisphosphate kinase 1 (ip6k1) activity is required for cytoplasmic dynein-driven transport," *Biochemical Journal*, vol. 473, no. 19, pp. 3031–3047, 2016.

[64] A. Saiardi, "Protein pyrophosphorylation: moving forward," *Biochemical Journal*, vol. 473, no. 21, pp. 3765–3768, 2016.

[65] D. Fiedler, H. Braberg, M. Mehta, G. Chechik, G. Cagney, P. Mukherjee, A. C. Silva, M. Shales, S. R. Collins, S. van Wageningen, P. Kemmeren, F. C. P. Holstege, J. S. Weissman, M.-C. Keogh,

D. Koller, K. M. Shokat, and N. J. Krogan, "Functional organization of the s. cerevisiae phosphorylation network," *Cell*, vol. 136, no. 5, pp. 952–963, 2009.

[66] A. Chakraborty, M. A. Koldobskiy, N. T. Bello, M. Maxwell, J. J. Potter, K. R. Juluri, D. Maag, S. Kim, A. S. Huang, M. J. Dailey, M. Saleh, A. M. Snowman, T. H. Moran, E. Mezey, and S. H. Snyder, "Inositol pyrophosphates inhibit akt signaling, thereby regulating insulin sensitivity and weight gain," *Cell*, vol. 143, no. 6, pp. 897–910, 2010.

[67] D. Wylie, A. Stock, C.-Y. Wong, and J. Stock, "Sensory transduction in bacterial chemotaxis involves phosphotransfer between che proteins," *Biochemical and Biophysical Research Communications*, vol. 151, no. 2, pp. 891–896, 1988.

[68] D. S. Sem and W. W. Cleland, "Phosphorylated aminosugars; synthesis, properties, and reactivity in enzymic reactions," *Biochemistry*, vol. 30, no. 20, pp. 4978–4984, 1991.

[69] E. A. Ruben, M. S. Chapman, and J. D. Evanseck, "Generalized anomeric interpretation of the "high-energy" n–p bond in n-methyl-n'-phosphorylguanidine - importance of reinforcing stereoelectronic effects in "high-energy" phosphoester bonds," *Journal of the American Chemical Society*, vol. 127, no. 50, pp. 17789–17798, 2005.

[70] Y. Shizuta, J. A. Beavo, P. J. Bechtel, F. Hofmann, and E. G. Krebs, "Reversibility of adenosine 3':5'-monophosphate-dependent protein kinase reactions.," *Journal of Biological Chemistry*, vol. 250, no. 17, pp. 6891–6896, 1975.

[71] L. Hubler, G. N. Gill, and P. J. Bertics, "Reversibility of the epidermal growth factor receptor self-phosphorylation reaction. evidence for formation of a high energy phosphotyrosine bond.," *Journal of Biological Chemistry*, vol. 264, no. 3, pp. 1558–1564, 1989.

[72] P. V. Attwood, M. J. Piggott, X. L. Zu, and P. G. Besant, "Focus on phosphohistidine," *Amino Acids*, vol. 32, no. 1, pp. 145–156, 2007.

[73] P. G. Besant, P. V. Attwood, and M. J. Piggott, "Focus on phosphoarginine and phospholysine," *Current Protein & Peptide Science*, vol. 10, no. 6, pp. 536–550, 2009.

[74] S. J. Benkovic and E. J. Sampson, "Structure-reactivity correlation for the hydrolysis of phosphoramidate monoanions," *Journal of the American Chemical Society*, vol. 93, no. 16, pp. 4009–4016, 1971.

[75] P. Boyer, M. Deluca, K. Ebner, D. Hultquist, and J. Peter, "Identification of phosphohistidine in digests from a probable intermediate of oxidative phosphorylation," *Journal of Biological Chemistry*, vol. 237, pp. PC3306–PC3308, 1962.

[76] A. M. Stock, V. L. Robinson, and P. N. Goudreau, "Two-component signal transduction," *Annual Review of Biochemistry*, vol. 69, no. 1, pp. 183–215, 2000.

[77] S. R. Fuhs and T. Hunter, "phisphorylation: the emergence of histidine phosphorylation as a reversible regulatory modification," *Current Opinion in Cell Biology*, vol. 45, pp. 8–16, 2017.

[78] C. M. Potel, M.-H. Lin, A. J. R. Heck, and S. Lemeer, "Widespread bacterial protein histidine phosphorylation revealed by mass spectrometry-based proteomics," *Nature Methods*, vol. 15, no. 3, pp. 187–190, 2018.

[79] S. K. Hindupur, M. Colombi, S. R. Fuhs, M. S. Matter, Y. Guri, K. Adam, M. Cornu, S. Piscuoglio, C. K. Y. Ng, C. Betz, D. Liko, L. Quagliata, S. Moes, P. Jenoe, L. M. Terracciano, M. H. Heim, T. Hunter, and M. N. Hall, "The protein histidine phosphatase lhpp is a tumour suppressor," *Nature*, vol. 555, p. 678, 2018.

[80] J. J. Petkowski, W. Bains, and S. Seager, "Natural products containing 'rare' organophosphorus functional groups," *Molecules*, vol. 24, no. 5, p. 866, 2019.

[81] J. Fuhrmann, A. Schmidt, S. Spiess, A. Lehner, K. Turgay, K. Mechtler, E. Charpentier, and T. Clausen, "Mcsb is a protein arginine kinase that phosphorylates and inhibits the heat-shock regulator ctsr," *Science*, vol. 324, no. 5932, pp. 1323–1327, 2009.

[82] A. K. W. Elsholz, K. Turgay, S. Michalik, B. Hessling, K. Gronau, D. Oertel, U. Mäder, J. Bernhardt, D. Becher, M. Hecker, and U. Gerth, "Global impact of protein arginine phosphorylation on the physiology of bacillus subtilis," *Proceedings of the National Academy of Sciences*, vol. 109, no. 19, pp. 7451–7456, 2012.

[83] S. Junker, S. Maaß, A. Otto, S. Michalik, F. Morgenroth, U. Gerth, M. Hecker, and D. Becher, "Spectral library based analysis of arginine phosphorylations in staphylococcus aureus," *Molecular & Cellular Proteomics*, vol. 17, no. 2, p. 335, 2018.

[84] S. Junker, S. Maaß, A. Otto, M. Hecker, and D. Becher, "Toward the quantitative characterization of arginine phosphorylations in staphylococcus aureus," *Journal of Proteome Research*, vol. 18, no. 1, pp. 265–279, 2019.

[85] S. Fu, C. Fu, Q. Zhou, R. Lin, H. Ouyang, M. Wang, Y. Sun, Y. Liu, and Y. Zhao, "Widespread arginine phosphorylation in human cells - a novel protein ptm revealed by mass spectrometry," *bioRxiv*, p. 725291, 2019.

[86] S. Fu, C. Fu, Q. Zhou, R. Lin, H. Ouyang, M. Wang, Y. Sun, Y. Liu, and Y. Zhao, "Widespread arginine phosphorylation in human cells - a novel protein ptm revealed by mass spectrometry," *Science China Chemistry*, vol. 63, no. 3, pp. 341–346, 2020.

[87] Ö. Zetterqvist and L. Engström, "Isolation of n-ϵ-[32p]phosphoryl-lysine from rat-liver cell sap after incubation with [32p]adenosine triphosphate," *Biochimica et Biophysica Acta (BBA) - General Subjects*, vol. 141, no. 3, pp. 523–532, 1967.

[88] Ö. Zetterqvist, "Further studies on acid-labile [32p]phosphate bound to high-molecular weight material from rat-liver cell sap after incubation with [32p]adenosine triphosphate," *Biochimica et Biophysica Acta (BBA) - General Subjects*, vol. 141, no. 3, pp. 533–539, 1967.

[89] Ö. Zetterqvist, "Studies on acid-labile [32p]phosphate in different chromatographic fractions of high-molecular weight material from rat-liver cell sap after incubation with [32p]adenosine triphosphate," *Biochimica et Biophysica Acta (BBA) - General Subjects*, vol. 141, no. 3, pp. 540–546, 1967.

[90] D. L. Smith, B. B. Bruegger, R. M. Halpern, and R. A. Smith, "New histone kinases in nuclei of rat tissues," *Nature*, vol. 246, no. 5428, pp. 103–104, 1973. 10.1038/246103a0.

[91] D. L. Smith, C.-C. Chen, B. B. Bruegger, S. L. Holtz, R. M. Halpern, and R. A. Smith, "Characterization of protein kinases forming acid-labile histone phosphates in walker-256 carcinosarcoma cell nuclei," *Biochemistry*, vol. 13, no. 18, pp. 3780–3785, 1974.

[92] C.-C. Chen, D. L. Smith, B. B. Bruegger, R. M. Halpern, and R. A. Smith, "Occurrence and distribution of acid-labile histone phosphates in regenerating rat liver," *Biochemistry*, vol. 13, no. 18, pp. 3785–3789, 1974.

[93] C. C. Chen, B. B. Bruegger, C. W. Kern, Y. C. Lin, R. M. Halpern, and R. A. Smith, "Phosphorylation of nuclear proteins in rat regenerating liver," *Biochemistry*, vol. 16, no. 22, pp. 4852–4855, 1977.

[94] T. Modro, *Phosphoric and Carboxylic Amides*, vol. 171 of *ACS Symposium Series*, pp. 128–619. AMERICAN CHEMICAL SOCIETY, 1981.

[95] E. Denehy, J. M. White, and S. J. Williams, "Electronic structure of the sulfonyl and phosphonyl groups: A computational and crystallographic study," *Inorganic Chemistry*, vol. 46, no. 21, pp. 8871–8886, 2007.

[96] S. J. Benkovic and P. A. Benkovic, "Hydrolytic mechanisms of phosphoramidates of aromatic amino acids," *Journal of the American Chemical Society*, vol. 89, no. 18, pp. 4714–4722, 1967.

[97] J. Bertran-Vicente, R. A. Serwa, M. Schümann, P. Schmieder, E. Krause, and C. P. R. Hackenberger, "Site-specifically phosphorylated lysine peptides," *Journal of the American Chemical Society*, vol. 136, no. 39, pp. 13622–13628, 2014.

[98] A. Schmidt, D. B. Trentini, S. Spiess, J. Fuhrmann, G. Ammerer, K. Mechtler, and T. Clausen, "Quantitative phosphoproteomics reveals the role of protein arginine phosphorylation in the bacterial stress response," *Molecular & Cellular Proteomics*, vol. 13, no. 2, pp. 537–550, 2014.

[99] K. Adam, S. Fuhs, J. Meisenhelder, A. Aslanian, J. Diedrich, J. Moresco, J. La Clair, J. R. Yates, and T. Hunter, "A non-acidic method using hydroxyapatite and phosphohistidine monoclonal antibodies allows enrichment of phosphopeptides containing non-conventional phosphorylations for mass spectrometry analysis," *bioRxiv*, p. 691352, 2019.

[100] G. Hardman, S. Perkins, P. J. Brownridge, C. J. Clarke, D. P. Byrne, A. E. Campbell, A. Kalyuzhnyy, A. Myall, P. A. Eyers, A. R. Jones, and C. E. Eyers, "Strong anion exchange-mediated phosphoproteomics reveals extensive human non-canonical phosphorylation," *The EMBO Journal*, vol. 38, no. 21, p. e100847, 2019.

[101] Y. Hu, Y. Weng, B. Jiang, X. Li, X. Zhang, B. Zhao, Q. Wu, Z. Liang, L. Zhang, and Y. Zhang, "Isolation and identification of phosphorylated lysine peptides by retention time difference combining dimethyl labeling strategy," *Science China Chemistry*, vol. 62, no. 6, pp. 708–712, 2019.

[102] E. Fischer and E. Fourneau, "Ueber einige derivate des glykocolls," *Berichte der deutschen chemischen Gesellschaft*, vol. 34, no. 2, pp. 2868–2877, 1901.

[103] M. Bergmann and L. Zervas, "Über ein allgemeines verfahren der peptid-synthese," *Berichte der deutschen chemischen Gesellschaft (A and B Series)*, vol. 65, no. 7, pp. 1192–1201, 1932.

[104] R. B. Merrifield, "Solid phase peptide synthesis. i. the synthesis of a tetrapeptide," *Journal of the American Chemical Society*, vol. 85, no. 14, pp. 2149–2154, 1963.

[105] R. B. Merrifield, "Solid phase synthesis (nobel lecture)," *Angewandte Chemie International Edition in English*, vol. 24, no. 10, pp. 799–810, 1985.

[106] R. Subirós-Funosas, R. Prohens, R. Barbas, A. El-Faham, and F. Albericio, "Oxyma: An efficient additive for peptide synthesis to replace the benzotriazole-based hobt and hoat with a lower risk of explosion[1]," *Chemistry – A European Journal*, vol. 15, no. 37, pp. 9394–9403, 2009.

[107] A. El-Faham and F. Albericio, "Peptide coupling reagents, more than a letter soup," *Chemical Reviews*, vol. 111, no. 11, pp. 6557–6602, 2011.

[108] J. M. Palomo, "Solid-phase peptide synthesis: an overview focused on the preparation of biologically relevant peptides," *RSC Advances*, vol. 4, no. 62, pp. 32658–32672, 2014.

[109] M. Amblard, J.-A. Fehrentz, J. Martinez, and G. Subra, "Methods and protocols of modern solid phase peptide synthesis," *Molecular Biotechnology*, vol. 33, no. 3, pp. 239–254, 2006.

[110] R. Behrendt, P. White, and J. Offer, "Advances in fmoc solid-phase peptide synthesis," *Journal of Peptide Science*, vol. 22, no. 1, pp. 4–27, 2016.

[111] K. D. Siebertz, *Application of chemoselective tools for the protein semi-synthesis of tau and the development of a novel photo-cleavable tag*. Thesis, Humboldt-Universität zu Berlin, 2019.

[112] F. T. Hofmann, C. Lindemann, H. Salia, P. Adamitzki, J. Karanicolas, and F. P. Seebeck, "A phosphoarginine containing peptide as an artificial sh2 ligand," *Chemical Communications*, vol. 47, no. 37, pp. 10335–10337, 2011.

[113] E. A. Hoyt, P. M. S. D. Cal, B. L. Oliveira, and G. J. L. Bernardes, "Contemporary approaches to site-selective protein modification," *Nature Reviews Chemistry*, vol. 3, no. 3, pp. 147–171, 2019.

[114] J. A. Shadish and C. A. DeForest, "Site-selective protein modification: From functionalized proteins to functional biomaterials," *Matter*, vol. 2, no. 1, pp. 50–77, 2020.

[115] K. Wals and H. Ovaa, "Unnatural amino acid incorporation in e. coli: current and future applications in the design of therapeutic proteins," *Frontiers in Chemistry*, vol. 2, no. 15, 2014.

[116] H. Chen, S. Venkat, P. McGuire, Q. Gan, and C. Fan, "Recent development of genetic code expansion for posttranslational modification studies," *Molecules*, vol. 23, no. 7, pp. 1662–1680, 2018.

[117] G. J. L. Bernardes, J. M. Chalker, J. C. Errey, and B. G. Davis, "Facile conversion of cysteine and alkyl cysteines to dehydroalanine on protein surfaces: Versatile and switchable access to functionalized proteins," *Journal of the American Chemical Society*, vol. 130, no. 15, pp. 5052–5053, 2008.

[118] M.-A. Kasper, M. Glanz, A. Stengl, M. Penkert, S. Klenk, T. Sauer, D. Schumacher, J. Helma, E. Krause, M. C. Cardoso, H. Leonhardt, and C. P. R. Hackenberger, "Cysteine-selective phosphonamidate electrophiles for modular protein bioconjugations," *Angewandte Chemie International Edition*, vol. 58, no. 34, pp. 11625–11630, 2019.

[119] A. L. Baumann, S. Schwagerus, K. Broi, K. Kemnitz-Hassanin, C. E. Stieger, N. Trieloff, P. Schmieder, and C. P. R. Hackenberger, "Chemically induced vinylphosphonothiolate electrophiles for thiol–thiol bioconjugations," *Journal of the American Chemical Society*, vol. 142, no. 20, pp. 9544–9552, 2020.

[120] J. A. Prescher, D. H. Dube, and C. R. Bertozzi, "Chemical remodelling of cell surfaces in living animals," *Nature*, vol. 430, no. 7002, pp. 873–877, 2004.

[121] E. Sletten and C. Bertozzi, "Bioorthogonal chemistry: Fishing for selectivity in a sea of functionality," *Angewandte Chemie International Edition*, vol. 48, no. 38, pp. 6974–6998, 2009.

[122] E. M. Sletten and C. R. Bertozzi, "From mechanism to mouse: A tale of two bioorthogonal reactions," *Accounts of Chemical Research*, vol. 44, no. 9, pp. 666–676, 2011.

[123] N. J. Agard, J. A. Prescher, and C. R. Bertozzi, "A strain-promoted [3 + 2] azide–alkyne cycloaddition for covalent modification of biomolecules in living systems," *Journal of the American Chemical Society*, vol. 126, no. 46, pp. 15046–15047, 2004.

[124] H.-S. Park, M. J. Hohn, T. Umehara, L.-T. Guo, E. M. Osborne, J. Benner, C. J. Noren, J. Rinehart, and D. Söll, "Expanding the genetic code of escherichia coli with phosphoserine," *Science*, vol. 333, no. 6046, pp. 1151–1154, 2011.

[125] N. L. Pirman, K. W. Barber, H. R. Aerni, N. J. Ma, A. D. Haimovich, S. Rogulina, F. J. Isaacs, and J. Rinehart, "A flexible codon in genomically recoded escherichia coli permits programmable protein phosphorylation," *Nature Communications*, vol. 6, no. 1, pp. 8130–8135, 2015.

[126] P. Zhu, P. R. Gafken, R. A. Mehl, and R. B. Cooley, "A highly versatile expression system for the production of multiply phosphorylated proteins," *ACS Chemical Biology*, vol. 14, no. 7, pp. 1564–1572, 2019.

[127] M. S. Zhang, S. F. Brunner, N. Huguenin-Dezot, A. D. Liang, W. H. Schmied, D. T. Rogerson, and J. W. Chin, "Biosynthesis and genetic encoding of phosphothreonine through parallel selection and deep sequencing," *Nature Methods*, vol. 14, no. 7, pp. 729–736, 2017.

[128] C. Fan, K. Ip, and D. Söll, "Expanding the genetic code of escherichia coli with phosphotyrosine," *FEBS Letters*, vol. 590, no. 17, pp. 3040–3047, 2016.

[129] C. Hoppmann, A. Wong, B. Yang, S. Li, T. Hunter, K. M. Shokat, and L. Wang, "Site-specific incorporation of phosphotyrosine using an expanded genetic code," *Nature Chemical Biology*, vol. 13, p. 842, 2017.

[130] X. Luo, G. Fu, R. E. Wang, X. Zhu, C. Zambaldo, R. Liu, T. Liu, X. Lyu, J. Du, W. Xuan, A. Yao, S. A. Reed, M. Kang, Y. Zhang, H. Guo, C. Huang, P.-Y. Yang, I. A. Wilson, P. G. Schultz, and F. Wang, "Genetically encoding phosphotyrosine and its nonhydrolyzable analog in bacteria," *Nature Chemical Biology*, vol. 13, no. 8, pp. 845–849, 2017.

[131] A. M. Marmelstein, J. Moreno, and D. Fiedler, *Chemical Approaches to Studying Labile Amino Acid Phosphorylation*, pp. 179–210. Cham: Springer International Publishing, 2017.

[132] K. P. Chooi, S. R. G. Galan, R. Raj, J. McCullagh, S. Mohammed, L. H. Jones, and B. G. Davis, "Synthetic phosphorylation of p38α recapitulates protein kinase activity," *Journal of the American Chemical Society*, vol. 136, no. 5, pp. 1698–1701, 2014.

[133] R. Meledin, S. M. Mali, S. K. Singh, and A. Brik, "Protein ubiquitination via dehydroalanine: development and insights into the diastereoselective 1,4-addition step," *Organic & Biomolecular Chemistry*, vol. 14, no. 21, pp. 4817–4823, 2016.

[134] A. M. Marmelstein, L. M. Yates, J. H. Conway, and D. Fiedler, "Chemical pyrophosphorylation of functionally diverse peptides," *Journal of the American Chemical Society*, vol. 136, no. 1, pp. 108–111, 2014.

[135] A. Marmelstein, J. A. M. Morgan, M. Penkert, D. T. Rogerson, J. W. Chin, E. Krause, and D. Fiedler, "Pyrophosphorylation via selective phosphoprotein derivatization," *Chemical Science*, vol. 9, no. 27, pp. 5929–5936, 2018.

[136] D. T. Rogerson, A. Sachdeva, K. Wang, T. Haq, A. Kazlauskaite, S. M. Hancock, N. Huguenin-Dezot, M. M. K. Muqit, A. M. Fry, R. Bayliss, and J. W. Chin, "Efficient genetic encoding of phosphoserine and its nonhydrolyzable analog," *Nature Chemical Biology*, vol. 11, no. 7, pp. 496–503, 2015.

[137] J. Fuhrmann, K. W. Clancy, and P. R. Thompson, "Chemical biology of protein arginine modifications in epigenetic regulation," *Chemical Reviews*, vol. 115, no. 11, pp. 5413–5461, 2015.

[138] Y.-F. Wei and H. R. Matthews, *[32] Identification of phosphohistidine in proteins and purification of protein-histidine kinases*, vol. Volume 200, pp. 388–414. Academic Press, 1991.

[139] T. Ruman, K. Długopolska, A. Jurkiewicz, D. Rut, T. Frączyk, J. Cieśla, A. Leś, Z. Szewczuk, and W. Rode, "Thiophosphorylation of free amino acids and enzyme protein by thiophosphoramidate ions," *Bioorganic Chemistry*, vol. 38, no. 2, pp. 74–80, 2010.

[140] J. M. Fujitaki, A. W. Steiner, S. E. Nichols, E. R. Helander, Y. C. Lin, and R. A. Smith, "A simple preparation of n-phosphorylated lysine and arginine," *Preparative Biochemistry*, vol. 10, no. 2, pp. 205–213, 1980.

[141] U. Beckman-Sundh, B. Ek, Ö. Zetterqvist, and P. Ek, "A screening method for phosphohistidine phosphatase 1 activity," *Upsala Journal of Medical Sciences*, vol. 116, no. 3, pp. 161–168, 2011.

[142] P. Ek, B. Ek, and Ö. Zetterqvist, "Phosphohistidine phosphatase 1 (phpt1) also dephosphorylates phospholysine of chemically phosphorylated histone h1 and polylysine," *Upsala Journal of Medical Sciences*, vol. 120, no. 1, pp. 20–27, 2015.

[143] H. Staudinger and J. Meyer, "Über neue organische phosphorverbindungen iii. phosphinmethylenderivate und phosphinimine," *Helvetica Chimica Acta*, vol. 2, no. 1, pp. 635–646, 1919.

[144] E. Saxon and C. R. Bertozzi, "Cell surface engineering by a modified staudinger reaction," *Science*, vol. 287, no. 5460, pp. 2007–2010, 2000.

[145] E. Saxon, J. I. Armstrong, and C. R. Bertozzi, "A "traceless" staudinger ligation for the chemoselective synthesis of amide bonds," *Organic Letters*, vol. 2, no. 14, pp. 2141–2143, 2000.

[146] B. Nilsson, L. Kiessling, and R. Raines, "Staudinger ligation: a peptide from a thioester and azide," *Organic Letters*, vol. 2, no. 13, pp. 1939–1941, 2000.

[147] Y. Gololobov and L. Kasukhin, "Recent advances in the staudinger reaction," *Tetrahedron*, vol. 48, no. 8, pp. 1353–1406, 1992.

[148] C. Bednarek, I. Wehl, N. Jung, U. Schepers, and S. Bräse, "The staudinger ligation," *Chemical Reviews*, vol. 120, no. 10, pp. 4301–4354, 2020.

[149] M. I. Kabachnik and V. A. Gilyarov *Bulletin of the Academy of Sciences of the USSR Division of chemical science*, vol. 5, pp. 809–816, 1956.

[150] R. Serwa, I. Wilkening, G. Del Signore, M. Muehlberg, I. Claussnitzer, C. Weise, M. Gerrits, and C. Hackenberger, "Chemoselective staudinger-phosphite reaction of azides for the phosphorylation of proteins," *Angewandte Chemie International Edition*, vol. 48, no. 44, pp. 8234–8239, 2009.

[151] R. Serwa, P. Majkut, B. Horstmann, J.-M. Swiecicki, M. Gerrits, E. Krause, and C. P. R. Hackenberger, "Site-specific pegylation of proteins by a staudinger-phosphite reaction," *Chemical Science*, vol. 1, no. 5, pp. 596–602, 2010.

[152] V. Böhrsch, R. Serwa, P. Majkut, E. Krause, and C. P. R. Hackenberger, "Site-specific functionalisation of proteins by a staudinger-type reaction using unsymmetrical phosphites," *Chemical Communications*, vol. 46, no. 18, pp. 3176–3178, 2010.

[153] J. Bertran-Vicente, M. Schümann, P. Schmieder, E. Krause, and C. P. R. Hackenberger, "Direct access to site-specifically phosphorylated-lysine peptides from a solid-support," *Organic & Biomolecular Chemistry*, vol. 13, no. 24, pp. 6839–6843, 2015.

[154] N. Nischan, A. Chakrabarti, R. A. Serwa, P. H. M. Bovee-Geurts, R. Brock, and C. P. R. Hackenberger, "Stabilization of Peptides for Intracellular Applications by Phosphoramidate-Linked

Polyethylene Glycol Chains," *Angewandte Chemie International Edition*, vol. 52, no. 45, pp. 11920–11924, 2013.

[155] E. Hoffmann, K. Streichert, N. Nischan, C. Seitz, T. Brunner, S. Schwagerus, C. P. R. Hackenberger, and M. Rubini, "Stabilization of bacterially expressed erythropoietin by single site-specific introduction of short branched peg chains at naturally occurring glycosylation sites," *Molecular BioSystems*, vol. 12, no. 6, pp. 1750–1755, 2016.

[156] V. Böhrsch, T. Mathew, M. Zieringer, M. R. J. Vallée, L. M. Artner, J. Dernedde, R. Haag, and C. P. R. Hackenberger, "Chemoselective staudinger-phosphite reaction of symmetrical glycosyl-phosphites with azido-peptides and polygycerols," *Organic & Biomolecular Chemistry*, vol. 10, no. 30, pp. 6211–6216, 2012.

[157] R. A. Serwa, J.-M. Swiecicki, D. Homann, and C. P. R. Hackenberger, "Phosphoramidate-peptide synthesis by solution- and solid-phase staudinger-phosphite reactions," *Journal of Peptide Science*, vol. 16, no. 10, pp. 563–567, 2010.

[158] D. R. Buckler and A. M. Stock, "Synthesis of [32p]phosphoramidate for use as a low molecular weight phosphodonor reagent," *Analytical Biochemistry*, vol. 283, no. 2, pp. 222–227, 2000.

[159] Y. Gololobov, I. Zhmurova, and L. Kasukhin, "Sixty years of staudinger reaction," *Tetrahedron*, vol. 37, no. 3, pp. 437–472, 1981.

[160] M. R. J. Vallée, P. Majkut, I. Wilkening, C. Weise, G. Müller, and C. P. R. Hackenberger, "Staudinger-phosphonite reactions for the chemoselective transformation of azido-containing peptides and proteins," *Organic Letters*, vol. 13, no. 20, pp. 5440–5443, 2011.

[161] M. R. J. Vallée, L. M. Artner, J. Dernedde, and C. P. R. Hackenberger, "Alkyne phosphonites for sequential azide–azide couplings," *Angewandte Chemie International Edition*, vol. 52, no. 36, pp. 9504–9508, 2013.

[162] M. R. J. Vallée, P. Majkut, D. Krause, M. Gerrits, and C. P. R. Hackenberger, "Chemoselective bioconjugation of triazole phosphonites in aqueous media," *Chemistry – A European Journal*, vol. 21, no. 3, pp. 970–974, 2015.

[163] K. D. Siebertz and C. P. R. Hackenberger, "Chemoselective triazole-phosphonamidate conjugates suitable for photorelease," *Chemical Communications*, vol. 54, no. 7, pp. 763–766, 2018.

[164] M.-A. Kasper, M. Glanz, A. Oder, P. Schmieder, J. P. von Kries, and C. P. R. Hackenberger, "Vinylphosphonites for staudinger-induced chemoselective peptide cyclization and functionalization," *Chemical Science*, vol. 10, no. 25, pp. 6322–6329, 2019.

[165] M.-A. Kasper, A. Stengl, P. Ochtrop, M. Gerlach, T. Stoschek, D. Schumacher, J. Helma, M. Penkert, E. Krause, H. Leonhardt, and C. P. R. Hackenberger, "Ethynylphosphonamidates for the rapid and cysteine-selective generation of efficacious antibody–drug conjugates," *Angewandte Chemie International Edition*, vol. 58, no. 34, pp. 11631–11636, 2019.

[166] M. Glanz, *Chemoselective conjugation of biological active peptides to functional scaffolds*. Thesis, Humboldt-Universität zu Berlin, 2019.

[167] A. Yang, K. Cho, and H.-S. Park, "Chemical biology approaches for studying posttranslational modifications," *RNA Biology*, vol. 15, no. 4-5, pp. 427–440, 2018.

[168] T. S. Elliott, A. Slowey, Y. Ye, and S. J. Conway, "The use of phosphate bioisosteres in medicinal chemistry and chemical biology," *MedChemComm*, vol. 3, no. 7, pp. 735–751, 2012.

[169] E. A. Bienkiewicz and K. J. Lumb, "Random-coil chemical shifts of phosphorylated amino acids," *Journal of Biomolecular NMR*, vol. 15, no. 3, pp. 203–206, 1999.

[170] J. Léger, M. Kempf, G. Lee, and R. Brandt, "Conversion of serine to aspartate imitates phosphorylation-induced changes in the structure and function of microtubule-associated protein tau," *Journal of Biological Chemistry*, vol. 272, no. 13, pp. 8441–8446, 1997.

[171] S. Pearlman, Z. Serber, and J. Ferrell Jr., "A mechanism for the evolution of phosphorylation sites," *Cell*, vol. 147, no. 4, pp. 934–946, 2011.

[172] W. Zheng, Z. Zhang, S. Ganguly, J. L. Weller, D. C. Klein, and P. A. Cole, "Cellular stabilization of the melatonin rhythm enzyme induced by nonhydrolyzable phosphonate incorporation," *Nature Structural & Molecular Biology*, vol. 10, no. 12, pp. 1054–1057, 2003.

[173] A. P. Combs, "Recent advances in the discovery of competitive protein tyrosine phosphatase 1b inhibitors for the treatment of diabetes, obesity, and cancer," *Journal of Medicinal Chemistry*, vol. 53, no. 6, pp. 2333–2344, 2010.

[174] T. R. Burke, H. K. Kole, and P. P. Roller, "Potent inhibition of insulin receptor dephosphorylation by a hexamer peptide containing the phosphotyrosyl mimetic f2pmp," *Biochemical and Biophysical Research Communications*, vol. 204, no. 1, pp. 129–134, 1994.

[175] M. Hussain, V. Ahmed, B. Hill, Z. Ahmed, and S. D. Taylor, "A re-examination of the difluoromethylenesulfonic acid group as a phosphotyrosine mimic for ptp1b inhibition," *Bioorganic & Medicinal Chemistry*, vol. 16, no. 14, pp. 6764–6777, 2008.

[176] L. Berlicki, "Inhibitors of glutamine synthetase and their potential application in medicine," *Mini-Reviews in Medicinal Chemistry*, vol. 8, pp. 869–878, 2008.

[177] R. E. Silversmith and R. B. Bourret, "Synthesis and characterization of a stable analog of the phosphorylated form of the chemotaxis protein chey.," *Protein Engineering, Design and Selection*, vol. 11, no. 3, pp. 205–212, 1998.

[178] R. L. Saxl, G. S. Anand, and A. M. Stock, "Synthesis and biochemical characterization of a phosphorylated analogue of the response regulator cheb," *Biochemistry*, vol. 40, no. 43, pp. 12896–12903, 2001.

[179] C. J. Halkides, M. M. McEvoy, E. Casper, P. Matsumura, K. Volz, and F. W. Dahlquist, "The 1.9 å resolution crystal structure of phosphono-chey, an analogue of the active form of the response regulator, chey," *Biochemistry*, vol. 39, no. 18, pp. 5280–5286, 2000.

[180] D. B. Lookadoo, M. S. Beyersdorf, and C. J. Halkides, *Synthesis of a Stable Analog of the Phosphorylated Form of CheY: Phosphono-CheY BT - Bacterial Chemosensing: Methods and Protocols*, pp. 337–343. New York, NY: Springer New York, 2018.

[181] R. C. Stewart, "Activating and inhibitory mutations in the regulatory domain of cheb, the methylesterase in bacterial chemotaxis.," *Journal of Biological Chemistry*, vol. 268, no. 3, pp. 1921–30, 1993.

[182] L. M. Yates and D. Fiedler, "A stable pyrophosphoserine analog for incorporation into peptides and proteins," *ACS Chemical Biology*, vol. 11, no. 4, pp. 1066–1073, 2016.

[183] C. Schenkels, B. Erni, and J.-L. Reymond, "Phosphofurylalanine, a stable analog of phosphohistidine," *Bioorganic & Medicinal Chemistry Letters*, vol. 9, no. 10, pp. 1443–1446, 1999.

[184] J.-M. Kee, B. Villani, L. R. Carpenter, and T. W. Muir, "Development of stable phosphohistidine analogues," *Journal of the American Chemical Society*, vol. 132, no. 41, pp. 14327–14329, 2010.

[185] T. E. McAllister, M. G. Nix, and M. E. Webb, "Fmoc-chemistry of a stable phosphohistidine analogue," *Chemical Communications*, vol. 47, no. 4, pp. 1297–1299, 2011.

[186] T. E. McAllister and M. E. Webb, "Triazole phosphohistidine analogues compatible with the fmoc-strategy," *Organic & Biomolecular Chemistry*, vol. 10, no. 20, pp. 4043–4049, 2012.

[187] S. Fuhs, J. Meisenhelder, A. Aslanian, L. Ma, A. Zagorska, M. Stankova, A. Binnie, F. Al-Obeidi, J. Mauger, G. Lemke, J. Yates, and T. Hunter, "Monoclonal 1- and 3-phosphohistidine antibodies: New tools to study histidine phosphorylation," *Cell*, vol. 162, no. 1, pp. 198–210, 2015.

[188] J.-M. Kee, R. C. Oslund, D. H. Perlman, and T. W. Muir, "A pan-specific antibody for direct detection of protein histidine phosphorylation," *Nat Chem Biol*, vol. 9, no. 7, pp. 416–421, 2013.

[189] M. Lilley, B. Mambwe, M. J. Thompson, R. F. W. Jackson, and R. Muimo, "4-phosphopyrazol-2-yl alanine: a non-hydrolysable analogue of phosphohistidine," *Chemical Communications*, vol. 51, no. 34, pp. 7305–7308, 2015.

[190] J.-M. Kee, R. C. Oslund, A. D. Couvillon, and T. W. Muir, "A second-generation phosphohistidine analog for production of phosphohistidine antibodies," *Organic Letters*, vol. 17, no. 2, pp. 187–189, 2015.

[191] J. Fuhrmann, V. Subramanian, and P. R. Thompson, "Synthesis and use of a phosphonate amidine to generate an anti-phosphoarginine-specific antibody," *Angewandte Chemie International Edition*, vol. 54, no. 49, pp. 14715–14718, 2015.

[192] J. Fuhrmann, V. Subramanian, D. Kojetin, and P. Thompson, "Activity-based profiling reveals a regulatory link between oxidative stress and protein arginine phosphorylation," *Cell Chemical Biology*, vol. 23, no. 8, pp. 967–977, 2016.

[193] H. Ouyang, C. Fu, S. Fu, Z. Ji, Y. Sun, P. Deng, and Y. Zhao, "Development of a stable phosphoarginine analog for producing phosphoarginine antibodies," *Organic & Biomolecular Chemistry*, vol. 14, no. 6, pp. 1925–1929, 2016.

[194] J. Cieśla, T. Fraczyk, and W. Rode, "Phosphorylation of basic amino acid residues in proteins: Important but easily missed," *Acta biochimica Polonica*, vol. 58, no. 2, pp. 137–148, 2011.

[195] L. S. Smith, C. W. Kern, R. M. Halpern, and R. A. Smith, "Phosphorylation on basic amino acids in myelin basic protein," *Biochemical and Biophysical Research Communications*, vol. 71, no. 2, pp. 459–465, 1976.

[196] L. M. Yates and D. Fiedler, "Establishing the stability and reversibility of protein pyrophosphorylation with synthetic peptides," *ChemBioChem*, vol. 16, no. 3, pp. 415–423, 2015.

[197] M. J. Suskiewicz, B. Hajdusits, R. Beveridge, A. Heuck, L. D. Vu, R. Kurzbauer, K. Hauer, V. Thoeny, K. Rumpel, K. Mechtler, A. Meinhart, and T. Clausen, "Structure of mcsb, a protein kinase for regulated arginine phosphorylation," *Nature Chemical Biology*, vol. 15, no. 5, pp. 510–518, 2019.

[198] D. B. Trentini, J. Fuhrmann, K. Mechtler, and T. Clausen, "Chasing phosphoarginine proteins: Development of a selective enrichment method using a phosphatase trap," *Molecular & Cellular Proteomics*, vol. 13, no. 8, pp. 1953–1964, 2014.

[199] K. Adam, J. Lesperance, T. Hunter, and P. Zage, "The potential functional roles of nme1 histidine kinase activity in neuroblastoma pathogenesis," *International Journal of Molecular Sciences*, vol. 21, no. 9, pp. 3319–3337, 2020.

[200] J. Zheng, X. Dai, H. Chen, C. Fang, J. Chen, and L. Sun, "Down-regulation of lhpp in cervical cancer influences cell proliferation, metastasis and apoptosis by modulating akt," *Biochemical and Biophysical Research Communications*, vol. 503, no. 2, pp. 1108–1114, 2018.

[201] Y. Li, X. Zhang, X. Zhou, and X. Zhang, "Lhpp suppresses bladder cancer cell proliferation and growth via inactivating akt/p65 signaling pathway," *Bioscience Reports*, vol. 39, no. 7, 2019.

[202] Y. Choi, S. H. Shin, H. Jung, O. Kwon, J. K. Seo, and J.-M. Kee, "Specific fluorescent probe for protein histidine phosphatase activity," *ACS Sensors*, vol. 4, no. 4, pp. 1055–1062, 2019.

[203] H. Hiraishi, T. Ohmagari, Y. Otsuka, F. Yokoi, and A. Kumon, "Purification and characterization of hepatic inorganic pyrophosphatase hydrolyzing imidodiphosphate," *Archives of Biochemistry and Biophysics*, vol. 341, no. 1, pp. 153–159, 1997.

[204] H. Hiraishi, F. Yokoi, and A. Kumon, "3-phosphohistidine and 6-phospholysine are substrates of a 56-kda inorganic pyrophosphatase from bovine liver," *Archives of Biochemistry and Biophysics*, vol. 349, no. 2, pp. 381–387, 1998.

[205] F. Yokoi, H. Hiraishi, and K. Izuhara, "Molecular cloning of a cdna for the human phospholysine phosphohistidine inorganic pyrophosphate phosphatase," *Journal of Biochemistry*, vol. 133, no. 5, pp. 607–614, 2003.

[206] S. Fahs, P. Lujan, and M. Köhn, "Approaches to study phosphatases," *ACS Chemical Biology*, vol. 11, no. 11, pp. 2944–2961, 2016.

[207] H. Cai, B. Huang, R. Lin, P. Xu, Y. Liu, and Y. Zhao, "A "turn-off" sers assay for kinase detection based on arginine n-phosphorylation process," *Talanta*, vol. 189, pp. 353–358, 2018.

[208] M. D. Shults, D. A. Pearce, and B. Imperiali, "Modular and tunable chemosensor scaffold for divalent zinc," *Journal of the American Chemical Society*, vol. 125, no. 35, pp. 10591–10597, 2003.

[209] M. D. Shults and B. Imperiali, "Versatile fluorescence probes of protein kinase activity," *Journal of the American Chemical Society*, vol. 125, no. 47, pp. 14248–14249, 2003.

[210] M. D. Shults, K. A. Janes, D. A. Lauffenburger, and B. Imperiali, "A multiplexed homogeneous fluorescence-based assay for protein kinase activity in cell lysates," *Nature Methods*, vol. 2, no. 4, pp. 277–284, 2005.

[211] E. Luković, J. A. González-Vera, and B. Imperiali, "Recognition-domain focused chemosensors: Versatile and efficient reporters of protein kinase activity," *Journal of the American Chemical Society*, vol. 130, no. 38, pp. 12821–12827, 2008.

[212] H. Jung, Y. Choi, D. Lee, J. K. Seo, and J.-M. Kee, "Distinct phosphorylation and dephosphorylation dynamics of protein arginine kinases revealed by fluorescent activity probes," *Chem. Commun.*, vol. 55, pp. 7482–7485, 2019.

[213] H. Jung, S. H. Shin, and J.-M. Kee, "Recent updates on protein n-phosphoramidate hydrolases," *ChemBioChem*, vol. 20, no. 5, pp. 623–633, 2019.

[214] D. Perrett, "From 'protein' to the beginnings of clinical proteomics," *PROTEOMICS – Clinical Applications*, vol. 1, no. 8, pp. 720–738, 2007.

[215] G. Prus, A. Hoegl, B. T. Weinert, and C. Choudhary, "Analysis and interpretation of protein post-translational modification site stoichiometry," *Trends in Biochemical Sciences*, vol. 44, no. 11, pp. 943–960, 2019.

[216] N. M. Riley and J. J. Coon, "Phosphoproteomics in the age of rapid and deep proteome profiling," *Analytical Chemistry*, vol. 88, no. 1, pp. 74–94, 2016.

[217] S. Lemeer and A. J. R. Heck, "The phosphoproteomics data explosion," *Current Opinion in Chemical Biology*, vol. 13, no. 4, pp. 414–420, 2009.

[218] B. A. Garcia, S. Mollah, B. M. Ueberheide, S. A. Busby, T. L. Muratore, J. Shabanowitz, and D. F. Hunt, "Chemical derivatization of histones for facilitated analysis by mass spectrometry," *Nature Protocols*, vol. 2, no. 4, pp. 933–938, 2007.

[219] Z. A. Knight, B. Schilling, R. H. Row, D. M. Kenski, B. W. Gibson, and K. M. Shokat, "Phosphospecific proteolysis for mapping sites of protein phosphorylation," *Nature Biotechnology*, vol. 21, no. 9, pp. 1047–1054, 2003.

[220] Y. Hu, Y. Li, H. Gao, B. Jiang, X. Zhang, X. Li, Q. Wu, Z. Liang, L. Zhang, and Y. Zhang, "Cleavable hydrophobic derivatization strategy for enrichment and identification of phosphorylated lysine peptides," *Analytical and Bioanalytical Chemistry*, vol. 411, no. 18, pp. 4159–4166, 2019.

[221] P. Voigt and D. Reinberg, "Histone tails: Ideal motifs for probing epigenetics through chemical biology approaches," *ChemBioChem*, vol. 12, no. 2, pp. 236–252, 2011.

[222] S. Sidoli, Z.-F. Yuan, S. Lin, K. Karch, X. Wang, N. Bhanu, A. M. Arnaudo, L.-M. Britton, X.-J. Cao, M. Gonzales-Cope, Y. Han, S. Liu, R. C. Molden, S. Wein, L. Afjehi-Sadat, and B. A. Garcia, "Drawbacks in the use of unconventional hydrophobic anhydrides for histone derivatization in bottom-up proteomics ptm analysis," *PROTEOMICS*, vol. 15, no. 9, pp. 1459–1469, 2015.

[223] J. Fíla and D. Honys, "Enrichment techniques employed in phosphoproteomics," *Amino acids*, vol. 43, no. 3, pp. 1025–1047, 2012. 22002794[pmid] PMC3418503[pmcid].

[224] L. Pieroni, F. Iavarone, A. Olianas, V. Greco, C. Desiderio, C. Martelli, B. Manconi, M. T. Sanna, I. Messana, M. Castagnola, and T. Cabras, "Enrichments of post-translational modifications in proteomic studies," *Journal of Separation Science*, vol. 43, no. 1, pp. 313–336, 2020.

[225] W. Qiu, C. Evans, A. Landels, T. K. Pham, and P. C. Wright, "Phosphopeptide enrichment for phosphoproteomic analysis - a tutorial and review of novel materials," *Analytica Chimica Acta*, 2020.

[226] X. Yue, A. Schunter, and A. B. Hummon, "Comparing multistep immobilized metal affinity chromatography and multistep tio2 methods for phosphopeptide enrichment," *Analytical Chemistry*, vol. 87, no. 17, pp. 8837–8844, 2015.

[227] G. Mamone, G. Picariello, P. Ferranti, and F. Addeo, "Hydroxyapatite affinity chromatography for the highly selective enrichment of mono- and multi-phosphorylated peptides in phosphoproteome analysis," *PROTEOMICS*, vol. 10, no. 3, pp. 380–393, 2010.

[228] J. H. Conway and D. Fiedler, "An affinity reagent for the recognition of pyrophosphorylated peptides," *Angewandte Chemie International Edition*, vol. 54, no. 13, pp. 3941–3945, 2015.

[229] E. Kinoshita, A. Yamada, H. Takeda, E. Kinoshita-Kikuta, and T. Koike, "Novel immobilized zinc(ii) affinity chromatography for phosphopeptides and phosphorylated proteins," *Journal of Separation Science*, vol. 28, no. 2, pp. 155–162, 2005.

[230] E. Greenfield, *Generating Monoclonal Antibodies*, pp. 201–221. Cold Spring Harbor Laboratory Press, 2nd ed., 2014.

[231] R. Kalagiri, K. Adam, and T. Hunter, *Empirical Evidence of Cellular Histidine Phosphorylation by Immunoblotting Using pHis mAbs BT - Histidine Phosphorylation: Methods and Protocols*, pp. 181–191. New York, NY: Springer US, 2020.

[232] J. Fuhrmann, B. Mierzwa, D. Trentini, S. Spiess, A. Lehner, E. Charpentier, and T. Clausen, "Structural basis for recognizing phosphoarginine and evolving residue-specific protein phosphatases in gram-positive bacteria," *Cell Reports*, vol. 3, no. 6, pp. 1832–1839, 2013.

[233] P. Roepstorff and J. Fohlman, "Proposal for a common nomenclature for sequence ions in mass spectra of peptides," *Biomedical Mass Spectrometry*, vol. 11, no. 11, pp. 601–601, 1984.

[234] C. M. Potel, S. Lemeer, and A. J. R. Heck, "Phosphopeptide fragmentation and site localization by mass spectrometry: An update," *Analytical Chemistry*, vol. 91, no. 1, pp. 126–141, 2019.

[235] M. Penkert, A. Hauser, R. Harmel, D. Fiedler, C. P. R. Hackenberger, and E. Krause, "Electron transfer/higher energy collisional dissociation of doubly charged peptide ions: Identification of labile protein phosphorylations," *Journal of the American Society for Mass Spectrometry*, vol. 30, no. 9, pp. 1578–1585, 2019.

[236] J. Bertran-Vicente, M. Schümann, C. P. R. Hackenberger, and E. Krause, "Gas-phase rearrangement in lysine phosphorylated peptides during electron-transfer dissociation tandem mass spectrometry," *Analytical Chemistry*, vol. 87, no. 14, pp. 6990–6994, 2015.

[237] M. Penkert, L. M. Yates, M. Schümann, D. Perlman, D. Fiedler, and E. Krause, "Unambiguous identification of serine and threonine pyrophosphorylation using neutral-loss-triggered electron-transfer/higher-energy collision dissociation," *Analytical Chemistry*, vol. 89, no. 6, pp. 3672–3680, 2017.

[238] C. M. Potel, M.-H. Lin, N. Prust, H. W. P. van den Toorn, A. J. R. Heck, and S. Lemeer, "Gaining confidence in the elusive histidine phosphoproteome," *Analytical Chemistry*, vol. 91, no. 9, pp. 5542–5547, 2019.

[239] M. Penkert, *Massenspektrometrische Charakterisierung von labilen Protein- und Peptidphosphorylierungen*. Thesis, Humboldt-Universität zu Berlin, 2019.

[240] M. P. Gamcsik, S. M. Ludeman, E. M. Shulman-Roskes, I. J. McLennan, M. E. Colvin, and O. M. Colvin, "Protonation of phosphoramide mustard and other phosphoramides," *Journal of Medicinal Chemistry*, vol. 36, no. 23, pp. 3636–3645, 1993.

[241] E. F. Mooney and P. H. Winson, *Nitrogen Magnetic Resonance Spectroscopy*, vol. 2, pp. 125–152. Academic Press, 1969.

[242] F. Seel and N. Klein, "Bildung von amidophosphaten und amidophosphorsäure aus n-methylcarbamoylphosphaten / formation of amidophosphates and amidophosphoric acid from n-methylcarbamoyl phosphates," 1983.

[243] H. Guo, R. Liu, J. Yang, B. Yang, X. Liang, and C. Chu, "A novel click lysine zwitterionic stationary phase for hydrophilic interaction liquid chromatography," *Journal of Chromatography A*, vol. 1223, pp. 47–52, 2012.

[244] E. D. Goddard-Borger and R. V. Stick, "An efficient, inexpensive, and shelf-stable diazo-transfer reagent imidazole-1-sulfonyl azide hydrochloride," *Organic Letters*, vol. 9, no. 19, pp. 3797–3800, 2007.

[245] A. K. Pandiakumar, S. P. Sarma, and A. G. Samuelson, "Mechanistic studies on the diazo transfer reaction," *Tetrahedron Letters*, vol. 55, no. 18, pp. 2917–2920, 2014.

[246] R. E. Wasylishen, "15n–13c spin–spin coupling constants in some aniline derivatives," *Canadian Journal of Chemistry*, vol. 54, no. 5, pp. 833–839, 1976.

[247] F. Kateb, P. Pelupessy, and G. Bodenhausen, "Measuring fast hydrogen exchange rates by nmr spectroscopy," *Journal of Magnetic Resonance*, vol. 184, no. 1, pp. 108–113, 2007.

[248] R. Nepravishta, B. Yu, and J. Iwahara, "Hydrogen-exchange kinetics studied through analysis of self-decoupling of nuclear magnetic resonance," *Journal of Magnetic Resonance*, vol. 312, p. 106687, 2020.

[249] H. Hiraishi, F. Yokoi, and A. Kumon, "Bovine liver phosphoamidase as a protein histidine/lysine phosphatase," *The Journal of Biochemistry*, vol. 126, no. 2, pp. 368–374, 1999.

[250] A. Gohla, "Do metabolic had phosphatases moonlight as protein phosphatases?," *Biochimica et Biophysica Acta (BBA) - Molecular Cell Research*, vol. 1866, no. 1, pp. 153–166, 2019.

[251] M.-A. Kasper, *Chemoselective synthesis of functional drug conjugates*. Thesis, Humboldt-Universität zu Berlin, 2020.

[252] H. Jakubowski, *Homocysteine-Thiolactone*, pp. 19–53. Vienna: Springer Vienna, 2013.

[253] S. Kato, A. Hori, M. Mitsuta, T. Katada, H. Ishihara, K. Fujieda, and Y. Ikebe, "On carbon-13 spectra of thio- and dithiocarboxylic acids triorgano group 14 metal esters," *Journal of Organometallic Chemistry*, vol. 420, no. 1, pp. 13–22, 1991.

[254] D. E. Petrillo, D. R. Mowrey, S. P. Allwein, and R. P. Bakale, "A general preparation of protected phosphoamino acids," *Organic Letters*, vol. 14, no. 5, pp. 1206–1209, 2012.

[255] W. Beck and G. Jung, "Convenient reduction of s-oxides in synthetic peptides, lipopeptides and peptide libraries," *Letters in Peptide Science*, vol. 1, no. 1, pp. 31–37, 1994.

[256] J. A. Gerlt, P. C. Demou, and S. Mehdi, "Oxygen-17 nmr spectral properties of simple phosphate esters and adenine nucleotides," *Journal of the American Chemical Society*, vol. 104, no. 10, pp. 2848–2856, 1982.

[257] H. J. Vogel and W. A. Bridger, "Phosphorus-31 nuclear magnetic resonance studies of the methylene and fluoro analogs of adenine nucleotides. effects of ph and magnesium ion binding," *Biochemistry*, vol. 21, no. 2, pp. 394–401, 1982.

[258] L. H. Schliselfeld, C. T. Burt, and R. J. Labotka, "Phosphorus-31 nuclear magnetic resonance of phosphonic acid analogs of adenosine nucleotides as functions of ph and magnesium ion concentration," *Biochemistry*, vol. 21, no. 2, pp. 317–320, 1982.

[259] M. R. Webb, "A continuous spectrophotometric assay for inorganic phosphate and for measuring phosphate release kinetics in biological systems," *Proceedings of the National Academy of Sciences*, vol. 89, no. 11, pp. 4884–4887, 1992.

[260] R. A. Friesner, J. L. Banks, R. B. Murphy, T. A. Halgren, J. J. Klicic, D. T. Mainz, M. P. Repasky, E. H. Knoll, M. Shelley, J. K. Perry, D. E. Shaw, P. Francis, and P. S. Shenkin, "Glide - a new approach for rapid, accurate docking and scoring. 1. method and assessment of docking accuracy," *Journal of Medicinal Chemistry*, vol. 47, no. 7, pp. 1739–1749, 2004.

[261] T. A. Halgren, R. B. Murphy, R. A. Friesner, H. S. Beard, L. L. Frye, W. T. Pollard, and J. L. Banks, "Glide - a new approach for rapid, accurate docking and scoring. 2. enrichment factors in database screening," *Journal of Medicinal Chemistry*, vol. 47, no. 7, pp. 1750–1759, 2004.

[262] R. A. Friesner, R. B. Murphy, M. P. Repasky, L. L. Frye, J. R. Greenwood, T. A. Halgren, P. C. Sanschagrin, and D. T. Mainz, "Extra precision glide - docking and scoring incorporating a model of hydrophobic enclosure for protein–ligand complexes," *Journal of Medicinal Chemistry*, vol. 49, no. 21, pp. 6177–6196, 2006.

[263] N. Homeyer, A. H. C. Horn, H. Lanig, and H. Sticht, "Amber force-field parameters for phosphorylated amino acids in different protonation states: phosphoserine, phosphothreonine, phosphotyrosine, and phosphohistidine," *Journal of Molecular Modeling*, vol. 12, no. 3, pp. 281–289, 2006.

[264] M. Aldeghi, V. Gapsys, and B. L. de Groot, "Accurate estimation of ligand binding affinity changes upon protein mutation," *ACS Central Science*, vol. 4, no. 12, pp. 1708–1718, 2018.

[265] M. Aldeghi, B. L. de Groot, and V. Gapsys, *Accurate Calculation of Free Energy Changes upon Amino Acid Mutation*, pp. 19–47. New York, NY: Springer New York, 2019.

[266] B. Hess, C. Kutzner, D. van der Spoel, and E. Lindahl, "Gromacs 4: algorithms for highly efficient, load-balanced, and scalable molecular simulation," *Journal of Chemical Theory and Computation*, vol. 4, no. 3, pp. 435–447, 2008.

[267] M. J. Abraham, T. Murtola, R. Schulz, S. Páll, J. C. Smith, B. Hess, and E. Lindahl, "Gromacs: high performance molecular simulations through multi-level parallelism from laptops to supercomputers," *SoftwareX*, vol. 1-2, pp. 19–25, 2015.

[268] D. Seeliger and B. L. de Groot, "Protein thermostability calculations using alchemical free energy simulations," *Biophysical journal*, vol. 98, no. 10, pp. 2309–2316, 2010.

[269] A. Kukol, *Molecular modeling of proteins*. New York; Heidelberg; Dordrecht: Humana Press, 2015.

[270] A. Furka, F. Sebestyén, M. Asgedom, and G. Dibó, "General method for rapid synthesis of multicomponent peptide mixtures," *International Journal of Peptide and Protein Research*, vol. 37, no. 6, pp. 487–493, 1991.

[271] M. Villain, J. Vizzavona, and K. Rose, "Covalent capture - a new tool for the purification of synthetic and recombinant polypeptides," *Chemistry & Biology*, vol. 8, no. 7, pp. 673–679, 2001.

[272] P. Giron, L. Dayon, N. Mihala, J.-C. Sanchez, and K. Rose, "Cysteine-reactive covalent capture tags for enrichment of cysteine-containing peptides," *Rapid Communications in Mass Spectrometry*, vol. 23, no. 21, pp. 3377–3386, 2009.

[273] F. Lopez-Tapia, C. Brotherton-Pleiss, P. Yue, H. Murakami, A. C. Costa Araujo, B. Reis dos Santos, E. Ichinotsubo, A. Rabkin, R. Shah, M. Lantz, S. Chen, M. A. Tius, and J. Turkson, "Linker variation and structure–activity relationship analyses of carboxylic acid-based small molecule stat3 inhibitors," *ACS Medicinal Chemistry Letters*, vol. 9, no. 3, pp. 250–255, 2018.

[274] S. W. Wright, D. L. Hageman, A. S. Wright, and L. D. McClure, "Convenient preparations of t-butyl esters and ethers from t-butanol," *Tetrahedron Letters*, vol. 38, no. 42, pp. 7345–7348, 1997.

[275] H. D. Jain, C. Zhang, S. Zhou, H. Zhou, J. Ma, X. Liu, X. Liao, A. M. Deveau, C. M. Dieckhaus, M. A. Johnson, K. S. Smith, T. L. Macdonald, H. Kakeya, H. Osada, and J. M. Cook, "Synthesis and structure–activity relationship studies on tryprostatin a, an inhibitor of breast cancer resistance protein," *Bioorganic & Medicinal Chemistry*, vol. 16, no. 8, pp. 4626–4651, 2008.

[276] S. Koch, D. Schollmeyer, H. Löwe, and H. Kunz, "C-glycosyl amino acids through hydroboration–cross-coupling of exo-glycals and their application in automated solid-phase synthesis," *Chemistry – A European Journal*, vol. 19, no. 22, pp. 7020–7041, 2013.

[277] E. Boz, N. S. Tüzün, and M. Stein, "Computational investigation of the control of the thermodynamics and microkinetics of the reductive amination reaction by solvent coordination and a co-catalyst," *RSC Adv.*, vol. 8, pp. 36662–36674, 2018.

[278] R. H. Burdon and p. H. van Knippenberg, eds., *Chapter 3 Peptide—carrier conjugation*, vol. 19, pp. 95–130. Elsevier, 1988.

[279] G. T. Hermanson, *Chapter 2 - Functional Targets for Bioconjugation*, pp. 127–228. Boston: Academic Press, 3rd ed., 2013.

[280] G. T. Hermanson, *Chapter 19 - Vaccines and Immunogen Conjugates*, pp. 839–865. Boston: Academic Press, 3rd ed., 2013.

[281] L. F. Tietze, M. Arlt, M. Beller, K.-H. Gl üsenkamp, E. Jähde, and M. F. Rajewsky, "Anticancer agents, 15. squaric acid diethyl ester: A new coupling reagent for the formation of drug biopolymer conjugates. synthesis of squaric acid ester amides and diamides," *Chemische Berichte*, vol. 124, no. 5, pp. 1215–1221, 1991.

[282] P. Kováč and P. Xu, *Controlled and highly efficient preparation of carbohydrate-based vaccines: squaric acid chemistry is the way to go*, vol. 42, pp. 83–115. The Royal Society of Chemistry, 2017.

[283] D. Straßburger, M. Glaffig, N. Stergiou, S. Bialas, P. Besenius, E. Schmitt, and H. Kunz, "Synthetic muc1 antitumor vaccine with incorporated 2,3-sialyl-t carbohydrate antigen inducing strong immune responses with isotype specificity," *ChemBioChem*, vol. 19, no. 11, pp. 1142–1146, 2018.

[284] D. Straßburger, N. Stergiou, M. Urschbach, H. Yurugi, D. Spitzer, D. Schollmeyer, E. Schmitt, and P. Besenius, "Mannose-decorated multicomponent supramolecular polymers trigger effective uptake into antigen-presenting cells," *ChemBioChem*, vol. 19, no. 9, pp. 912–916, 2018.

[285] D. Shechter, H. L. Dormann, C. D. Allis, and S. B. Hake, "Extraction, purification and analysis of histones," *Nat. Protocols*, vol. 2, no. 6, pp. 1445–1457, 2007. 10.1038/nprot.2007.202.

[286] K. H. Valkonen and R. Piha, "Isoelectric focusing and isoelectric points of bovine liver histones," *Analytical Biochemistry*, vol. 104, no. 2, pp. 499–505, 1980.

[287] G. Wu, A. G. McArthur, A. Fiser, A. Šali‡, M. L. Sogin, and M. M, "Core histones of the amitochondriate protist, giardia lamblia," *Molecular Biology and Evolution*, vol. 17, no. 8, pp. 1156–1163, 2000.

[288] B. A. Garcia, S. A. Busby, C. M. Barber, J. Shabanowitz, C. D. Allis, and D. F. Hunt, "Characterization of phosphorylation sites on histone h1 isoforms by tandem mass spectrometry," *Journal of Proteome Research*, vol. 3, no. 6, pp. 1219–1227, 2004.

[289] T. Y. Wang, "The isolation, properties, and possible functions of chromatin acidic proteins," *The Journal of Biological Chemistry*, vol. 242, no. 6, pp. 1220–1226, 1967.

[290] D. R. Lide, *CRC handbook of chemistry and physics*, pp. 7.1–7.2. Boca Raton: CRC Press, 1991.

[291] T. Yang, X.-M. Li, X. Bao, Y. M. E. Fung, and X. D. Li, "Photo-lysine captures proteins that bind lysine post-translational modifications," *Nature Chemical Biology*, vol. 12, no. 2, pp. 70–72, 2016.

[292] K. Panigrahi, M. Eggen, J.-H. Maeng, Q. Shen, and D. B. Berkowitz, "The α,α-difluorinated phosphonate l-pser-analogue: An accessible chemical tool for studying kinase- dependent signal transduction," *Chemistry & Biology*, vol. 16, no. 9, pp. 928–936, 2009.

[293] K. J. Dykema, T. N. Truong, and M. S. Gordon, "Studies of silicon-phosphorus bonding," *Journal of the American Chemical Society*, vol. 107, no. 15, pp. 4535–4541, 1985.

[294] D. L. Haire, E. G. Janzen, V. J. Robinson, and I. Hrvoic, "Electron spin resonance study of phosphorus-nitroxides from 1,3-additions of silicon-phosphorus reagents to nitrones," *Magnetic Resonance in Chemistry*, vol. 42, no. 10, pp. 835–843, 2004.

[295] M. Findeisen, T. Brand, and S. Berger, "A 1h-nmr thermometer suitable for cryoprobes," *Magnetic Resonance in Chemistry*, vol. 45, no. 2, pp. 175–178, 2007.

[296] A. Bax and M. F. Summers, "Proton and carbon-13 assignments from sensitivity-enhanced detection of heteronuclear multiple-bond connectivity by 2d multiple quantum nmr," *Journal of the American Chemical Society*, vol. 108, no. 8, pp. 2093–2094, 1986.

[297] D. O. Cicero, G. Barbato, and R. Bazzo, "Sensitivity enhancement of a two-dimensional experiment for the measurement of heteronuclear long-range coupling constants, by a new scheme of coherence selection by gradients," *Journal of Magnetic Resonance*, vol. 148, no. 1, pp. 209–213, 2001.

[298] M. Piotto, V. Saudek, and V. Sklenář, "Gradient-tailored excitation for single-quantum nmr spectroscopy of aqueous solutions," *Journal of Biomolecular NMR*, vol. 2, no. 6, pp. 661–665, 1992.

[299] B. Yan and W. Li, "Rapid fluorescence determination of the absolute amount of aldehyde and ketone groups on resin supports," *The Journal of Organic Chemistry*, vol. 62, no. 26, pp. 9354–9357, 1997.

[300] W. S. Hancock and J. E. Battersby, "A new micro-test for the detection of incomplete coupling reactions in solid-phase peptide synthesis using 2,4,6-trinitrobenzene-sulphonic acid," *Analytical Biochemistry*, vol. 71, no. 1, pp. 260–264, 1976.

[301] J. H. Kaplan, B. Forbush, and J. F. Hoffman, "Rapid photolytic release of adenosine 5'-triphosphate from a protected analog: utilization by the sodium:potassium pump of human red blood cell ghosts," *Biochemistry*, vol. 17, no. 10, pp. 1929–1935, 1978.

[302] E. D. Goddard-Borger and R. V. Stick, "An efficient, inexpensive, and shelf-stable diazotransfer reagent imidazole-1-sulfonyl azide hydrochloride," *Organic Letters*, vol. 13, no. 9, pp. 2514–2514, 2011.

[303] R. H. Herpel, P. Vedantham, D. L. Flynn, and P. R. Hanson, "High-load, oligomeric phosphonyl dichloride: facile generation via rom polymerization and application to scavenging amines," *Tetrahedron Letters*, vol. 47, no. 36, pp. 6429–6432, 2006.

[304] A. D. Becke, "Density-functional thermochemistry. iii. the role of exact exchange," *The Journal of Chemical Physics*, vol. 98, no. 7, pp. 5648–5652, 1993.

[305] C. Lee, W. Yang, and R. G. Parr, "Development of the colle-salvetti correlation-energy formula into a functional of the electron density," *Physical Review B*, vol. 37, no. 2, pp. 785–789, 1988. PRB.

[306] S. H. Vosko, L. Wilk, and M. Nusair, "Accurate spin-dependent electron liquid correlation energies for local spin density calculations: a critical analysis," *Canadian Journal of Physics*, vol. 58, no. 8, pp. 1200–1211, 1980.

[307] F. Weigend, "Accurate coulomb-fitting basis sets for h to rn," *Physical Chemistry Chemical Physics*, vol. 8, no. 9, pp. 1057–1065, 2006.

[308] F. Weigend and R. Ahlrichs, "Balanced basis sets of split valence, triple zeta valence and quadruple zeta valence quality for h to rn: Design and assessment of accuracy," *Physical Chemistry Chemical Physics*, vol. 7, no. 18, pp. 3297–3305, 2005.

[309] TURBOMOLE, "Turbomole v7.0," *V7.0; a development of the University of Karlsruhe and Forschungszentrum Karlsruhe GmbH, 1989-2007, Turbomole GmbH since 2007; available from http://www.turbomole.com*, 2015.

[310] O. Treutler and R. Ahlrichs, "Efficient molecular numerical integration schemes," *The Journal of Chemical Physics*, vol. 102, no. 1, pp. 346–354, 1995.

[311] K. Eichkorn, F. Weigend, O. Treutler, and R. Ahlrichs, "Auxiliary basis sets for main row atoms and transition metals and their use to approximate coulomb potentials," *Theoretical Chemistry Accounts*, vol. 97, no. 1-4, pp. 119–124, 1997.

[312] G. Schaftenaar, E. Vlieg, and G. Vriend, "Molden 2.0: quantum chemistry meets proteins," *Journal of Computer-Aided Molecular Design*, vol. 31, no. 9, pp. 789–800, 2017.

[313] G. Schaftenaar and J. H. Noordik, "Molden: a pre- and post-processing program for molecular and electronic structures*," *Journal of Computer-Aided Molecular Design*, vol. 14, no. 2, pp. 123–134, 2000.

[314] L. Schrodinger, "The pymol molecular graphics system, version 1.8," *The PyMOL Molecular Graphics System, Version 1.8*, 2015.

[315] G. E. Crooks, "Entropy production fluctuation theorem and the nonequilibrium work relation for free energy differences," *Physical Review E*, vol. 60, no. 3, pp. 2721–2726, 1999.

[316] V. Gapsys, S. Michielssens, D. Seeliger, and B. L. de Groot, "pmx: Automated protein structure and topology generation for alchemical perturbations," *Journal of Computational Chemistry*, vol. 36, no. 5, pp. 348–354, 2015.

[317] G. Köhler and C. Milstein, "Continuous cultures of fused cells secreting antibody of predefined specificity," *Nature*, vol. 256, no. 5517, pp. 495–497, 1975.

Appendices

Chromatograms of Synthesized Peptides

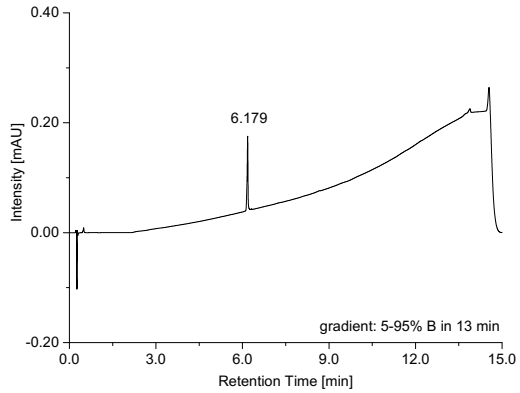

(A) ^{Ac}Tyr-Lys(NPO(OTc)$_2$)-Gly^{CONH_2} **4**

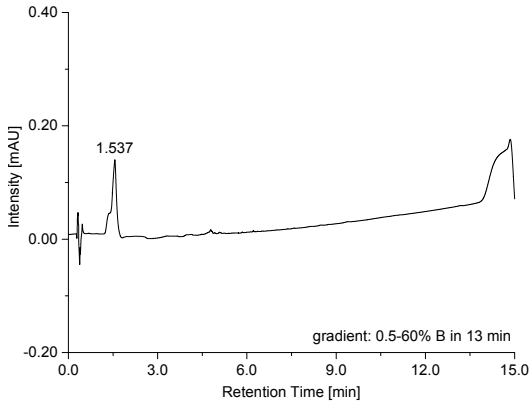

(B) ^{Ac}Tyr-pLys-Gly^{CONH_2} **5**

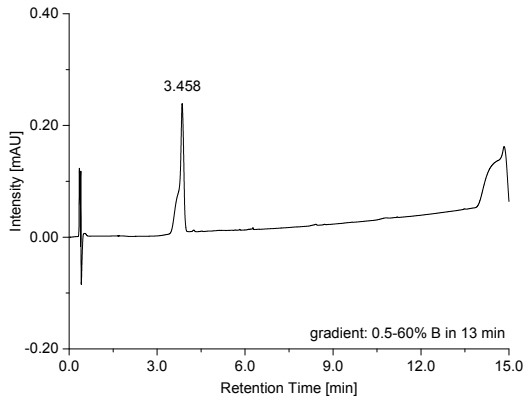

(C) ^{Ac}Tyr-Lys^{N_3}-Gly^{CONH_2} **6**

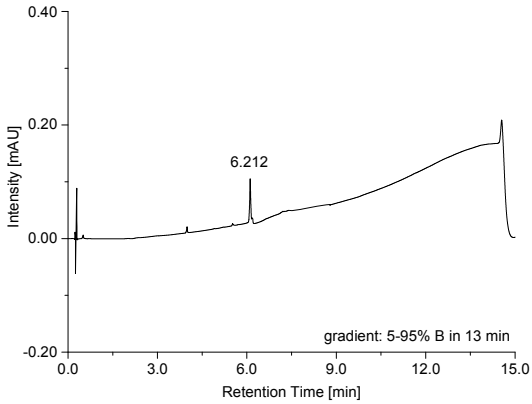

(D) ^{Ac}Tyr-Lys(NPO(ONPE)$_2$)-Gly^{CONH_2} **7**

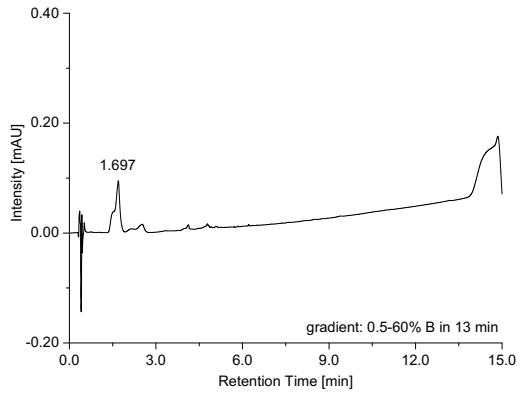

(E) ^{Ac}Tyr-pLys-$^{15}N_2$-Gly^{CONH_2} **10**

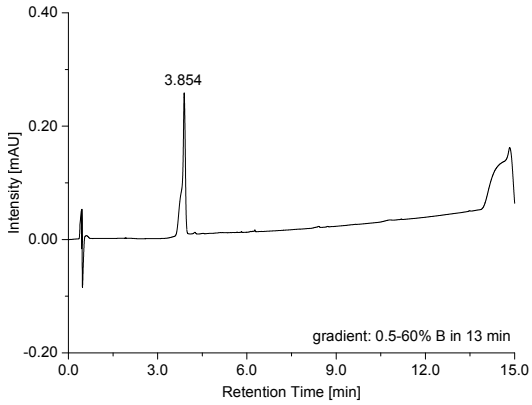

(F) ^{Ac}Tyr-Lys^{N_3}-$^{15}N_2$-Gly^{CONH_2} **14**

Figure A1: UPLC-traces (220 nm) of **4**, **5**, **6**, **7**, **10** and **14**.

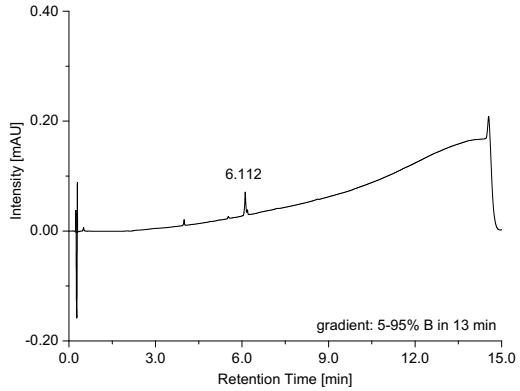

(A) ^{Ac}Tyr(NPO(ONPE)$_2$)-$^{15}N_2$-Gly^{CONH_2} **15**

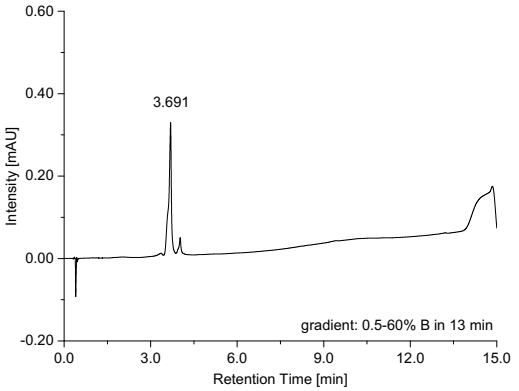

(B) ^{Ac}Tyr-hCys(EtPO(OH)$_2$)-Gly^{CONH_2} **23**

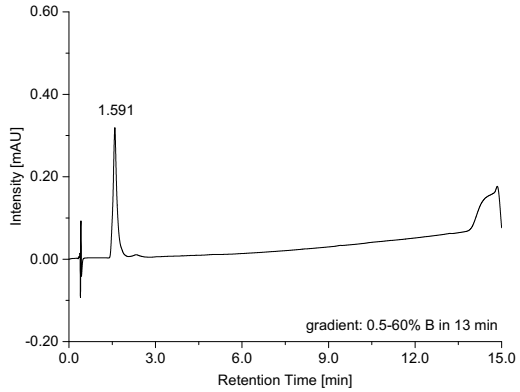

(C) ^{Ac}Tyr-Nle(OPO(OH)$_2$)-Gly^{CONH_2} **24**

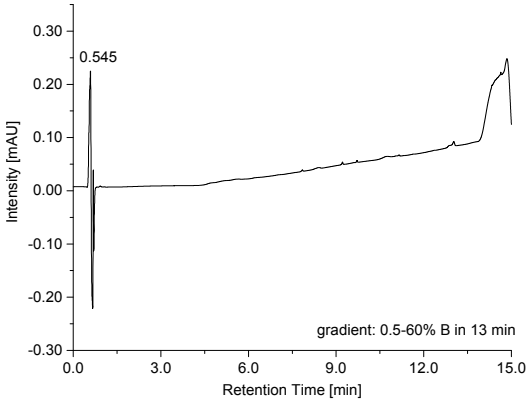

(D) pLys **25a**

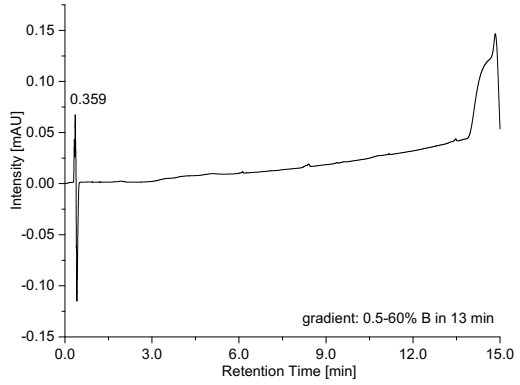

(E) pSer **25b**

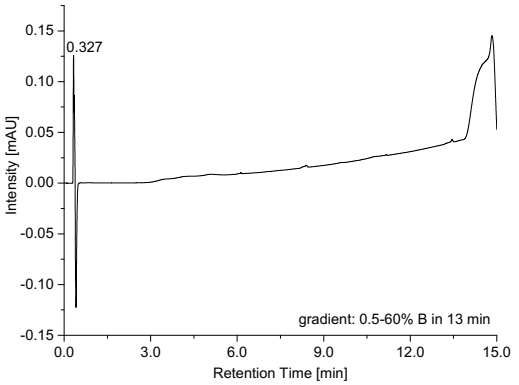

(F) pThr **25c**

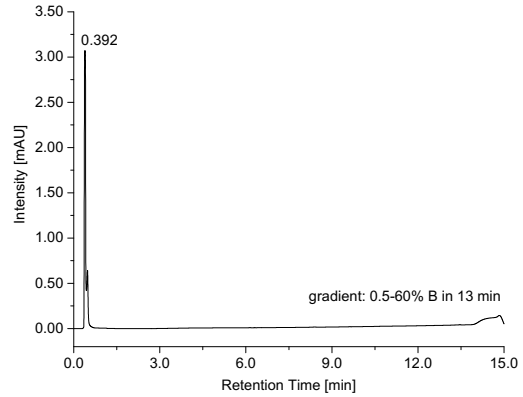

(G) pTyr **25d**

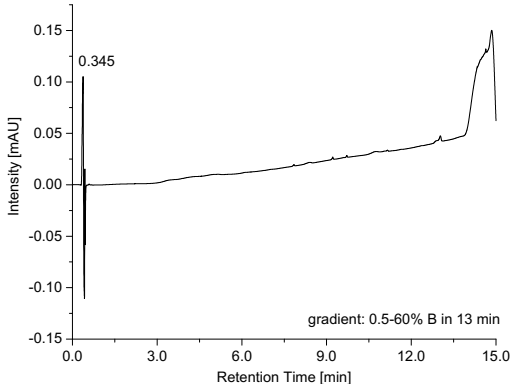

(H) pArg **25e**

Figure A2: UPLC-traces (220 nm) of **15**, **23**, **24**, **25a**, **25b**, **25c**, **25d** and **25e**.

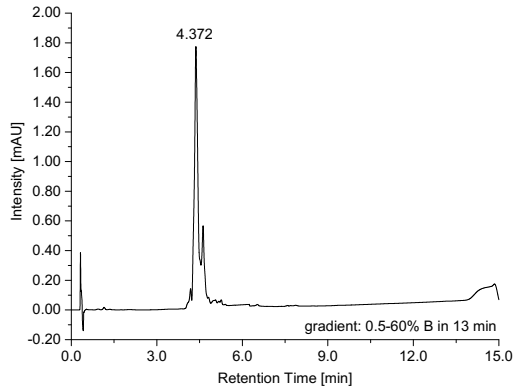

(A) ^{H_2N}APAPAEpKTPVKKKA^{CONH_2} **26a**

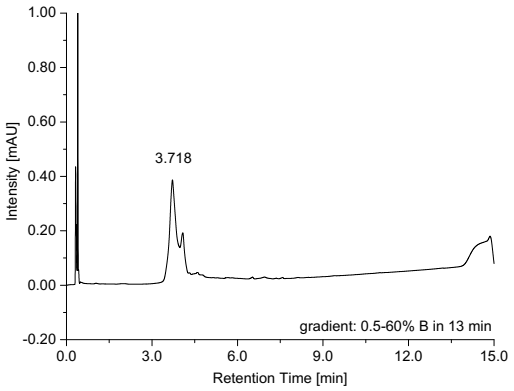

(B) ^{H_2N}KKKARpKSAGAAKRKASG^{CONH_2} **26b**

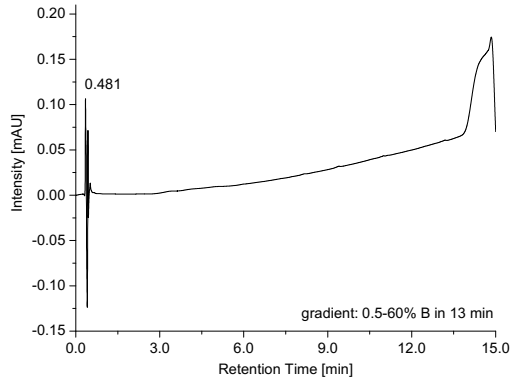

(C) ^{Ac}GGpKGG^{CONH_2} **27a**

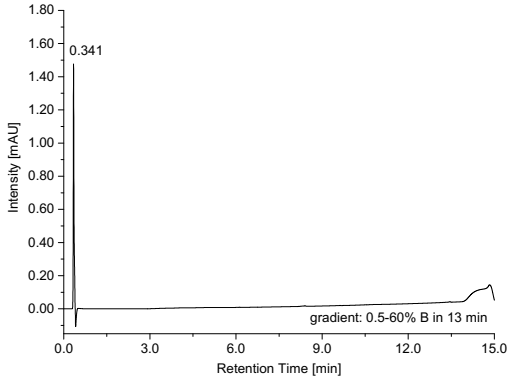

(D) ^{Ac}GGpSGG^{CONH_2} **27b**

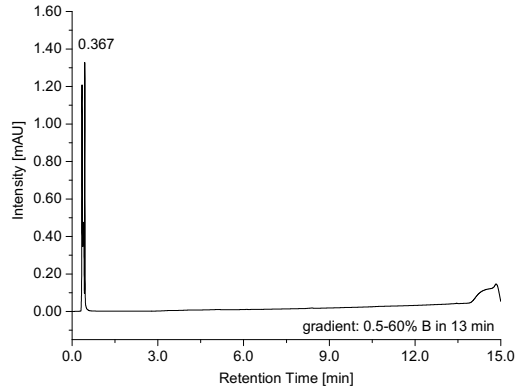

(E) ^{Ac}GGpTGG^{CONH_2} **27c**

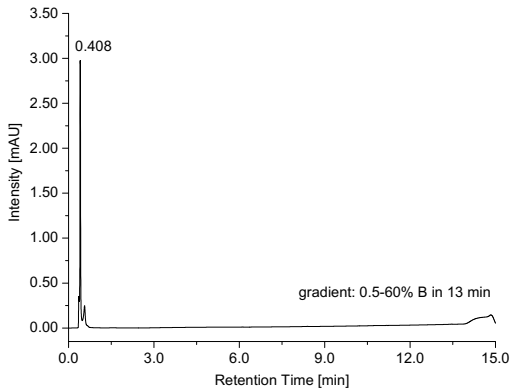

(F) ^{Ac}GGpYGG^{CONH_2} **27d**

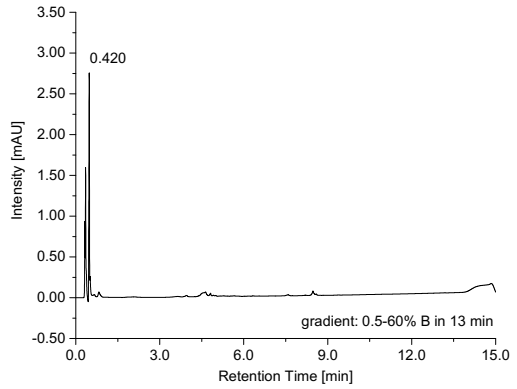

(G) ^{Ac}GGpRGG^{CONH_2} **27e**

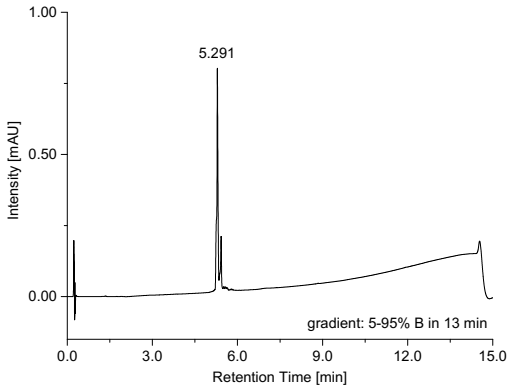

(H) ^{Ac}GGcpRGG^{CONH_2} **27e***

Figure A3: UPLC-traces (220 nm) of **26a**, **26b**, **27a**, **27b**, **27c**, **27d**, **27e** and **27e***.

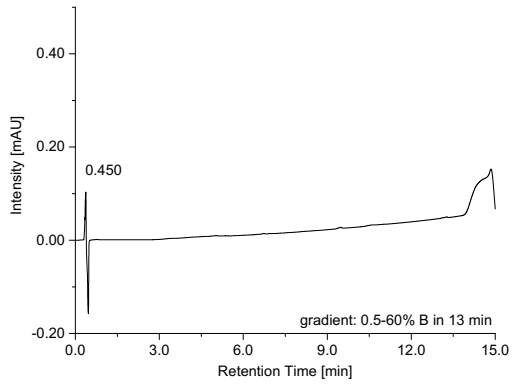

(A) ^{Ac}GApKGG^{CONH_2} **28a**

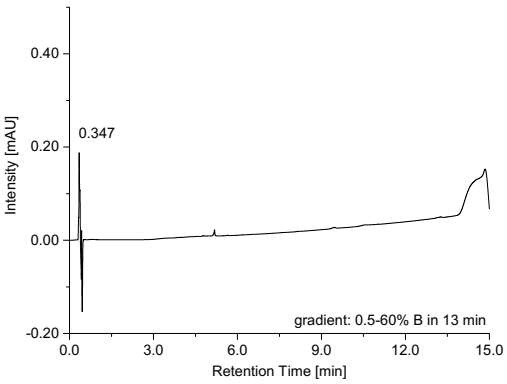

(B) ^{Ac}GCpKGG^{CONH_2} **28b**

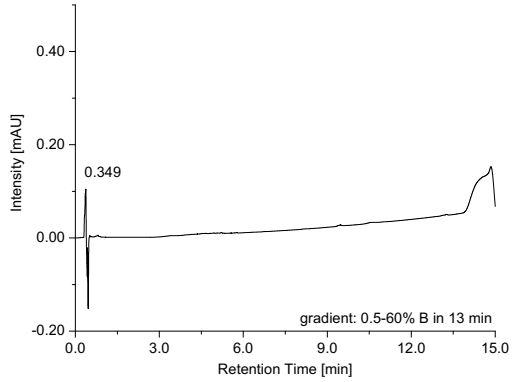

(C) ^{Ac}GDpKGG^{CONH_2} **28c**

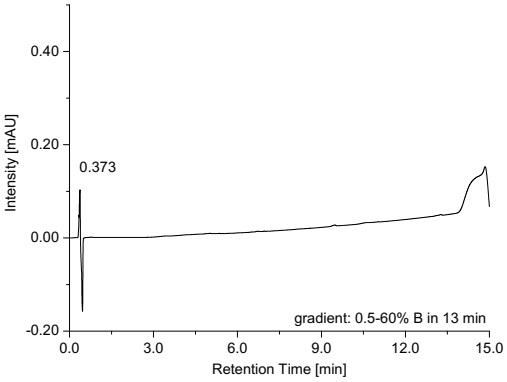

(D) ^{Ac}GFpKGG^{CONH_2} **28d**

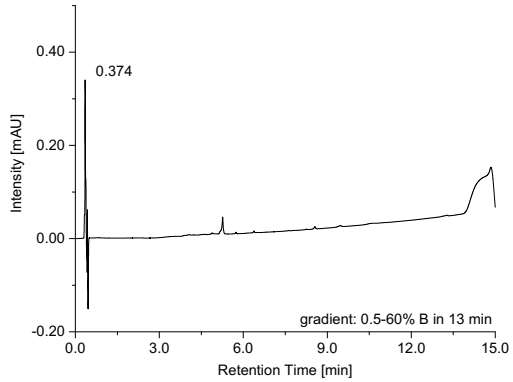

(E) ^{Ac}GIpKGG^{CONH_2} **28e**

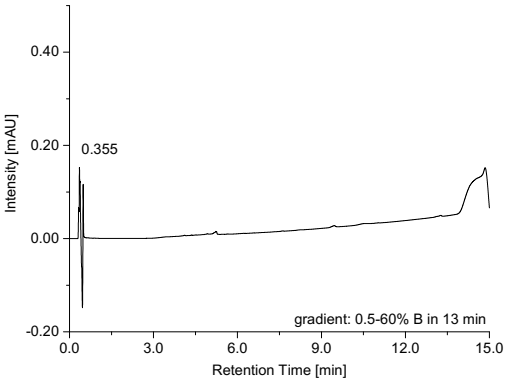

(F) ^{Ac}GKpKGG^{CONH_2} **28f**

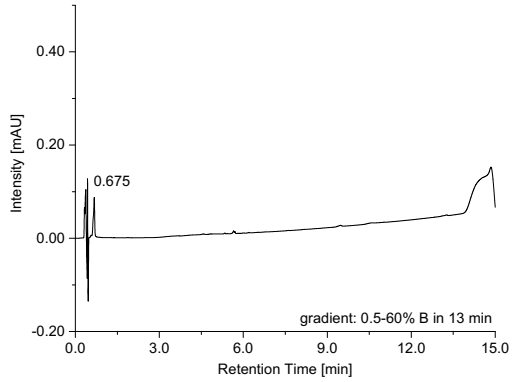

(G) ^{Ac}GPpKGG^{CONH_2} **28g**

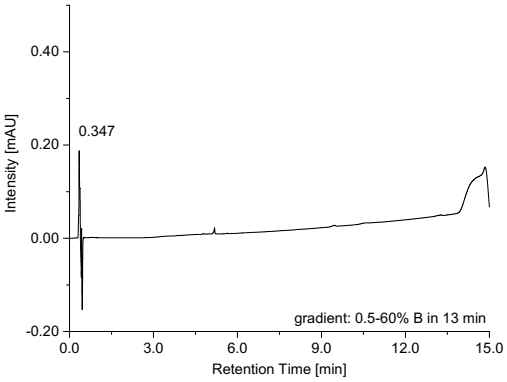

(H) ^{Ac}GQpKGG^{CONH_2} **28h**

Figure A4: UPLC-traces (220 nm) of **28a**, **28b**, **28c**, **28d**, **28e**, **28f**, **28g** and **28h**.

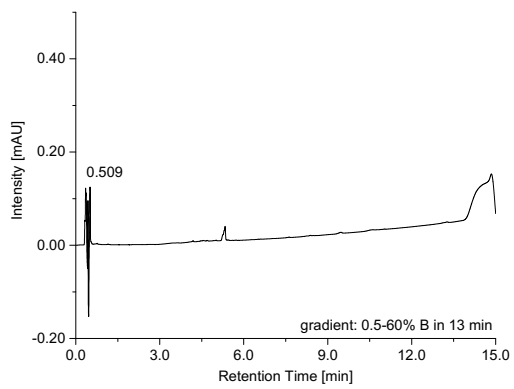

(A) ^{Ac}GRpKGG^{CONH_2} **28i**

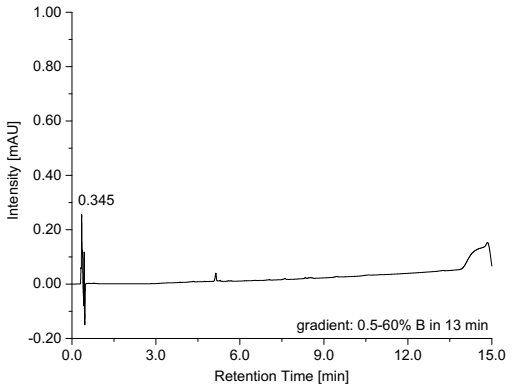

(B) ^{Ac}GSpKGG^{CONH_2} **28j**

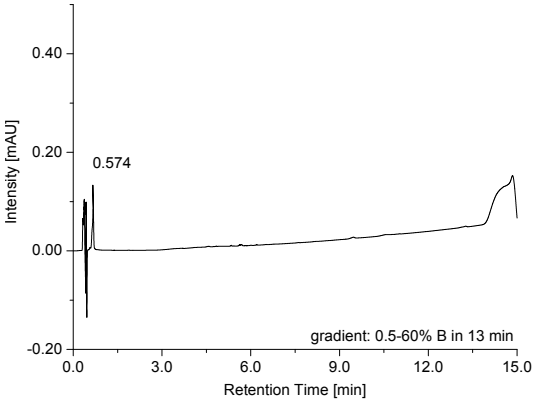

(C) ^{Ac}GGpKAG^{CONH_2} **29a**

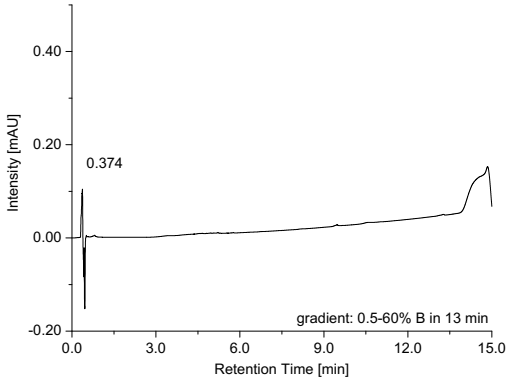

(D) ^{Ac}GGpKCG^{CONH_2} **29b**

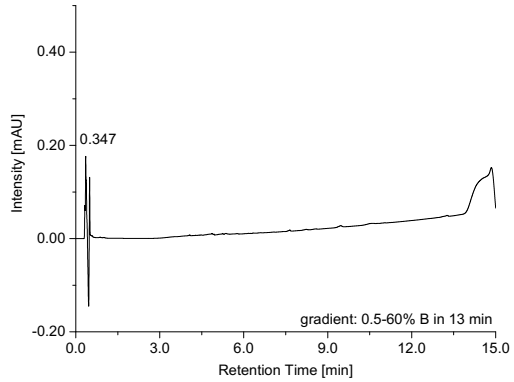

(E) ^{Ac}GGpKDG^{CONH_2} **29c**

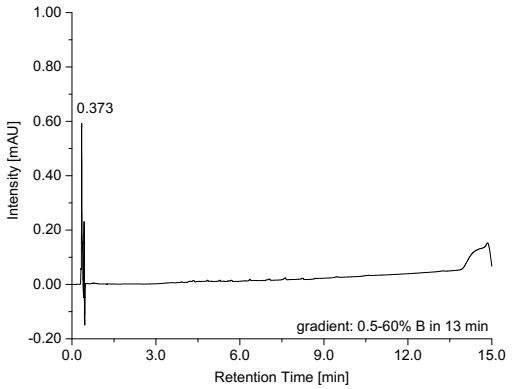

(F) ^{Ac}GGpKFG^{CONH_2} **29d**

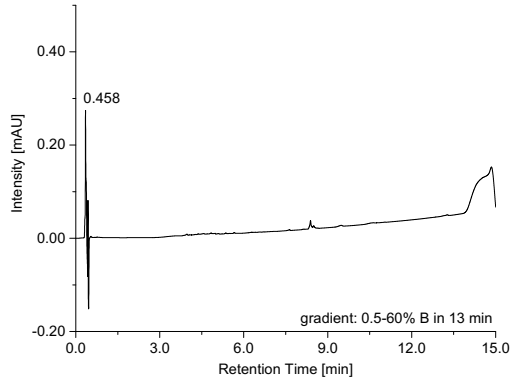

(G) ^{Ac}GGpKIG^{CONH_2} **29e**

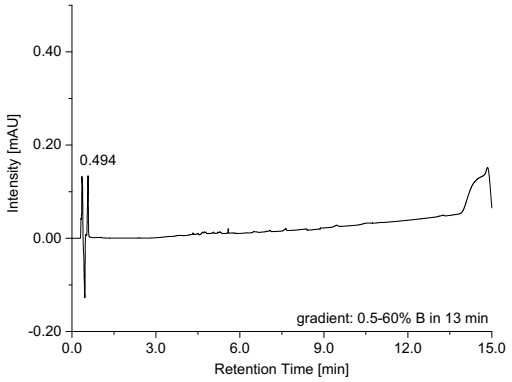

(H) ^{Ac}GGpKKG^{CONH_2} **29f**

Figure A5: UPLC-traces (220 nm) of **28i**, **28j**, **29a**, **29b**, **29c**, **29d**, **29e** and **29f**.

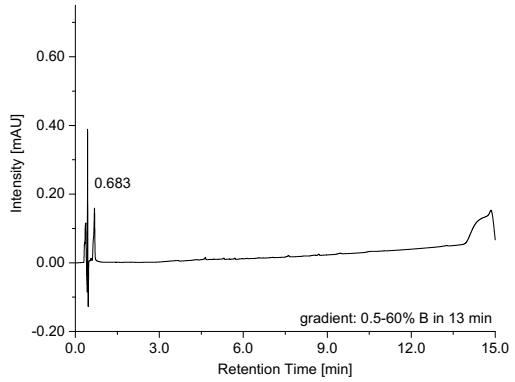

(A) ^{Ac}GGpKPG^{CONH_2} **29g**

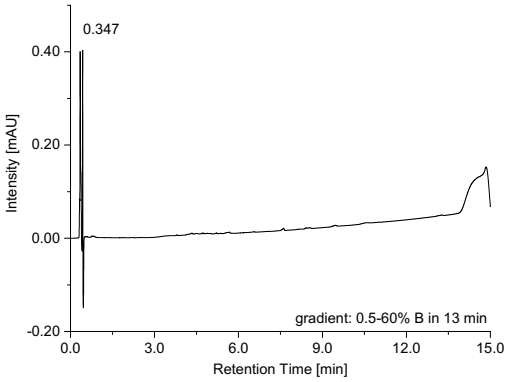

(B) ^{Ac}GGpKQG^{CONH_2} **29h**

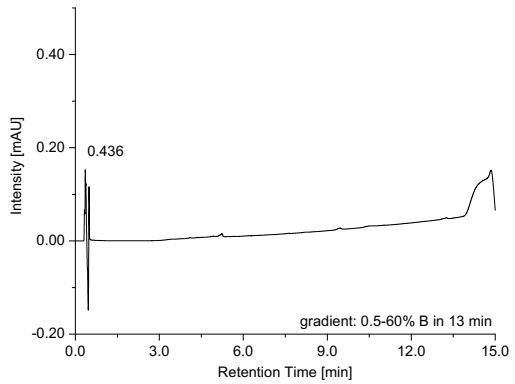

(C) ^{Ac}GGpKRG^{CONH_2} **29i**

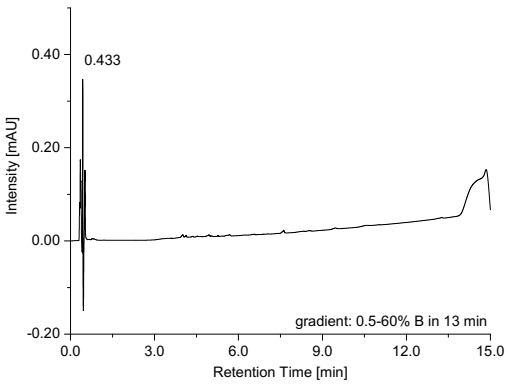

(D) ^{Ac}GGpKSG^{CONH_2} **29j**

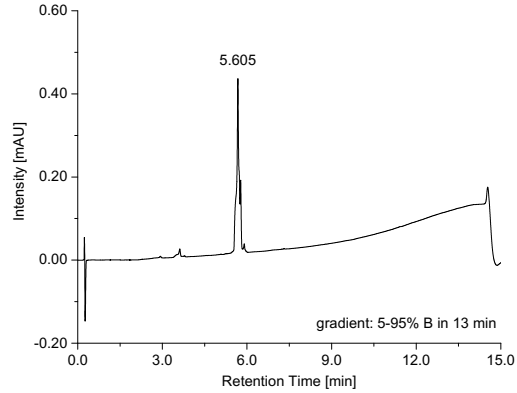

(E) NH_2-Lys(NPO(ONPE)$_2$)-OH **30**

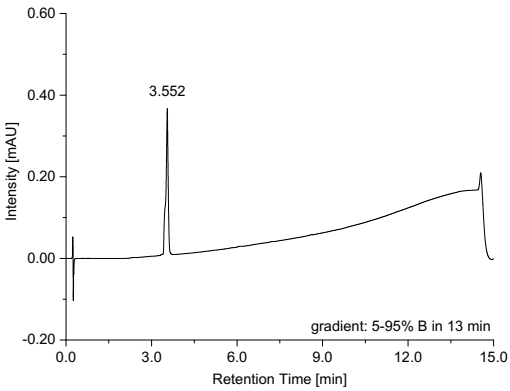

(F) ^{H_2N}APAPAEK^{N_3}TPVKKKA^{CONH_2} **31a**

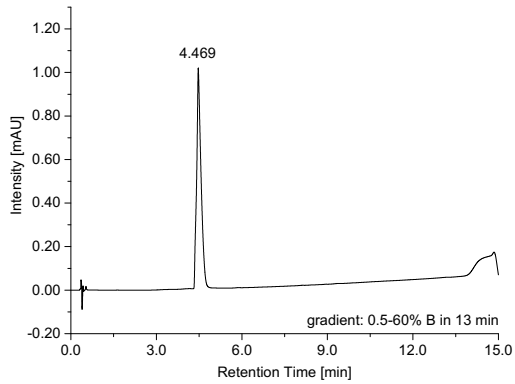

(G) ^{H_2N}KKKARK^{N_3}SAGAAKRKASG^{CONH_2} **31b**

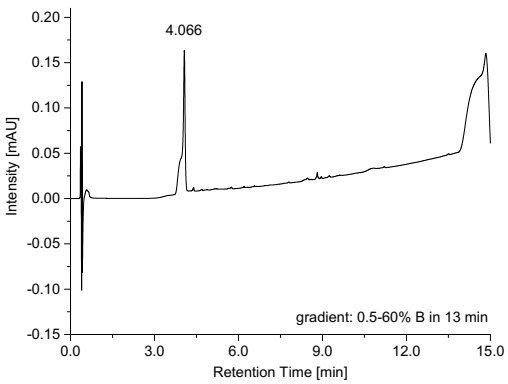

(H) ^{Ac}GGK^{N_3}GG^{CONH_2} **31c**

Figure A6: UPLC-traces (220 nm) of **29g**, **29h**, **29i**, **29j**, **30**, **31a**, **31b** and **31c**.

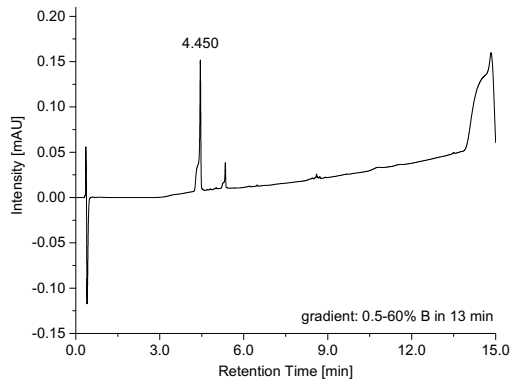

(A) ^{Ac}GAK^{N_3}GG^{CONH_2} **31d**

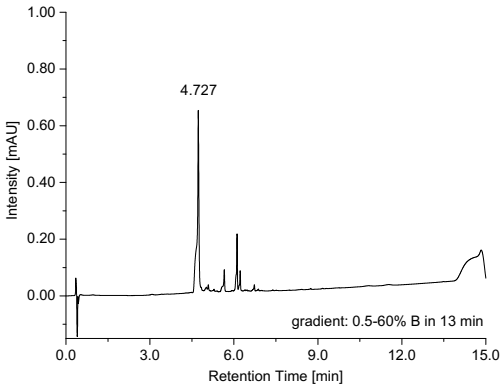

(B) ^{Ac}GCK^{N_3}GG^{CONH_2} **31e**

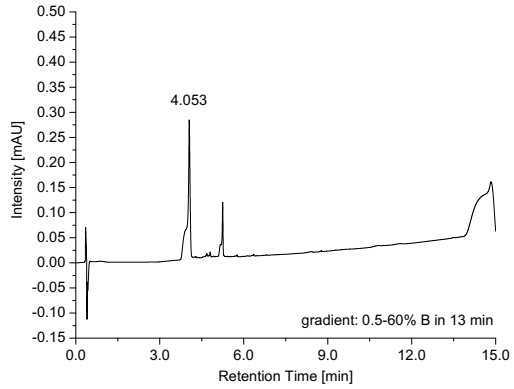

(C) ^{Ac}GDK^{N_3}GG^{CONH_2} **31f**

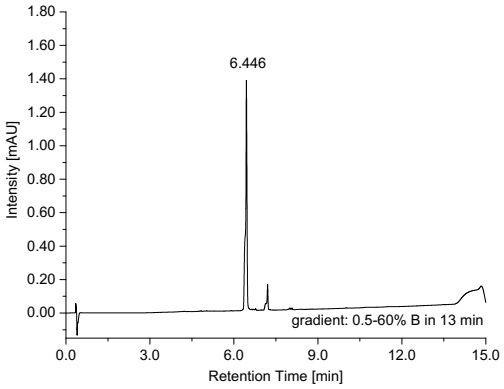

(D) ^{Ac}GFK^{N_3}GG^{CONH_2} **31g**

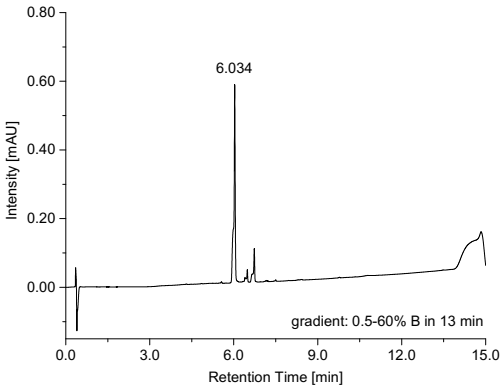

(E) ^{Ac}GIK^{N_3}GG^{CONH_2} **31h**

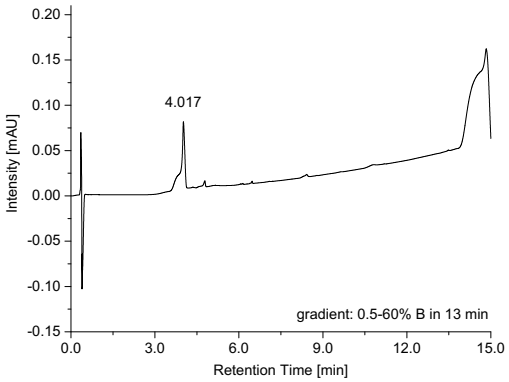

(F) ^{Ac}GKK^{N_3}GG^{CONH_2} **31i**

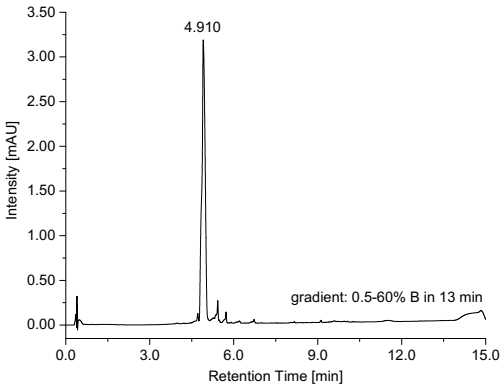

(G) ^{Ac}GPK^{N_3}GG^{CONH_2} **31j**

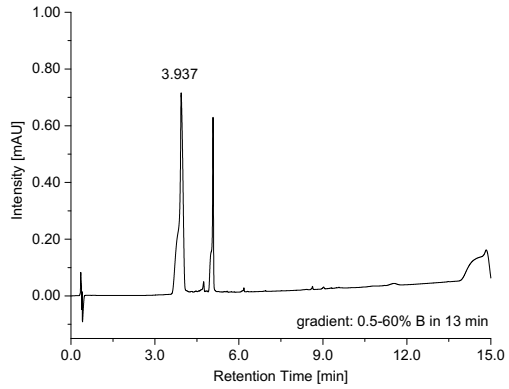

(H) ^{Ac}GQK^{N_3}GG^{CONH_2} **31k**

Figure A7: UPLC-traces (220 nm) of **31d**, **31e**, **31f**, **31g**, **31h**, **31i**, **31j** and **31k**.

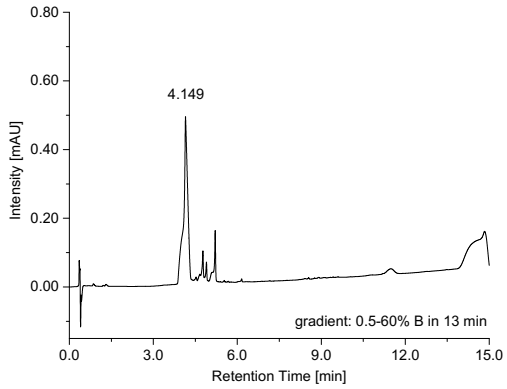

(A) ^{Ac}GRK^{N_3}GG^{CONH_2} **31l**

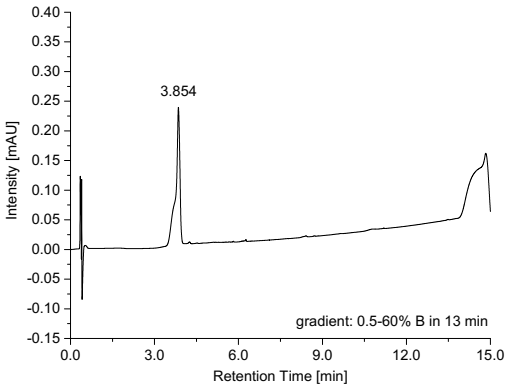

(B) ^{Ac}GSK^{N_3}GG^{CONH_2} **31m**

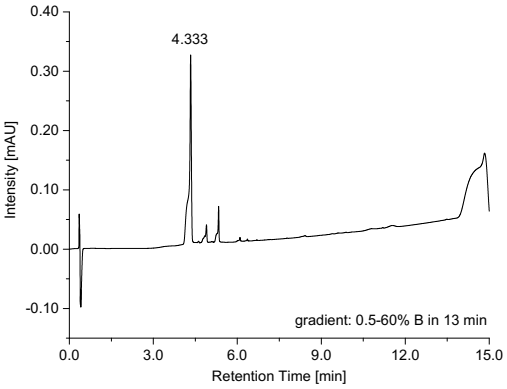

(C) ^{Ac}GGK^{N_3}AG^{CONH_2} **31n**

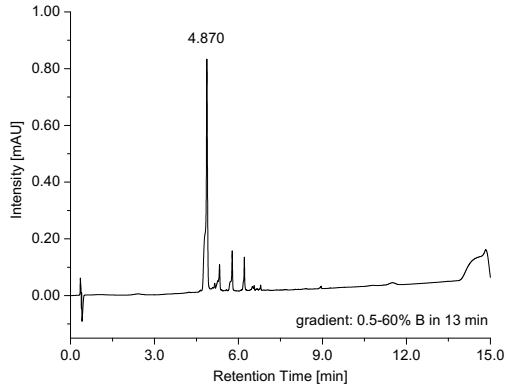

(D) ^{Ac}GGK^{N_3}CG^{CONH_2} **31o**

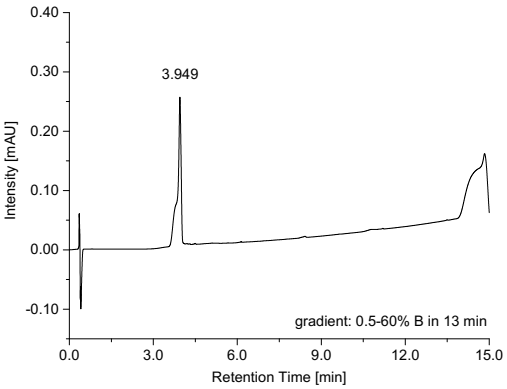

(E) ^{Ac}GGK^{N_3}DG^{CONH_2} **31p**

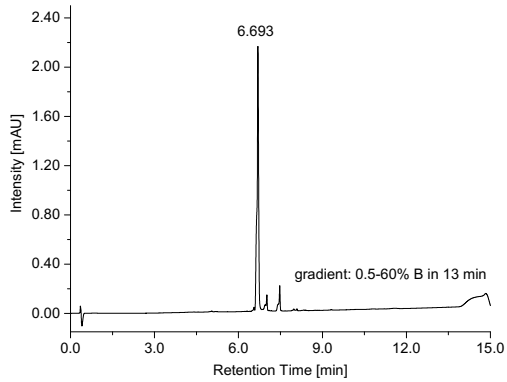

(F) ^{Ac}GGK^{N_3}FG^{CONH_2} **31q**

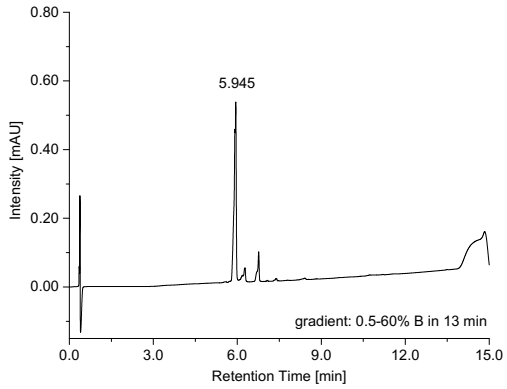

(G) ^{Ac}GGK^{N_3}IG^{CONH_2} **31r**

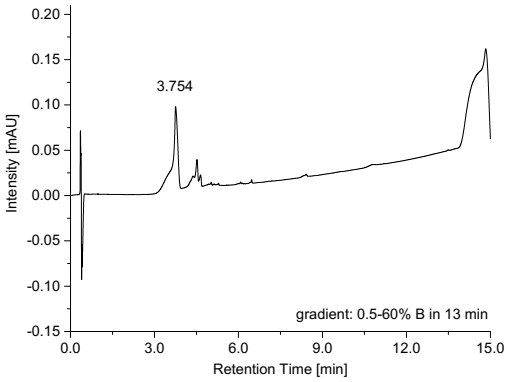

(H) ^{Ac}GGK^{N_3}KG^{CONH_2} **31s**

Figure A8: UPLC-traces (220 nm) of **31l**, **31m**, **31n**, **31o**, **31p**, **31q**, **31r** and **31s**.

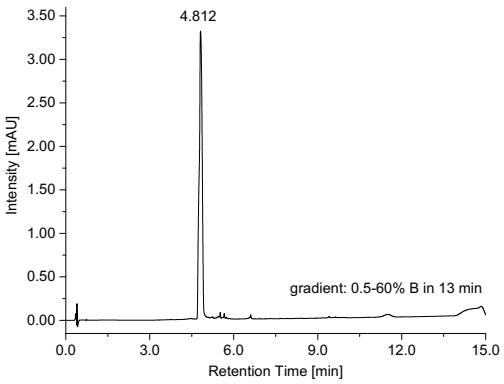

(A) ^{Ac}GGK^{N_3}PG^{CONH_2} **31t**

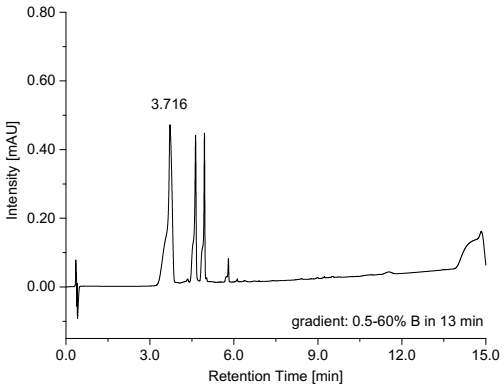

(B) ^{Ac}GGK^{N_3}QG^{CONH_2} **31u**

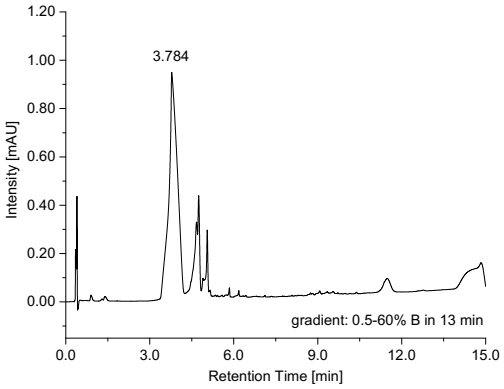

(C) ^{Ac}GGK^{N_3}RG^{CONH_2} **31v**

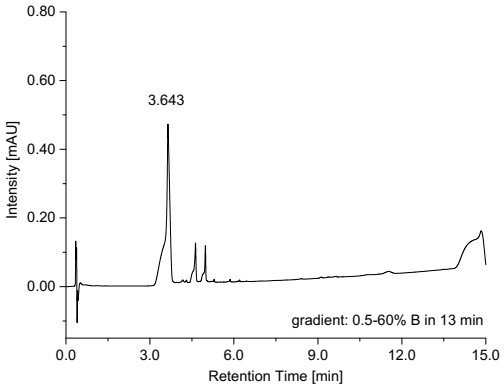

(D) ^{Ac}GGK^{N_3}SG^{CONH_2} **31w**

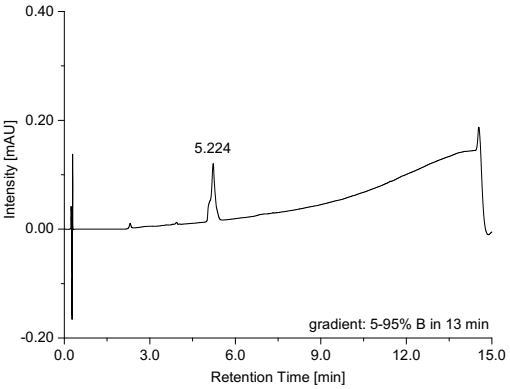

(E) ^{H_2N}APAPAEcpKTPVKKKA^{CONH_2} **32a**

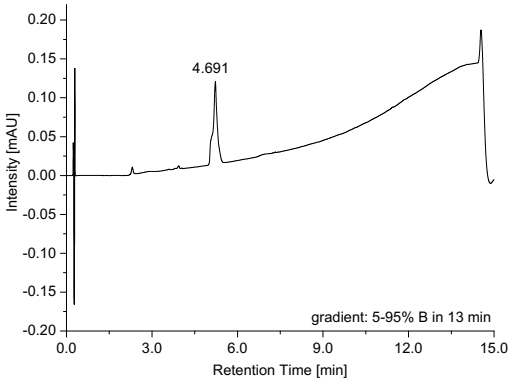

(F) ^{H_2N}KKKARcpKSAGAAKRKASG^{CONH_2} **32b**

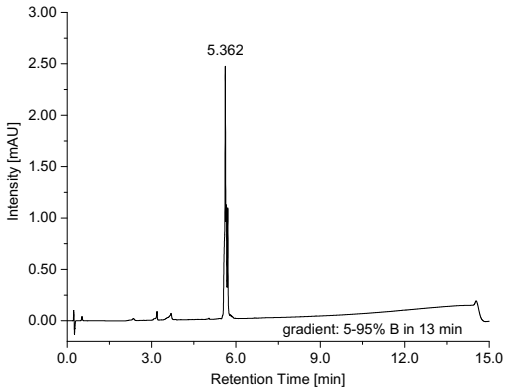

(G) ^{Ac}GGcpKGG^{CONH_2} **32c**

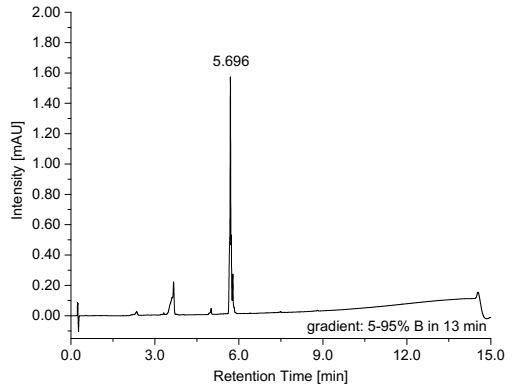

(H) ^{Ac}GAcpKGG^{CONH_2} **32d**

Figure A9: UPLC-traces (220 nm) of **31t**, **31u**, **31v**, **31w**, **32a**, **32b**, **32c** and **32d**.

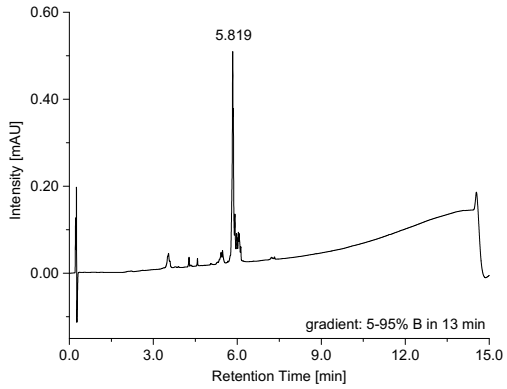

(A) ^{Ac}GCcpKGG^{CONH_2} **32e**

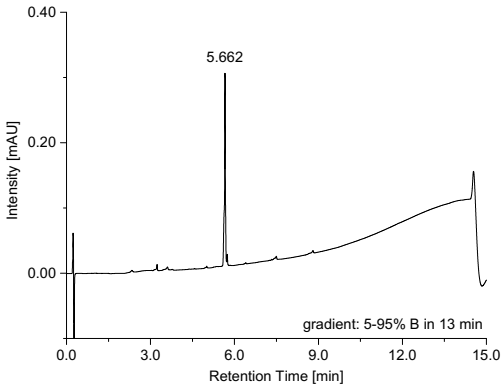

(B) ^{Ac}GDcpKGG^{CONH_2} **32f**

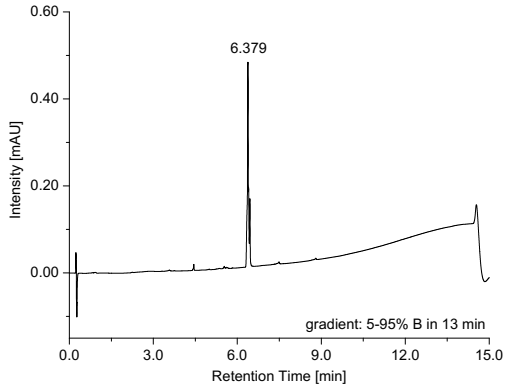

(C) ^{Ac}GFcpKGG^{CONH_2} **32g**

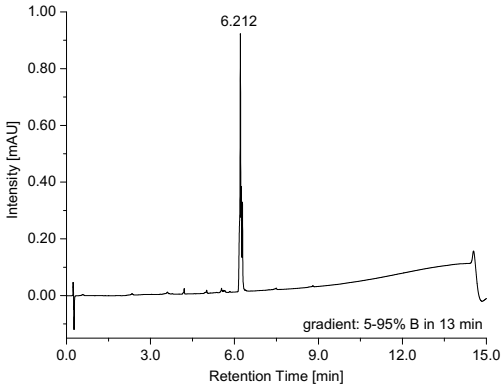

(D) ^{Ac}GIcpKGG^{CONH_2} **32h**

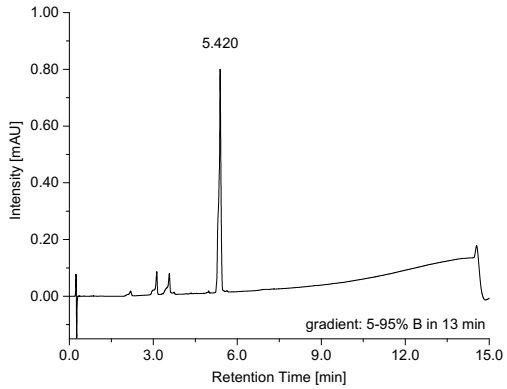

(E) ^{Ac}GKcpKGG^{CONH_2} **32i**

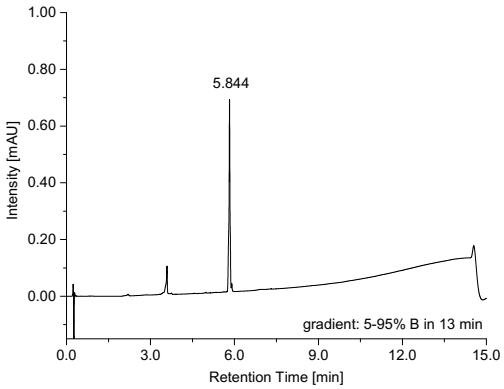

(F) ^{Ac}GPcpKGG^{CONH_2} **32j**

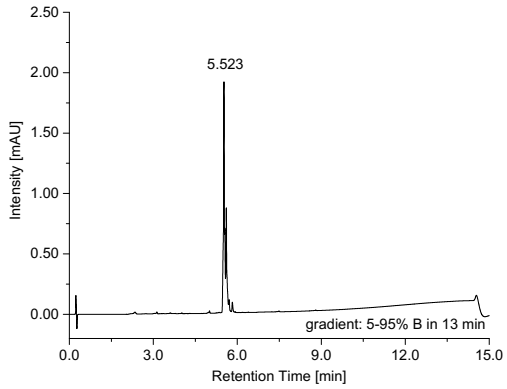

(G) ^{Ac}GQcpKGG^{CONH_2} **32k**

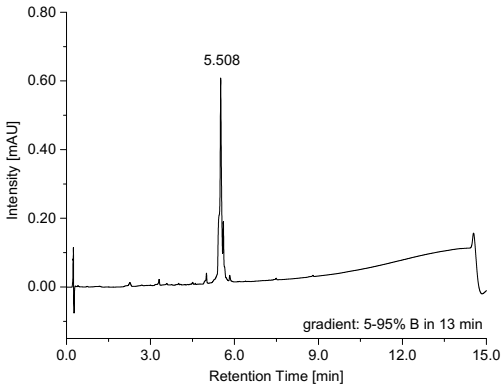

(H) ^{Ac}GRcpKGG^{CONH_2} **32l**

Figure A10: UPLC-traces (220 nm) of **32e**, **32f**, **32g**, **32h**, **32i**, **32j**, **32k** and **32l**.

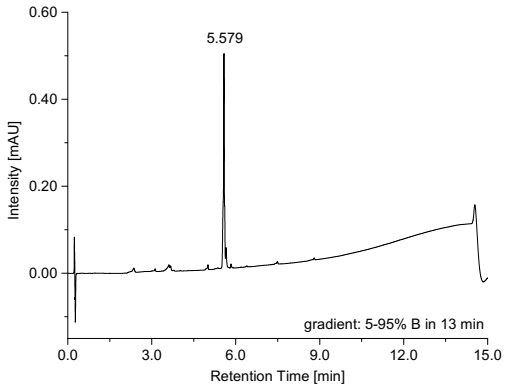

(A) ^{Ac}GScpKGG^{CONH_2} **32m**

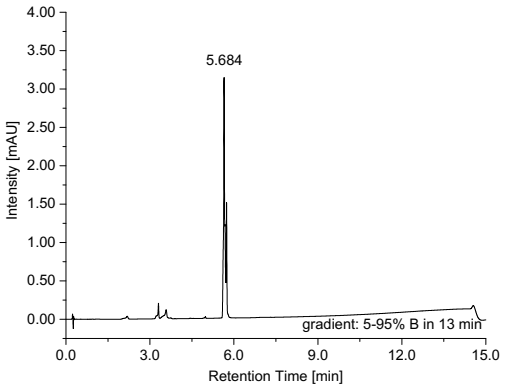

(B) ^{Ac}GGcpKAG^{CONH_2} **32n**

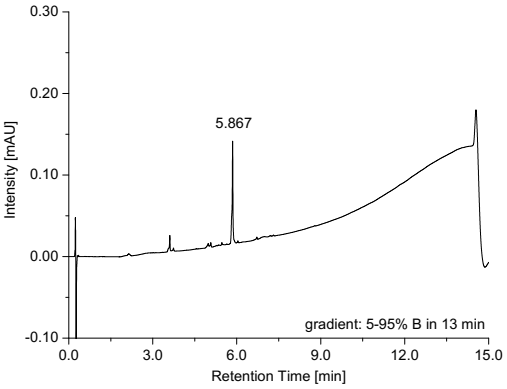

(C) ^{Ac}GGcpKCG^{CONH_2} **32o**

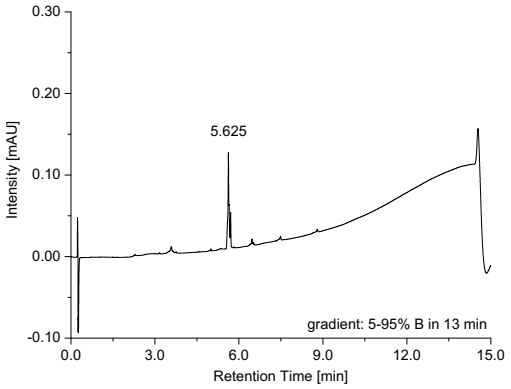

(D) ^{Ac}GGcpKDG^{CONH_2} **32p**

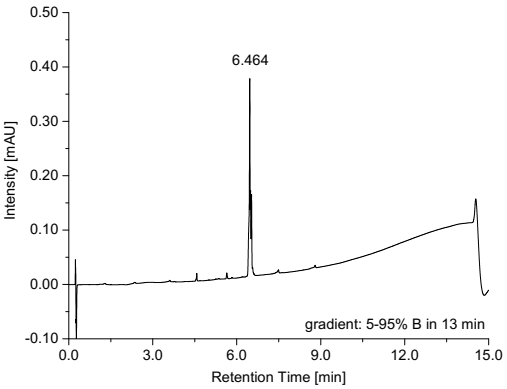

(E) ^{Ac}GGcpKFG^{CONH_2} **32q**

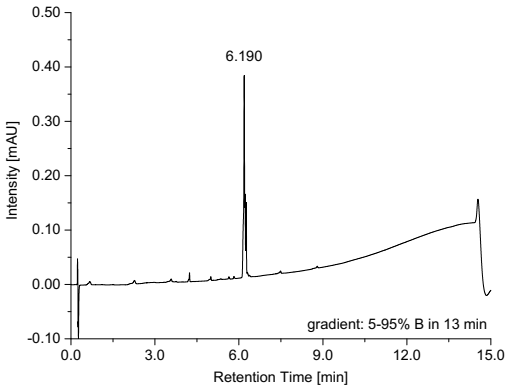

(F) ^{Ac}GGcpKIG^{CONH_2} **32r**

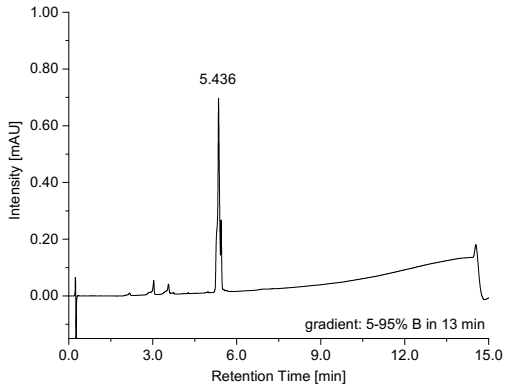

(G) ^{Ac}GGcpKKG^{CONH_2} **32s**

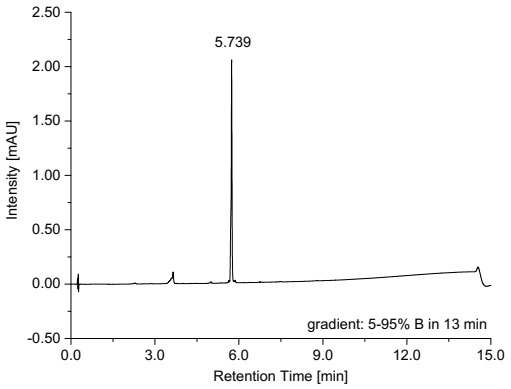

(H) ^{Ac}GGcpKPG^{CONH_2} **32t**

Figure A11: UPLC-traces (220 nm) of **32m**, **32n**, **32o**, **32p**, **32q**, **32r**, **32s** and **32t**.

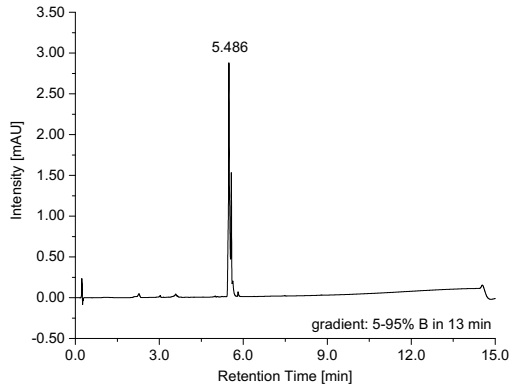

(A) ^{Ac}GGcpKQG^{CONH_2} **32u**

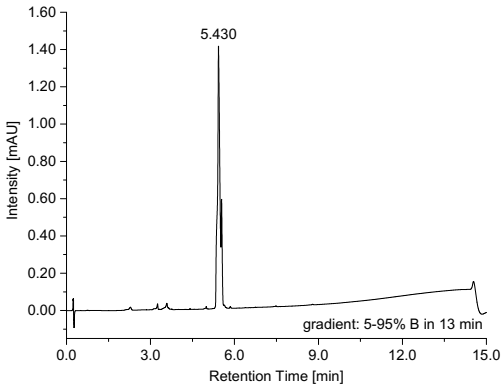

(B) ^{Ac}GGcpKRG^{CONH_2} **32v**

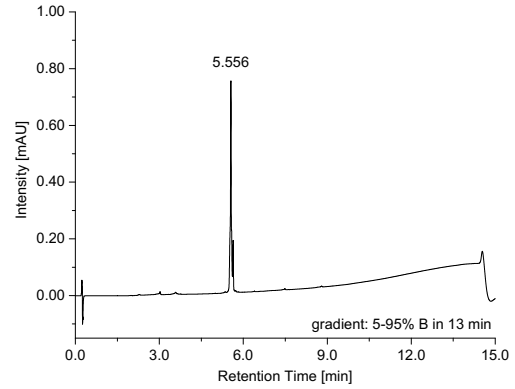

(C) ^{Ac}GGcpKSG^{CONH_2} **32w**

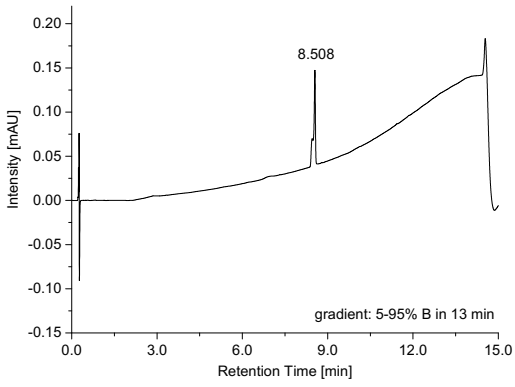

(D) Fmoc-Arg(NPO(OTc$_2$))-OH **34**

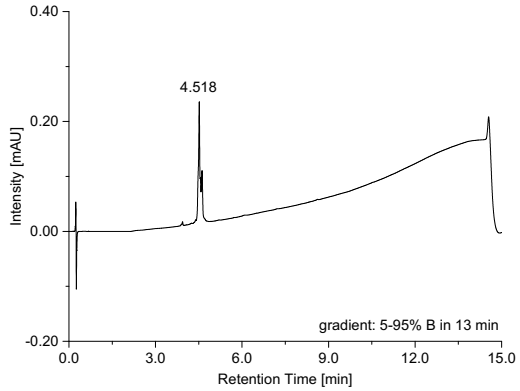

(E) ^{H_2N}E$^{PEG\text{-}biotin}$-TTAVEID*h*CDSLK^{CONH_2} **62**

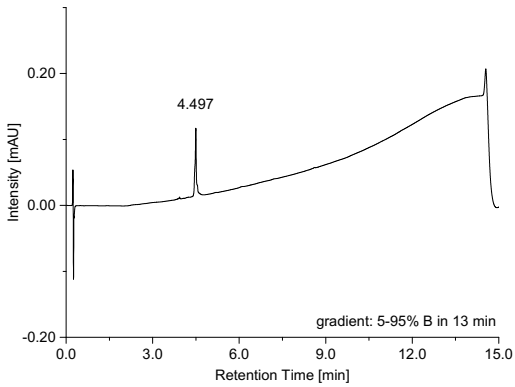

(F) ^{H_2N}E$^{PEG\text{-}biotin}$-TTAVEID*Nle*DSLK^{CONH_2} **63**

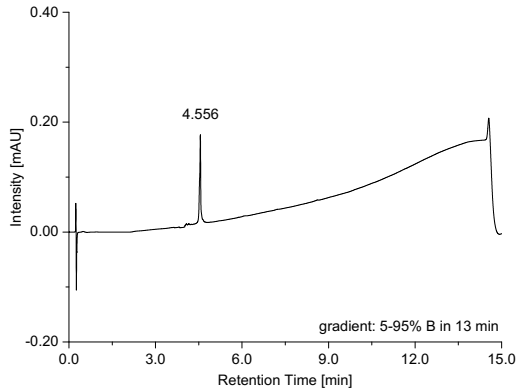

(G) ^{H_2N}E$^{PEG\text{-}biotin}$-TTAVEIDYDSLK^{CONH_2} **64**

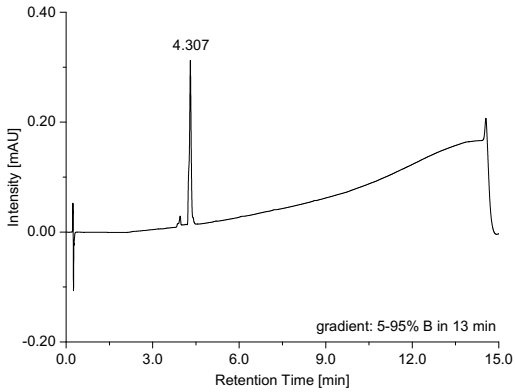

(H) ^{H_2N}E$^{PEG\text{-}biotin}$-TTAVEIDKDSLK^{CONH_2} **65**

Figure A12: UPLC-traces (220 nm) of **32u**, **32v**, **32w**, **34**, **62**, **63**, **64** and **65**.

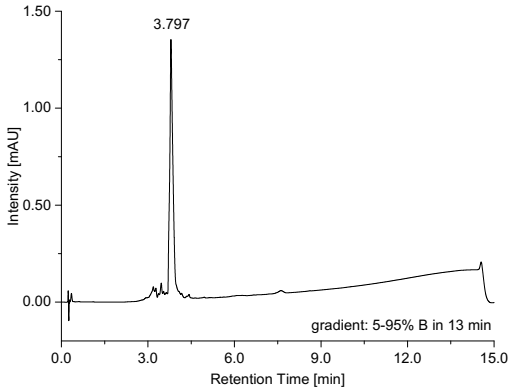

(A) ^{H_2N}E$^{PEG\text{-}biotin}$-TTAVEIDK^{N_3}DSLK^{CONH_2} **66**

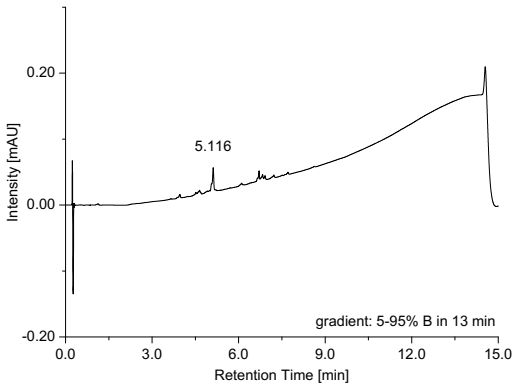

(B) ^{H_2N}E$^{PEG\text{-}biotin}$-TTAVEIDK^{N_3}DSLK^{COOH} **67**

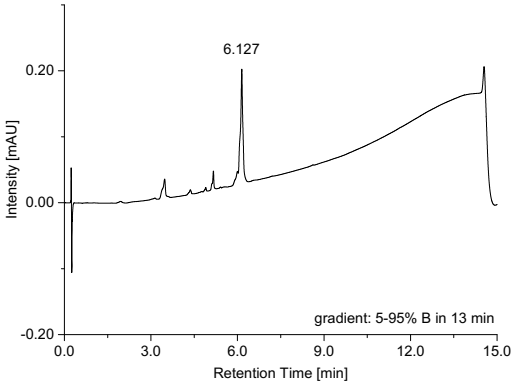

(C) ^{H_2N}E$^{PEG\text{-}biotin}$-TTAVEIDcpKDSLK^{CONH_2} **68**

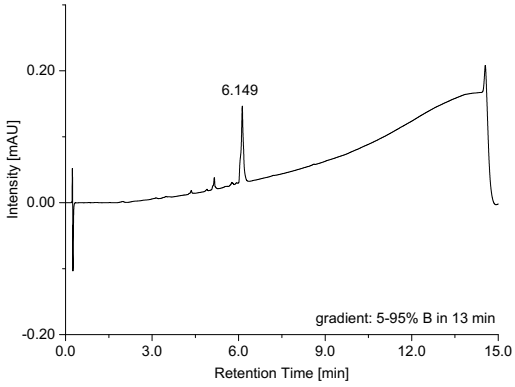

(D) ^{H_2N}E$^{PEG\text{-}biotin}$-TTAVEIDcpKDSLK^{COOH} **69**

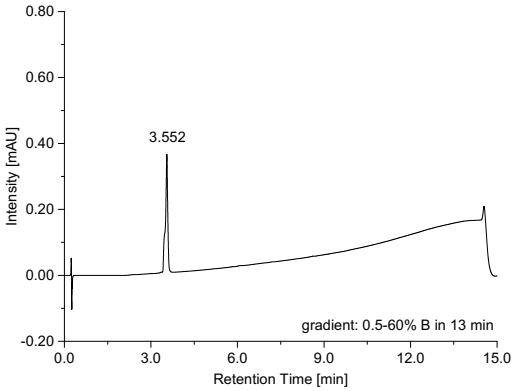

(E) ^{H_2N}E$^{PEG\text{-}biotin}$-TTAVEIDpKDSLK^{CONH_2} **70**

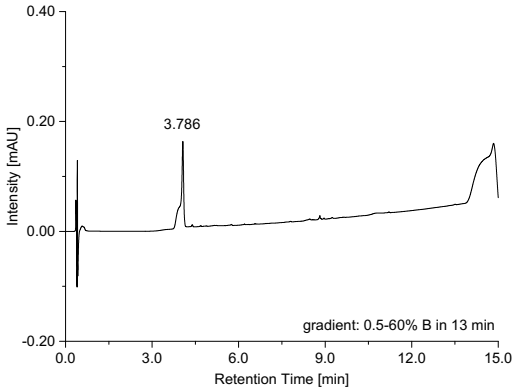

(F) ^{H_2N}E$^{PEG\text{-}biotin}$-TTAVEIDpKDSLK^{COOH} **71**

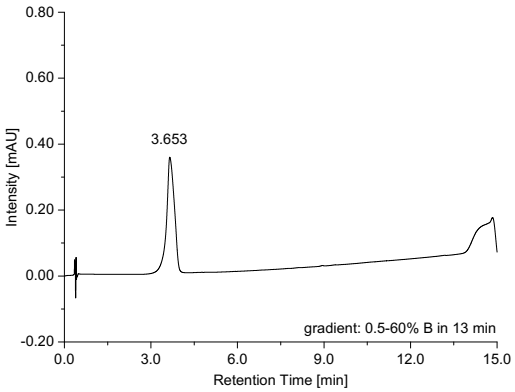

(G) ^{H_2N}KKKARKSAGAAKRKASG^{CONH_2} **72**

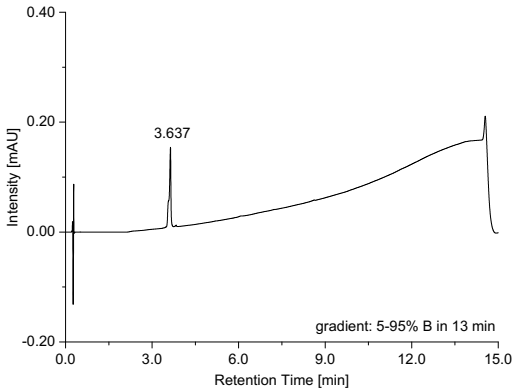

(H) ^{H_2N}EYGAG*Sox*KAGAG^{CONH_2} **73**

Figure A13: UPLC-traces (220 nm) of **66**, **67**, **68**, **69**, **70**, **71**, **72** and **73**.

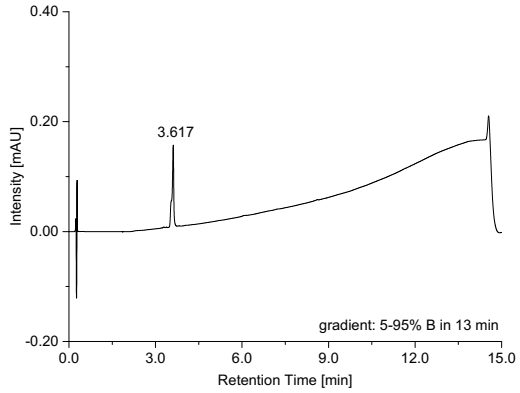

(A) ^{H_2N}EYGAG*Sox*GKGAG^{CONH_2} **74**

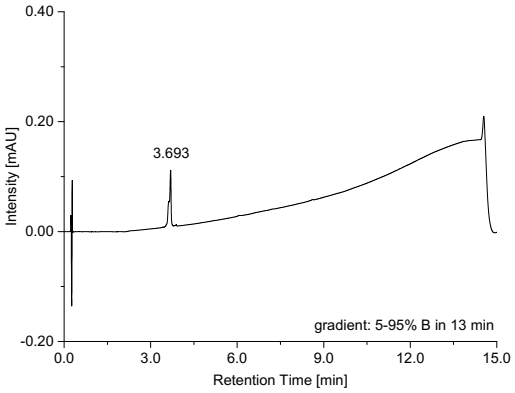

(B) ^{H_2N}EYGAG*Sox*GAKAG^{CONH_2} **75**

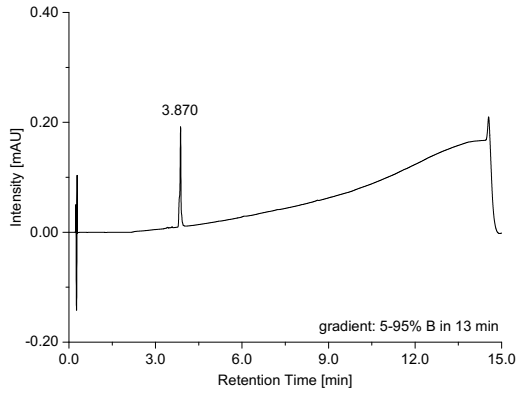

(C) ^{Ac}EYGAG*Sox*KAGAG^{CONH_2} **76**

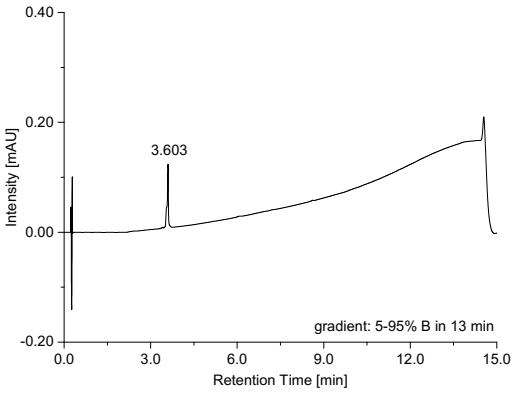

(D) ^{Ac}EAGAG*Sox*KAGAG^{CONH_2} **77**

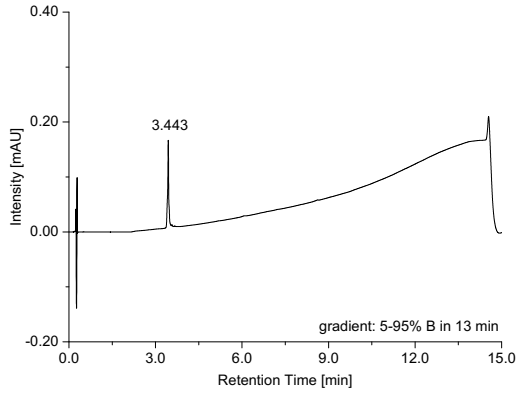

(E) ^{H_2N}EYGAG*Sox*G**pS**GAG^{CONH_2} **78**

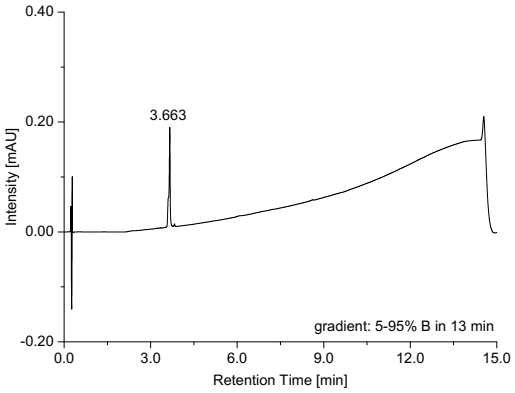

(F) ^{H_2N}EYGAG*Sox*G**S**KAG^{CONH_2} **79**

Figure A14: UPLC-traces (220 nm) of **74**, **75**, **76**, **77**, **78** and **79**.

NMR Spectra of Synthesized Compounds

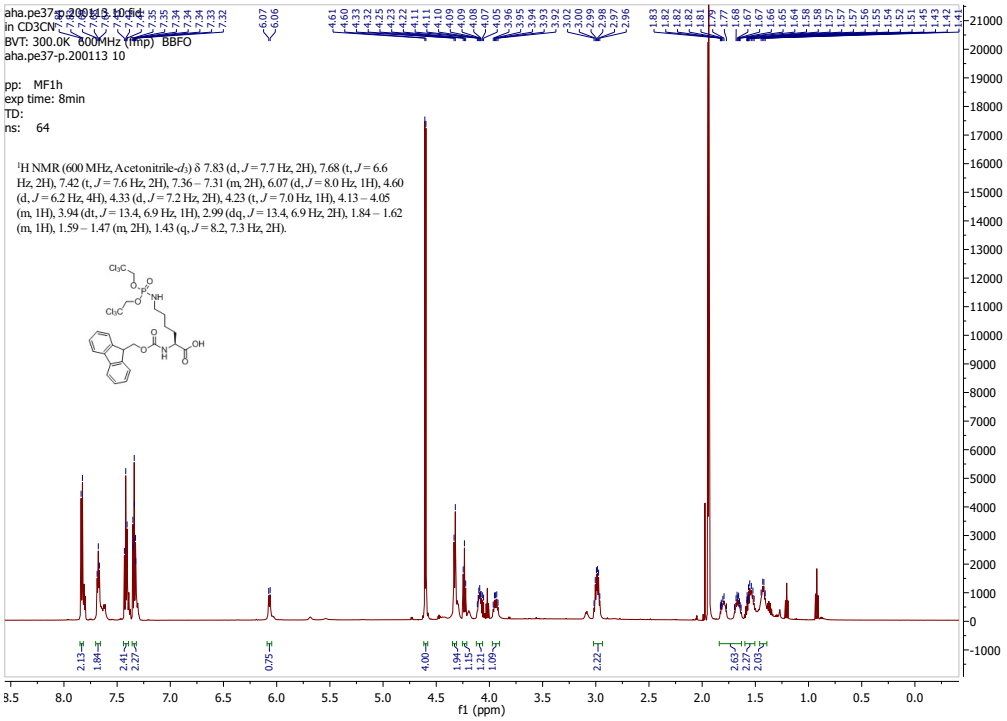

Figure A15: ^{1}H NMR spectrum of compound **1** (600 MHz, CD_3CN).

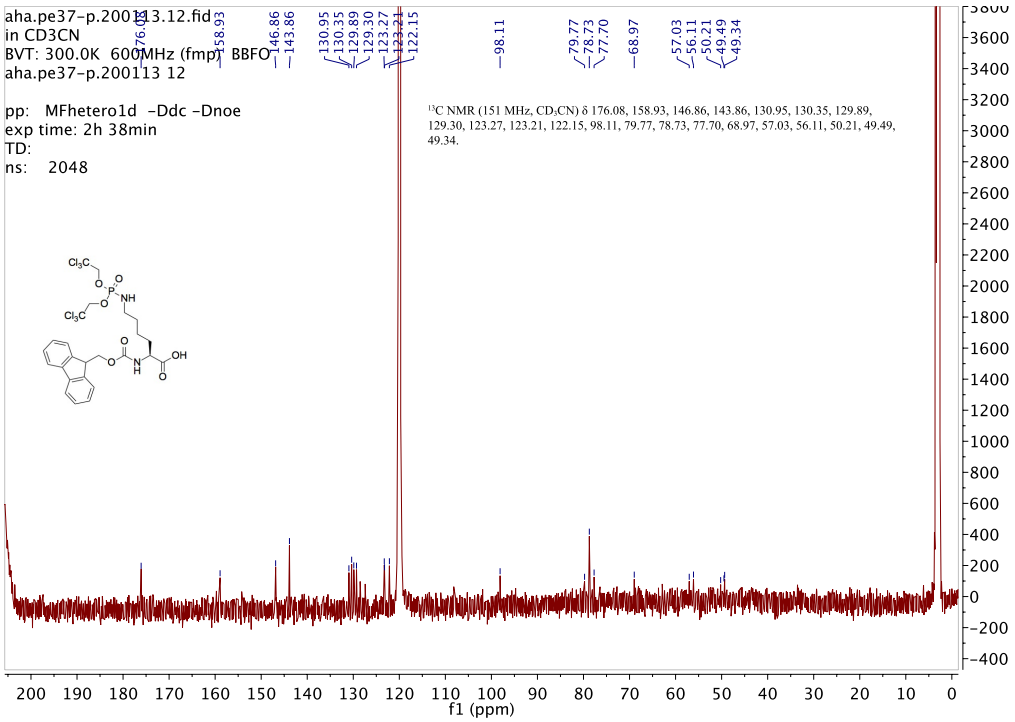

Figure A16: ^{13}C NMR spectrum of compound **1** (151 MHz, CD_3CN).

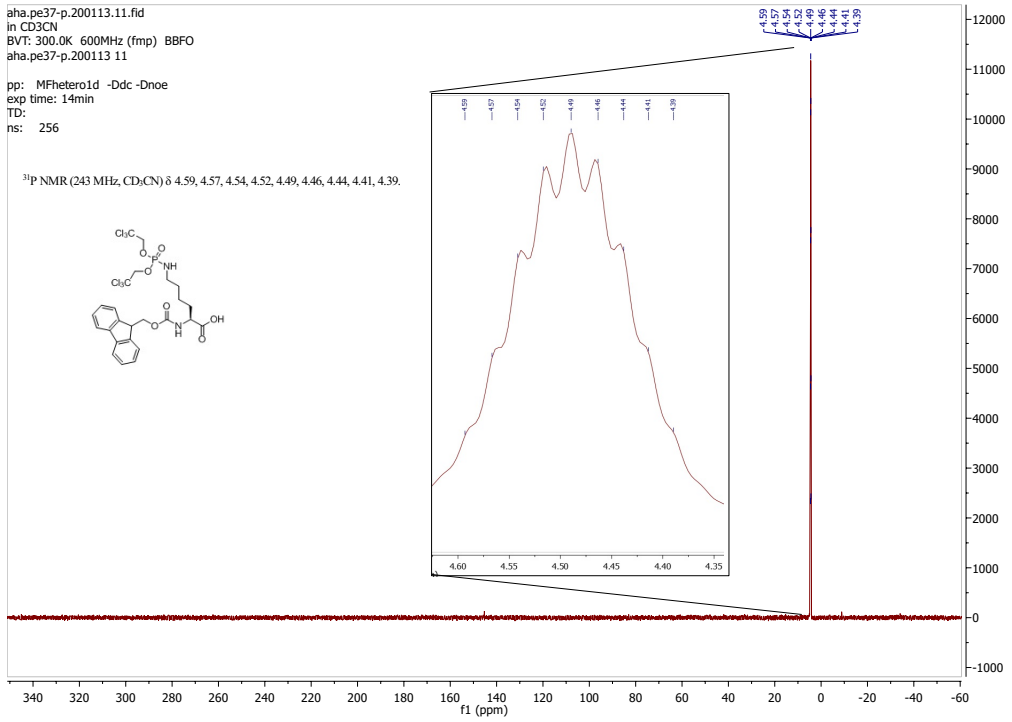

Figure A17: ^{31}P NMR spectrum of compound **1** (243 MHz, CD_3CN).

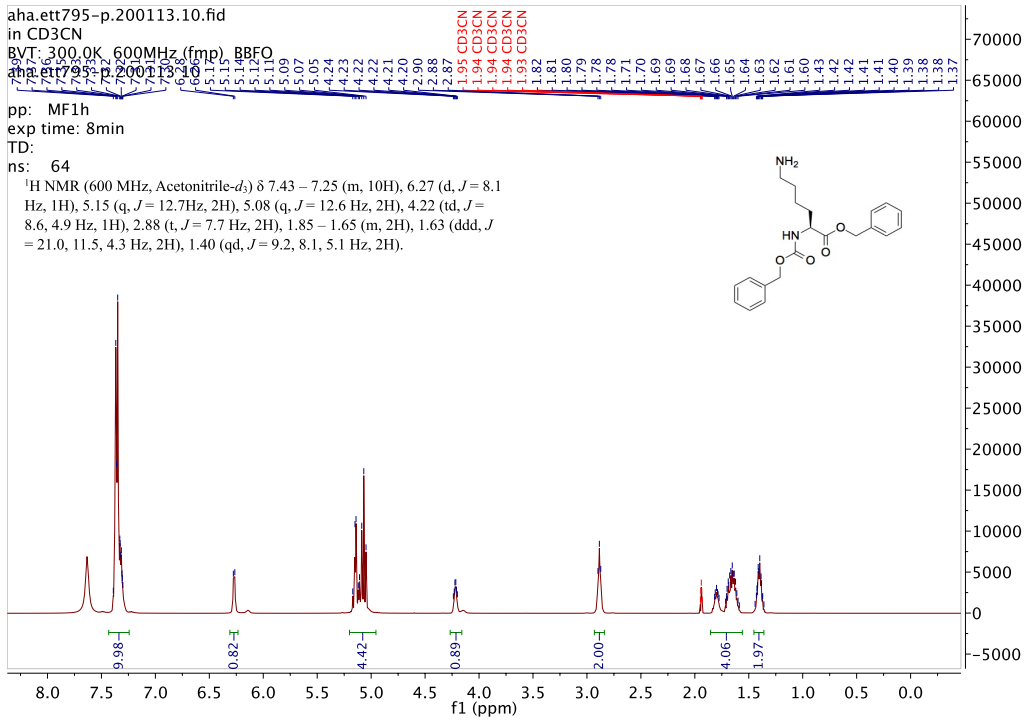

Figure A18: ^{1}H NMR spectrum of compound **2** (600 MHz, CD_3CN).

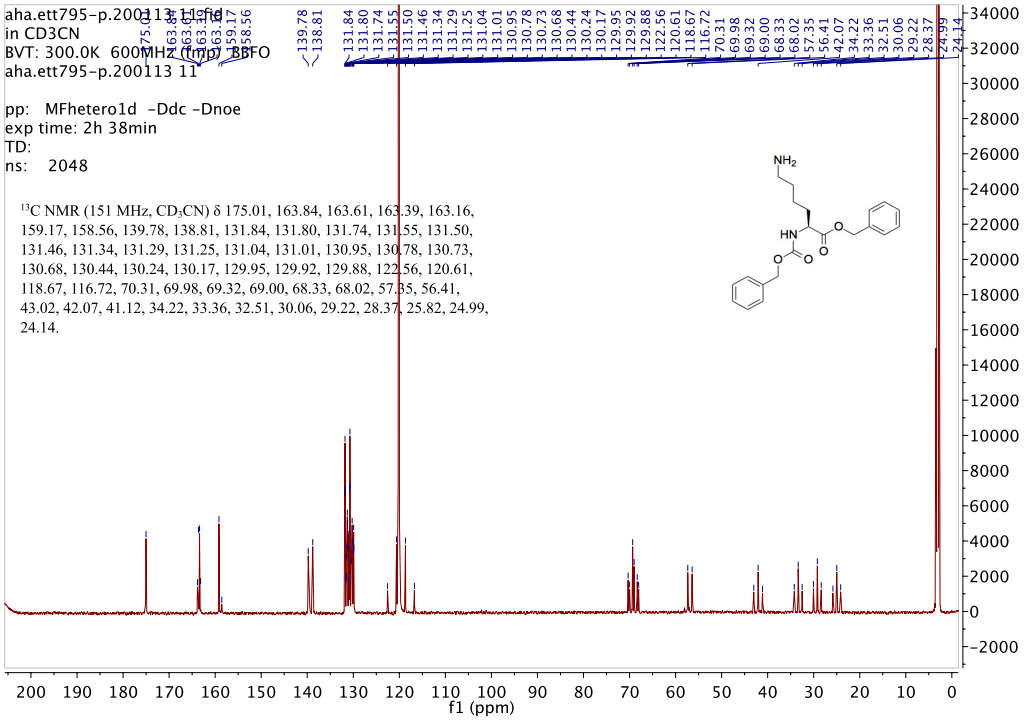

Figure A19: ^{13}C NMR spectrum of compound **2** (151 MHz, CD_3CN).

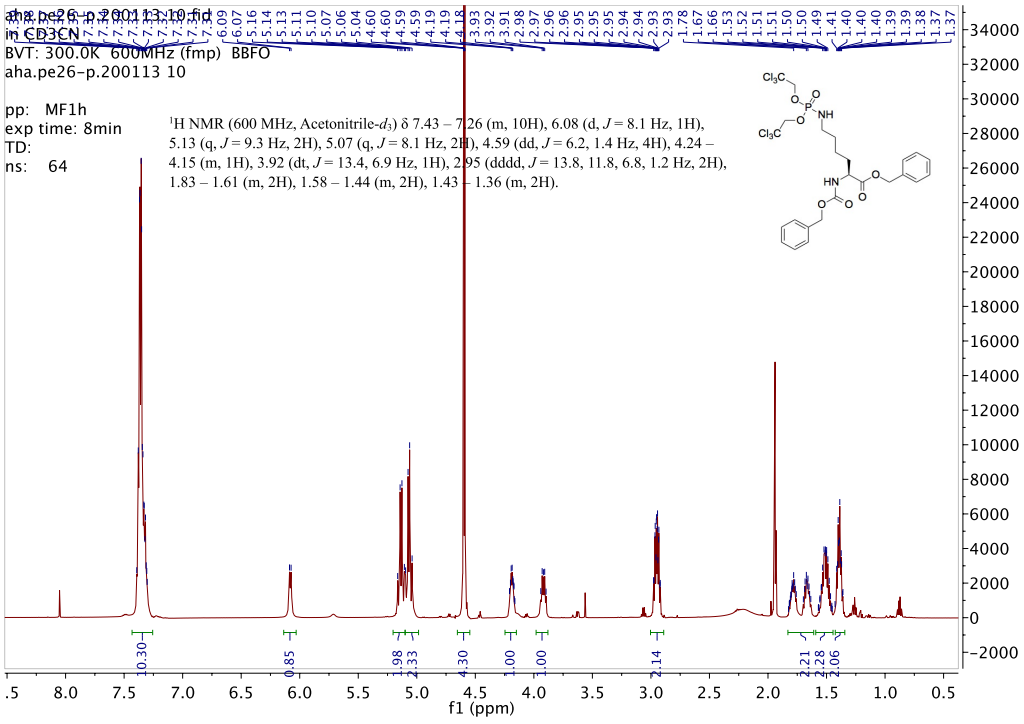

Figure A20: ^{1}H NMR spectrum of compound **3** (600 MHz, CD_3CN).

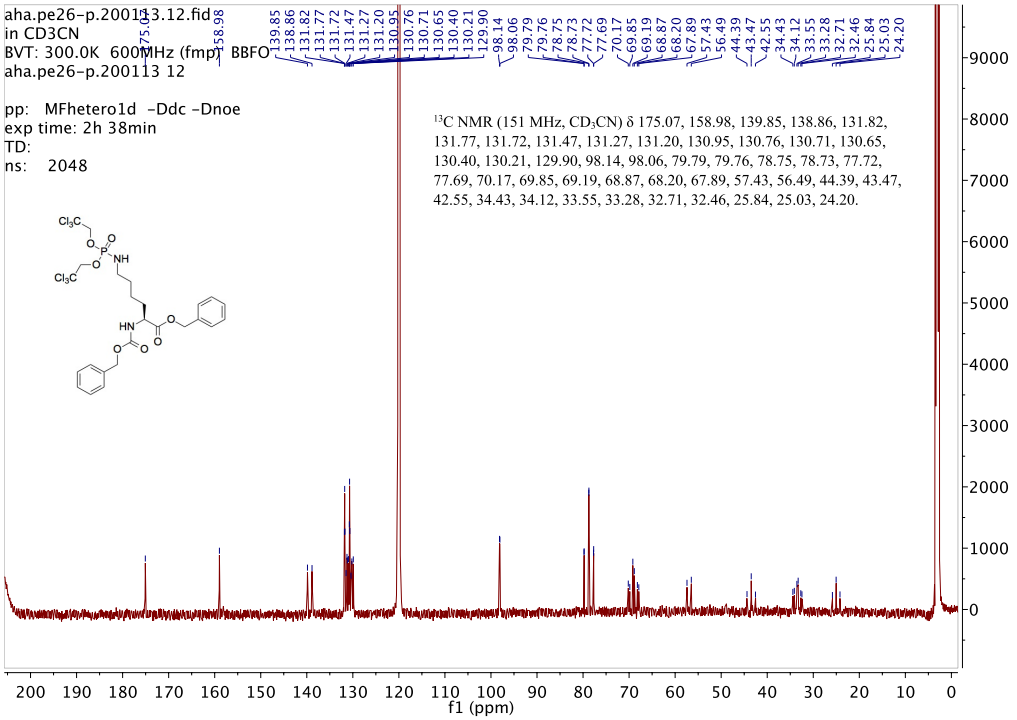

Figure A21: ^{13}C NMR spectrum of compound **3** (151 MHz, CD_3CN).

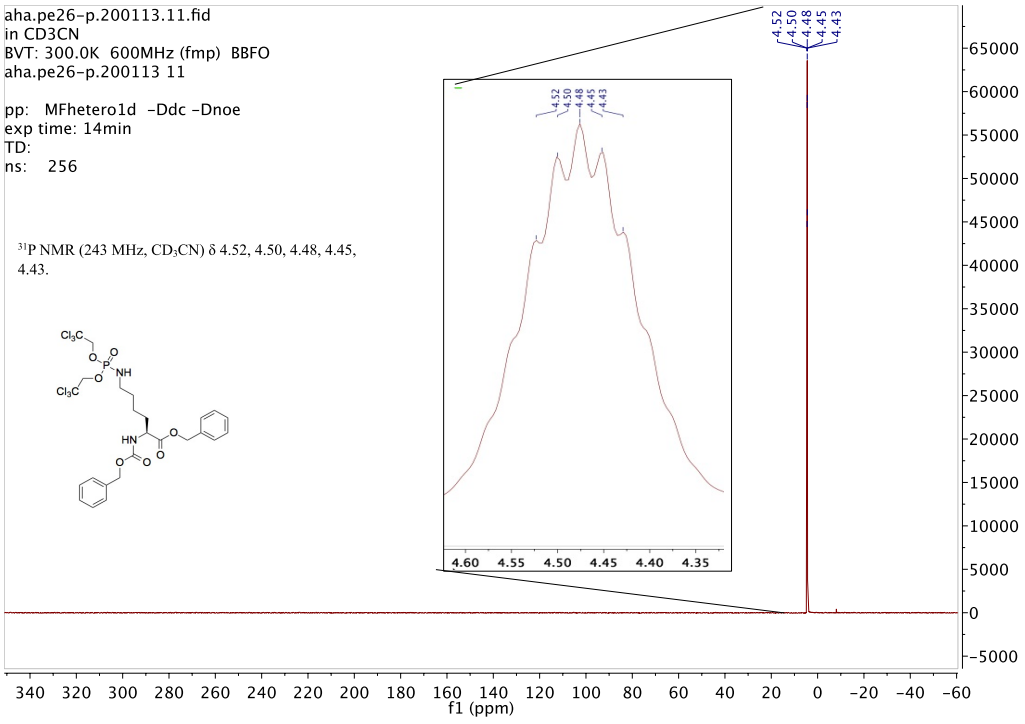

Figure A22: ^{31}P NMR spectrum of compound **3** (243 MHz, CD_3CN).

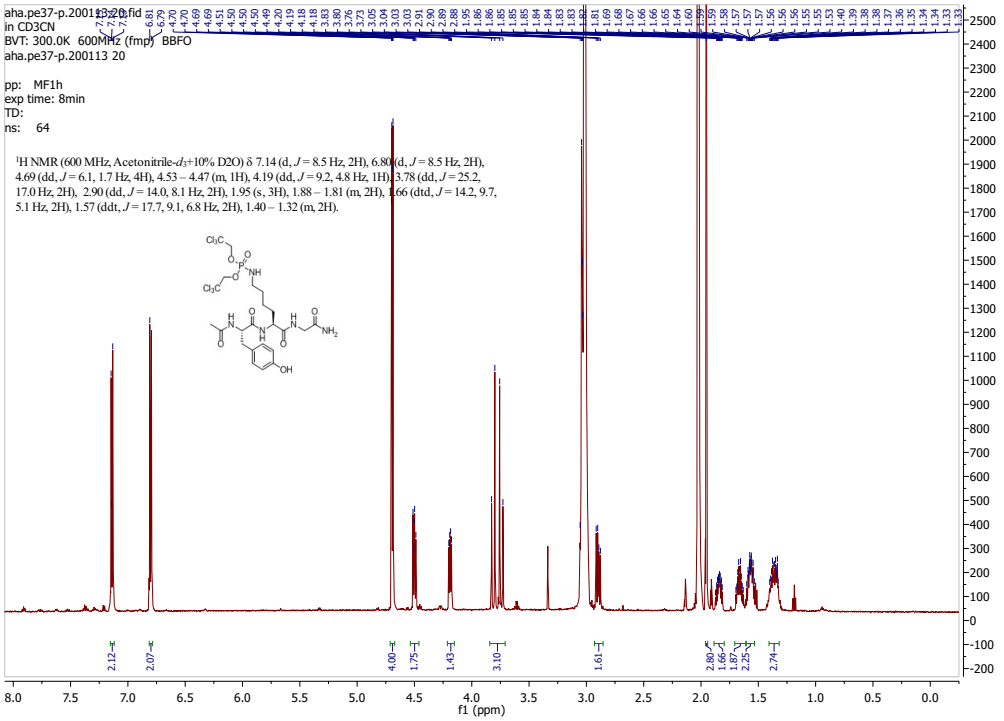

Figure A23: ^{1}H NMR spectrum of peptide **4** (600 MHz, CD_3CN+10% D_2O).

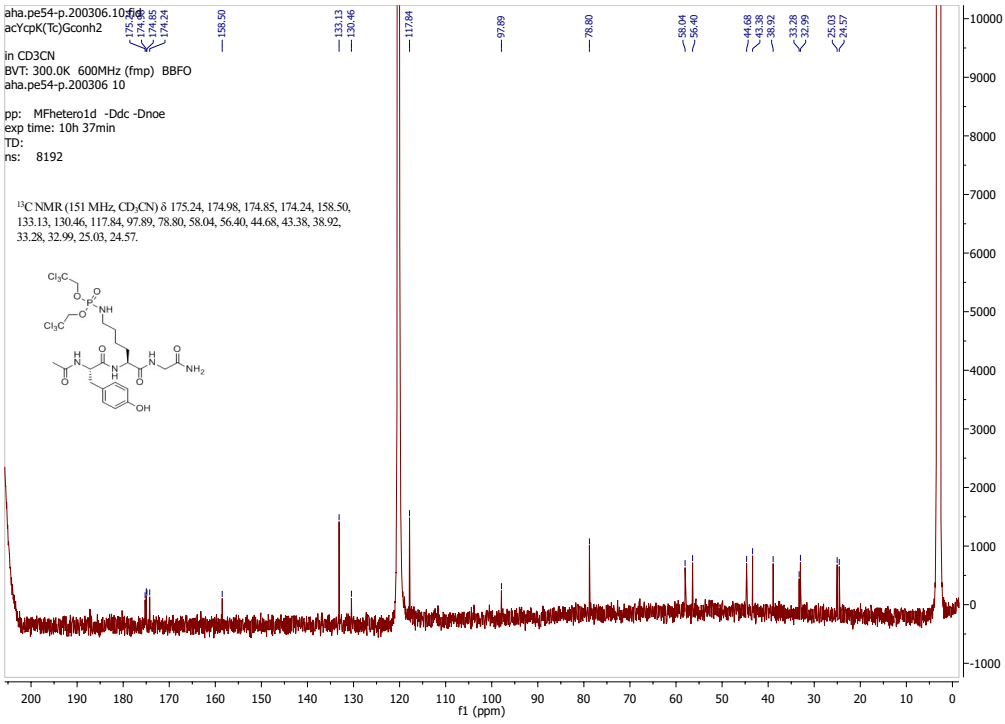

Figure A24: ^{13}C NMR spectrum of peptide **4** (151 MHz, CD_3CN+10% D_2O).

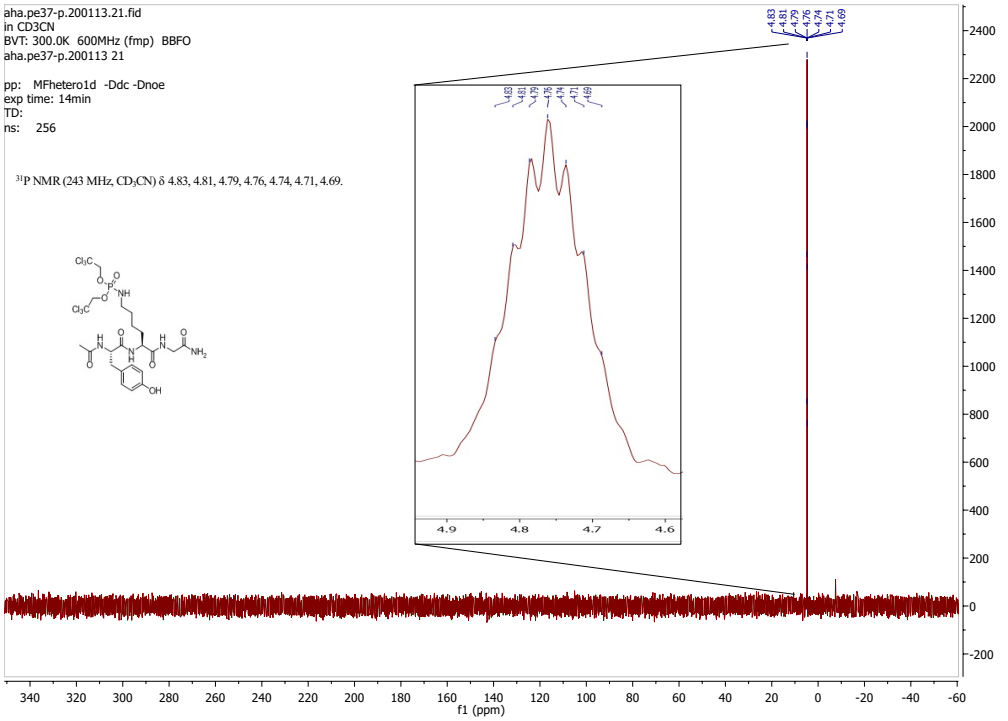

Figure A25: ^{31}P NMR spectrum of peptide **4** (243 MHz, CD_3CN+10% D_2O).

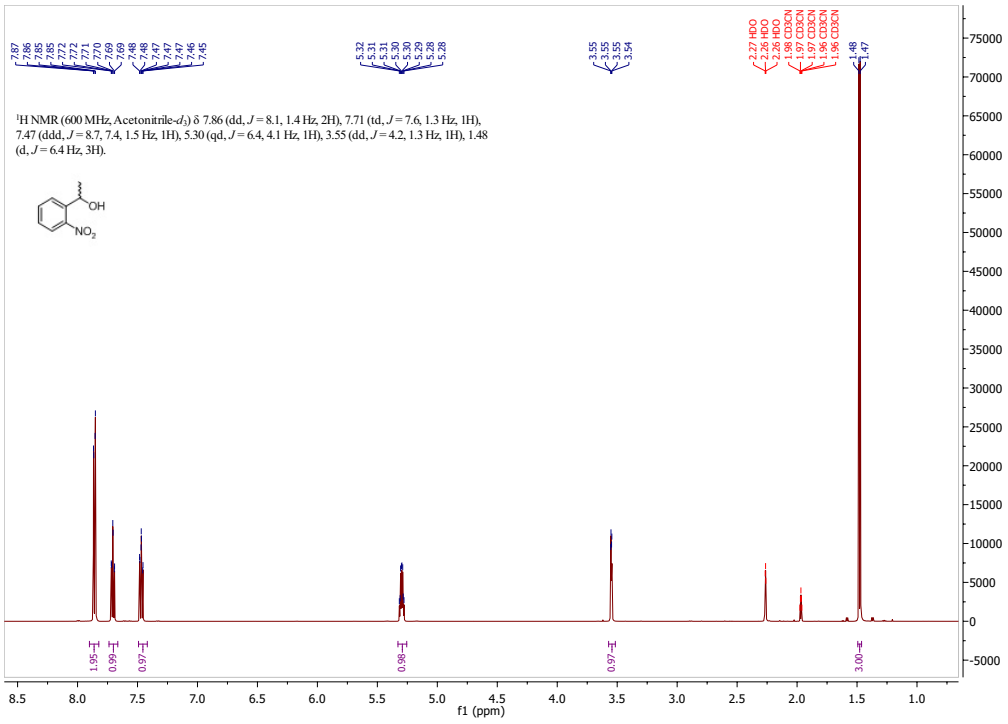

Figure A26: ^{1}H NMR spectrum of compound **8** (600 MHz, CD_3CN).

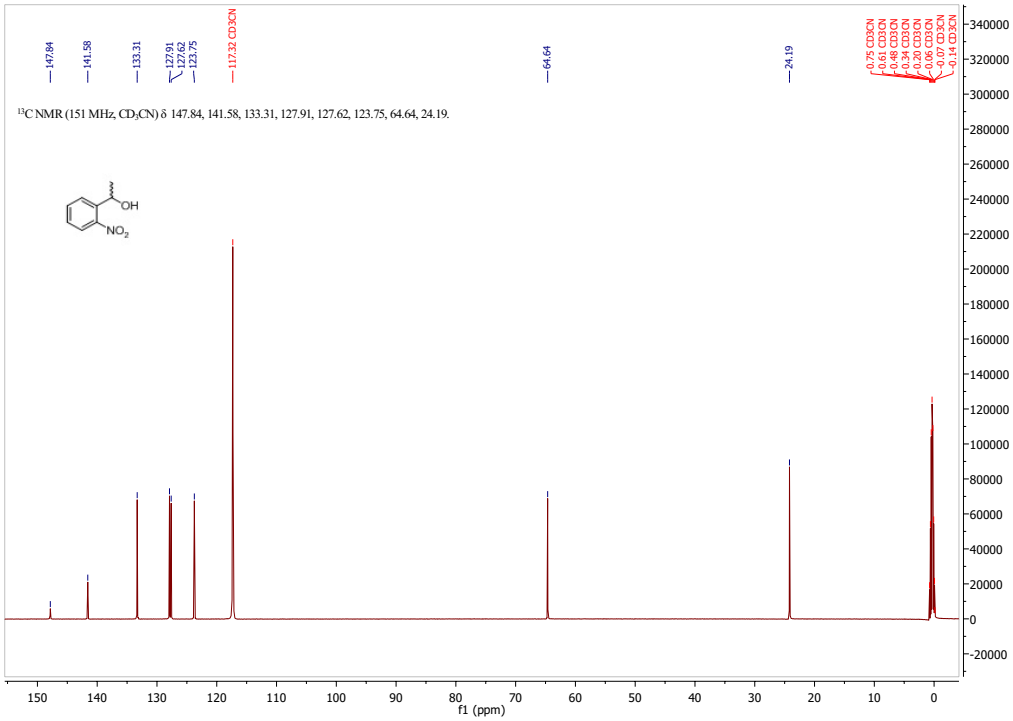

Figure A27: ^{13}C NMR spectrum of compound **8** (151 MHz, CD_3CN).

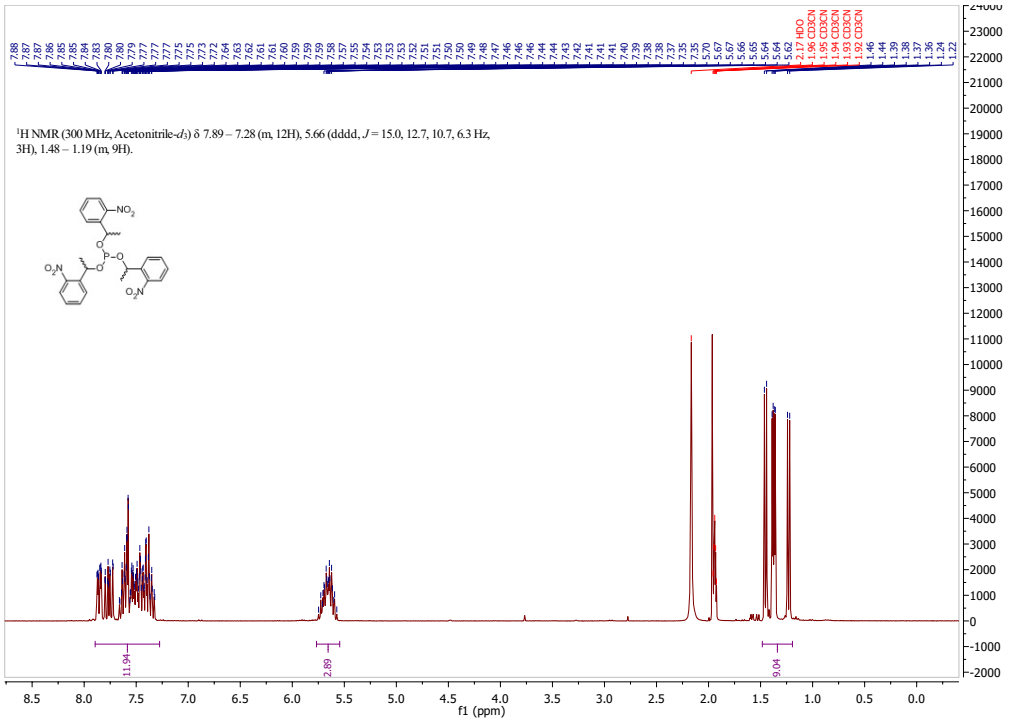

Figure A28: ^{1}H NMR spectrum of compound **9** (300 MHz, CD_3CN).

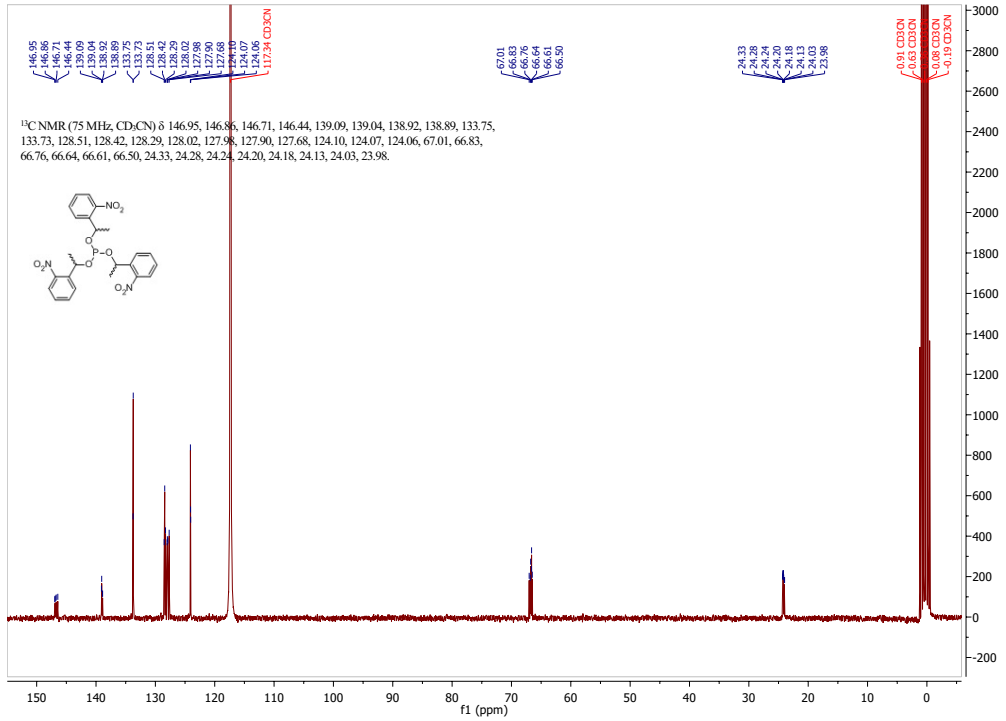

Figure A29: ^{13}C NMR spectrum of compound **9** (75 MHz, CD_3CN).

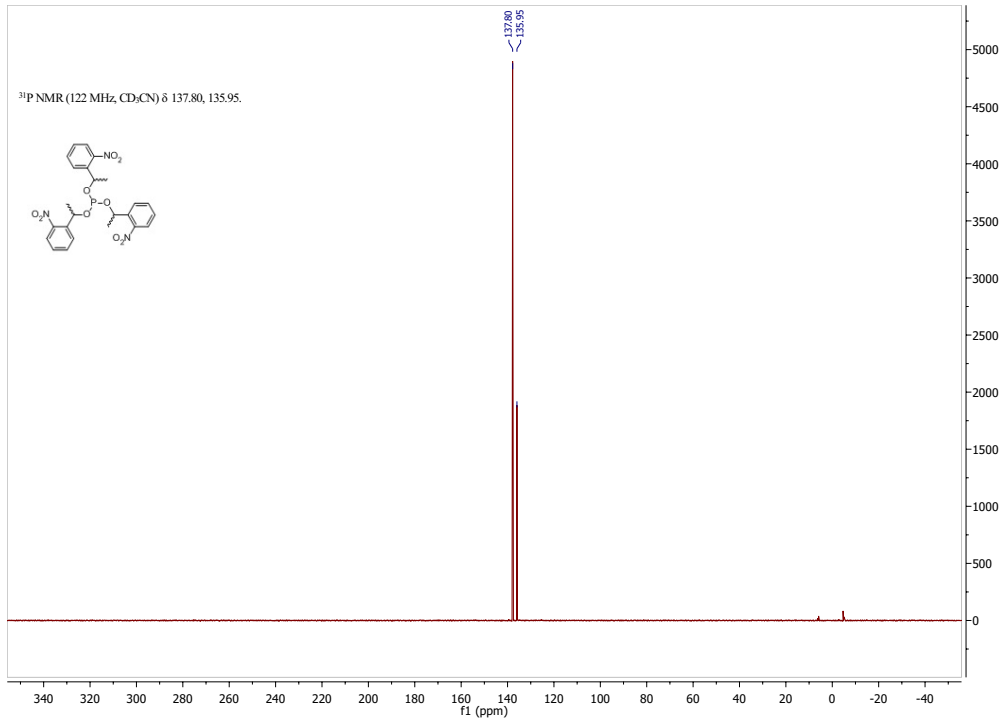

Figure A30: ^{31}P NMR spectrum of compound **9** (122 MHz, CD_3CN).

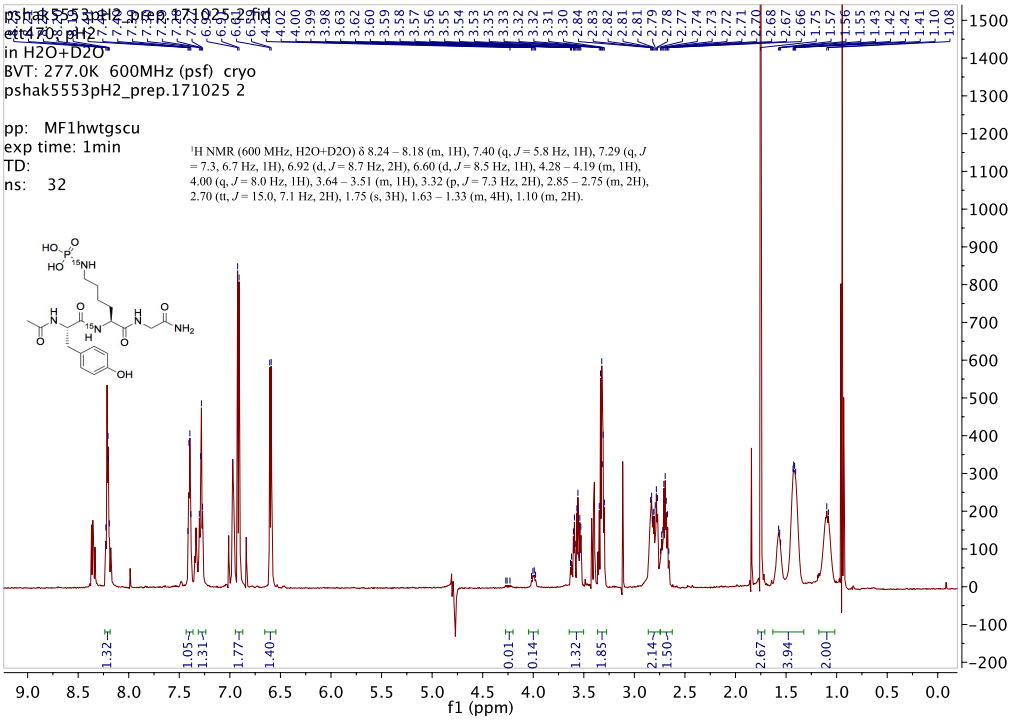

Figure A31: ^{1}H NMR spectrum of peptide **10** (600 MHz, 0.1% TFA + D_2O).

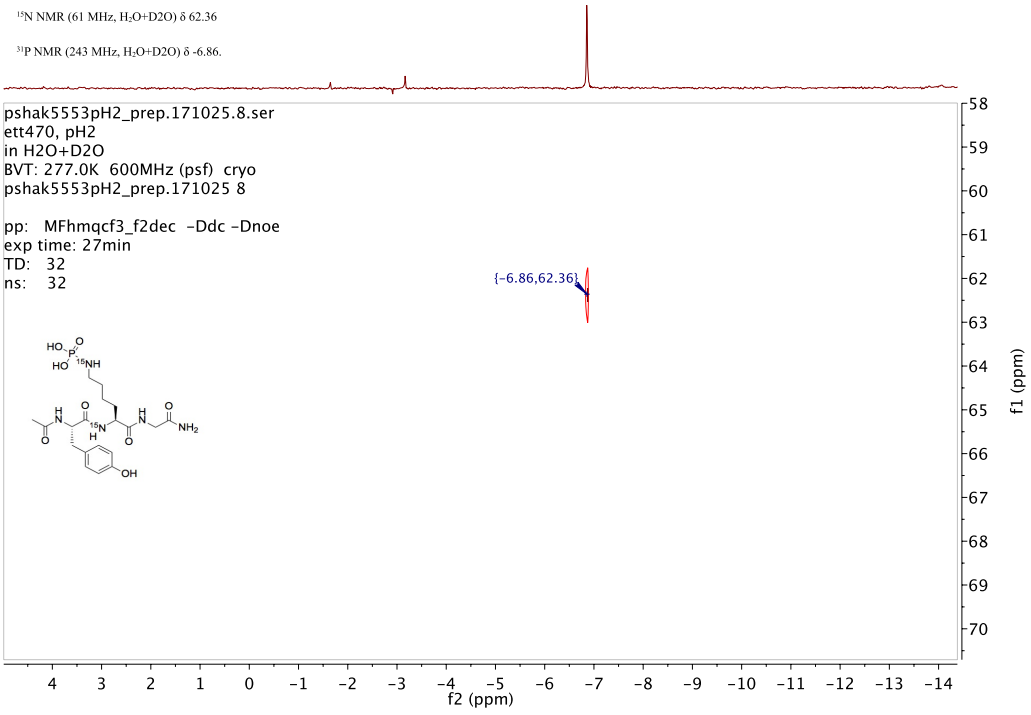

Figure A32: ^{31}P-^{15}N-HMBC NMR spectrum of peptide **10** (243 MHz, 0.1% TFA + D_2O).

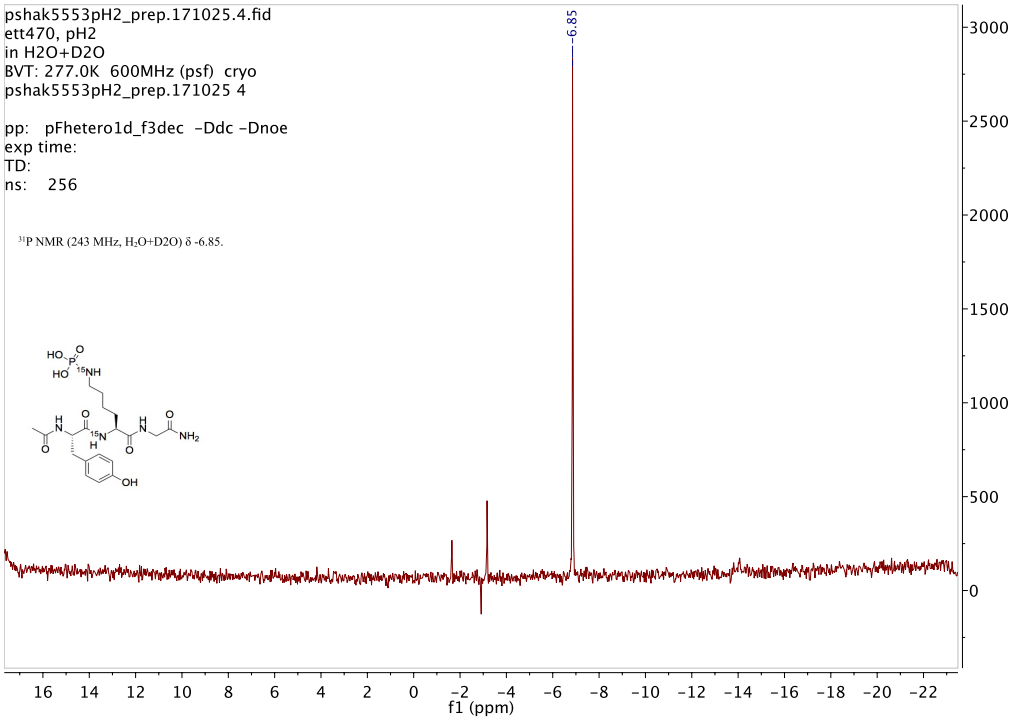

Figure A33: ^{31}P NMR spectrum of peptide **10** (243 MHz, 0.1% TFA + D_2O).

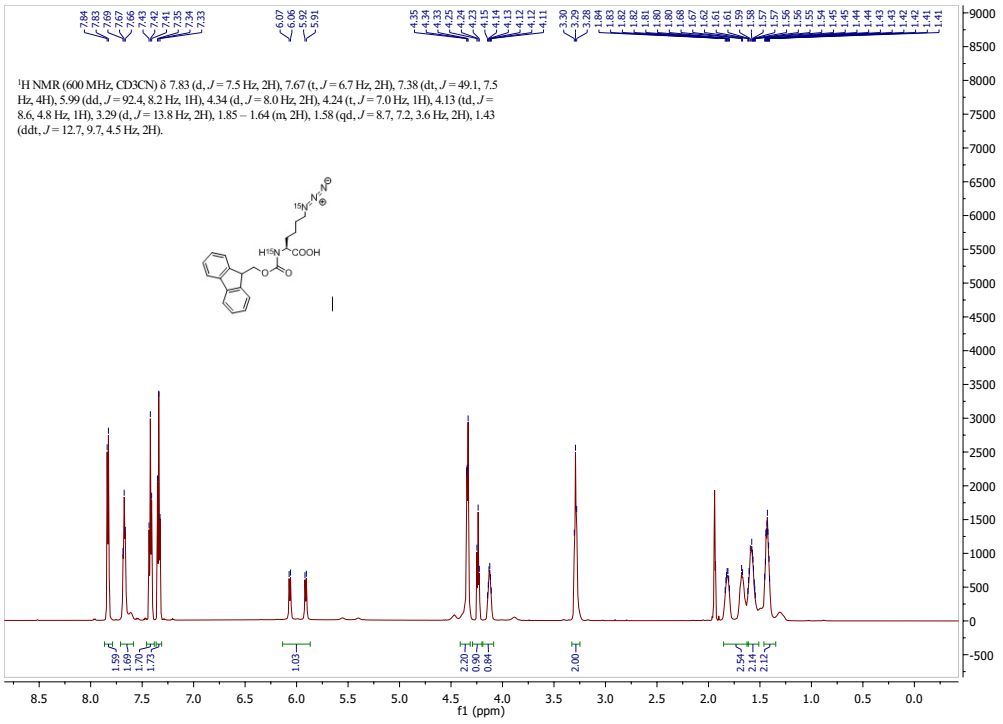

Figure A34: ^{1}H NMR spectrum of compound **13** (600 MHz, CD_3CN).

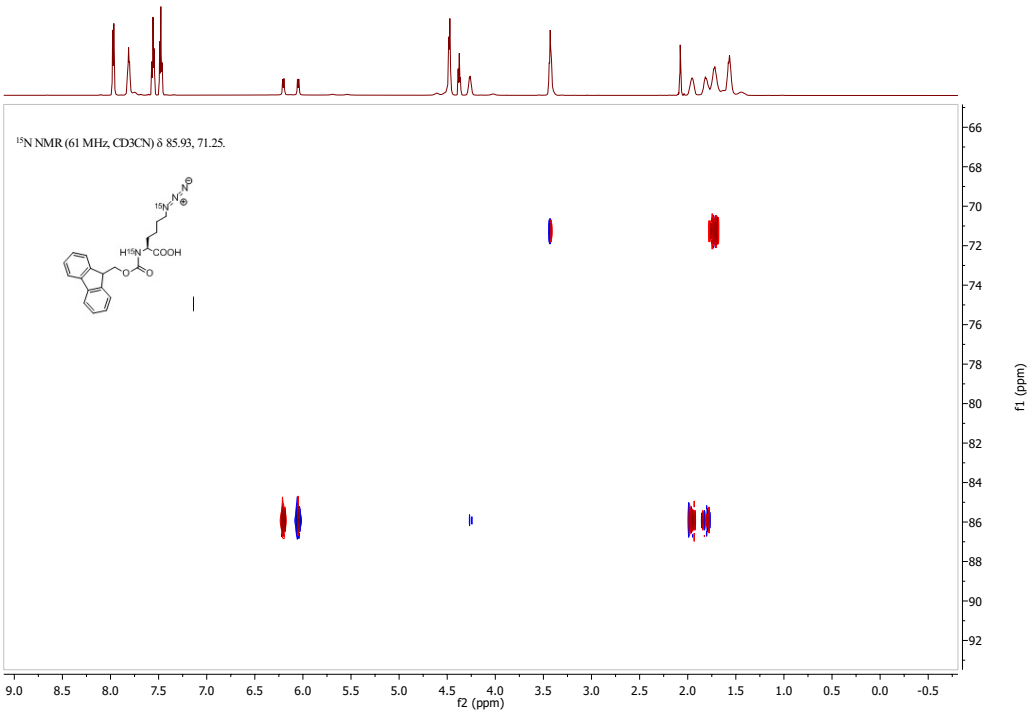

Figure A35: ^{1}H-^{15}N-HMBC NMR spectrum of compound **13** (600 MHz, CD_3CN).

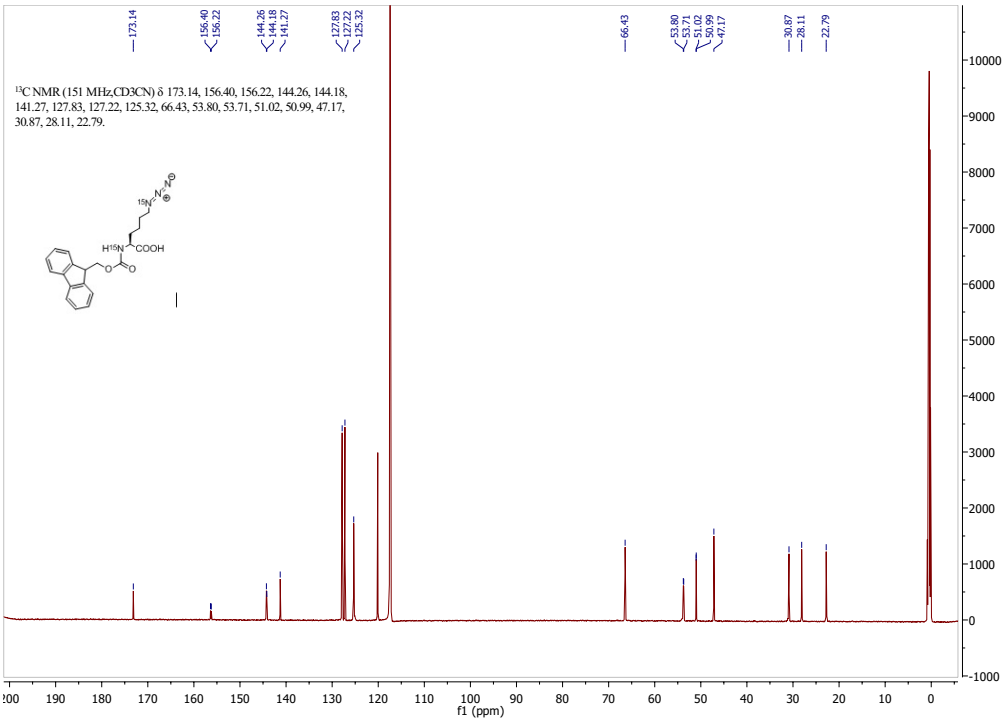

Figure A36: ^{13}C NMR spectrum of compound **13** (151 MHz, CD_3CN).

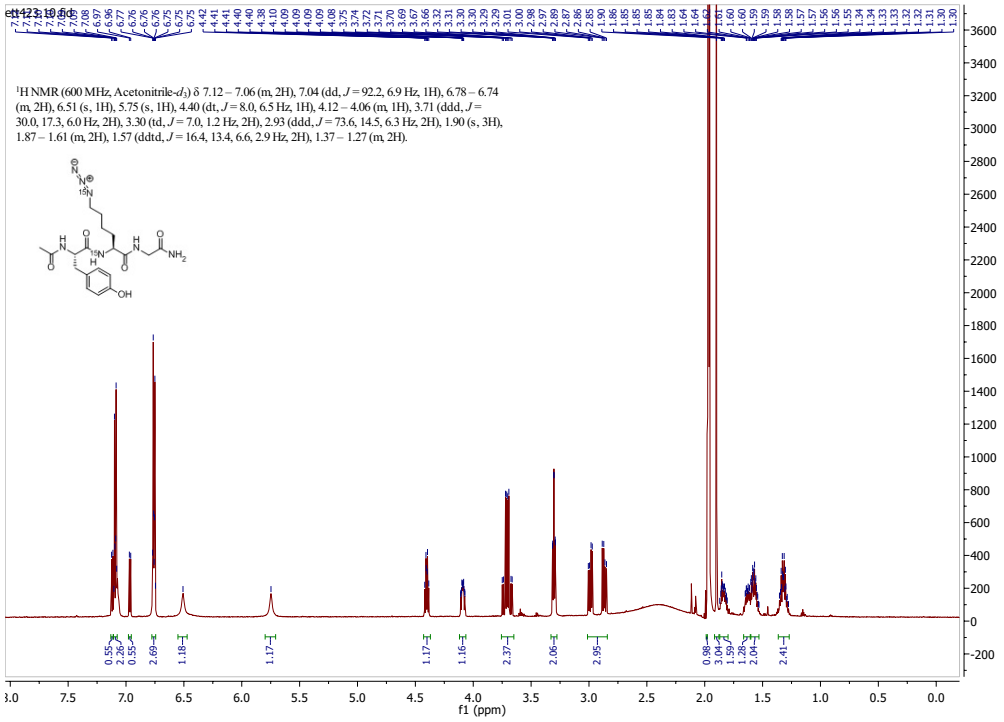

Figure A37: ^{1}H NMR spectrum of peptide **14** (600 MHz, CD_3CN).

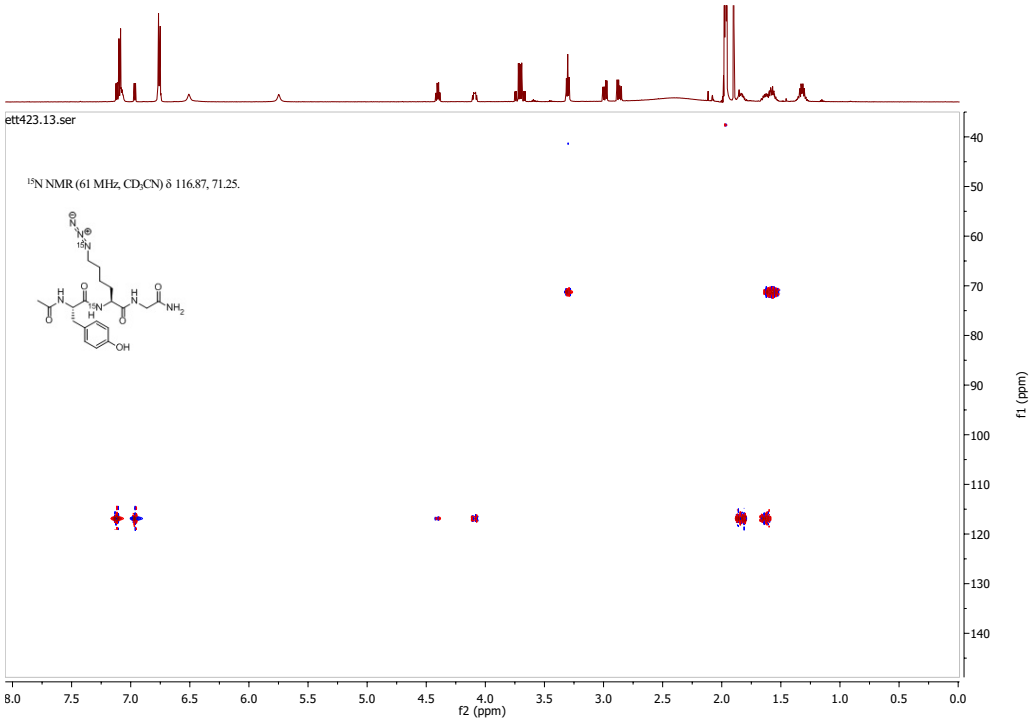

Figure A38: ^{1}H-^{15}N-HMBC NMR spectrum of peptide **14** (600 MHz, CD_3CN).

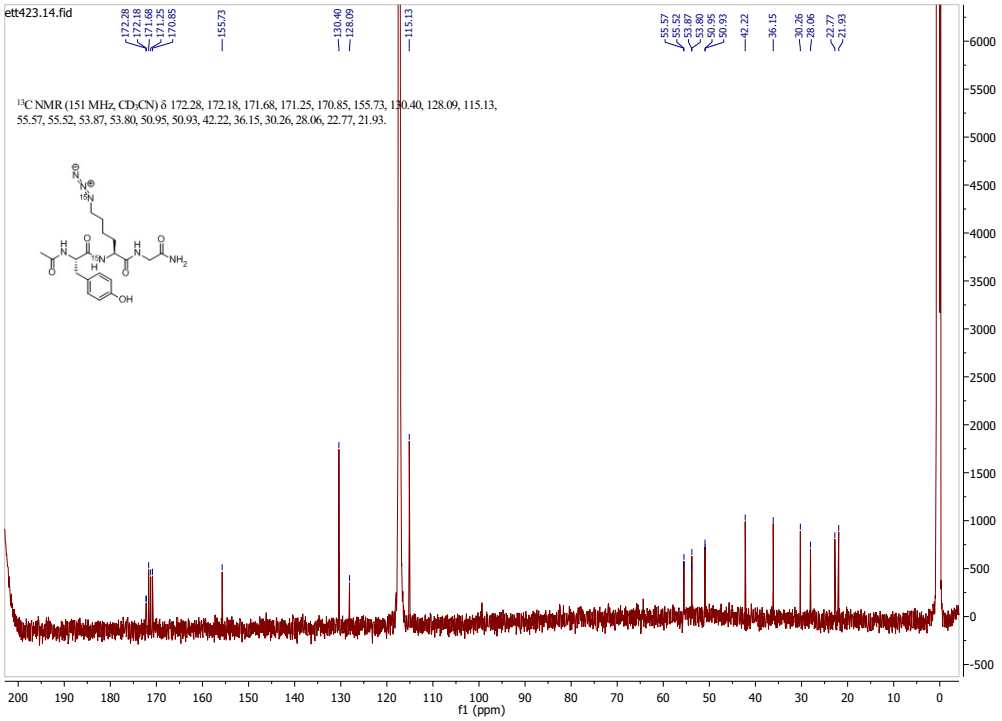

Figure A39: ^{13}C NMR spectrum of peptide **14** (151 MHz, CD_3CN).

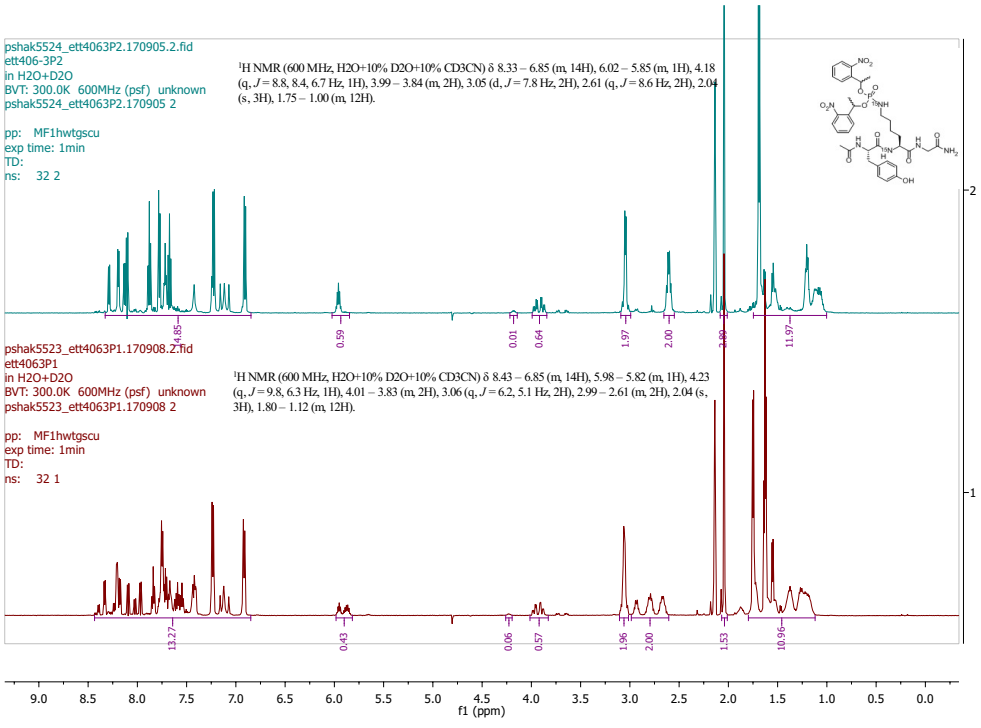

Figure A40: ^{1}H NMR spectra of peptide **15** (600 MHz, 0.1% TFA + D_2O + CD_3CN), isomers separated.

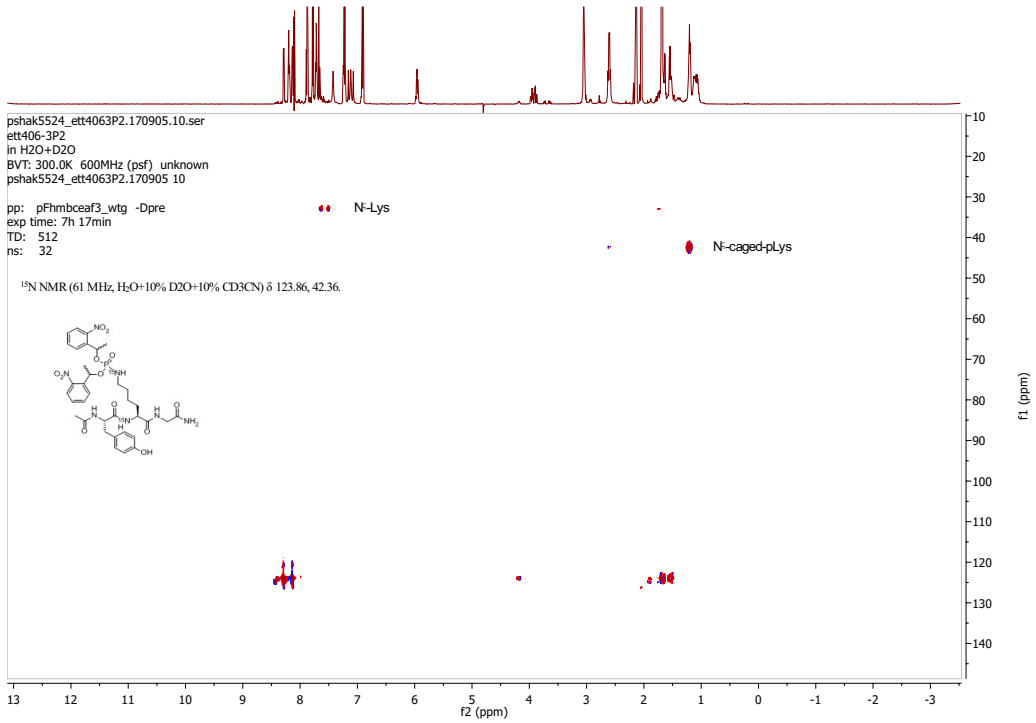

Figure A41: ^{1}H-^{15}N-HMBC NMR spectrum of peptide **15** (600 MHz, 0.1% TFA + D_2O + CD_3CN).

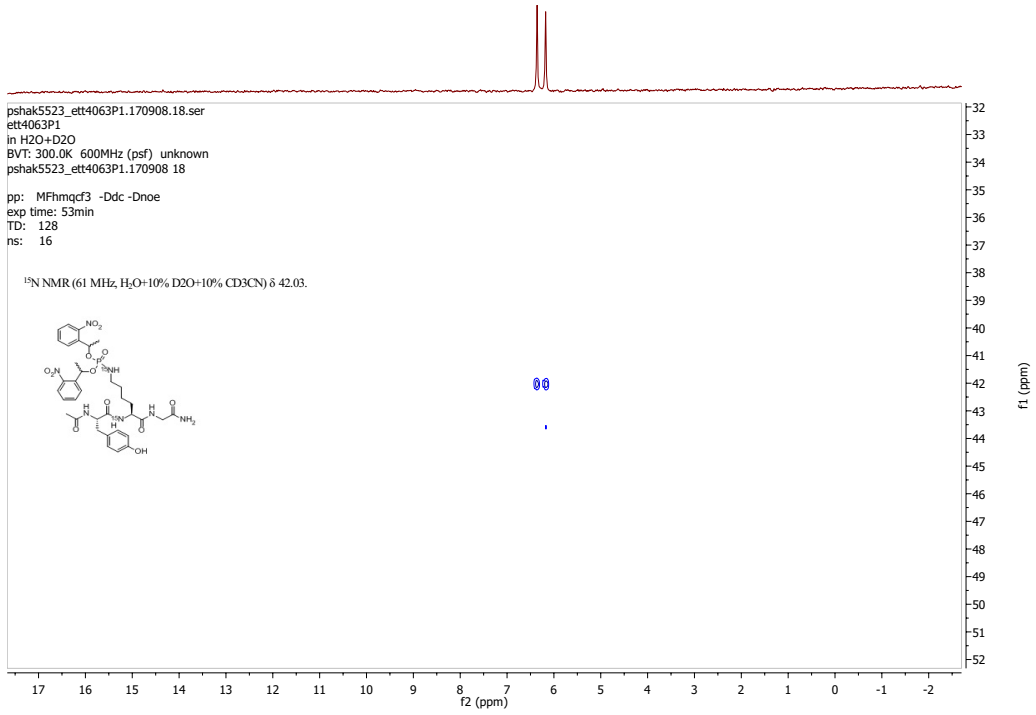

Figure A42: ^{31}P-^{15}N-HMQC NMR spectrum of peptide **15** (243 MHz, 0.1% TFA + D_2O + CD_3CN).

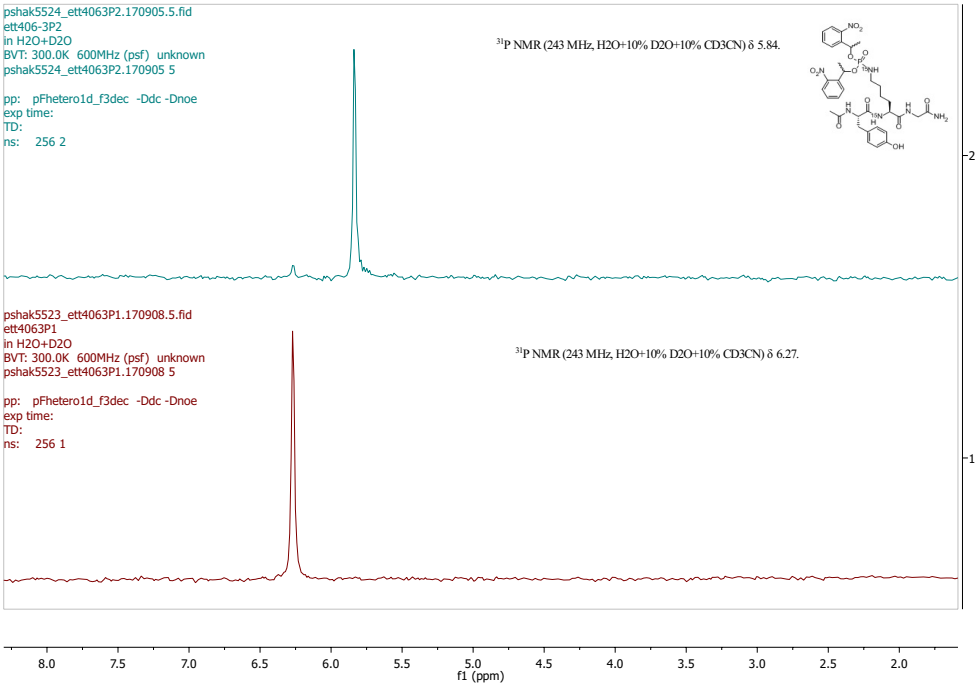

Figure A43: $^{31}P\{^{15}N\}$ NMR spectra of peptide **15** (243 MHz, 0.1% TFA + D_2O + CD_3CN), isomers separated.

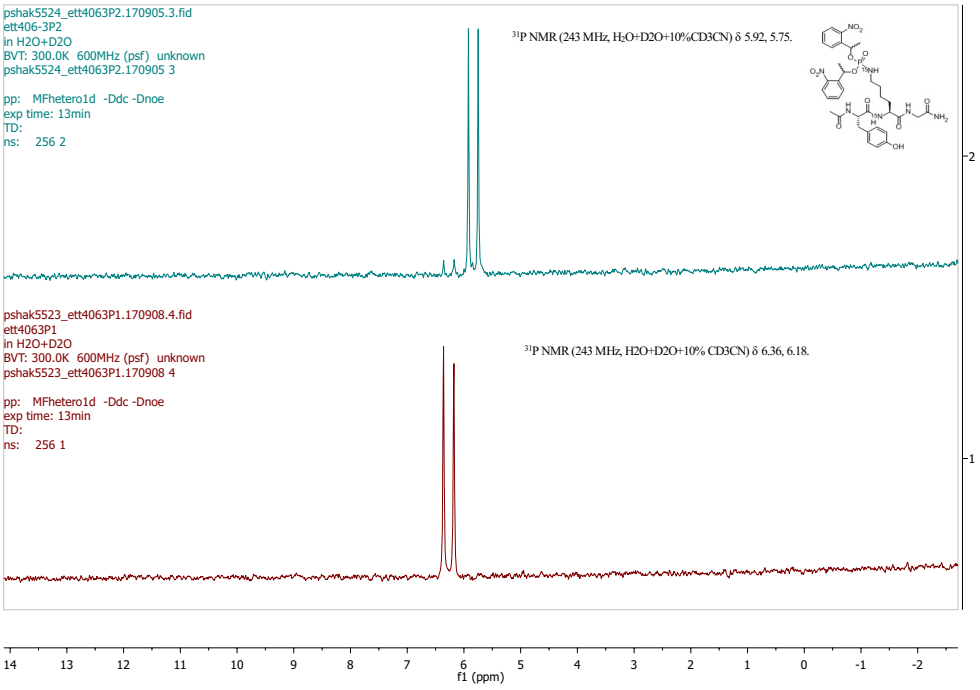

Figure A44: ^{31}P NMR spectra of peptide **15** (243 MHz, 0.1% TFA + D_2O + CD_3CN), isomers separated.

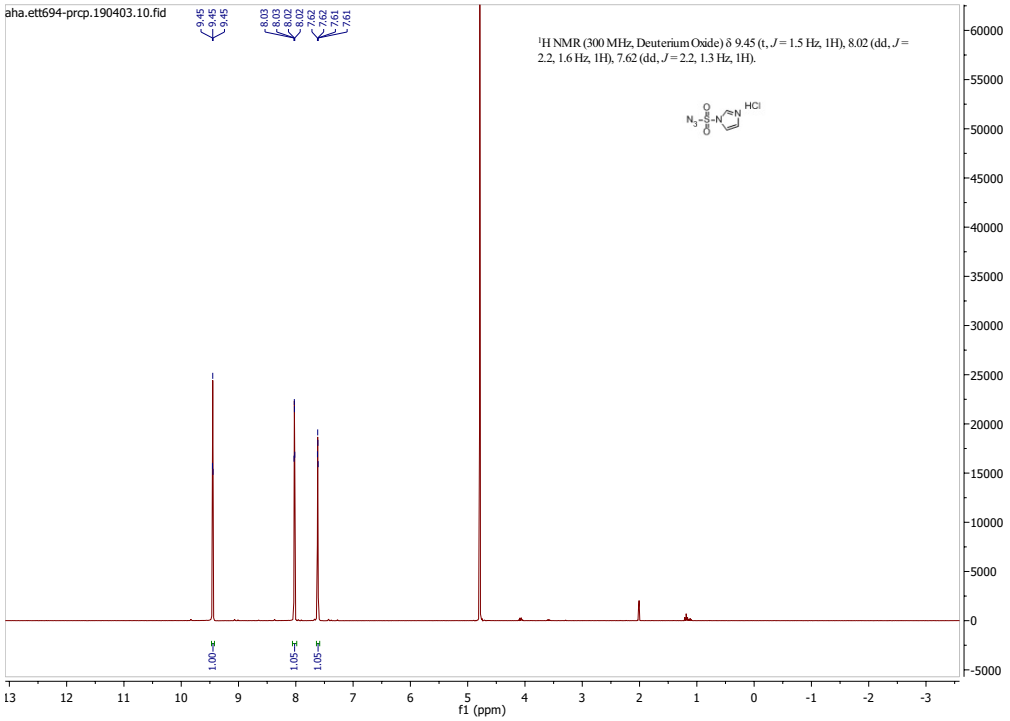

Figure A45: ^{1}H NMR spectrum of compound **17** (300 MHz, D_2O).

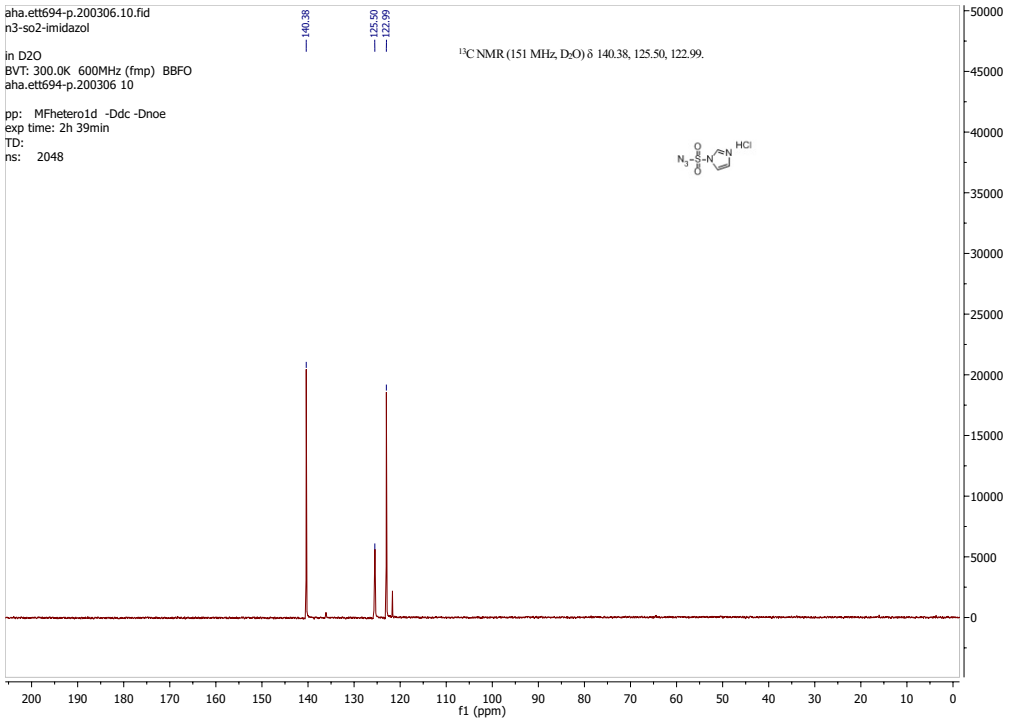

Figure A46: ^{13}C NMR spectrum of compound **17** (75 MHz, D_2O).

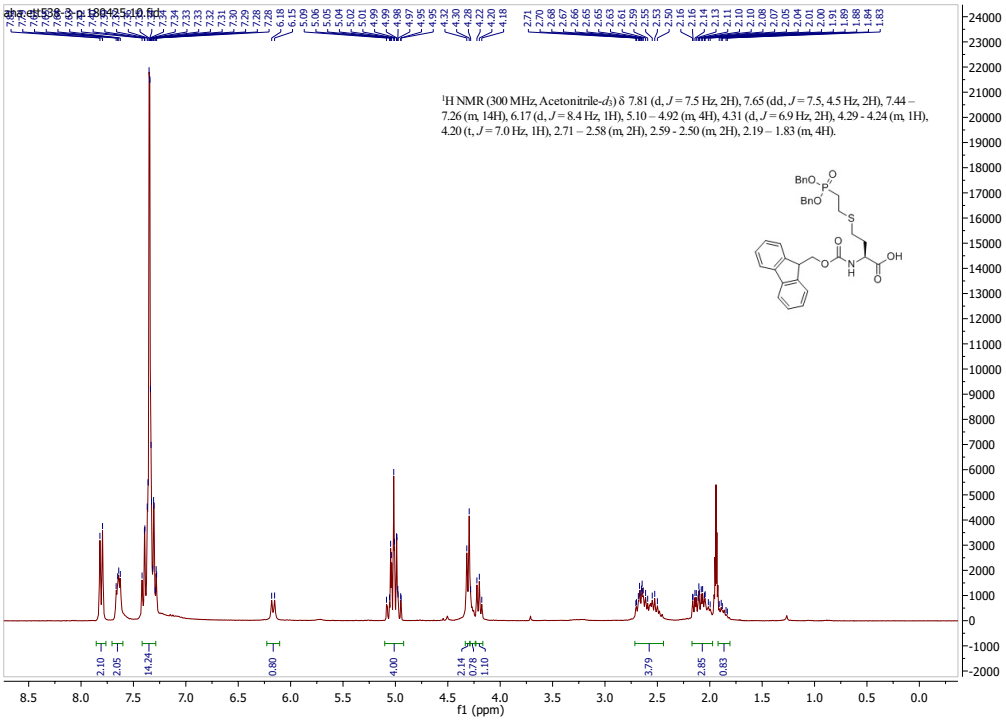

Figure A47: ^{1}H NMR spectrum of compound **18** (600 MHz, CD_3CN).

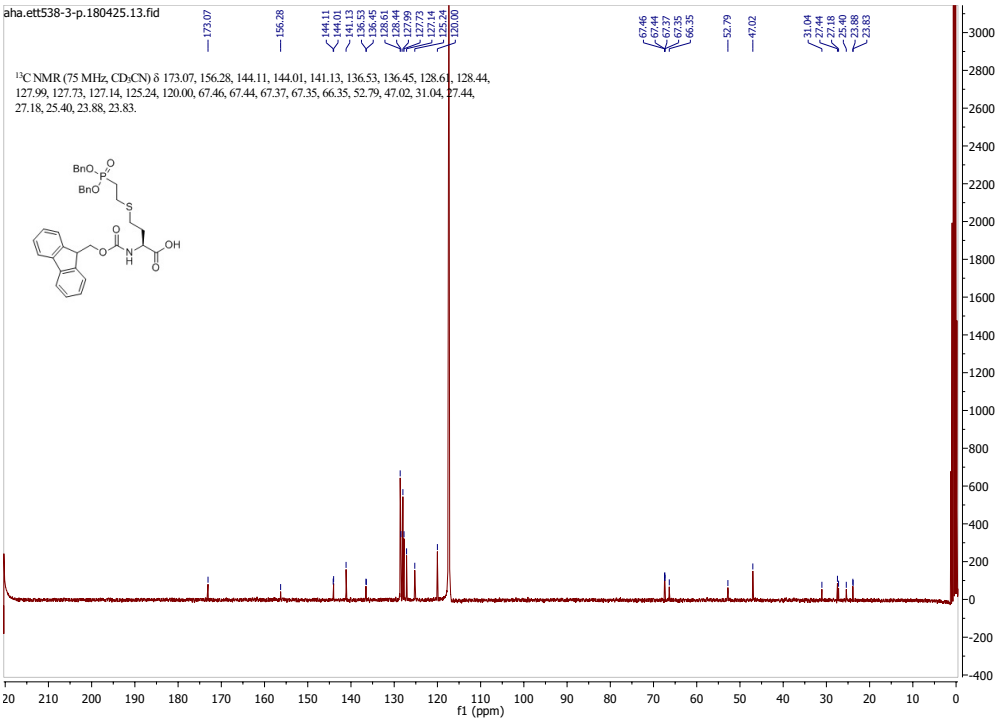

Figure A48: ^{13}C NMR spectrum of compound **18** (151 MHz, CD_3CN).

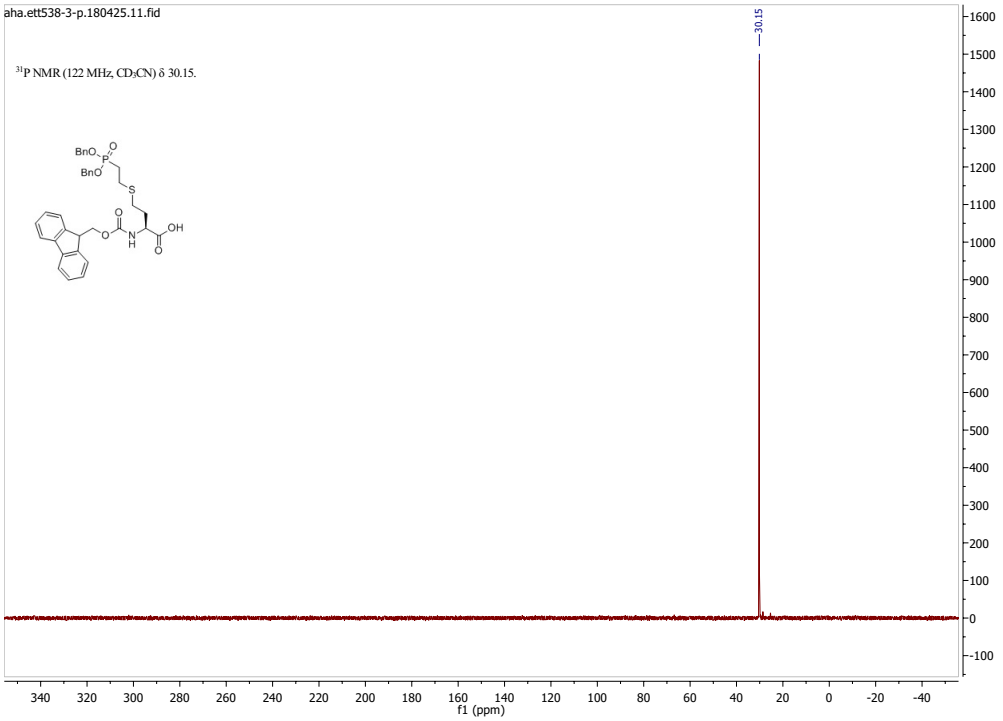

Figure A49: ^{31}P NMR spectrum of compound **18** (243 MHz, CD_3CN).

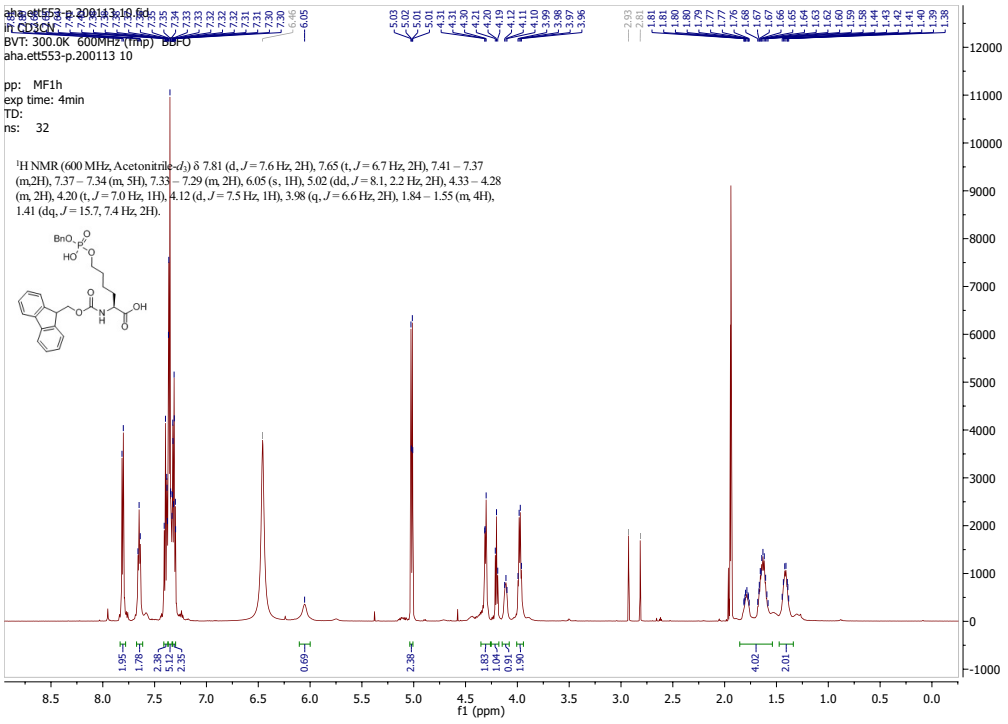

Figure A50: ^{1}H NMR spectrum of compound **19** (600 MHz, CD_3CN).

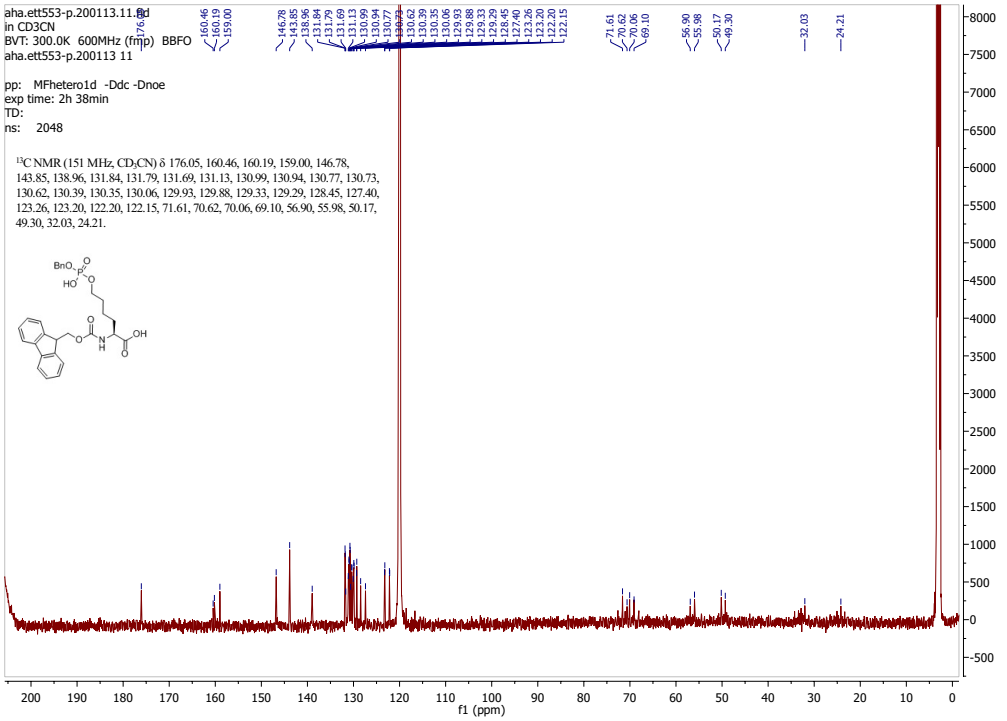

Figure A51: ^{13}C NMR spectrum of compound **19** (151 MHz, CD_3CN).

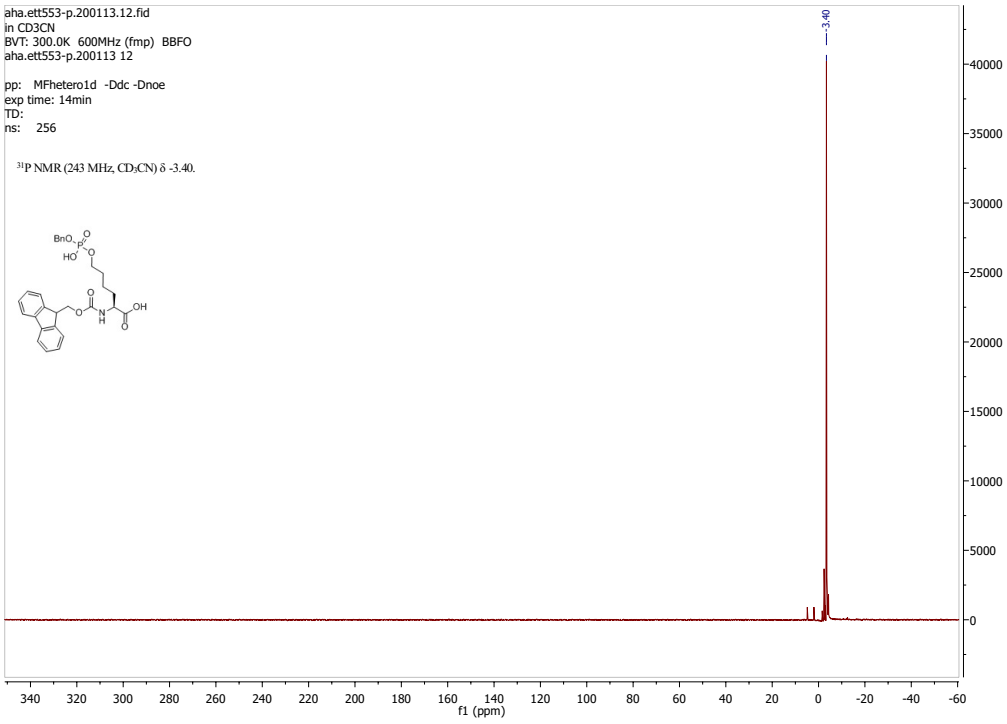

Figure A52: ^{31}P NMR spectrum of compound **19** (243 MHz, CD_3CN).

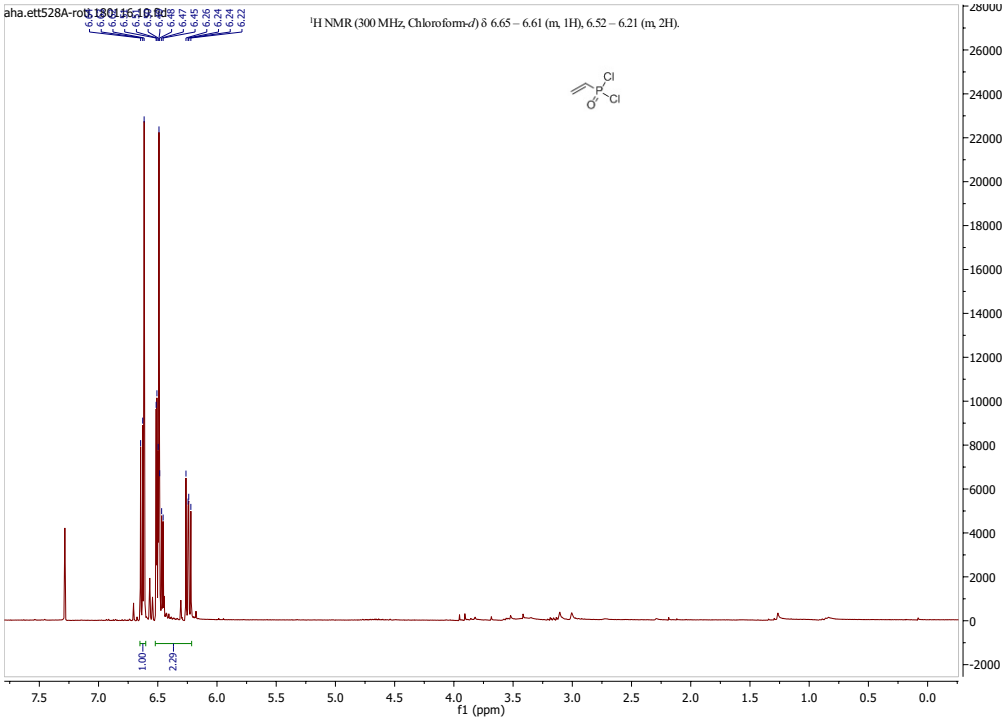

Figure A53: ^{1}H NMR spectrum of compound **20** (300 MHz, $CDCl_3$).

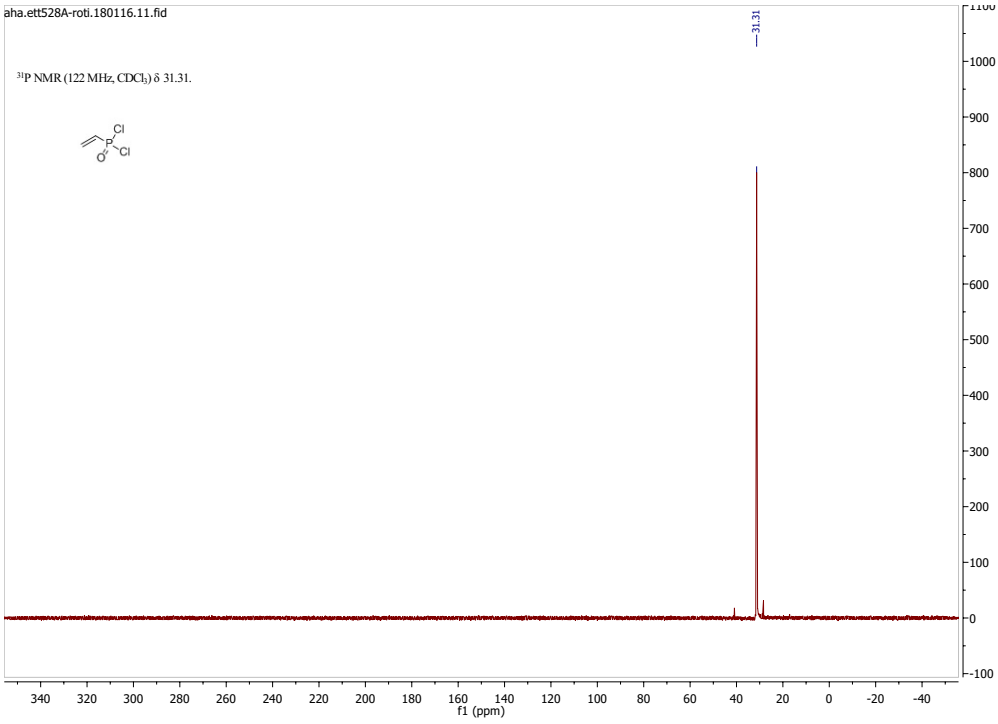

Figure A54: ^{31}P NMR spectrum of compound **20** (122 MHz, $CDCl_3$).

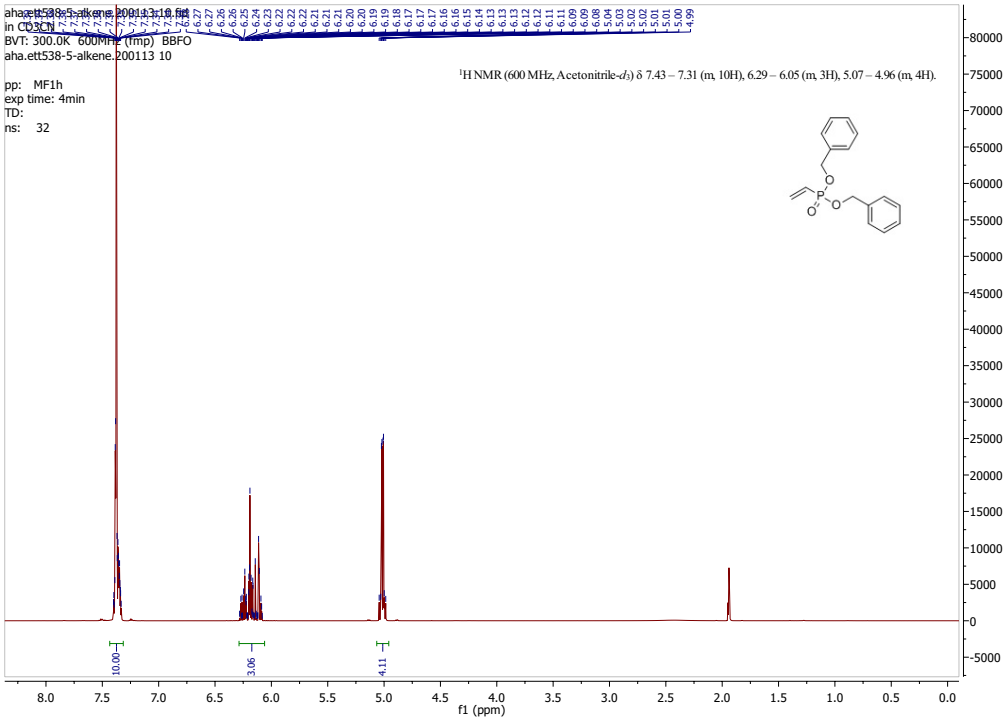

Figure A55: ^{1}H NMR spectrum of compound **21** (600 MHz, CD_3CN).

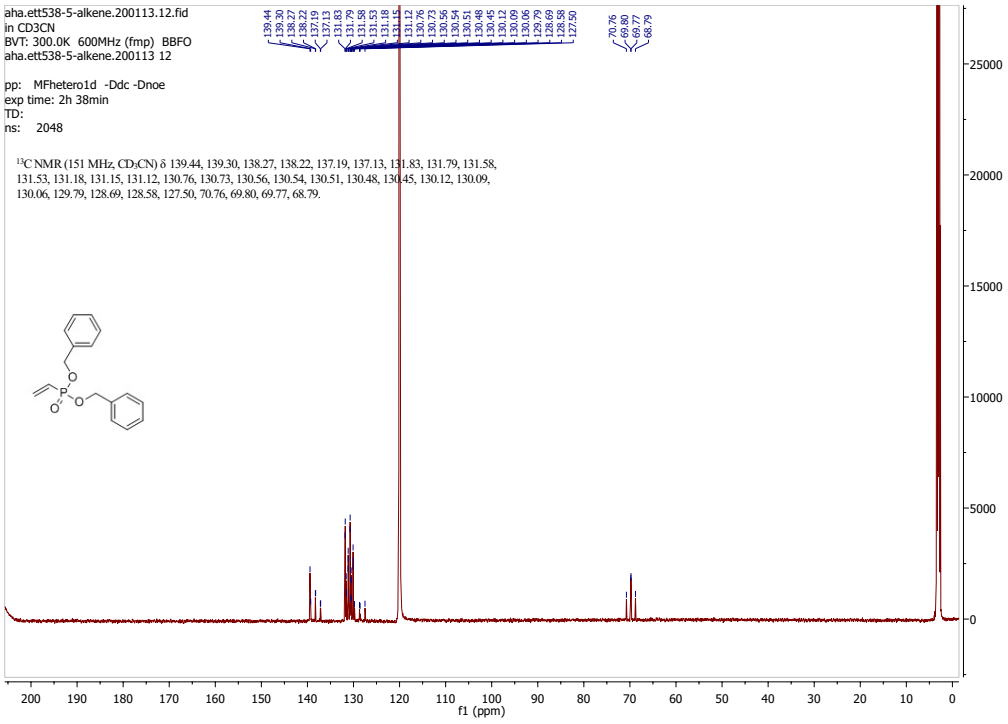

Figure A56: ^{13}C NMR spectrum of compound **21** (151 MHz, CD_3CN).

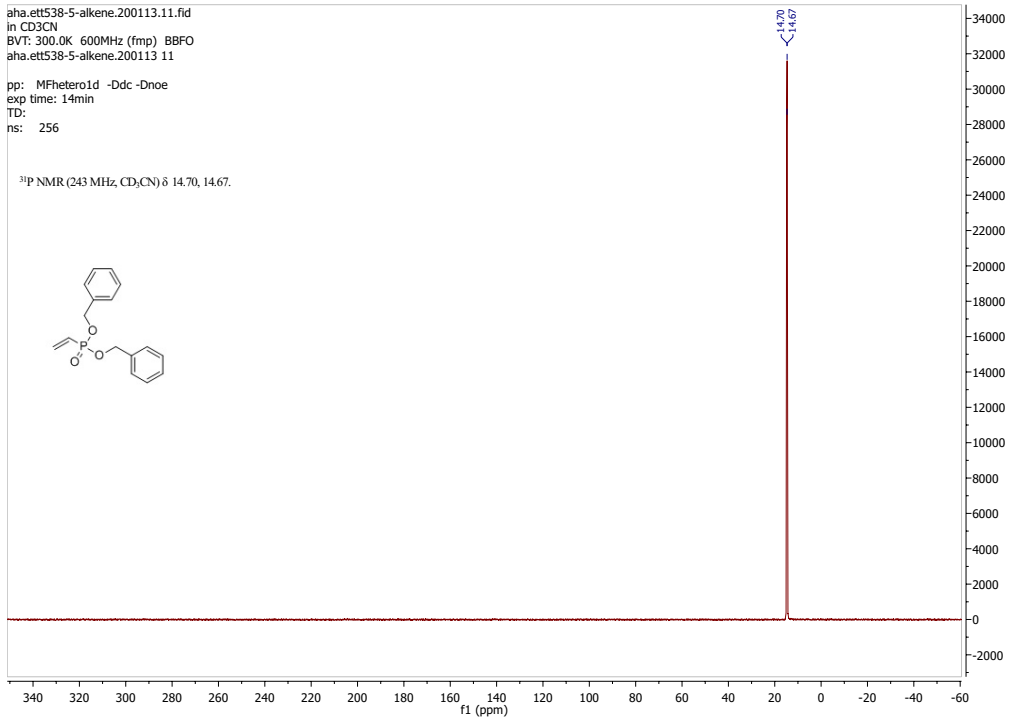

Figure A57: ^{31}P NMR spectrum of compound **21** (243 MHz, CD_3CN).

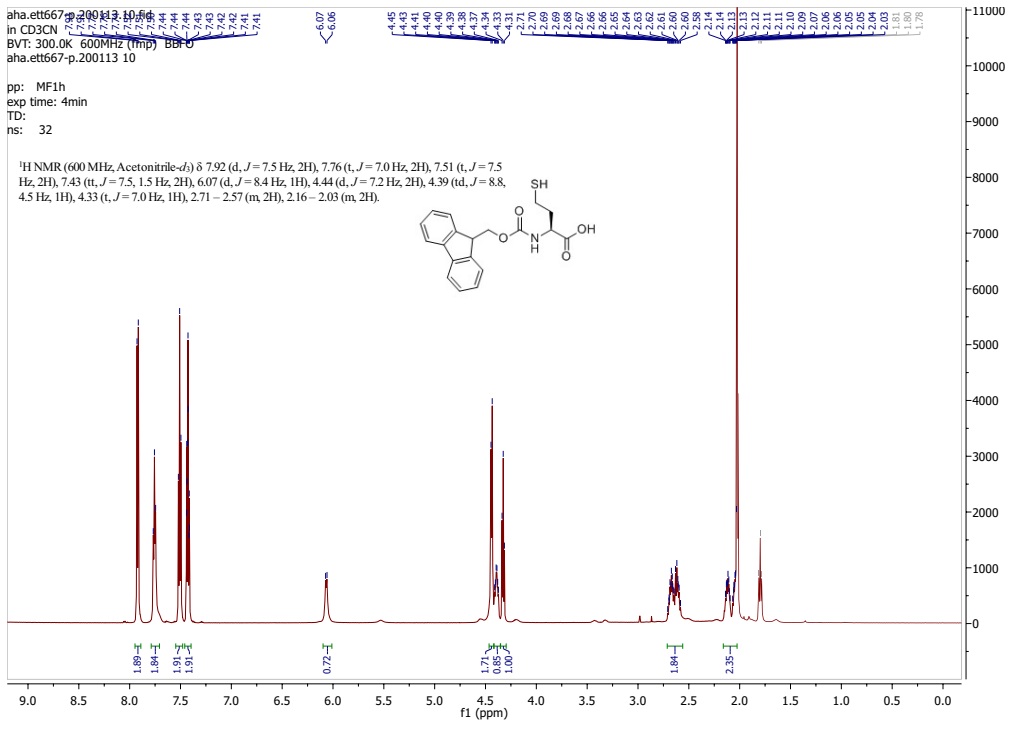

Figure A58: ^{1}H NMR spectrum of compound **22** (600 MHz, CD_3CN).

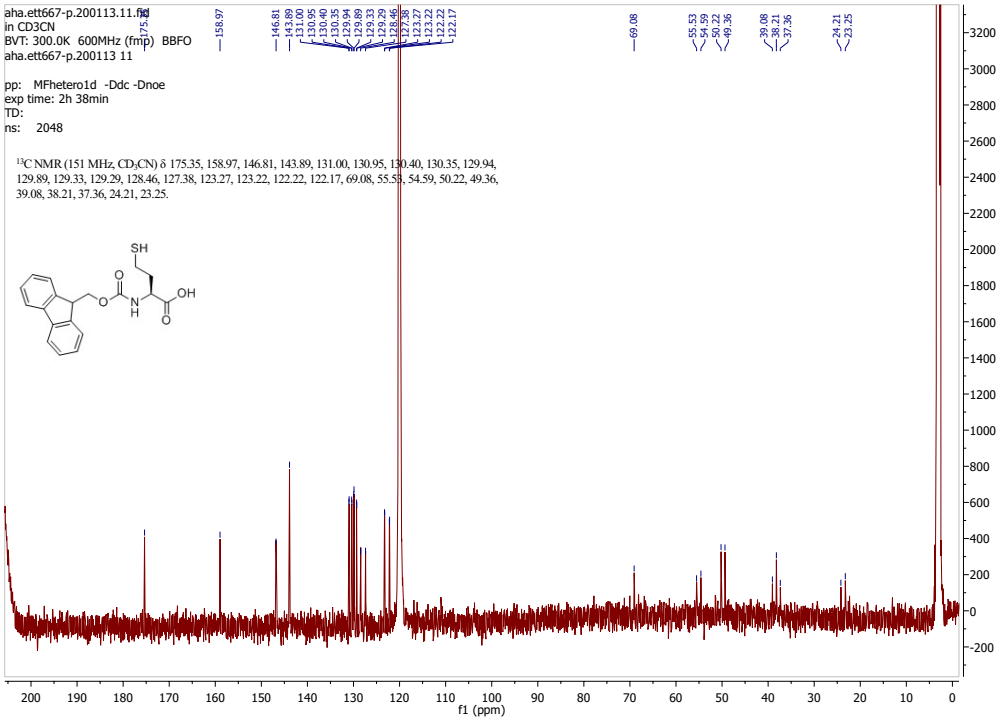

Figure A59: ^{13}C NMR spectrum of compound **22** (151 MHz, CD_3CN).

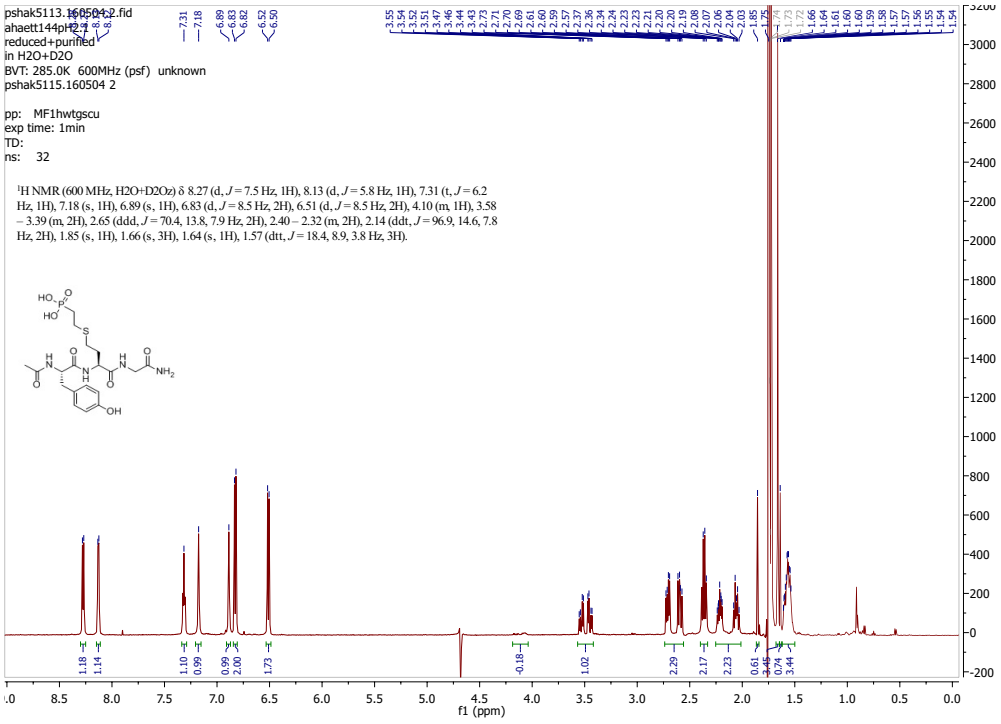

Figure A60: ^{1}H NMR spectrum of peptide **23** (600 MHz, H_2O + 10% D_2O).

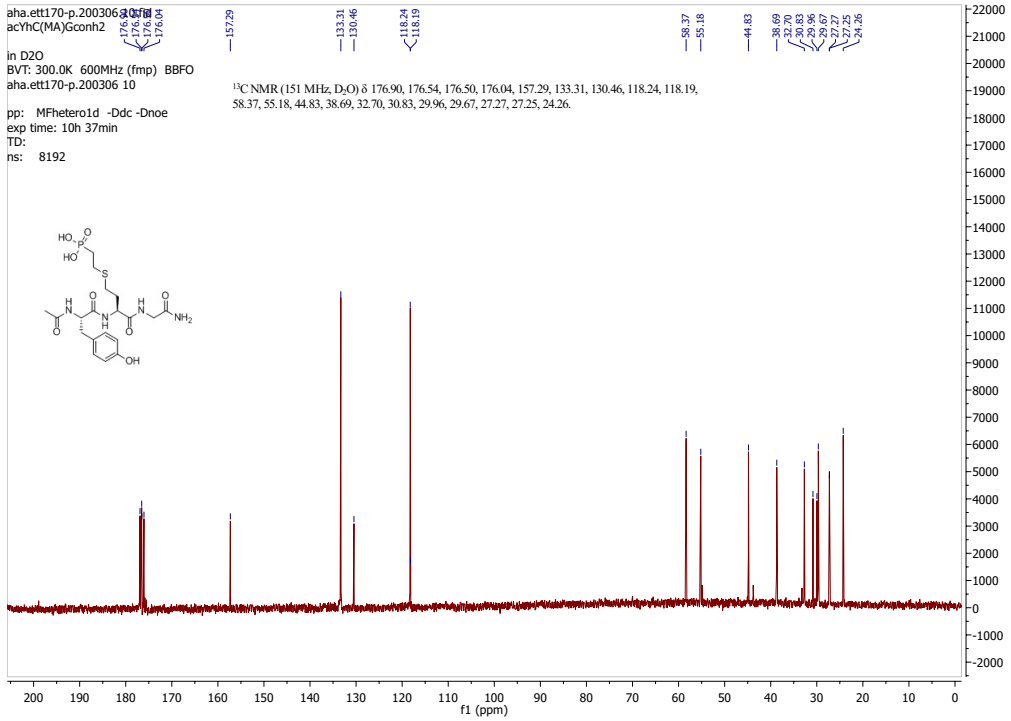

Figure A61: ^{13}C NMR spectrum of peptide **23** (151 MHz, H_2O + 10% D_2O).

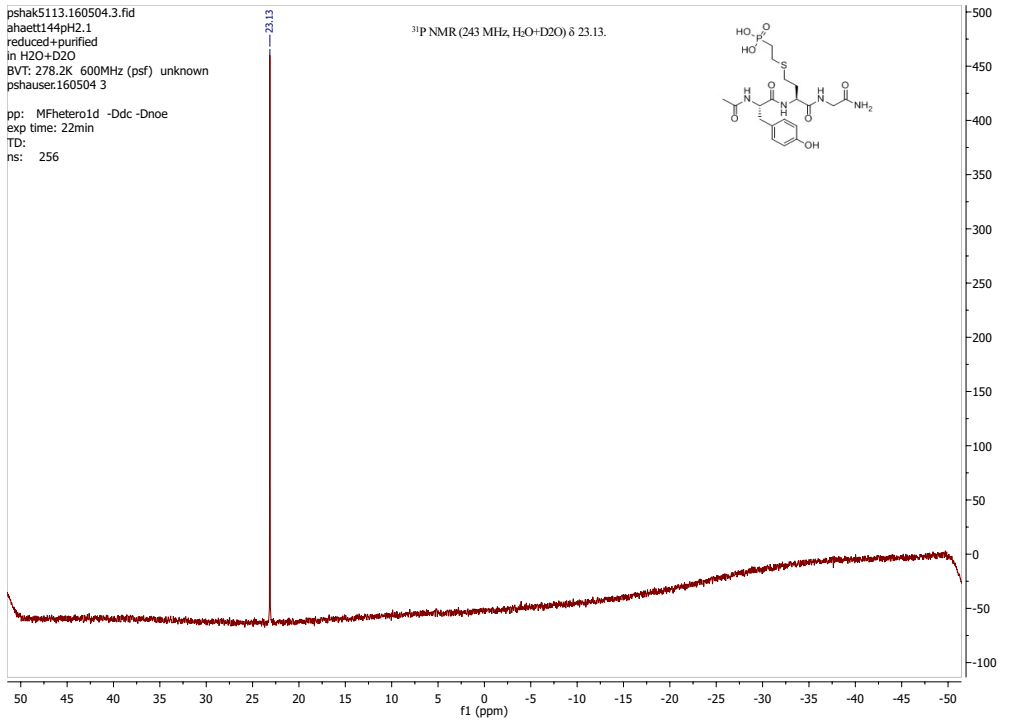

Figure A62: ^{31}P NMR spectrum of peptide **23** (243 MHz, H_2O + 10% D_2O).

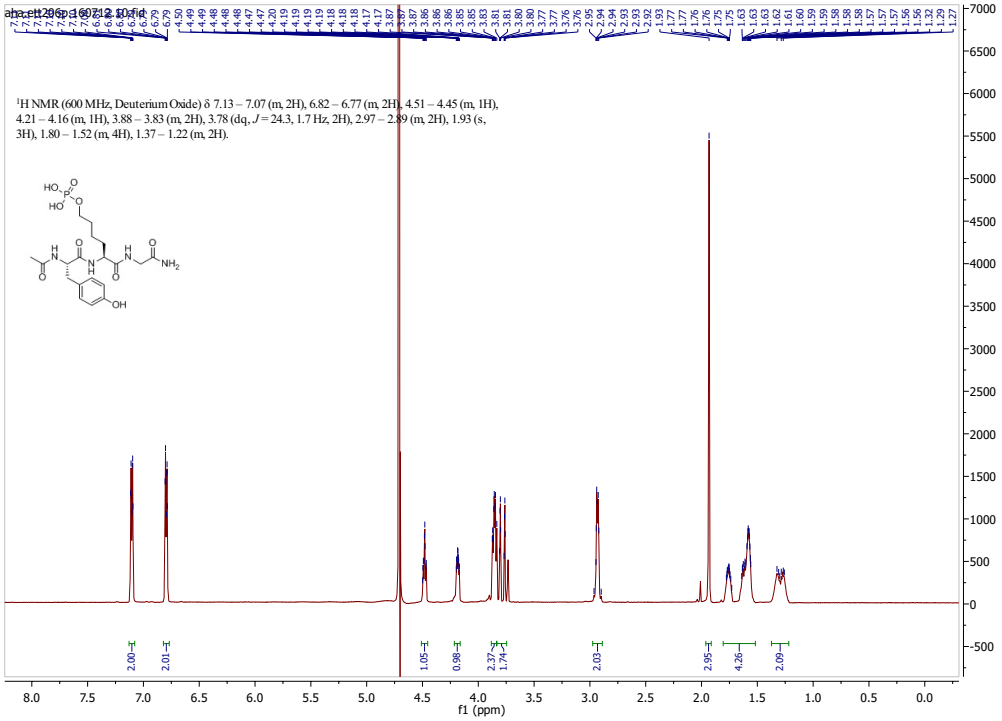

Figure A63: ^{1}H NMR spectrum of peptide **24** (600 MHz, D_2O).

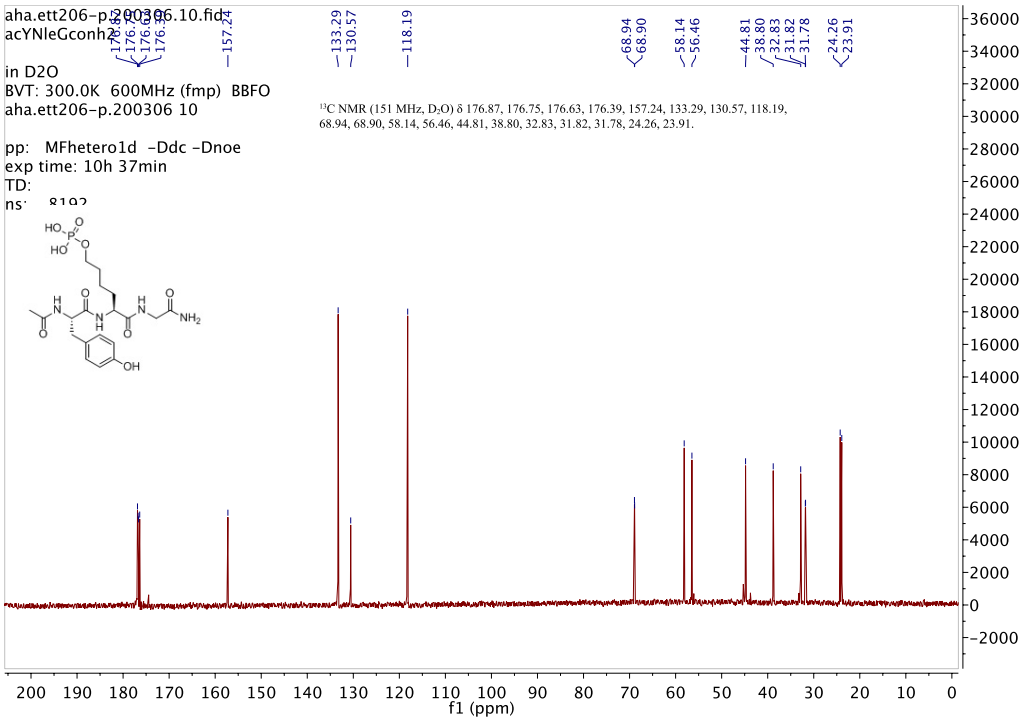

Figure A64: ^{13}C NMR spectrum of peptide **24** (151 MHz, D_2O).

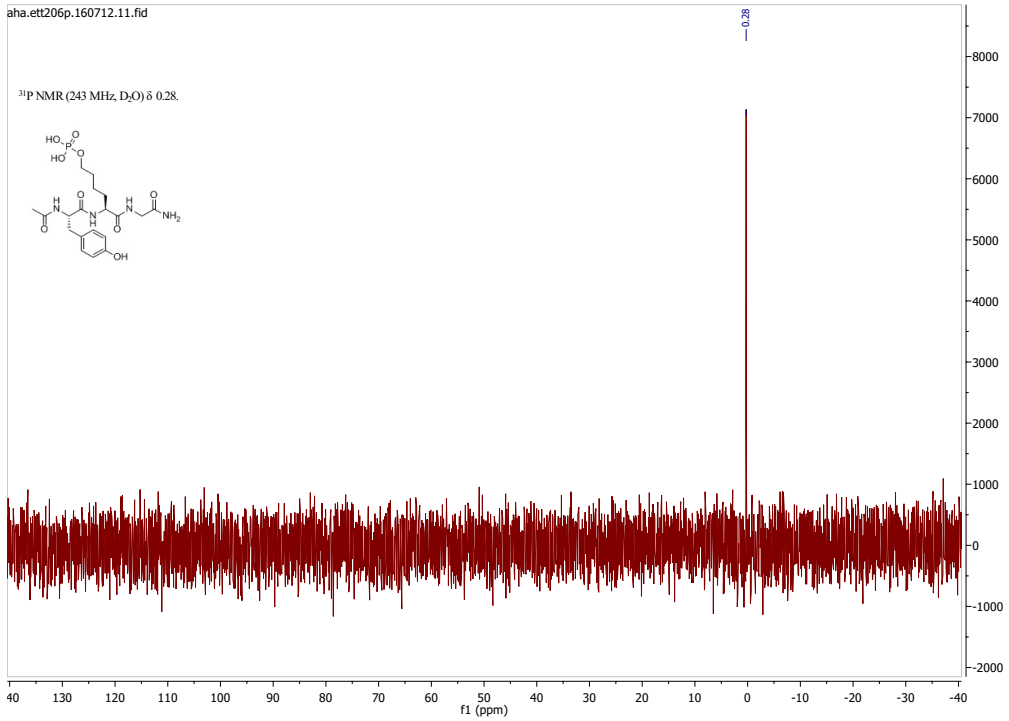

Figure A65: ^{31}P NMR spectrum of peptide **24** (243 MHz, D_2O).

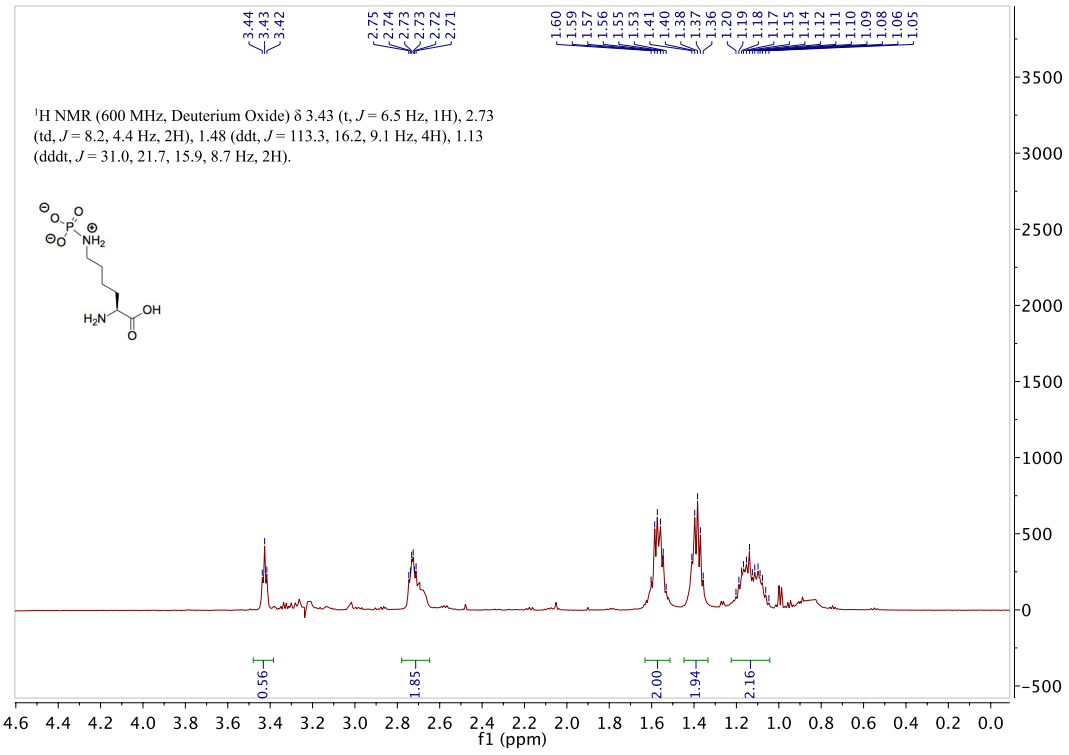

Figure A66: ^{1}H NMR spectrum of compound **25a** (600 MHz, D_2O).

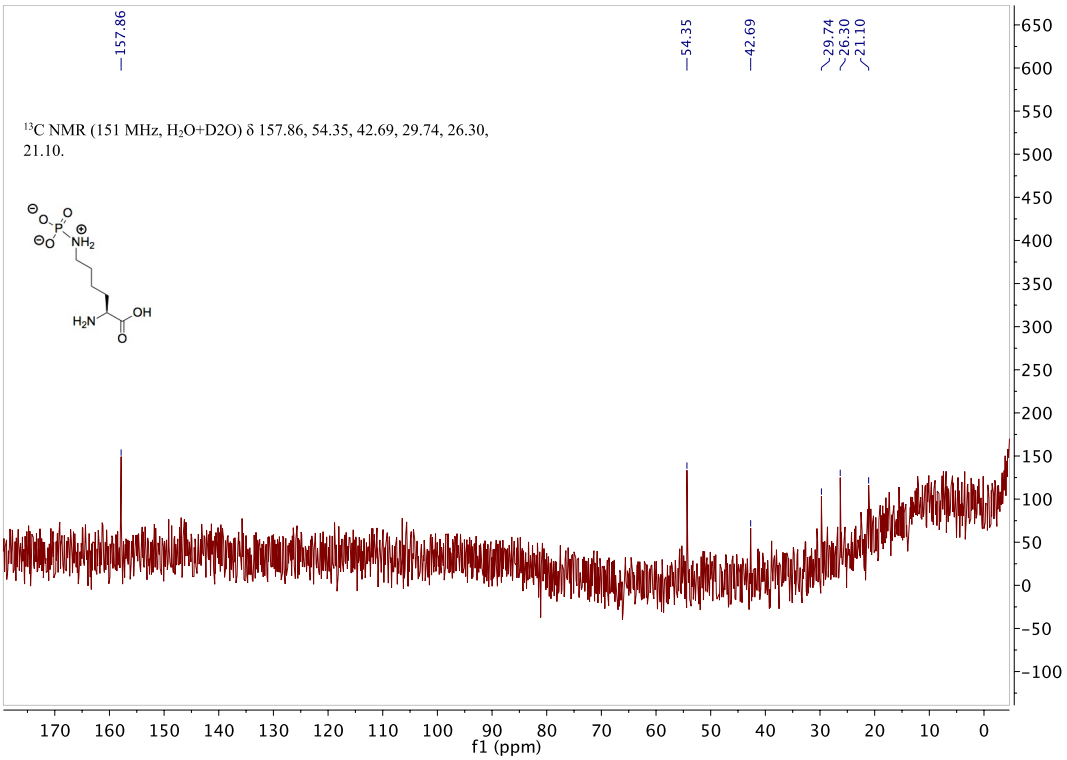

Figure A67: ^{13}C NMR spectrum of compound **25** (151 MHz, D_2O).

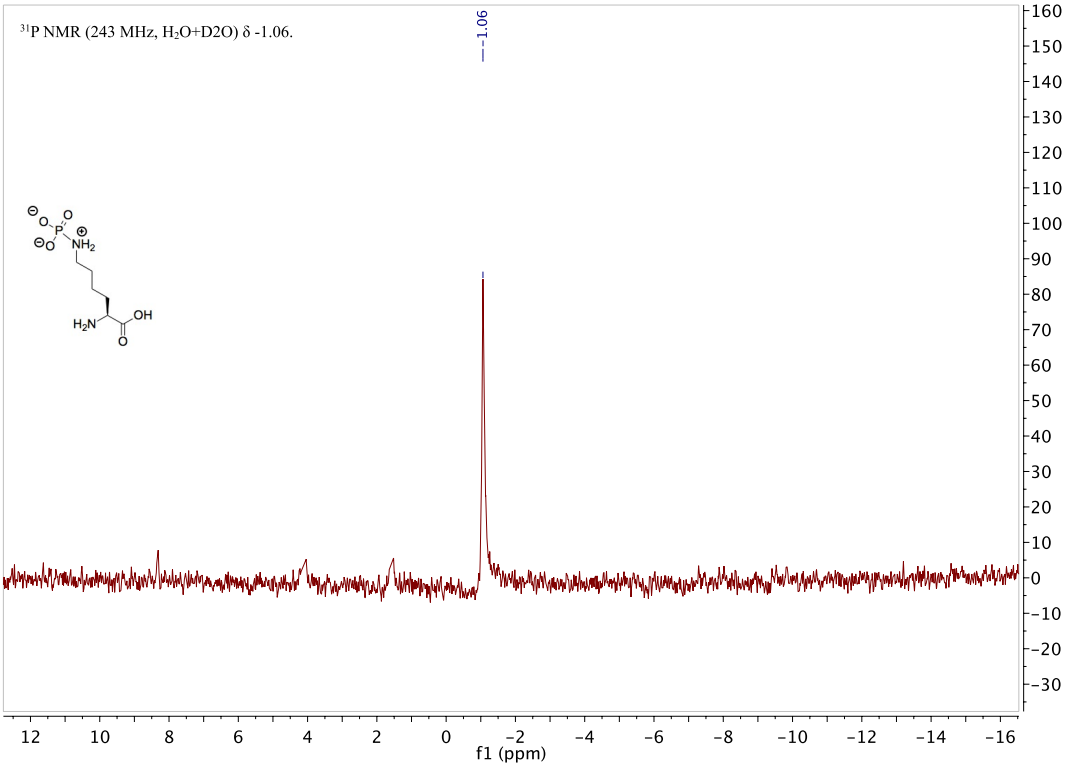

Figure A68: ^{31}P NMR spectrum of compound **25a** (243 MHz, D_2O).

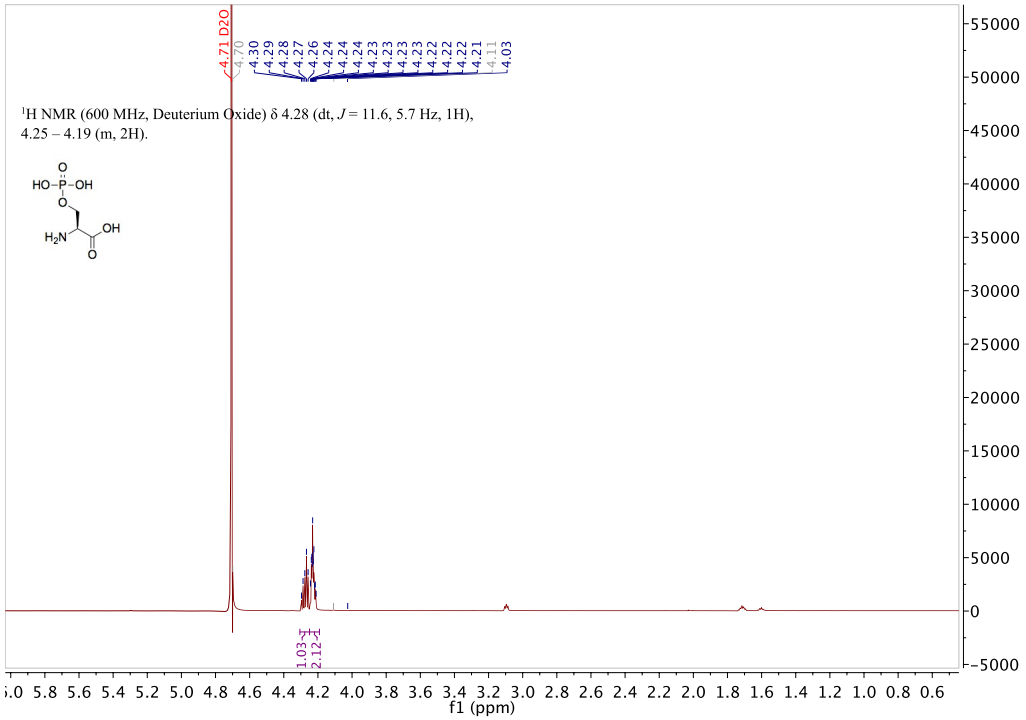

Figure A69: ^{1}H NMR spectrum of compound **25b** (600 MHz, D_2O).

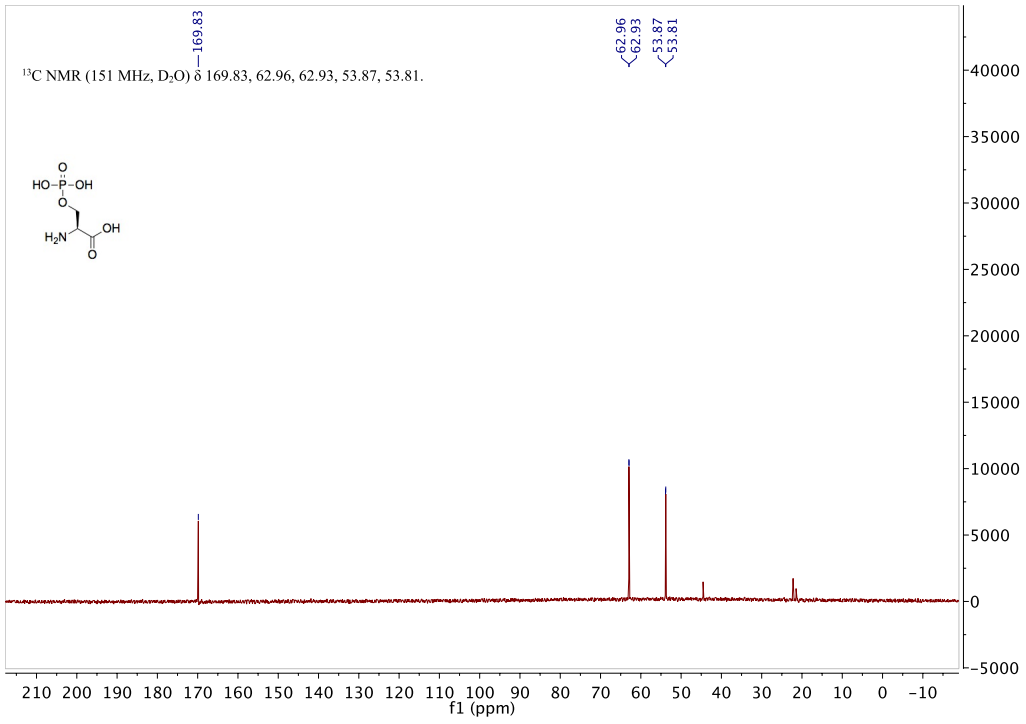

Figure A70: ^{13}C NMR spectrum of compound **25b** (151 MHz, D_2O).

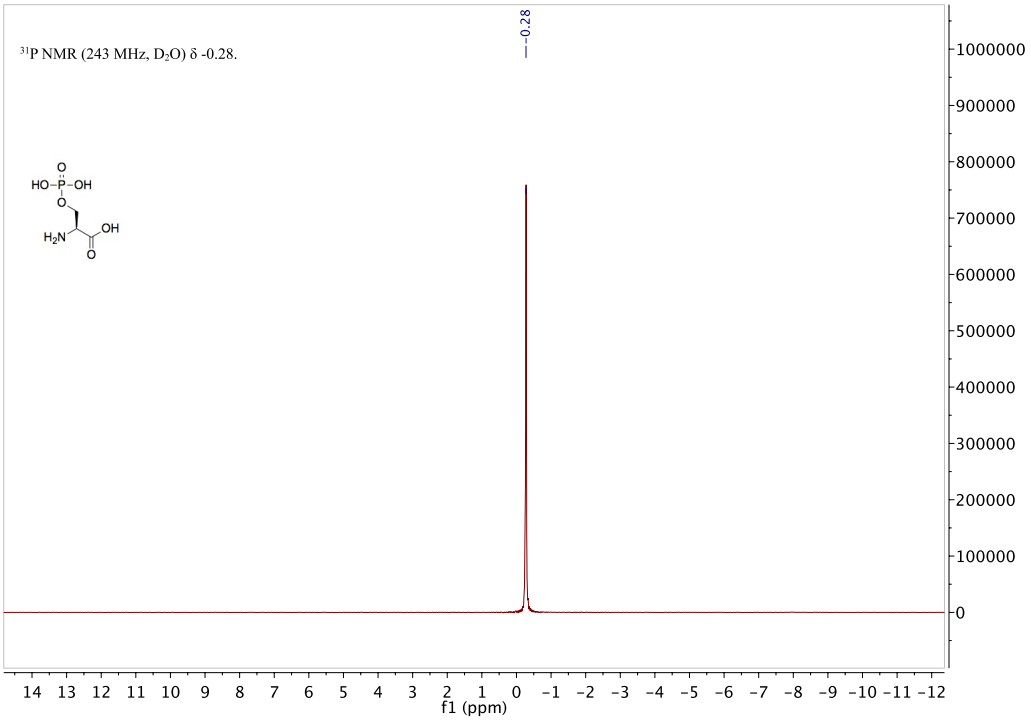

Figure A71: ^{31}P NMR spectrum of compound **25b** (243 MHz, D_2O).

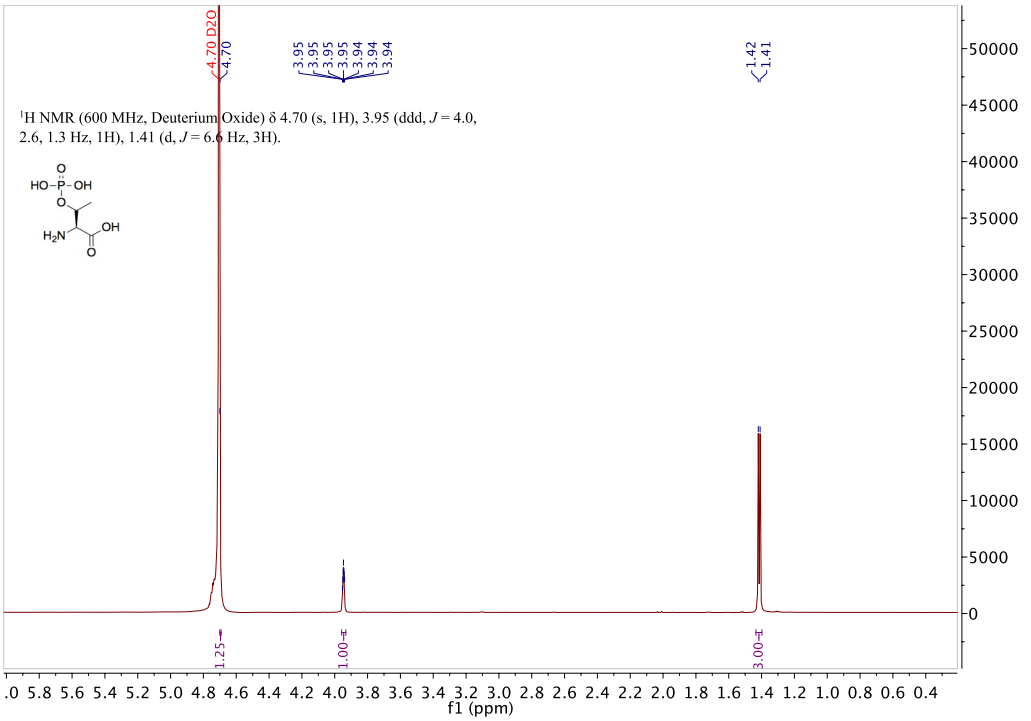

Figure A72: ^{1}H NMR spectrum of compound **25c** (600 MHz, D_2O).

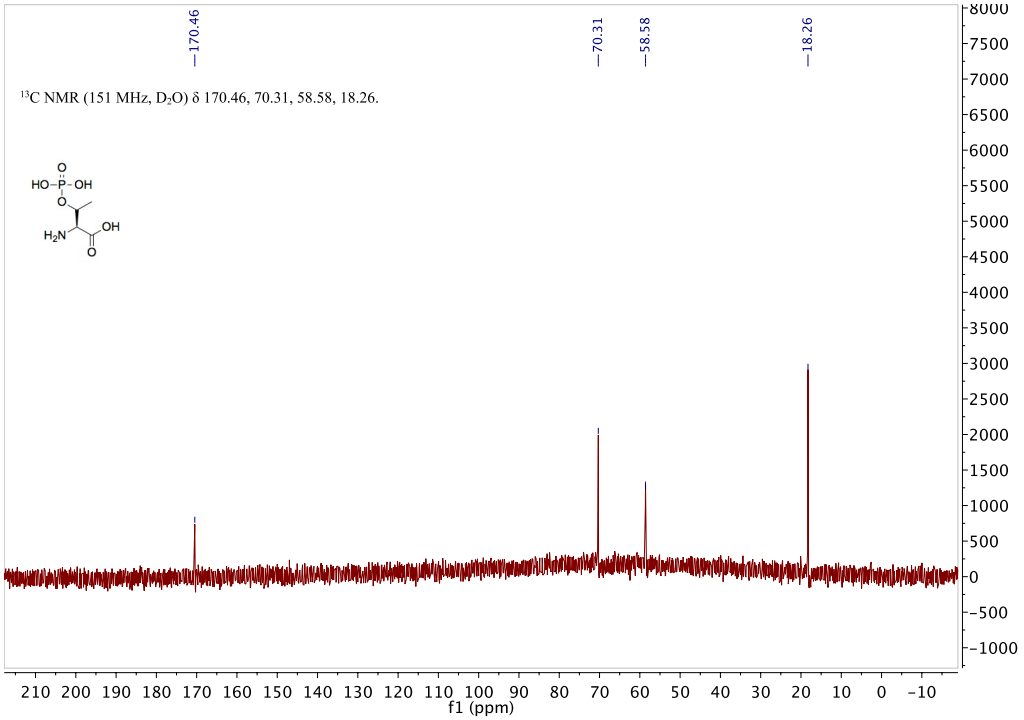

Figure A73: ^{13}C NMR spectrum of compound **25c** (151 MHz, D_2O).

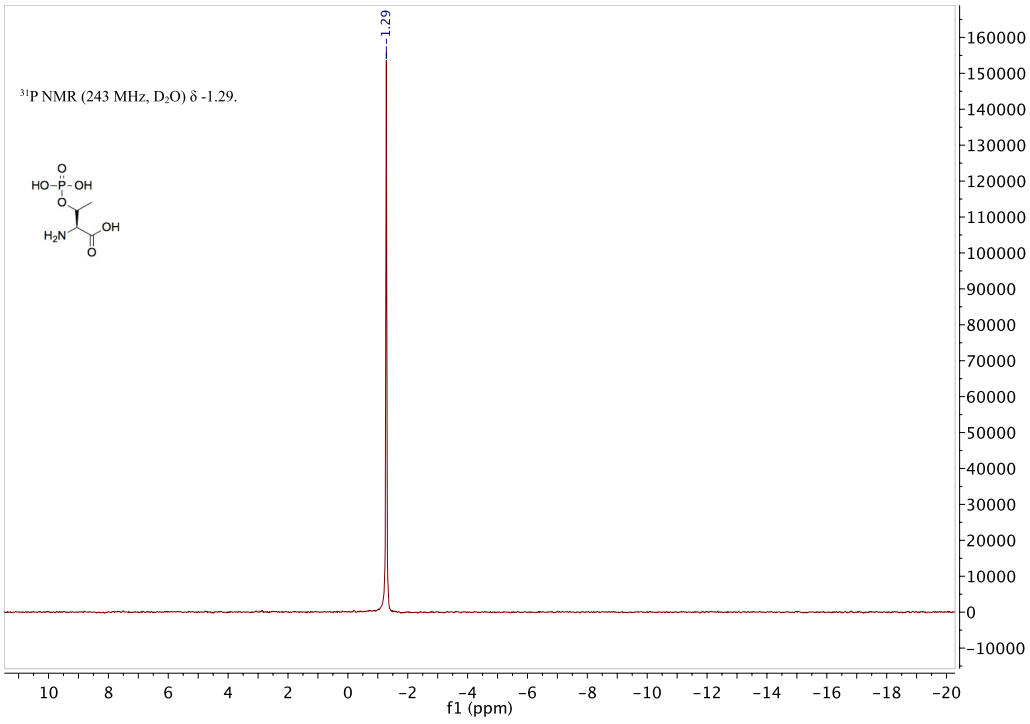

Figure A74: ^{31}P NMR spectrum of compound **25c** (243 MHz, D_2O).

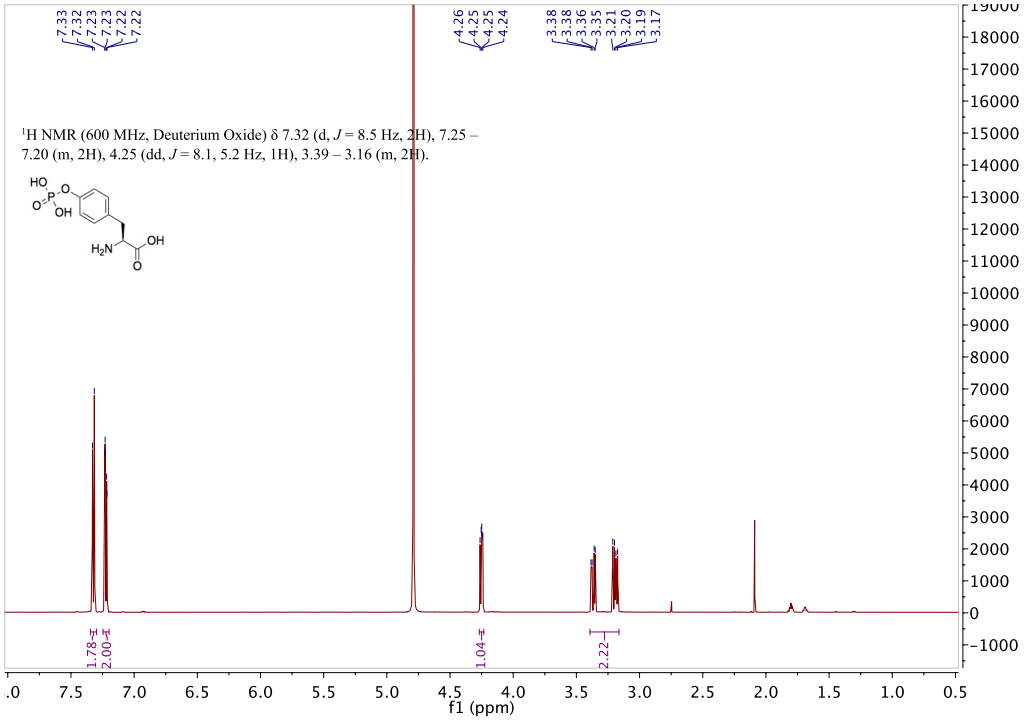

Figure A75: ^{1}H NMR spectrum of compound **25d** (600 MHz, D_2O).

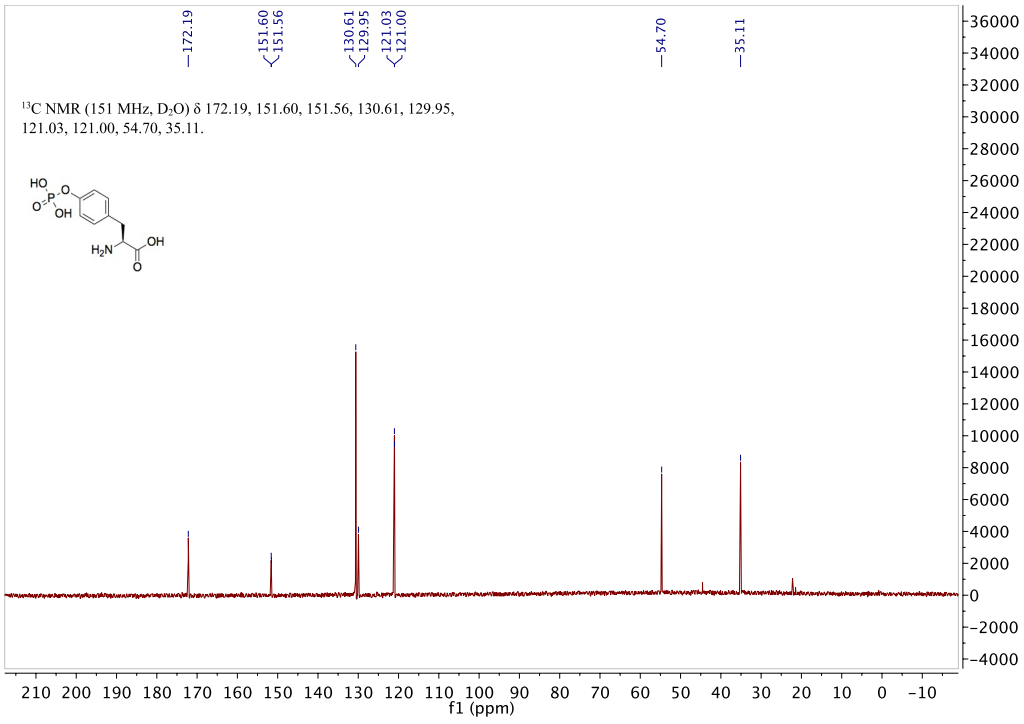

Figure A76: ^{13}C NMR spectrum of compound **25d** (151 MHz, D_2O).

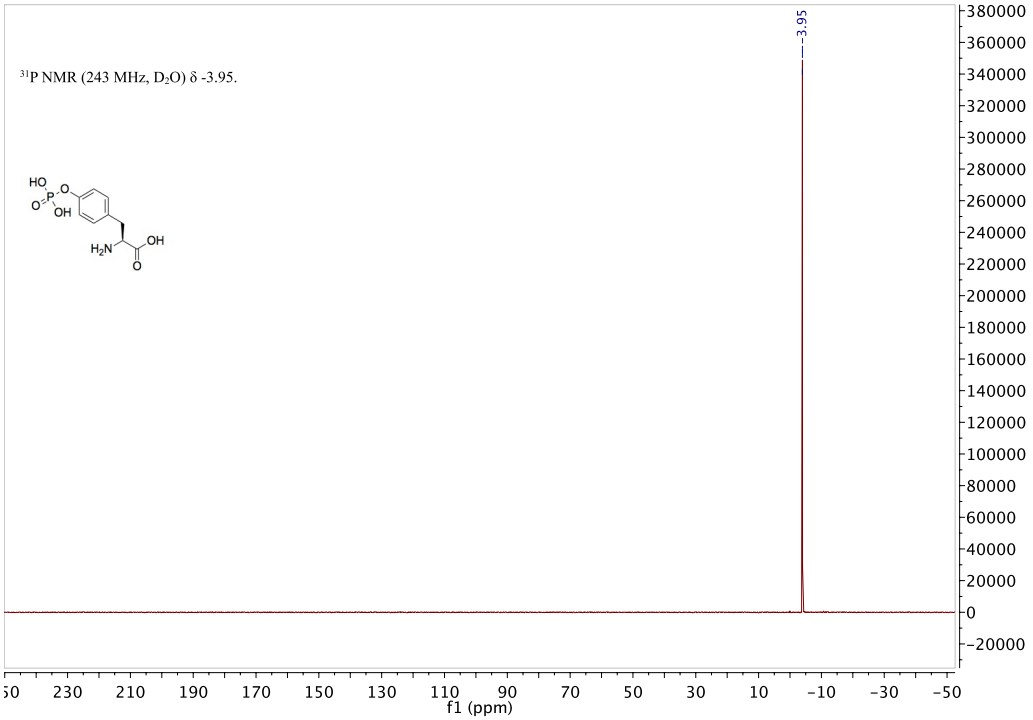

Figure A77: ^{31}P NMR spectrum of compound **25d** (243 MHz, D_2O).

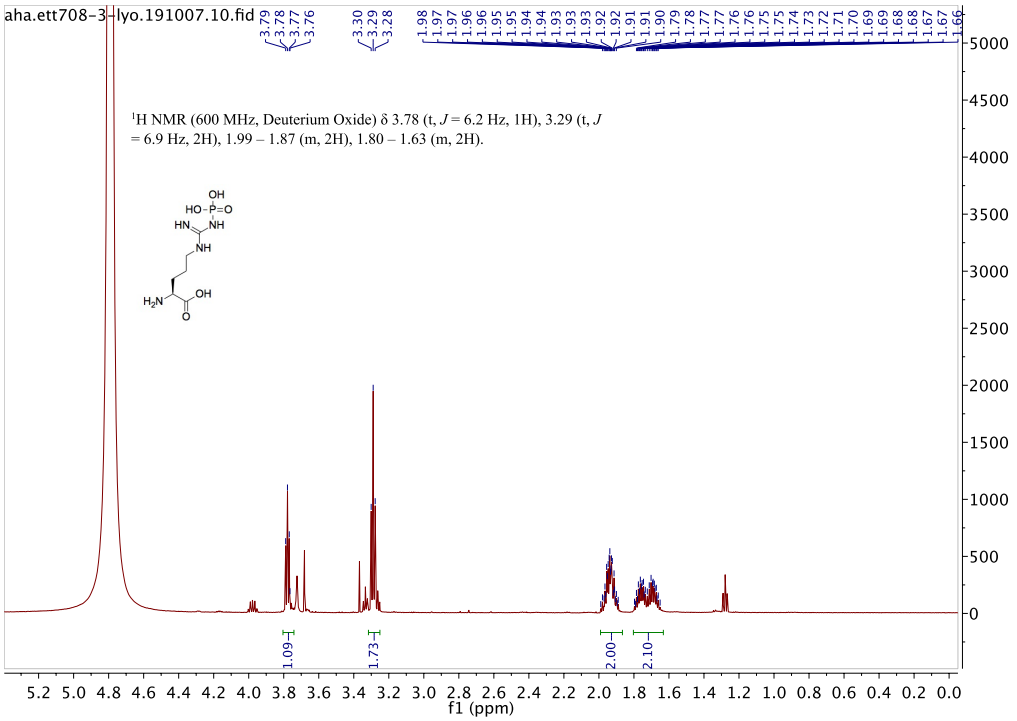

Figure A78: ^{1}H NMR spectrum of compound **25e** (600 MHz, D_2O).

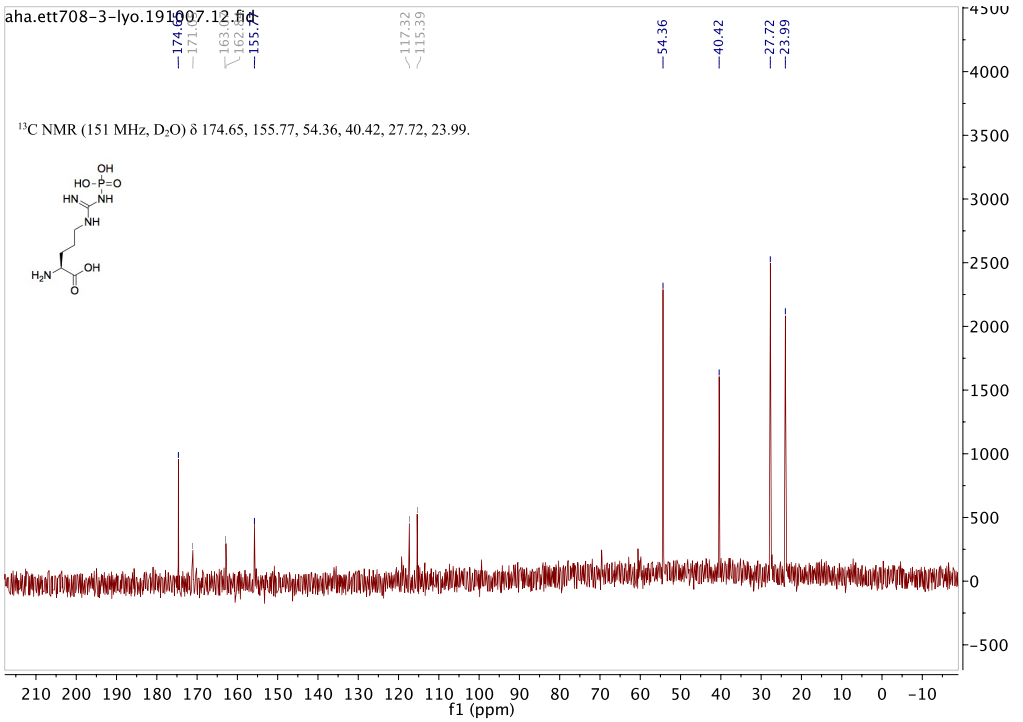

Figure A79: ^{13}C NMR spectrum of compound **25e** (151 MHz, D_2O).

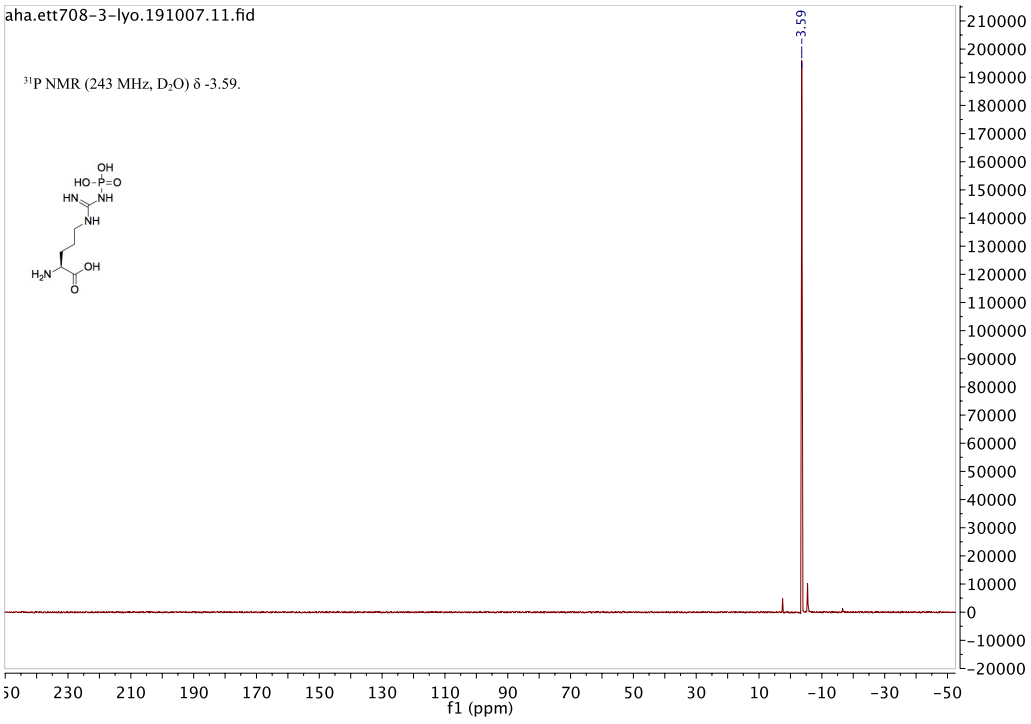

Figure A80: ^{31}P NMR spectrum of compound **25e** (243 MHz, D_2O).

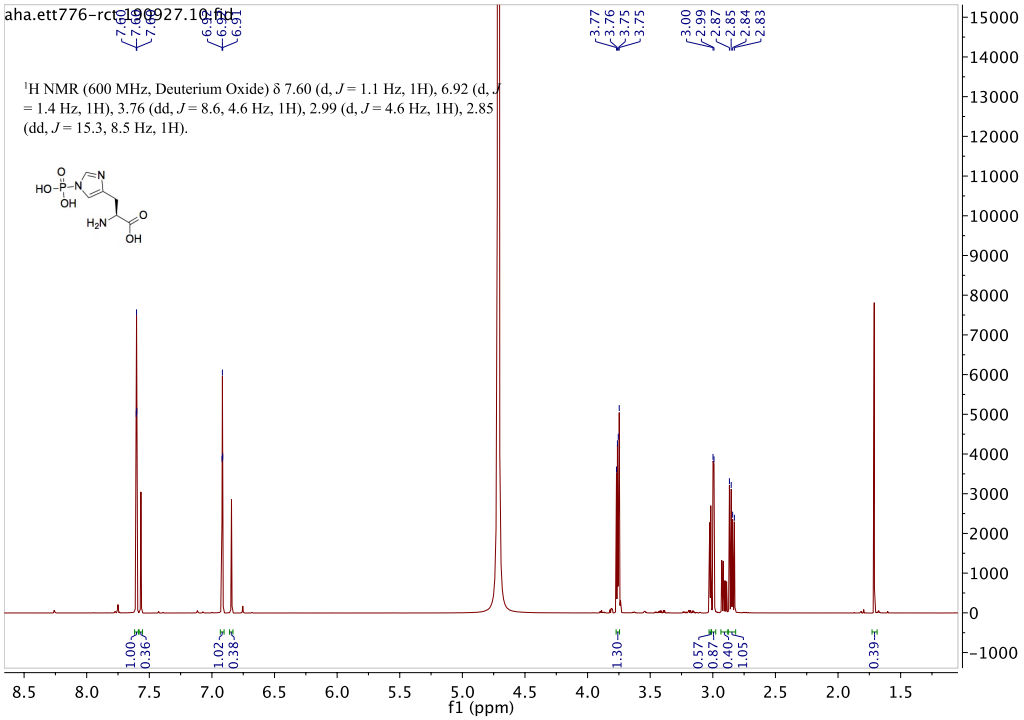

Figure A81: ^{1}H NMR spectrum of compound **25f** (600 MHz, D_2O).

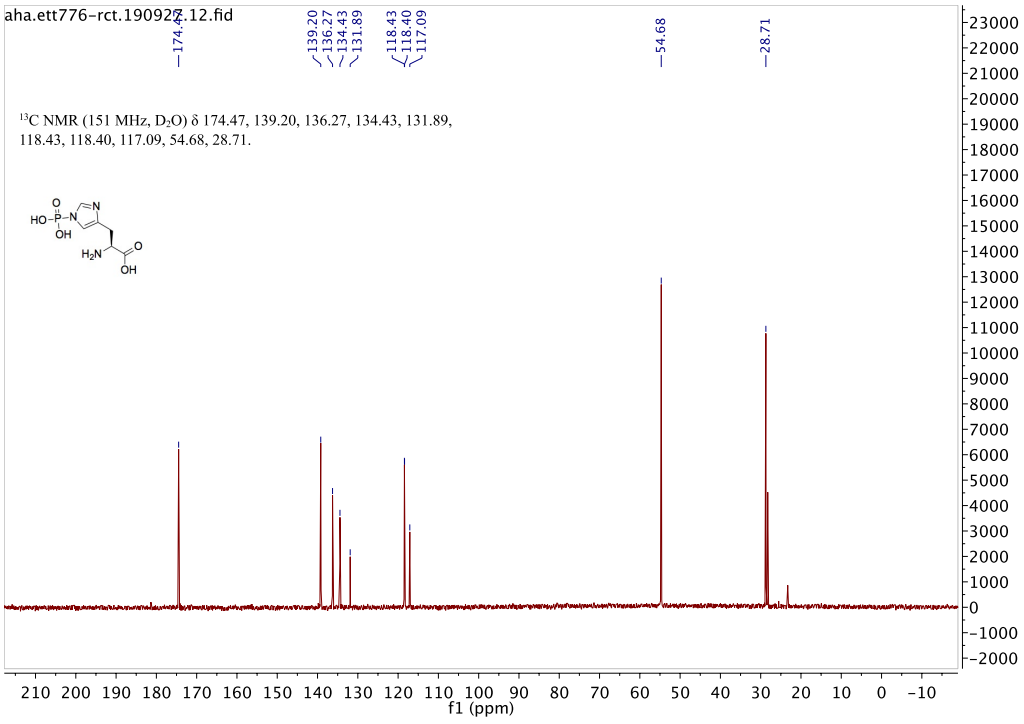

Figure A82: ^{13}C NMR spectrum of compound **25f** (151 MHz, D_2O).

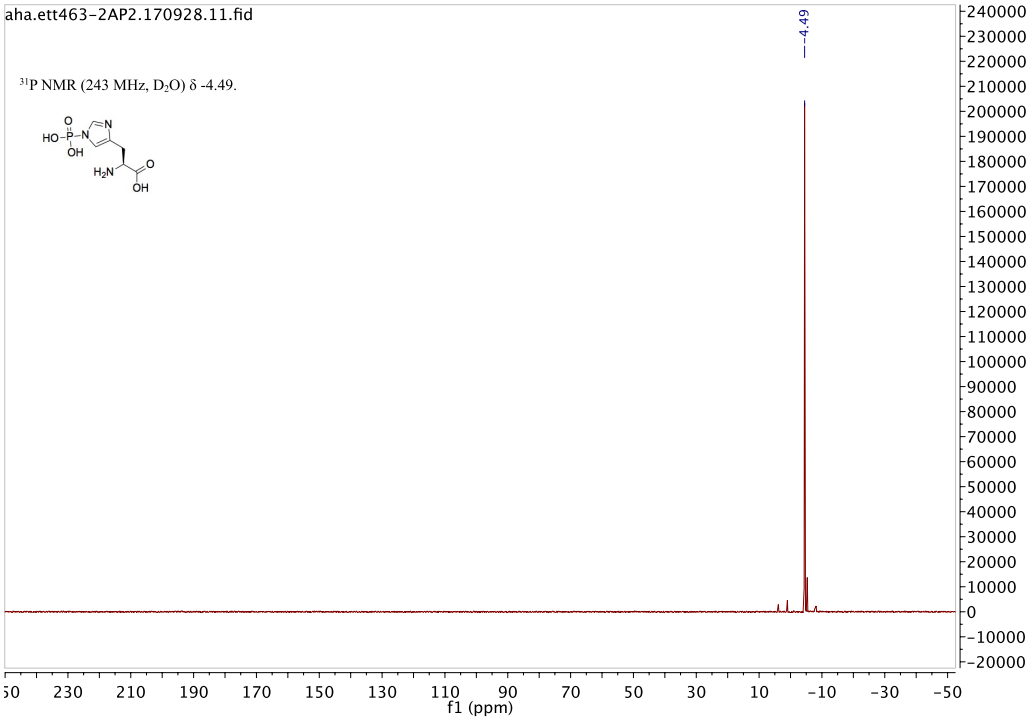

Figure A83: ^{31}P NMR spectrum of compound **25f** (243 MHz, D_2O).

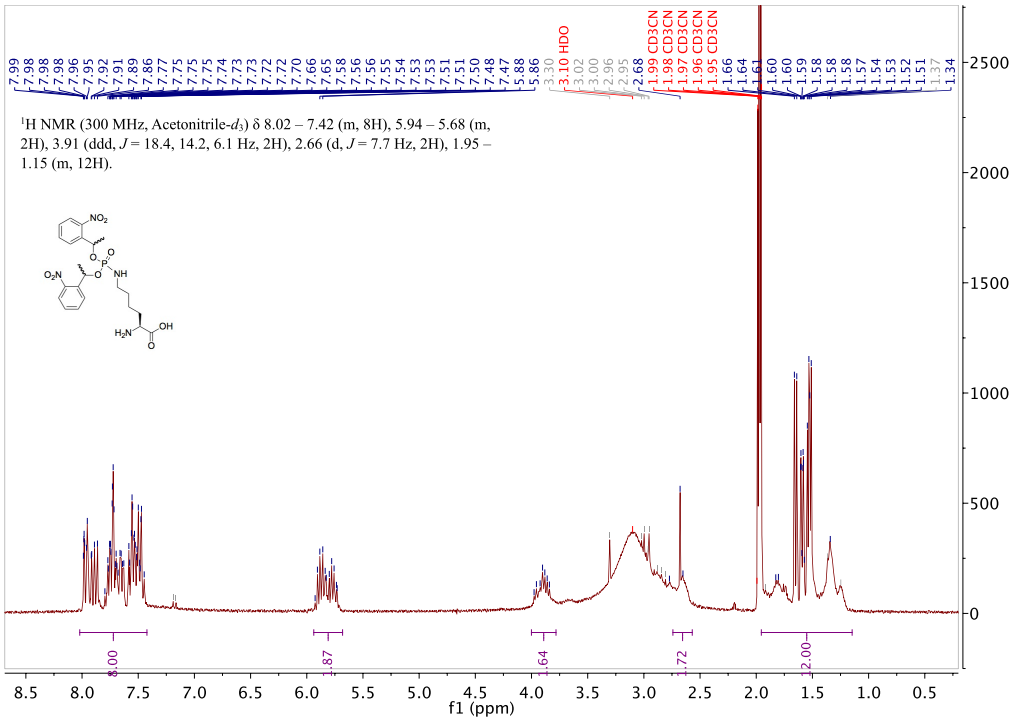

Figure A84: ^{1}H NMR spectrum of compound **30** (300 MHz, CD_3CN).

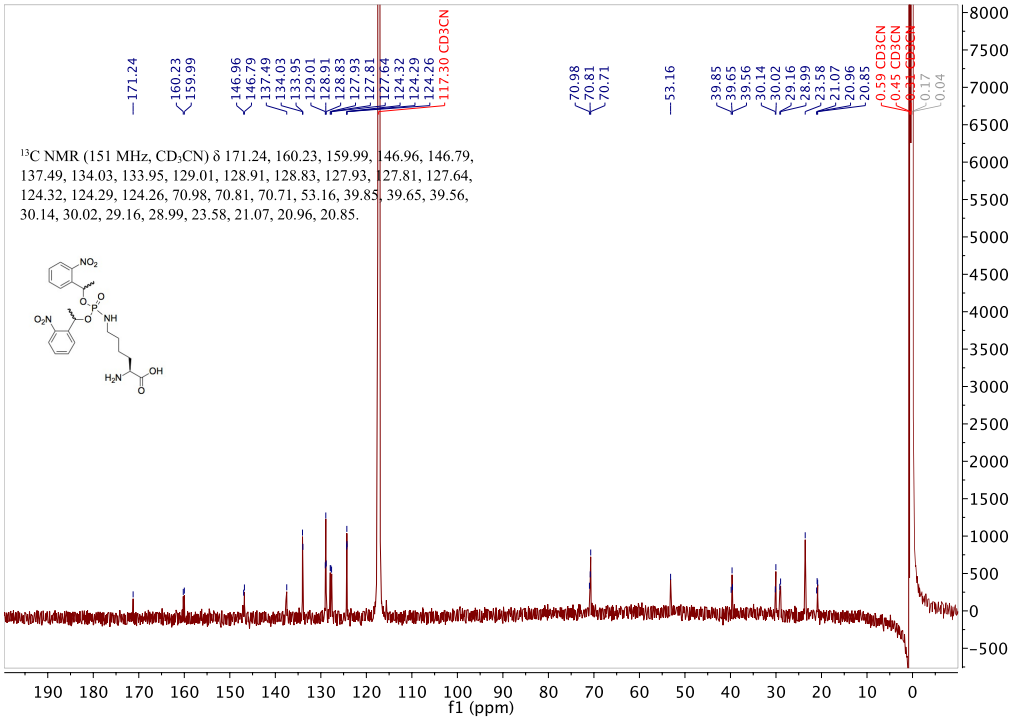

Figure A85: ^{13}C NMR spectrum of compound **30** (151 MHz, CD_3CN).

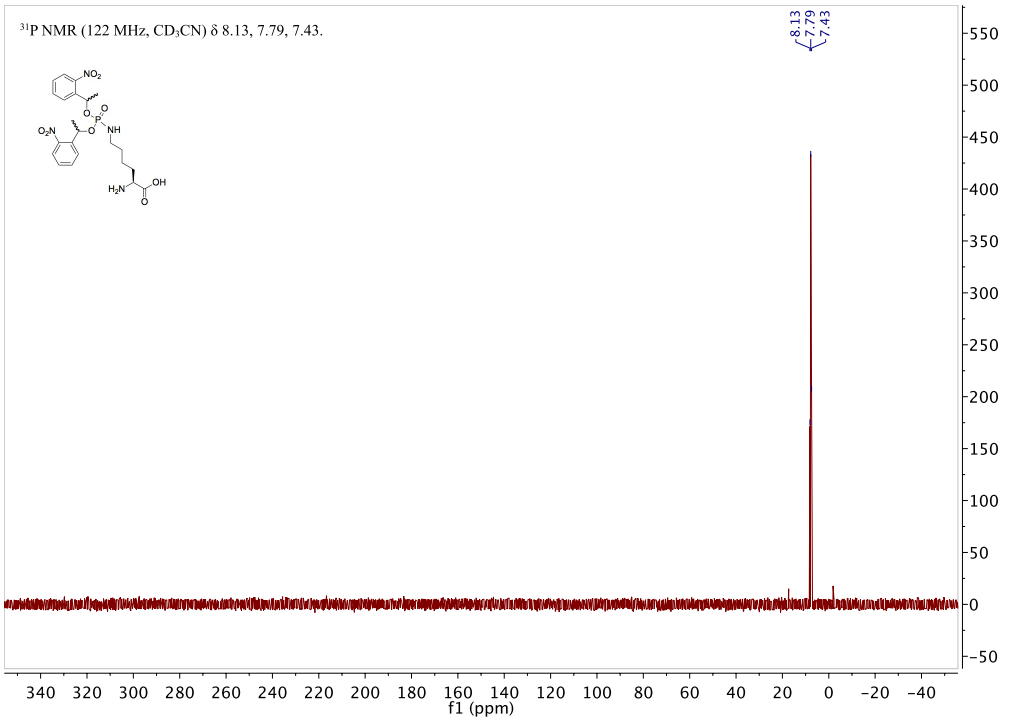

Figure A86: ^{31}P NMR spectrum of compound **30** (122 MHz, CD_3CN).

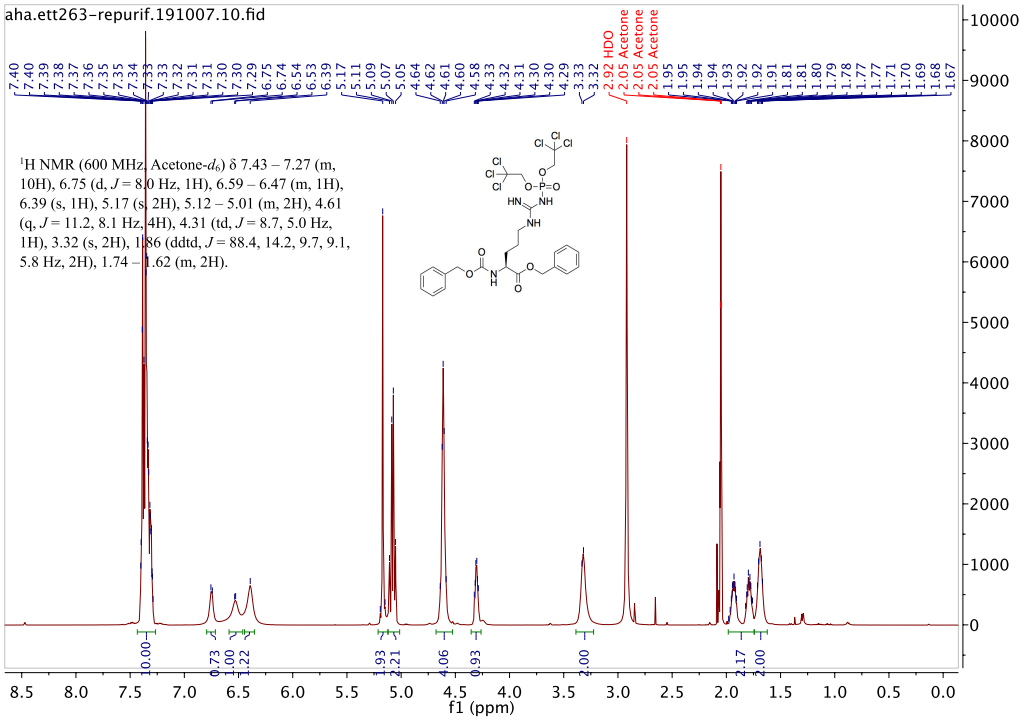

Figure A87: ^{1}H NMR spectrum of compound **30** (600 MHz, acetone-d_6).

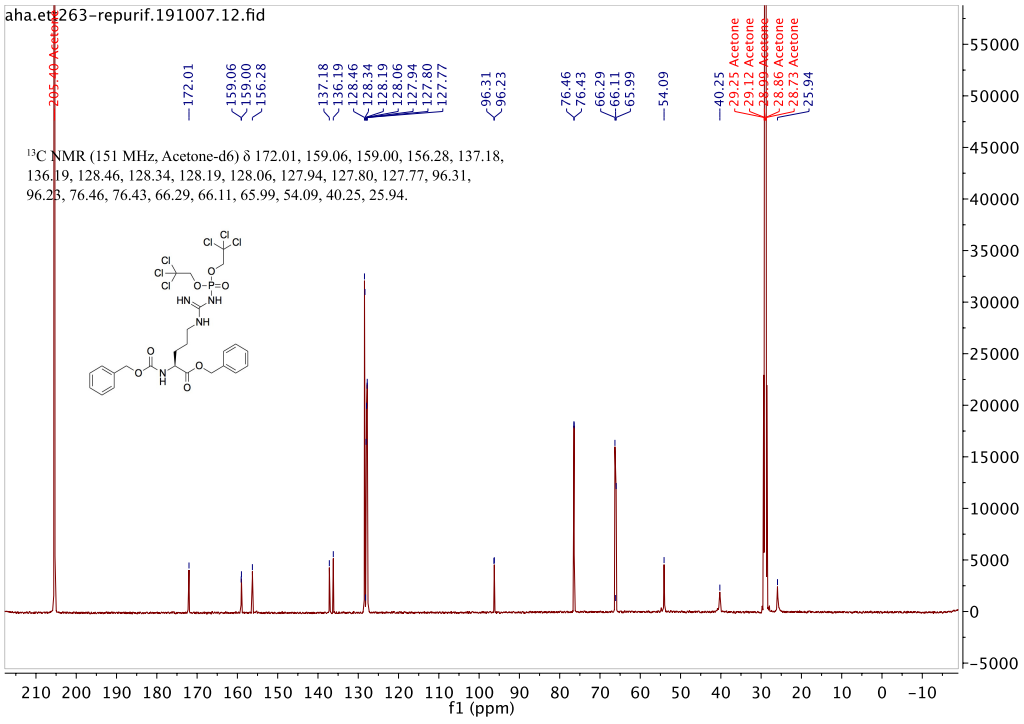

Figure A88: ^{13}C NMR spectrum of compound **30** (151 MHz, acetone-d_6).

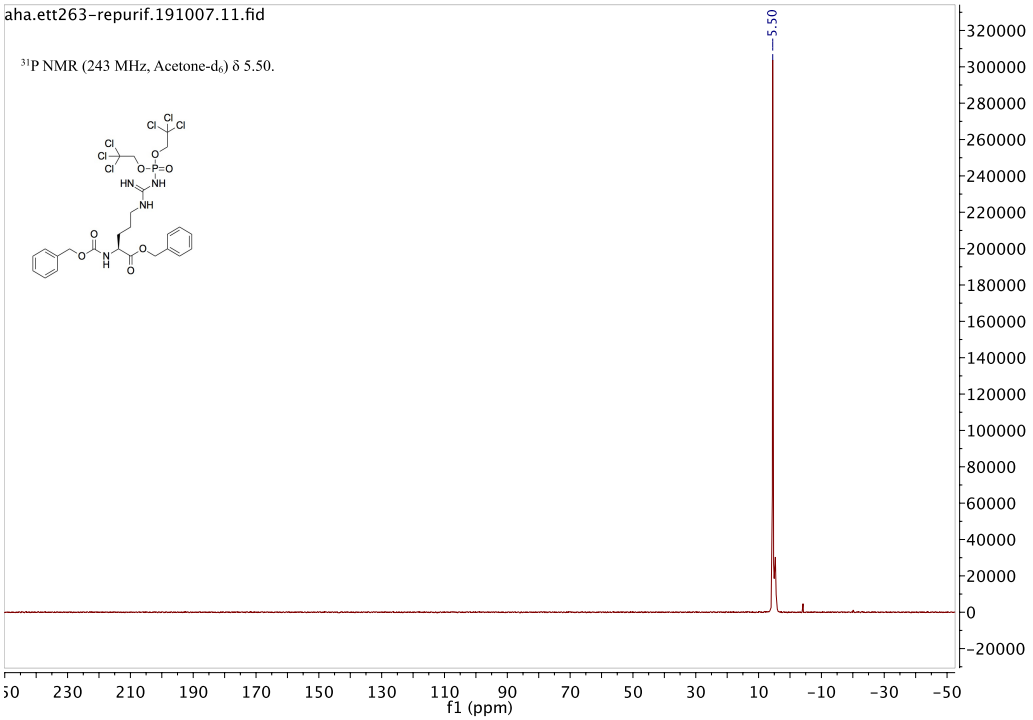

Figure A89: ^{31}P NMR spectrum of compound **30** (243 MHz, acetone-d_6).

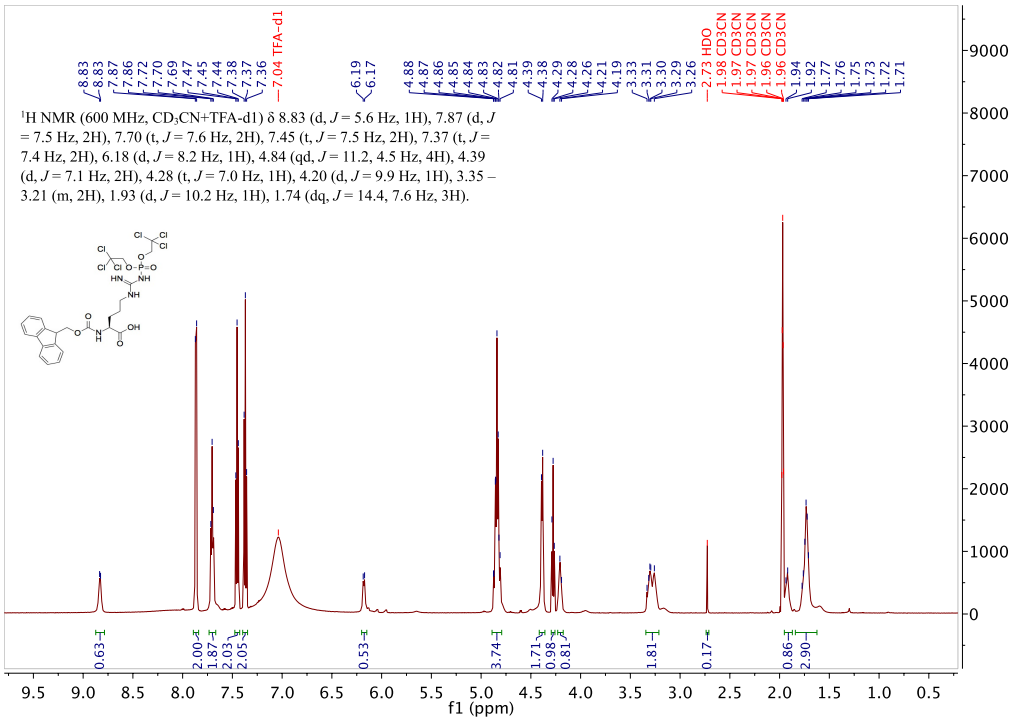

Figure A90: ^{1}H NMR spectrum of compound **34** (600 MHz, CD_3CN + TFA).

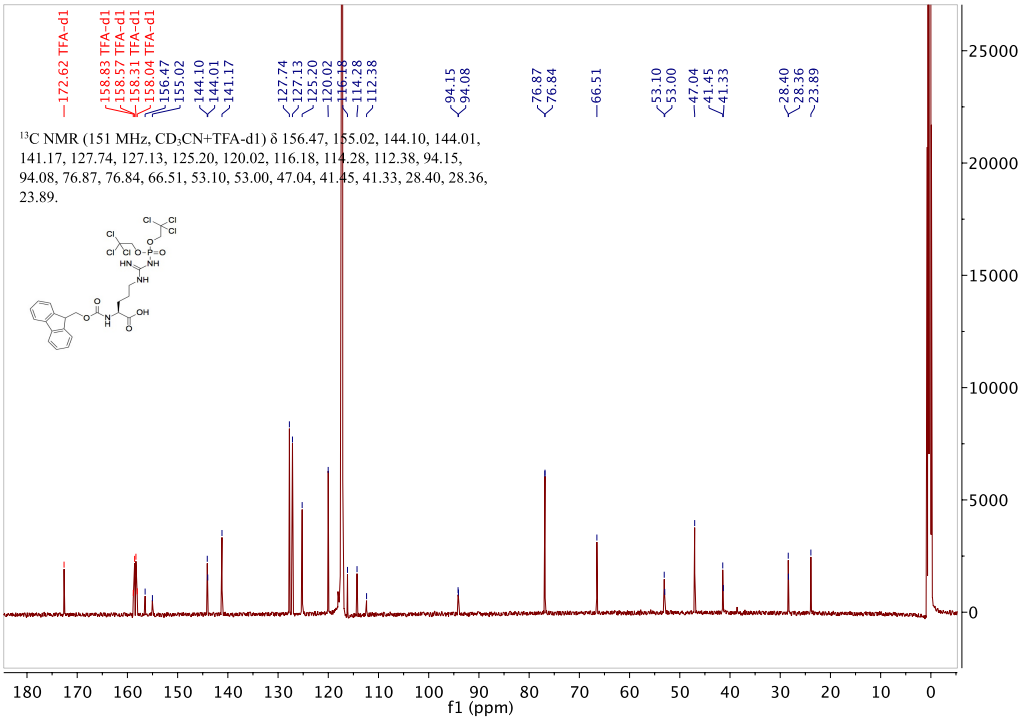

Figure A91: ^{13}C NMR spectrum of compound **34** (151 MHz, CD_3CN + TFA).

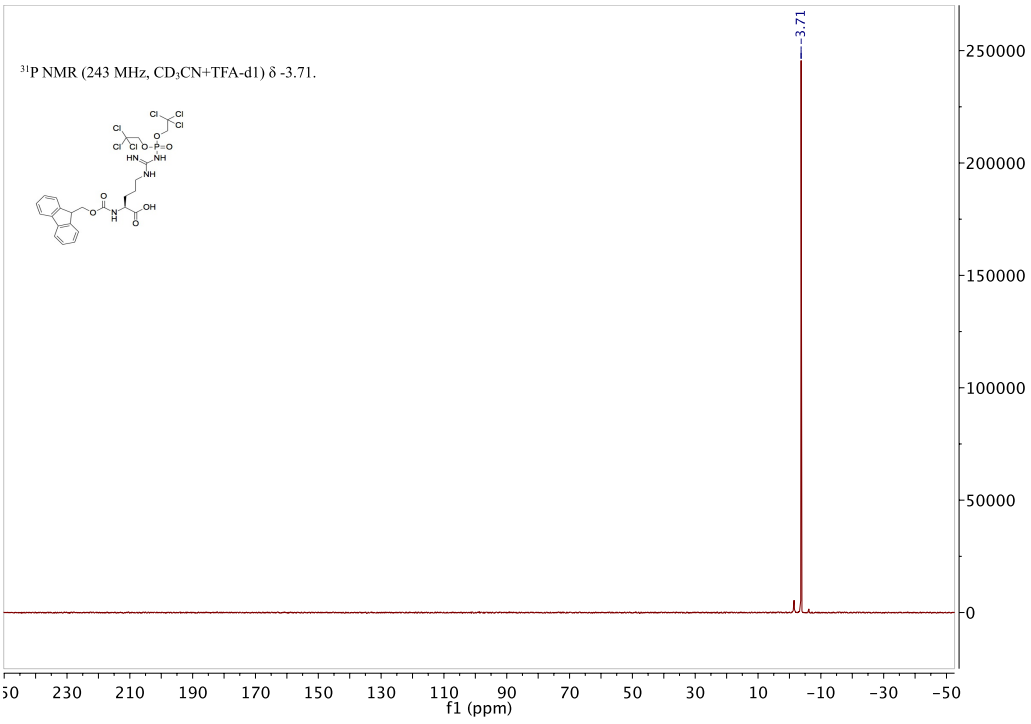

Figure A92: ^{31}P NMR spectrum of compound **34** (243 MHz, CD_3CN + TFA).

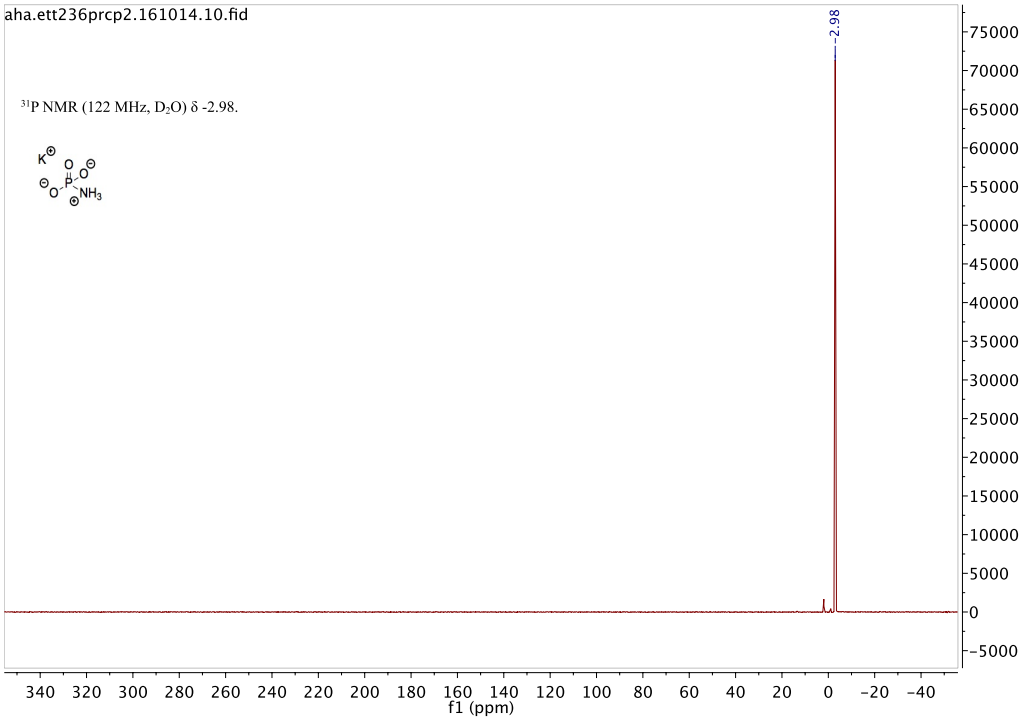

Figure A93: ^{31}P NMR spectrum of compound **35** (122 MHz, D_2O).

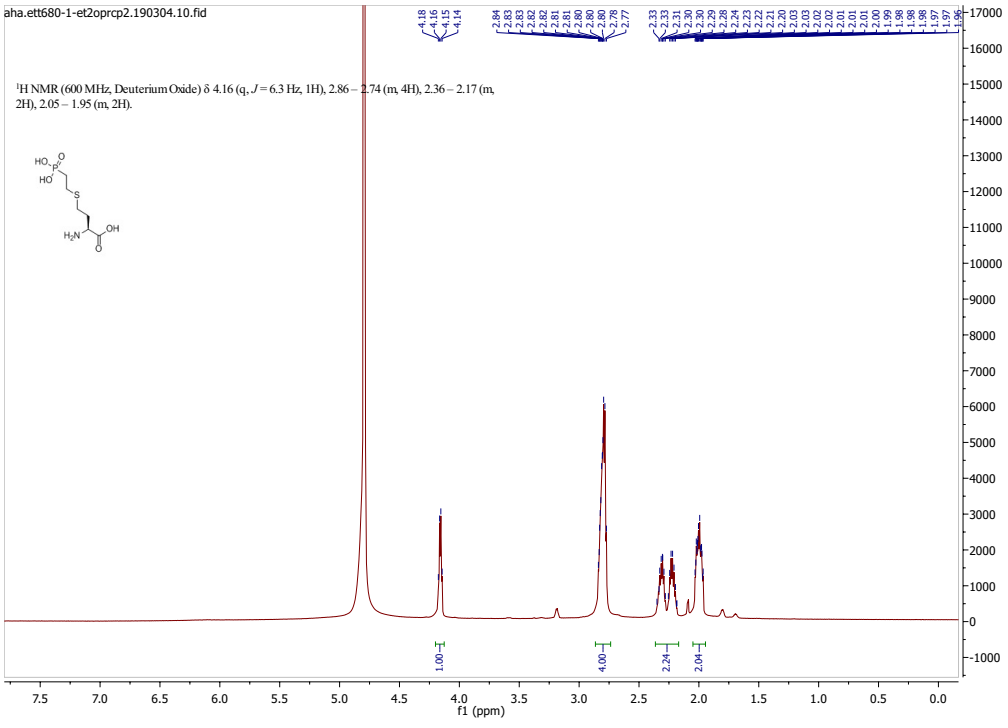

Figure A94: ^{1}H NMR spectrum of compound **59a** (600 MHz, D_2O).

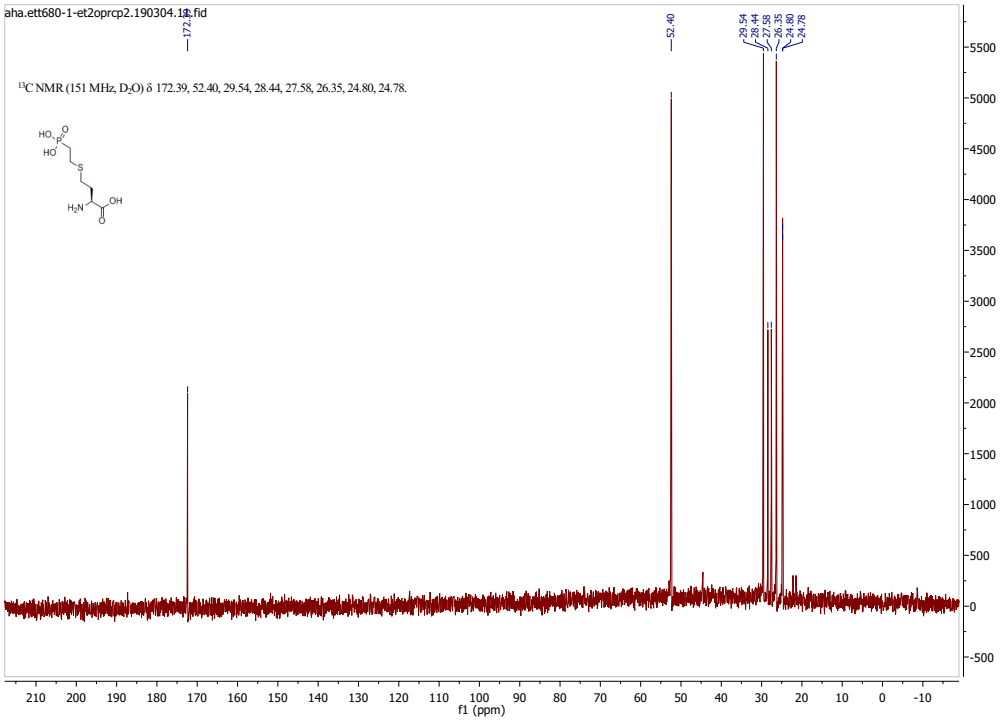

Figure A95: ^{13}C NMR spectrum of compound **59a** (151 MHz, D_2O).

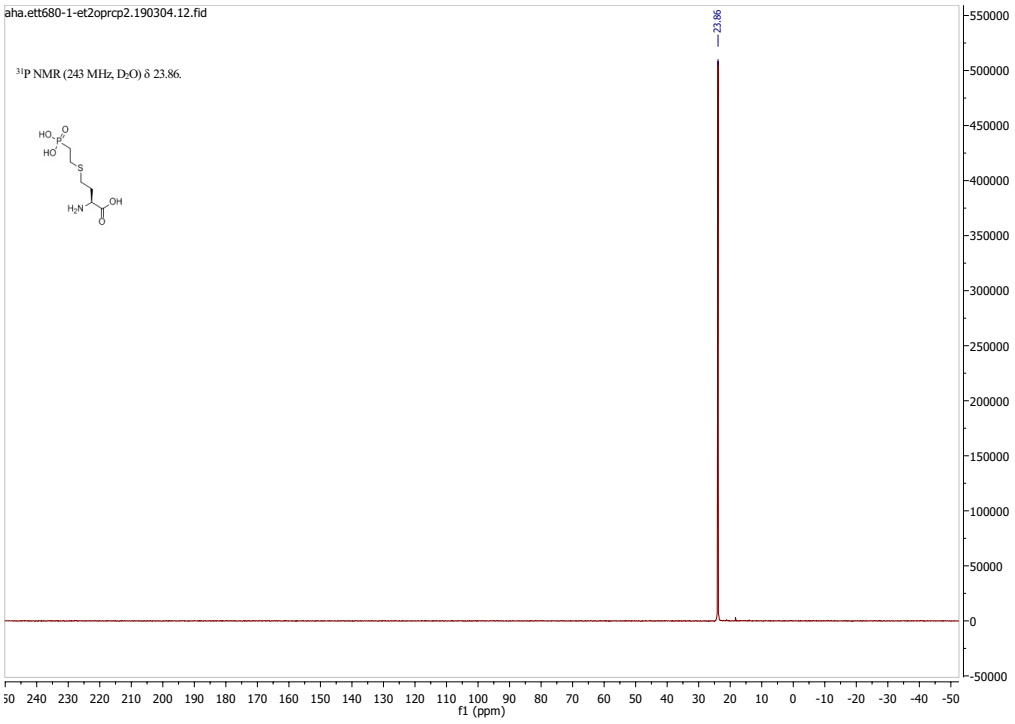

Figure A96: ^{31}P NMR spectrum of compound **59a** (243 MHz, D_2O).

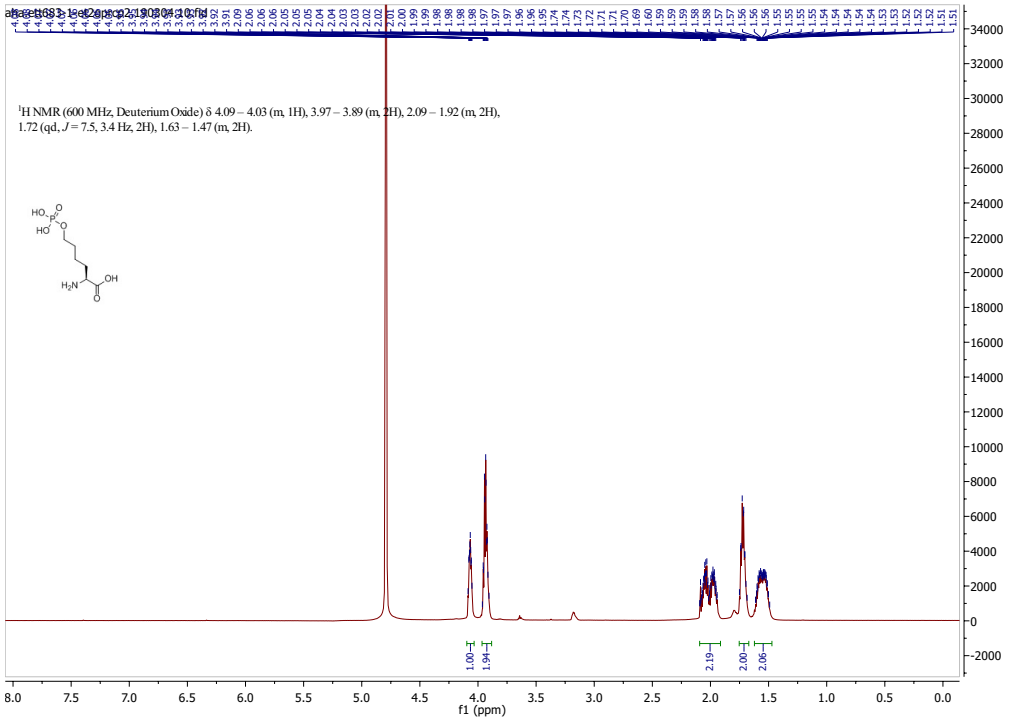

Figure A97: ^{1}H NMR spectrum of compound **59b** (600 MHz, D_2O).

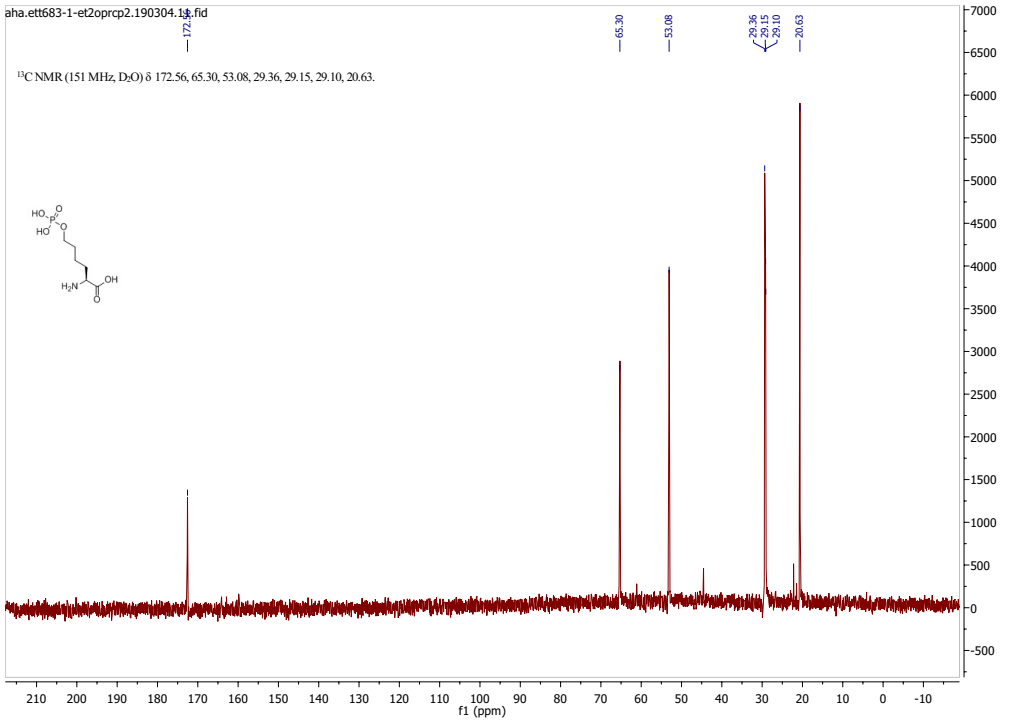

Figure A98: ^{13}C NMR spectrum of compound **59b** (151 MHz, D_2O).

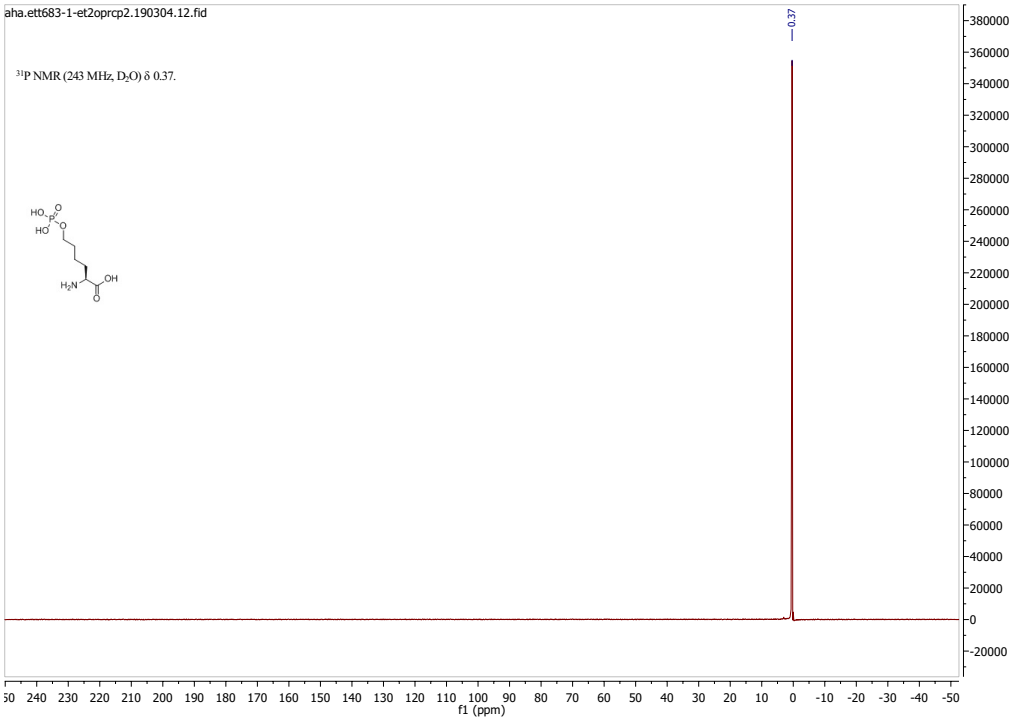

Figure A99: ^{31}P NMR spectrum of compound **59b** (243 MHz, D_2O).

Acknowledgements

First, I would like to thank my supervisor Prof. Christian Hackenberger for the opportunity to pursue my doctoral studies in his group. The project he entrusted me with was many things, just not boring. I was able to grow professionally and above all personally every day of my PhD. His supervision enabled me to learn how to find my own path as well as to act and argue at eye level and I am grateful for our occasional get-togethers when I got the opportunity to share my impressions.

In addition, I would like to thank Prof. Dorothea Fiedler and Prof. Christian Hedberg for reviewing my work. Thank you Dr. Franziska Emmerling and Prof. Julia Stähler for being part of my doctoral degrees committee.

I am also very grateful to the Evonik Foundation for the financial support over three years of my doctoral thesis.They also enabled me to see many exciting places and meet people inside and outside of chemical industry and academia, both of which have shaped my future path. Mrs. Peitzmann was a wonderful caregiver in all those years. Special thanks go to my fellows David Karl, who infected me with his curiosity for everything, and Lydia, who helped me discuss my results.

Thinking about the FMP, I highly appreciated working in such a professional and yet familiar environment. The diversity in research at the institute gave me the opportunity to learn a lot outside of my field. I'm especially grateful to the kind-hearted elves, who cared for all the small details in the background, helped me organizing my work and shared their wisdom with me. Here I would like to name Marianne, Katta, Jenni, Kristin, Dagmar, Ines, Beate, Heike N., Heike S., Michael, Michal, Brigitte, Monika, Nils, Andreas and Herr Reich.

Also, I would like to thank the whole Hackenberger group. The "We're all in this together" spirit among us made my PhD life so much more bearable. Special thanks to lab B3.02 in its recent and former composition for the stories, jokes and music even when it came from the neighbors: Jordi – the pLys pioneer and my start-up support, Tom, Sergej – my brother from another mother, Alice – thank you for all your caring and open words, Wenyi, Bingja, Reihaneh – taking the project to the next level, Eleftheria – Queen, you've grown so much and made me grow. I'm also grateful for the other labile phosphorylation companions, who fought with me: Martin – Marty McFly, my MS buddy, Simon, Deba and Chris.
Un grand merci à Antoine, qui m'a aidé à traverser une phase difficile de mon doctorat grâce à ses connaissances, ses coups de pouce dans la vie et son français.
Thank you Oliver and Dominik for all your knowledge about antibodies and proteins in general.
I should not forget the great performance of the UPLC team in all these years. Thanks to Tom, Lorenzo and Lutz for courting the lady with me.
Besides all of us being awesome together, some group members will always have a special place in

my heart: Olaia, Kristina – un vin chaud à Paris rend le monde meilleur, Klenki, Maria – let's go to this concert or back to Leipzig, Jahzy – thanks for your natural and yet progressive mind and words, Alec – look what we have become, Don – thanks for your empathy and coolness, Bro.

This thesis would have never been completed without my interns, who struggled, succeeded and failed with me – Alina, Jeannine and Elef, and my collaboration partners, who were at my side with continuous support and advise. Thank you Dr. Schepers, Peter S., Han, Martin and Fabian. I also would like to thank Maja Köhn, Hubert Kalbacher, Sabryna, Peter C. and Timm for fruitful discussion about my work. Un gran agradecimiento y un gran abrazo a Olalla, que ha estado a mi lado desde mi Master thesis y es un modelo a seguir para mí como WINS.

I further would like to thank my proofreading team either for actual proofreading and correcting or just for trying to do it, which made me stick to my own deadlines after all. Thanks to Mathi, Jahzy, Carsten, Claudia, Martin, Alec and Philipp.

Besides my work life, many people supported me during the last years either by encouraging me, listening to my complaints, distracting me or also staying away when it was necessary. Danke an meine Familie und besonders an meine Mutter und Antje, die bei mir waren, als ich mich aus dem warmen Schoß einer sicheren Festanstellung ins Studium wagte und auch jetzt hier sind, wenn ich dieses Abenteuer nach gefühlt endlos vielen Jahren beende.

I highly appreciate all the people from our Kaffeekränzchen club and the hortus refugio, who enjoy afternoons and evenings full of vegan/gluten free food, good wine or gin and laughter with us. Your diversity nourishes me: Rebekka, Mathi, Monsieur Meunier, Matthias, Timm, Lena, Alec, Jahzy, Antje, Alice, Simon, Philipp, Elef, Frédéric, Johnny, Pablo, Francesco, David and your specialawesomeones.
Also, I am grateful for my specialawesomeones, who accompanied me for a little while, through countless personal struggles regarding the thesis or otherwise: Carsten, Ani, Anghi, Johnny and Claudia. Thank you 2m6 for letting space in our togetherness – without you I'm just < .

Additionally, I would like to thank the people I met during various volunteering and political activism experiences and who have been in my life for short or long time. All of you helped me making up my mind about my future path.
Special thanks to my fellows from the Journey in August 2019. It was such a fun, intense and deliberating experience with you. Big hugs for Val, El, Sanne, Anaïs, Meyssoun, Anisja and Carlos.

List of Publications, Posters and Oral Presentations

Publications

- Bhabak, K.P., Hauser, A., Redmer, S., Banhart, S., Heuer, D. and Arenz, C., "Development of a Novel FRET Probe for the Real-Time Determination of Ceramidase Activity", *ChemBioChem* **2013**, *14*(9), 1049-1052. DOI: 10.1002/cbic.201300207
- Hauser, A. and Bohlmann, R., "Preparation of Aldehydes by Oxidation of Benzylic Amines with Selectfluor™ (F-TEDA-BF4)", *Synlett* **2016**, *27*(12), 1870-1872. DOI: 10.1055/s-0035-1561642
- Di Pisa, M., Hauser, A. and Seitz, O., "Maximizing Output in RNA-Programmed Peptidyl-Transfer Reactions", *ChemBioChem* **2017**, *18*(9), 872–879. DOI: 10.1002/cbic.201600687
- Hauser, A., Penkert, M. and Hackenberger, C.P.R., "Chemical Approaches to Investigate Labile Peptide and Protein Phosphorylation", *Accounts of Chemical Research* **2017**, *50*(8), 1883-1893. DOI: 10.1021/acs.accounts.7b00170
- Penkert, M., Hauser, A., Harmel, R., Fiedler, D., Hackenberger, C.P.R. and Krause, E., "Electron-Transfer/Higher-Energy Collision Dissociation of Doubly Charged Peptide Ions: Identification of Labile Protein Phosphorylations", *Journal of the American Society for Mass Spectrometry* **2019**, *30*(9), 1578-1585. DOI: 10.1007/s13361-019-02240-4
- Hauser, A.,* Stieger, C.E.* and Hackenberger, C.P.R., "Beyond phosphate esters – synthesis of unusually phosphorylated peptides and proteins for proteomic research", in Brik, A., Dawson, P. and Liu, L. (Ed.) "Total Chemical Synthesis of Proteins" **2020**, John Wiley & Sons, Inc., New York, *manuscript accepted.* *both authors contributed equally
- Hauser, A., Hwang, S., Sun, H. and Hackenberger, C.P.R. "Combining free energy calculations with tailored enzyme activity assays to elucidate substrate binding of a phospho-lysine phosphatase", *Chemical Science* **2020**, *11*, 12655-12661. DOI: 10.1039/D0SC03930F
- Hauser, A., Poulou, E., Müller, F., Schmieder, P. and Hackenberger, C.P.R., "Synthesis and evaluation of non-hydrolyzable phospholysine peptide mimics" *Chemistry—A European Journal* **2020**. DOI: 10.1002/chem.202003947

Posters

- Bertran-Vicente, J., Reiske, S., Hauser, A. and Hackenberger, C.P.R., "Chemoselective tools to study protein phosphorylation", *ICBS/ECBS* **2015**, Berlin.
- Reiske, S., Hauser, A., Bertran-Vicente, J. and Hackenberger, C.P.R., "Chemoselective tools to study protein phosphorylation", *FMP/MDC PhD Retreat* **2015**, Bad Saarow.

- Hauser, A., Bertran-Vicente, J., Penkert, M. and Hackenberger, C.P.R., "Chemoselective Tools to Decipher Lysine Phosphorylation", *EPS* **2016**, Leipzig.
- Hauser, A., Bhowmick, D. Bertran-Vicente, J., Penkert, M., Krause, E. and Hackenberger, C.P.R., "Chemoselective Tools to Decipher Uncommon Phosphorylations", *GDCh-Wissenschaftsforum* **2017**, Berlin.
- Hauser, A., Bertran-Vicente, J., Penkert, M., Krause, E. and Hackenberger, C.P.R., "Chemoselective Tools to Decipher Lysine Phosphorylation", *EMBO Workshop Chemical Biology* **2018**, Heidelberg.

Oral Presentations

- Hauser, A., "Understanding Lysine Phosphorylation – Chemical Methods for the Proteomic Analysis and Elucidation of the Biological Role" *Evonik Scientific Colloquium* **2016**, Darmstadt.

Selbstständigkeitserklärung

Ich, Anett Hauser, erkläre, dass ich die Dissertation selbstständig und nur unter Verwendung der von mir gemäß § 7 Abs. 3 der Promotionsordnung der Mathematisch-Naturwissenschaftlichen Fakultät, veröffentlicht im Amtlichen Mitteilungsblatt der Humboldt-Universität zu Berlin Nr. 42/2018 am 11.07.2018 angegebenen Hilfsmittel angefertigt habe. Alle Zitate sind als solche kenntlich gemacht. Diese Dissertation wurde bisher nicht in gleicher oder ähnlicher Form bei anderen Prüfungsausschüssen eingereicht.

_____ Berlin, den

Hereby, I, Anett Hauser, declare that I have authored the present dissertation independently and only by means of the stated resources in accordance to § 7 Abs. 3 of the Promotionsordnung of the Faculty of Mathematics and Natural Sciences, published in the Official Gazette of Humboldt-Universität zu Berlin (Amtliches Mitteilungsblatt) no. 42/2018 on 11/07/2018. All citations are marked as such. This thesis was not submitted to other examination boards in the same or similar form before.

_____ Berlin